

POLITECNICO DI MILANO

Facoltà di Ingegneria Civile, Ambientale e Territoriale

Corso di laurea specialistica in Ingegneria Civile



Updated overview of concentrated head losses in pressure pipelines' devices

Relatore: Prof. Alberto Bianchi

Correlatore: Ing. Emiliano Veronese

Tesi di laurea di

Andrea Cappelletti

Matricola 770873

ANNO ACCADEMICO 2012/2013

Index

1.	List of figures	1
2.	List of tables	4
3.	List of graphs	7
4.	Abstract (italian)	15
5.	Abstract (english)	18
6.	Introduction	20
6.1.	General directions	22
6.2.	Theoretical framework	26
6.2.1.	Properties of the fluid	26
6.2.2.	Equations and definitions	30
6.2.2.1.	Equilibrium of fluids	30
6.2.2.2.	Motion of fluids	32
6.2.3.	Bernoulli's theorem	37
6.2.4.	Flow in pipes	40
6.2.5.	Friction head losses	41
6.2.6.	Local head losses	53
7.	Smooth contractions and Inlets	57
7.1.	Smooth contractions	58
7.2.	Conduit inlets	61
8.	Sudden Enlargements and Orifices	63
8.1.	Introduction	65
8.1.1.	Sudden Enlargements	65
8.1.2.	Orifices	73
8.2.	Graphs of head loss coefficients	81
9.	Diffusers	99
9.1.	Introduction	101
9.2.	Graphs of head loss coefficients	115
10.	Bends	145
10.1.	Introduction	146
10.2.	Circular arc bends	147
10.3.	Mitre bends	151
11.	Junctions	152
11.1.	Introduction	153
11.2.	Sharp-edged combining tees	155
11.3.	Sharp-edged dividing tees	160
11.4.	Symmetrical division of flow	164
11.5.	Tee junction edges	166
12.	Grids, screens and bar gratings	168
12.1.	Grids	170

12.2.	Screens	178
12.3.	Bar gratings	182
13.	Valves	186
13.1.	Introduction	188
13.1.1.	Theoretical approach	190
13.1.2.	Loss coefficient ζ and flow coefficients C_v , K_v	193
13.1.3.	Limitation in using data	197
13.1.4.	Valves with contractions at inlet/outlet	198
13.1.5.	Classification of valves	199
13.2.	Gate valves	202
13.2.1.	Fully open gate valves	204
13.2.2.	Other types of gate valves	210
13.2.3.	Partial opening of gate valves	211
13.3.	Globe valves	213
13.3.1.	Fully open globe valves	215
13.3.2.	Globe valves with contractions at inlet and outlet	223
13.3.3.	Globe valves with reduced seat	224
13.3.4.	Partial opening of globe valves	225
13.3.5.	Other types of globe valves	226
13.4.	Lift check valves	230
13.4.1.	Standard Lift Check Valves	231
13.4.2.	Ball check-valves	235
13.5.	Disc check-valves	238
13.6.	Conical check-valves	242
13.7.	Nozzle valves	245
13.7.1.	Solid disc nozzle check valves	247
13.7.2.	Ring disc nozzle check valves	251
13.8.	Plug Valves	253
13.8.1.	Fully open plug valves	254
13.8.2.	Plug valves with contractions at inlet and outlet	257
13.9.	Ball Valves	258
13.9.1.	Fully open ball valves	259
13.9.2.	Ball valves with contractions at inlet and outlet	261
13.10.	Stopcocks	262
13.11.	Butterfly valves	263
13.11.1.	Fully open central pattern	268
13.11.2.	Fully open double eccentric pattern	273
13.11.3.	Partial opening of butterfly valves	275
13.12.	Flaps	278
13.13.	Swing check-valves	279
13.14.	Wafer check valves	284
13.14.1.	Swing type wafer check valves	284

	13.14.2.	Split disk wafer check valves	285
13.15.		Tilting-disc check-valves	287
	13.15.1.	Fully open Tilting-disc check-valves	288
	13.15.2.	Partial opening of tilting disc-check valves	291
13.16.		Diaphragm valves	292
14.		New valve introduction	295
14.1.		Main inlet valve for hydro power turbines	295
14.2.		VAG CHECKtronic pump safety valve	297
15.		Conclusions	304
15.1.		Introduction	305
15.2.		Valves comparisons and conclusions	308
	15.2.1.	Gate valves	309
	15.2.2.	Globe valves	315
	15.2.3.	Nozzle valves	336
	15.2.4.	Plug valves	341
	15.2.5.	Ball valves	352
	15.2.6.	Butterfly valves	356
	15.2.7.	Swing check valves	367
	15.2.8.	Tilting disc check valves	373
15.3.		Future developments	379
16.		Bibliography	381
17.		Acknowledgements	

1 List of figures

6	Introduction			
	Figure:	1	infinitesimal volume with volume and surface forces	30
	Figure:	2	fluid flow regimes	33
	Figure:	3	velocity distributions over the pipe cross section for laminar and turbulent flow	34
	Figure:	4	stretch of stream with parameters	35
	Figure:	5	geometrical interpretation of the Bernoulli's theorem	38
	Figure:	6	Bernoulli's theorem extension to streams	39
	Figure:	7	stream separation and formation of eddies in a diffuser	53
	Figure:	8	schematic representation of a local head loss measuring	55
7	Smooth contractions and Inlets			
	Figure:	1	smooth contractions	58
	Figure:	2	schematic view of a smooth contraction with geometrical parameters	59
	Figure:	3	schematic view of a conduit inlet with rounded boundary	61
8	Sudden Enlargements and Orifices			
	Figure:	1	flow pattern at sudden expansion	65
	Figure:	2	equilibrium equation	66
	Figure:	3	smooth diffuser $\alpha = 8^\circ$ to 10°	69
	Figure:	4	general case of a stream flow from one volume into another through an orifice	73
9	Diffusers			
	Figure:	1	diffuser's geometrical schematic shape	101
	Figure:	2	main measures contributing to an improvement of flow in diffusers	110
	Figure:	3	Initial Zone	115
	Figure:	4	Conical diffuser in a line	118
	Figure:	5	Pyramidal diffuser in a line	121
	Figure:	6	Plane diffuser in a line	125
	Figure:	7	Transition diffusers	131
	Figure:	8	Curved diffusers' geometrical parameters	132
	Figure:	9	Stepped conical diffuser's geometrical parameters	135
	Figure:	10	Stepped pyramidal diffuser's geometrical parameters	138
	Figure:	11	Stepped plane diffuser's geometrical parameters	141
10	Bends			
	Figure:	1	Bend geometry	146
11	Junctions			
	Figure:	1	Notation for combining flow and dividing flow	153
12	Grids, screens and bar gratings			
	Figure:	1	schematic view of a plane grid (perforated sheet)	172
	Figure:	2	schematic view of beveled edges grid	174
	Figure:	3	schematic view of rounded orifices grid	176
13	Valves			
	Figure:	1	flow pattern and turbulences in double disk check valve	188
	Figure:	2	throttling device (gate valve)	190

Figure:	3	head lines and piezometrical lines before and after a throttling component	191
Figure:	4	gate valve closure member	202
Figure:	5	VAG BETA® 200 Gate Valve	202
Figure:	6	VAG EKOPlus Gate valve	202
Figure:	7	VAG IKOPlus Gate valve	202
Figure:	8	EKO and IKO VAG models schematic view	203
Figure:	9	geometrical parameters associated with gate valves	211
Figure:	10	VAG Dura control globe valve	213
Figure:	11	Different types of globe valves	214
Figure:	12	seating configuration frequently employed in Globe valves	215
Figure:	13	standard globe valve models: vertical (90°) and 45° walls	219
Figure:	14	direct-flow globe valve with geometrical parameters	226
Figure:	15	schematic representation and section view of a lift check valve (standard pattern)	230
Figure:	16	VAG KRV ball check-valve	235
Figure:	17	schematic view of VAG KRV ball check-valve	235
Figure:	18	VAG KRV Ball Check Valve	237
Figure:	19	schematic functioning of disk check valves	238
Figure:	20	Conical valve with geometric parameters	242
Figure:	21	conical valve types with geometrical parameters	242
Figure:	22	solid disc nozzle check valve	247
Figure:	23	Idel'chik spherical closure member and geometrical parameters	248
Figure:	24	ring disc nozzle check valves	251
Figure:	25	Schematic View of a plug valve	253
Figure:	26	Throttling positions of plug valves	253
Figure:	27	ball valve	258
Figure:	28	Functioning of a ball valve	258
Figure:	29	stopcock with its schematic opening angle representation	262
Figure:	30	VAG Cerex 300-L Butterfly valve	263
Figure:	31	schematic view of the VAG Cerex-L butterfly valve	263
Figure:	32	definition of opening angle for butterfly valves	264
Figure:	33	high friction during the stroke of the closure member	265
Figure:	34	moving the center of rotation back	265
Figure:	35	imperfect watertight closure	266
Figure:	36	vertical moving of the rotation line of the closure member	266
Figure:	37	VAG EKN Butterfly Valve schematic	267
Figure:	38	VAG EKN Butterfly Valve	267
Figure:	39	geometrical parameters that define the thickness ratio factor	268
Figure:	40	VAG CEREX-L Butterfly Valve	271
Figure:	41	VAG CEREX-W Butterfly Valve	271
Figure:	42	VAG EKN Butterfly Valve	273
Figure:	43	3D view of VAG EKN Butterfly valve	273
Figure:	44	flap valve	279
Figure:	45	VAG RSK Check valve	279
Figure:	46	VAG RSK Disk Check valve (swing check valve)	280
Figure:	47	VAG RSK Disk Check Valve AL	282
Figure:	48	VAG RETO-STOP Non-Return Valve	283

	Figure:	49	sectional veiw of a wafer check valve	284
	Figure:	50	VAG ZETKA Non-return valve	285
	Figure:	51	wafer double disk check valve schematic view	285
	Figure:	52	VAG SKR Slanted Seat Tilting-disk check valve	287
	Figure:	53	VAG SKR Slanted Seat Tilting-disk check valve (CUT VIEW)	287
	Figure:	54	tilting-disk valve opening angle definition	288
	Figure:	55	schematic view of VAG TOP-STOP valve	292
	Figure:	56	difference between straight-through type and the weir type of diaphragm valve	292
	Figure:	57	VAG TOP-STOP Diaphragm Non-Return Valve	293
	Figure:	58	VAG TOP-STOP diaphragm non-return valve (technical illustration)	293
14	New valve introduction			
	Figure:	59	VAG Main Inlet Valve	295
	Figure:	60	components of Main Inlet Valve	295
	Figure:	61	CFD computation of velocity	296
	Figure:	62	VAG CHECKtronic Pump Safety Valve	297
	Figure:	63	Checktroinc valve features illustration	298
	Figure:	64	VAG CHECKtronic pump safety valve with gearbox and electric actuator	299
	Figure:	65	VAG CHECKtronic pump safety valve with electric actuator and without gearbox	299
15	Conclusions			
	Figure:	1	Excel screenshot choosing the trend-lines' model	306

2 List of tables

6	Introduction			
	Table:	1	values of density for water on different temperatures for 101325 Pa (1 atm) pressure	26
	Table:	2	conversion factors for dynamic viscosity	28
	Table:	3	conversion factors for kinematic viscosity	28
	Table:	4	dynamic and kinematic viscosity of water as function of temperature	29
	Table:	5	other simplified formulas for friction coefficients	50
	Table:	6	roughness of pipe and channels	51
7	Smooth contractions and Inlets			
	Table:	1	loss coefficients for smooth contractions	60
8	Sudden Enlargements and Orifices			
	Table:	1	formulas for different types of restrictor at $Re > 10^5$	79
	Table:	2	formulas for different types of restrictor at $Re < 10^5$	79
9	Diffusers			
	Table:	1	number of dividing walls	111
	Table:	2	values of k_1	116
	Table:	3	values of ζ_{exp}	119
	Table:	4	values of ζ_{fr}	120
	Table:	5	values of ζ_{exp}	123
	Table:	6	values of $\Delta\zeta_{fr}$ and $\Delta\zeta'_{fr}$ on α, β	124
	Table:	7	values ζ_{exp} on θ	126
	Table:	8	values of ζ_{fr} on θ , for different a_0/b_0 ratios	127
	Table:	9	values of φ_0	133
	Table:	10	values of σ_0 and d	134
	Table:	11	values of ζ_{min}	136
	Table:	12	values of θ_{opt}	137
	Table:	13	values of ζ_{min}	139
	Table:	14	values of θ_{opt}	140
	Table:	15	values of ζ_{min}	142
	Table:	16	values of θ_{opt}	143
12	Grids, screens and bar gratings			
	Table:	1	Coefficients for different bar type	174
	Table:	2	values of k_1	185
13	Valves			
	Table:	1	conversion factors between litres, UK gallons and US gallons	194
	Table:	2	coefficients conversion with diameters in [mm]	196
	Table:	3	friction factors for clean steel pipe in complete turbulence zone	197
	Table:	4	determination of the head loss coefficient values for sudden (gradual) contraction and enlargement	198
	Table:	5	classification of valves according to functional features	199
	Table:	6	classification of valves according to their basic design	201
	Table:	7	VAG Gate valves products	202
	Table:	8	examples of approximate minor loss coefficient associated to standard gate valve from different sources	204
	Table:	9	formulas for calculating loss coefficient for gate valves	209

	Table:	10	particular types of gate valve	210
	Table:	11	examples of approximate minor loss coefficient associated to standard globe valve from different sources	215
	Table:	12	resistance coefficient for straight-way globe valves formulas	226
	Table:	13	particular globe valve types	229
	Table:	14	Head loss coefficients ζ for plug valves	254
	Table:	15	Head loss coefficients for ball valves	259
	Table:	16	Bianchi and Sanfilippo values of loss coefficients	268
	Table:	17	VAG VALVES data for tilting disk check valve without damper unit	290
	Table:	18	head loss coefficients from Miller (1973)	294
	Table:	19	head loss coefficients from Zappe (1998)	294
14	New valve introduction			
	Table:	20	head loss coefficients computation	301
	Table:	21	comparison between statistical parameters of CHECKtronic and globe oblique pattern	303
15	Conclusions			
	Table:	1	average ζ values for fully open gate valves	310
	Table:	2	statistical parameters for fully open gate valves	312
	Table:	3	average ζ values for fully open globe valves (standard pattern)	316
	Table:	4	statistical parameters for fully open globe valves (standard pattern)	318
	Table:	5	average ζ values for fully open globe valves (angle pattern)	321
	Table:	6	statistical parameters for fully open globe valves (angle pattern)	323
	Table:	7	average ζ values for fully open globe valves (oblique pattern)	326
	Table:	8	statistical parameters for fully open globe valves (oblique pattern)	328
	Table:	9	comparison between head loss coefficients from standard and reduced seat globe valves (standard models)	330
	Table:	10	comparison between vertical dividing walls and 45° dividing walls for standard globe valves	331
	Table:	11	comparison of loss coefficient values ζ at different opening percentage between different globe valve models	332
	Table:	12	comparison between corresponding models of lift-check valves and globe valves	333
	Table:	13	average ζ values for fully open nozzle valves	337
	Table:	14	statistical parameters for fully open nozzle valves	338
	Table:	15	comparison between ranges of different plug valve's patterns	342
	Table:	16	average ζ values for fully open plug valves (tapered pattern)	343
	Table:	17	statistical parameters for fully open plug valves (tapered pattern)	344
	Table:	18	average ζ values for fully open plug valves (cylindrical pattern)	346
	Table:	19	statistical parameters for fully open plug valves (cylindrical pattern)	347
	Table:	20	average ζ values for fully open plug valves (3-way pattern)	349
	Table:	21	statistical parameters for fully open plug valves (3-way pattern)	350
	Table:	22	average ζ values for fully open ball valves	353
	Table:	23	statistical parameters for fully open ball valves	354
	Table:	24	average ζ values for fully open butterfly valves (central pattern)	357
	Table:	25	statistical parameters for fully open butterfly valves (central pattern)	358
	Table:	26	average ζ values for butterfly valves (central pattern) on the opening angle δ	361

	Table:	27	statistical parameters for fully open butterfly valves (central pattern)	362
	Table:	28	loss coefficients ζ for fully open butterfly valve double eccentric pattern	364
	Table:	29	comparison between loss coefficients ζ for central model and double eccentric model and percentage differences at same DN	365
	Table:	30	average ζ values for swing check valves	368
	Table:	31	statistical parameters for swing check valves	369
	Table:	32	comparison between average ζ values for swing check valves, single wafer check valves and double wafer check valves	371
	Table:	33	comparison between ranges of different plug valve's patterns	372
	Table:	34	average ζ values for tilting disc check valves ($\alpha = 5^\circ$)	374
	Table:	35	average ζ values for tilting disc check valves ($\alpha = 15^\circ$)	375
	Table:	36	statistical parameters for tilting-disc check valves	377

3 List of graphs

6	Introduction			
	Graph:	1	kinematic viscosity on temperature at 101325 Pa (1 atm)	39
	Graph:	2	values of λ for circular sections and smooth walls at laminar flow	46
	Graph:	3	values of k_1 for rectangular sections and smooth walls at laminar flow	46
	Graph:	4	values of λ for circular and rectangular section and smooth walls at transitional flow	47
	Graph:	5	values of friction coefficient for circular and rectangular section and smooth walls for turbulent flow	47
	Graph:	6	Nikuradse Graph	48
	Graph:	7	Prandtl v.Karaman expression plotted on different values of relative roughness	49
	Graph:	8	Moody Graph	50
7	Smooth contractions and Inlets			
	Graph:	1	loss coefficients for smooth convergences with different area ratio	60
	Graph:	2	loss coefficients for rounded conduit inlet	62
8	Sudden Enlargements and Orifices			
	Graph:	1	Velocity distribution in plane diffusers with divergence angle not wider than 8°	71
	Graph:	2	Non-symmetric velocity distribution behind an elbow or diffuser with cause the stream separation	72
	Graph:	3	Values of ζ' for straight entrance into a conduit for different values of b/D_h (legend)	75
	Graph:	4	Values of ζ' for entrance at an arbitrary angle δ into a conduit	76
	Graph:	5	Values of ζ' for smooth entrance made by an arc of a circle, without screen, at $Re > 10^4$	77
	Graph:	6	values of ζ' for conical converging entrance at various angle of convergence α , at $Re > 10^4$	77
	Graph:	7	ζ with sudden expansion of a stream with uniform velocity distribution - $Re > 3,5 \times 10^3$	81
	Graph:	8	ζ with sudden expansion of a stream with uniform velocity distribution $10 < Re < 3,5 \times 10^3$	82
	Graph:	9	values of M and N in exponential velocity	83
	Graph:	10	ζ with circular or rectangular cross section	83
	Graph:	11	values of M and N in exponential velocity	84
	Graph:	12	ζ with plane and straight stretches or plane diffusers	84
	Graph:	13	values of M and N after plane plane and straight stretches, plane diffuser, etc., with exponential velocity distribution	85
	Graph:	14	ζ with sudden enlargement of a plane channel behind orifice plates, baffles in elbows, etc., with sinusoidal velocity distribution	85
	Graph:	15	values of ζ with sudden expansion behind plane diffusers with $\alpha > 10^\circ$, elbows, etc., with asymmetric velocity distribution	86
	Graph:	16	values of ζ for sudden expansion after stretches with parabolic velocity distribution	86

	Graph:	17	values of ζ with stream deformation in a straight conduit with exponential velocity profile	87
	Graph:	18	values of ζ with sharp-edged orifice at the passage of the stream from a conduit of one size to another	88
	Graph:	19	values of ε_0 and $\zeta\varphi$ for sharp-edged orifice at the passage of the stream from a conduit of one size to another - $Re < 10^5$	90
	Graph:	20	values of ζ_0 for sharp-edged orifice at the passage of the stream from a conduit of one size to another - $Re < 10^5$	90
	Graph:	21	values of τ for thick-edged orifice at the passage of the stream from a conduit of one size to another	91
	Graph:	22	values of ζ' for thick-edged orifice with orifice beveled or rounded at the passage of the stream from a conduit of one size to another	92
	Graph:	23	values of ζ for sharp edged orifice in straight conduit	93
	Graph:	24	values of ζ for thick edged orifice in straight conduit, with $Re > 10^5$	95
	Graph:	25	values of ζ for orifice with edges beveled facing the stream flow in straight pipe	96
	Graph:	26	values of ζ for orifice with rounded edges in straight pipe	97
	Graph:	27	values of k_M for perforated plate at high Mach numbers	98
9	Diffusers			
	Graph:	1	performance chart resulting from Gibson experience	103
	Graph:	2	velocity profiles in plane diffusers with different divergence angles	105
	Graph:	3	values of k_1 on divergence angle θ	116
	Graph:	4	values of V_{max}/V_0 for Initial Zone (straight pipe)	117
	Graph:	5	values of V_{max}/V_0 for Initial Zone (straight pipe)	117
	Graph:	6	values of ζ_{exp} on divergence angle θ	119
	Graph:	7	values of ζ_{fr} on θ angle	120
	Graph:	8	values of ζ_{exp}	123
	Graph:	9	values of $\Delta\zeta_{fr}$ and $\Delta\zeta'_{fr}$ on α, β	124
	Graph:	10	values of ζ_{exp} on θ	126
	Graph:	11	values of ζ_{fr} at $a_0/b_0 = 0,5$ on θ values	128
	Graph:	12	values of ζ_{fr} at $a_0/b_0 = 0,75$	129
	Graph:	13	values of ζ_{fr} at $a_0/b_0 = 1,0$	129
	Graph:	14	values of ζ_{fr} at $a_0/b_0 = 1,5$	130
	Graph:	15	values of ζ_{fr} at $a_0/b_0 = 2,0$	130
	Graph:	16	values of φ_0 on L_d/D_h (L_d/α_0)	133
	Graph:	17	values of d and d, σ_0 on F_0/F_1	134
	Graph:	18	values of σ on F_0/F_1	135
	Graph:	19	values of ζ_{min} on L_d/D_0	136
	Graph:	20	values of θ_{opt} on L_d/D_0	137
	Graph:	21	values of σ on F_0/F_1	138
	Graph:	22	values of ζ_{min} on L_d/D_h	139
	Graph:	23	values of θ_{opt} on L_d/D_h	140
	Graph:	24	values of σ on F_0/F_1	141
	Graph:	25	values of ζ_{min} on L_d/θ_0	142
	Graph:	26	values of θ_{opt} on l_d/θ_0	143
10	Bends			
	Graph:	1	loss coefficient for circular cross-section bends	149
	Graph:	2	loss coefficients for square cross-section bends	149

	Graph:	3	loss coefficients for rectangular cross-section bends (aspect ratio = 0,5)	149
	Graph:	4	loss coefficients for rectangular cross-section bends (aspect ratio = 2)	149
	Graph:	5	Reynolds number correction factor	150
	Graph:	6	outlet tangent length correction	150
	Graph:	7	loss coefficients for single mitre bends	151
	Graph:	8	loss coefficients for 90 degree composite bends	151
11	Junctions			
	Graph:	1	Loss coefficients ζ_{23} for 45 degrees sharp-edged combining tees (r=3)	156
	Graph:	2	Loss coefficients ζ_{13} for 45 degrees sharp-edged combining tees (r=1)	156
	Graph:	3	Loss coefficients ζ_{13} for 45 degrees sharp-edged combining tees (r=1)	157
	Graph:	4	Loss coefficients ζ_{23} for 90 degrees sharp-edged combining tees (r=3)	158
	Graph:	5	Loss coefficients ζ_{13} for 90 degrees sharp-edged combining tees (r=1)	159
	Graph:	6	Loss coefficients ζ_{13} for 90 degrees sharp-edged combining tees (r=1)	159
	Graph:	7	Loss coefficients ζ_{32} sharp-edged dividing tees	161
	Graph:	8	Loss coefficients ζ_{31} for 90 degrees sharp-edged dividing tees (r=1)	162
	Graph:	9	Loss coefficients ζ_{31} for 90 degrees sharp-edged dividing tees (r=1)	162
	Graph:	10	Loss coefficients ζ_{31} for 45 degrees sharp-edged dividing tees (r=1)	163
	Graph:	11	Loss coefficients ζ_{31} for 45 degrees sharp-edged dividing tees (r=1)	163
	Graph:	12	Loss coefficients for symmetrical division of flow (A1=A2=A3)	164
	Graph:	13	Loss coefficients for symmetrical division of flow (A1=A2 and A1+A2=A3)	165
	Graph:	14	correction factors C13 for 90 degrees combining tees with a radius of 0,1D ₁	166
	Graph:	15	correction factors C23 for 90 degrees combining tees with a radius of 0,1D ₁	167
	Graph:	16	correction factors C31 for 90 degrees combining tees with a radius of 0,1D ₁	167
12	Grids, screens and bar gratings			
	Graph:	1	loss coefficients for plane grid (perforated sheet) with sharp edged orifices and Reynolds Number > 10 ⁵	172
	Graph:	2	ζ_{φ} coefficients for plane grid with sharp-edged orifices Re < 10 ⁵	173
	Graph:	3	loss coefficients fro grid with orifices edges beveled facing the flow	174
	Graph:	4	loss coefficients for thickened grid (perforated plate or laths) with l/dh > 0,015	175
	Graph:	5	loss coefficients for grid with rounded orifices edges	176
	Graph:	6	values of km plotted on Mach Number varying <i>f</i>	177
	Graph:	7	loss coefficients for screens with Reynolds number larger than 400	180
	Graph:	8	kRe coefficients for screens	180
	Graph:	9	values of coefficient k'M that allow for Mach influence	181
	Graph:	10	geometrical parameters of grantings	184
	Graph:	11	values of k ₁ coefficients for bar grating (Re10 ⁴)	185
13	Valves			
	Graph:	1	loss coefficients for fully open gate valves	205
	Graph:	2	loss coefficients for fully open gate valves (Crane)	205
	Graph:	3	VAG valves performance charts	205
	Graph:	4	loss coefficients for fully open gate valves (oppo.it)	206

	Graph:	5	loss coefficients for fully open gate valves (metropumps.com)	206
	Graph:	6	loss coefficients for fully open gate valve (crbnet.com)	207
	Graph:	7	comparison between head loss coefficients from different gate valves's sources	208
	Graph:	8	loss coefficients for gate valves	211
	Graph:	9	loss coefficients for wedge-type gate valves	212
	Graph:	10	loss coefficients for fully open globe valves three types (Miller)	216
	Graph:	11	loss coefficients for fully open globe valves three types (Miller)	217
	Graph:	12	loss coefficients for fully open globe valves (metropumps.com)	217
	Graph:	13	Idel'chik values of Loss coefficient for standard globe valves	219
	Graph:	14	loss coefficients for Y-pattern (oblique) globe valve	220
	Graph:	15	loss coefficients for fully open globe standard values	221
	Graph:	16	loss coefficients for fully open globe angle valves	221
	Graph:	17	loss coefficients for fully open oblique valves	222
	Graph:	18	loss coefficients for open globe standard valves with reduced seat for Crane	223
	Graph:	19	loss coefficients for open globe standard valves with reduced seat for Miller	224
	Graph:	20	loss coefficients for the three models of globe valve against opening percentage	225
	Graph:	21	loss coefficients for direct-flow globe valve, $Re > 3 \times 10^5$ for complete opening	227
	Graph:	22	loss coefficients for direct-flow globe valve, $Re > 3 \times 10^5$ for incomplete opening	228
	Graph:	23	Determination of k_{Re}	228
	Graph:	24	loss coefficients for fully open lift check valve standard pattern (Crane)	231
	Graph:	25	loss coefficients for fully open lift check valve oblique pattern (Crane)	231
	Graph:	26	loss coefficients for fully open lift check valve standard pattern with reduced seat (Crane)	232
	Graph:	27	loss coefficients for fully open lift check valve oblique pattern with reduced seat (Crane)	232
	Graph:	28	loss coefficient values for fully open lift check valves	233
	Graph:	29	comparison between Crane data and metropumps.com data	234
	Graph:	30	loss coefficients ζ for ball check valve (Bianchi, Sanfilippo)	236
	Graph:	31	head loss coefficients for different values of flow velocity (ball check valve VAG)	237
	Graph:	32	values of coefficient G1 for disk valves with bottom guides	240
	Graph:	33	values of coefficient G2 for disk valves with bottom guides	240
	Graph:	34	loss coefficient for disk check valves (Idel'chik)	241
	Graph:	35	loss coefficients for conical valve on conical seat (Idel'chik)	243
	Graph:	36	loss coefficients ζ for conical valve on flat seat (Idel'chik)	244
	Graph:	37	loss coefficients for nozzle check valves (Bianchi and Sanfilippo)	247
	Graph:	38	loss coefficients ζ for nozzle check valves	248
	Graph:	39	loss coefficients for nozzle solid disc check valves (Goodwin International)	249
	Graph:	40	loss coefficients for nozzle solid disc check valves (Erhard)	249

	Graph:	41	loss coefficients for solid disc check valve (NoReVa)	250
	Graph:	42	loss coefficients ζ for nozzle ring disc check valve (Goodwin international)	252
	Graph:	43	loss coefficients ζ for plug valves (metropumps.com)	254
	Graph:	44	loss coefficient for plug valves (Crane book)	254
	Graph:	45	comparison between Crane book and metropumps.com for cylindrical open plug valves	255
	Graph:	46	comparison between Crane book and metropumps.com for tapered open plug valves	255
	Graph:	47	comparison between Crane book and metropumps.com for 3-way open plug valves	256
	Graph:	48	loss coefficient for fully open plug valves	257
	Graph:	49	loss coefficients ζ for fully open ball valve	259
	Graph:	50	loss coefficients ζ for fully open ball valve (metropumps.com)	260
	Graph:	51	comparison between the two sources for head loss coefficient of fully open ball valve	260
	Graph:	52	coefficients ζ for fully open ball valve with contraction and enlargement	261
	Graph:	53	loss coefficients for stopcocks (Idel'chik)	262
	Graph:	54	loss coefficients for fully open butterfly valve against thickness ratio	268
	Graph:	55	Loss coefficients for fully open valves from metropumps.com	269
	Graph:	56	loss coefficients for fully open valves from Crane book	269
	Graph:	57	loss coefficients for fully open valves from valvias.com	270
	Graph:	58	loss coefficients for fully open valves from valvemate.com	270
	Graph:	59	loss coefficients for fully open VAG CEREX Butterfly Valve	271
	Graph:	60	comparison between loss coefficients of central pattern of butterfly valves	272
	Graph:	61	VAG EKN Butterfly Valve loss coefficients	274
	Graph:	62	loss coefficients for butterfly valve against opening angle values between 40° and 70° (water.me.vccs.edu)	275
	Graph:	63	Loss coefficients for butterfly valve against opening angle values between 0° and 40° (water.me.vccs.edu)	275
	Graph:	64	Loss coefficients for butterfly valve against opening angle values between 0° - 40° (Idel'chik)	275
	Graph:	65	Loss coefficients for butterfly valve against opening angle values between 40° - 70° (Idel'chik)	275
	Graph:	66	Loss coefficients for butterfly valve against opening angle (valvias.com)	276
	Graph:	67	Loss coefficients for butterfly valve against opening angle (valvemate.com)	276
	Graph:	68	Comparison between loss coefficients of different sources (opening percentage)	277
	Graph:	69	Loss coefficient for flap valves in logarithmic scale (Idel'chik)	278
	Graph:	70	loss coefficients for swing check valves (Idel'chik)	280
	Graph:	71	Loss coefficients for VAG RSK Disk Check Valve AL	282
	Graph:	72	Loss coefficients for VAG RETO-STOP Non-Return Valve	283
	Graph:	73	loss coefficient ζ for wafer swing check valve (sureflowequipment.com)	284

	Graph:	74	loss coefficients for wafer double disk valve (sureflowequipment.com)	286
	Graph:	75	Loss coefficients for tilting disk check valve at $\alpha = 5^\circ$ and $\alpha = 15^\circ$ (Crane)	288
	Graph:	76	Loss coefficients for tilting disk check valve at $\alpha = 5^\circ$ and $\alpha = 15^\circ$ (metropumps.com)	288
	Graph:	77	comparison between head loss values from metropumps.com and Crane	289
	Graph:	78	head loss coefficients for VAG SKR slanted seat tilting disk check valve	290
	Graph:	79	loss coefficients against opening angle for tilting disk check valve	291
	Graph:	80	Loss coefficients for VAG TOP-STOP Diaphragm Non-Return Valve	294
14	New valve introduction			
	Graph:	81	local head losses of CHECKtronic valve against the flow	301
	Graph:	82	loss coefficients ζ for CHECKtronic valve	302
	Graph:	83	comparison between loss coefficients ζ of a standard globe valve oblique pattern and the CHECKtronic valve	303
15	Conclusions			
	Graph:	1	Loss coefficients ζ for fully open gate valves - comparison between sources	309
	Graph:	2	average ζ values for fully open gate valves	310
	Graph:	3	average values ζ and trend-line y for fully open gate valves	311
	Graph:	4	average values ζ and trend-line y for fully open gate valves	311
	Graph:	5	comparisons between metallic and resilient type of gate valves	314
	Graph:	6	Loss coefficients ζ for fully open globe valves standard pattern - comparison between sources	315
	Graph:	7	average ζ values for fully open globe valves (standard pattern)	316
	Graph:	8	average values ζ and trend-line y for fully open globe valves (standard pattern)	317
	Graph:	9	average values ζ and trend-line y for fully open globe valves (standard pattern)	317
	Graph:	10	Loss coefficients ζ for fully open globe valves angle pattern - comparison between sources	320
	Graph:	11	average ζ values for fully open globe valves (angle pattern)	321
	Graph:	12	average values ζ and trend-line y for fully open globe valves (angle pattern)	322
	Graph:	13	average values ζ and trend-line y for fully open globe valves (angle pattern)	322
	Graph:	14	Loss coefficients ζ for fully open globe valves oblique pattern - comparison between sources	325
	Graph:	15	average ζ values for fully open globe valves (oblique pattern)	326
	Graph:	16	average values ζ and trend-line y for fully open globe valves (oblique pattern)	327
	Graph:	17	average values ζ and trend-line y for fully open globe valves (oblique pattern)	327

	Graph:	18	comparison between head loss coefficients from standard and reduced seat globe valves (standard models)	330
	Graph:	19	comparison between vertical dividing walls and 45° dividing walls for standard globe valves	331
	Graph:	20	comparison of loss coefficient values ζ at different opening percentage between different globe valve models	332
	Graph:	21	comparison between corresponding models of lift-check valves and globe valves	333
	Graph:	22	loss coefficients ζ for fully open nozzle valves - comparison between sources	336
	Graph:	23	average ζ values for fully open nozzle valves	337
	Graph:	24	average values ζ and trend-line y for fully open nozzle valves	338
	Graph:	25	loss coefficients ζ for fully open plug valves - comparison between sources	341
	Graph:	26	average ζ values for fully open plug valves (tapered pattern)	343
	Graph:	27	average values ζ and trend-line y for fully open plug valves (tapered pattern)	344
	Graph:	28	average ζ values for fully open plug valves (cylindrical pattern)	346
	Graph:	29	average values ζ and trend-line y for fully open plug valves (cylindrical pattern)	347
	Graph:	30	average ζ values for fully open plug valves (3-way pattern)	349
	Graph:	31	average values ζ and trend-line y for fully open plug valves (3-way pattern)	350
	Graph:	32	loss coefficients ζ for fully open ball valves - comparison between sources	352
	Graph:	33	average ζ values for fully open ball valves	353
	Graph:	34	average values ζ and trend-line y for fully open ball valves	354
	Graph:	35	loss coefficients ζ for fully open butterfly valves (central pattern) - comparison between sources	356
	Graph:	36	average ζ values for fully open butterfly valves (central pattern)	357
	Graph:	37	average values ζ and trend-line y for fully open butterfly valves (central pattern)	358
	Graph:	38	loss coefficients ζ for butterfly valves (central pattern) on the opening angle δ - comparison between sources	360
	Graph:	39	average ζ values for butterfly valves (central pattern) on the opening angle δ	361
	Graph:	40	average values ζ and trend-line y for butterfly valves (central pattern) against the opening angle δ	362
	Graph:	41	loss coefficients ζ for fully open butterfly valve double eccentric pattern at different PN	364
	Graph:	42	comparison between loss coefficients ζ for central model and double eccentric model	365
	Graph:	43	loss coefficients ζ for fully open swing check valves - comparison between sources	367
	Graph:	44	average ζ values for swing check valves	368
	Graph:	45	average values ζ and trend-line y for swing check valves	369
	Graph:	46	comparison between average ζ values for swing check valves, single wafer check valves and double wafer check valves	371
	Graph:	47	loss coefficients ζ for tilting disc check valves - comparison between sources	373
	Graph:	48	average ζ values for tilting disc check valves ($\alpha = 5^\circ$)	374

	Graph:	49	average ζ values for tilting disc check valves ($\alpha = 15^\circ$)	375
	Graph:	50	average values ζ and trend-line y for tilting disc check valves ($\alpha = 5^\circ$)	376
	Graph:	51	average values ζ and trend-line y for tilting disc check valves ($\alpha = 15^\circ$)	376

4 Abstract (italian)

Il problema dello studio del moto nelle correnti in pressione di liquidi incomprimibili è uno degli argomenti principali dell'ingegneria idraulica e il calcolo delle perdite di carico è il fattore centrale di tale problema. Da un punto di vista pratico, indipendentemente dalla complessità delle reti di condotte in pressione, la precisione nel calcolo delle perdite di carico comporta vantaggi economici rilevanti.

Questo lavoro è nato, in collaborazione con la ditta VAG-Armaturen GmbH, dall'esigenza pratica di poter disporre di un manuale che consentisse il calcolo delle perdite di carico, con valori e formule, accompagnato da una stima dell'affidabilità. Pertanto, il fine del lavoro è consistito nella stesura di un manuale pratico per il calcolo delle perdite di carico dei più diffusi dispositivi idraulici, accompagnato da uno studio della variabilità e dell'affidabilità dei dati reperiti in letteratura e in rete.

I destinatari di tale manuale sono compresi in un ampio campo di specialisti: progettisti, tecnici operativi, ingegneri, studenti universitari e d'istituti tecnici.

Dal punto di vista teorico, lo studio delle correnti in pressione può essere visto come la ricerca della relazione esistente fra le perdite di carico della corrente e tutte le altre grandezze fisiche da cui dipendono. Tali grandezze possono suddividersi in tre categorie:

- grandezze relative al condotto: area e forma della sezione, scabrezza delle pareti, lunghezza;
- grandezze cinematiche: portata e velocità media della corrente fluida;
- grandezze relative al fluido: viscosità, densità, (comprimibilità);

Determinata questa relazione e, quindi, determinato il valore delle perdite di carico, è possibile studiare il moto di liquidi incomprimibili nelle condotte in pressione attraverso il teorema di Bernoulli, per la cui applicazione dovranno essere soddisfatte le seguenti ipotesi:

1. moto permanente;
2. correnti lineari;

Le perdite di carico possono essere suddivise in perdite distribuite e perdite localizzate; queste ultime rappresentano il principale oggetto di studio del presente lavoro.

Le perdite di carico localizzate sono l'effetto di disturbi in tratti limitati al regolare flusso delle correnti, che appaiono come separazione dalle superfici di contorno dei dispositivi e la conseguente formazione di vortici nelle zone di distacco. Questi vortici comportano la trasformazione di parte dell'energia meccanica totale del flusso in calore che, a sua volta, implica la dissipazione di tale energia. La geometria interna dei dispositivi in esame è il principale fattore d'influenza sulle perdite di carico localizzate: la separazione dai confini dei dispositivi è dovuta a brusche variazioni geometriche nei corpi degli stessi che provocano destabilizzazioni del profilo medio della velocità nel condotto e la conseguente formazione di turbolenze.

Le perdite di carico localizzate ΔH sono proporzionali al termine cinetico del trinomio di Bernoulli e, perciò, sono esprimibili mediante la seguente relazione:

$$\Delta H = \zeta \frac{V^2}{2g}$$

Il coefficiente di proporzionalità, detto coefficiente perdita di carico localizzata, si calcola, perciò, mediante la seguente espressione:

$$\zeta = \frac{\Delta H}{\frac{V^2}{2g}}$$

La perdita di carico localizzata, che si determina mediante la relazione precedente è, in realtà, la somma della perdita localizzata provocata dal dispositivo idraulico in esame e della perdita di carico distribuita presente nel tratto in esame.

Per quanto riguarda questo aspetto, i dispositivi trattati, fatta eccezione per i diffusori, hanno una lunghezza (nella direzione della condotta) ridotta e ciò implica che la perdita localizzata vera e propria, possa essere considerata uguale alla somma delle due perdite senza errori eccessivi.

Ci sono varie modalità formali di esprimere il valore delle perdite di carico localizzate associate al relativo dispositivo: coefficiente di perdita di carico localizzata ζ , coefficienti di flusso C_V o K_V , e altri ancora. La validità di tutte le modalità è equivalente e non è oggetto di discussione, ma in questa sede si è preferito l'uso dell'espressione mediante coefficiente di perdita di carico localizzata ζ . Il vantaggio di tale scelta è legato all'adimensionalità e, quindi, all'applicabilità immediata del coefficiente ai calcoli ingegneristici.

La struttura del lavoro è articolata nei seguenti punti principali:

1. introduzione teorica;
2. presentazione dei coefficienti ζ e delle formule per il loro calcolo associati ai relativi dispositivi idraulici;
3. confronto fra i coefficienti ζ trovati per le valvole e conclusioni;

Nella parte teorica introduttiva sono fornite indicazioni generali necessarie alla corretta lettura della tesi in tutti i suoi aspetti, comprese le ipotesi idrauliche basilari che non possono essere trascurate. In seguito si elencano le basi matematiche principali che consentono di capire la collocazione del problema e gli strumenti che consentono di affrontare analiticamente lo studio delle correnti in pressione. Infine sono forniti gli strumenti per il calcolo delle perdite di carico distribuite, qualora non fossero trascurabili.

Nella sezione di presentazione dei coefficienti di perdita di carico localizzata i coefficienti ζ sono presentati in varie modalità: valori puntuali, formule e grafici i quali possono essere ricavati dalle formule e dai dati o semplicemente riportati nelle fonti bibliografiche. Le risorse bibliografiche dalle quali sono stati reperiti i dati sono letteratura cartacea e siti web, richiamati sia nella bibliografia sia nei capitoli dove sono espressamente utilizzati.

I dispositivi idraulici che sono stati trattati sono imbocchi e convergenti, bruschi allargamenti e orifizi, diffusori, gomiti, giunti, griglie, filtri, e, infine, le valvole.

Il capitolo delle valvole è di gran lunga il più esteso per il grande numero di tipologie e per l'innovazione tecnologica che propone sempre nuovi modelli e nuove varianti. Le tipologie di valvola trattate sono molteplici (saracinesche, valvole a sfera, valvole a palla, valvole coniche, valvole di non ritorno, rubinetti, valvole a diaframma, valvole a farfalla ecc) e sono state classificate secondo lo standard europeo EN 736-1.

La parte conclusiva della tesi riguarda esclusivamente le valvole e il paragone fra i valori dei coefficienti e delle formule trovate da diverse fonti per gli stessi modelli di valvola. Nel capitolo sono presenti grafici di confronto, tabelle e una breve valutazione statistica che consente di determinare l'affidabilità dei dati reperiti.

Il lavoro è presentato in lingua inglese per richiesta della ditta VAG e in ogni suo capitolo è presente la lista dei simboli utilizzati in quel capitolo associati alle unità di misura, nel rispetto del Sistema Internazionale di unità di misura SI.

5 Abstract

The field of application of this paper is pipe flow calculation of weighted and incompressible fluid, one of the most important issues of the hydraulic engineering. The object of research is the head loss calculation, the fundamental issue of the pressure pipeline systems design, both from the theoretical and from the practical point of view. The paper is born, in collaboration with VAG-Armaturen GmbH, from the necessity to have a practical handbook containing the tools for calculating the friction losses and the loss coefficients ζ for specific hydraulic pressure devices. The other aim of the paper is to test the reliability of the data found, making comparisons between sources (literature and websites).

The handbook is intended for a wide range of specialists: designing and operating engineers, students of universities and technical institutes. The data of the paper are coming from both bibliographic resources and websites and are presented in different ways: graphs, figures, tables and formulas.

The head losses are divided in two main categories: local (or concentrated) head losses and friction losses. The local head losses are the object of this paper. They are due to sudden changes in the geometry of the system, for example in presence of particular additional devices like valves, diffusers or junctions.

There are different parameters which allow to present the local head losses, but the choice of the author is to use the head loss coefficients ζ (or resistance coefficients):

$$\zeta = \frac{\Delta H}{\frac{V^2}{2g}}$$

This head loss coefficient expresses the direct proportionality between the local head loss and the kinetic part of the Bernoulli's trio. From the hydraulic point of view, the Bernoulli's approach to the problem implies the hypothesis of steady flow and linear streams.

The structure of the paper is divided into three main sections.

In the introductory part are collected the general indications to have a correct reading of the paper, the theoretical framework with the mathematical tools, which make the reader able to fight the problem analytically and the formulas to compute the friction head losses.

In the second part there's the complete presentation of the head loss coefficients ζ associated to the following devices:

- Contractions and inlets;
- Sudden enlargements and orifices;
- Diffusers;
- Bends;
- Junctions;
- Grids and screens;
- Bar gratings;
- Valves;

The valves' data are treated also in the third part, in which there is the comparison of the data for same models but from different sources. Moreover, there are the relative conclusions and a statistical analysis of the reliability.

6 Introduction

List of the chapter symbols

Latin characters:

- a_0, b_0 = sides of the rectangular cross section of a conduit [m];
- ds = infinitesimal space distance, [m];
- dt = infinitesimal time instant, [t];
- D = conduit diameter [m];
- D_h = hydraulic diameter [m];
- D_0 = internal conduit diameter [m];
- DN = Nominal diameter [m];
- F = area of the conduit cross-section [m²];
- g = standard gravity [m/s²];
- G = mass flow rate [kg/m³];
- H = hydraulic head [m];
- J = friction slope;
- L, l = generical length of correlated object, [m];
- m = mass, [kg];
- M = Mach number;
- p = pressure [Pa];
- Q = volumetric flow rate [m³/s];
- Re = Reynolds number;
- s = space linear coordinate in direction of the average flow [m];
- F_V = volume force per unit of mass, [m/s²];
- S_F = resultant of surface forces, [N];
- t = time variable, [s];
- T = fluid temperature [°C];
- v = velocity vector of a fluid particle [m/s];
- V = mean velocity of a stream [m/s];
- Vol = volume, [m³];
- V_F = resultant of volume forces, [N];
- z = elevation of the point above a reference plane [m]

Greek characters:

- α = Coriolis coefficient, [adim];
- γ = specific weight, [N/m^3];
- δ = difference between piezometric heights [m];
- ΔH = head losses [m];
- ΔH_{fr} = friction head losses [m];
- ΔH_{L} = local head losses [m];
- ΔH_{sys} = total system head loss [m]
- ε = absolute geometric roughness [m];
- ε/D = equivalent (or hydraulic) roughness [m];
- ε/D_{h} = relative roughness;
- ζ = resistance coefficient;
- ζ_{fr} = friction resistance coefficient;
- ζ_{L} = local resistance coefficient;
- λ = friction coefficient;
- μ = dynamic viscosity [Ns/m^2];
- ν = kinematic viscosity [m^2/s];
- Π = perimeter of the conduit section [m];
- ρ = density, [kg/m^3];
- τ = shear stresses [Pa];

6.1 General directions

Foreward

The problem of pipe flow calculation of weighted and incompressible fluid is one of the most important practical issues of the hydraulic branch of engineering. In this context, the head loss computation represents one of the central points of all the pressure pipelines design: regardless of the complexity of the pressure pipeline system, the correct calculation of the fluid resistance of these systems is necessary in all the cases to have practical and economical benefits.

This paper is born from this necessity as a practical handbook containing friction coefficients and coefficients of local resistances associated to a variety of pipeline devices, in particular inlets, contractions, sudden enlargements, orifices, diffusers, bends, junctions, grids, screens, gratings and valves.

The handbook is intended for a wide range of specialists: designing and operating engineers, students of universities and technical institutes.

The importance of the problem is testified also by the number of textbooks, hydraulic and scientific papers, experiments, data reports, professional data sheets and internet websites which treat the argument, with data, formulas and practical indications: this paper is the result of an operation of synthesis, standardisation and processing of the data contained in these sources.

Because of the variety of the sources the difficulties encountered during the realization of the paper were considerable and concerned the different range of local resistance, the geometrical differences of considered elements, the different theoretical approach to the issue, the different originating contexts of the textbook and websites consulted. For what it concerns the differences founded in the units of measurement, they were all adapted and converted to the International System of Units SI.

The accuracy of the presented data are variable depending on the devices treated and on the sources' accuracy: one of the aim of this paper is precisely to identify this accuracy, trying to estimate the reliability of the data.

All the symbols that appear in the general direction chapter are accurately defined in the theoretical framework chapter and over the pages of the paper.

The object of research

The basic reference data given in this paper are the friction coefficients ζ_{fr} and the coefficients of local fluid resistance ζ_L of pipe fittings, throttles, obstructions and other industrial instruments.

In this paper it is assumed that all the magnitudes, including all the geometric parameters of the system considered, are given in the known formula for calculating the head losses are given except for the total coefficient of fluid resistance ζ_{sum} :

$$\Delta H_{sum} = \zeta_{sum} \frac{V^2}{2g}$$

the only unknowns are ζ_{sum} and its components ζ_{fr} and ζ_L .

The coefficient of local resistance ζ_L can be considered equal to ζ_{sum} in all the cases in which the value of ζ_{fr} can be neglected if compared to the magnitude of ζ_L . These considerations are true typically for short element's components and thus for the most of the devices treated in this paper.

The values of ζ_L given include the local head losses in the immediate proximity of variation in the system configuration and also the head losses associated with the subsequent equalization of velocities over the straight exit section. Since, however, local losses are arbitrarily determined as the difference between the total and frictional losses in the exit section, the frictional losses have to be taken in account.

All values of local resistance coefficients, with certain exceptions, are given for conditions of uniform velocity distribution in the inlet section of element considered.

The influence of the local resistance of the element, due to fittings, obstructions, or lengthy straight stretches located downstream, is not allowed for the values given of ζ in the handbook, except as noted. In certain cases this influence causes an increase in the value of ζ_L of the element considered, while in other cases a decrease. As yet there is no general method of allowing for this.

The structure of the work

The paper can be divided in three main parts:

- the first one is the introductory part, which contains a forward, the general indications, the theoretical framework and all the necessary indications for the correct usability of the paper itself;
- the second part is the practical collection of the proper coefficients for every device treated;
- the third part contains the comparison between the data obtained from the different sources for the listed devices and the conclusions based on them;

The paper contains 11 chapters, neglecting the bibliography and the lists of graphs, figures and tables.

At the beginning of every chapter is positioned the list of the symbols used in the chapter itself, in alphabetical order and distinguishing between latin and greek characters. Every symbol is presented with its units of measurement according to International System of Units.

The first chapter, the abstract, is a short descriptive summary of the work.

The second chapter is the introduction, which contains the foreward, a list of general directions for the correct usage of the book, the theoretical framework containing general equations and the hydraulics and mechanics of fluids definitions used in the paper and a theoretical treatment of flow in pipes.

The following chapters are titled with the name of the corresponding pipe device and reports all the coefficients, formulas and graph which allows the user to compute the head losses connected to the device itself in the indicated conditions and with the listed limitations.

The last chapter contains the comparison between results obtained from the different sources and a processing of this data in order to get the reliability of the sources and of the data itself.

Reading data

It is important to specify that data are presented in different forms depending on the origin. Because of this fact there were adopted different way to report the coefficients:

- if the data were presented in tables, they were copied as themselves with a graphical plot obtained from them;
- if were presented only functions, the data were obtained using the function on different variables (DN, opening angles, etc.);
- if data were presented in different forms or in different units of measurement (as C_V or K_V for example) the data were obtained converting in loss coefficients in SI units;
- if data were presente only in graphical form (as for Miller book, 1973), they were reported in the paper by optical reconstruction of the curves;

Reynolds number and Mach number

The dependence of the coefficients of local resistance on the Reynolds number Re , is only given in those cases where the influence of the latter is known or can be estimated. In practice, Re has an influence on the local resistance in the range $Re < 2 \times 10^5$. For $Re > 2 \times 10^5$ we can consider the local resistance coefficient as independent on Re . If there is no indication of the values of Re for which the values given for ζ_L were obtained, it can be assumed that, for turbulent flow the values of local resistance are independent on Re . In case of laminar flow, $Re < 10^3$, the given coefficients are only a rough estimation of the real resistance given by the element considered.

All the values given in this paper, except for what is noted, were obtained for Mach numbers $M < 0,3$. In practice, however, the values given for ζ_L and ζ_{fr} are correct even for higher subsonic velocities, roughly up to $M = 0,7 \div 0,8$.

Cross-sections and mean velocity

The basic reference of cross-sectional shape of the pipe considered in the paper is circular and rectangular. When cross-section is not specified as a parameter that has an influence to the result, all the values of resistance coefficient given for polygonal rectangular section of ratio $0,6 \leq a_0/b_0 \leq 1,7$ are available also for circular sections.

In the introduction of this paper it is stated that the head loss due to fittings (and so also to valves) is proportional to a constant power of the velocity head (kinetic head). In the turbulent flow range, the value of the exponent of V has been found to vary from 1,8 to 2,1 for different designs of valves. However, for the practical purposes that this paper has, it can be assumed that this value is 2 for turbulent range.

6.2 Theoretical framework

6.2.1 Properties of the fluid

Density and specific weight

The density, or more precisely, the volumetric mass density, ρ of a substance is defined as its mass per unit volume:

$$\rho = \frac{m}{Vol}$$

In this paper, as it's specified in the introduction, the only fluid take in account is water, so in Table 1 are given the values of water density expressed in kg/m^3 , as imposed from SI.

The specific weight γ is the weight per unit volume of a material, and can be expressed according to SI with N/m^3 . The relation between the two specific properties is the well-known equation:

$$\gamma = \rho g$$

where g is the standard gravity, considered constant and equal to $9,806 \text{ m}/\text{s}^2$.

From a theoretical point of view, both density and specific weight are influenced by pressure and temperature $\rho = \rho(p, T)$. But in the practical field of application, when the fluid is a liquid (as in this paper) the influence of the pressure can be neglected. The dependence of water density on temperature at 101325 Pa is given in Table 1.

Table 1: values of density for water on different temperatures for 101325 Pa (1 atm) pressure

T [°C]	0	10	20	30	40	50	60	70	80	90	100
ρ [kg/m^3]	999,8	999,7	998,2	995,7	992,2	988,1	983,2	977,1	971,8	965,3	958,4

If sea water is analyzed in the system it is obvious that there are variations in density: at 15°C , sea water specific weight is taken from the range $1,020 \div 1,030 \text{ N}/\text{m}^3$.

Viscosity

The viscosity is a property of all the fluids and manifests itself as internal friction during motion as a consequence of internal shear stresses in the fluid. There are two types of viscosity:

1. the dynamic viscosity μ , defined as the ratio of the shear stress τ to the velocity gradient $\frac{dV}{dy}$ in the direction of the normal to the motion direction y :

$$\mu = \frac{\tau}{\frac{dV}{dy}} = \left[\frac{Ns}{m^2} \right] = \left[\frac{kg}{m \cdot s} \right]$$

2. the kinematic viscosity ν , defined as the ratio between the dynamic viscosity of the fluid and its density:

$$\nu = \frac{\mu}{\rho} = \left[\frac{m^2}{s} \right]$$

In the industry it is not unusual that this physical quantity is expressed in poise (P) according to c.g.s. system and corresponding to 0,1 Ns/m², or centipoise (cP) corresponding to 0,001 Ns/m². It is also possible that the units of measurement of the dynamic viscosity is $\frac{kg}{m \times hour}$, or $\frac{kg_p \times s}{m^2}$ (where kg_p is the unit of force corresponding to 9,806 N).

In the c.g.s. system the kinematic viscosity is measured in stokes (St), equivalent to cm²/s.

The conversion factors necessary to pass from c.g.s. system to SI system are given in Table 2 and

Table 3.

Table 2: conversion factors for dynamic viscosity

Unit of measurement	μPs	cPs	Ps	$\text{kg}/(\text{m} \times \text{s})$	$\text{kg}/(\text{m} \times \text{h})$	$(\text{kg} \times \text{s})/\text{m}^2$	$\text{lb}/(\text{ft} \times \text{s})$	$\text{lb}/(\text{ft} \times \text{h})$
μPs	1	10^{-4}	10^{-6}	10^{-7}	$3,6 \times 10^{-4}$	$1,02 \times 10^{-3}$	$6,72 \times 10^{-3}$	$2,42 \times 10^{-4}$
cPs	10^4	1	10^{-2}	10^{-3}	3,6	$1,02 \times 10^{-4}$	$6,72 \times 10^{-4}$	2,42
Ps	10^6	10^2	1	10^{-1}	$3,6 \times 10^2$	$1,02 \times 10^{-2}$	$6,72 \times 10^{-2}$	$2,42 \times 10^2$
$\text{kg}/(\text{m} \times \text{s})$	10^7	10^3	10	1	$3,6 \times 10^3$	$1,02 \times 10^{-1}$	$6,72 \times 10^{-1}$	$2,42 \times 10^3$
$\text{kg}/(\text{m} \times \text{h})$	$2,78 \times 10^9$	$2,78 \times 10^{-1}$	$2,78 \times 10^{-3}$	$2,78 \times 10^{-4}$	1		$1,863 \times 10^{-4}$	$6,72 \times 10^{-1}$
$(\text{kg} \times \text{s})/\text{m}^2$	$9,81 \times 10^7$	$9,81 \times 10^3$	$9,81 \times 10^2$	9,81	$3,53 \times 10^4$	1	6,592	$2,374 \times 10^4$
$\text{lb}/(\text{ft} \times \text{s})$	$1,488 \times 10^7$	$1,488 \times 10^3$	$1,488 \times 10$	1,488	$4,13 \times 10^3$	$1,52 \times 10^{-1}$	1	$3,6 \times 10^3$
$\text{lb}/(\text{ft} \times \text{h})$	$4,13 \times 10^9$	$4,13 \times 10^{-1}$	$4,13 \times 10^{-3}$	$4,13 \times 10^{-4}$	1,488	$4,21 \times 10^{-5}$	$2,77 \times 10^{-4}$	1

Table 3: conversion factors for kinematic viscosity

Unit of measurement	cSt	St	m^2/s	m^2/h	ft^2/s	ft^2/h
cSt	1	10^{-2}	10^{-6}	$3,60 \times 10^{-3}$	$1,07 \times 10^{-5}$	$3,85 \times 10^{-2}$
St	10^2	1	10^{-4}	$3,60 \times 10^{-1}$	$1,07 \times 10^{-3}$	3,85
m^2/s	10^6	10^4	1	$3,60 \times 10^3$	$1,07 \times 10$	$3,85 \times 10^4$
m^2/h	$2,78 \times 10^2$	2,78	$2,78 \times 10^{-4}$	1	$2,98 \times 10^{-3}$	$1,07 \times 10$
ft^2/s	$9,35 \times 10^4$	$9,35 \times 10^2$	$9,35 \times 10^{-2}$	36×10^2	1	$3,60 \times 10^3$
ft^2/h	$2,60 \times 10$	$2,60 \times 10^{-1}$	$2,60 \times 10^{-5}$	$9,35 \times 10^{-2}$	$2,78 \times 10^{-4}$	1

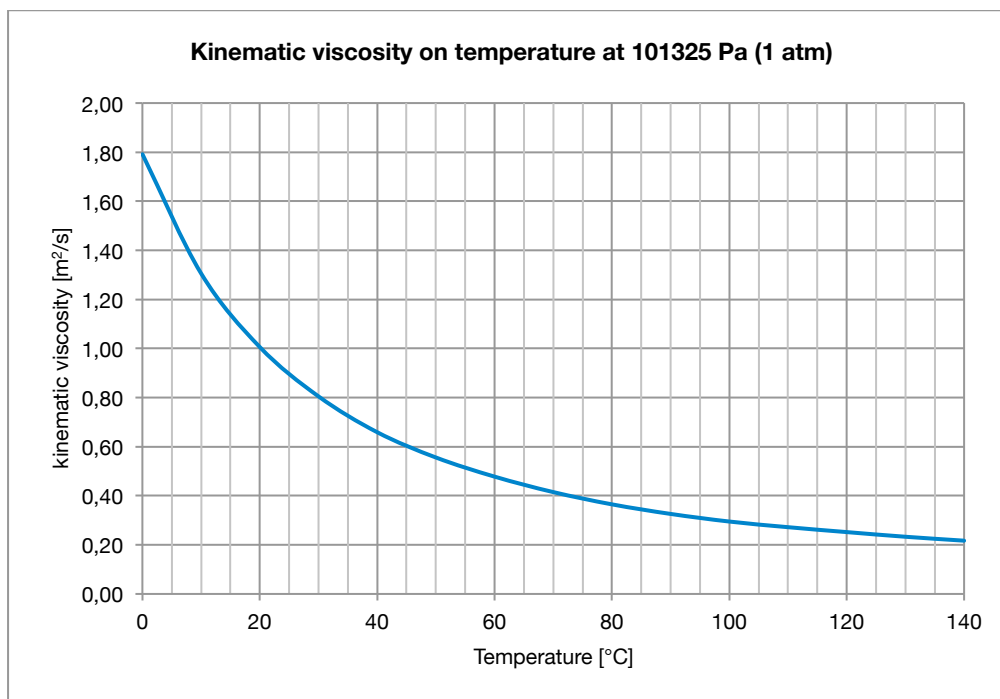
The dynamic and kinematic viscosities depend on the characteristics of the medium. The dynamic viscosity of fluids is a function of the temperature only. The kinematic viscosity of liquids and gases is a function of both temperature and pressure.

The dependence of the dynamic and kinematic viscosities of water on temperature is given in Table 4 and the dependence of the kinematic viscosity is given also in Graph 1.

Table 4

T [°C]	0	10	20	30	40	50	60	70	80	90	100
$\mu \times 10^6$ [(kg x s)/m ²]	182,3	133,1	102,4	81,7	66,6	56,0	47,9	41,4	36,2	32,1	28,8
$\nu \times 10^6$ [m ² /s]	1,792	1,306	1,006	0,805	0,659	0,556	0,478	0,415	0,365	0,326	0,295

Table 4: dynamic and kinematic viscosity of water as function of temperature



Graph 1: kinematic viscosity on temperature at 101325 Pa (1 atm)

6.2.2 Equations and definitions

6.2.2.1 Equilibrium of fluid

When a fluid is at rest, no shear stresses are possible between its particles because there are not relative displacements between themselves. In equilibrium condition of a fluid mass, every internal stress admits only normal component. This means that the stress in a generic point belonging to a fluid mass at rest has always direction normal to the surface element on which is applied and its module is independent of the positioning passing through the point itself. The module of the stress is defined as pressure p , expressed in pascal [Pa].

In Figure 1 is represented an infinitesimal volume of fluid mass at rest, with a vertex in a generic point O , where ρ is the density and p is the pressure. and with The sides of the volume are dx , dy and dz are parallel to a reference system x,y,z centered in O .

It is defined also the three-dimensional Cartesian coordinate system with origin in O and versors i , j and k .

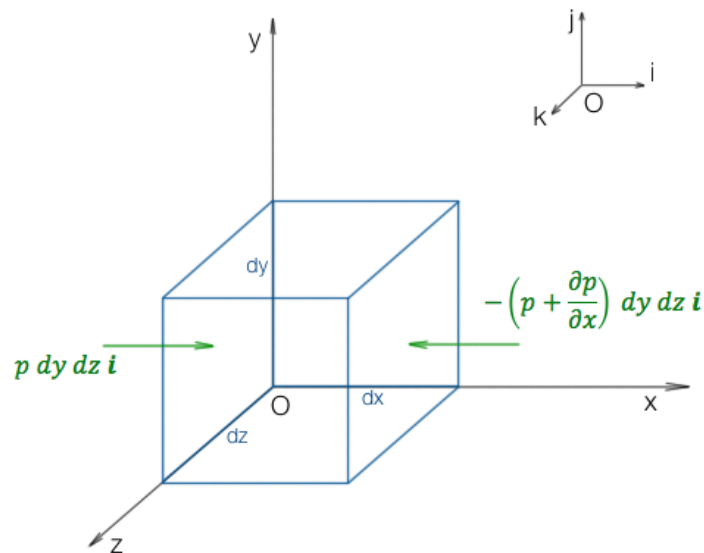


Figure 1: infinitesimal volume with surface forces

On this volume there are many forces that exert influence:

1. Volume force, the resultant of all the external forces acting on the mass at rest;
2. Surface forces, the forces which are transmitted through the boundary surface of the volume on the fluid mass contained;

The overall value of the resultant volume force V_F , defining F_V as the volume force for unit of mass, is:

$$V_F = \rho F_V dx dy dz$$

Simplifying the related components of the surface forces, the resultant of all surface forces S_F is:

$$S_F = -\left(\frac{\partial p}{\partial x} i + \frac{\partial p}{\partial y} j + \frac{\partial p}{\partial z} k\right) dx dy dz = -grad(p) dx dy dz$$

Imposing the equilibrium condition to the volume, the resultant of S_F and V_F has to be equal to zero, and so it can be written the following expression, corresponding to the undefined equation of the fluid static:

$$\rho F_V = grad(p)$$

Defining z as the elevation of the considered point above a reference plane and considering fluid at rest subject only to the gravitational force, it is possible to define the volume force per unit of mass as:

$$F_V = -g \cdot grad(z)$$

with g is considered constant.

Making the further hypothesis of incompressibility of the fluid, and so considering ρ as a constant for all the fluid mass, it is possible to obtain the Stevin law (fundamental equation of the static):

$$z + \frac{p}{\gamma} = const.$$

6.2.2.2 Motion of fluids

Stream, Rate of flow and mean flow velocity

The term stream indicates the wide range of flow motion types characterized by the fact that all the fluid paths have significantly the same direction; this fluid motion is what takes place in piping systems, the application field of this paper.

With the term cross-section it will be identified a surface that cuts the pipe and that is normal, in every point and in a generic time, to the velocity vector v in the same point. The area of the cross-section will be indicated with F .

The amount of fluid flowing across a given cross-section F of a pipe per unit of time is called flow rate. This amount can be measured in m^3 or in kg : in the first case the flow rate is known as volumetric flow rate Q [m^3/s], in the second case the flow rate is known as mass flow rate G [kg/s].

At any flow-velocity distribution over a pipe cross-section, the volumetric flow rate is represented in its general form by the formula:

$$Q = \int_F dQ = \int_F v dF$$

where v is the velocity at the given point of conduit cross-section [m/s].

When the volumetric flow rate is known, the mass flow rate is computable multiplying Q by the fluid density ρ :

$$G = \rho Q$$

The distribution of velocities over the conduit cross-section is practically never uniform. The analysis of the problem is simplified by the introduction of the mean flow velocity V , [m/s]:

$$V = \frac{Q}{F} = \frac{1}{F} \int_F v dF$$

whence: $Q = V \cdot F$.

From this point of the paper, when the term “rate of flow” will be used, it will mean “volumetric rate of flow”.

Fluid flow states

The flow state characterized by fluid properties that don't depend on time is the steady flow: the velocity vector is function only of the space coordinates. Otherwise, flow is called unsteady.

Reynolds experiment underlined that the regime of a fluid in a conduit in pressure can be laminar or turbulent. In the first case, the flow is stable, the fluid layers move without mixing each other and flow smoothly past in obstacles in their way. The second type of flow is characterized by a random motion of finite masses of fluid together mixing strongly.

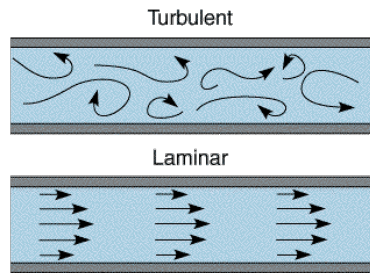


Figure 2: fluid flow regimes

The state of fluid flow is function of the Reynolds number Re , dependent on the dynamic viscosity μ , the mean velocity V of the fluid across the cross-section considered, and the pipe diameter D :

$$Re = \frac{\rho VD}{\mu}$$

For each installation there exists a certain range of “critical” values of Reynolds number at which the passage from laminar to turbulent flow takes place. The lower limit of the critical Reynolds Number for a circular pipe is about 2000-2300. The upper limit of Re depends strongly on the inlet conditions and the state of the wall surface.

When a viscous fluid flows between solid boundaries, the layer contiguous to the solid surface adheres to it, leading to a transverse velocity gradient: the velocity increases in the region near the solid surface from zero to the velocity V of the undisturbed stream (Figure 3). The region in which this variation of the velocity takes place is called boundary layer.

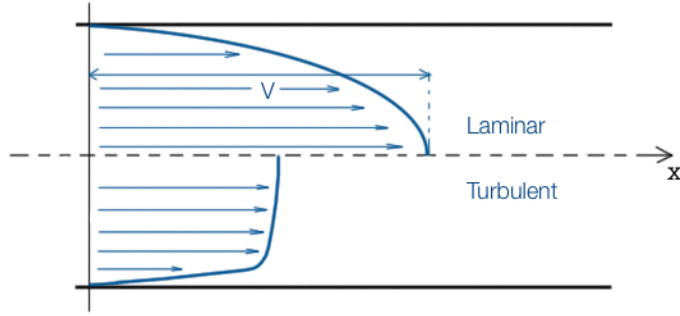


Figure 3: velocity distributions over the pipe cross section for laminar and turbulent flow

The definition of turbulent flow states that this flow regime is essentially characterized by a superposition of a basic motion of transport and an irregular agitation motion that doesn't contribute to the flow developing. Strictly speaking this kind of flow must be considered as unsteady because the field of velocity varies in time. However, turbulent mean flow will be considered as steady, because transport motion is steady.

Continuity equation of a stream

In piping calculation the stream is treated as a whole in a one-dimensional fluid treatment because the study is focused on different cross-section and not on every single point of the fluid mass.

The stream is practically determined when are known the value of the volumetric flow rate Q (or the mean velocity V) and the cross-section F value for every space coordinate s and for every time t . If it is considered a compressible flow, the density ρ has to be known for ever s and t as well. Using this analysis approach does not allow to know every aspect of the flow motion; in particular it is not possible to determine the velocity distribution and the density distribution across all the cross-sections. However, the experience has shown that this vision of the flow as a whole is very effective for practical application.

After these assumptions about the stream characteristics, it is considered a stream stretch between two cross-section at infinitesimal distance ds (Figure 4). In an infinitesimal time instant dt from the inlet cross-section the fluid mass quantity m_{in} enters, and from the outlet section the fluid mass quantity m_{out} exits, where these two magnitudes are defined as following:

$$m_{in} = \rho Q dt$$

$$m_{out} = \left[\rho Q + \frac{\partial(\rho Q)}{\partial s} ds \right] dt$$

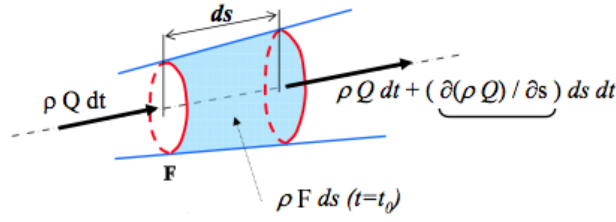


Figure 4: stretch of stream with parameters

making a balance between the two masses, the outgoing mass is greater than the entering mass of the quantity:

$$\frac{\partial(\rho Q)}{\partial s} ds dt$$

for the principle of mass conservation this quantity must be balanced with a diminution of the inside mass, computable as $\rho A ds$, of the value:

$$-\frac{\partial(\rho F)}{\partial t} ds dt$$

it is now possible to write the following expression, which represent the equation of continuity of a stream:

$$\frac{\partial(\rho Q)}{\partial s} + \frac{\partial(\rho F)}{\partial t} = 0$$

making the hypothesis of incompressible fluid ($\rho = const.$), the previous equation is simplified as following:

$$\frac{\partial Q}{\partial s} + \frac{\partial F}{\partial t} = 0$$

in the further hypothesis of steady flow ($\frac{\partial F}{\partial t} = 0$), the previous equation is reduced as following:

$$\frac{\partial Q}{\partial s} = 0$$

in piping flow field of application this condition is the same because even if the flow could be considered unsteady, the cross-section value F , which varies with s , is invariant with the time.

This means that, instant after instant, Q is the same for every cross section, and it is only a function of the time t . In most cases, F is not dependent on s and so it can be written:

$$\frac{\partial Q}{\partial s} = \frac{\partial FV}{\partial s} = F \frac{\partial V}{\partial s} = 0$$

and so the following expression is derived:

$$\frac{\partial V}{\partial s} = 0$$

6.2.3 Bernoulli's theorem

Bernoulli equation is a particular expression of the energy conservation law that can be derived from the Euler Equation for perfect fluids. It states that in steady flow of a perfect, weighty and incompressible fluid, the hydraulic head H is constant along every path:

$$H = z + \frac{p}{\gamma} + \frac{V^2}{2g} = \text{const.}$$

The hydraulic head H represents the total mechanical energy associated to the weight unit, that can be called also specific energy. The total value of H is composed by three members, respectively representing the elevation z , the piezometric height p/γ and the kinetic height (or velocity head) $\frac{V^2}{2g}$. The sum of the piezometric height and the elevation is called piezometric head.

This particular formulation of Bernoulli's theorem is obtained from the Euler equation under the previous hypothesis and the hypothesis of linear streams, in which the radius of curvature of the single paths are extremely large. Because of this the pressure distribution over the cross-section can be considered as hydrostatic.

Bernoulli's theorem is particularly suitable to be geometrically interpreted: considering the Figure 5, there are represented a series of point A, B, and C along a particular fluid path. Points A', B' and C' are vertically elevated over the path points by the piezometric height values in points A, B and C respectively. These points are positioned on a continuous line called piezometric line of the path. Points A'', B'' and C'' are vertically elevated over the points A', B' and C' by the velocity head value in A', B' and C' respectively. These points belong to a continuous line called energy grade line.

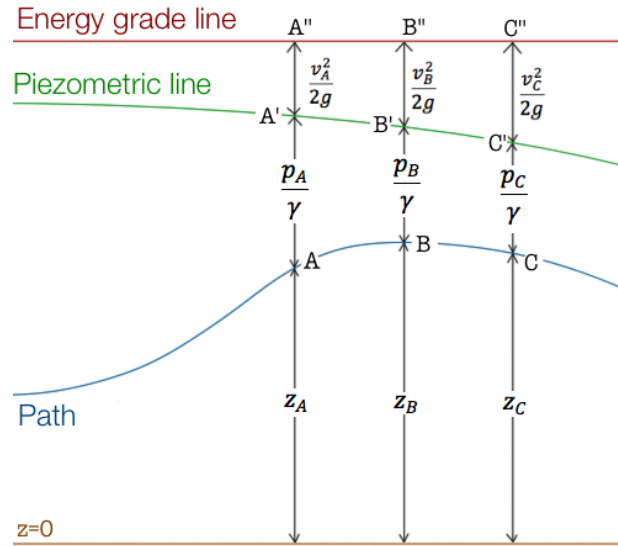


Figure 5: geometrical interpretation of the Bernoulli's theorem

In order to use this theorem in practical cases it is necessary to remove the hypothesis of perfect fluid and to extend it to real fluids. The subsequent step is to extend the results from the single fluid particle to the whole stream.

Considering a real fluid instead of a perfect fluid means that it is necessary to introduce the effects of the viscosity. The introduction of viscosity imposes that mechanical energy cannot be considered as constant along the flow motion because of the shear stresses. The work associated with them is the responsible of the conversion into heat of a part of the total mechanical energy belonging to the particles. These mechanical energy dissipations are called head losses ΔH .

The total head of a generic fluid particle, i.e. its mechanical energy, is not constant during its steady flow but decreases progressively. This implies that the energy grade line is sloping in the flow direction. If the geometrical conditions of the conduit are constant (roughness included) this slope is constant: it is defined as friction slope J , the decreasing of the energy grade line per unit of path:

$$J = -\frac{\partial H}{\partial s}$$

the integration of this equation between two cross-sections brings to an integral formulation of the head losses along the path, in terms of J :

$$H(s) - H_0 = -Js$$

the friction slope J resumes the head loss effects that develop along the flow path and this continuous head loss is called frictional head loss ΔH_f . It can be anticipated that exists another type of head losses, identified as local ΔH_L which are the main topic of this paper.

In order to extend the meaning of Bernoulli's theorem to streams (linear streams), it is necessary to introduce the Coriolis coefficient α defined as the ratio between the real kinetic power of the stream and the kinetic power of a fictive stream that has a uniform distribution of the velocities on the cross-sections.

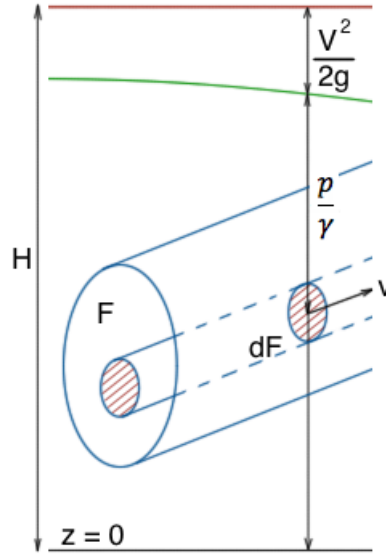


Figure 6: Bernoulli's theorem extension to streams

The Bernoulli's trinomial is modified as following and now H represents the mean specific energy of the flow crossing the cross-section:

$$H = z + \frac{p}{\gamma} + \alpha \frac{V^2}{2g} = \text{const.}$$

This Coriolis coefficient, for turbulent flow state, that will be the prevailing state analyzed in this paper, is 6-7% greater than the unit and so can be assumed as unit. For laminar flow state the velocity distribution is parabolic and the Coriolis coefficient is equal to 2 (so it can't be neglected). Another formal specification is necessary: the total head value H presented in the previous expression is the mean value of the total head over the cross-section, but it will be indicated again with the symbol H .

6.2.4 Flow in pipes

As anticipated previously, the field of application of this paper is pipe flow calculation. The study of the uniform water flow in pipes represents one of the most important issues of the hydraulic engineering. It is possible to synthesize the problem in the research of the relation between the head losses ΔH in pipes and the factors on which it depends. A simple qualitative analysis leads to recognize that these factors are essentially:

- The geometry of the conduit (including the roughness value);
- The kinematic quantities of the stream (Q , V);
- The physical factors related to the medium fluid (water), including viscosity and density;

It is important to underline some hydraulic hypothesis that are necessary and that simplify the theoretical analysis of the problem. The flow motion is always considered uniform (steady and constant all over the space coordinates) which involves cylindrical shape of the pipes, with circular or rectangular cross-section. Moreover, we will consider straight pipes and so linear streams. The Bernoulli's hypothesis underlined before are obviously considered here again (fluid, i.e. water, must be considered weighty and incompressible).

Under the conditions stated previously, a one-dimensional mathematical model can be effectively applied to analyze the problem.

As we said before the fluid energy losses in the course of the motion are due to the irreversible transformation of the mechanical energy into heat. This transformation is due to the molecular and turbulent viscosity of the moving medium and involves head losses. There are two different types of fluid energy losses:

1. The frictional losses ΔH_f ;
2. The local losses ΔH_L ;

6.2.5 Friction head losses

The friction losses are due to the viscosity (molecular and turbulent) of the fluids, which manifests itself during their motion and is a result of the exchange of momentum between molecules at laminar flow and between individual particles of adjacent fluid layers moving at different velocities, at turbulent flow. These losses take place along the entire length of the pipe and they depends on the friction slope J . Calling L the generical length of a pipe stretch, the frictional head losses are expressed by the following equation:

$$\Delta H_{fr} = J \cdot L$$

The previous expression can be considered as the uniform flow motion equation. In the following pages there will be a chapter completely dedicated to the computation of this type of losses but in general, it is possible to say that J depends also on the type of the flow motion, in particular from the flow state.

The friction losses through a straight stretch conduit of constant cross section and length equal to L , are calculated by the following formula:

$$\Delta H_{fr} = JL \quad [m]$$

where, the friction slope J defined before, can be expressed with the experimentally obtained Darcy-Weisbach formula:

$$J = \lambda \frac{V^2}{2gD_h}$$

Where $D_h = D$ for circular sections and $D_h = 2 \frac{a_0 b_0}{a_0 + b_0}$ for rectangular sections.

λ is the friction factor or resistance factor, which in general depends on the Reynolds number, and so on the flow state (regime), and on the pipe roughness:

$$\lambda = \lambda(Re; \varepsilon/D)$$

The resistance to fluid motion for laminar flow is due to the viscosity forces which occur during the motion of one layer of a fluid relative to an adjacent one. Viscosity forces are proportional to the stream velocity and a small amount of roughness has no effects on the resistance magnitude: the friction coefficient is only function of Reynolds number.

At a certain value of Reynolds the flow becomes turbulent. This flow condition is characterized by the appearance of cross-current velocities and by the resulting mixing of the fluid in the whole stream. In turbulent flow, the resistance is greater than in laminar condition, because of the greater exchange of momentum due to the random motion of fluid particles.

In the case of a rough wall surface the flow is accompanied by a jet separation and the friction coefficient is a function not only of the Reynolds number but also of the equivalent roughness $\frac{\varepsilon}{D}$. Conduits can be either smooth or rough, and the roughness can be uniform or not uniform. The two types of roughness differ in the shape of protuberances, dimensions, spacing, etc. and most industrial pipes are non-uniformly rough so it is very difficult to formerly define a parameter which includes all the features of the pipe roughness.

In order to better understand the meaning of the equivalent roughness it is necessary to introduce the mean height ε [m] of the roughness protuberances, called absolute geometric roughness, and the ratio $\frac{\varepsilon}{D_h}$ that is called relative roughness. Since the geometric characteristics of the roughness cannot uniquely define the pipe resistance, it is introduced the concept of the equivalent roughness (or hydraulic roughness) that is calculated measuring directly the resistance in the pipe, looking at the consequences that it has on the flow motion.

The equivalent roughness is a function of:

1. the material and method of manufacture of a pipe;
2. the properties of the medium flowing through a pipe;
3. the length of time the pipe has been in use;

The variation of the coefficient λ in function of Re and the relative roughness was established for the first time by Nikuradse treatment, for conduits with uniform roughness (Graph 6). The treatment shows clearly the three different regimes of flow:

1. laminar, created at low Re numbers (up to $Re = 2000$), and independent from roughness factors; this regime is regulated by the Hagen-Poiseuille formula: $\lambda = 64/Re$ (Graph 2);
2. the transition regime, that in the graph, includes three portions of the head loss curves for regular roughness:
 - a. middle zone (critical) between laminar and turbulent flow (for $2000 < Re < 4000$, roughly) in which the head loss coefficient increases quickly with Re but doesn't vary with roughness;
 - b. the zone, where λ is decreasing with the increasing of Re in which the curves obtained for pipe with different roughness coincide with the Blasius curve:

$$\lambda = \frac{0,3164}{Re^{0,25}}$$

- c. the zone in which the resistance curves diverge from each other and from the straight line for pipes at different roughness; in this zone λ is increasing with the increasing of relative roughness;
3. the square-law flow or turbulent flow, characterized by friction coefficients independent of Re and constant for given roughness;

The same three regions are present also for non-uniform roughness (industrial pipes); for this pipe types the referring graph is the Moody abach (Graph 8). The Moody graph is a double-logarithmic scale diagram in which are represented the different formulations of the functional relation $\lambda = \lambda(Re; \varepsilon/D)$.

In the Moody abach it is possible to distinguish:

1. the laminar flow zone, characterized by $Re < 2000$, in which λ depends only on Re number; in this region the relative roughness has no influence on the head losses computation but this situation is realized for very small pipes or extremely viscous fluids;
2. the turbulent flow zone, for $Re > 2000 - 4000$; this region is bounded below by the curve associated to the turbulent flow in smooth walls, in which λ depends only on Re number. The resistance law in turbulent flow conditions is described by different curves based on the relative roughness value that are detached from the smooth curve described before; the turbulent flow zone is, in turn, divided in two sub-zones: the first is associated to the dependence of λ on Re and the relative roughness and is called transition region; the second sub-zone is the fully turbulent flow zone and here λ depends only on the relative roughness;

In the following pages are presented the indication for the determination of the friction coefficient λ in case of smooth pipe walls for rectangular cross-section and circular cross-section (Graph 2, Graph 3, Graph 4 and Graph 5), walls with uniform roughness (Graph 6) and commercial pipes (Graph 7 and Graph 8). Different values of ε for different commercial materials are listed in Table 6 and other experimental simplified formulas for λ computation are listed in Table 5.

Pipes can be considered hydraulically smooth in the condition of:

$$\frac{\varepsilon}{D} < \left(\frac{\varepsilon}{D}\right)_{\text{lim}}$$

the formula which allows to compute this factor are different depending on the roughness conditions:

- For uniform roughness the formula is the following:

$$\left(\frac{\varepsilon}{D}\right)_{\text{lim}} = \frac{18 \log \text{Re} - 16,4}{\text{Re}}$$

from this it follows, using Blasius formula, that for $\text{Re} < 10^5$:

$$\left(\frac{\varepsilon}{D}\right)_{\text{lim}} \cong 17,85 \text{Re}^{-0,875}$$

- For non-uniform roughness (commercial pipes) the formula is the following:

$$\left(\frac{\varepsilon}{D}\right)_{\text{lim}} \cong \frac{23}{\text{Re}}$$

from the previous expressions, it follows that the Reynolds Number at which the influence of roughness can be felt are different depending on the roughness pipe again:

- For uniform roughness the formula is the following:

$$\text{Re}'_{\text{lim}} = \frac{26,9}{\left(\frac{\varepsilon}{D}\right)^{1,143}}$$

- For non-uniform roughness (commercial pipes) the formula is the following:

$$\text{Re}'_{\text{lim}} = \frac{23}{\left(\frac{\varepsilon}{D}\right)}$$

The limiting value of Reynolds number at which the square law of resistance can be applied is determined from the following expressions depending on the roughness type again:

- For uniform roughness the formula is the following:

$$Re''_{lim} = \frac{217,6 - 382,2 \log\left(\frac{\varepsilon}{D}\right)}{\left(\frac{\varepsilon}{D}\right)}$$

- For non-uniform roughness (commercial pipes) the formula is the following:

$$Re''_{lim} = \frac{560}{\left(\frac{\varepsilon}{D}\right)}$$

For smooth walls, the friction coefficient λ can be determined:

- At laminar flow ($Re \leq 2000$):

- For circular cross-sections: (Graph 2)

$$\lambda = 64/Re$$

- For rectangular cross-sections: (k_1 is plotted in Graph 3)

$$\lambda_{rect} = k_1 \lambda$$

- At transitional flow ($2000 < Re < 4000$):

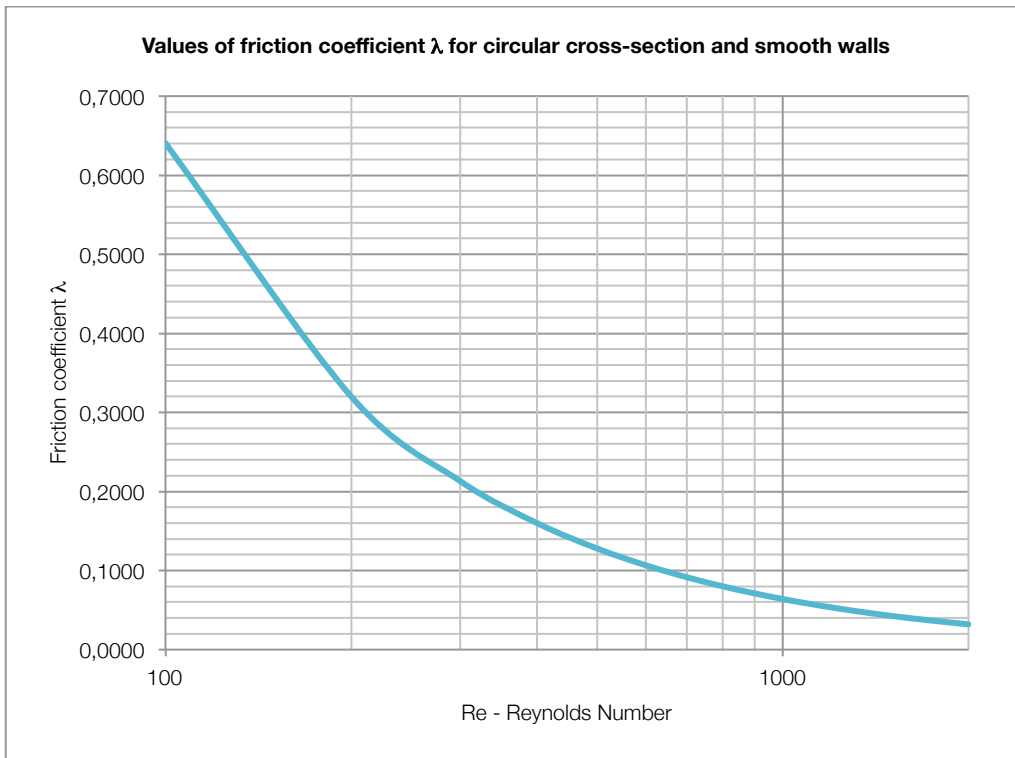
- For circular and rectangular ($0,5 < a_0/b_0 < 2$) cross-sections: (Graph 4)

$$\lambda = \frac{\Delta H}{\frac{V_0^2 l}{2g D_h}} = \frac{0,3164}{\sqrt[4]{Re}}$$

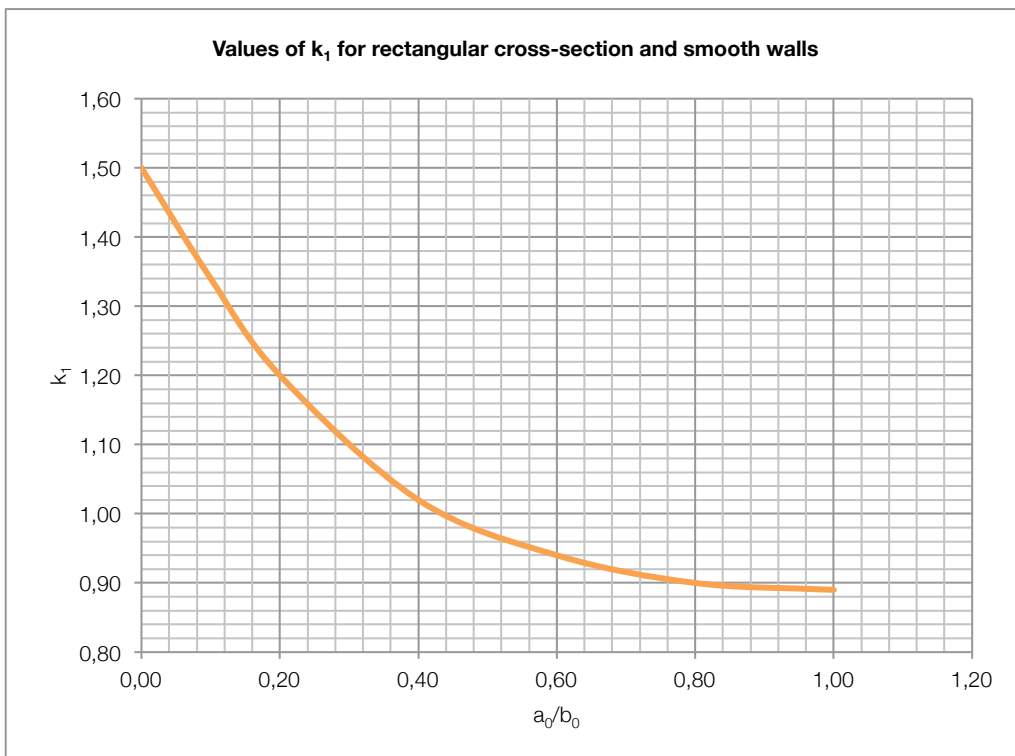
- At turbulent flow ($Re > 4000$):

- For circular and rectangular ($0,5 < a_0/b_0 < 2$) cross-sections:

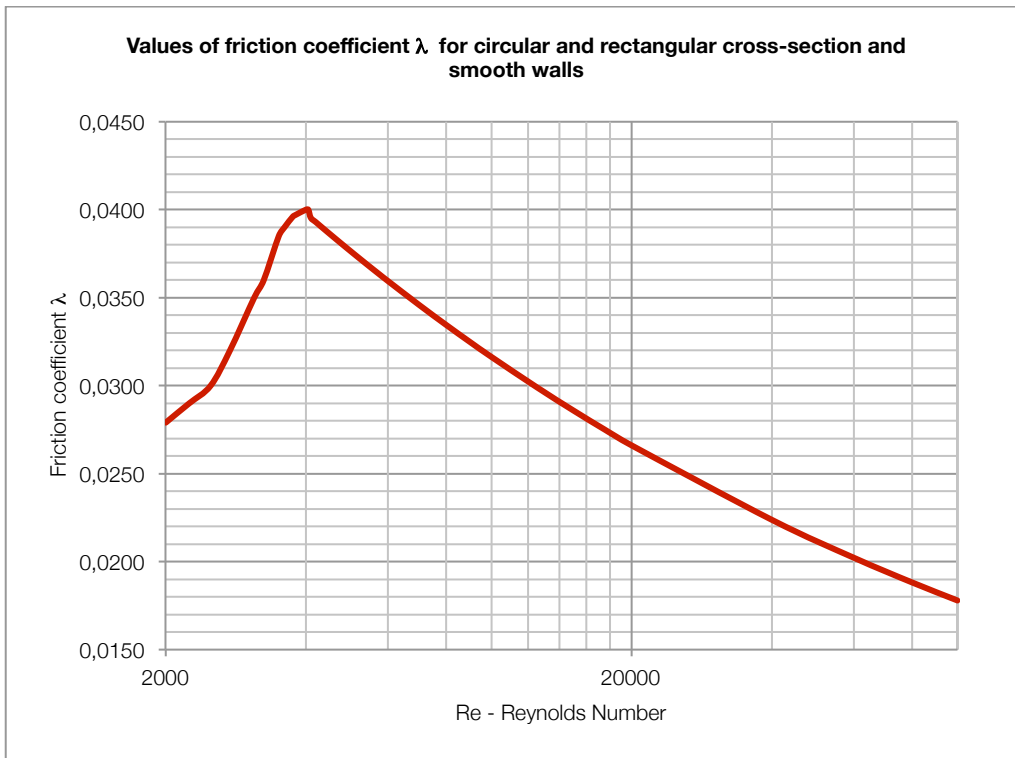
$$\lambda = \frac{\Delta H}{\frac{V_0^2 l}{2g D_h}} = \frac{1}{(1,8 \log Re - 1,64)^2}$$



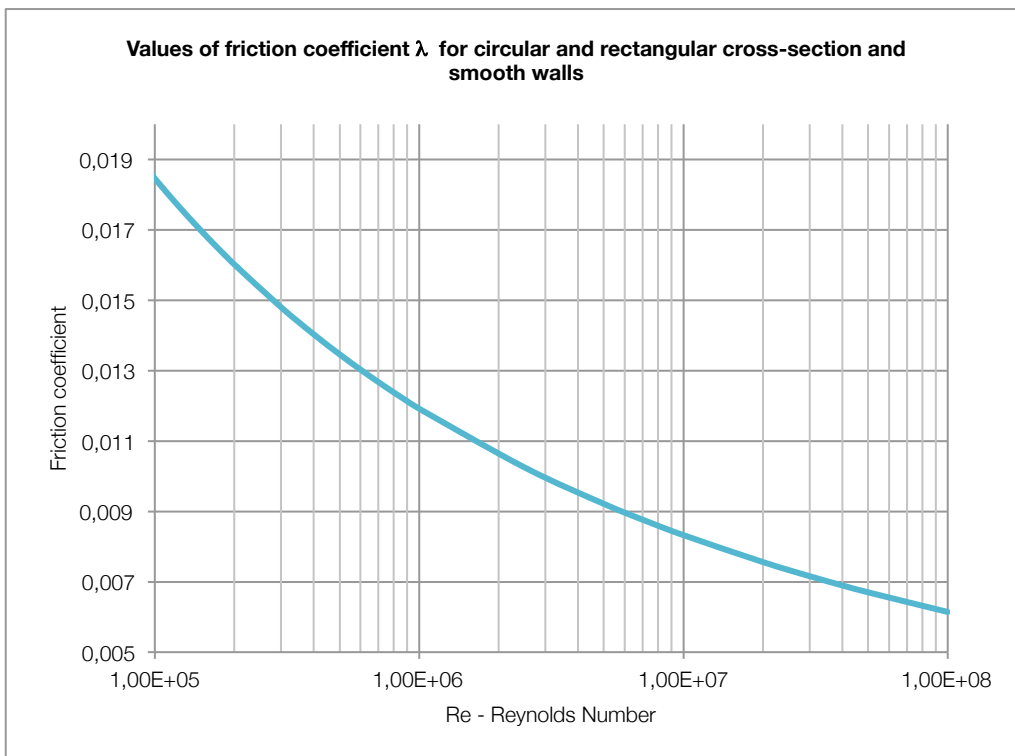
Graph 2: values of λ for circular sections and smooth walls at laminar flow



Graph 3: values of k_1 for rectangular sections and smooth walls at laminar flow



Graph 4: Values of λ for circular and rectangular section and smooth walls at transitional flow



Graph 5: values of friction coefficient for circular and rectangular section and smooth walls for turbulent flow

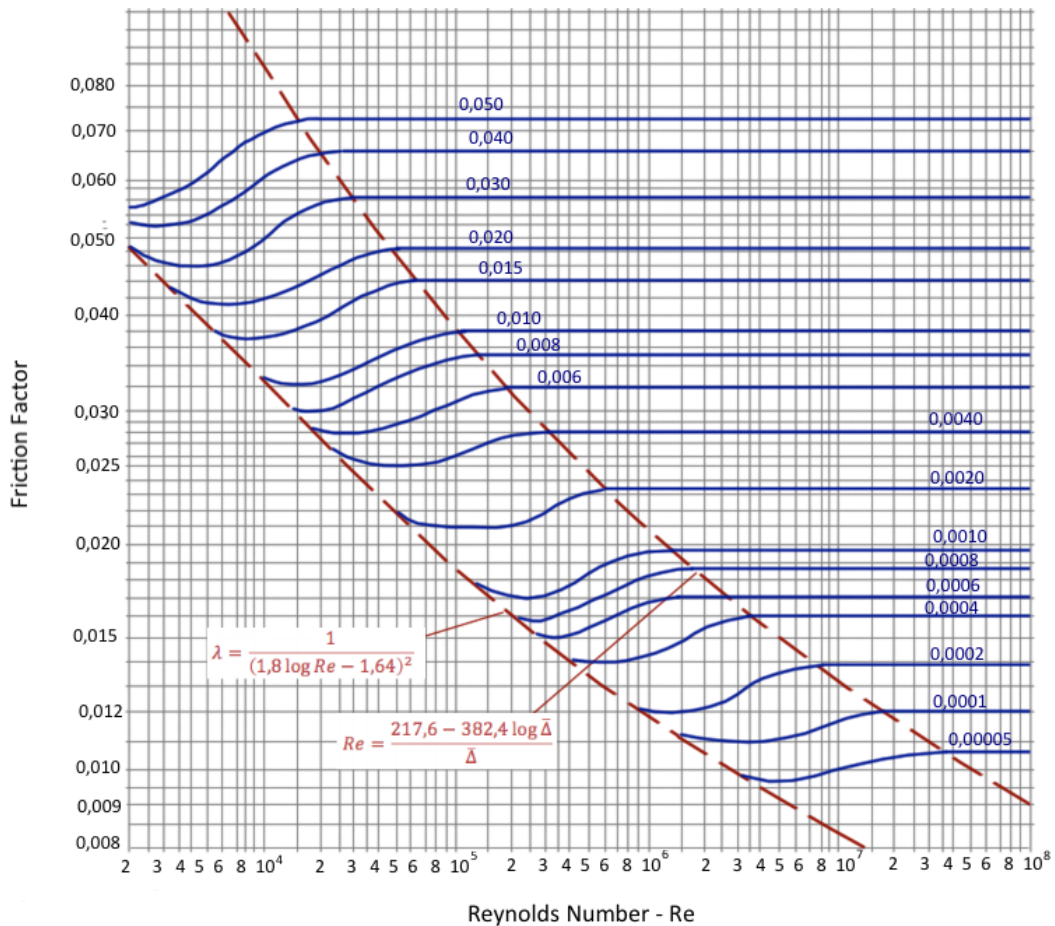
The friction coefficient λ of circular pipe with uniform roughness in the transition region, within the limits:

$$\frac{26,9}{\left(\frac{\varepsilon}{D}\right)^{1,143}} < Re < \frac{217,6 - 382,4 \log\left(\frac{\varepsilon}{D}\right)}{\left(\frac{\varepsilon}{D}\right)}$$

is determined from Graph 6 where in blue color are represented the various $\left(\frac{\varepsilon}{D}\right)$, based on Nikuradse formula:

$\left(\frac{\varepsilon}{D}\right) Re\sqrt{\lambda}$	a_1	b_1	c_1
3,6 - 10,0	-0,800	2,000	0,000
10,0 - 20,0	0,068	1,130	-0,870
20,0 - 40,0	1,538	0,000	-2,000
40,0 - 191,2	2,471	-0,588	-2,588
> 191,2	1,138	0,000	-2,000

$$\lambda = \frac{1}{\left[a_1 + b_1 \log(Re\sqrt{\lambda}) + c_1 \log\left(\frac{\varepsilon}{D}\right)\right]^2}$$



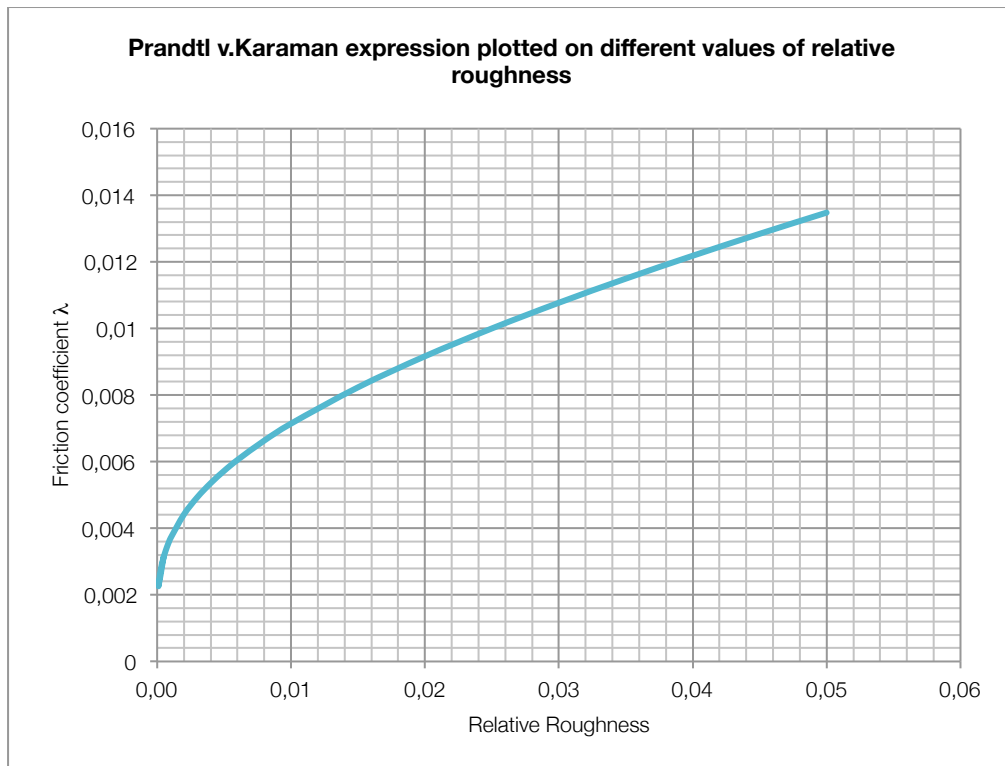
Graph 6: Nikuradse Graph

With the exception of special pipes (for which the values of λ are given separately from manufacturers), the friction coefficient λ of all commercial pipes can be determined, for transition region, from the Colebrook-White formula, plotted in the Moody Graph (Graph 8):

$$\lambda = \frac{1}{\left[-2 \log \frac{2,51}{Re\sqrt{\lambda}} + \frac{(\frac{\epsilon}{D})}{3,71} \right]^2}$$

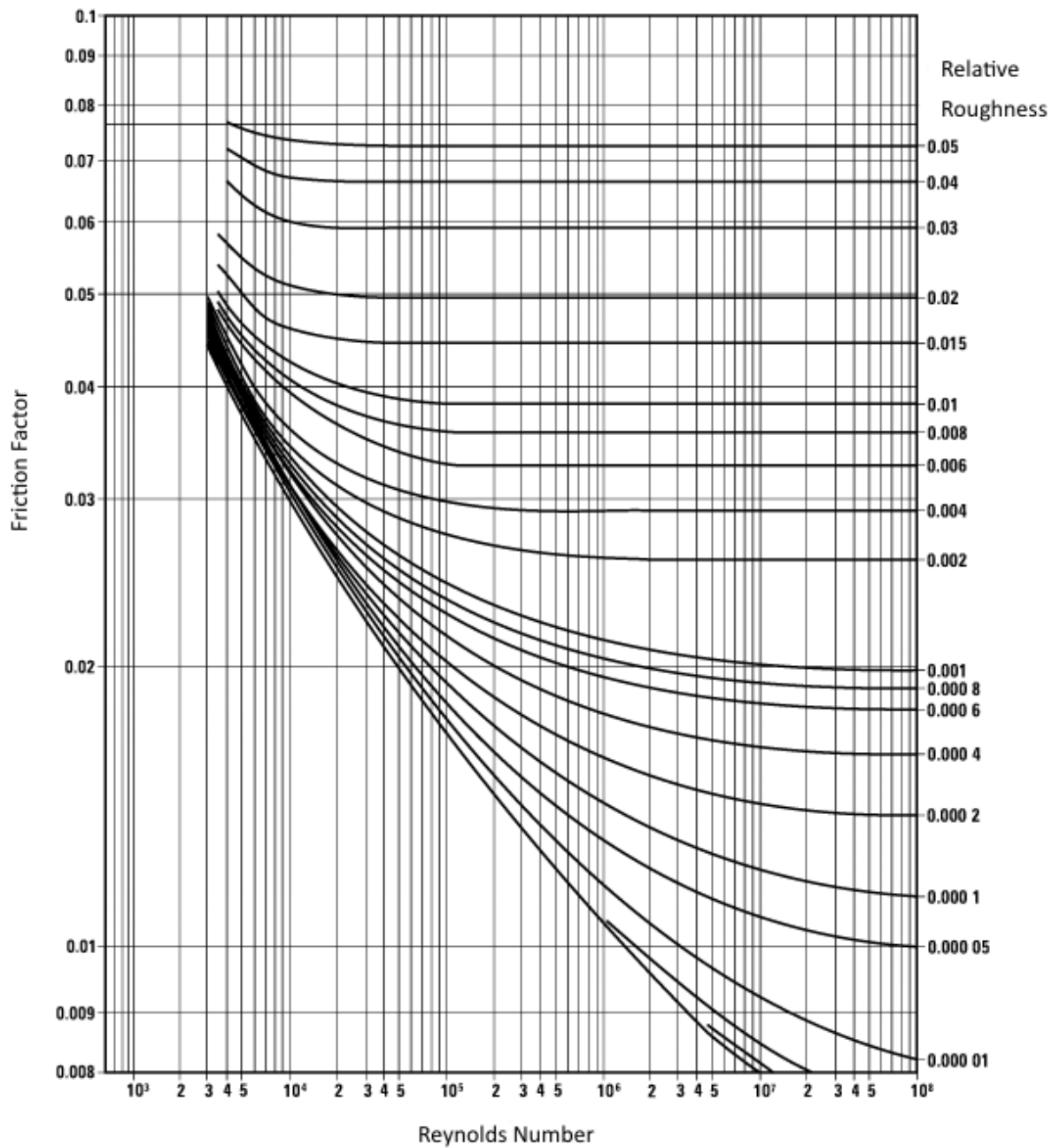
The Colebrook-White formula can be simplified, for turbulent region and so for high Re number (roughly for $Re > \frac{560}{(\frac{\epsilon}{D})}$) into the Prandtl-v.Karaman formula, plotted in Graph 7:

$$\lambda = \frac{1}{\left[2 \log \frac{3,71}{(\frac{\epsilon}{D})} \right]^2}$$



Graph 7: Prandtl v.Karaman expression plotted on different values of relative roughness

λ values for commercial pipes with non-uniform roughness (Colebrook formula)



Graph 8: Moody Graph

Table 5: other simplified formulas for friction coefficients

<p>Al'tshul':</p> $0,00008 < \left(\frac{\varepsilon}{D}\right) < 0,0125$ $\lambda = 0,1 \left(1,46 \left(\frac{\varepsilon}{D}\right) + \frac{100}{Re} \right)^{0,25}$	<p>Lobaev:</p> $0,0001 < \left(\frac{\varepsilon}{D}\right) < 0,01$ $\lambda = \frac{1,42}{\left[\log \frac{Re}{\left(\frac{\varepsilon}{D}\right)} \right]^2}$
--	--

Table 6: roughness of pipe and channels

Type of pipe and material	State of pipe surface and condition of use	Roughness ε [mm]
Metal pipes		
Seamless pipes made from brass, copper lead or aluminum	Commercially smooth	0,0015 – 0,01
	The same	0,015 - 0,06
Seamless steel pipes (commercial)	New, unused	0,02 – 0,10
	Cleaned after many years of use	Up to 0,04
	Bituminized	Up to 0,04
	Superheated-steam pipes of heating systems and water pipes of heating systems with de-aeration and chemical treatment of running water	0,10
	After one year of use in gas pipelines	0,12
	After several years of use as tubing in gas wells under various conditions	0,04 – 0,20
	After several years of use as casings in gas wells under various conditions	0,06 – 0,022
	Saturated-steam pipes and water pipes of heating systems with insignificant water leakages (up to 0,5%) and de-aeration of water added for making up leakage losses	0,20
	Heating-system water pipes independent of their feed source	0,20
	Oil pipelines for medium condition of operation	0,20
	Slightly corroded	$\approx 0,4$
	Small deposition of scale	$\approx 0,4$
	Steam pipes in intermittent operation, and condensate pipes in an open condensate system	0,5
	Compressed-air ducts from piston compressors and turbocompressors	0,8
	After several years of use under various condition, i.e. corroded or with small scale deposits	0,15 – 1,0
	Condensate pipes working intermittently, and water-heating pipes in the absence of deaeration and chemical treatment of the water, with large leakage (up to 1,5-3%)	1,0
	Water pipelines in operation	1,2 – 1,5
	Large depositions of scale	$\approx 3,0$
Pipe surface in poor state. Nonuniform overlapping of pipe joints	> 5,0	
Welded steel pipes	New or old pipes in satisfactory state; welded or rivedet pipe joints	0,04 – 0,1
	New, bituminized pipes	$\approx 0,15$
	Used pipes, corroded bitumen partially dissolved	$\approx 0,10$
	Used pipes, uniform corrosion	$\approx 0,15$
	Without noticeable unevenness at the joints; laquered on the inside (layer thickness about 10 mm); satisfactory state of surface	0,3 – 0,4
	Gas main after many years of use	$\approx 0,5$
	With simple or double transverse riveted joints; inside lacquered (layer thickness 10 mm) or without lacquer but not corroded	0,6 – 0,7
	Lacquer-coated on the inside, but not rust-free; soiled in the process of carrying water, but not corroded	0,95 – 1,0
	Layer deposits; gas mains after 20 years of use	1,1
	With double transverse riveted joints, not corroded; soiled by passage of water	1,2 – 1,5
	Small deposits	1,5
	With double transverse riveted joint, heavily corroded	2,0
	Considerable deposits	2,0 – 4,0
	25 years use in municipal gas mains, uneven depositions of resin and naphthalene	2,4
Pipe surface in poor state; uneven overlap of joints	> 5,0	

Riveted steel pipe	Riveted along and across with one line of rivets; lacquered on the inside (layer thickness 10 mm); satisfactory state of the surface	0,3 – 0,4
	With double longitudinal riveted joints and simple transverse riveted joints lacquered on the inside (layer thickness 10 mm), or without lacquer but not corroded	0,6 – 0,7
	With simple transverse and double longitudinal riveted joints; coated on the inside with tar or lacquer (layer thickness 10 to 20 mm)	1,2 – 1,3
	With four to six longitudinal rows of rivets; long period of use	2,0
	With four transverse and six longitudinal rows of rivets; joints overlapped on the inside	4,0
	Pipe surface in very poor state; uneven overlap of the joints	> 5,0
Roofing steel sheets	Not oiled	0,02 – 0,04
	Oiled	0,10 – 0,15
Galvanized steel pipes	Bright galvanization, new pipes	0,07 – 0,10
	Ordinary galvanization	0,1 – 0,15
Galvanized sheet steel	New pipes	0,15
	Used (in water pipelines)	0,18
Cast-iron pipes	New ones	0,25 – 1,0
	New, bituminized	0,10 – 0,15
	Asphalt-coated	0,12 – 0,30
	Used water pipes	1,4
	Used and corroded pipes	1,0 – 1,5
	With deposit	1,0 – 1,5
	Considerable deposit	2,0 – 4,0
	Cleaned after many years of use	0,3 – 1,5
Strongly corroded	Up to 3,0	

Conduits made from concrete, cement or other materials

Concrete pipes	Good surface, plaster finish	0,3 – 0,8
	Average conditions	2,5
	Coarse (rough) surface	3,0 – 9,0
Reinforced concrete pipes		2,5
Asbestos – cement pipes	New	0,05 – 0,10
	Average	≈ 0,60
Cement pipes	Smoothed surfaces	0,3 – 0,8
	Nonsmoothed surfaces	1,0 – 2,0
	Mortar in the joints not smoothed	1,9 – 6,4
Channel with a cement-mortar plaster	Good plaster from pure cement with smoothed connections; all unevennesses removed	0,5 – 0,22
Plaster over a metallic grid		10 – 15
Slag-concrete tiles		1,5
Slag and alabaster-filling tiles	Carefully finished plates	1,0 – 1,5

Wood, plywood and glass pipes

Wooden pipes	Very thoroughly dressed boards	0,15
	Dressed boards	0,30
	Undressed boards	1,0
	Wood-stave pipes	0,6
Plywood pipes	From good-quality birch plywood with transverse grain	0,12
	From good-quality birch plywood with longitudinal grain	0,0015 – 0,010
Glass pipes	Plain glass	0,0015 – 0,010

6.2.6 Local head losses

The local losses, that are the main topic of this paper, are due to sudden changes in the geometry of the system, for example in presence of additional devices like valves, diffusers or junctions. In these places the stream cannot be considered linear and so it is strictly impossible to talk about a total head line for all the stream flow.

Local losses appear as a disturbance of the normal flow of the stream, such as its separation from the wall and the formation of eddies at places of alteration of the pipe configuration or at obstacles in the pipe. The losses of kinetic height occurring with the discharge of the stream from a pipe into a large volume (such as atmosphere) must also be classified as local losses.

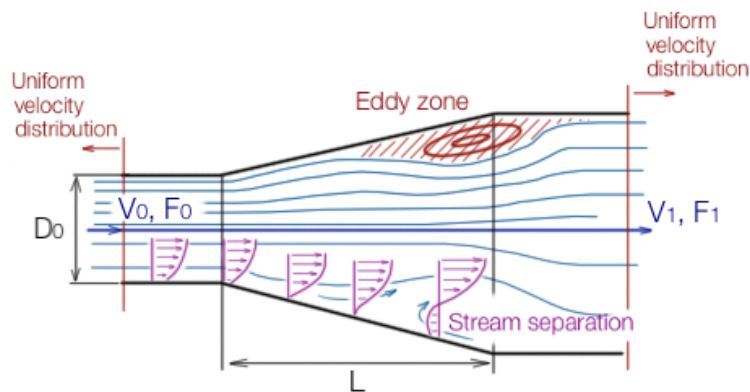


Figure 7: stream separation and formation of eddies in a diffuser

The cause of the energy dissipation in local head losses is the separation of the flow from the channel walls and the consequent formation of eddies which convert the mechanical energy of the stream into heat. Moreover, at the end of this turbulence zones there's always pipe stretches in which the stream is extremely delayed where the turbulence state acquires a lot of importance. This phenomenon cause an abrupt falling of the energy grade line.

The phenomenon of flow separation and eddy formation is linked with the difference between the flow velocities in the cross-section, and with a positive pressure gradient along the stream, which appears when the motion is slowed down in an expanding channel, in accordance with Bernoulli's equation. The difference between the velocities in the cross section at negative pressure gradient doesn't lead to flow separation. The flow in smoothly converging stretches is even more stable than in stretches of constant section.

All kinds of local head losses, except for the kinetic head losses at exit of a pipe, occur along a more or less extended stretch of the pipe and cannot be separated from the frictional losses that occur in the same stretch. For ease of calculation, they are arbitrarily assumed to be concentrated in one section; it is also assumed that they do not include friction losses. The summing is conducted according to the principle of

superposition of losses, according to which the total loss is equal to the arithmetic sum of the friction and local losses:

$$\Delta H_{sum} = \Delta H_{fr} + \Delta H_L$$

In practice, it is necessary to take ΔH_r in account only for relatively long fittings or when its value is commensurable with ΔH_L .

It is important to better specify the meaning of this assumption in relation to the modalities in which the local head losses are measured. Normally, local head losses are experimentally determined with a differential pressure gauge, connected with an upstream and a downstream section (N and M respectively in Figure 8). In this two cross-sections the stream flow can be considered linear and the pressure gauge determines the difference δ between the two piezometric heads.

Looking at Figure 8 the pressure gauge will determine the local head loss value as follows:

$$\Delta H = \delta + \frac{V_1^2 - V_2^2}{2g}$$

The local head loss value determined in this way is the sum of the local head loss $\Delta H'$ caused by the device and the friction loss $Y'+Y''$ caused by the corresponding pipe stretch. From a theoretical point of view this value has to be purified from the friction loss value (that can be calculated assuming the device as a stretch of pipe) in order to obtain the local head loss. This operation is not always possible but it's important to underline that for the devices that will be considered in this paper the friction loss value is extremely lower than the local head loss value. Moreover, for some comparison between different device models can be important to take in account also the friction and so the “deputation” of the value loses its meaning.

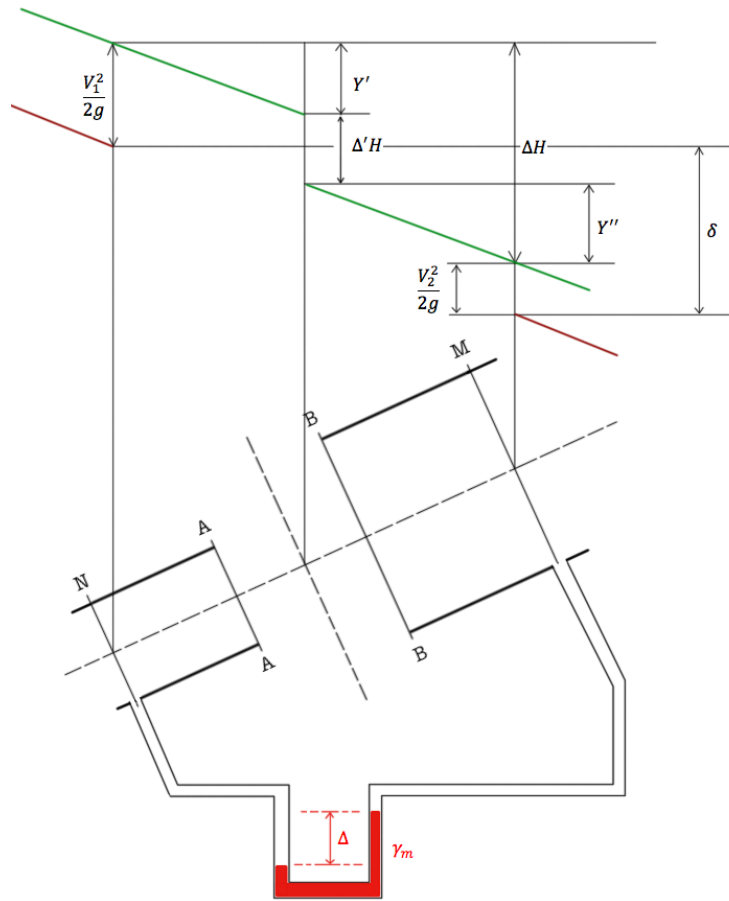


Figure 8: schematic representation of a local head loss measuring

In hydraulic calculation one of the possibilities to express this head loss is to use the dimensionless coefficient of fluid resistance ζ , which has the same value in dynamically similar streams, i.e., streams having geometrically similar stretches, equal values of Re , and equal values of other similitude criteria, independent of the nature of the fluid. This is especially true of the flow velocity and the dimensions of the stretches being calculated.

The fluid resistance coefficient ζ represents the ratio of the head loss ΔH to the kinetic height in section F considered:

$$\zeta = \frac{\Delta H}{\frac{V^2}{2g}}$$

The numerical value of ζ is thus a function of the kinetic height, and therefore of the cross-section. These values are the data which this paper is based on.

The total fluid resistance of any element of the pipe, according to what seen before, is thus determined by the formula:

$$\Delta H_{sum} = \zeta_{sum} \frac{V^2}{2g}$$

In accordance with the principle of superposition of losses:

$$\zeta_{sum} = \zeta_{fr} + \zeta_L$$

The friction coefficient of entire element is expressed through the friction coefficient per unit relative length by:

$$\zeta_{fr} = \lambda \frac{l}{D_h}$$

Where l is the length of the considered element, D_h is the hydraulic diameter, expressed by $D_h = 4F/\Pi$ (Π is the perimeter of the section) and λ is the friction coefficient.

The friction coefficient λ , and hence ζ_{fr} , at constant values of $\frac{l}{D_h}$ is a function of two factors:

1. Reynolds number Re ;
2. The roughness of the pipe walls;

The coefficient of local resistance ζ_L is function of several parameters, including the geometry of the fitting considered, but also motion parameters:

1. Reynolds number Re ;
2. Mach number M ;

The velocity profile at the inlet of the element; this in turn is a function of the state of flow, the inlet shape, the shape and the distance of various fittings or obstacles located ahead of the element;

The principle of superposition of losses is used not only with respect to a separate element of the conduit, but also in the hydraulic calculation of the entire system. This means that the losses found for separate elements of the system are summed arithmetically which gives the total resistance of the entire system ΔH_{sys} .

7 Smooth contractions and Inlets

List of the chapter symbols

Latin symbols:

- D_n = pipe diameter of the n stretch [m²];
- F_n = pipe cross-sectional area of the n stretch [m²];
- r = radius of contraction in conduit inlets [m²];

Greek symbols:

- α = angle of convergence (Figure 2) [°];
- η = area ratio F_2/F_1 ;

7.1 Smooth contractions

In general, it is not wrong to say that pipe stretches which present a smooth convergence don't imply the rising of appreciable head losses from the practical point of view: in most cases project designers used to take in account the local head loss caused by the convergence as the friction loss which it would be if the convergence was a straight stretch of pipe with the smallest diameter.

Although the differences, from the practical point of view, are negligible, the experience shows that there are different smooth convergence devices more or less efficient in terms of head losses caused.

In the following figure, are showed the most diffused contraction devices used in engineering.

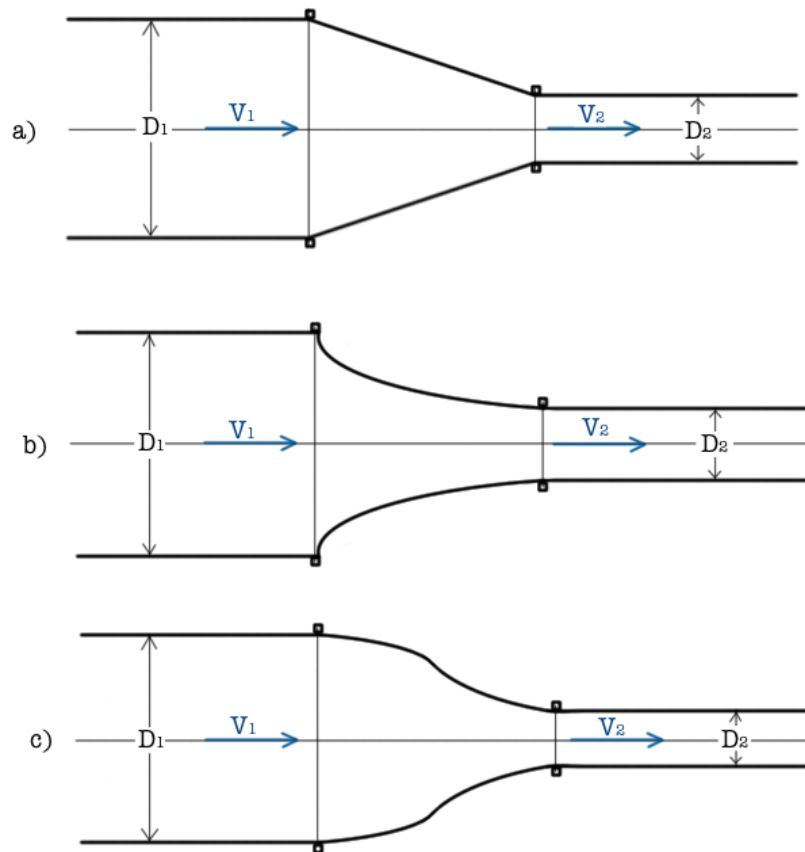


Figure 1: smooth contractions

Following the trend of the stream profile after an abrupt contraction it is clear that the smooth contractor type b) is the most efficient device for limiting the turbulences.

On the contrary the first type (a) is the worst model from the performance point of view, causing a lot of eddies but it is interesting to analyze the head loss in such type of contractor because is the most diffused in hydraulic projects.

Although this model has a contraction geometry equal to a reversal of flow direction in a conduit expansion, the flows in the two elements are expected to be fundamentally different.

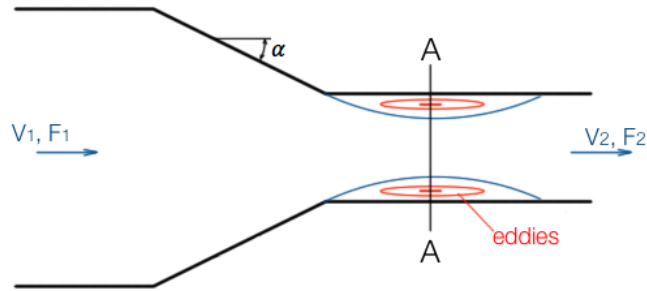


Figure 2: schematic view of a smooth contraction with geometrical parameters

As schematically represented in Figure 2, the flow in a sharp-edged contraction experiences an additional contraction in section A-A and expands downstream to the full cross-sectional area F_2 .

As it is stated before, a contracted flow is nearly free of energy loss and the loss in the contraction element must be attributed to the expansion downstream of the contracted flow.

Contraction flow is essentially influenced by the angle of contraction α and the area ratio η defined as:

$$\eta = \frac{F_2}{F_1} < 1$$

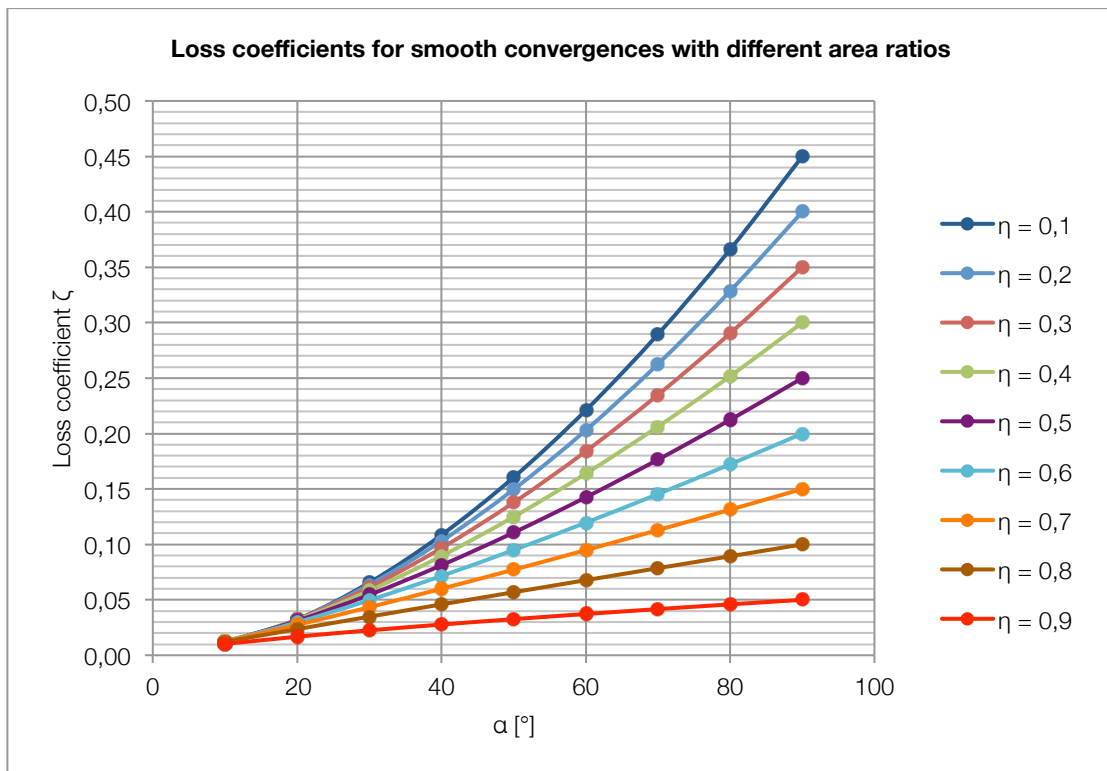
where F_1 and F_2 are the inlet and the outlet cross-sectional areas respectively, in which the stream is completely expanded towards the pipe boundary.

Few experimental studies exist for conduit contractions. One of particular relevance is a paper by Gardel (1962) which derived the following relationship for the loss coefficient ζ taken from Idel'chik (Idel'chik, 1966) and plotted in Graph 1.

$$\zeta = \frac{\Delta H}{V^2/2g} = \frac{1}{2}(1 - \eta) \left(\frac{\alpha}{90^\circ} \right)^{1,83(1-\eta)^{0,4}}$$

Table 1: loss coefficients for smooth contractions

α [°]	Area ratios values η								
	0,1	0,2	0,3	0,4	0,5	0,6	0,7	0,8	0,9
10	0,01	0,01	0,01	0,01	0,01	0,01	0,01	0,01	0,01
20	0,03	0,03	0,03	0,03	0,03	0,03	0,03	0,02	0,02
30	0,07	0,06	0,06	0,06	0,05	0,05	0,04	0,03	0,02
40	0,11	0,10	0,10	0,09	0,08	0,07	0,06	0,05	0,03
50	0,16	0,15	0,14	0,12	0,11	0,09	0,08	0,06	0,03
60	0,22	0,20	0,18	0,16	0,14	0,12	0,09	0,07	0,04
70	0,29	0,26	0,23	0,21	0,18	0,15	0,11	0,08	0,04
80	0,37	0,33	0,29	0,25	0,21	0,17	0,13	0,09	0,05
90	0,45	0,40	0,35	0,30	0,25	0,20	0,15	0,10	0,05



Graph 1: loss coefficients for smooth convergences with different area ratio

7.2 Conduit inlets

A *conduit inlet* (Figure 3) can be treated as a special case of a contraction element with the area ratio tending to zero. It follows, from the previous equation that:

$$\zeta = \frac{\Delta H}{V^2/2g} = \frac{1}{2}(1-0) \left(\frac{\alpha}{90^\circ}\right)^{1,83(1-0)^{0,4}} = \frac{1}{2} \left(\frac{\alpha}{90^\circ}\right)^{1,83}$$

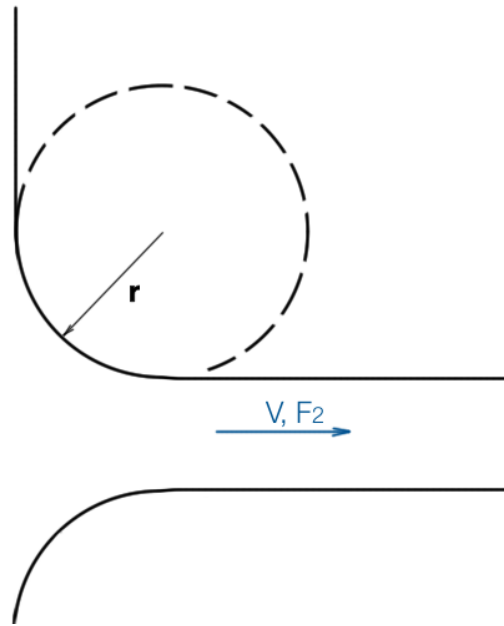


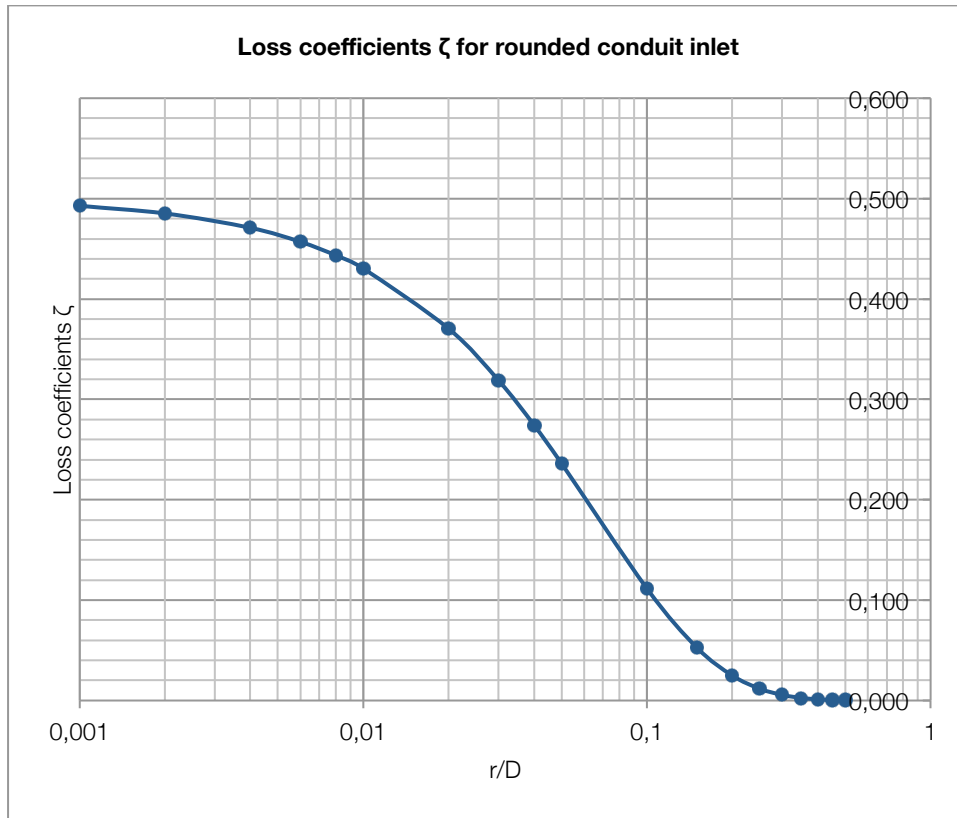
Figure 3: schematic view of a conduit inlet with rounded boundary

For a sharp-edged conduit inlet $\alpha = 90^\circ$, therefore, the head loss is half the pipe velocity head $\zeta = 0,5$. This “high” value of head loss could be reduced rounding the contraction inlet with radius r . the data from Idel’chik book of resistance can be approximated as:

$$\zeta = \frac{\Delta H}{V^2/2g} = \frac{1}{2} e^{-15r/D}$$

the results computed by this formula are plotted in Graph 2.

Looking at the graph it is interesting to observe that for $r/D > 0,5$ the head loss coefficient is negligible and so there’s no practical head loss. On the contrary, it can be stated that for $r/D < 0,001$ the head loss is equal to half kinetic head.



Graph 2: loss coefficients for rounded conduit inlet

r/D	ζ
0,001	0,493
0,002	0,485
0,004	0,471
0,006	0,457
0,008	0,443
0,01	0,430
0,02	0,370
0,03	0,319
0,04	0,274
0,05	0,236
0,1	0,112
0,15	0,053
0,2	0,025
0,25	0,012
0,3	0,006
0,35	0,003
0,4	0,001
0,45	0,001
0,5	0,000

8 Sudden Enlargements and Orifices

List of chapter symbols

Latin characters:

- b = depth of the penetration of a conduit inlet in the wall [m];
- b_0 = width of the plane channel [m];
- D_0 = diameter of the passage cross-section of the throttling device or internal diameter of the pipe where specified [m];
- D_h = hydraulic diameter of the passage [m];
- DN = nominal diameter of the device [mm];
- F_0 = cross-section area at the inlet of the device [m²];
- F_C = cross-section area of the contracted jet after the orifice [m²];
- F_n = area of the n cross-section [m²];
- k = generical integer number;
- k_m = coefficient that permits to allow for the Mach influence;
- l = length of the orifice in the direction of the flow [m];
- m = exponent which can generally vary from case to case;
- n = area ratio;
- M = coefficient of momentum at exit from the narrow channel into the wide one;
- N = coefficient of kinetic energy of the stream in the section;
- R_θ = the radius of the section, [m];
- Re = Reynolds number;
- v = velocity in a given point over the cross-section, [m/s];
- V_n = mean stream velocity in the n section [m/s];
- v_{\max} = maximum velocity over the section [m/s];
- y = generical distance from the pipe axis [m];
- Z = where specified is the equivalent of ζ ;

Greek characters:

- α = angle of convergence of the walls of a conduit [°];
- δ = angle between the conduit direction and the wall [°];
- δ_1 = thickness of the wall of the conduit [m];
- Δp = pressure drop [Pa];
- ΔV = deviation of the velocity at the given point of a narrow channel section from the mean velocity V_0 over the section [m/s];

- ε_0^{Re} = coefficient of filling of the section of a sharp-edged orifice at $\frac{F_0}{F_1} = 0$;
- λ = friction coefficient (see theoretical framework);
- ζ = head loss coefficient (see theoretical framework);
- $\zeta_0 = 1 + 0,707 \sqrt{1 - \frac{F_0}{F_1}}$ = head loss coefficient;
- ζ_{fr} = friction loss coefficient;
- ζ_M = resistance coefficient of the restrictor at large Mach numbers;
- $\zeta_\varphi = \frac{1}{\varphi^2} - 1$ = head loss coefficient;
- Π_0 = perimeter of the cross-section [m];
- τ = coefficient which permits to take in account for the thickness of the wall, the inlet shape, and conditions of the stream passage into the orifice;
- φ = velocity coefficient at discharge from a sharp edged orifice.

8.1 Introduction

8.1.1 Sudden enlargements

This particular type of singularity can be assumed as the basic model of discontinuities in pipe flow: a lot of other studies can be reconnected to it.

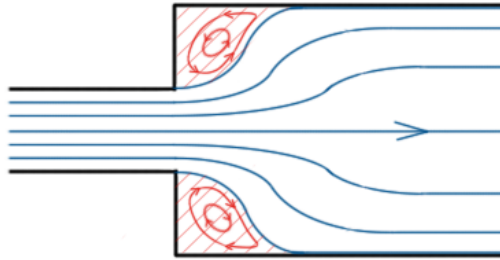


Figure 1: flow pattern at sudden expansion

The first analysis connected to this model date back in the work of the French scientist Borda who analyzed the shock phenomena. He assumed that the energy dissipation due to the sudden expansion singularity can be seen as an inelastic shock between the flow upstream and the downstream of the section. Nowadays we know that the energetic dissipation is due to the flow vein detachment from the boundary walls of the pipe but the Borda intuition simplified a lot the mathematical approach to the problem.

Considering a stretch of conduit in which is contained a sudden enlargement (Figure 2), it is possible to define two sections, one upstream and one downstream of the discontinuity: the section 1 is the last in which it is possible to consider linear stream before the discontinuity, and section 2 is the nearest section in which the stream can be reconsidered linear after the discontinuity.

Using the fluid dynamic equilibrium equation between the upstream and the downstream section (Figure 2) under the hypothesis of horizontal, smooth pipe and hydrostatic distribution of the pressure in the two sections (and in the connecting section between the two stretches) it is possible to write the following expression:

$$p_1 F_1 + p_1 (F_2 - F_1) + \rho Q V_1 = p_2 F_2 + \rho Q V_2$$

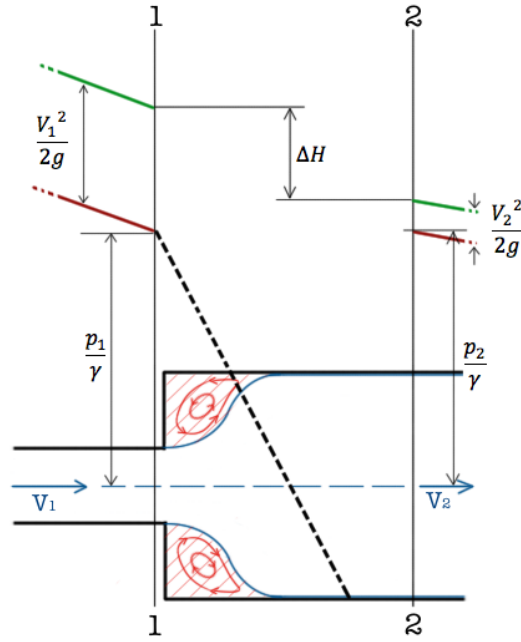


Figure 2: equilibrium equation

Where F_1 e F_2 are the area section of the two pipes considered, Q is the flow considered, V_1 and V_2 the mean velocities of the stream at inlet and outlet of the volume considered. β , the coefficient of mean velocities, is neglected because is made equal to 1.

Assumed that $Q = F_2 V_2$:

$$\rho F_2 V_2 (V_1 - V_2) = F_2 (p_2 - p_1)$$

For the continuity it is certainly $V_1 > V_2$, and from this assumption derives that the left term of the equation is certainly positive. Consequently it must be positive also the right term of the equation and so $p_2 > p_1$.

Considering an inclined duct, it can be written that:

$$\left(\frac{p_2}{\gamma} + z_2\right) > \left(\frac{p_1}{\gamma} + z_1\right)$$

So, for the head loss computation it can be written the following equation:

$$\Delta H = \frac{p_1}{\gamma} + \frac{V_1^2}{2g} - \frac{p_2}{\gamma} - \frac{V_2^2}{2g} = \frac{1}{2g} (V_1^2 - V_2^2) + \frac{1}{\gamma} (p_1 - p_2)$$

From the previous formula:

$$(p_1 - p_2) = -\rho V_2 (V_1 - V_2) = \rho V_2 (V_2 - V_1)$$

And then, substituting in the previous expression we have the Borda's formula in the following expression:

$$\begin{aligned}\Delta H &= \frac{1}{2g}(V_1^2 - V_2^2) + \frac{1}{\gamma}\rho V_2(V_2 - V_1) = \frac{1}{2g}(V_1^2 - V_2^2) + \frac{1}{2\rho g}\rho V_2(2V_2 - 2V_1) \\ &= \frac{1}{2g}(V_1^2 - V_2^2 - 2V_2V_1 + 2V_2^2) \\ &\rightarrow \Delta H = \frac{(V_1 - V_2)^2}{2g}\end{aligned}$$

The result is that the head loss in the passage through a sudden enlargement is the differential dynamic pressure of the flow. This head loss can be called "shock-loss".

The resistance coefficient ζ of a "shock", following the Borda expression, with uniform distribution of velocity over the section before the expansion and turbulent flow, is a function of the area ratio $n = \frac{F_2}{F_1}$ only, and can be calculated with Borda formula:

$$\zeta = \frac{\Delta H}{\frac{V_1^2}{2g}} = \left(1 - \frac{F_1}{F_2}\right)^2 = \left(1 - \frac{1}{n}\right)^2$$

As we've already written, the energy loss in this particular singularity is due to the separation of the flow from the boundaries of the pipe: in the section, when the flow suddenly expands, a jet is formed in the expanded section. This jet disintegrates into powerful eddies, which are the main cause of the dissipation of mechanical energy into heat. These eddies have a gradual reabsorption along the pipe, and the complete re-expansion of the flow in a complete spreading over the section takes place after 8/10 downstream diameters after the enlargement.

8.1.1.1 Reynolds number influence

- For $1 < Re < 10$ the resistance coefficient is a function only of Reynolds number and it can be assumed the Karev formula:

$$\zeta = \frac{\Delta H}{\frac{V_1^2}{2g}} = \frac{26}{Re}$$

- Within the Reynolds number $10 < Re < 3500$, the resistance coefficient of shock is a function not only of the area ratio $\frac{F_2}{F_1}$ but also of the Re number itself. The values of ζ in these conditions can be found from Graph 8;
- For $Re > 3500$ the resistance coefficient can be referred to the Graph 7;

8.1.1.2 Velocity profiles influence

Actually, velocity profiles in the sudden expansion can be rarely assumed as regular, or, to say better, they're non-uniform. This fact has a great influence in the losses computation, in particular it increases the head losses seen before, and so it's basic to consider this factor. From this point of the paragraph it will be indicated with the subscript "0" all the quantities referred to the inlet of the enlargement, and with the subscript "2" all the quantities referred to the down stream of the previous section 2 (Figure 2).

In order to calculate the resistance coefficient in such conditions, it is necessary to have a general formula of the shock, which allows for this non-uniformity if the velocity distribution over the channel section is known:

$$\zeta = \frac{\Delta H}{\frac{V_0^2}{2g}} = \frac{1}{n^2} + N - \frac{2M}{n}$$

Where:

$M = \frac{1}{F_0} \int_{F_0} \left(\frac{V}{V_0}\right)^2 dF$ is the coefficient of momentum at exit from the narrow channel into the wide one;

$N = \frac{1}{F_0} \int_{F_0} \left(\frac{V}{V_0}\right)^3 dF$ is the coefficient of kinetic energy of the stream in the same section;

It can be approximated that:

$$N \cong 3M - 2$$

Using the last expression, the following approximate formula is obtained for the resistance coefficients:

$$\zeta = \frac{\Delta H}{\frac{V^2}{2g}} \cong \frac{1}{n^2} + N \left(1 - \frac{2}{3n} \right) - \frac{4}{3n}$$

The determination of N and M is easy if the velocity distribution is known, but also if the distribution is not known, they can be determined by numerical integration (empirically) on the profiles obtained.

The velocity distribution is roughly exponential in the sections of expanding channels of divergence angle $\alpha = 8^\circ$ to 10° (Figure 3), in lengthy stretches of constant cross-section with developed turbulent velocity profile and other stretches. Defining v and v_{max} as the velocity at given point and the maximum velocity over the section, R_0 as the radius of the section, y as the distance from the pipe axis and m as the exponent which can generally vary from case to case, it is possible to write the following expression which identifies the exponential profile of the velocity:

$$\frac{v}{v_{max}} = \left(1 - \frac{y}{R_0} \right)^{\frac{1}{m}}$$

- At $m = 1$ the velocity profiles resembles a triangle;
- At $m = \infty$ the velocity profiles resembles a rectangle, meaning that the velocity distribution in the section is completely regular;
- In practice a velocity profile approximating a rectangle is obtained for m as low as 8 to 10; these values are valid for lengthy stretches with turbulent flow;
- The values $m = 2$ to 6 can be assumed for lengthy diffusers ($n > 2$), in accordance with the following table:

$\alpha = 2^\circ$	$m \cong 6$
$\alpha = 4^\circ$	$m \cong 4$
$\alpha = 6^\circ$	$m \cong 3$
$\alpha = 8^\circ$	$m \cong 2$

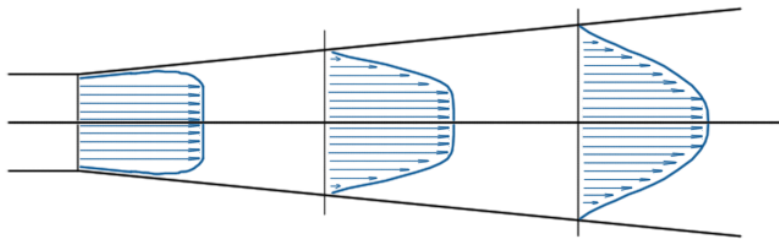


Figure 3: smooth diffuser $\alpha = 8^\circ$ to 10°

The values of N and M can be calculated at the exponential velocity profile from the following formulas obtained by Idel'cik (Idel'chik, 1966):

1. in the case of conduits of circular and square sections (Graph 9 and Graph 10);

$$M = \frac{(2m+1)^2(m+1)}{4m^2(m+2)} \quad \text{and} \quad N = \frac{(2m+1)^3(m+1)^3}{4m^4(2m+3)(m+3)}$$

2. in the case of a plane pipe or diffuser with sides ratio of the rectangular section $0,3 < a_0/b_0 < 3,0$ (Graph 11 and Graph 12):

$$M = \frac{(m+1)^2}{m(m+2)} \quad \text{and} \quad N = \frac{(m+1)^3}{m^2(m+3)}$$

The velocity profile in lengthy straight stretches of conduits, with a distance from the inlet larger than $10D_h$ and laminar flow, is parabolic:

$$\frac{v}{v_{max}} = 1 - \left(\frac{y}{R_0}\right)^2$$

The values of N and M can be calculated here are:

	M	N
Circular or square section	1,33	2,00
Plane pipe	1,20	1,55

The velocity profile is roughly sinusoidal in conduits near grids, elbows behind guide vanes, and other similar obstructions; in the case of a plane channel it is calculated by the following formula (Graph 13 and Graph 14):

$$\frac{v}{V_0} = 1 + \frac{\Delta V}{V_0} \sin 2k\pi \frac{2y}{b_0}$$

Where b_0 is the width of the plane channel, ΔV is the deviation of the velocity at the given point of a narrow channel section from the mean velocity V_1 over the section and k is an integer number.

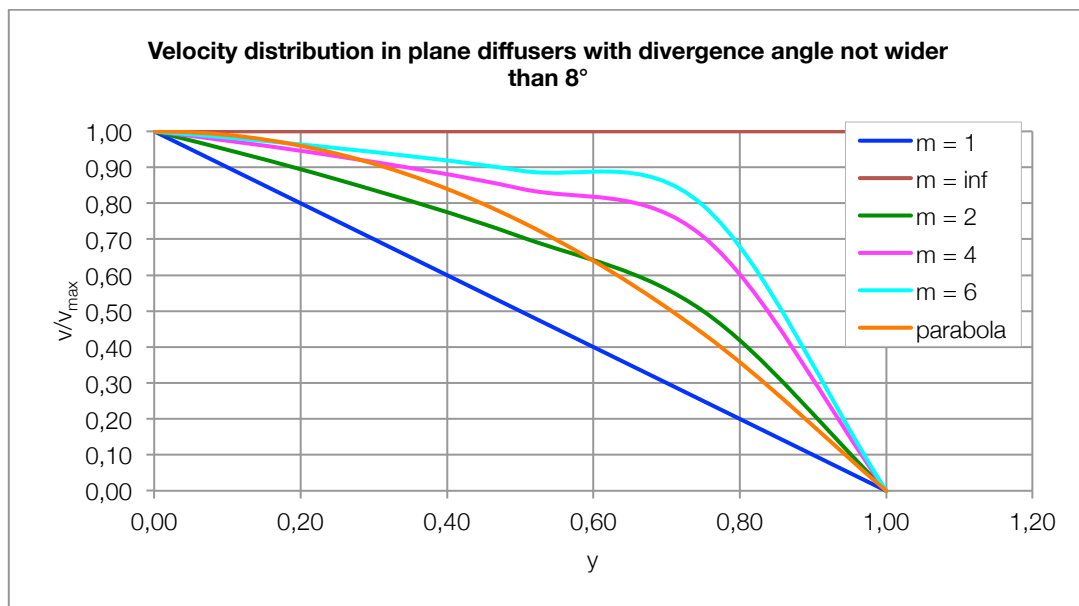
For the sinusoidal profile, the coefficients N and M can be calculated as:

$$M = 1 + \frac{1}{2} \left(\frac{\Delta V}{V_0}\right)^2 \quad \text{and} \quad N = 1 + \frac{3}{2} \left(\frac{\Delta V}{V_0}\right)^2$$

A non-symmetrical velocity profile is established behind diffusers with divergence angle greater than 10° , angle that is the minimum to cause the stream separation, behind elbows branches etc. (Graph 15). In particular, for $15^\circ < \alpha < 20^\circ$ and straight elbows (of angle 90°) we can use the formula (plotted in Graph 2):

$$\frac{V}{V_0} = 0,585 + 1,64 \sin\left(0,2 + 1,95 \frac{2y}{b_0}\right)$$

Here the values of N and M are 3,7 and 1,87 respectively.



Graph 1: Velocity distribution in plane diffusers with divergence angle not wider than 8°

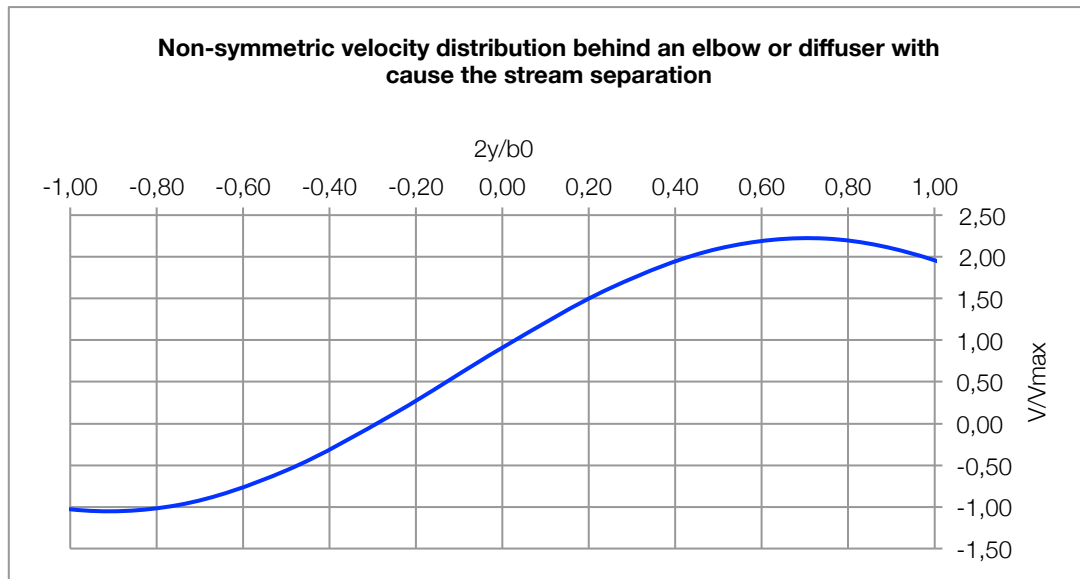
When a non-uniform velocity distribution is established in a conduit of constant cross section, the equalization of the stream is accompanied by an irreversible head loss, which is calculated by the following formulas:

$$\zeta = \frac{\Delta H}{\frac{V^2}{2g}} \cong 1 + N - 2M$$

or

$$\zeta = \frac{\Delta H}{\frac{V^2}{2g}} \cong \frac{1}{3}(N - 1)$$

Where N and M are determined in accordance with the non-uniform pattern obtained. These losses are taken into account only where they've been neglecting in determining the local resistance of fittings or obstructions in the straight stretches.



Graph 2: Non-symmetric velocity distribution behind an elbow or diffuser which causes the stream separation

The resistance of a stretch with a sudden enlargement can be reduced by installing baffles (Graph 7). The correct installation of these baffles can reduce the loss by 35%-40%, so the formula used to calculate the concentrated head loss is:

$$\zeta' = \frac{\Delta H}{\frac{V^2}{2g}} \cong 0,6 \cdot \zeta$$

Where ζ is the coefficient obtained without baffles.

8.1.2 Orifices

In the general case, the passage of a stream from one volume to another through a hole in a wall, is accompanied by the phenomena illustrated in Figure 4. The stream passes from channel 1 through an orifice of diameter D_0 , into the channel 2. The two channels can have cross-sections of arbitrary dimensions, but not smaller than the orifice diameter. The passage through the orifice is accompanied by the bending of the trajectories of the particles and the inertial forces causing them to continue their motion toward the orifice axis. This leads to a decrease of the jet section from its initial area F_1 to an area F_C smaller than the area F_0 of the orifice section.

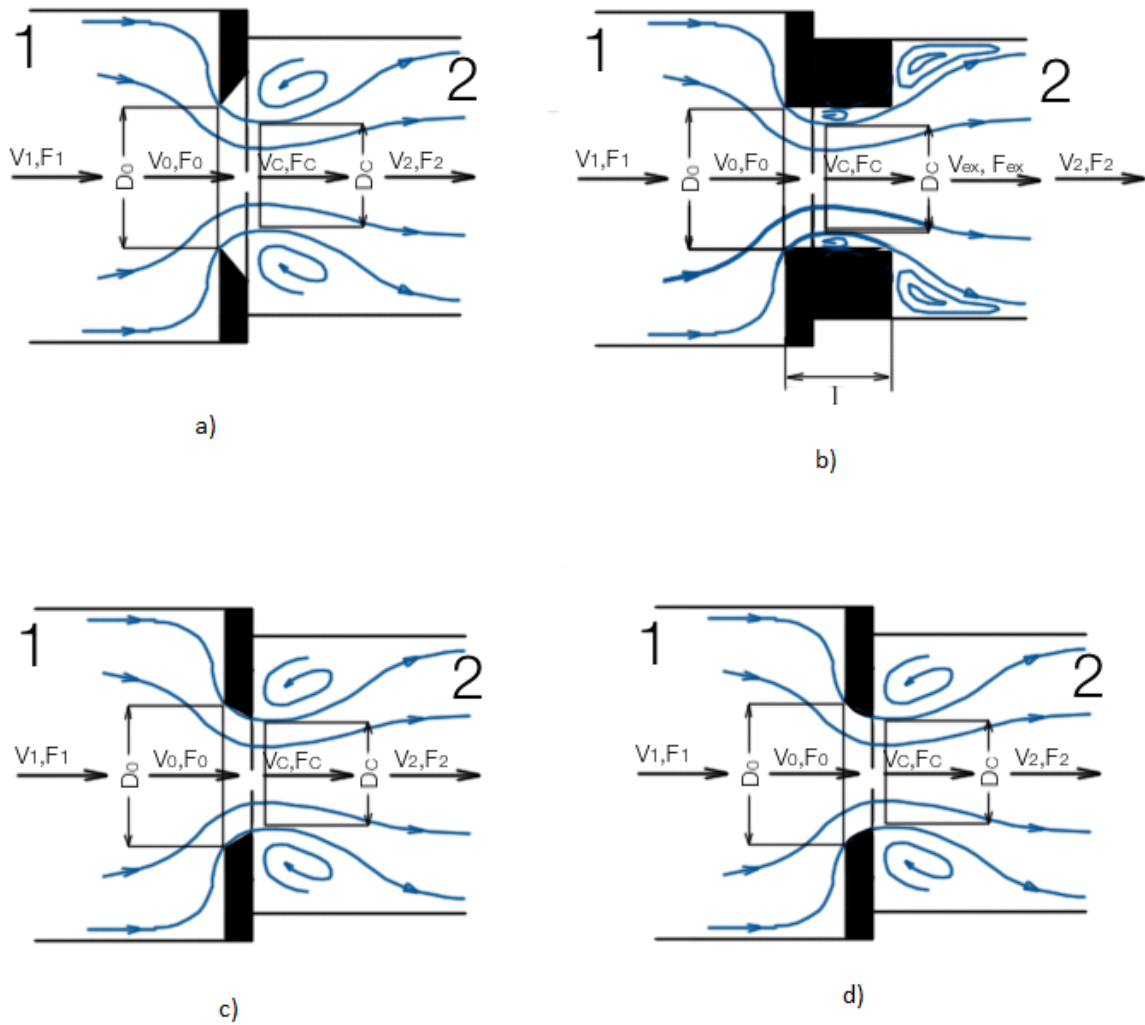


Figure 4: general case of a stream flow from one volume into another through an orifice

Looking at Figure 4, it's clear that there are different type of orifices in pipe flow field:

- a. Sharp-edged orifice ($l/D_h = 0$)
- b. Thick-walled orifice ($l/D_h > 0$);
- c. Orifice with edges beveled in the flow direction;
- d. Orifice edges rounded in the flow direction;

For Sharp-edged orifices ($l/D_h = 0$), case a), the resistance coefficient can be calculated in two different way, in relation to the Reynolds number:

Reynolds Number	Formula
$> 10^5$	$\zeta = \frac{\Delta H}{V^2} = \left(1 + 0,707 \sqrt{1 - \frac{F_0}{F_1} - \frac{F_0}{F_2}} \right)^2$
$< 10^5$	$\zeta = \frac{\Delta H}{V^2} \cong \left(\frac{1}{\varphi^2} - 1 \right) + \frac{0,342}{(\varepsilon_0^{Re})^2} \left(1 + 0,707 \sqrt{1 - \frac{F_0}{F_1} - \frac{F_0}{F_2}} \right)^2 = \zeta_\varphi + \overline{\varepsilon_0^{Re}} \left(\zeta_0 - \frac{F_0}{F_2} \right)^2$

Where φ is the velocity coefficient at discharge from a sharp edged orifice, depending on Re and on $\frac{F_0}{F_1}$; $\varepsilon_0^{Re} = \frac{F_c}{F_0}$ is the coefficient of filling of the section of a sharp-edged orifice at $\frac{F_0}{F_1} = 0$, depending on Re; $\zeta_\varphi = \frac{1}{\varphi^2} - 1$ is determined from the curves of the Graph 19; $\overline{\varepsilon_0^{Re}} = \frac{0,342}{(\varepsilon_0^{Re})^2}$ is determined from the curve on the same graph; $\zeta_0 = 1 + 0,707 \sqrt{1 - \frac{F_0}{F_1}}$;

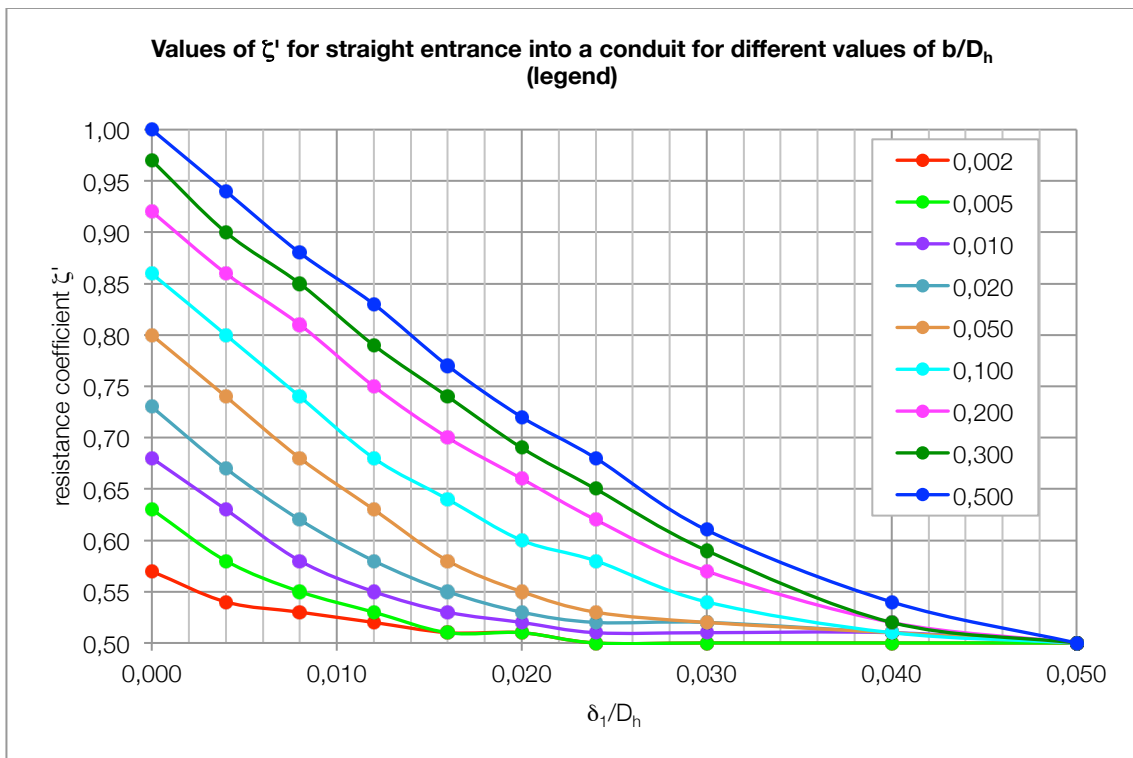
The thickening, beveling or rounding (cases b), c), and d) respectively) of the orifice edges leads, in general, to a reduction of the resistance of the discontinuity because of his influence in the reduction of velocity in the narrowest section and, consequently, of the shock.

The resistance coefficient of the passage of a stream through a wall orifice of arbitrary edge shape and thickness is calculated, at high Reynolds numbers ($Re > 10^5$, practically) by the following formula:

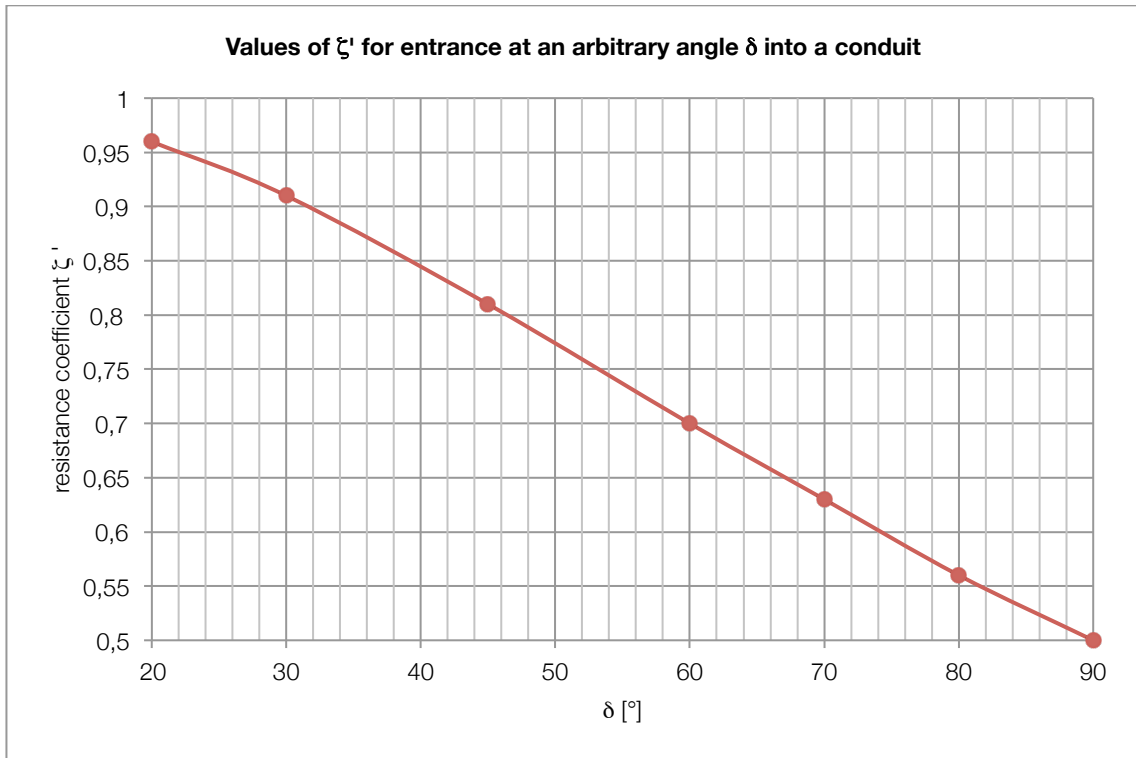
$$\zeta = \frac{\Delta H}{V^2} = \zeta' \left(1 - \frac{F_0}{F_1} \right) + \left(1 - \frac{F_0}{F_2} \right)^2 + \tau \sqrt{1 - \frac{F_0}{F_1} \left(1 - \frac{F_0}{F_2} \right)} + \zeta_{fr}$$

Where ζ' is a coefficient, depending on the shape of the inlet edge of the orifice, and is determined from the Graph 3, Graph 4, Graph 5 and Graph 6.

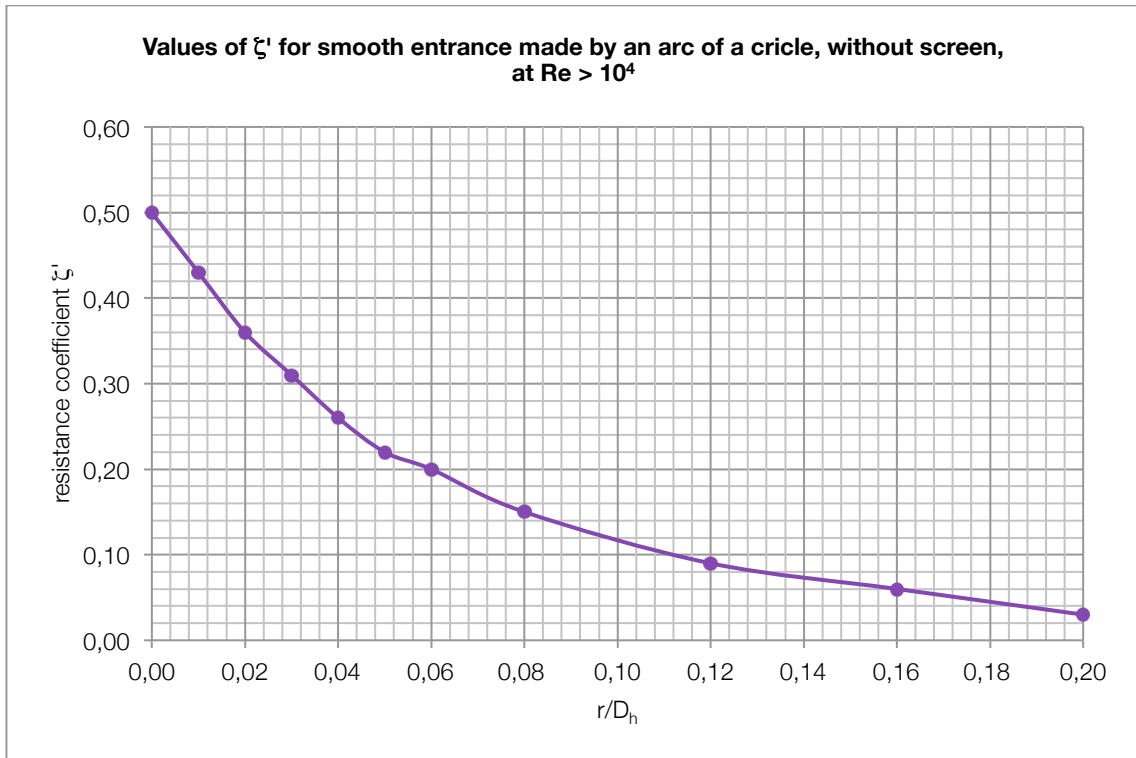
<p>Graph 3 Values of ζ' for straight entrance into a conduit for different values of b/D_h (legend)</p>	<p>Graph 4 Values of ζ' for entrance at an arbitrary angle δ into a conduit</p>
<p>Graph 5 Values of ζ' for smooth entrance made by an arc of a circle, without screen, at $Re > 10^4$</p>	<p>Graph 6 Values of ζ' for conical converging entrance at various angle of convergence α, at $Re > 10^4$</p>



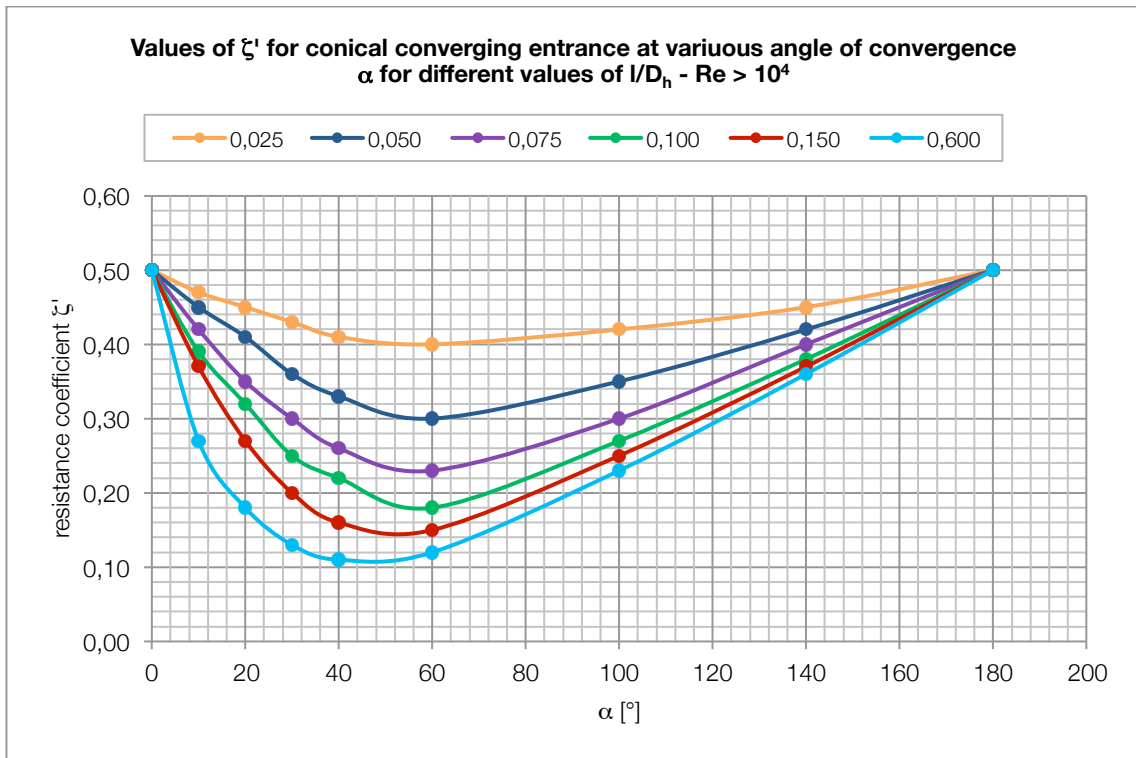
Graph 3: Values of ζ' for straight entrance into a conduit for different values of b/D_h (legend)



Graph 4: Values of ζ' for entrance at an arbitrary angle δ into a conduit



Graph 5: Values of ζ' for smooth entrance made by an arc of a circle, without screen, at $Re > 10^4$



Graph 6: Values of ζ' for conical converging entrance at various l/D_h and angle of convergence α , at $Re > 10^4$

τ is a coefficient which permits to take in account for the thickness of the wall, the inlet shape, and conditions of the stream passage into the orifice. It is determined from Graph 21 for thick-walled orifices and, approximately, for rounded and beveled edges by the formula $\tau = 2\sqrt{\zeta'}$;

$\zeta_{fr} = \lambda \frac{l}{D_h}$ is the friction loss coefficient for the entire depth of the orifice (in case of beveled or rounded edges is to be equal to zero, Graph 22);

The resistance coefficient of the passage of a stream through a wall orifice of arbitrary edge shape and thickness is calculated, at low Reynolds numbers ($Re < 10^5$, practically) by the following formula:

$$\zeta = \frac{\Delta H}{\frac{V^2}{2g}} \cong \zeta_\varphi + \varepsilon_0^{Re} \left[0,5 \left(1 - \frac{F_0}{F_1}\right) + \left(1 - \frac{F_0}{F_2}\right)^2 + \tau \sqrt{1 - \frac{F_0}{F_1}} \left(1 - \frac{F_0}{F_2}\right) \right] + \zeta_{fr}$$

In general, the flow through an orifice in a wall can assume several distinct forms, and, in relation to this fact, the formulas seen till here can be simplified as follow:

a) $F_1 = F_0$ (sudden expansion of the section)

$$\zeta = \frac{\Delta H}{\frac{V^2}{2g}} = \left(1 - \frac{F_0}{F_2}\right)$$

b) $F_2 = F_0$ (sudden contraction of the section)

$$\zeta = \frac{\Delta H}{\frac{V^2}{2g}} = \zeta' \left(1 - \frac{F_0}{F_1}\right)$$

c) $F_1 \rightarrow \infty$ (entrance with sudden enlargement, through a perforated plate for example)

$$\zeta = \frac{\Delta H}{\frac{V^2}{2g}} = \left[\zeta' + \left(1 - \frac{F_0}{F_2}\right)^2 + \tau \left(1 - \frac{F_0}{F_2}\right) + \zeta_{fr} \right] \left(\frac{F_2}{F_0}\right)^2$$

d) $F_1 = F_2$ (resitrictor)

$$\zeta = \frac{\Delta H}{\frac{V^2}{2g}} = \left[\left(\zeta' + \tau \sqrt{1 - \frac{F_0}{F_1}} \right) + \left(1 - \frac{F_0}{F_1}\right) + \left(1 - \frac{F_0}{F_1}\right)^2 + \zeta_{fr} \right] \left(\frac{F_1}{F_0}\right)^2$$

The resistance coefficients of a restrictor, reduces the previous equations to the following expressions at different shapes of the orifice edges and $Re > 10^5$ (Table 1).

Table 1: formulas for different types of restrictor at $Re > 10^5$

Shape of resistor edges	Conditions	Reduced formula
<i>Sharp-edged orifice</i> Graph 23	$\zeta' = 0,5$ $\tau = 1,41$	$\zeta = \frac{\Delta H}{V^2} = \left[0,707 \sqrt{1 - \frac{F_0}{F_1} + 1 - \frac{F_0}{F_1}} \right]^2 \left(\frac{F_1}{F_0} \right)^2$
<i>Thick-walled orifice</i> Graph 24	$\zeta' = 0,5$	$\zeta = \frac{\Delta H}{V^2} = \left[\left(0,5 + \tau \sqrt{1 - \frac{F_0}{F_1}} \right) \left(1 - \frac{F_0}{F_1} \right) + \left(1 - \frac{F_0}{F_1} \right)^2 + \zeta_{fr} \right]^2 \left(\frac{F_1}{F_0} \right)^2$
<i>Orifice with edges beveled or rounded</i> Graph 25, Graph 26	$\tau = 2\sqrt{\zeta'}$ $\zeta_{fr} = 0$	$\zeta = \frac{\Delta H}{V^2} = \left[1 + \sqrt{\zeta' \left(1 - \frac{F_0}{F_1} \right) - \frac{F_0}{F_1}} \right]^2 \left(\frac{F_1}{F_0} \right)^2$

For $Re < 10^5$ the resistance coefficients of a restrictor can be computed as specified in the Table 2.

Table 2: formulas for different types of restrictor at $Re < 10^5$

Shape of resistor edges	Conditions	Reduced formula
<i>Sharp-edged orifice</i>	$\zeta' = 0,5$ $\tau = 1,41$	$\zeta = \frac{\Delta H}{V^2} \cong \left[\left(\frac{1}{\varphi^2} - 1 \right) + \frac{0,342}{(\varepsilon_0^{Re})^2} \left(1 + 0,707 \sqrt{1 - \frac{F_0}{F_1} - \frac{F_0}{F_1}} \right)^2 \right] \left(\frac{F_1}{F_0} \right)^2$ $= \left[\zeta_\varphi + \overline{\varepsilon_0^{Re}} \left(\zeta_0 - \frac{F_0}{F_1} \right)^2 \right] \left(\frac{F_1}{F_0} \right)^2$
<i>Thick-edged orifice</i>	$\zeta' = 0,5$	$\zeta = \frac{\Delta H}{V^2} \cong \left\{ \zeta_\varphi + \overline{\varepsilon_0^{Re}} \left[\left(0,5 + \tau \sqrt{1 - \frac{F_0}{F_1}} \right) \left(1 - \frac{F_0}{F_1} \right) + \left(1 - \frac{F_0}{F_2} \right)^2 \right] + \zeta_{fr} \right\} \left(\frac{F_1}{F_0} \right)^2$

At low cross-section coefficients $\frac{F_0}{F_1}$ of the restrictors, large velocities are obtained in its orifice even at relatively low stream velocities in the pipe. The influence of compression begin to felt here, leading to an increase in the resistance coefficient of the restrictor.

The resistance coefficient of a restrictor in such conditions, taking the influence of the compression into account, can be determined by the formula:

$$\zeta_M = \frac{\Delta H}{\frac{V_1^2}{2g}} \cong k_m \zeta$$

Where ζ_M is the resistance coefficient of the restrictor at large Mach numbers; ζ is the resistance coefficient of the restrictor at low Mach numbers, determined as seen before; k_m is the coefficient that permits to allow for the influence of compressibility in the vena contracta of the jet, determined by the Graph 27.

In the following pages are presented the graphs for the various cases previously listed.

8.2 Graphs of head loss coefficients

Sudden expansion of a stream with uniform velocity distribution

$D_h = 4F_0/\Pi_0$; Π_0 is the perimeter

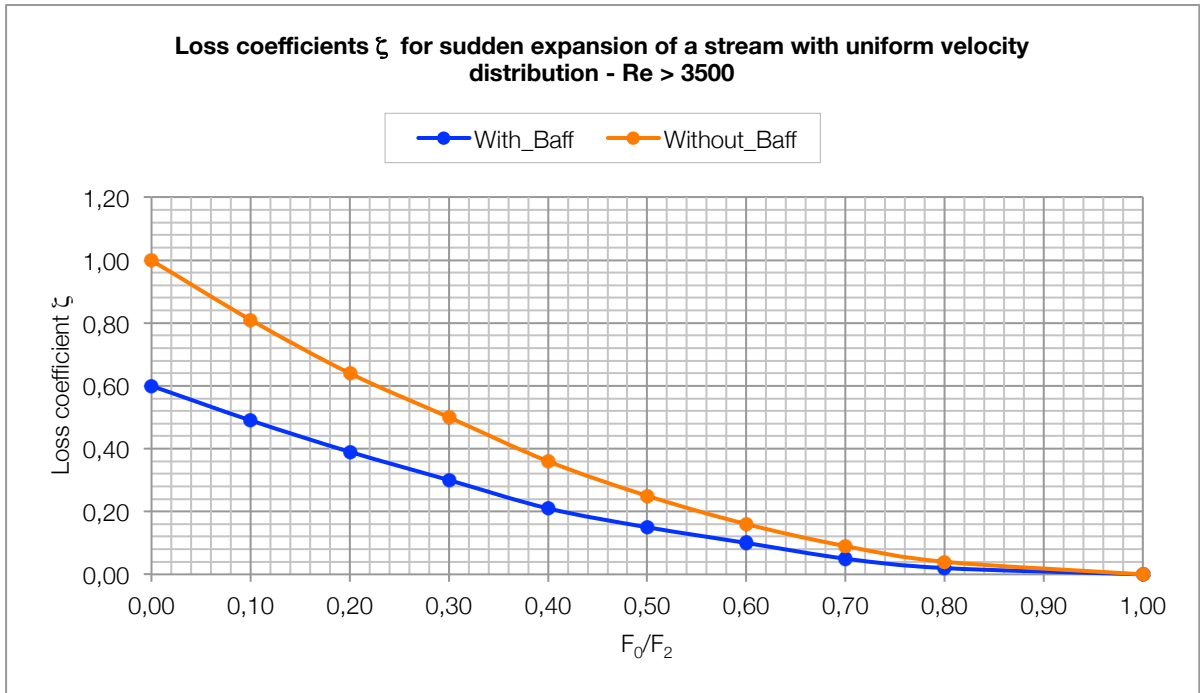
Re > 3,5 x 10³

Without baffles

$$\zeta = \frac{\Delta H}{\frac{V_0^2}{2g}} = \left(1 - \frac{F_0}{F_2}\right)^2$$

With baffles

$$\zeta = \frac{\Delta H}{\frac{V_0^2}{2g}} \cong 0,6 \left(1 - \frac{F_0}{F_2}\right)^2$$

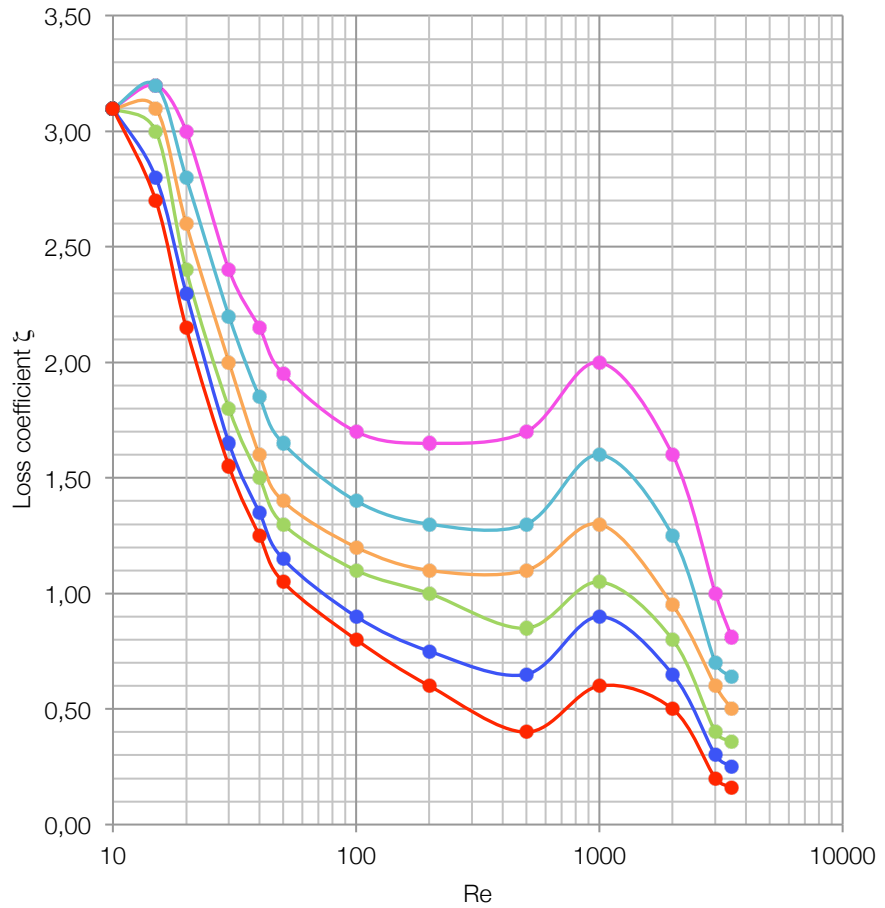


Graph 7: ζ with sudden expansion of a stream with uniform velocity distribution - Re > 3,5 x 10³

F_0/F_2	With Baffles	Without Baffles
0,00	0,60	1,00
0,10	0,49	0,81
0,20	0,39	0,64
0,30	0,30	0,50
0,40	0,21	0,36
0,50	0,15	0,25
0,60	0,10	0,16
0,70	0,05	0,09
0,80	0,02	0,04
1,00	0,00	0,00

Loss coefficients ζ for sudden expansion of a stream with uniform velocity distribution
 $10 < Re < 3,5 \times 10^3$

—●— 0,10 —●— 0,20 —●— 0,30 —●— 0,40 —●— 0,50 —●— 0,60



$10 < Re < 3,5 \times 10^3$

$$\zeta = \frac{\Delta H}{\frac{V_0^2}{2g}}$$

Determined from Graph 8

$1 < Re < 10$

$$\zeta = \frac{\Delta H}{\frac{V_0^2}{2g}} = \frac{26}{Re}$$

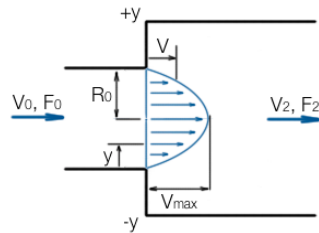
Graph 8: ζ with sudden expansion of a stream with uniform velocity distribution $10 < Re < 3,5 \times 10^3$

	Reynolds Numbers												
F_0/F_2	10	15	20	30	40	50	100	200	500	1000	2000	3000	3500
0,10	3,10	3,20	3	2,4	2,15	1,95	1,7	1,65	1,7	2	1,6	1	0,81
0,20	3,10	3,20	2,8	2,2	1,85	1,65	1,4	1,3	1,3	1,6	1,25	0,7	0,64
0,30	3,10	3,10	2,6	2	1,6	1,4	1,2	1,1	1,1	1,3	0,95	0,6	0,5
0,40	3,10	3,00	2,4	1,8	1,5	1,3	1,1	1	0,85	1,05	0,8	0,4	0,36
0,50	3,10	2,80	2,3	1,65	1,35	1,15	0,9	0,75	0,65	0,9	0,65	0,3	0,25
0,60	3,10	2,70	2,15	1,55	1,25	1,05	0,8	0,6	0,4	0,6	0,5	0,2	0,16

Sudden expansion after a long straight stretch, diffuser, etc. with exponential velocity distribution (circular or rectangular cross section, $Re > 3500$)

$$D_h = 4F_0/\Pi_0; \Pi_0 \text{ is the perimeter; } n = F_2/F_0$$

$$\frac{v}{v_{max}} = 1 - \left(\frac{y}{R_0}\right)^2 \text{ velocity profile}$$



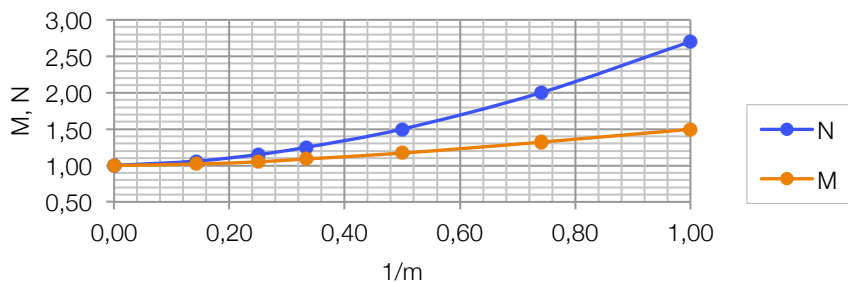
$$\zeta = \frac{\Delta H}{V_0^2} = \frac{1}{n^2} + N - \frac{2M}{n}$$

Determined on Graph 10

$$\begin{cases} M = \frac{(2m+1)^2(m+1)}{4m^2(m+1)} \\ N = \frac{(2m+1)^3(m+1)^3}{4m^4(2m+3)(m+3)} \end{cases}$$

Determined on Graph 9

M and N values - Sudden expansion after a long straight stretch, diffuser, etc., with exponential velocity distribution - Circular or rectangular cross section

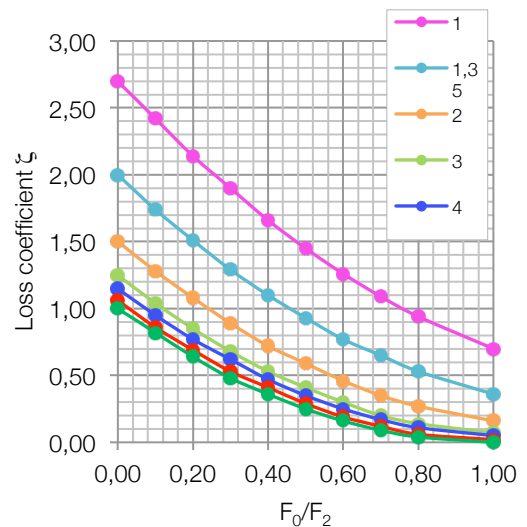


m	1/m	N	M
1,00	1,00	2,70	1,50
1,35	0,74	2,00	1,32
2,00	0,50	1,50	1,17
3,00	0,33	1,25	1,09
4,00	0,25	1,15	1,05
7,00	0,14	1,06	1,02
∞	0,00	1,00	1,00

Graph 9: values of M and N in exponential velocity

F_0/F_2	m values						
	1,00	1,35	2,00	3,00	4,00	7,00	∞
0,00	2,70	2,00	1,50	1,25	1,15	1,06	1,00
0,10	2,42	1,74	1,28	1,04	0,95	0,86	0,82
0,20	2,14	1,51	1,08	0,85	0,77	0,69	0,64
0,30	1,90	1,29	0,89	0,68	0,62	0,53	0,48
0,40	1,66	1,10	0,72	0,53	0,47	0,41	0,36
0,50	1,45	0,93	0,59	0,41	0,35	0,29	0,25
0,60	1,26	0,77	0,46	0,30	0,25	0,19	0,16
0,70	1,09	0,65	0,35	0,20	0,17	0,12	0,09
0,80	0,94	0,53	0,27	0,14	0,11	0,06	0,04
1,00	0,70	0,36	0,16	0,07	0,05	0,02	0,00

Loss coefficients ζ for sudden expansion after a long straight stretch, diffuser, etc., with exponential velocity distribution - Circular or rectangular cross section

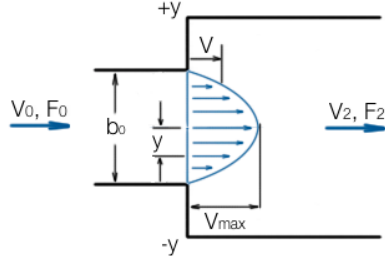


Graph 10: ζ with circular or rectangular cross section

Sudden expansion after a long plane and straight stretches, plane diffusers, etc. with exponential velocity distribution, $Re > 3500$

$$D_h = 4F_0/\Pi_0; \Pi_0 \text{ is the perimeter; } n = F_2/F_0$$

$$\frac{v}{v_{max}} = 1 - \left(\frac{2y}{b_0}\right)^2 \text{ velocity profile}$$



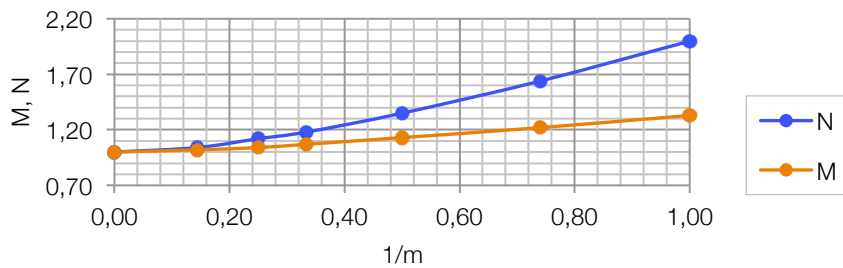
$$\zeta = \frac{\Delta H}{\frac{V_0^2}{2g}} = \frac{1}{n^2} + N - \frac{2M}{n}$$

Determined on Graph 12

$$\begin{cases} M = \frac{(m+1)^2}{m(m+2)} \\ N = \frac{(m+1)^3}{m^2(m+3)} \end{cases}$$

Determined on Graph 11

M and N values - Sudden expansion after long plane and straight stretches, plane diffuser, etc., with exponential velocity distribution

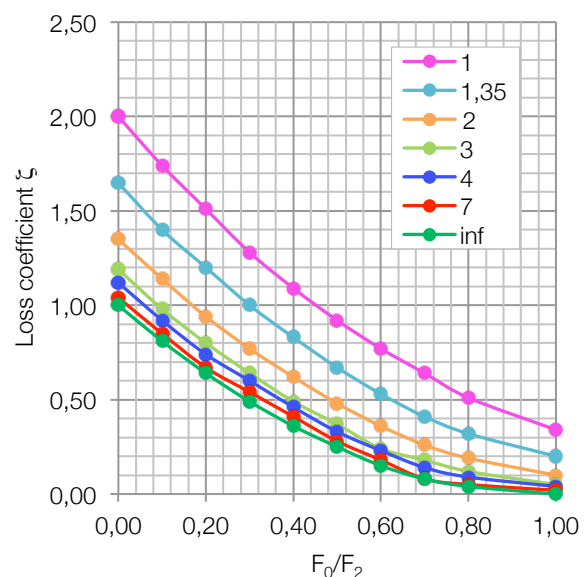


Graph 11: values of M and N in exponential velocity

m	1/m	N	M
1,00	1,00	2,00	1,33
1,35	0,74	1,64	1,22
2,00	0,50	1,35	1,13
3,00	0,33	1,18	1,07
4,00	0,25	1,12	1,04
7,00	0,14	1,04	1,02
∞	0,00	1,00	1,00

F_0/F_2	m values						
	1,00	1,35	2,00	3,00	4,00	7,00	∞
0,00	2,00	1,65	1,35	1,19	1,12	1,04	1,00
0,10	1,74	1,40	1,14	0,98	0,92	0,85	0,81
0,20	1,51	1,20	0,94	0,80	0,74	0,67	0,64
0,30	1,28	1,00	0,77	0,64	0,60	0,54	0,49
0,40	1,09	0,83	0,62	0,49	0,46	0,41	0,36
0,50	0,92	0,67	0,48	0,37	0,33	0,28	0,25
0,60	0,77	0,53	0,36	0,24	0,23	0,18	0,15
0,70	0,64	0,41	0,26	0,18	0,14	0,08	0,08
0,80	0,51	0,32	0,19	0,12	0,09	0,05	0,04
1,00	0,34	0,20	0,10	0,05	0,04	0,02	0,00

Loss coefficients ζ for sudden expansion after long plane and straight stretches, plane diffuser, etc., with exponential velocity distribution

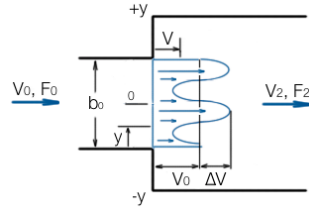


Graph 12: ζ with plane and straight stretches or plane diffusers

Sudden enlargement of a plane channel behind orifice plates, baffles in elbows, etc., with sinusoidal velocity distribution, $Re > 3500$

$$D_h = 4F_0/\Pi_0; \Pi_0 \text{ is the perimeter; } n = F_2/F_0$$

$$\frac{v}{V_0} = 1 + \frac{\Delta V}{V_0} \sin 2k\pi \frac{2y}{b_0} \text{ velocity profile, where } k \text{ is an integer number}$$



$$\zeta = \frac{\Delta H}{V_0^2} = \frac{1}{n^2} + N - \frac{2M}{n}$$

Determined on Graph 12

$$\begin{cases} M = 1 + \frac{1}{2} \left(\frac{\Delta V}{V_0} \right)^2 \\ N = 1 + \frac{3}{2} \left(\frac{\Delta V}{V_0} \right)^2 \end{cases}$$

Determined on Graph 11

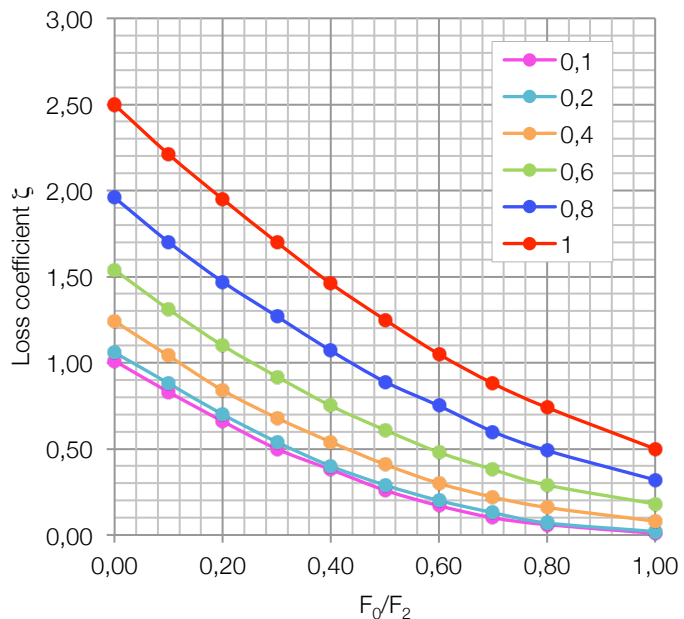
M and N for sudden enlargement of a plane channel behind orifice plates, baffles in elbows, etc., with sinusoidal velocity distribution



$\Delta V/V_0$	M	N
0,10	1,00	1,00
0,20	1,02	1,06
0,30	1,04	1,13
0,40	1,08	1,24
0,50	1,12	1,37
0,60	1,18	1,54
0,70	1,24	1,73
0,80	1,32	1,96
0,90	1,40	2,22
1,00	1,50	2,50

Graph 13: values of M and N after plane plane and straight stretches, plane diffuser, etc., with exponential velocity distribution

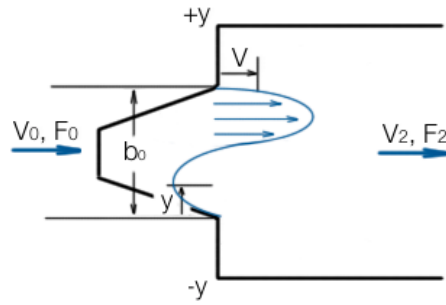
Loss coefficients for ζ for sudden enlargement of a plane channel behind orifice plates, baffles in elbows, etc., with sinusoidal velocity distribution



F_0/F_2	$\Delta V/V_0$					
	0,1	0,2	0,4	0,6	0,8	1
0,00	1,01	1,06	1,24	1,54	1,96	2,50
0,10	0,83	0,88	1,04	1,31	1,70	2,21
0,20	0,66	0,70	0,84	1,10	1,47	1,95
0,30	0,5	0,54	0,68	0,92	1,27	1,70
0,40	0,38	0,40	0,54	0,75	1,07	1,46
0,50	0,26	0,29	0,41	0,61	0,89	1,25
0,60	0,17	0,20	0,30	0,48	0,75	1,05
0,70	0,10	0,13	0,22	0,38	0,60	0,88
0,80	0,06	0,07	0,16	0,29	0,49	0,74
1,00	0,01	0,02	0,08	0,18	0,32	0,50

Graph 14: ζ with sudden enlargement of a plane channel behind orifice plates, baffles in elbows, etc., with sinusoidal velocity distribution

Sudden expansion after stretches with parabolic velocity distribution, $Re > 3500$



$$D_h = 4F_0/\Pi_0; \Pi_0 \text{ is the perimeter; } n = F_2/F_0$$

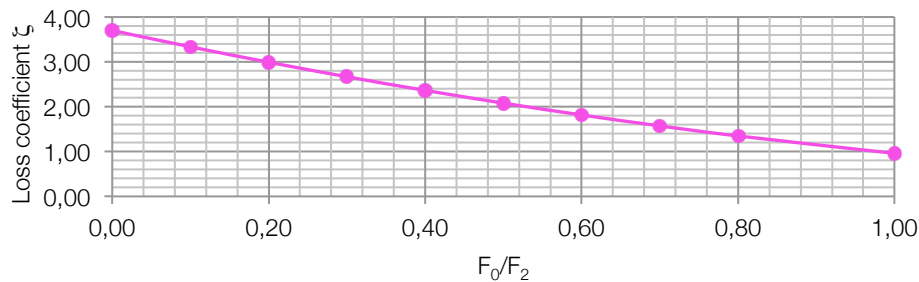
$$\frac{v}{v_0} = 0,585 + 1,64 \sin\left(0,2 + 1,95 \frac{2y}{b_0}\right)$$

velocity profile, where k is an integer number

$$\zeta = \frac{\Delta H}{\frac{V_0^2}{2g}} = \frac{1}{n^2} + 3,7 - \frac{3,74}{n}$$

Determined on Graph 15

Loss coefficient ζ for sudden expansion behind plane diffusers with $\alpha > 10^\circ$, elbows, etc., with asymmetric velocity distribution



F_0/F_2	n	ζ
0,00	∞	3,70
0,10	10,00	3,34
0,20	5,00	2,99
0,30	3,33	2,67
0,40	2,50	2,36
0,50	2,00	2,08
0,60	1,67	1,82
0,70	1,43	1,57
0,80	1,25	1,35
1,00	1,00	0,96

Graph 15: values of ζ with sudden expansion behind plane diffusers with $\alpha > 10^\circ$, elbows, etc., with asymmetric velocity distribution

$$D_h = 4F_0/\Pi_0; \Pi_0 \text{ is the perimeter; } n = F_2/F_0$$

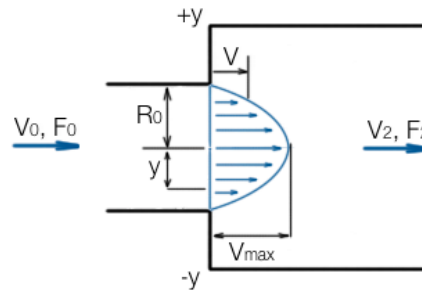
Circular Pipe

$$\zeta = \frac{\Delta H}{\frac{V_0^2}{2g}} = \frac{1}{n^2} + 2 - \frac{2,66}{n}$$

Rectangular Pipe

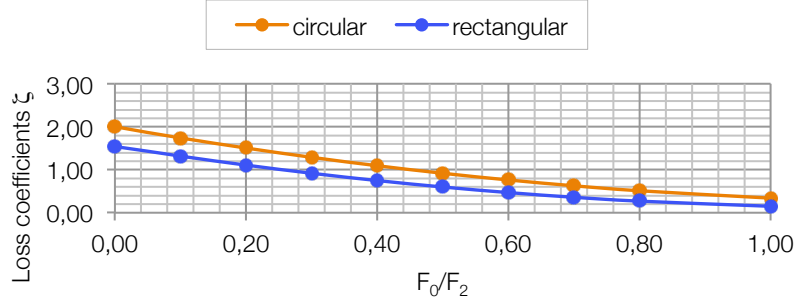
$$\zeta = \frac{\Delta H}{\frac{V_0^2}{2g}} = \frac{1}{n^2} + 1,55 - \frac{2,4}{n}$$

Determined from Graph 16



F_0/F_2	n	circular	rectangular
0,00	∞	2,00	1,55
0,10	10,00	1,74	1,32
0,20	5,00	1,51	1,11
0,30	3,33	1,29	0,92
0,40	2,50	1,10	0,75
0,50	2,00	0,92	0,60
0,60	1,67	0,76	0,47
0,70	1,43	0,63	0,36
0,80	1,25	0,51	0,27
1,00	1,00	0,34	0,15

Loss coefficients ζ for sudden expansion after stretches with parabolic velocity distribution



Graph 16: values of ζ for sudden expansion after stretches with parabolic velocity distribution

Stream deformation in a straight conduit with exponential velocity profile, $Re > 3500$

EXPONENTIAL VELOCITY PROFILE

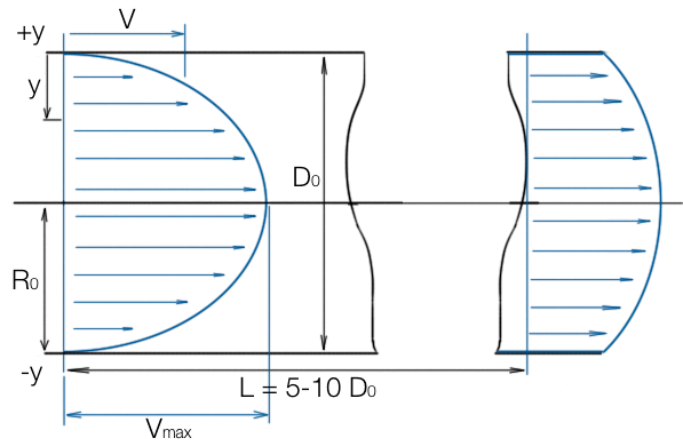
$D_h = 4F_0/\Pi_0$; Π_0 is the perimeter;

$$\frac{v}{V_{max}} = \left(1 - \frac{y}{R_0}\right)^{\frac{1}{m}}; \text{ with } m > 1$$

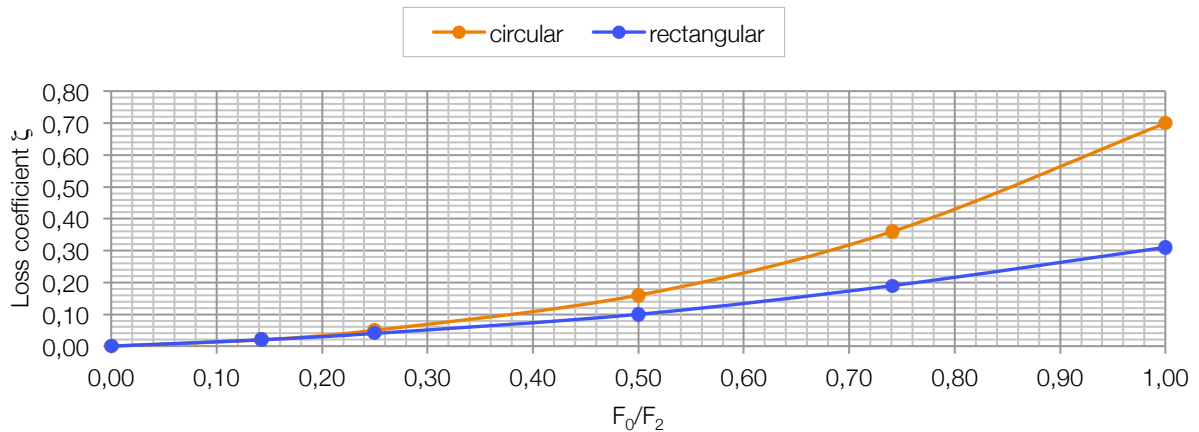
$$\zeta = \frac{\Delta H}{\frac{V_0^2}{2g}} = 1 + N - 2M$$

M and N are determined from Graph 9 and Graph 11

m	1/m	Circular	Rectangular
1,00	1,00	0,70	0,31
1,35	0,74	0,36	0,19
2,00	0,50	0,16	0,10
4,00	0,25	0,05	0,04
7,00	0,14	0,02	0,02
∞	0,00	0,00	0,00



Loss coefficients for stream deformation in a straight conduit with exponential velocity profile



Graph 17: values of ζ with stream deformation in a straight conduit with exponential velocity profile

PARABOLIC VELOCITY PROFILE

$D_h = 4F_0/\Pi_0$; Π_0 is the perimeter;

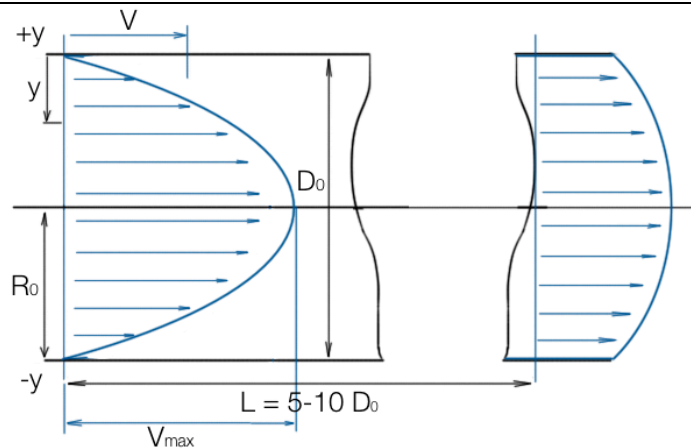
$$\frac{v}{V_{max}} = \left(1 - \frac{y}{R_0}\right)^2;$$

Circular pipe

$$\zeta = \frac{\Delta H}{\frac{V_0^2}{2g}} = 0,34$$

Rectangular pipe

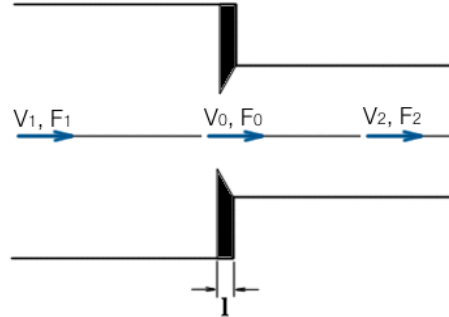
$$\zeta = \frac{\Delta H}{\frac{V_0^2}{2g}} = 0,15$$



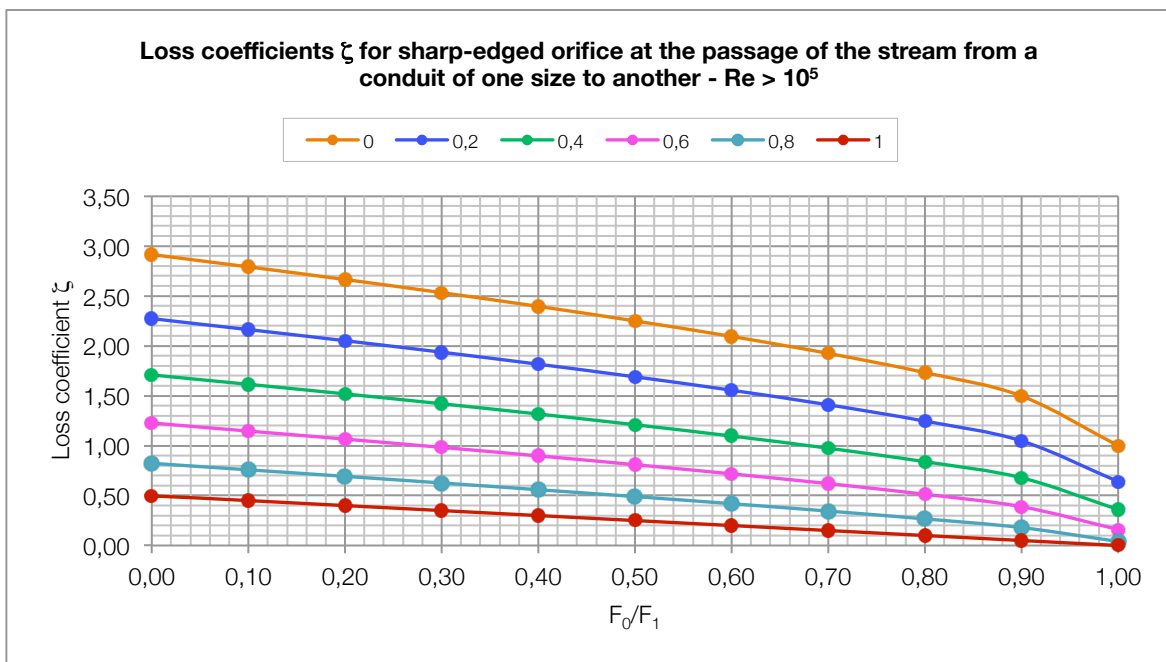
Sharp-Edged ($l/D_h = 0 \div 0,015$) orifice at the passage of the stream from a conduit to one size to another, $Re > 3,5 \times 10^5$

$$D_h = 4F_0/\Pi_0; \Pi_0 \text{ is the perimeter;}$$

$$\zeta = \frac{\Delta H}{\frac{V_0^2}{2g}} = \left(1 + 0,707 \sqrt{1 - \frac{F_0}{F_1} - \frac{F_0}{F_2}} \right)^2$$



F_0/F_1	F_0/F_2					
	0	0,2	0,4	0,6	0,8	1
0,00	2,91	2,27	1,71	1,23	0,82	0,50
0,10	2,79	2,16	1,61	1,15	0,76	0,45
0,20	2,66	2,05	1,52	1,07	0,69	0,40
0,30	2,53	1,94	1,42	0,98	0,63	0,35
0,40	2,40	1,82	1,32	0,90	0,56	0,30
0,50	2,25	1,69	1,21	0,81	0,49	0,25
0,60	2,09	1,56	1,10	0,72	0,42	0,20
0,70	1,92	1,41	0,97	0,62	0,34	0,15
0,80	1,73	1,25	0,84	0,51	0,27	0,10
0,90	1,50	1,05	0,68	0,39	0,18	0,05
1,00	1,00	0,64	0,36	0,16	0,04	0,00

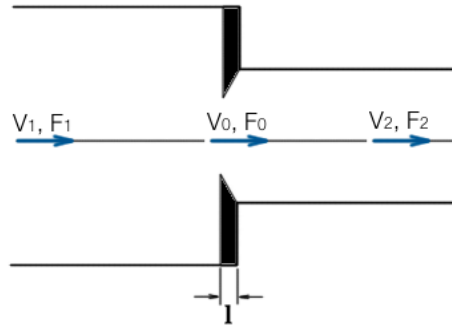


Graph 18: values of ζ with sharp-edged orifice at the passage of the stream from a conduit of one size to another - $Re > 10^5$

Sharp-Edged ($l/D_h = 0 \div 0,015$) orifice at the passage of the stream from a conduit to one size to another, $Re < 3,5 \times 10^5$

$$\zeta = \frac{\Delta H}{\frac{V_0^2}{2g}} \cong \left(\frac{1}{\varphi^2} - 1 \right) + \frac{0,342}{(\varepsilon_0^{Re})^2} \left(1 + 0,707 \sqrt{1 - \frac{F_0}{F_1} - \frac{F_0}{F_2}} \right)^2 = \zeta_\varphi + \varepsilon_0^{Re} \left(\zeta_0 - \frac{F_0}{F_2} \right)^2$$

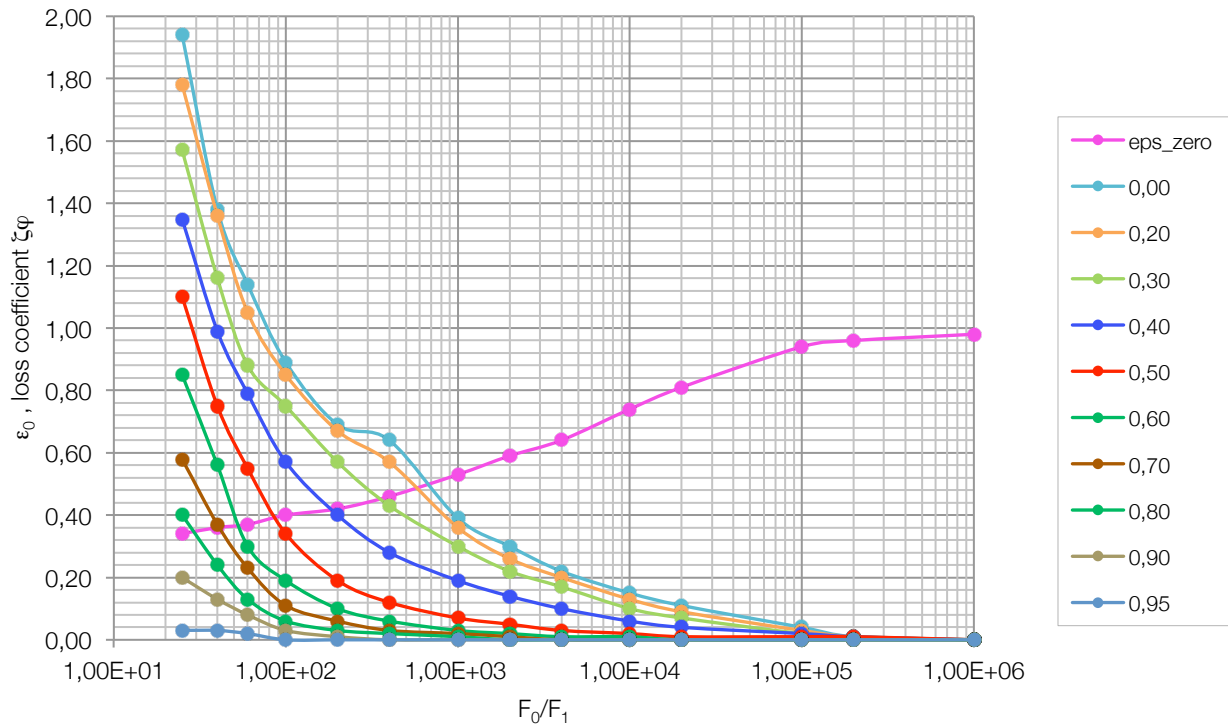
Where ζ_φ and ε_0^{Re} are determined on Graph 19; ζ_0 is determined on Graph 20;



$D_h = 4F_0/\Pi_0$; Π_0 is the perimeter;

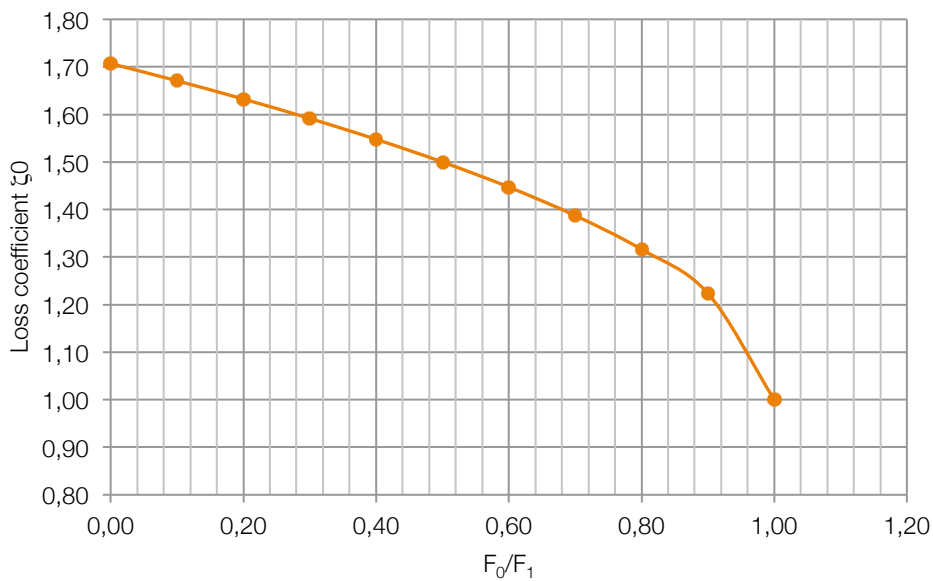
Re	ε_0^{Re}	F_0/F_1									
		0,00	0,20	0,30	0,40	0,50	0,60	0,70	0,80	0,90	0,95
2,50E+01	0,34	1,94	1,78	1,57	1,35	1,10	0,85	0,58	0,40	0,20	0,03
4,00E+01	0,36	1,38	1,36	1,16	0,99	0,75	0,56	0,37	0,24	0,13	0,03
6,00E+01	0,37	1,14	1,05	0,88	0,79	0,55	0,30	0,23	0,13	0,08	0,02
1,00E+02	0,40	0,89	0,85	0,75	0,57	0,34	0,19	0,11	0,06	0,03	0,00
2,00E+02	0,42	0,69	0,67	0,57	0,40	0,19	0,10	0,06	0,03	0,01	0,00
4,00E+02	0,46	0,64	0,57	0,43	0,28	0,12	0,06	0,03	0,02	0,00	0,00
1,00E+03	0,53	0,39	0,36	0,30	0,19	0,07	0,03	0,02	0,01	0,00	0,00
2,00E+03	0,59	0,30	0,26	0,22	0,14	0,05	0,02	0,01	0,00	0,00	0,00
4,00E+03	0,64	0,22	0,20	0,17	0,10	0,03	0,01	0,00	0,00	0,00	0,00
1,00E+04	0,74	0,15	0,13	0,10	0,06	0,02	0,01	0,00	0,00	0,00	0,00
2,00E+04	0,81	0,11	0,09	0,07	0,04	0,01	0,00	0,00	0,00	0,00	0,00
1,00E+05	0,94	0,04	0,03	0,02	0,02	0,01	0,00	0,00	0,00	0,00	0,00
2,00E+05	0,96	0,01	0,01	0,01	0,01	0,01	0,00	0,00	0,00	0,00	0,00
1,00E+06	0,98	0,00	0,00	0,00	0,00	0,00	0,00	0,00	0,00	0,00	0,00

Loss coefficients ζ_φ and ε_0 for sharp-edged orifice at the passage of the stream from a conduit of one size to another - $Re < 10^5$



Graph 19: values of ε_0 and ζ_φ for sharp-edged orifice at the passage of the stream from a conduit of one size to another - $Re < 10^5$

Loss coefficients ζ_0 for sharp-edged orifice at the passage of the stream from a conduit of one size to another - $Re < 10^5$



F_0/F_1	ζ_0
0,00	1,71
0,10	1,67
0,20	1,63
0,30	1,59
0,40	1,55
0,50	1,50
0,60	1,45
0,70	1,39
0,80	1,32
0,90	1,22
1,00	1,00

Graph 20: values of ζ_0 for sharp-edged orifice at the passage of the stream from a conduit of one size to another - $Re < 10^5$

Thick-Edged ($l/D_h > 0,015$) orifice at the passage of the stream from a conduit to one size to another

$Re > 10^5$

$$\zeta = \frac{\Delta H}{\frac{V_0^2}{2g}} = 0,5 \left(1 - \frac{F_0}{F_1}\right) + \left(1 - \frac{F_0}{F_2}\right)^2 + \tau \sqrt{1 - \frac{F_0}{F_1} \left(1 - \frac{F_0}{F_2}\right)} + \zeta_{fr}$$

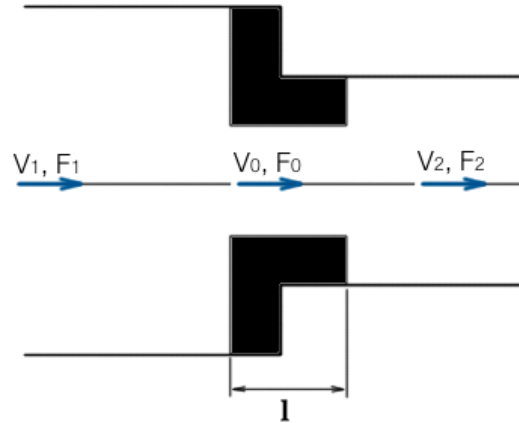
Where $\zeta_{fr} = \lambda \frac{l}{D_h}$, is determined as a function of Re and relative roughness (Moody graph); τ is determined on Graph 21;

$Re < 10^5$

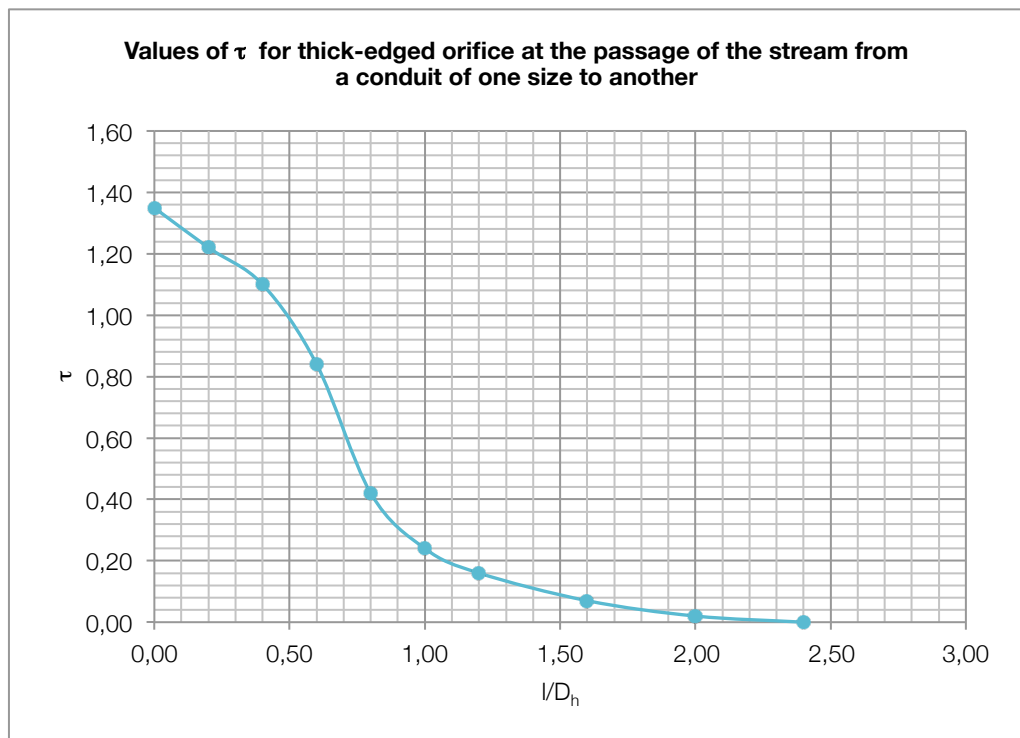
$$\zeta = \frac{\Delta H}{\frac{V_0^2}{2g}} \cong \zeta_\varphi + \overline{\varepsilon_0^{Re}} \left[0,5 \left(1 - \frac{F_0}{F_1}\right) + \left(1 - \frac{F_0}{F_2}\right)^2 + \tau \sqrt{1 - \frac{F_0}{F_1} \left(1 - \frac{F_0}{F_2}\right)} \right]$$

Where ζ_φ and $\overline{\varepsilon_0^{Re}}$ are determined on Graph 19; ζ_0 is determined on Graph 20;

$D_h = 4F_0/\Pi_0$; Π_0 is the perimeter;



l/D_h	τ
0,00	1,35
0,20	1,22
0,40	1,10
0,60	0,84
0,80	0,42
1,00	0,24
1,20	0,16
1,60	0,07
2,00	0,02
2,40	0,00



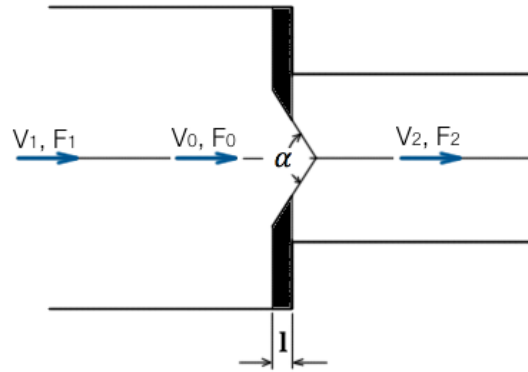
Graph 21: values of τ for thick-edged orifice at the passage of the stream from a conduit of one size to another

Thick-Edged ($l/D_h > 0,015$) orifice with edges beveled or rounded at the passage of a stream from a conduit of one size to another

Orifice with beveled edges

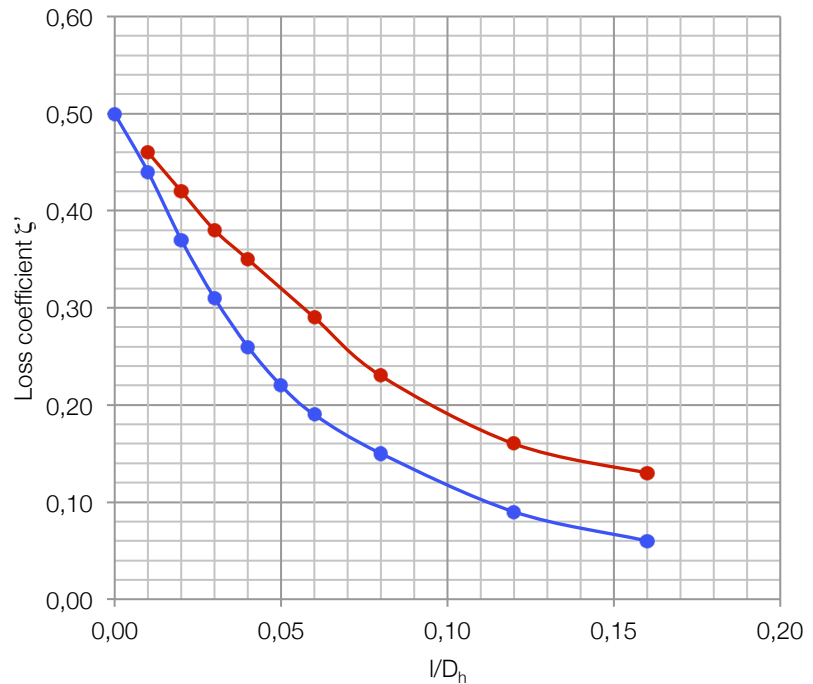
$$\zeta = \frac{\Delta H}{\frac{V_0^2}{2g}} \cong \zeta' \left(1 - \frac{F_0}{F_1}\right) + \left(1 - \frac{F_0}{F_2}\right)^2 + 2 \sqrt{\zeta' \left(1 - \frac{F_0}{F_1}\right) \left(1 - \frac{F_0}{F_2}\right)}$$

Where ζ' is determined on Graph 22;



l/D_h	beveled	l/D_h	rounded
0,01	0,46	0,00	0,50
0,02	0,42	0,01	0,44
0,03	0,38	0,02	0,37
0,04	0,35	0,03	0,31
0,06	0,29	0,04	0,26
0,08	0,23	0,05	0,22
0,12	0,16	0,06	0,19
0,16	0,13	0,08	0,15
		0,12	0,09
		0,16	0,06

Loss coefficients ζ' for thick-edged orifice with orifice beveled or rounded at the passage of the stream from a conduit of one size to another

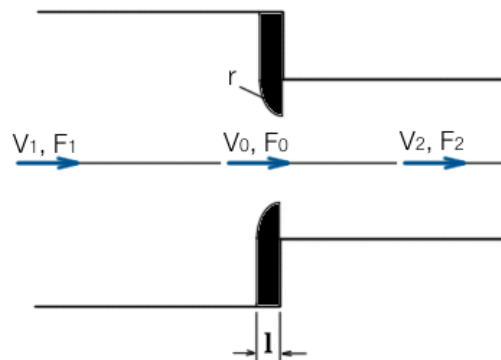


Graph 22: values of ζ' for thick-edged orifice with orifice beveled or rounded at the passage of the stream from a conduit of one size to another

Orifice with rounded edges

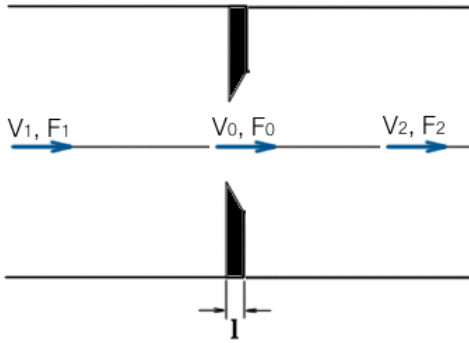
$$\zeta = \frac{\Delta H}{\frac{V_0^2}{2g}} \cong \zeta' \left(1 - \frac{F_0}{F_1}\right) + \left(1 - \frac{F_0}{F_2}\right)^2 + 2 \sqrt{\zeta' \left(1 - \frac{F_0}{F_1}\right) \left(1 - \frac{F_0}{F_2}\right)}$$

Where ζ' is determined on Graph 22;



Sharp-Edged ($l/D_h = 0 \div 0,015$) orifice in a straight conduit

$D_h = 4F_0/\Pi_0$; Π_0 is the perimeter;



$Re > 10^5$

$$\zeta = \frac{\Delta H}{\frac{V_0^2}{2g}} = \left[0,707 \sqrt{1 - \frac{F_0}{F_1} + 1 - \frac{F_0}{F_1}} \right]^2 \left(\frac{F_1}{F_0} \right)^2$$

Where $\zeta_{fr} = \lambda \frac{l}{D_h}$, is determined as a function of Re and relative roughness (Moody graph); τ is determined on Graph 21;

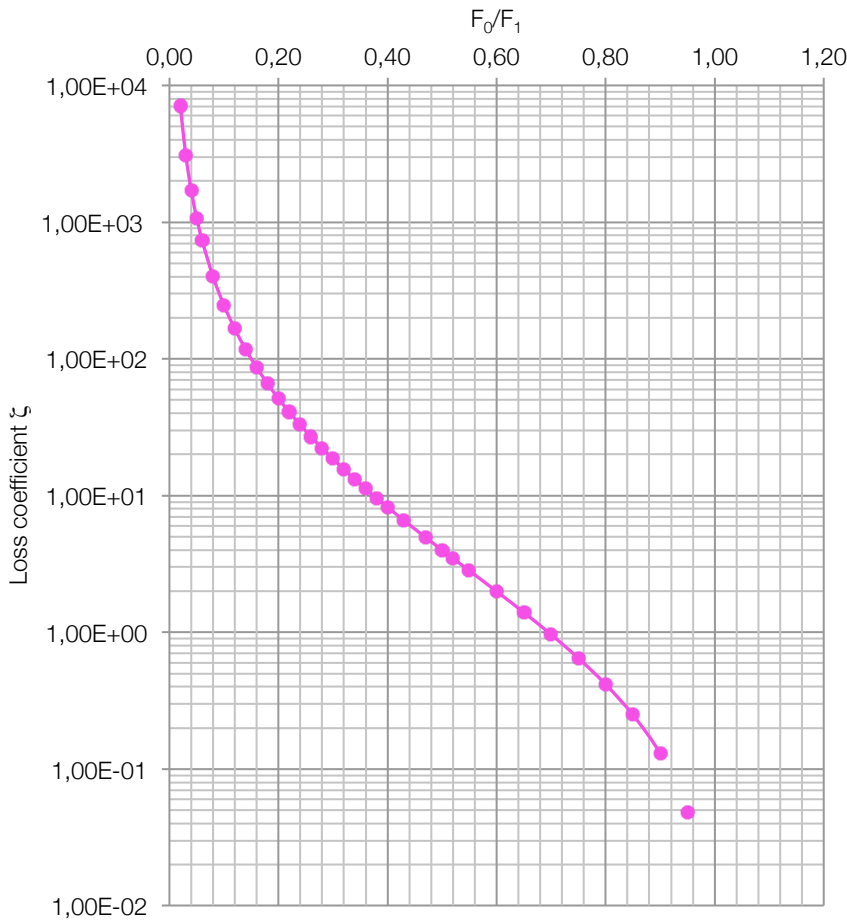
$Re < 10^5$

$$\zeta = \frac{\Delta H}{\frac{V_0^2}{2g}} \cong \left[\left(\frac{1}{\varphi^2} - 1 \right) + \frac{0,342}{(\varepsilon_0^{Re})^2} \left(1 + 0,707 \sqrt{1 - \frac{F_0}{F_1} - \frac{F_0}{F_1}} \right)^2 \right] \left(\frac{F_1}{F_0} \right)^2$$

$$= \left[\zeta_\varphi + \varepsilon_0^{Re} \left(\zeta_0 - \frac{F_0}{F_1} \right)^2 \right] \left(\frac{F_1}{F_0} \right)^2$$

Where ζ_φ and ε_0^{Re} are determined on Graph 19; ζ_0 is determined on Graph 20;

Loss coefficient ζ for sharp edged orifice in straight conduit



Graph 23: values of ζ for sharp edged orifice in straight conduit

F_0/F_1	ζ
0,02	7000,00
0,03	3100,00
0,04	1670,00
0,05	1050,00
0,06	730,00
0,08	400,00
0,12	165,00
0,14	117,00
0,18	65,50
0,22	40,60
0,24	32,00
0,28	22,30
0,32	15,60
0,34	13,10
0,38	9,55
0,40	8,25
0,50	4,00
0,55	2,85
0,60	2,00
0,70	0,97
0,75	0,65
0,80	0,42
0,85	0,25
0,90	0,13
0,95	0,05
1,00	0,00

Thick-Edged ($l/D_h > 0,015$) orifice in a straight conduit

$Re > 10^5$

$$\zeta = \frac{\Delta H}{\frac{V_0^2}{2g}} = \left[\left(0,5 + \tau \sqrt{1 - \frac{F_0}{F_1}} \right) \left(1 - \frac{F_0}{F_1} \right) + \left(1 - \frac{F_0}{F_1} \right)^2 + \zeta_{fr} \right]^2 \left(\frac{F_1}{F_0} \right)^2$$

Where $\zeta_{fr} = \lambda \frac{l}{D_h}$, is determined as a function of Re and relative roughness (Moody graph); τ is determined on Graph 21;

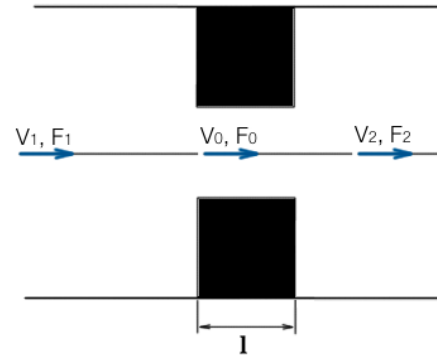
ζ is determined for $\lambda = 0,02$ on Graph 24;

$Re < 10^5$

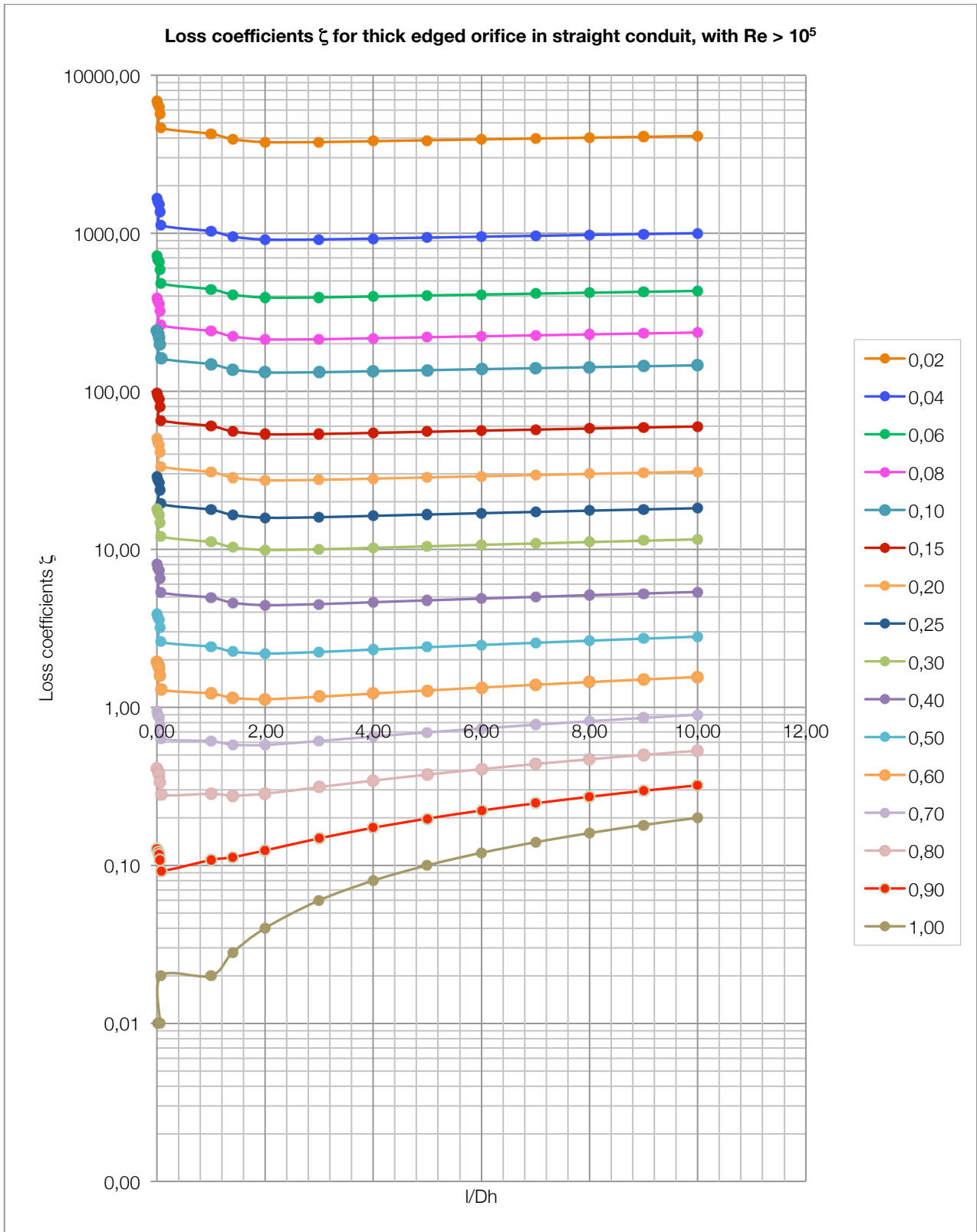
$$\zeta = \frac{\Delta H}{\frac{V_0^2}{2g}} \cong \left\{ \zeta_\varphi + \overline{\varepsilon_0^{Re}} \left[\left(0,5 + \tau \sqrt{1 - \frac{F_0}{F_1}} \right) \left(1 - \frac{F_0}{F_1} \right) + \left(1 - \frac{F_0}{F_2} \right)^2 \right] + \zeta_{fr} \right\} \left(\frac{F_1}{F_0} \right)^2$$

Where ζ_φ and $\overline{\varepsilon_0^{Re}}$ are determined on Graph 19;
 ζ_0 is determined on Graph 20;

$D_h = 4F_0/\Pi_0$; Π_0 is the perimeter;



		F_0/F_1															
l/D_h	τ	0,02	0,04	0,06	0,08	0,10	0,15	0,20	0,25	0,30	0,40	0,50	0,60	0,70	0,80	0,90	1,00
0,00	1,35	6900	1669	717,7	390,2	241,2	98,02	50,15	29,03	18,12	8,05	3,91	1,95	0,94	0,41	0,13	0,00
0,02	1,22	6586	1593	684,9	372,4	230,2	93,51	47,83	27,69	17,28	7,67	3,73	1,86	0,90	0,39	0,12	0,01
0,04	1,10	6296	1523	654,6	355,9	220,0	89,35	45,70	26,44	16,50	7,33	3,56	1,78	0,86	0,37	0,12	0,01
0,06	0,84	5666	1370	588,9	320,1	197,8	80,31	41,06	23,75	14,81	6,57	3,19	1,59	0,77	0,34	0,11	0,01
0,08	0,42	4649	1123	482,7	262,2	162,0	65,70	33,55	19,39	12,08	5,35	2,60	1,30	0,63	0,28	0,09	0,02
1,00	0,24	4258	1029	442,3	240,3	148,4	60,25	30,79	17,81	11,12	4,95	2,42	1,22	0,61	0,28	0,11	0,02
1,40	0,10	3939	952	409,0	222,2	137,3	55,73	28,49	16,49	10,30	4,59	2,25	1,15	0,58	0,28	0,11	0,03
2,00	0,02	3775	912	392,1	213,1	131,7	53,47	27,36	15,85	9,91	4,43	2,19	1,13	0,58	0,28	0,12	0,04
3,00	0,00	3776	913	392,6	213,5	132,0	53,67	27,50	15,96	10,00	4,50	2,24	1,17	0,61	0,31	0,15	0,06
4,00	0,00	3826	926	398,2	216,6	134,0	54,56	28,00	16,28	10,22	4,63	2,32	1,22	0,65	0,34	0,17	0,08
5,00	0,00	3876	938	403,7	219,7	136,0	55,44	28,50	16,60	10,44	4,75	2,40	1,28	0,69	0,38	0,20	0,10
6,00	0,00	3926	951	409,3	222,8	138,0	56,33	29,00	16,92	10,67	4,88	2,48	1,33	0,73	0,41	0,22	0,12
7,00	0,00	3976	963	414,8	226,0	140,0	57,22	29,50	17,24	10,89	5,00	2,56	1,39	0,78	0,44	0,25	0,14
8,00	0,00	4026	976	420,4	229,1	142,0	58,11	30,00	17,56	11,11	5,13	2,64	1,44	0,82	0,47	0,27	0,16
9,00	0,00	4076	988	426,0	232,2	144,0	59,00	30,50	17,88	11,33	5,25	2,72	1,50	0,86	0,50	0,30	0,18
10,00	0,00	4126	1001	431,5	235,3	146,0	59,89	31,00	18,20	11,56	5,38	2,80	1,56	0,90	0,53	0,32	0,20

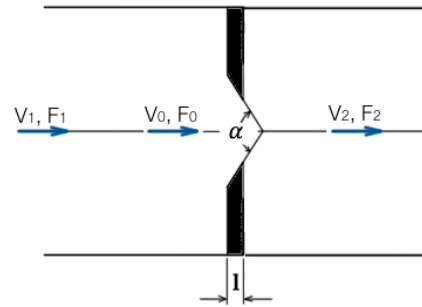


Graph 24: values of ζ for thick edged orifice in straight conduit, with $Re > 10^5$

Orifice with edges beveled facing the stream flow ($\alpha = 40-60$) in a straight pipe, $Re > 10^4$

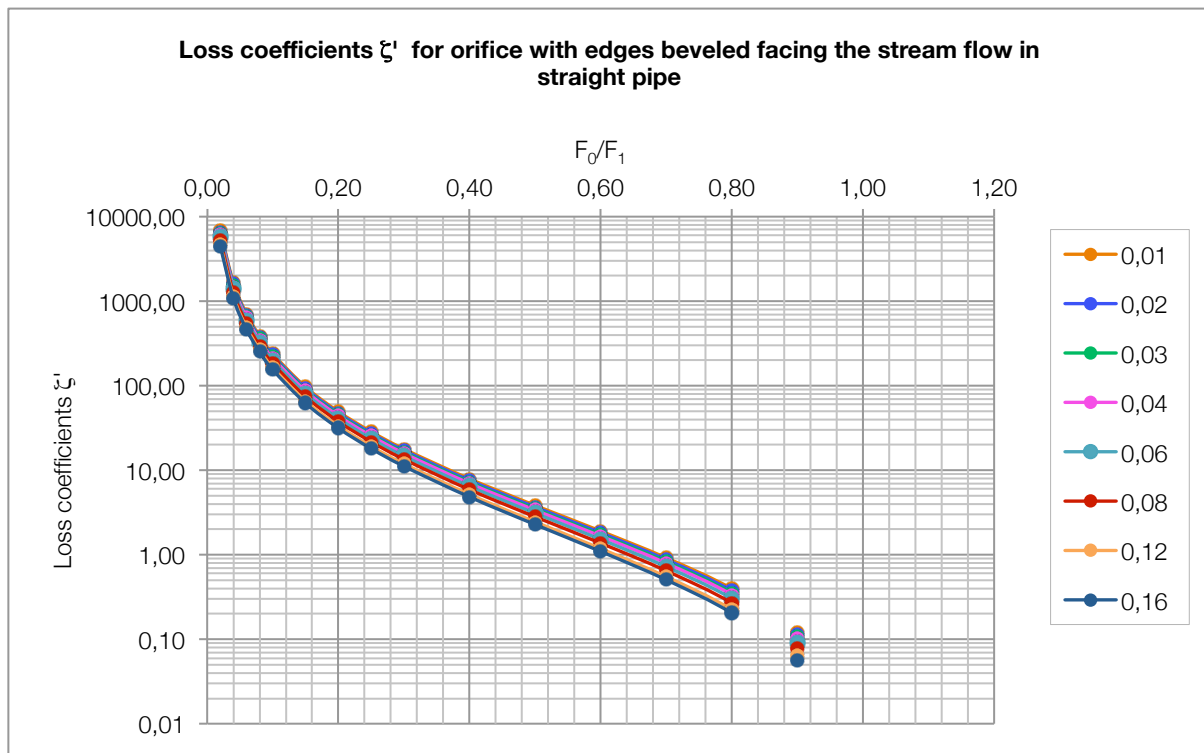
$$\zeta = \frac{\Delta H}{\frac{V_0^2}{2g}} = \left[1 + \sqrt{\zeta' \left(1 - \frac{F_0}{F_1}\right) - \frac{F_0}{F_1}} \right]^2 \left(\frac{F_1}{F_0}\right)^2$$

Where ζ' can be found in Graph 22;
 ζ is determined by Graph 25;



$$D_h = 4F_0/\Pi_0; \Pi_0 \text{ is the perimeter;}$$

l/D _h	ζ'	F ₀ /F ₁															
		0,02	0,04	0,06	0,08	0,10	0,15	0,20	0,25	0,30	0,40	0,50	0,60	0,70	0,80	0,90	1,00
0,01	0,46	6817	1649	709	385	238,2	96,73	49,47	28,62	17,85	7,92	3,84	1,91	0,92	0,40	0,12	0,00
0,02	0,42	6573	1589	683	371	229,4	93,12	47,59	27,51	17,15	7,59	3,67	1,82	0,88	0,37	0,11	0,00
0,03	0,38	6322	1528	657	357	220,4	89,41	45,65	26,37	16,42	7,26	3,50	1,73	0,83	0,35	0,11	0,00
0,04	0,35	6128	1481	636	345	213,5	86,54	44,17	25,50	15,87	7,00	3,37	1,66	0,79	0,34	0,10	0,00
0,06	0,29	5724	1383	593	322	199,0	80,58	41,07	23,67	14,71	6,47	3,10	1,52	0,72	0,30	0,09	0,00
0,08	0,23	5291	1278	548	298	183,6	74,21	37,76	21,73	13,47	5,90	2,82	1,37	0,65	0,27	0,08	0,00
0,12	0,16	4733	1142	489	266	163,7	66,02	33,51	19,23	11,89	5,17	2,45	1,18	0,55	0,22	0,06	0,00
0,16	0,13	4468	1078	461	250	154,2	62,14	31,50	18,05	11,15	4,83	2,28	1,10	0,51	0,20	0,06	0,00

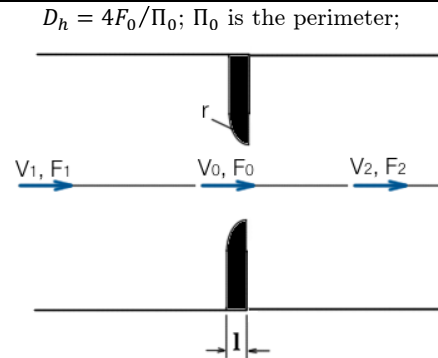


Graph 25: values of ζ for orifice with edges beveled facing the stream flow in straight pipe

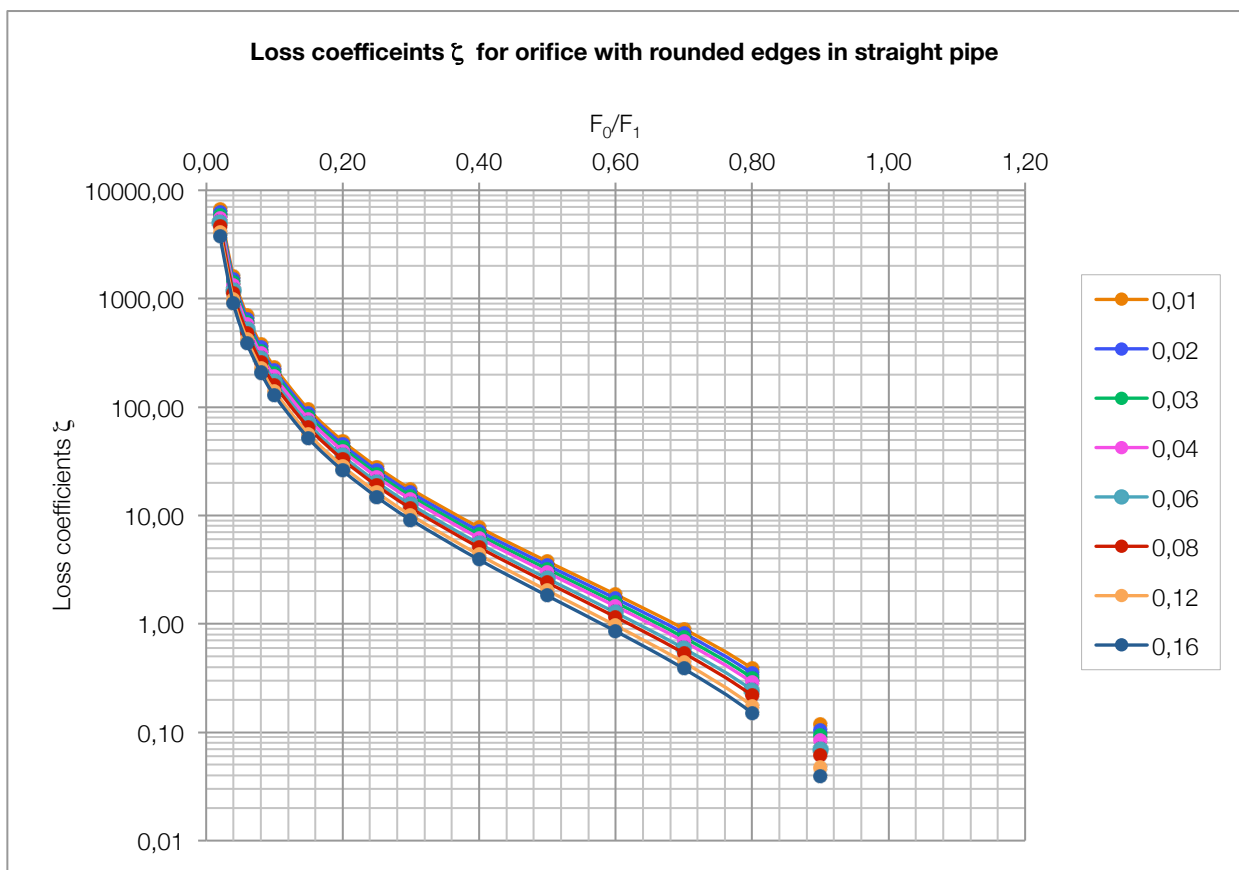
Orifice with rounded edges in a straight pipe, $Re > 10^4$

$$\zeta = \frac{\Delta H}{\frac{V_0^2}{2g}} = \left[1 + \sqrt{\zeta' \left(1 - \frac{F_0}{F_1} \right) - \frac{F_0}{F_1}} \right]^2 \left(\frac{F_1}{F_0} \right)^2$$

Where ζ' can be found in Graph 22;
 ζ is determined by Graph 26;



r/D_h	ζ'	F_0/F_1															
		0,02	0,04	0,06	0,08	0,10	0,15	0,20	0,25	0,30	0,40	0,50	0,60	0,70	0,80	0,90	1,00
0,01	0,44	6696	1619	696	378	233,8	94,94	48,53	28,07	17,50	7,75	3,76	1,87	0,90	0,39	0,12	0,00
0,02	0,37	6258	1513	650	353	218,1	88,46	45,16	26,08	16,24	7,17	3,46	1,71	0,82	0,35	0,11	0,00
0,03	0,31	5861	1416	608	330	203,9	82,61	42,12	24,29	15,10	6,65	3,19	1,57	0,75	0,31	0,09	0,00
0,04	0,26	5511	1331	571	310	191,4	77,45	39,44	22,72	14,10	6,19	2,96	1,45	0,68	0,29	0,08	0,00
0,06	0,19	4980	1202	515	279	172,5	69,65	35,39	20,34	12,60	5,49	2,61	1,27	0,59	0,24	0,07	0,00
0,08	0,15	4647	1121	480	260	160,6	64,76	32,86	18,85	11,65	5,06	2,40	1,16	0,54	0,22	0,06	0,00
0,12	0,09	4076	982	420	227	140,3	56,41	28,53	16,32	10,05	4,33	2,03	0,97	0,44	0,17	0,05	0,00
0,16	0,06	3736	900	385	208	128,2	51,44	25,96	14,81	9,10	3,90	1,81	0,86	0,38	0,15	0,04	0,00

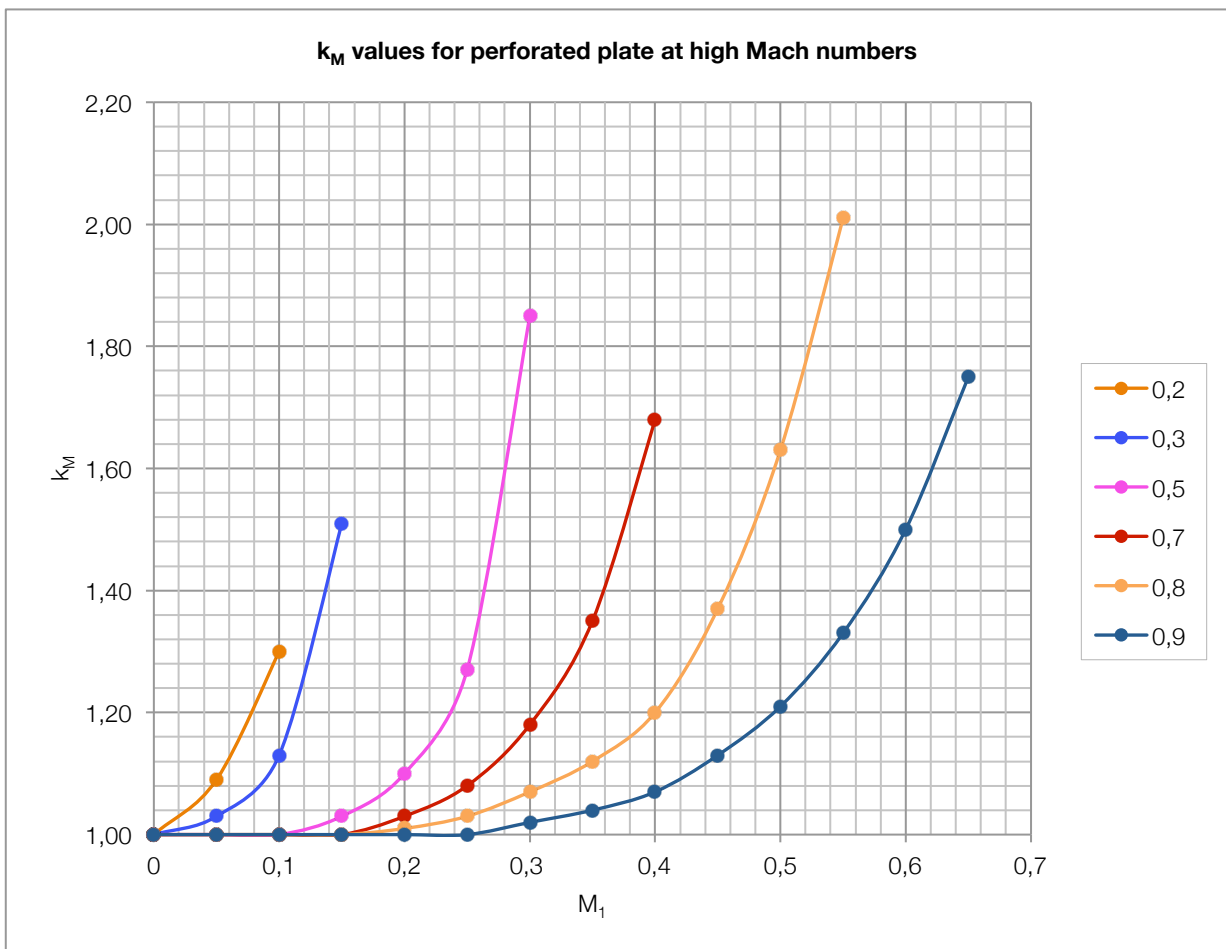


Graph 26: values of ζ for orifice with rounded edges in straight pipe

Perforated plate at high Mach numbers

Sharp-edged orifices	$\zeta_M = k_M \zeta$ <p>Where ζ is determined as in the previous cases, for sharp-edged orifices; k_M is determined from Graph 27; $M_1 = \frac{v_1}{a}$ where a is velocity of sound</p>
Orifice edges beveled or rounded	$\zeta_M = k'_M \zeta$ <p>Where ζ is determined as in the previous cases, for sharp-edged orifices; k'_M is determined from grid chapter</p>

f	M ₁													
	0	0,05	0,1	0,15	0,2	0,25	0,3	0,35	0,4	0,45	0,5	0,55	0,6	0,65
0,2	1,00	1,09	1,30	-	-	-	-	-	-	-	-	-	-	-
0,3	1,00	1,03	1,13	1,51	-	-	-	-	-	-	-	-	-	-
0,5	1,00	1,00	1,00	1,03	1,10	1,27	1,85	-	-	-	-	-	-	-
0,7	1,00	1,00	1,00	1,00	1,03	1,08	1,18	1,35	1,68	-	-	-	-	-
0,8	1,00	1,00	1,00	1,00	1,01	1,03	1,07	1,12	1,20	1,37	1,63	2,01	-	-
0,9	1,00	1,00	1,00	1,00	1,00	1,00	1,02	1,04	1,07	1,13	1,21	1,33	1,50	1,75



Graph 27: values of k_M for perforated plate at high Mach numbers

9 Diffusers

List of chapter symbols

Latin characters:

- a_0, b_0 = sides of the rectangular narrow section of a rectangular diffuser [m];
- a_1, b_1 = sides of the rectangular wide section of a rectangular diffuser [m];
- D_0 = diameter of the narrow section of a diffuser [m];
- D_1 = diameter of the narrow section of a diffuser [m];
- D_h = hydraulic diameter of the narrow section of a diffuser [m];
- F_0 = cross-section area of the narrow section of the diffuser [m²];
- F_1 = cross-section area of the wide section of the diffuser [m²];
- F_2 = cross-section area of the widest section of the multistage diffuser [m²];
- F_{sep} = cross-section area in which begins the separation of the path from the walls [m²];
- k_1 = coefficient which allow for the boundary condions;
- k_2 = coefficient which allow for the cross-section shape;
- k_3 = coefficient which allow for the shape of generatrix;
- l_d = diffuser length [m];
- n = total area ratio of the multistage diffuser, defined as the ratio between F_2 and F_0 ;
- n_1 = area ratio of the diffuser, defined as the ratio between F_1 and F_0 ;
- n_2 = area ratio of the sudden enalrgement of a multistage diffuser, defined as the ratio between F_2 and F_1 ;
- V_0, V_1 = mean stream velocity in the narrow and wide sections of the diffuser, respectively [m/s];
- V_{max} = maximum stream velocity over the cross section [m/s];
- z = number of dividing walls;

Greek characters:

- α = divergence angle in the vertical plane for pyramidal diffuser [°];
- β = divergence angle in the horizontal plane for pyramidal diffuser [°];
- ΔH_{dif} = total head loss of the diffuser [m];
- ΔH_{exp} = local head loss of the diffuser [m];
- ΔH_{fr} = friction head loss occurring in the diffuser [m];

- $\Delta\zeta_{fr}$ = friction loss coefficient associated to the angle α for pyramidal diffusers;
- $\Delta\zeta'_{fr}$ = friction loss coefficient associated to the angle β for pyramidal diffusers;
- ζ_{dif} = total head loss coefficient for the diffusers;
- ζ_{exp} = local head loss coefficient;
- ζ_{fr} = friction loss coefficient;
- θ = central angle of divergence of a diffuser of arbitrary shape [$^{\circ}$];
- φ_0 = coefficient depending on the relative length $\frac{l_d}{D_h}$ of the curved diffuser;
- φ_d = total coefficient of shock allowing for the total losses in the diffuser;
- φ_{exp} = coefficient of shock allowing for the local losses due to the diffuser enlargement only;
- Π_0 = perimeter of the narrow section of a diffuser [m];
- σ = corrective factor;

9.1 Introduction

A diffuser is a gradually widening passage to make the transition from a narrow conduit to a wide one, with minimum head losses. In such a divergent pipe the intensity of turbulence is greater both than in the straight pipe and in the converging components, and the local friction are also greater. The increase in the pipe section is accompanied by a drop in the mean stream velocity.

Therefore, the total resistance coefficient of the diffuser, expressed in terms of the velocity in the initial section, is less for divergence angles below a certain value, than for the equivalent length of a constant-section pipe, whose area is equal to the initial section of the diffuser. An increase of the divergence angle beyond this limit leads to a considerable increase in the resistance coefficient, so that it finally becomes much larger than for the equivalent length of straight pipe.

In Figure 1 are represented the principal section's type of conical diffusers used in hydraulic commerce.

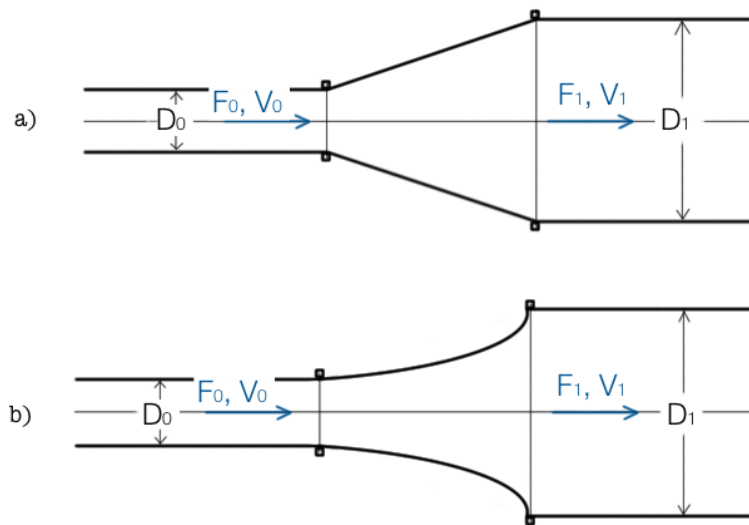


Figure 1: diffuser's geometrical schematic shape

From the historical point of view, there's so much material and a lot of experience that treated the diffusers' topic. One of the most important of these experiences was the Gibson's one.

The experiences of English scientist Gibson, show perfectly how the detachment of the fluid vein occurs in the initial section of the diffusers type a), while in the diffuser type b) it occurs in downstream sections from the initial one, after a considerable slowdown of the flow.

Gibson, through a lot of experiments, first varying the type of diffuser, than keeping constant the initial and the final diameters, and in the end varying the convergence angle, pointed out that the local head losses in the diffusers was very similar to Borda's one. And so it can be written as:

$$\Delta H = \zeta \frac{(V_1 - V_2)^2}{2g}$$

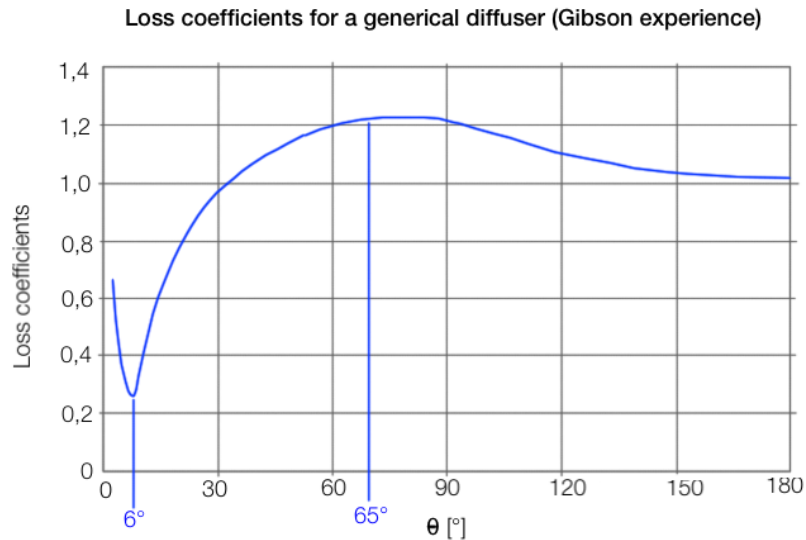
Where ζ is the loss coefficient which varies with the divergence angle. Moreover, Gibson pointed out that the coefficient ζ assumes minimum value when the angle is $\theta = 6^\circ$, and the maximum value for $\theta = 65^\circ$. In this last case, for $\theta = 6$ the coefficient value is $\zeta = 1,2$, and so a value 20% higher than the Borda's one for the abrupt enlargement.

The result, apparently no-sense, is explainable because Gibson didn't purify the head loss value pointed out from the head loss grown in the trunk pipe corresponding to the diffuser, because of the friction.

The fact that the maximum value of ζ occurs for $\alpha = 65^\circ$, means that from this value, the friction head losses decrease faster than the local head losses increases: therefore the overall head losses decreases.

When θ decreases, instead, the continue friction losses will increase, because of the increment of the length of the stretch pipe of the diffuser: when $\theta \rightarrow 0^\circ$ the length of the diffuser tends to infinite. This is why we've the minimum of ζ for $\theta = 6^\circ$.

From the graphical point of view, calling θ the divergence angle, F_0 the inlet area, the F_1 the outlet area and fixing their ratio, we can represent the chart this can be represented as in the Graph 1.



Graph 1: performance chart resulting from Gibson experience

The Gibson experience pointed out a lot of key points of the diffusers' head losses: the comparison between diffusers and abrupt expansions, the dependence of the head losses from the divergence angle, the possibility to distinguish between losses caused by friction and losses due to abrupt expansion, the turbulence caused by the detachment of the fluid vein in the first section of the diffuser.

The increase of the resistance coefficient of a diffuser with the increase of its divergence angle, is mainly a result of the separation of the boundary layer from the diffuser walls, and of intensification of the stream turbulence with the resulting formation of turbulence in the entire stream.

The separation of the boundary layer from the walls is due to a positive pressure gradient existing in the diffuser as a result of the velocity drop which accompanies the increase in cross section (Bernoulli equation).

The beginning of stream separation in a plane diffuser: can be approximately determined from the following relation, proposed by Levin:

$$\frac{F_{sep}}{F_0} = \frac{1}{1 - \frac{1,95}{\theta^{4/5} \sqrt[5]{Re}}}$$

Where F_{sep} is the area of the section in which the stream separation starts.

Other experiments, like the Escande ones, had pointed out that the separation of the fluid vein from the duct wall, with the resulting formation of turbulence, contributes directly to the local head loss: using small holes in the duct and creating a depression over them, Escande sucked the small vortices, obtaining that the detachment of the flow vein and the concentrated head loss were decreased. The experience of Escande underlines another important point: the reduction of the eddies, caused by the turbulence, is a key point in the head losses and the possibility to reduce them can be

achievable by different technological improvements in diffusers' manufacturing. In fact, technologic innovation brought to the continuous development of various types of diffusers, for trying to keep small concentrated head losses and for practical/economic necessities.

9.1.1 Head loss coefficients

The head loss coefficient ζ of a diffuser is a function of several parameters:

1. The divergence angle θ ;
2. The area ratio $n_1 = \frac{F_1}{F_0}$ where F_1 is the outlet area and F_0 is the inlet area;
3. The cross-section shape, characterized by the coefficient k_2 ;
4. The shape of the generatrix, characterized by the coefficient k_3 ;
5. The inlet conditions in terms of the state of boundary layer (the velocity distribution), characterized by the coefficient k_1 ;
6. The regime of flow (value of Re)
7. The Mach number M

$$\zeta = \frac{\Delta H}{\frac{V_0^2}{2g}} = f(Re, M, \theta, n_1, k_1, k_2, k_3)$$

In practice an arbitrary method of loss separation is used. This is due to the scarcity of available data on the dependence of diffuser resistance on these parameters, and particularly on the Reynolds number. With this method, the total head loss of the diffuser ΔH_{dif} is considered as the sum of the local resistance ΔH_{exp} , due to the stream expansion, and the frictional resistance ΔH_{fr} . The total head loss coefficient ζ_{dif} is correspondingly considered as the sum of the local head loss coefficient ζ_{exp} and the friction coefficient ζ_{fr} .

$$\zeta_{dif} = \frac{\Delta H}{\frac{V_0^2}{2g}} = \zeta_{exp} + \zeta_{fr}$$

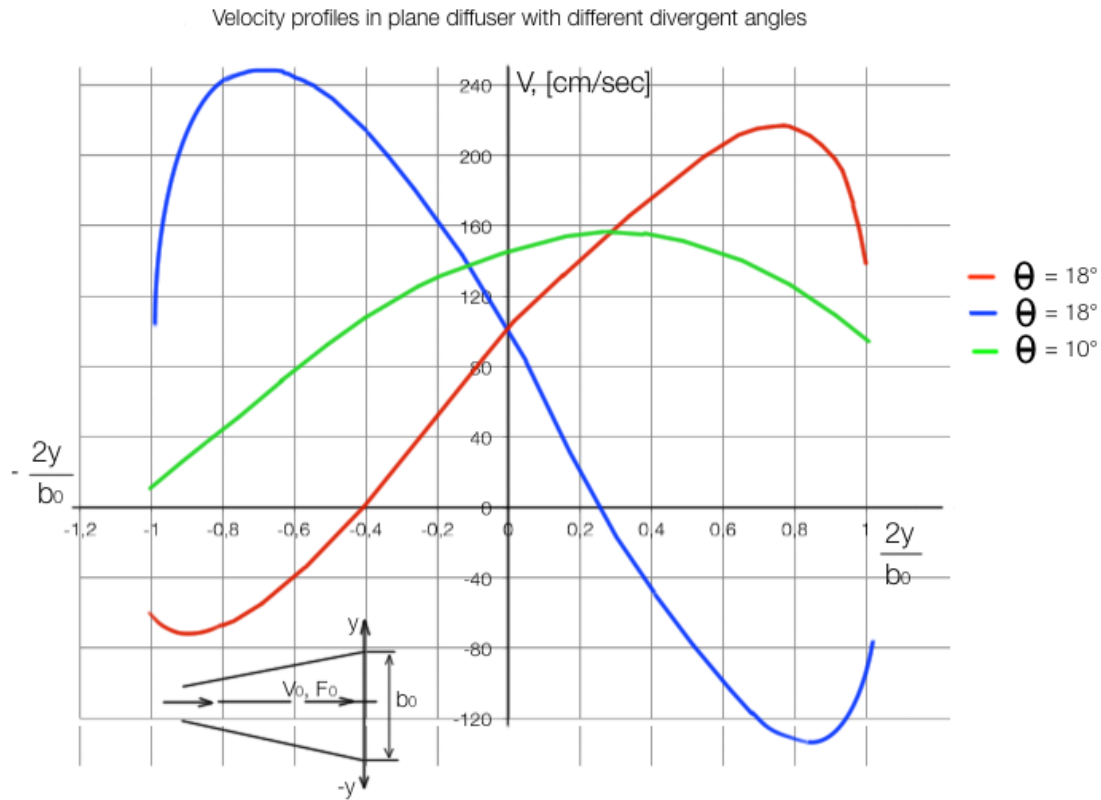
Making this distinction, we can consider the influence of the Re number only applied on the friction coefficient ζ_{fr} , while ζ_{exp} is practically independent of Re .

9.1.2 Velocity profiles

The velocities over the cross section in narrow-angle diffusers with non-separating boundary layers are distributed symmetrically about the longitudinal axis (Graph 2).

The separation in wide-angle diffusers (up to $\theta = 50^\circ - 60^\circ$) generally starts from only one of the walls, in particular from the wall where the velocity is lowest. With the

beginning of stream separation from one of the walls, the pressure increase through the diffuser is interrupted or reduced, and as a result there will be no stream separation from the opposite wall. Consequently, the distribution of velocities over the diffuser section will be asymmetric.



Graph 2: velocity profiles in plane diffusers with different divergence angles

9.1.3 Shock coefficient

It is convenient to express the expansion losses by the coefficient of shock, defined as the ratio of expansion losses in a smooth diffuser to the theoretical losses at shock, in the case of sudden expansion of the cross section ($\theta = 180^\circ$):

$$\varphi_{exp} = \frac{\Delta H}{\frac{1}{2g}(V_0 - V_1)^2}$$

In the case of uniform velocity distribution at the inlet ($k_1 = 1,0$) the coefficient of shock of diffusers with divergence angles ($\theta = 0^\circ - 40^\circ$) can be calculated by the following expression (approximate):

$$\varphi_{exp} = k_2 \tan \frac{\theta}{2} \left(\tan \frac{\theta}{2} \right)^{\frac{1}{4}}$$

Where θ is the general divergence angle (in the case of a pyramidal diffuser with unequal divergence angles in the two planes, θ is the larger angle).

The value of φ_{exp} for the entire range of θ from 0 to 180 degrees is determined from the curves in Graph 6, Graph 8 and Graph 10.

The coefficient of local resistance of expansion is expressed through the coefficient of shock as follows:

$$\zeta_{exp} = \frac{\Delta H}{\frac{V_0^2}{2g}} = \varphi_{exp} \left(1 - \frac{1}{n_1} \right)^2 = k_2 \tan \frac{\theta}{2} \left(\tan \frac{\theta}{2} \right)^{\frac{1}{4}} \left(1 - \frac{1}{n_1} \right)^2$$

9.1.4 Cross-section shape

The following value of k_2 is used for conical and plane diffusers:

$$k_2 \approx 3,2$$

The following value is tentatively used for more accurate experimental data for pyramidal diffusers with expansion in two planes:

$$k_2 \approx 4,0$$

9.1.5 Friction coefficient

The friction coefficient of a diffuser of circular or rectangular section, with equal divergence angles in the two planes, is calculated by the formula:

$$\zeta_{fr} = \frac{\Delta H}{\frac{V_0^2}{2g}} = \frac{\lambda}{8 \sin \frac{\theta}{2}} \left(1 - \frac{1}{n_1^2} \right)$$

Where λ is the friction coefficient of unit length of the diffuser, determined from the corresponding graphs as a function of the Reynolds number and the relative roughness (theoretical framework).

The friction coefficient of a pyramidal diffuser with unequal divergence angles in the two planes ($\alpha \neq \beta$) is calculated by the following formula:

$$\zeta_{fr} = \frac{\Delta H}{\frac{V_0^2}{2g}} = \frac{\lambda}{16 \sin \frac{\alpha}{2}} \left(1 - \frac{1}{n_1^2}\right) + \frac{\lambda}{16 \sin \frac{\beta}{2}} \left(1 - \frac{1}{n_1^2}\right) = \Delta\zeta_{fr} + \Delta\zeta'_{fr}$$

The friction coefficient of a plane diffuser with inlet-section sides a_0 and b_0 , where b_0 is constant along diffuser, is calculated by:

$$\zeta_{fr} = \frac{\Delta H}{\frac{V_0^2}{2g}} = \frac{\lambda}{4} \left[\frac{a_0}{b_0 \tan \frac{\theta}{2}} \left(1 - \frac{1}{n_1^2}\right) + \frac{1}{2 \sin \frac{\theta}{2}} \left(1 - \frac{1}{n_1^2}\right) \right]$$

This formula can be simplified to be used in practice:

$$\zeta_{fr} = \frac{\lambda}{4} \left[\frac{a_0}{b_0 \tan \frac{\theta}{2}} \left(1 - \frac{1}{n_1^2}\right) + 0,5 \left(1 - \frac{1}{n_1^2}\right) \right]$$

9.1.6 Interaction circular-to-rectangular

The head loss coefficients of diffusers where the rectangular section changes to circular or vice versa, can be determined from the data for pyramidal diffusers with equivalent divergence angles. The equivalent angle θ_e is determined on the basis of the following formulae:

- Transition from circle to rectangle:

$$\tan \frac{\theta_e}{2} = \frac{2\sqrt{\frac{a_1 b_1}{\pi}} - D_0}{2l_d}$$

- Transition from rectangle to circle:

$$\tan \frac{\theta_e}{2} = \frac{D_1 - 2\sqrt{\frac{a_0 b_0}{\pi}}}{2l_d}$$

9.1.7 Non-uniform velocity at inlet section

In the case of a non-uniform velocity distribution at inlet section, i.e., at $k_1 > 1,0$, as when the diffuser is placed behind a long straight stretch or any other fitting, behind a throttle, etc., the coefficient of local resistance due to expansion in the diffuser is determined by the formula:

$$\zeta_{exp} = k_1 \zeta'_{exp}$$

Where ζ'_{exp} is determined as ζ_{exp} of a diffuser with uniform velocity distribution at the inlet.

k_1 is determined as a function of the velocity profile at the inlet of the diffuser and of its divergence angle.

At the inlet, the dependence of the diffuser head loss coefficients on the state of the boundary layer, (the velocity distribution) is complex.

In narrow-angle diffusers a non-uniform symmetric velocity profile with a maximum at the center and minimum at the walls leads to a decrease of the total resistance, since the frictional stress at the walls is decreased. At the same time this velocity profile increases the possibility of stream separation and displaces the point of separation toward the initial section of the diffuser, so that with the subsequent increase of the divergence angle the resistance will increase compared with resistance at a uniform velocity distribution.

In a non-uniform velocity profile, with lower velocities at the center and higher ones at the walls, the opposite will be observed; the total resistance of the diffuser being higher: at small divergence angles and lower at larger ones.

The dependence of the coefficient k_1 on the divergence angle for a symmetric velocity profile at the inlet has been plotted in Graph 3 for different values of the ratio of the maximum to the mean velocities $\frac{V_{max}}{V}$ over the section. The dependence of the ratio $\frac{V_{max}}{V}$ on the relative length $\frac{l}{D_h}$ of the initial straight stretch has likewise been plotted in the same graph for different values of Re.

In the case of a non-symmetric velocity profile, which exists behind various fittings, throttles, etc., limited use can be made of the values of k_1 .

9.1.8 Considerations on shock coefficient

Up to $\theta = 40^\circ$ to 50° , the shock coefficient φ_{exp} is smaller than unity. This shows that losses in a diffuser are smaller than shock losses in the case of sudden expansion ($\theta = 180^\circ$).

At divergence angle $50^\circ \leq \theta \leq 90^\circ$ the value of φ_{exp} becomes larger than unity, i.e., losses in a diffuser increase slightly compared with losses at shock. Starting with $\theta = 90^\circ$, and up to $\theta = 180^\circ$, the value of φ_{exp} again drops and approaches unity, indicating that the losses in the diffuser approach to the losses at sudden expansion.

If, therefore, a uniform velocity distribution at the diffuser exit is not required, it will be inexpedient to use diffusers with convergence angle $\theta > 40^\circ$ to 50° . If a very short

transition stretch is required by design considerations, this can be achieved by means of sudden expansion ($\theta = 180^\circ$).

If it is required to obtain a uniform velocity profile behind the transition stretch and if this purpose is to be achieved by means of baffles, dividing walls, or grids, then any diffuser, even with a large divergence angle ($\theta > 50^\circ$), is to be preferred to sudden expansion ($\theta = 180^\circ$).

9.1.9 Optimum angle of divergence θ_{opt}

Since the smooth increase of a pipe section with narrow divergence angles leads to a decrease in the head losses compared with those in a pipe of constant section, and at wide divergence angles to the increase of these losses, there must obviously exist an optimum divergence angle at which minimum losses are obtained. This angle can be calculated for the case of a straight diffuser of circular section by:

$$\theta_{opt} = 0,43 \left(\frac{\lambda}{k_1} \cdot \frac{n_1 + 1}{n_1 - 1} \right)^{\frac{4}{9}}$$

Thus, at $\lambda = 0,015$, $n_1 = 2,25$ and $k_1 = 1,0$ one obtains $\alpha_{opt} = 6^\circ$. For a diffuser of rectangular section, θ_{opt} lies approximately within the same limits. For a plane diffuser this angle lies within the limits $\theta_{opt} = 10^\circ$ to 12° .

9.1.10 Technological improvements

The flow conditions of a stream in short wide-angled diffusers can be considerably improved by preventing stream separation or reducing the formation of eddies.

The main measures contributing to an improvement of flow in diffusers are (Figure 2):

- 1) the suction of the boundary layer;
- 2) the blowing away of the boundary layer;
- 3) the installation of baffles or guide vanes;
- 4) the installation of dividing walls;
- 5) the use of curved walls;
- 6) the use of stepped walls;

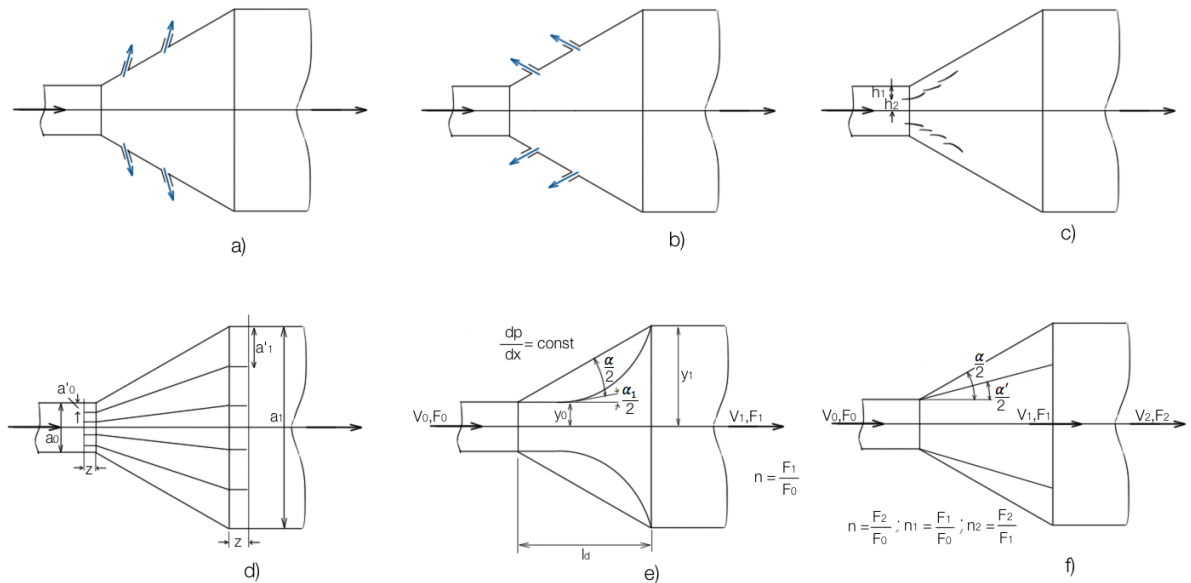


Figure 2: main measures contributing to an improvement of flow in diffusers

- When the boundary layer is sucked (Figure 2, a), the part of the stream separated from the wall again adheres to the surface, and as a result the zone of separation is displaced downstream, the flow becomes smoother, and the resistance decreases. A 30% to 50% reduction of losses can be achieved as a result.
- The blowing away of the boundary layer (Figure 2, b) leads to an increase of stream velocity near the walls. As a result, the separation zone is also displaced downstream.
- Guide vanes or baffles (Figure 2, c) deflect a part of the high-velocity stream core toward the boundary zone of separation. The latter is reduced or even completely eliminated as a result. The effect of guide vanes is greatest at wide divergence. At $\theta = 50^\circ$ to 180° the head loss coefficient is reduced by a factor of almost two. Several general rules can be given for positioning the baffles in the diffuser:
 - a) The vanes should be placed before and behind the entrance angle to the diffuser (Figure 2, c), and their number should be increased with the increase of the divergence angle.
 - b) The channels between the vanes and the walls must contract as a rule; however, at wide divergence angles, satisfactory results can be obtained even with expanding channels. It is necessary to permit the stream to expand in the peripheral channels just as in the main channel.
 - c) The relative distance $\frac{h_1}{h_2}$ must be equal to 0.95 for $\theta = 90^\circ$, and to 1,4 for $\theta = 180^\circ$ (Figure 2, c).
 - d) The vanes must have a small curvature and can be made of sheet metal.

- e) The chord of the vanes can represent 20% to 25% of the diameter or the height of the diffuser section.
 - f) The best angle of inclination of the vanes can be selected by arranging them first one behind the other and rotating each of them through an angle until the diffuser resistance becomes minimum.
- The dividing walls divide a wide-angle diffuser into several narrow-angle diffusers (Figure 2, d). As a result, the resistance is decreased and a more uniform velocity distribution over the section is achieved. The dividing walls are more efficient with the increase of the total divergence angle of the diffuser. At relatively narrow divergence angles the dividing walls can even increase the diffuser resistance, since they increase the total friction surface. The following procedure is used when selecting and installing dividing walls in wide-angle diffusers:
 - a) The number z of dividing walls is selected from the following table as a function of the divergence angle.

Table 1: number of dividing walls

θ [°]	30	45	60	90	120
z	2	4	4	6	8

- b) The dividing walls are positioned so that the distance a'_0 between them at the diffuser inlet are exactly equal, and the distance a'_1 between them at the exit are approximately equal.
 - c) The dividing walls extend in both directions beyond the diffuser, with protruding parts parallel to the diffuser axis. The length of the protruding parts must not be smaller than $0,1 \cdot a_0$ and $0,1 \cdot a_1$ respectively.
- The variation of the pressure gradient along the diffuser is smoother in a diffuser with curved walls (Figure 2, e), in which the rate of increase of the cross-section area is lower in the initial section than in the end section. As a result, the main cause of stream separation is weakened, and the main source of losses is attenuated. A diffuser in which the pressure gradient remains constant along the channel $\frac{dp}{dx} = const$ at potential flow will be the best choice. The losses in such diffusers may be as much as 40% lower than corresponding straight diffusers at divergence angles $25^\circ \leq \theta \leq 90^\circ$, the reduction increasing with an increase of the divergence angle within the limits. At lower divergence angles, e. g., curved diffusers is therefore expedient at wide divergence angles only.

The equation of the generatrix of a curved diffuser with a section which fulfills the condition $\frac{dp}{dx} = \text{const}$ is:

$$y = \frac{y_1}{\sqrt[4]{1 + \left[1 + \left[\left(\frac{y_1}{y_0}\right)^4 - 1\right]\right] \frac{x}{l_d}}}$$

The equation of the generatrix of a plane diffuser is:

$$y = \frac{y_1}{\sqrt{1 + \left[1 + \left[\left(\frac{y_1}{y_0}\right)^2 - 1\right]\right] \frac{x}{l_d}}}$$

The head loss coefficient of a curvilinear diffuser at $\frac{dp}{dx} = \text{const}$ within the limits $0,1 \leq \frac{F_0}{F_1} \leq 0,9$ can be calculated by the following approximate formula:

$$\zeta = \frac{\Delta H}{\frac{V_0^2}{2g}} = \varphi_0 \left(1,43 - \frac{1,3}{n_1}\right) \left(1 - \frac{1}{n}\right)^2$$

Where φ_0 is a coefficient depending on the relative length $\frac{l_d}{D_h}$ of the curved diffuser and determined from data of the Graph 16.

- In a multistage diffuser (Figure 2, f), in which a sudden expansion takes place after a smooth variation of cross-section area, the main shock losses occur at relatively low velocities. As a result, the losses in the diffuser are reduced by a factor of two to three. The coefficient of total resistance of a multistage diffuser of circular or rectangular section can be approximately calculated by the following formula:

$$\zeta = \frac{\Delta H}{\frac{V_0^2}{2g}} = (1 + \sigma) \left[\frac{\lambda}{8 \sin \frac{\theta}{2}} \cdot \frac{\left(1 + 2 \frac{l_d}{D_h} \tan \frac{\theta}{2}\right)^2 + 1}{\left(1 + 2 \frac{l_d}{D_h} \tan \frac{\theta}{2}\right)^2 - 1} + k_2 \tan \frac{\theta}{2} \sqrt{\tan \frac{\theta}{2}} \right] \cdot \left[1 - \frac{1}{\left(1 + 2 \frac{l_d}{D_h} \tan \frac{\theta}{2}\right)^2} \right]^2 + \left[\frac{1}{\left(1 + 2 \frac{l_d}{D_h} \tan \frac{\theta}{2}\right)^2} - \frac{1}{n} \right]^2$$

Where: $k_2 = 3,2$ for diffuser of circular section; $k_2 = 4$ to 6 for diffuser of rectangular section; $n = \frac{F_2}{F_0}$ is total area ratio of the multistage diffuser, i.e.,

ratio of the area of the widest part of the diffuser to the area of its narrowest part (Figure 2, f).

The coefficient of total resistance of a plane multistage diffuser can be approximately calculated as follows:

$$\zeta = \frac{\Delta H}{\frac{V_0^2}{2g}} = (1 + \sigma) \left[\frac{\lambda}{8 \frac{l_d}{a_0} \tan \frac{\theta}{2}} \cdot \left[\frac{a_0}{b_0} \frac{1}{\tan \frac{\theta}{2}} \left(1 + 2 \frac{l_d}{D_h} \tan \frac{\theta}{2} \right) + \frac{1}{\sin \frac{\theta}{2}} \left(1 + \frac{l_d}{D_h} \tan \frac{\theta}{2} \right) \right] \right. \\ \left. + 3,2 \tan \frac{\theta}{2} \sqrt{\tan \frac{\theta}{2}} \right] \cdot \left[1 - \frac{1}{\left(1 + 2 \frac{l_d}{D_h} \tan \frac{\theta}{2} \right)^2} \right]^2 + \left[\frac{1}{\left(1 + 2 \frac{l_d}{D_h} \tan \frac{\theta}{2} \right)^2} - \frac{1}{n} \right]^2$$

With b_0 constant along the diffuser.

To each area ratio n and each relative length $\frac{l_d}{D_h}$ (or $\frac{l_d}{a_0}$) of the multistage diffuser, there corresponds an optimum divergence angle θ_{opt} at which the total coefficient of resistance is minimum. The use of multistage diffusers with optimum expansion angles is recommended.

The head loss coefficient for such diffusers is determined by the formula:

$$\zeta = \frac{\Delta H}{\frac{V_0^2}{2g}} = (1 + \sigma) \zeta_{min}$$

Where ζ_{min} = minimum head loss coefficient, depending on the relative length of the smooth part of the diffuser $\frac{l_d}{D_h}$ (or $\frac{l_d}{a_0}$), and the total area ratio n of the multistage diffuser; this relationship has been plotted in Graph 19, Graph 22 and Graph 25; σ is a corrective factor, determined from Graph 18, Graph 21 and Graph 24 as a function of $\frac{F_0}{F_1}$.

The limiting divergence angle θ_{lim} of the smooth part of the multistage-diffuser, i. e., the angle at which, for the given overall area ratio n and relative length $\frac{l_d}{D_h}$ (or $\frac{l_d}{a_0}$) of the smooth part, a straight diffuser is obtained, is given by:

$$\left\{ \begin{array}{l} \tan \frac{\theta_{lim}}{2} = \frac{\sqrt{n} - 1}{2 \frac{l_d}{D_h}} \\ \tan \frac{\theta_{lim}}{2} = \frac{\sqrt{n} - 1}{2 \frac{l_d}{a_0}} \end{array} \right.$$

In practice, it is expedient to select the relative length $\frac{l_d}{D_h}$ of the multistage diffuser not on the basis of the minimum value ζ_{min} , but on a value approximately 10% higher, which makes possible a considerable reduction in diffuser length without noticeably increasing the losses in it.

The lines of optimum values of $\frac{l_d}{D_h}$ are represented in Graph 20, Graph 23 and Graph 26 by dotted lines.

9.2 Graphs of head loss coefficients

Diffusers of arbitrary shape located at the discharge of long stretches with non-uniform but symmetric velocity profile

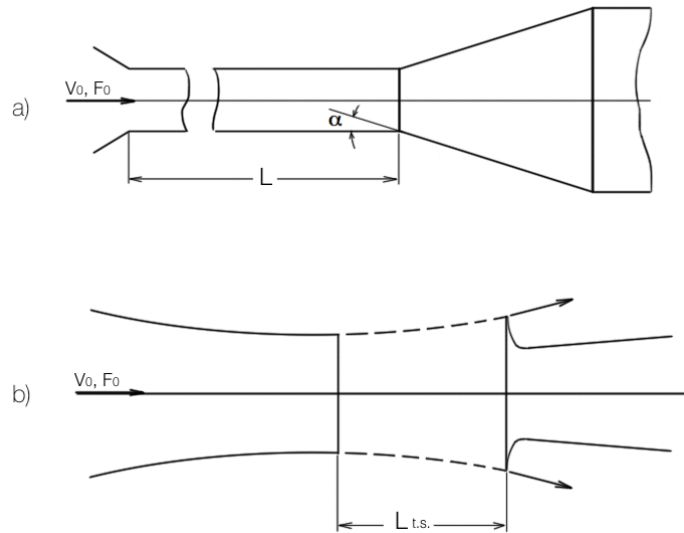


Figure 3: Initial Zone

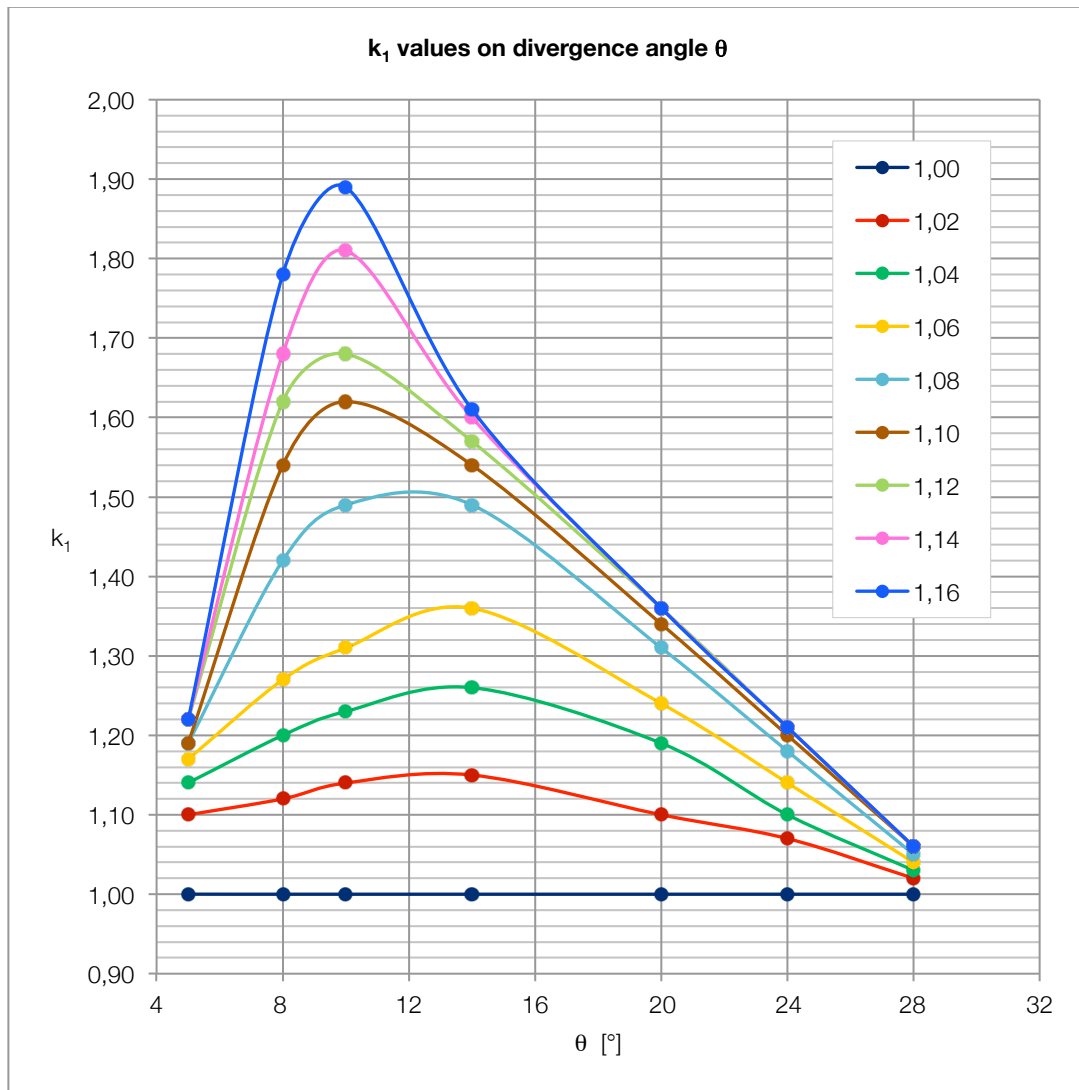
$$\zeta = \frac{\Delta H}{\frac{V_0^2}{2g}} = k_1 \zeta_{exp} + \zeta_{fr}$$

Where:

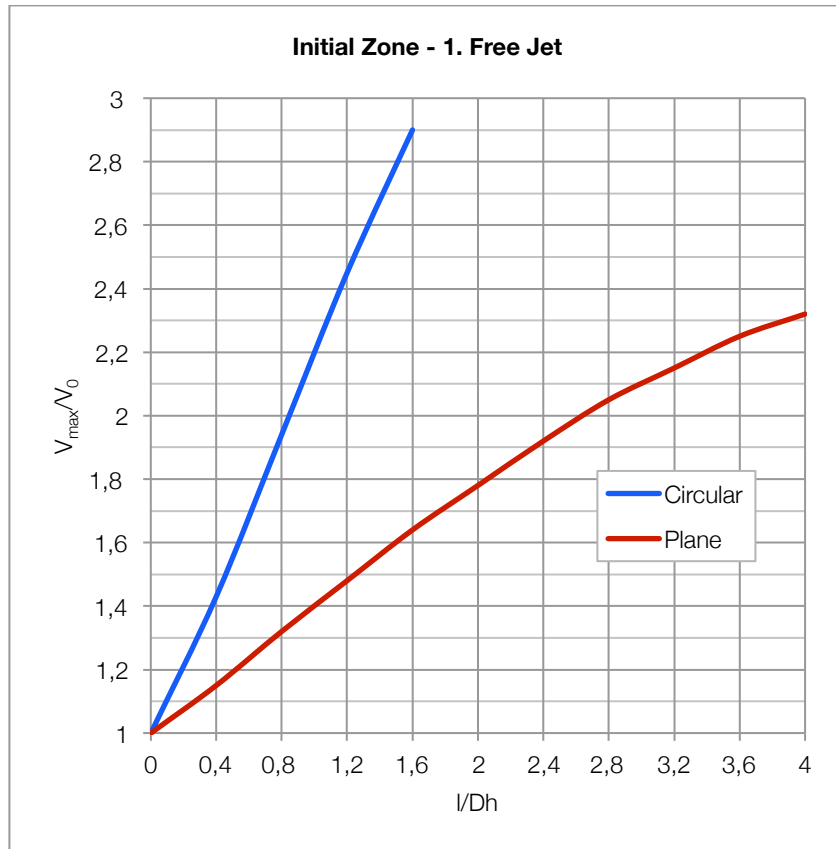
- ζ_{exp} and ζ_{fr} are taken from the diagrams of the following sections of this chapter;
- k_1 is determined as function of from the curves of corresponding to different $\frac{V_{max}}{V}$
- $\frac{V_{max}}{V}$ is determined as a function of $\frac{l}{D_h}$ from the curves of graphs 1b and 1c corresponding to different values of Re

Table 2: Values of k_1

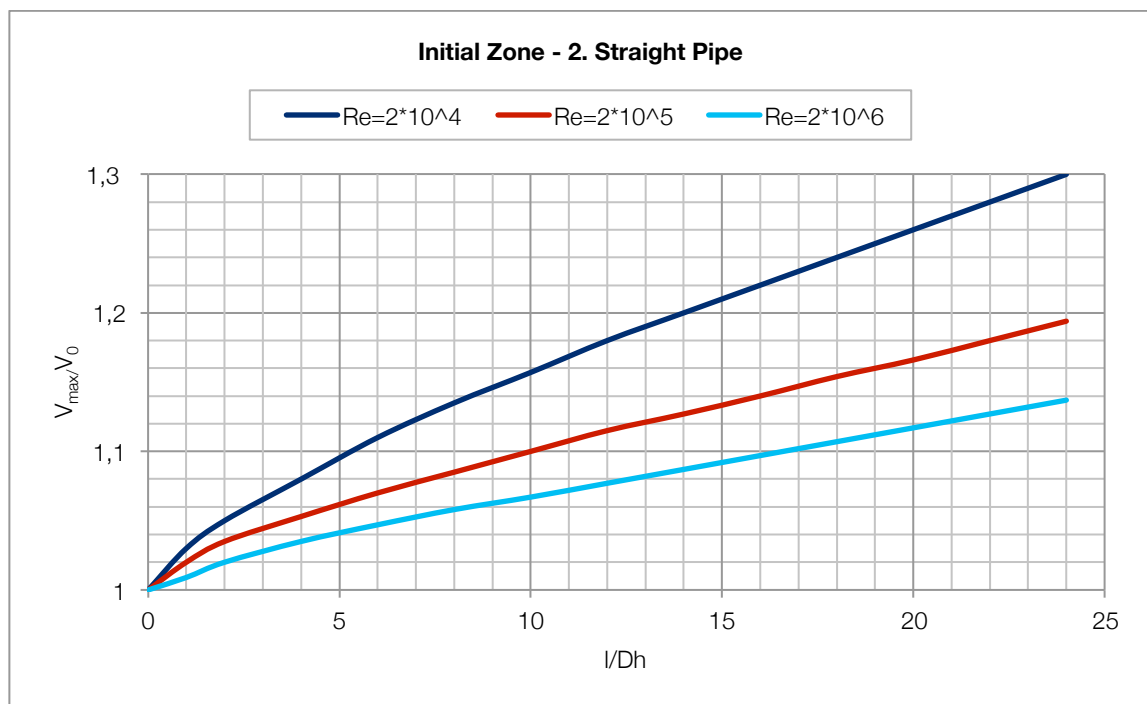
V_{\max}/V_0	θ [°]						
	5	8	10	14	20	24	28
1,00	1,00	1,00	1,00	1,00	1,00	1,00	1,00
1,02	1,10	1,12	1,14	1,15	1,10	1,07	1,02
1,04	1,14	1,20	1,23	1,26	1,19	1,10	1,03
1,06	1,17	1,27	1,31	1,36	1,24	1,14	1,04
1,08	1,19	1,42	1,49	1,49	1,31	1,18	1,05
1,10	1,19	1,54	1,62	1,54	1,34	1,20	1,06
1,12	1,22	1,62	1,68	1,57	1,36	1,21	1,06
1,14	1,22	1,68	1,81	1,60	1,36	1,21	1,06
1,16	1,22	1,78	1,89	1,61	1,36	1,21	1,06



Graph 3: values of k_1 on divergence angle θ



Graph 4: Values of V_{\max}/V_0 for Initial Zone (straight pipe)



Graph 5: Values of V_{\max}/V_0 for Initial Zone (straight pipe)

Conical diffuser in a line

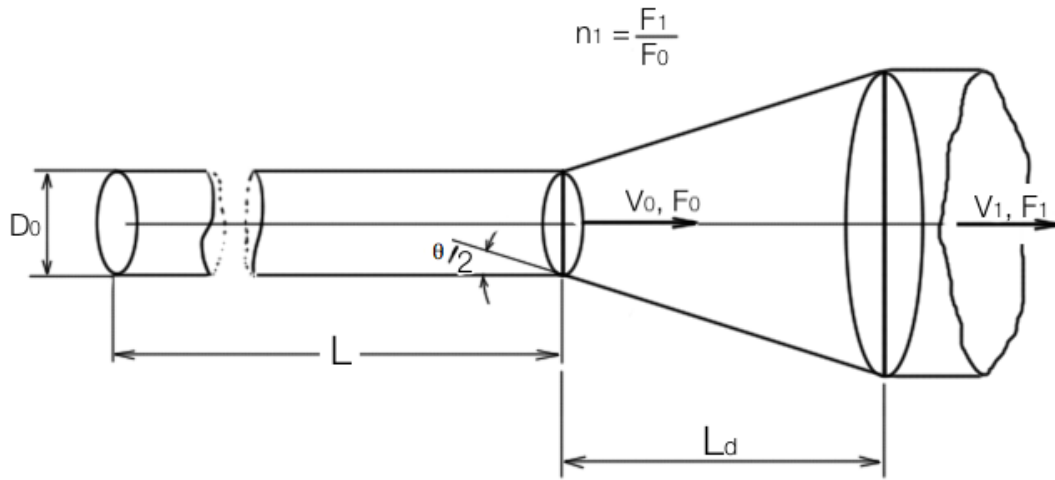


Figure 4: Conical diffuser in a line

Uniform velocity distribution at the diffuser inlet

$$\zeta = \frac{\Delta H}{\frac{V_0^2}{2g}} = \zeta_{exp} + \zeta_{fr} \qquad \zeta_{exp} = \varphi_{exp} \left(1 - \frac{F_0}{F_1}\right)^2$$

Where:

φ_{exp} is determined from the curve $\zeta_{exp} = f(\theta)$ at $\frac{F_0}{F_1} = 0$ on the Graph 6.

Within the limits $0^\circ \leq \theta \leq 40^\circ$:

$$\varphi_{exp} = 3,2 \tan \frac{\alpha}{2} \sqrt{\tan \frac{\theta}{2}}$$

The values of ζ_{exp} are determined from the curves $\zeta_{exp} = f\left(\alpha, \frac{F_0}{F_1}\right)$ of the Graph 6.

$$\zeta_{fr} = \frac{\lambda}{8 \sin \frac{\theta}{2}} \left[1 - \left(\frac{F_0}{F_1}\right)^2\right]$$

At $\lambda = 0,02$ ζ_{fr} is determined from the curves $\zeta_{fr} = f\left(\theta, \frac{F_0}{F_1}\right)$ on Graph 7;

λ is determined from Moody diagram available in the theoretical framework.

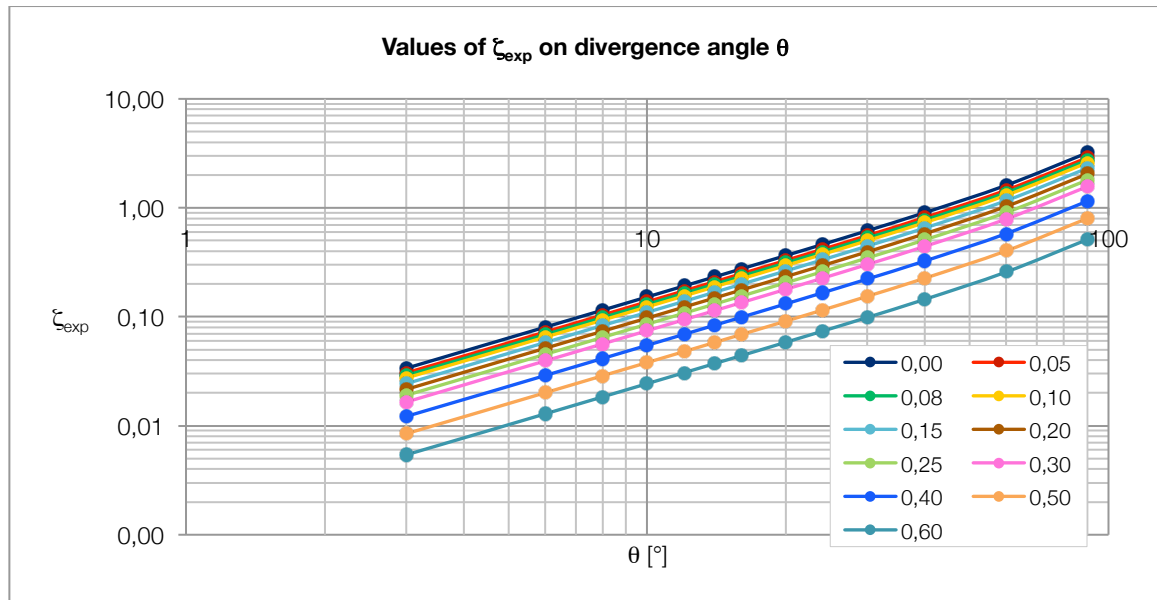
Non-uniform velocity distribution at the diffuser inlet

$$\zeta = \frac{\Delta H}{\frac{V_0^2}{2g}} = k_1 \zeta_{exp} + \zeta_{fr}$$

Where k_1 is determined from the Graph 3.

Table 3: Values of ζ_{exp}

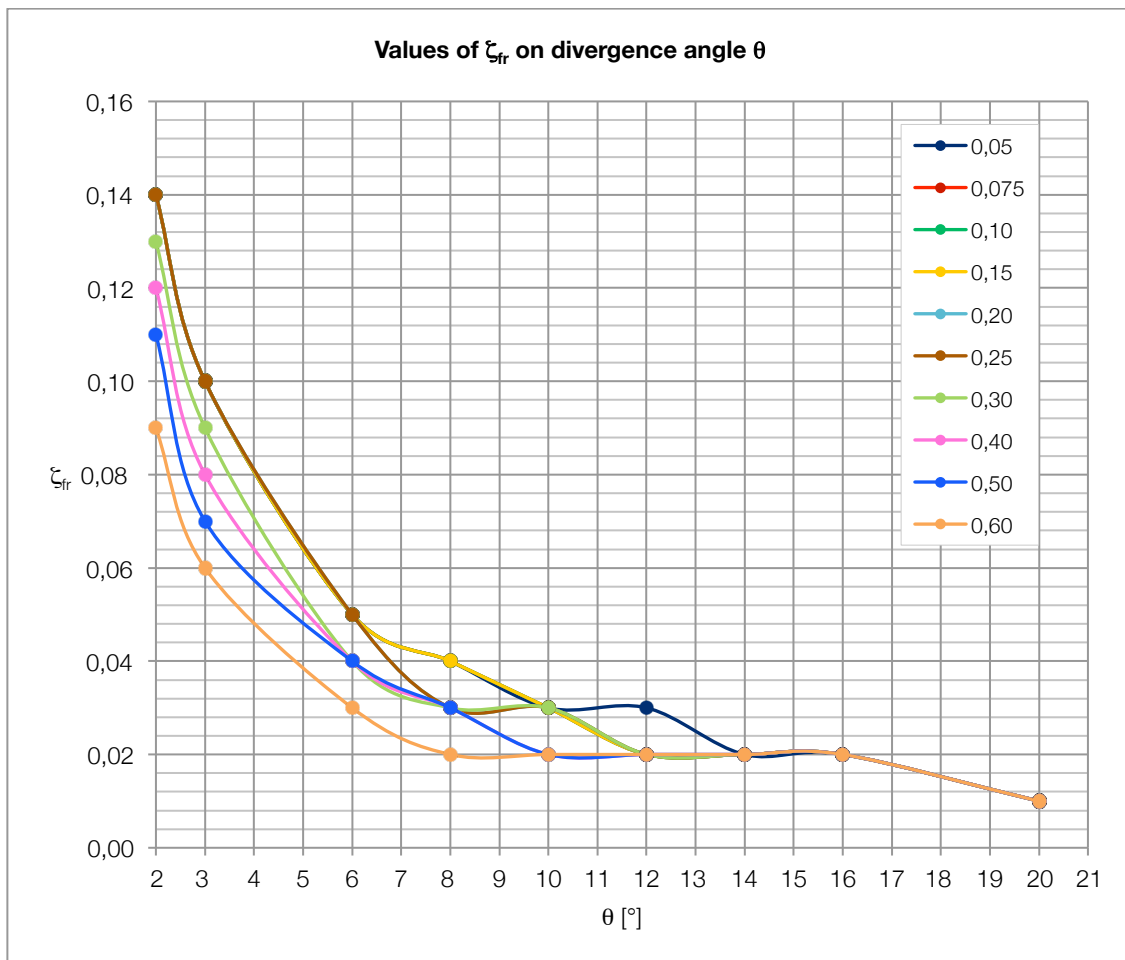
F_0/F_1	n_1	θ													
		3	6	8	10	12	14	16	20	24	30	40	60	90	180
0,00	∞	0,03	0,08	0,11	0,15	0,19	0,23	0,27	0,36	0,47	0,65	0,92	1,15	1,10	1,02
0,05	20,0	0,03	0,07	0,10	0,14	0,16	0,20	0,24	0,32	0,42	0,58	0,83	1,04	0,99	0,92
0,08	13,3	0,03	0,07	0,09	0,13	0,16	0,19	0,23	0,30	0,40	0,55	0,79	0,99	0,95	0,88
0,10	10,0	0,03	0,07	0,09	0,12	0,15	0,18	0,22	0,29	0,38	0,52	0,75	0,93	0,89	0,83
0,15	6,67	0,02	0,06	0,08	0,11	0,14	0,17	0,20	0,26	0,34	0,46	0,67	0,84	0,79	0,74
0,20	5,00	0,02	0,05	0,07	0,10	0,12	0,15	0,17	0,23	0,30	0,41	0,59	0,74	0,70	0,65
0,25	4,00	0,02	0,05	0,06	0,08	0,10	0,13	0,15	0,20	0,26	0,35	0,47	0,65	0,62	0,58
0,30	3,33	0,02	0,04	0,05	0,07	0,09	0,11	0,13	0,18	0,23	0,31	0,40	0,57	0,54	0,50
0,40	2,50	0,01	0,03	0,04	0,06	0,07	0,08	0,10	0,13	0,17	0,23	0,33	0,41	0,39	0,37
0,50	2,00	0,01	0,02	0,03	0,04	0,05	0,06	0,07	0,09	0,12	0,16	0,23	0,29	0,28	0,26
0,60	1,67	0,01	0,01	0,02	0,03	0,03	0,04	0,05	0,06	0,08	0,10	0,15	0,18	0,17	0,16



Graph 6: Values of ζ_{exp} on divergence angle θ

Table 4: values of ζ_{fr}

F_0/F_1	n_1	θ								
		2	3	6	8	10	12	14	16	20
0,05	20,00	0,14	0,10	0,05	0,04	0,03	0,03	0,02	0,02	0,01
0,075	13,33	0,14	0,10	0,05	0,04	0,03	0,02	0,02	0,02	0,01
0,10	10,00	0,14	0,10	0,05	0,04	0,03	0,02	0,02	0,02	0,01
0,15	6,67	0,14	0,10	0,05	0,04	0,03	0,02	0,02	0,02	0,01
0,20	5,00	0,14	0,10	0,05	0,03	0,03	0,02	0,02	0,02	0,01
0,25	4,00	0,14	0,10	0,05	0,03	0,03	0,02	0,02	0,02	0,01
0,30	3,33	0,13	0,09	0,04	0,03	0,03	0,02	0,02	0,02	0,01
0,40	2,50	0,12	0,08	0,04	0,03	0,02	0,02	0,02	0,02	0,01
0,50	2,00	0,11	0,07	0,04	0,03	0,02	0,02	0,02	0,02	0,01
0,60	1,67	0,09	0,06	0,03	0,02	0,02	0,02	0,02	0,02	0,01



Graph 7: Values of ζ_{fr} on θ angle

Pyramidal diffuser in a line

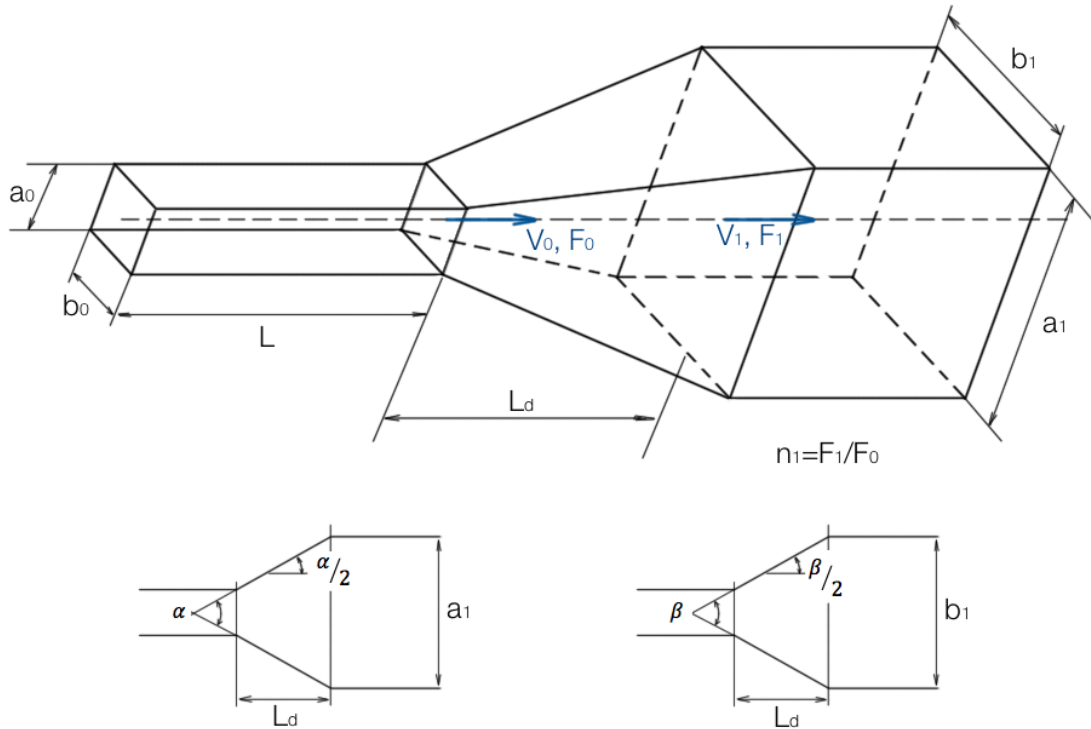


Figure 5: Pyramidal diffuser in a line

Uniform velocity distribution at the diffuser inlet

$$\zeta = \frac{\Delta H}{\frac{V_0^2}{2g}} = \zeta_{exp} + \zeta_{fr}$$

Where:

$$\zeta_{exp} = \varphi_{exp} \left(1 - \frac{F_0}{F_1}\right)^2$$

φ_{exp} is only approximately determined from the curve $\zeta_{exp} = f(\theta)$ at $\frac{F_0}{F_1} = 0$ on Graph 8.

Within the limits $0^\circ \leq \alpha \leq 25^\circ$:

$$\varphi_{exp} \cong 4,0 \tan \frac{\alpha}{2} \sqrt{\tan \frac{\alpha}{2}}$$

The values of ζ_{exp} are determined from the curves $\zeta_{exp} = f\left(\alpha, \frac{F_0}{F_1}\right)$ of Graph 8;

$$\zeta_{fr} \cong \frac{\lambda}{16 \sin \frac{\alpha}{2}} \left[1 - \left(\frac{F_0}{F_1} \right)^2 \right] + \frac{\lambda}{16 \sin \frac{\beta}{2}} \left[1 - \left(\frac{F_0}{F_1} \right)^2 \right] = \Delta\zeta_{fr} + \Delta\zeta'_{fr}$$

At $\alpha = \beta$:

$$\zeta_{fr} = \frac{\lambda}{8 \sin \frac{\alpha}{2}} \left[1 - \left(\frac{F_0}{F_1} \right)^2 \right] = 2\Delta\zeta_{fr}$$

At $\lambda = 0,02$ $\Delta\zeta_{fr}$ is determined from the curves $\Delta\zeta_{fr} = f(\alpha)$ on Graph 9;

$\Delta\zeta'_{fr}$ is determined from the curves $\Delta\zeta'_{fr} = f(\beta)$ on Graph 9;

λ is determined from the Moody abach (theoretical framework);

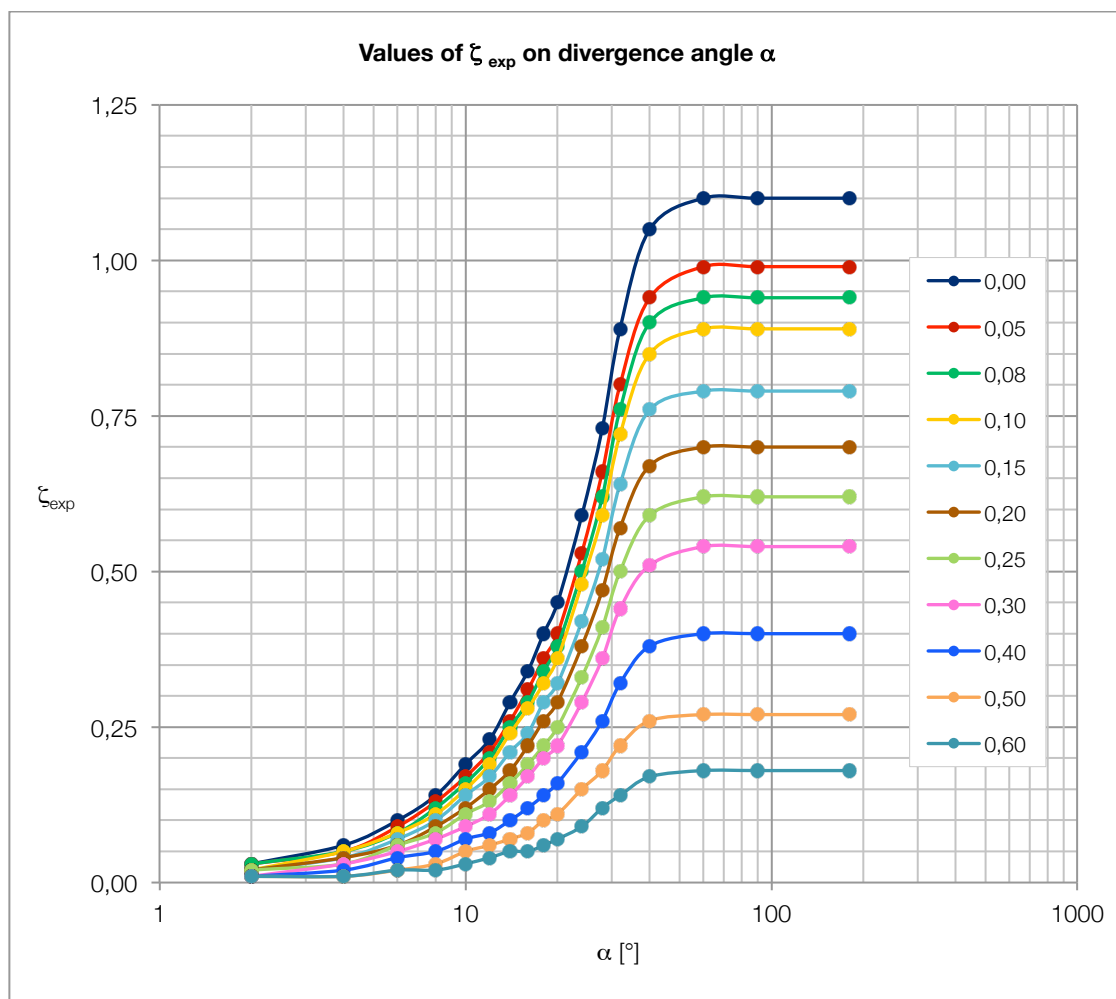
Non-uniform velocity distribution at the diffuser inlet

$$\zeta = \frac{\Delta H}{\frac{V_0^2}{2g}} = k_1 \zeta_{exp} + \zeta_{fr}$$

Where k_1 is determined from the Graph 3.

Table 5: values of ζ_{exp}

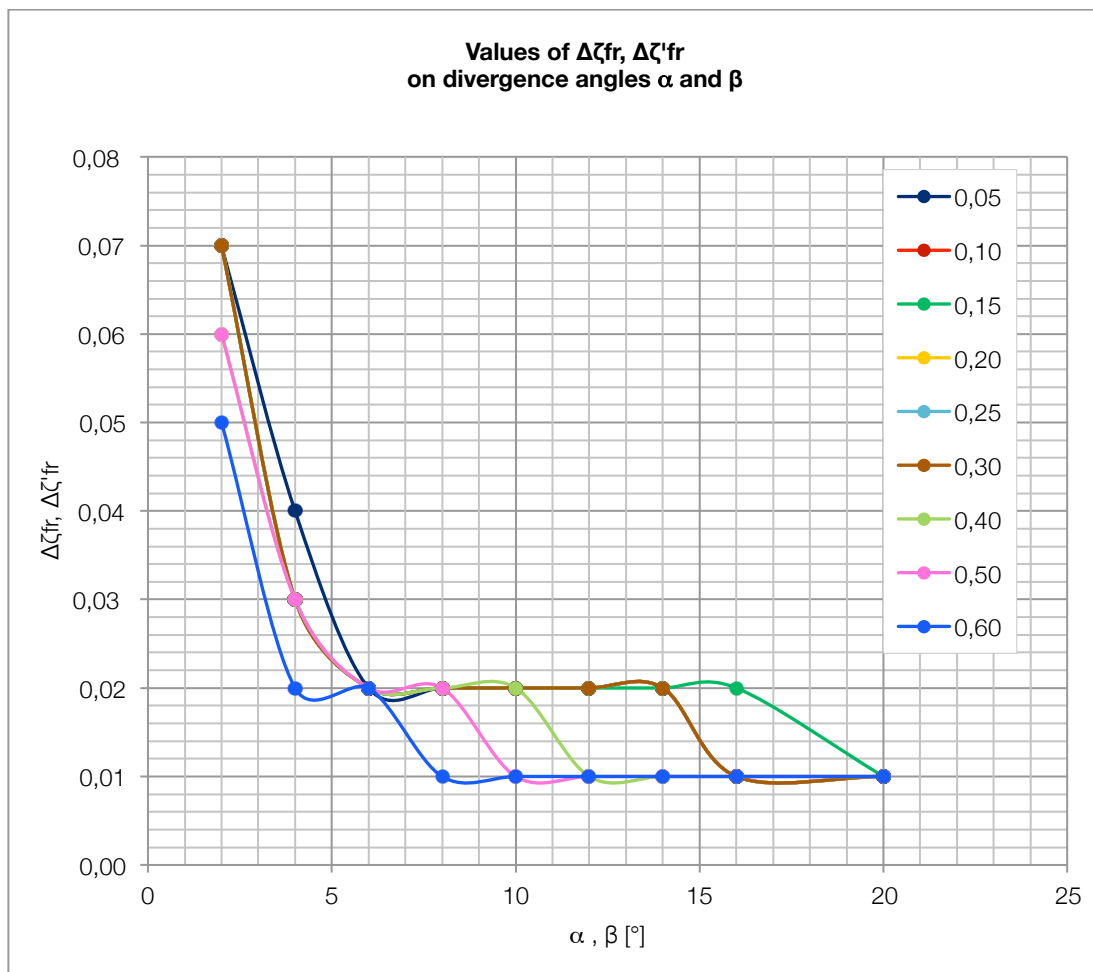
F_0/F_1	n_1	α [°]																
		2	4	6	8	10	12	14	16	18	20	24	28	32	40	60	90	180
0,00	∞	0,03	0,06	0,10	0,14	0,19	0,23	0,29	0,34	0,40	0,45	0,59	0,73	0,89	1,05	1,1	1,1	1,1
0,05	20,00	0,03	0,05	0,09	0,13	0,17	0,21	0,26	0,31	0,36	0,40	0,53	0,66	0,80	0,94	0,99	0,99	0,99
0,08	13,33	0,03	0,05	0,08	0,12	0,16	0,20	0,25	0,29	0,34	0,38	0,50	0,62	0,76	0,90	0,94	0,94	0,94
0,10	10,00	0,02	0,05	0,08	0,11	0,15	0,19	0,24	0,28	0,32	0,36	0,48	0,59	0,72	0,85	0,89	0,89	0,89
0,15	6,67	0,02	0,04	0,07	0,10	0,14	0,17	0,21	0,24	0,29	0,32	0,42	0,52	0,64	0,76	0,79	0,79	0,79
0,20	5,00	0,02	0,04	0,06	0,09	0,12	0,15	0,18	0,22	0,26	0,29	0,38	0,47	0,57	0,67	0,7	0,7	0,7
0,25	4,00	0,02	0,03	0,06	0,08	0,11	0,13	0,16	0,19	0,22	0,25	0,33	0,41	0,50	0,59	0,62	0,62	0,62
0,30	3,33	0,01	0,03	0,05	0,07	0,09	0,11	0,14	0,17	0,20	0,22	0,29	0,36	0,44	0,51	0,54	0,54	0,54
0,40	2,50	0,01	0,02	0,04	0,05	0,07	0,08	0,10	0,12	0,14	0,16	0,21	0,26	0,32	0,38	0,4	0,4	0,4
0,50	2,00	0,01	0,01	0,02	0,03	0,05	0,06	0,07	0,08	0,10	0,11	0,15	0,18	0,22	0,26	0,27	0,27	0,27
0,60	1,67	0,01	0,01	0,02	0,02	0,03	0,04	0,05	0,05	0,06	0,07	0,09	0,12	0,14	0,17	0,18	0,18	0,18



Graph 8: values of ζ_{exp}

Table 6: values of $\Delta\zeta_{fr}$ or $\Delta\zeta'_{fr}$ on α, β

F_0/F_1	n_1	α, β								
		2	4	6	8	10	12	14	16	20
0,05	20,00	0,07	0,04	0,02	0,02	0,02	0,02	0,02	0,01	0,01
0,10	10,00	0,07	0,03	0,02	0,02	0,02	0,02	0,02	0,01	0,01
0,15	6,67	0,07	0,03	0,02	0,02	0,02	0,02	0,02	0,02	0,01
0,20	5,00	0,07	0,03	0,02	0,02	0,02	0,02	0,02	0,01	0,01
0,25	4,00	0,07	0,03	0,02	0,02	0,02	0,02	0,02	0,01	0,01
0,30	3,33	0,07	0,03	0,02	0,02	0,02	0,02	0,02	0,01	0,01
0,40	2,50	0,06	0,03	0,02	0,02	0,02	0,01	0,01	0,01	0,01
0,50	2,00	0,06	0,03	0,02	0,02	0,01	0,01	0,01	0,01	0,01
0,60	1,67	0,05	0,02	0,02	0,01	0,01	0,01	0,01	0,01	0,01



Graph 9: Values of Δz_{fr} or $\Delta z'_{fr}$ on α, β

Plane diffuser in a line

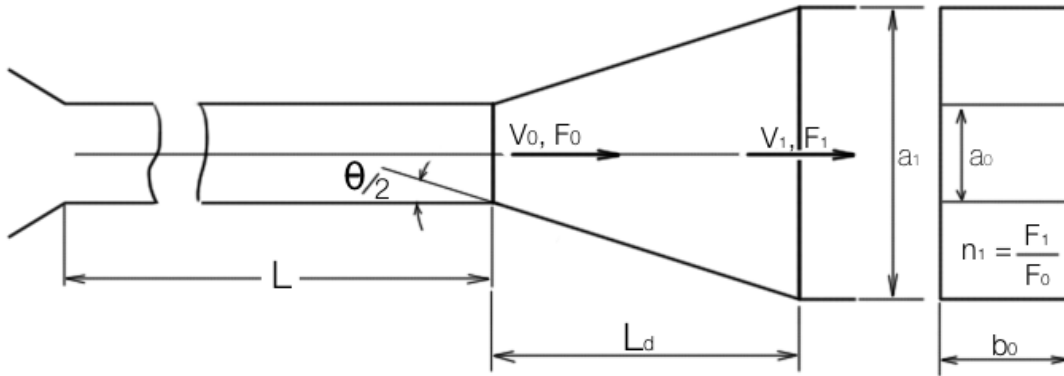


Figure 6: Plane diffuser in a line

Uniform velocity distribution at the diffuser inlet

$$\zeta = \frac{\Delta H}{\frac{V_0^2}{2g}} = \zeta_{exp} + \zeta_{fr}$$

Where:

$$\zeta_{exp} = \varphi_{exp} \left(1 - \frac{F_0}{F_1}\right)^2$$

φ_{exp} is only approximately determined from the curve $\zeta_{exp} = f(\theta)$ at $\frac{F_0}{F_1} = 0$ on Graph 10.

Within the limits $0^\circ \leq \theta \leq 40^\circ$:

$$\varphi_{exp} \cong 3,2 \tan \frac{\theta}{2} \sqrt{\tan \frac{\theta}{2}}$$

The values of ζ_{exp} are determined from the curves $\zeta_{exp} = f\left(\theta, \frac{F_0}{F_1}\right)$ on Graph 10;

$$\zeta_{fr} \cong \frac{\lambda}{4 \sin \frac{\theta}{2}} \left\{ \frac{a_0}{b_0} \left(1 - \frac{F_0}{F_1}\right) + 0,5 \left[1 - \left(\frac{F_0}{F_1}\right)^2\right] \right\}$$

At $\lambda = 0,02$ $\Delta\zeta_{fr}$ is determined from the curves $\zeta_{fr} = f\left(\theta, \frac{a_0}{b_0}, \frac{F_0}{F_1}\right)$ on Graph 11 to Graph 15;

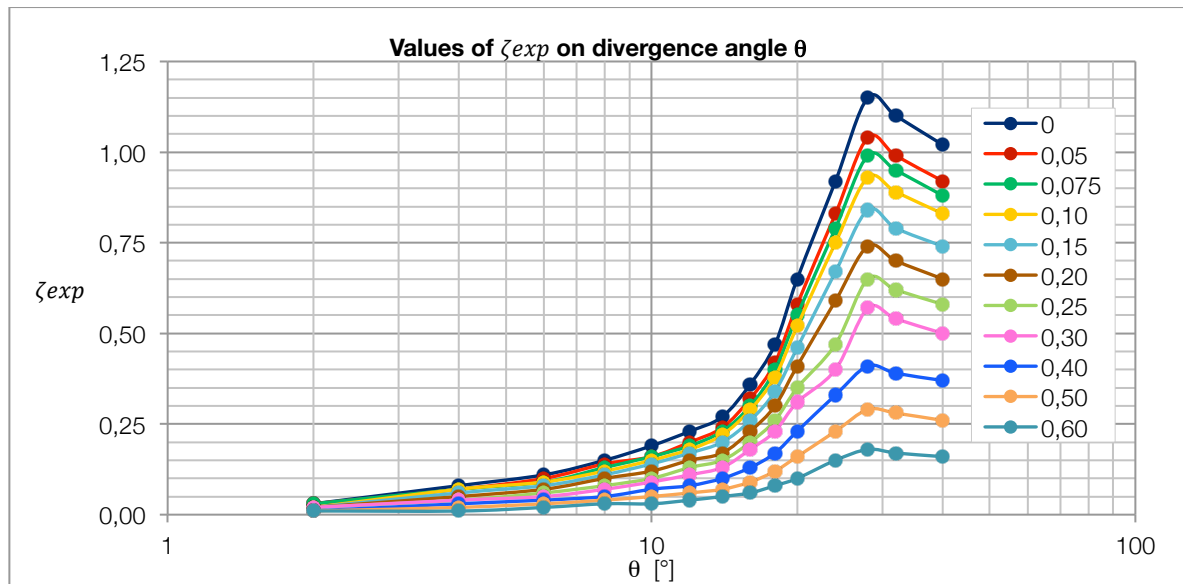
Non-uniform velocity distribution at the diffuser inlet

$$\zeta = \frac{\Delta H}{\frac{V_0^2}{2g}} = k_1 \zeta_{exp} + \zeta_{fr}$$

Where k_1 is determined from the Graph 3.

Table 7: values of ζ_{exp} on θ

F_0/F_1	n_1	θ													
		3	6	8	10	12	14	16	20	24	30	40	50	90	180
0	∞	0,03	0,08	0,11	0,15	0,19	0,23	0,27	0,36	0,47	0,65	0,92	1,15	1,10	1,02
0,05	20,00	0,03	0,07	0,10	0,14	0,16	0,20	0,24	0,32	0,42	0,58	0,83	1,04	0,99	0,92
0,075	13,33	0,03	0,07	0,09	0,13	0,16	0,19	0,23	0,30	0,40	0,55	0,79	0,99	0,95	0,88
0,10	10,00	0,02	0,07	0,09	0,12	0,15	0,18	0,22	0,29	0,38	0,52	0,75	0,93	0,89	0,83
0,15	6,67	0,02	0,06	0,08	0,11	0,14	0,17	0,20	0,26	0,34	0,46	0,67	0,84	0,79	0,74
0,20	5,00	0,02	0,05	0,07	0,10	0,12	0,15	0,17	0,23	0,30	0,41	0,59	0,74	0,70	0,65
0,25	4,00	0,02	0,04	0,06	0,08	0,10	0,13	0,15	0,20	0,26	0,35	0,47	0,65	0,62	0,58
0,30	3,33	0,02	0,04	0,05	0,07	0,09	0,11	0,13	0,18	0,23	0,31	0,40	0,57	0,54	0,50
0,40	2,50	0,01	0,03	0,04	0,05	0,07	0,08	0,10	0,13	0,17	0,23	0,33	0,41	0,39	0,37
0,50	2,00	0,01	0,02	0,03	0,04	0,05	0,06	0,07	0,09	0,12	0,16	0,23	0,29	0,28	0,26
0,60	1,67	0,01	0,01	0,02	0,03	0,03	0,04	0,05	0,06	0,08	0,10	0,15	0,18	0,17	0,16



Graph 10: values of ζ_{exp} on θ

Table 8: values of ζ_{fr} on θ , for different a_0/b_0 ratios

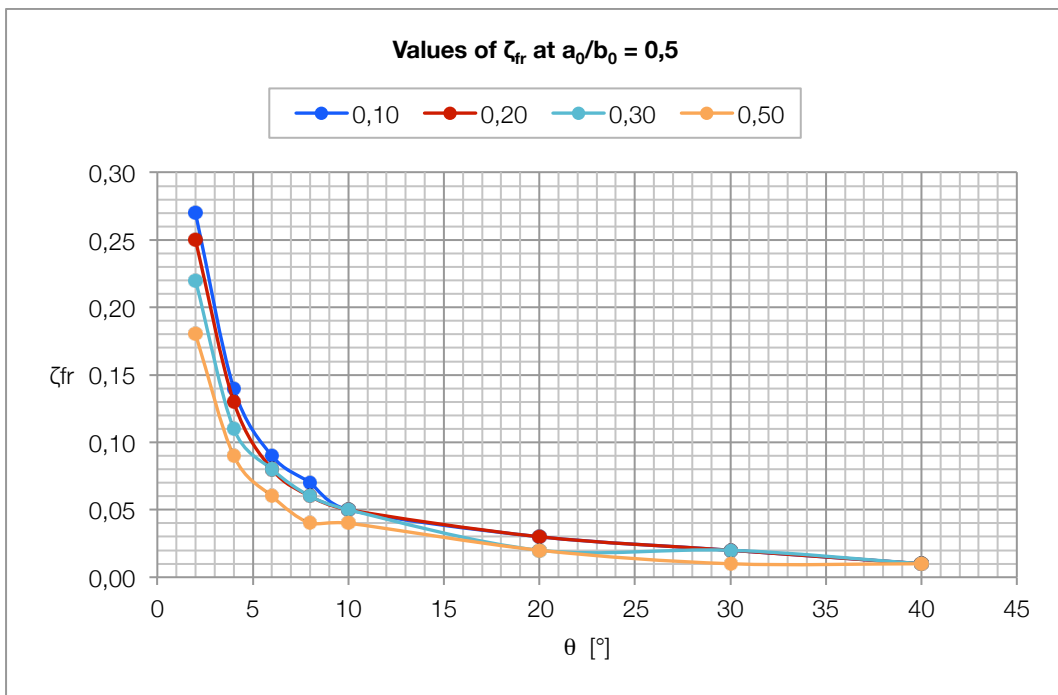
$a_0/b_0 = 0,5$									
F_0/F_1	n_1	θ							
		2	4	6	8	10	20	30	40
0,10	10,00	0,27	0,14	0,09	0,07	0,05	0,03	0,02	0,01
0,20	5,00	0,25	0,13	0,08	0,06	0,05	0,03	0,02	0,01
0,30	3,33	0,22	0,11	0,08	0,06	0,05	0,02	0,02	0,01
0,50	2,00	0,18	0,09	0,06	0,04	0,04	0,02	0,01	0,01

$a_0/b_0 = 0,75$									
F_0/F_1	n_1	θ							
		2	4	6	8	10	20	30	40
0,10	10,00	0,34	0,17	0,11	0,08	0,07	0,03	0,02	0,02
0,20	5,00	0,31	0,15	0,10	0,08	0,06	0,03	0,02	0,02
0,30	3,33	0,28	0,14	0,09	0,07	0,06	0,03	0,02	0,01
0,50	2,00	0,21	0,11	0,07	0,05	0,04	0,02	0,01	0,01

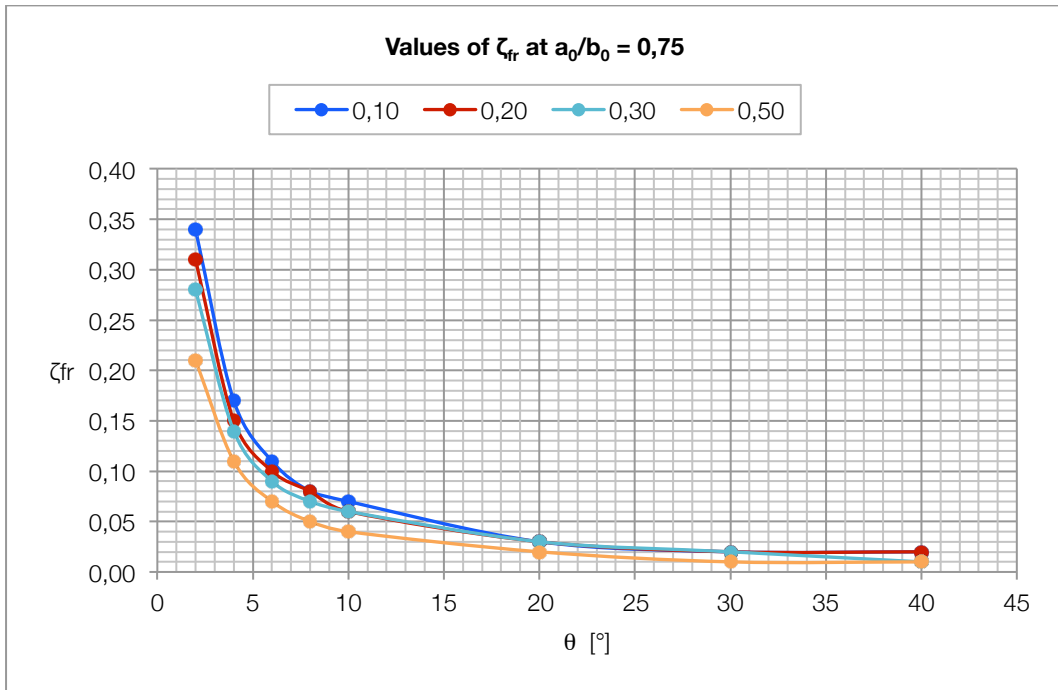
$a_0/b_0 = 1,0$										
F_0/F_1	n_1	θ								
		2	4	6	8	10	20	30	40	50
0,10	10,00	0,40	0,20	0,13	0,10	0,08	0,04	0,03	0,02	0,02
0,20	5,00	0,37	0,18	0,13	0,09	0,07	0,04	0,03	0,02	0,02
0,30	3,33	0,33	0,17	0,11	0,08	0,07	0,03	0,02	0,02	0,02
0,50	2,00	0,25	0,13	0,08	0,06	0,05	0,03	0,02	0,01	0,01

$a_0/b_0 = 1,5$									
F_0/F_1	n_1	θ							
		2	4	6	8	10	20	30	40
0,10	10,00	0,53	0,26	0,18	0,13	0,11	0,25	0,04	0,03
0,20	5,00	0,48	0,24	0,16	0,12	0,10	0,05	0,03	0,02
0,30	3,33	0,43	0,21	0,14	0,10	0,09	0,04	0,03	0,02
0,50	2,00	0,32	0,16	0,10	0,08	0,06	0,03	0,02	0,02

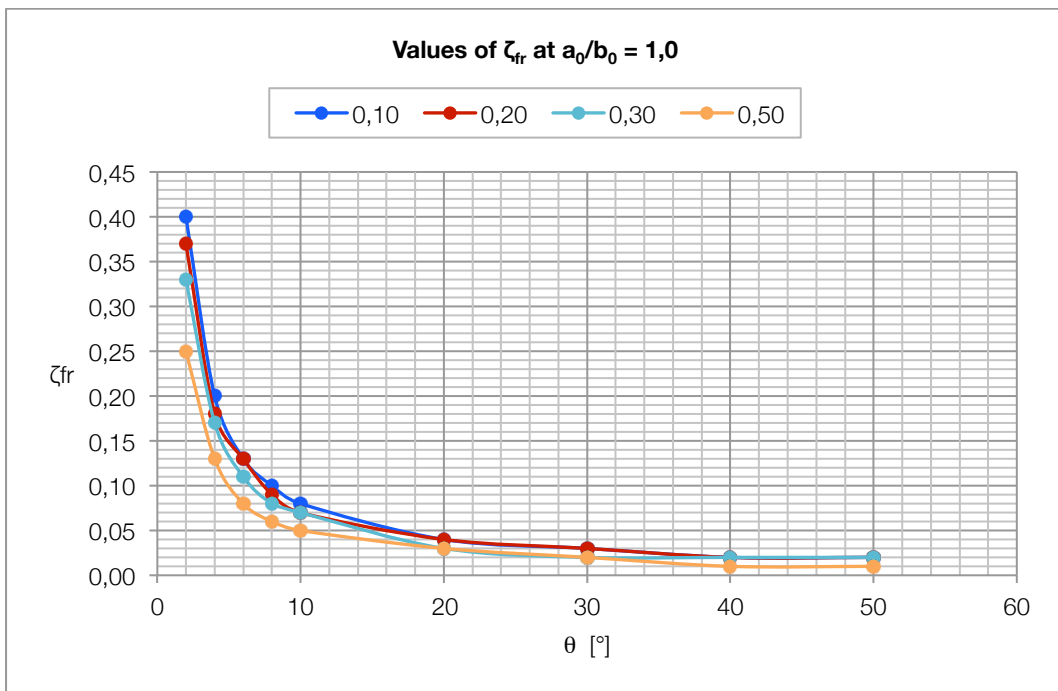
$a_0/b_0 = 2,0$											
F_0/F_1	n_1	θ									
		2	4	6	8	10	20	30	40	50	60
0,10	10,00	0,65	0,33	0,22	0,16	0,13	0,06	0,04	0,03	0,03	0,02
0,20	5,00	0,60	0,30	0,28	0,15	0,12	0,06	0,04	0,03	0,03	0,02
0,30	3,33	0,53	0,26	0,18	0,13	0,11	0,05	0,04	0,03	0,02	0,02
0,50	2,00	0,39	0,19	0,13	0,10	0,08	0,04	0,03	0,02	0,02	0,01



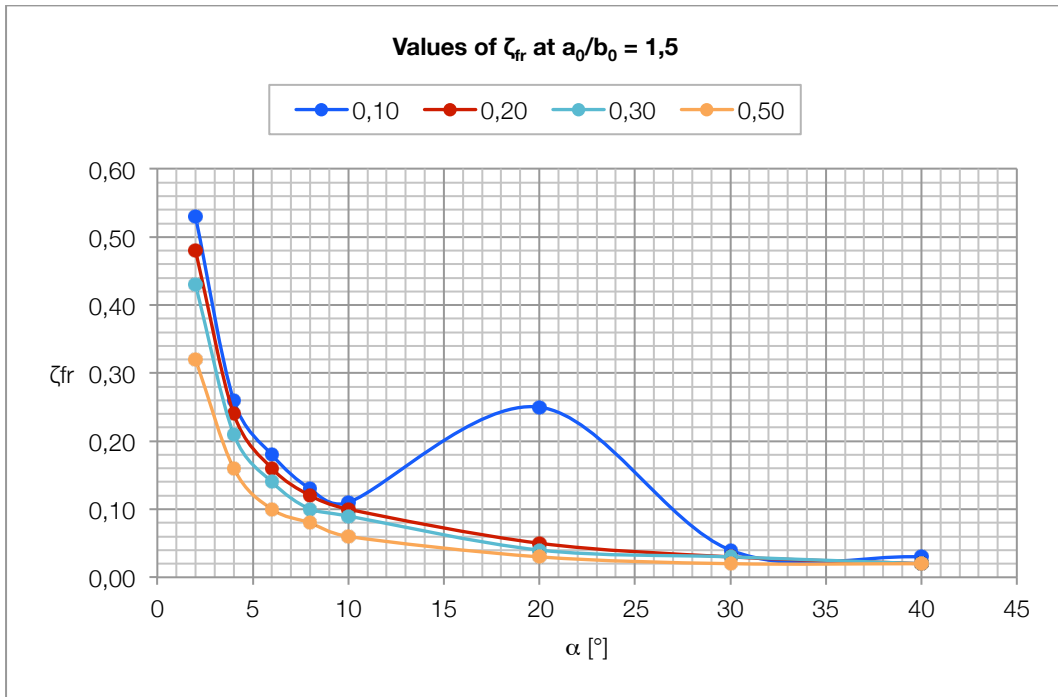
Graph 11: values of ζ_{fr} at $a_0/b_0 = 0,5$ on θ values



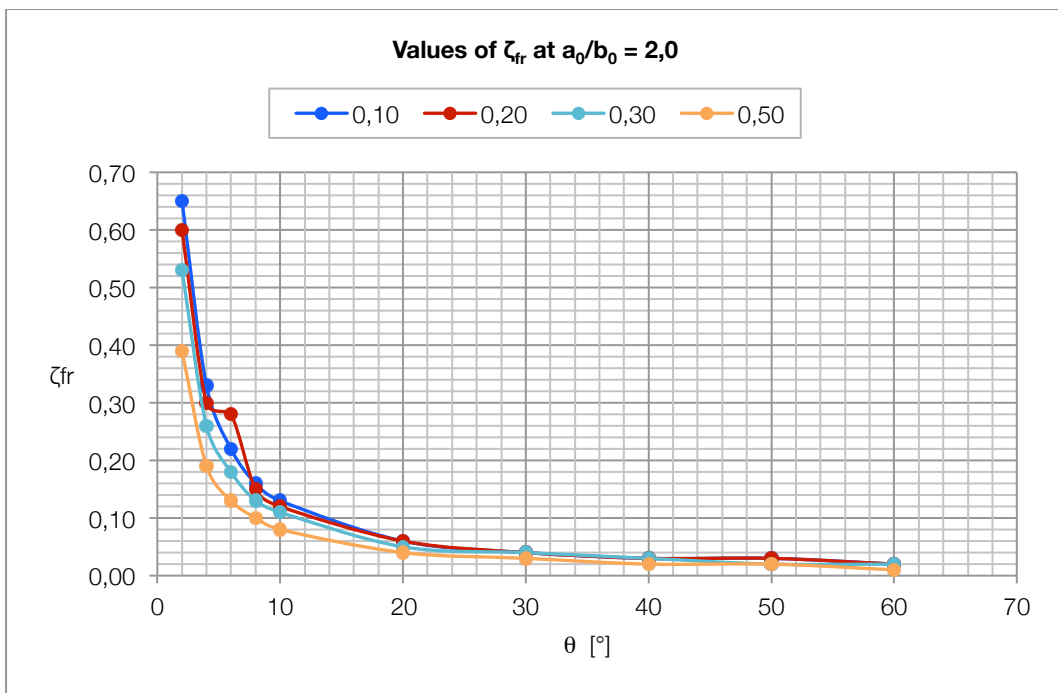
Graph 12: values of ζ_{fr} at $a_0/b_0 = 0,75$



Graph 13: values of ζ_{fr} at $a_0/b_0 = 1,0$



Graph 14: values of ζ_{fr} at $a_0/b_0 = 1,5$



Graph 15: values of ζ_{fr} at $a_0/b_0 = 2,0$

Transition diffusers

$$\zeta = \frac{\Delta H}{\frac{V_0^2}{2g}}$$

The resistance coefficient is determined by from the data in for pyramidal diffuser with equivalent divergence angle, determined from the following relations:

- a) Transition from circle to rectangle

$$\tan \frac{\theta}{2} = \frac{2\sqrt{\frac{a_1 b_1}{\pi}} - D_0}{2l_d}$$

- b) Transition from rectangle to circle

$$\tan \frac{\theta}{2} = \frac{D_1 - 2\sqrt{\frac{a_0 b_0}{\pi}}}{2l_d}$$

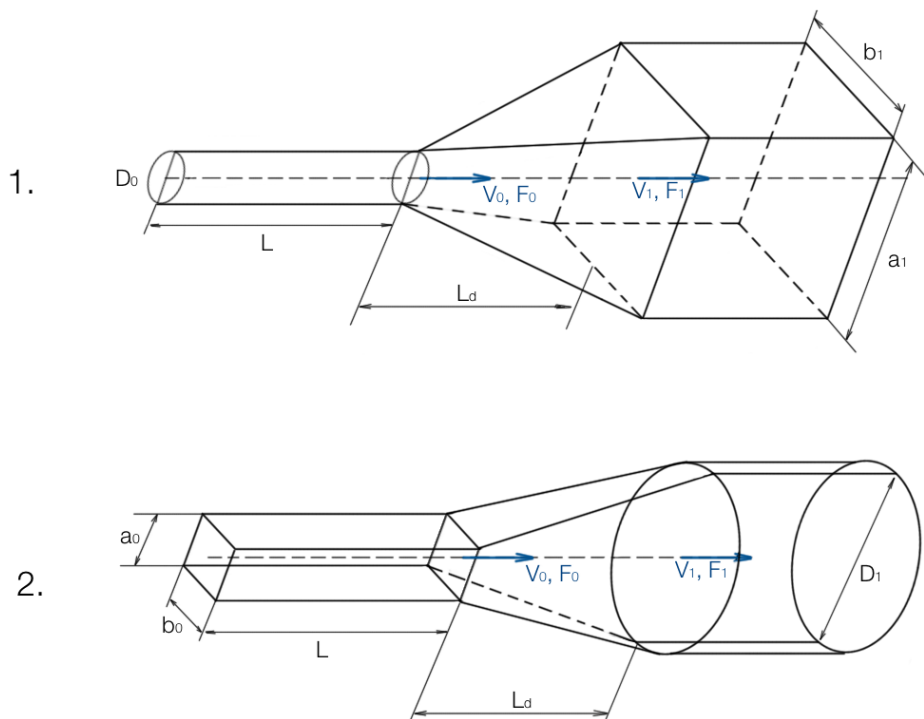


Figure 7: Transition diffusers

Curved diffusers

Within the limits $0,1 \leq F_0/F_1 \leq 0,9$:

$$\zeta = \frac{\Delta H}{\frac{V_0^2}{2g}} \cong \varphi_0 \sigma_0 d$$

Where:

$\sigma_0 = 1,43 - \frac{1,3F_0}{F_1}$ can be determined from the curve $\sigma_0 = f\left(\frac{F_0}{F_1}\right)$ of Graph 17

$d = \left(1 - \frac{F_0}{F_1}\right)^2$ can be determined from the curve $\sigma_0 = f\left(\frac{F_0}{F_1}\right)$ of Graph 17

$\varphi_0 = f\left(\frac{l}{D_h}\right)$ and $\varphi_0 = f\left(\frac{l}{a_0}\right)$ can be determined from the corresponding curves of Graph 16.

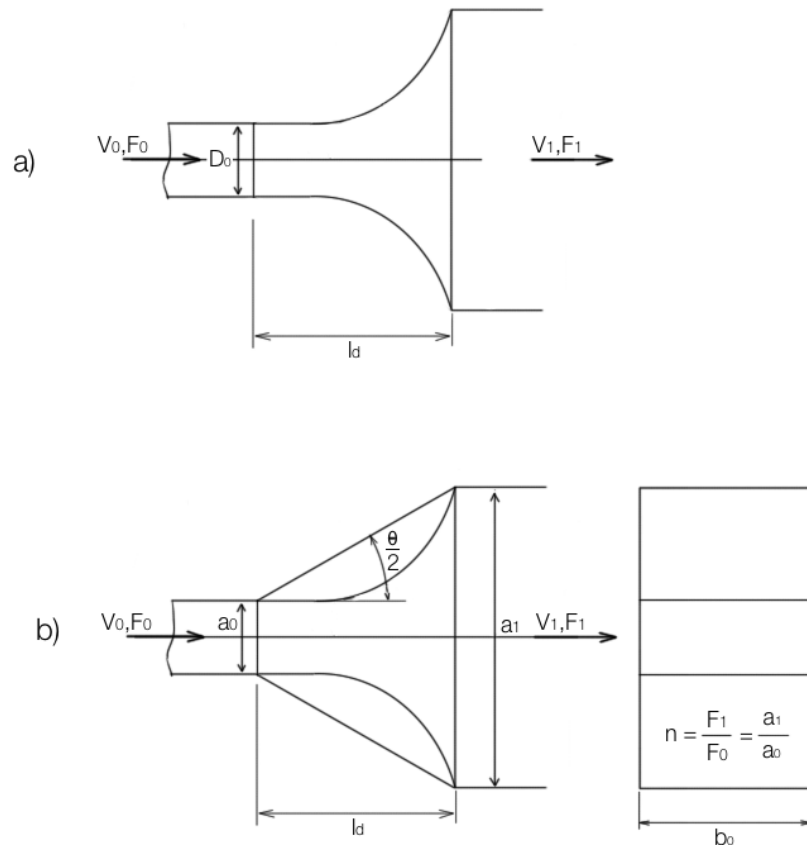
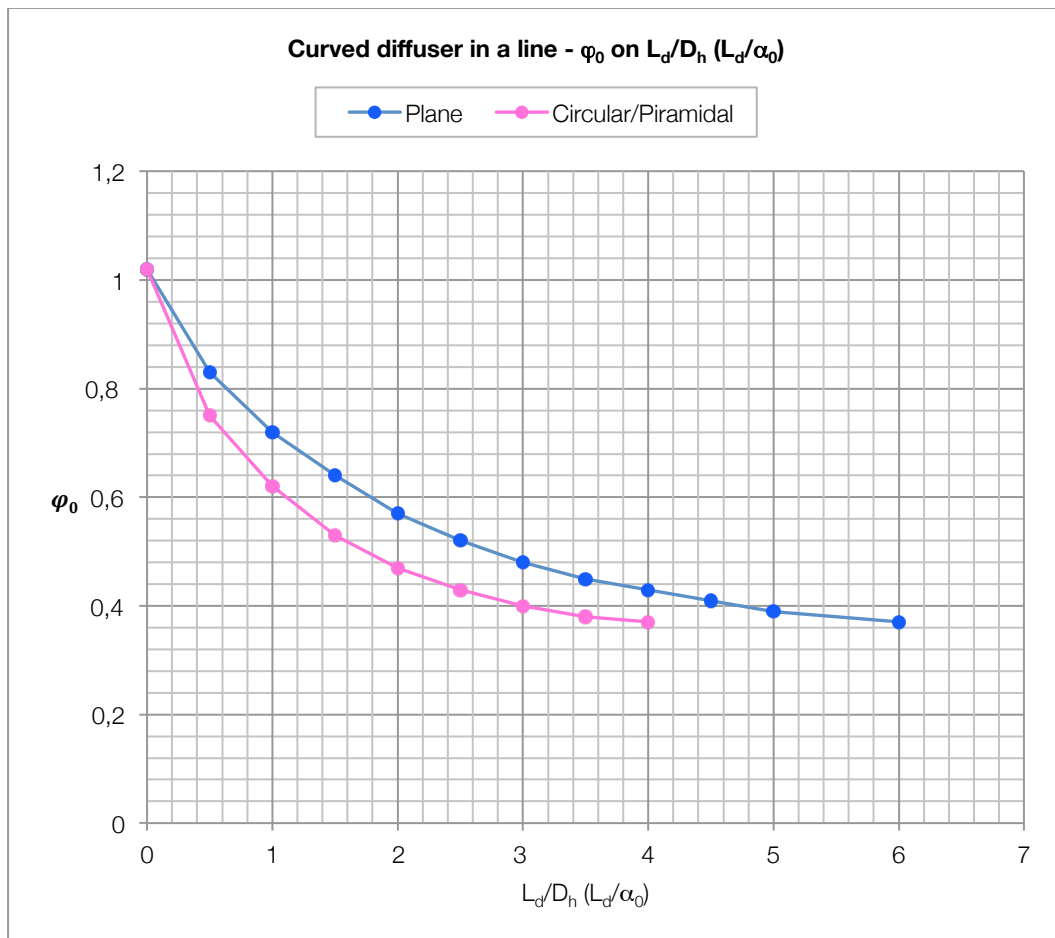


Figure 8: Curved diffusers' geometrical parameters

Table 9: values of φ_0

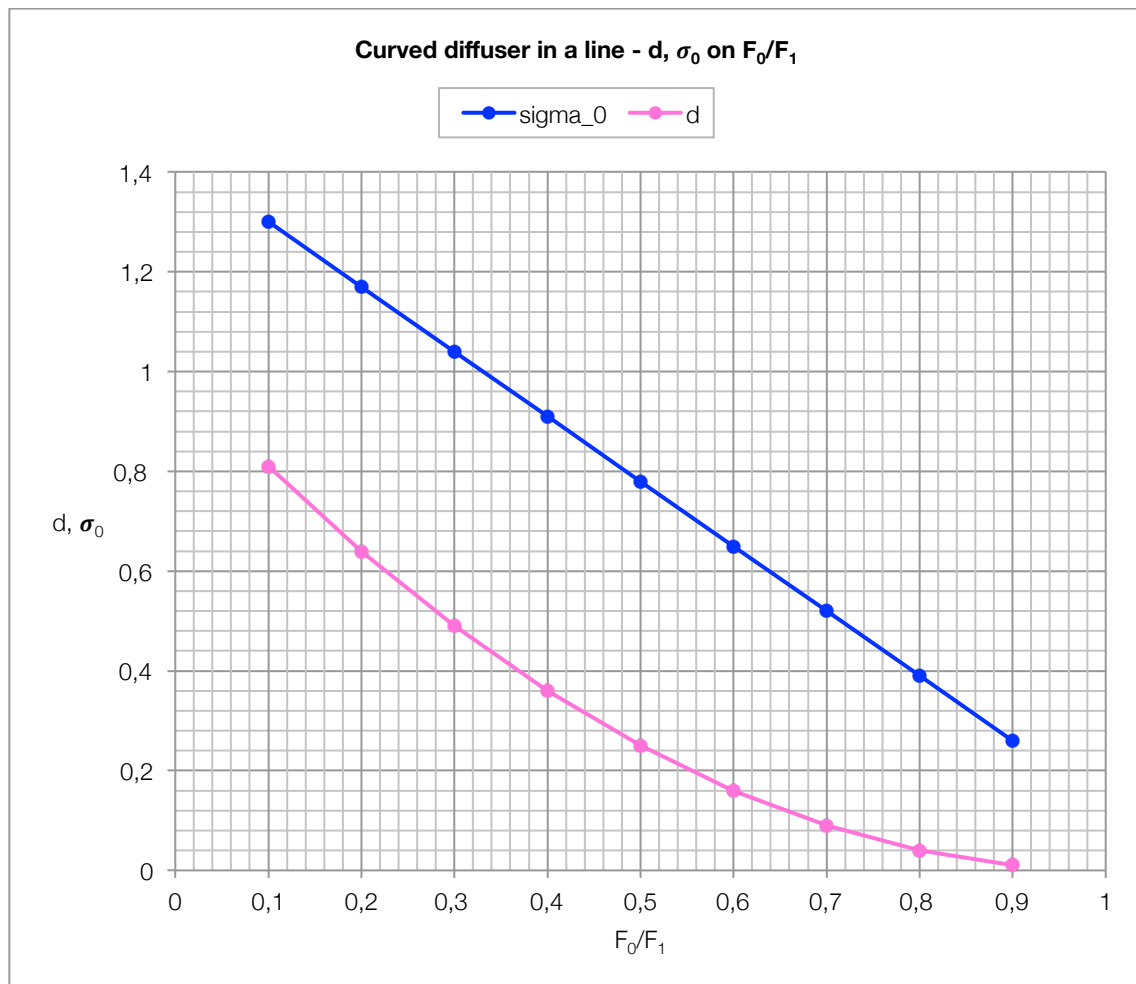
ld/Dh	φ_0	
	Circular/Piramidal	Plane
0	1,02	1,02
0,5	0,75	0,83
1,0	0,62	0,72
1,5	0,53	0,64
2,0	0,47	0,57
2,5	0,43	0,52
3,0	0,4	0,48
3,5	0,38	0,45
4,0	0,37	0,43
4,5	-	0,41
5,0	-	0,39
6,0	-	0,37



Graph 16: values of φ_0 on L_d/D_h (L_d/α_0)

Table 10: values of σ_0 and d

F_0/F_1	σ_0	d
0,1	1,3	0,81
0,2	1,17	0,64
0,3	1,04	0,49
0,4	0,91	0,36
0,5	0,78	0,25
0,6	0,65	0,16
0,7	0,52	0,09
0,8	0,39	0,04
0,9	0,26	0,01



Graph 17: values of d and σ_0 on F_0/F_1

Stepped Conical diffuser

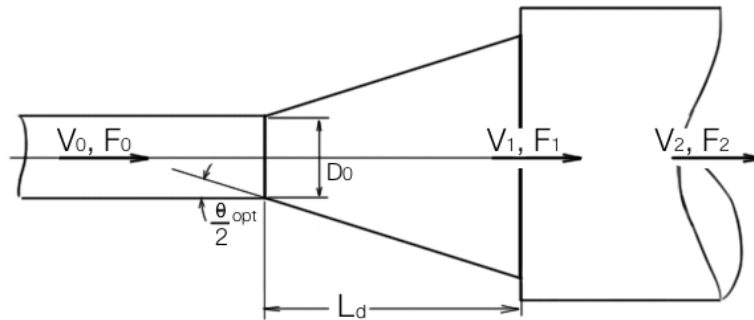


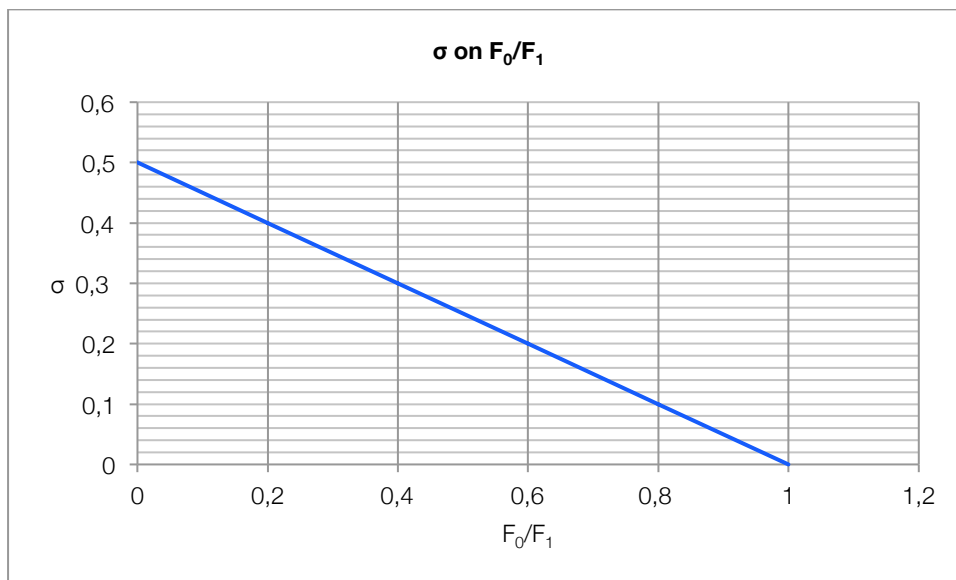
Figure 9: Stepped conical diffuser's geometrical parameters

$$\zeta = \frac{\Delta H}{\frac{V_0^2}{2g}} \cong (1 + \sigma)\zeta_{min}$$

The formula may be used for selecting the optimum angle α_{opt} from Graph 20

ζ_{min} is determined from Graph 19 as a function of L_d/D_0 and n

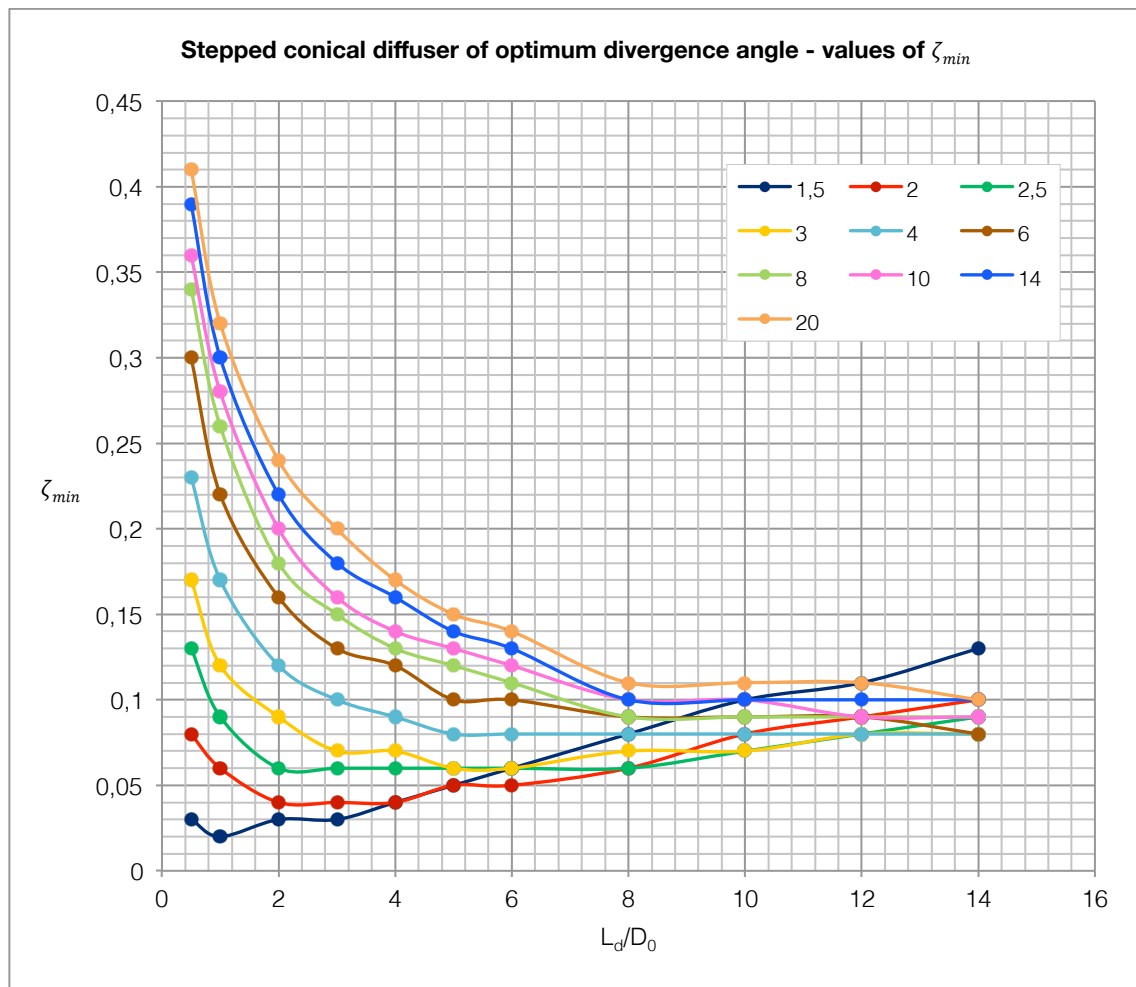
σ is determined approximately from Graph 18 as a function of F_0/F_1 .



Graph 18: values of σ on F_0/F_1

Table 11: values of ζ_{min}

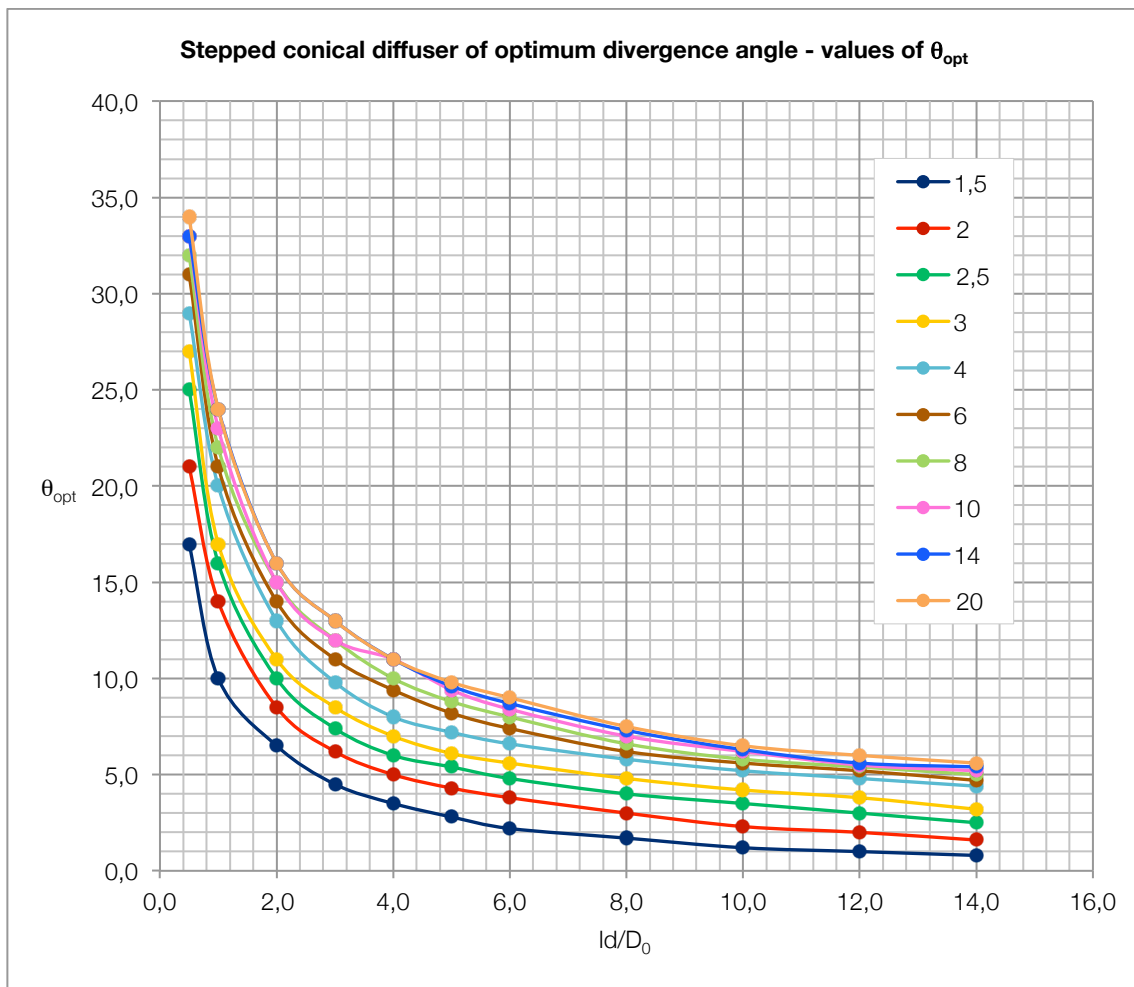
l_d/D_0	n									
	1,5	2	2,5	3	4	6	8	10	14	20
0,5	0,03	0,08	0,13	0,17	0,23	0,3	0,34	0,36	0,39	0,41
1	0,02	0,06	0,09	0,12	0,17	0,22	0,26	0,28	0,3	0,32
2	0,03	0,04	0,06	0,09	0,12	0,16	0,18	0,2	0,22	0,24
3	0,03	0,04	0,06	0,07	0,1	0,13	0,15	0,16	0,18	0,2
4	0,04	0,04	0,06	0,07	0,09	0,12	0,13	0,14	0,16	0,17
5	0,05	0,05	0,06	0,06	0,08	0,1	0,12	0,13	0,14	0,15
6	0,06	0,05	0,06	0,06	0,08	0,1	0,11	0,12	0,13	0,14
8	0,08	0,06	0,06	0,07	0,08	0,09	0,09	0,1	0,1	0,11
10	0,1	0,08	0,07	0,07	0,08	0,09	0,09	0,1	0,1	0,11
12	0,11	0,09	0,08	0,08	0,08	0,09	0,09	0,09	0,1	0,11
14	0,13	0,1	0,09	0,08	0,08	0,08	0,09	0,09	0,1	0,1



Graph 19: values of ζ_{min} on L_d/D_0

Table 12: values of θ_{opt}

L_d/D_0	n									
	1,5	2	2,5	3	4	6	8	10	14	20
0,5	17,0	21,0	25,0	27,0	29,0	31,0	32,0	33,0	33,0	34,0
1,0	10,0	14,0	16,0	17,0	20,0	21,0	22,0	23,0	24,0	24,0
2,0	6,5	8,5	10,0	11,0	13,0	14,0	15,0	15,0	16,0	16,0
3,0	4,5	6,2	7,4	8,5	9,8	11,0	12,0	12,0	13,0	13,0
4,0	3,5	5,0	6,0	7,0	8,0	9,4	10,0	11,0	11,0	11,0
5,0	2,8	4,3	5,4	6,1	7,2	8,2	8,8	9,4	9,6	9,8
6,0	2,2	3,8	4,8	5,6	6,6	7,4	8,0	8,4	8,7	9,0
8,0	1,7	3,0	4,0	4,8	5,8	6,2	6,6	7,0	7,3	7,5
10,0	1,2	2,3	3,5	4,2	5,2	5,6	5,8	6,2	6,3	6,5
12,0	1,0	2,0	3,0	3,8	4,8	5,2	5,4	5,5	5,6	6,0
14,0	0,8	1,6	2,5	3,2	4,4	4,7	5,0	5,2	5,4	5,6



Graph 20: values of θ_{opt} on L_d/D_0

Stepped Pyramidal diffuser

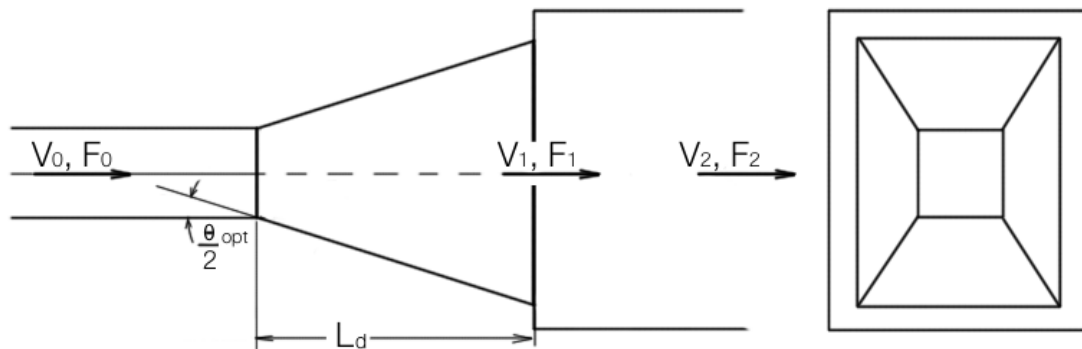


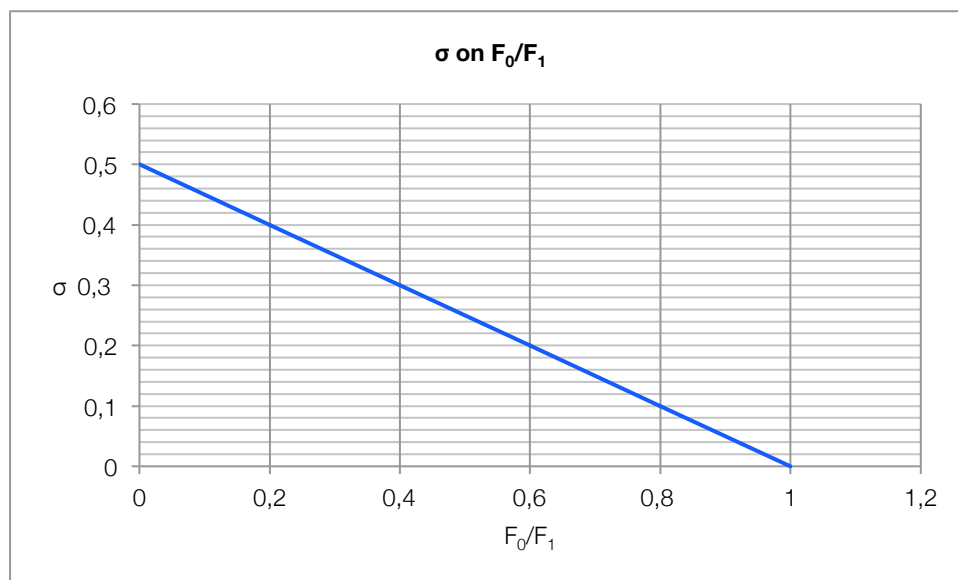
Figure 10: Stepped pyramidal diffuser's geometrical parameters

$$\zeta = \frac{\Delta H}{\frac{V_0^2}{2g}} \cong (1 + \sigma)\zeta_{min}$$

The formula may be used for selecting the optimum angle α_{opt} from Graph 23

ζ_{min} is determined from Graph 22 as a function of l_d/D_h and n

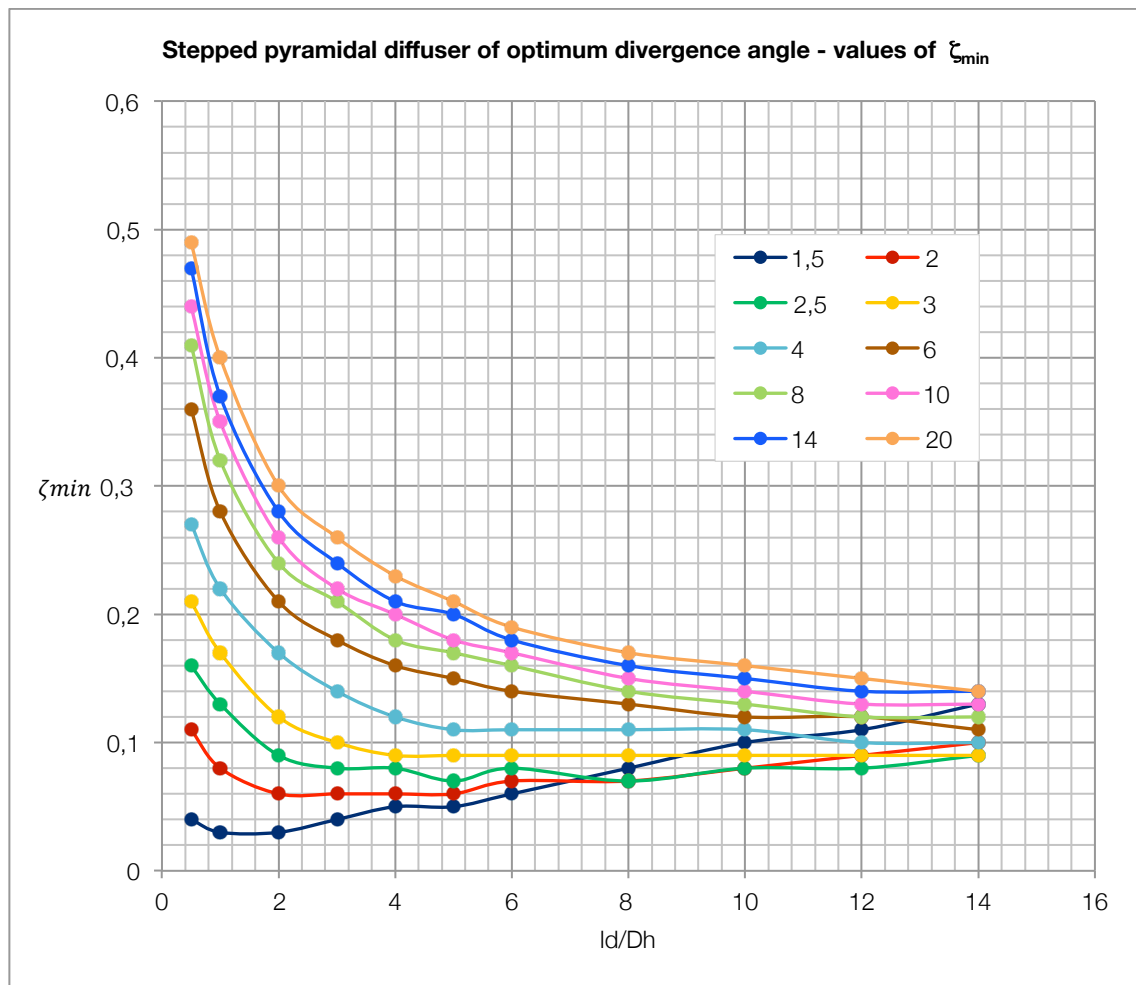
σ is determined approximately from Graph 21 graph as a function of F_0/F_1 .



Graph 21: values of σ on F_0/F_1

Table 13: values of ζ_{min}

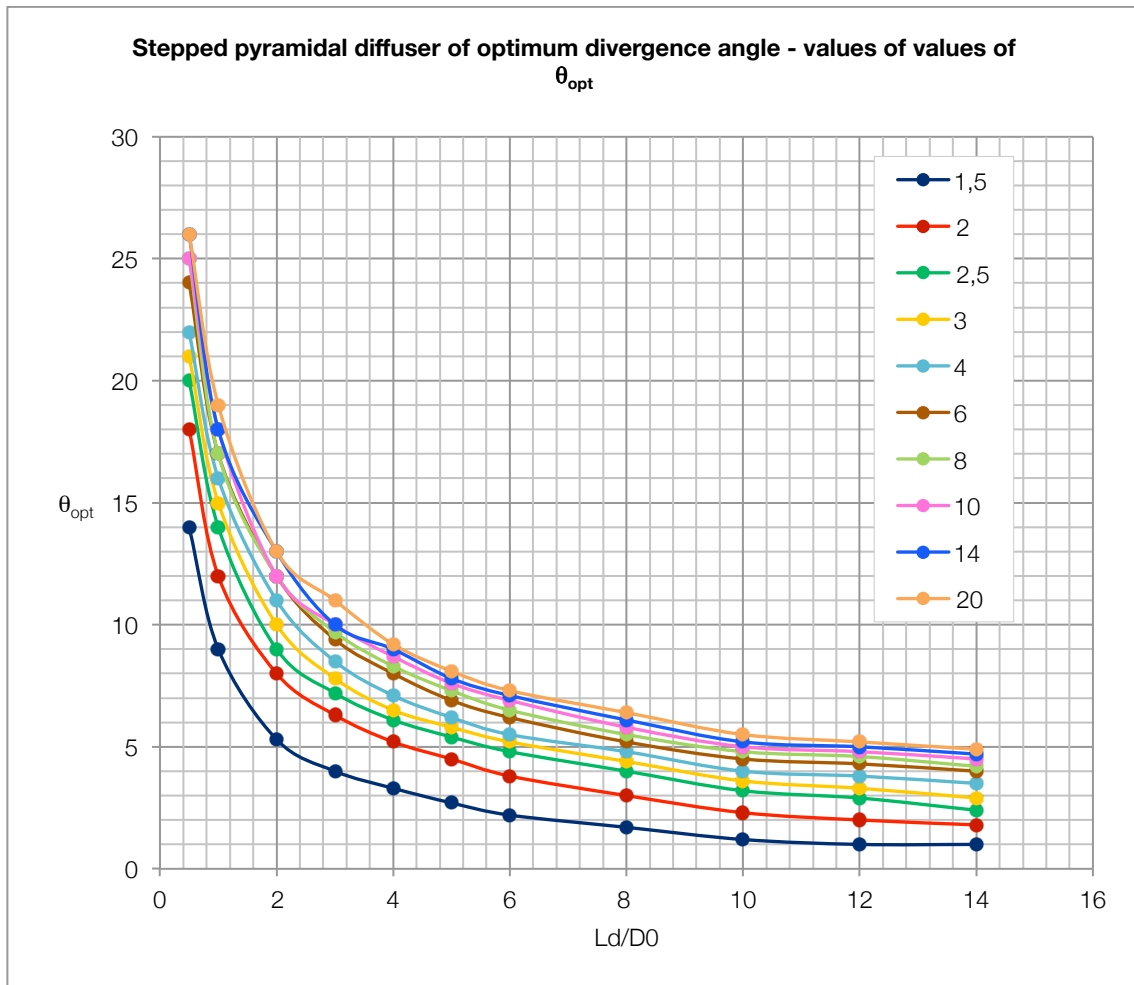
l_d/D_h	n									
	1,5	2	2,5	3	4	6	8	10	14	20
0,5	0,04	0,11	0,16	0,21	0,27	0,36	0,41	0,44	0,47	0,49
1	0,03	0,08	0,13	0,17	0,22	0,28	0,32	0,35	0,37	0,4
2	0,03	0,06	0,09	0,12	0,17	0,21	0,24	0,26	0,28	0,3
3	0,04	0,06	0,08	0,1	0,14	0,18	0,21	0,22	0,24	0,26
4	0,05	0,06	0,08	0,09	0,12	0,16	0,18	0,2	0,21	0,23
5	0,05	0,06	0,07	0,09	0,11	0,15	0,17	0,18	0,2	0,21
6	0,06	0,07	0,08	0,09	0,11	0,14	0,16	0,17	0,18	0,19
8	0,08	0,07	0,07	0,09	0,11	0,13	0,14	0,15	0,16	0,17
10	0,1	0,08	0,08	0,09	0,11	0,12	0,13	0,14	0,15	0,16
12	0,11	0,09	0,08	0,09	0,1	0,12	0,12	0,13	0,14	0,15
14	0,13	0,1	0,09	0,09	0,1	0,11	0,12	0,13	0,14	0,14



Graph 22: values of ζ_{min} on L_d/D_h

Table 14: values of θ_{opt}

l_d/D_0	n									
	1,5	2	2,5	3	4	6	8	10	14	20
0,5	14	18	20	21	22	24	25	25	26	26
1	9	12	14	15	16	17	17	18	18	19
2	5,3	8	9	10	11	12	12	12	13	13
3	4	6,3	7,2	7,8	8,5	9,4	9,7	10	10	11
4	3,3	5,2	6,1	6,5	7,1	8	8,3	8,7	9	9,2
5	2,7	4,5	5,4	5,8	6,2	6,9	7,3	7,6	7,8	8,1
6	2,2	3,8	4,8	5,2	5,5	6,2	6,5	6,9	7,1	7,3
8	1,7	3	4	4,4	4,8	5,2	5,5	5,8	6,1	6,4
10	1,2	2,3	3,2	3,6	4	4,5	4,8	5	5,2	5,5
12	1	2	2,9	3,3	3,8	4,3	4,6	4,8	5	5,2
14	1	1,8	2,4	2,9	3,5	4	4,2	4,5	4,7	4,9



Graph 23: values of θ_{opt} on l_d/D_h

Stepped Plane diffuser

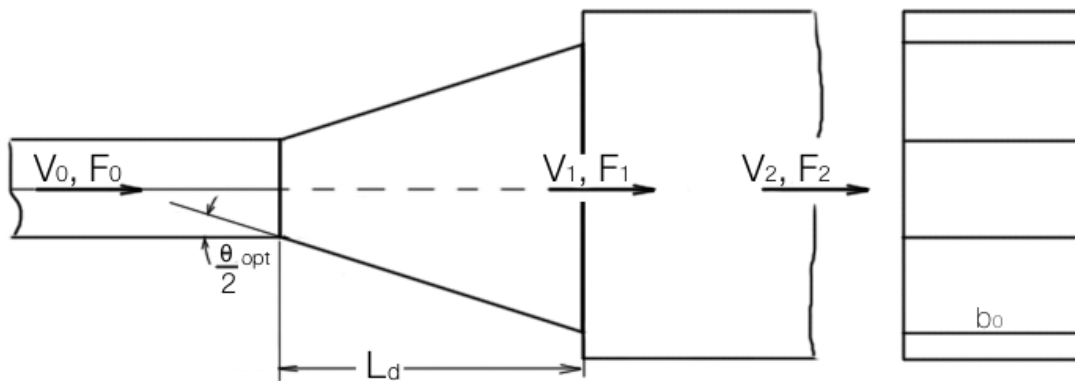


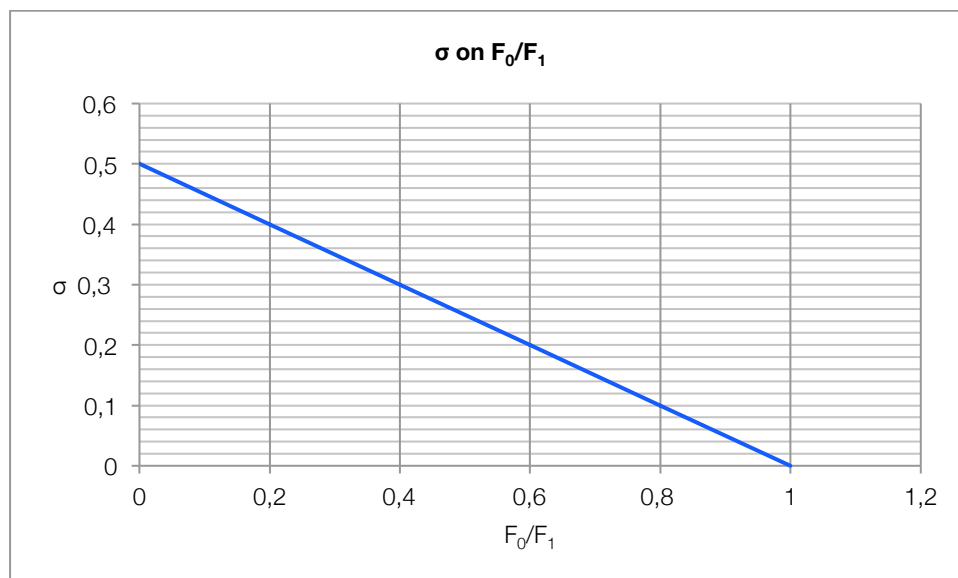
Figure 11: Stepped plane diffuser's geometrical parameters

$$\zeta = \frac{\Delta H}{\frac{V_0^2}{2g}} \cong (1 + \sigma)\zeta_{min}$$

The formula may be used for selecting the optimum angle θ_{opt} from Graph 26

ζ_{min} is determined from Graph 25 as a function of l_d/θ_0 and n

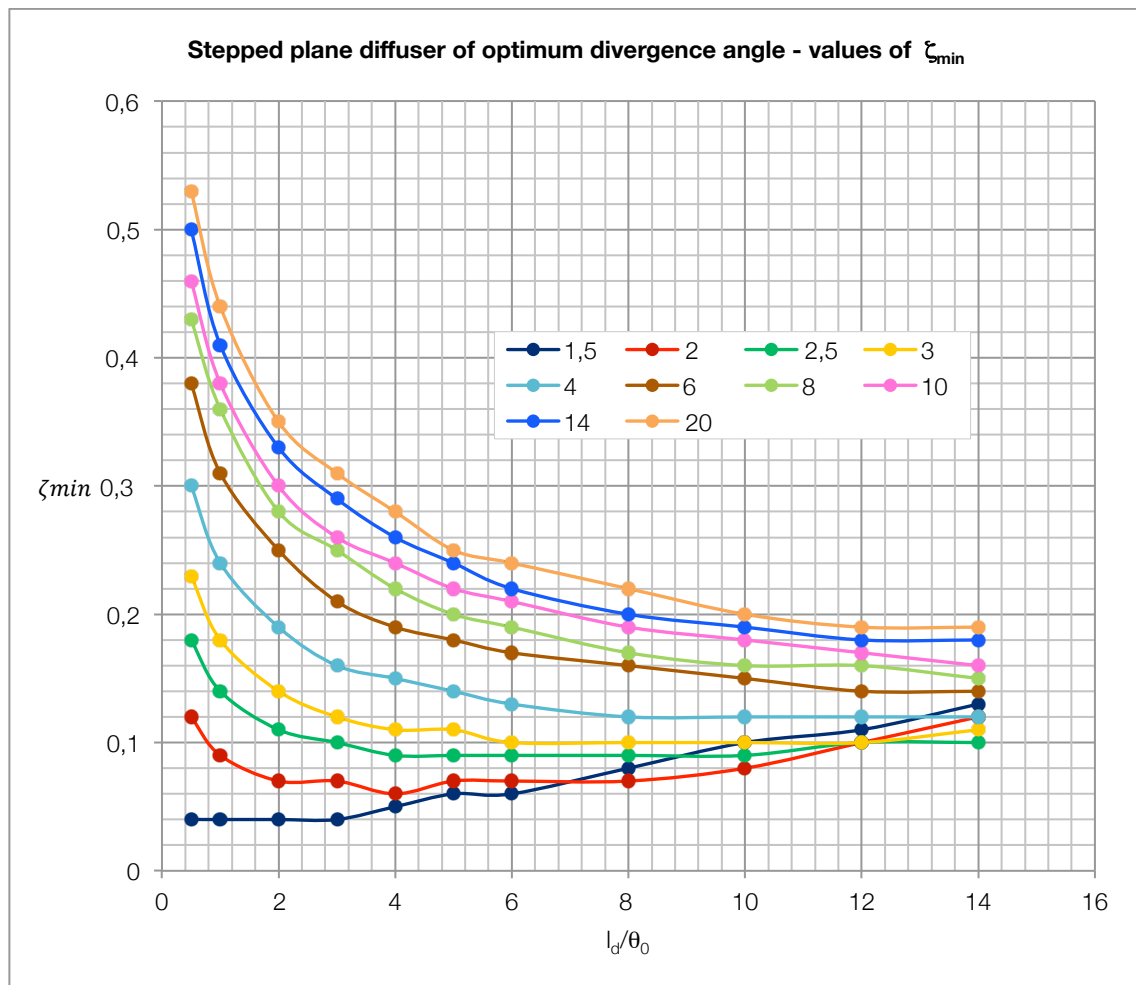
σ is determined approximately from Graph 24 as a function of F_0/F_1 .



Graph 24: values of σ on F_0/F_1

Table 15: values of ζ_{min}

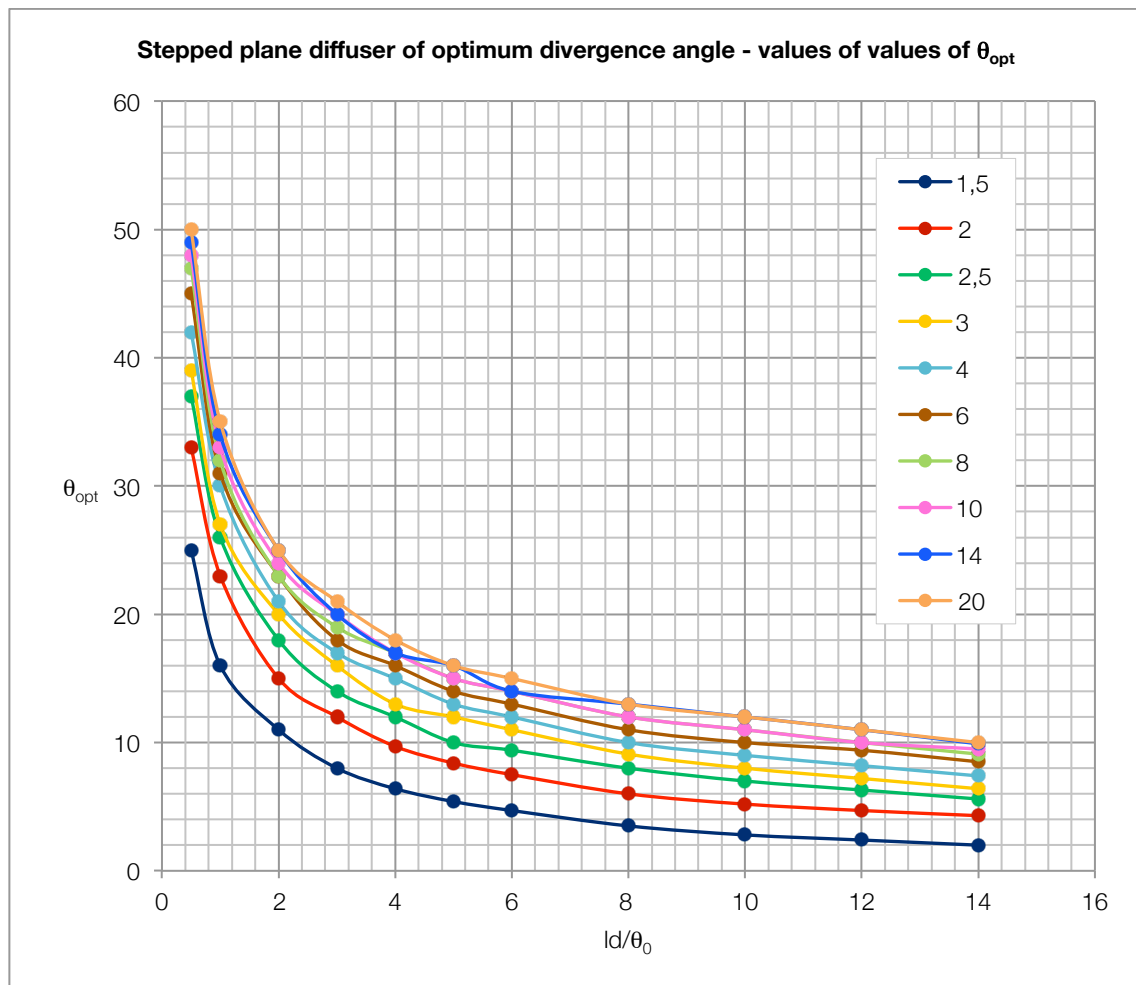
ld/θ_0	n									
	1,5	2	2,5	3	4	6	8	10	14	20
0,5	0,04	0,12	0,18	0,23	0,3	0,38	0,43	0,46	0,5	0,53
1	0,04	0,09	0,14	0,18	0,24	0,31	0,36	0,38	0,41	0,44
2	0,04	0,07	0,11	0,14	0,19	0,25	0,28	0,3	0,33	0,35
3	0,04	0,07	0,1	0,12	0,16	0,21	0,25	0,26	0,29	0,31
4	0,05	0,06	0,09	0,11	0,15	0,19	0,22	0,24	0,26	0,28
5	0,06	0,07	0,09	0,11	0,14	0,18	0,2	0,22	0,24	0,25
6	0,06	0,07	0,09	0,1	0,13	0,17	0,19	0,21	0,22	0,24
8	0,08	0,07	0,09	0,1	0,12	0,16	0,17	0,19	0,2	0,22
10	0,1	0,08	0,09	0,1	0,12	0,15	0,16	0,18	0,19	0,2
12	0,11	0,1	0,1	0,1	0,12	0,14	0,16	0,17	0,18	0,19
14	0,13	0,12	0,1	0,11	0,12	0,14	0,15	0,16	0,18	0,19



Graph 25: values of ζ_{min} on L_d/θ_0

Table 16: values of θ_{opt}

L_d/θ_0	n									
	1,5	2	2,5	3	4	6	8	10	14	20
0,5	25	33	37	39	42	45	47	48	49	50
1,0	16	23	26	27	30	31	32	33	34	35
2,0	11	15	18	20	21	23	23	24	25	25
3,0	8	12	14	16	17	18	19	20	20	21
4,0	6,4	9,7	12	13	15	16	17	17	17	18
5,0	5,4	8,4	10	12	13	14	15	15	16	16
6,0	4,7	7,5	9,4	11	12	13	14	14	14	15
8,0	3,5	6	8	9,1	10	11	12	12	13	13
10,0	2,8	5,2	7	8	9	10	11	11	12	12
12,0	2,4	4,7	6,3	7,2	8,2	9,4	10	10	11	11
14,0	2	4,3	5,6	6,4	7,4	8,5	9,1	9,5	9,9	10



Graph 26: values of θ_{opt} on l_d/θ_0

Short diffusers with guiding devices or with resistance at the exit

<i>Guiding device</i>	<i>Schematic Diagram</i>	<i>Resistance coefficient</i>												
<p>Dividing Walls</p> <p>Number of dividing walls</p> <table border="1" style="margin-left: auto; margin-right: auto; border-collapse: collapse;"> <tr> <td style="padding: 2px;">θ°</td> <td style="padding: 2px;">30</td> <td style="padding: 2px;">45</td> <td style="padding: 2px;">60</td> <td style="padding: 2px;">90</td> <td style="padding: 2px;">120</td> </tr> <tr> <td style="padding: 2px;">ζ</td> <td style="padding: 2px;">2</td> <td style="padding: 2px;">4</td> <td style="padding: 2px;">6</td> <td style="padding: 2px;">6</td> <td style="padding: 2px;">6+8</td> </tr> </table>	θ°	30	45	60	90	120	ζ	2	4	6	6	6+8		<p>$\zeta \cong 0,65\zeta_d$</p> <p>Where ζ_d is determined from the corresponding graphs.</p>
θ°	30	45	60	90	120									
ζ	2	4	6	6	6+8									
<p>Baffles</p>		<p>$\zeta \cong 0,65\zeta_d$</p> <p>Where ζ_d is determined from the corresponding graphs.</p>												

10 Bends

List of the chapter symbols

Latin characters:

- g = specific gravity [m/s^2];
- V = mean velocity of the stream [m/s];

Greek characters:

- α_b = Reynolds number correction factor;
- α_{rough} = roughness correction factor;
- β_b = outlet tangent correction factor;
- ΔH = head loss [m];
- ζ = resistance coefficient;
- ζ_{correct} = resistance coefficient obtained with correction factors;
- λ_{rough} = friction coefficient for rough pipe;
- λ_{smooth} = friction coefficient for smooth pipe;
- θ = angle of the bend [$^\circ$];

10.1 Introduction

The change of direction in duct systems is possible thanks to devices called bends. In this fittings there are minor head losses in both cases of mitre variation and of circular arc bends. The tangents refer to the section pipe at inlet and exit from the bend.

In Figure 1 is represented the geometry of bends with their geometric parameters that are used to compute the minor loss coefficient ζ that is defined as for the other fittings/devices in this thesis:

$$\zeta = \frac{\Delta H}{V^2/2g}$$

In this formula, the parameter V^2 is referred to the mean velocity at inlet section.

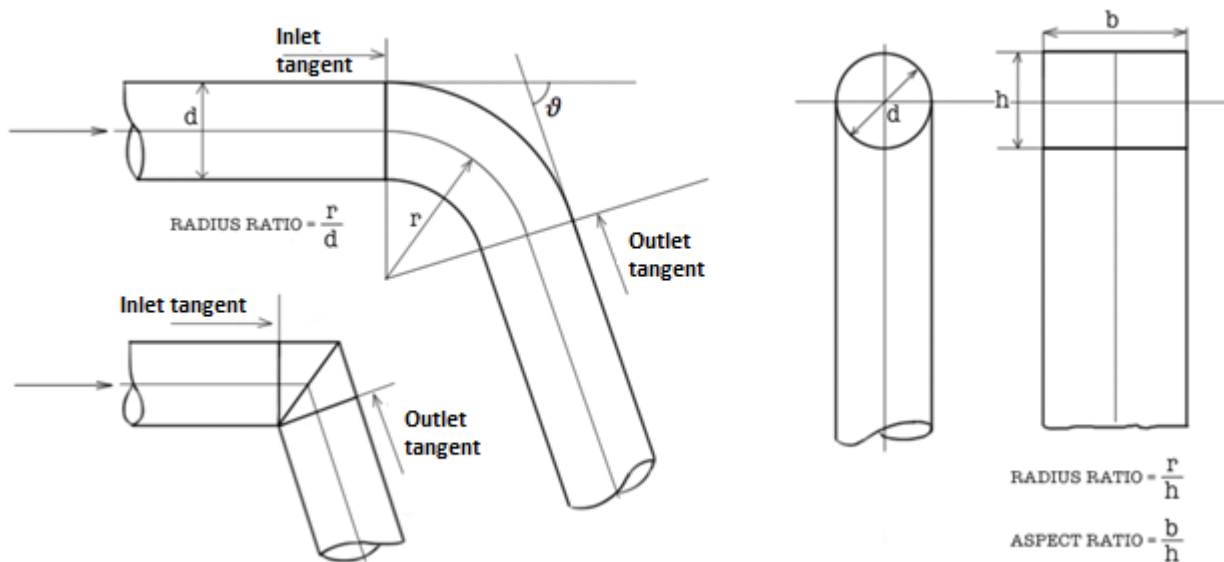


Figure 1: bend geometry

It is important to state that the minor loss coefficients defined here are the sum of the contributes of the head loss caused by the detachment of the flow path at the bend inlet and the loss caused by the redevelopment of the stream after the bend (at outlet bend). The former one could reach the value of the 50% of the head at inlet.

In commerce there are a lot of types of bend and every manufacturer gives the performance graph for every product. Looking for theoretical approaches to the subject, there are a lot of websites and literature about it, which makes loss coefficients available.

Miller (Miller, 1973) refers minor loss coefficients for circular arc bends with smooth internal surface and for mitre bends.

10.2 Circular arc bends

For circular arc bends the basic loss coefficients are quoted in performance graphs for Reynolds number 10^6 and they can be used without underestimating the head loss for outlet tangents of 3 diameters or more, and for the following conditions:

- Smooth internal surface
- For bends located 2 or more pipe diameters after another bend of radius ratio > 1 ;
- For bends located 4 or more pipe diameters after another bend of radius ratio < 1 , for a diffuser, for a sudden expansion or for any other component having a loss coefficient of less than one velocity head (dynamic pressure);
- For bends located 6 or more pipe diameters after any disturbance having a loss coefficient greater than one velocity head, such a partially open valve, pressure differential flow meter etc.

If the outlet tangent is shorter than 30 diameters a correction can be applied.

In the following graphs are represented curves that define the loss coefficients for the following cross sections:

- | | |
|-------------------------------------|---------|
| 1. Circular; | Graph 1 |
| 2. Square, aspect ratio = 1; | Graph 2 |
| 3. Rectangular, aspect ratio = 0,5; | Graph 3 |
| 4. Rectangular, aspect ratio = 2; | Graph 4 |

Correction factors

The Reynolds number correction factor α_b , given in graph has to be used to compute the correct minor loss factor with the formula:

$$\zeta_{correct} = \zeta \cdot \alpha_b$$

The roughness correction factor α_{rough} is used by multiplying the smooth bend loss coefficient by the ratio of the rough to smooth friction coefficients at the appropriate Reynolds Number:

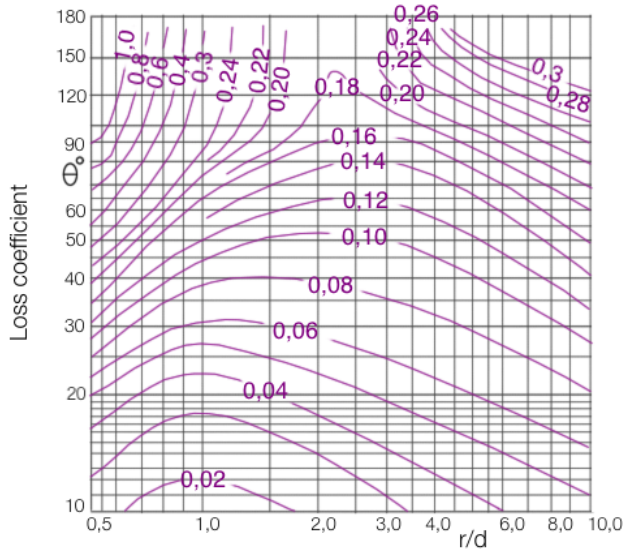
$$\zeta_{correct} = \zeta \cdot \alpha_{rough}$$

The outlet tangent correction factor β_b is used by multiplying the smooth bend loss coefficient by the coefficient itself, with the following formula:

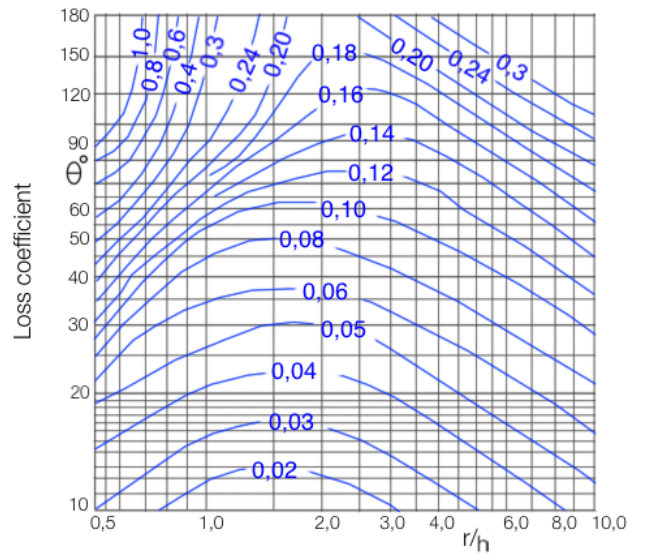
$$\zeta_{correct} = \zeta \cdot \beta_b$$

The values of the three correction factors are represented as following:

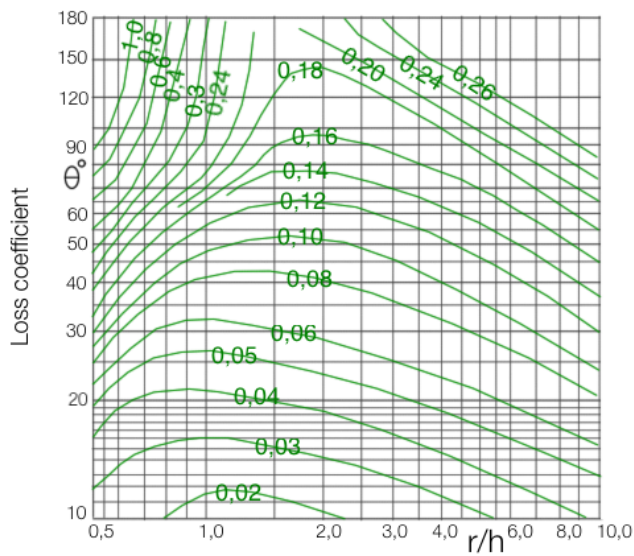
Reynolds Number correction factor α_b	Graph 5
roughness correction factor α_{rough}	$\alpha_{rough} = \frac{\lambda_{rough}}{\lambda_{smooth}}$ <p>And λ can be found in Moody graph in the introductory theoretical chapter.</p>
outlet tangent correction factor β_b	Graph 6



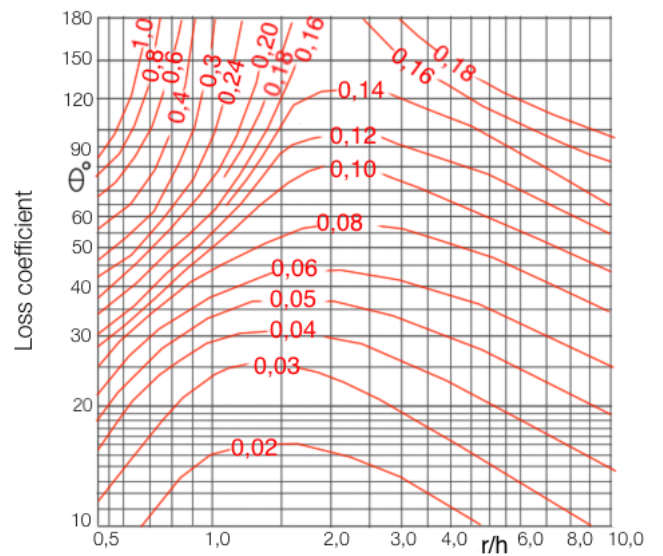
Graph 1: loss coefficient for circular cross-section bends



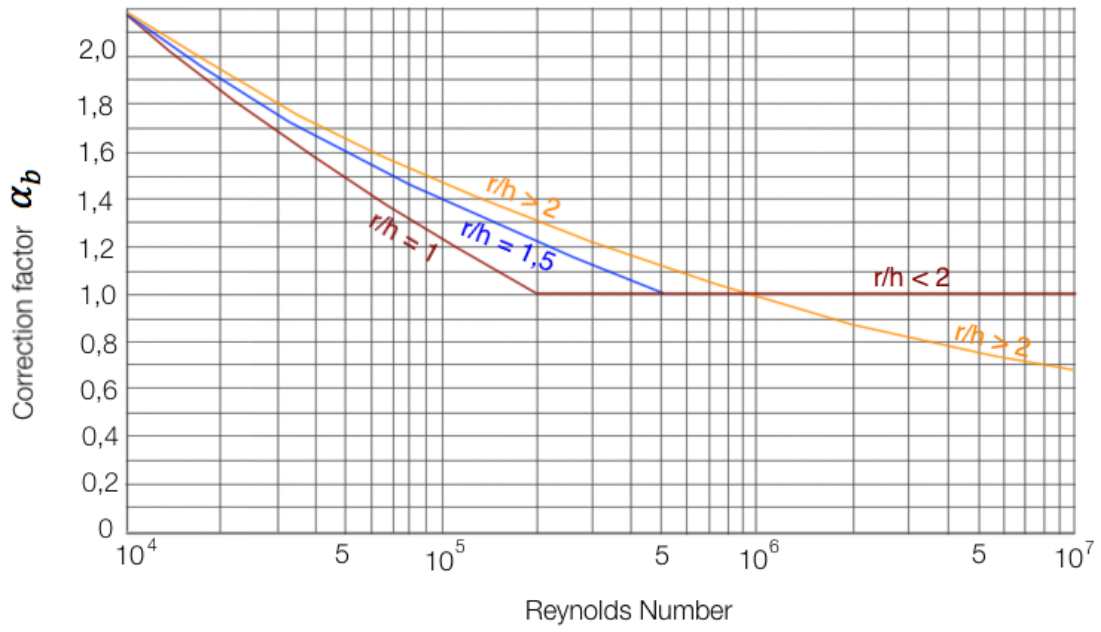
Graph 2: loss coefficients for square cross-section bends



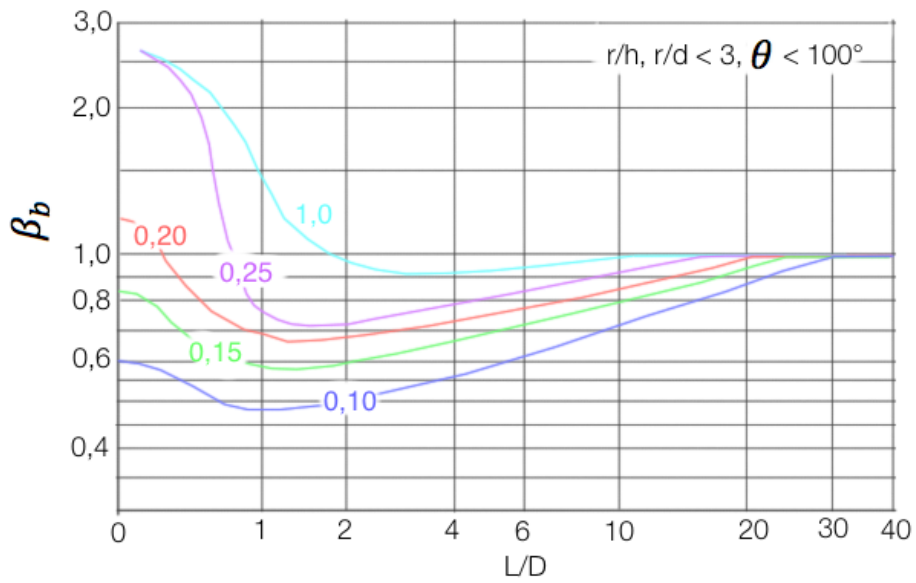
Graph 3: loss coefficients for rectangular cross-section bends (aspect ratio = 0,5)



Graph 4: loss coefficients for rectangular cross-section bends (aspect ratio = 2)



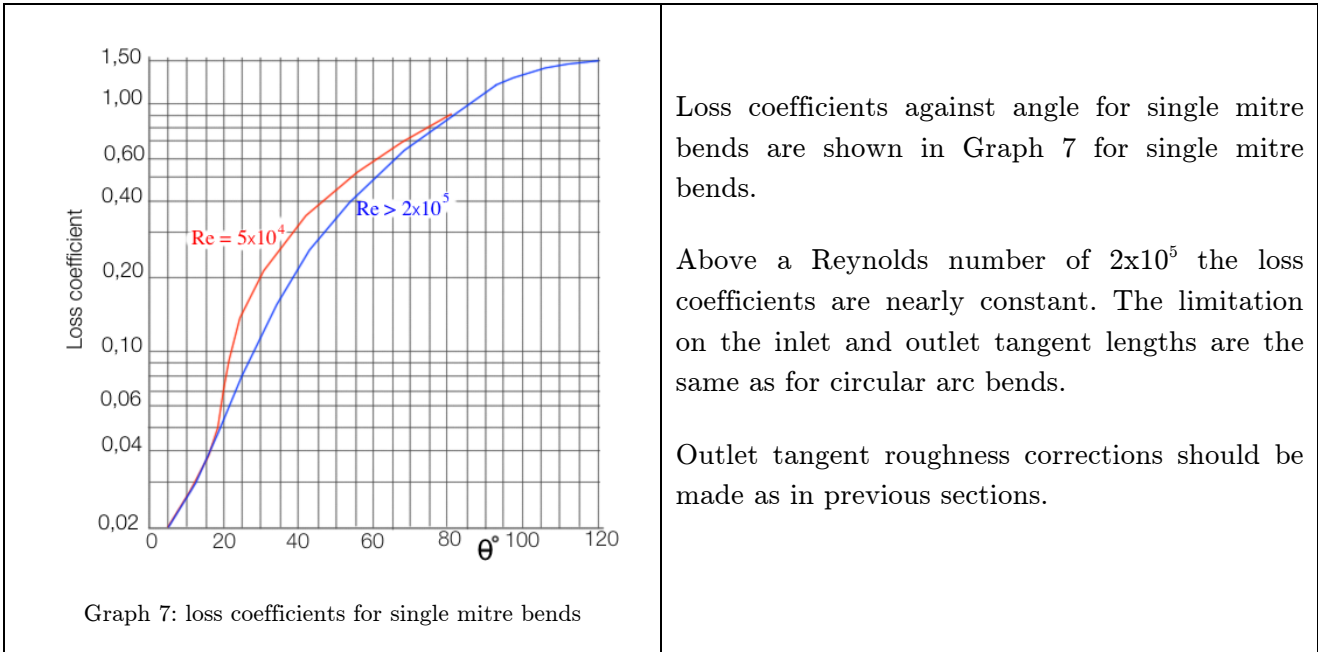
Graph 5: Reynolds number correction factor



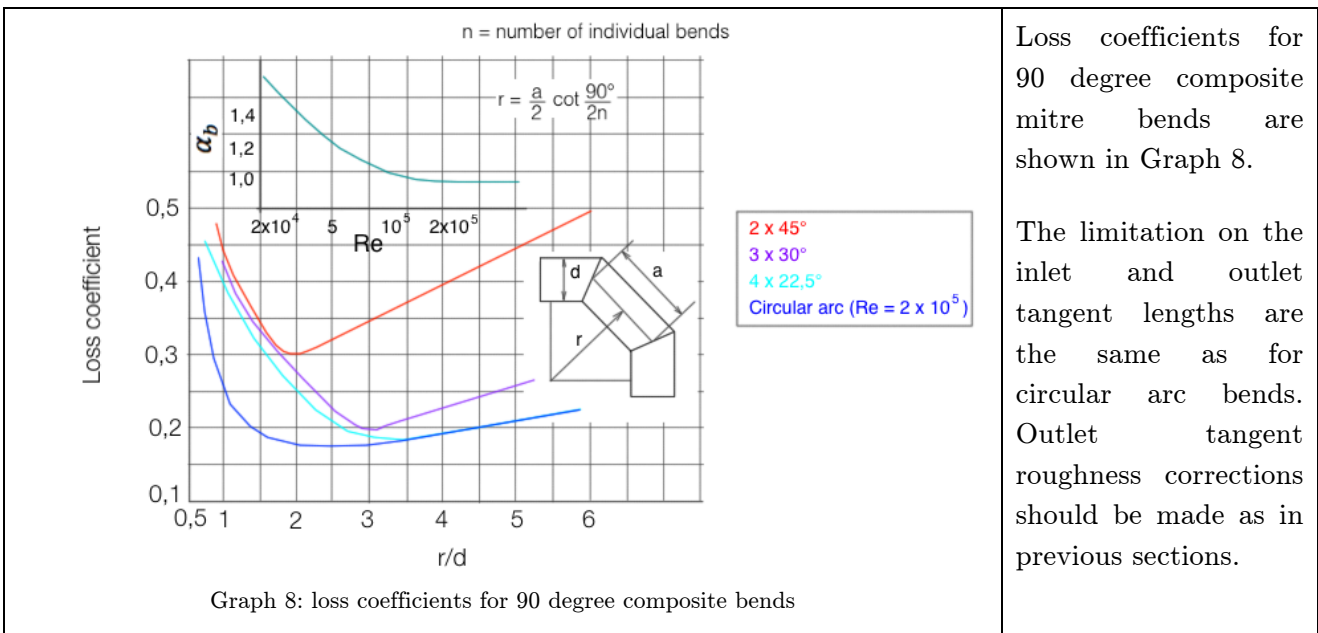
Graph 6: outlet tangent length correction

10.3 Mitre bends

Single mitre bends



90-degree composite mitre bends



11 Junctions

List of chapter symbols

Latin symbols:

- a = ratio of branch to main cross-sectional area;
- A_n = cross-sectional area of the branch n [m^2];
- C_{ij} = combining flow correction factor associate to loss coefficient ζ_{ij} ;
- q = ratio of flow in branch to the combined flow;
- Q_n = flow in the n branch, [m^3/s];
- r = ratio of radius at branch to main junction to the branch diameter;
- V_n = mean velocity value referred to the n leg of the junction [m/s];

Greek symbols:

- θ = angle of the junction, [$^\circ$]; (see Figure 1)
- ζ_{ij} = loss coefficient for flow direction i to j ; (see introduction)

11.1 Introduction

The loss coefficients given in this section are made combining and dividing flow tee junctions with Reynolds number above 10^5 in the leg carrying the combined flow. We can divide the junctions in two types, as we can see in the following figure (Figure 1): *combining flow* and *dividing flow*.

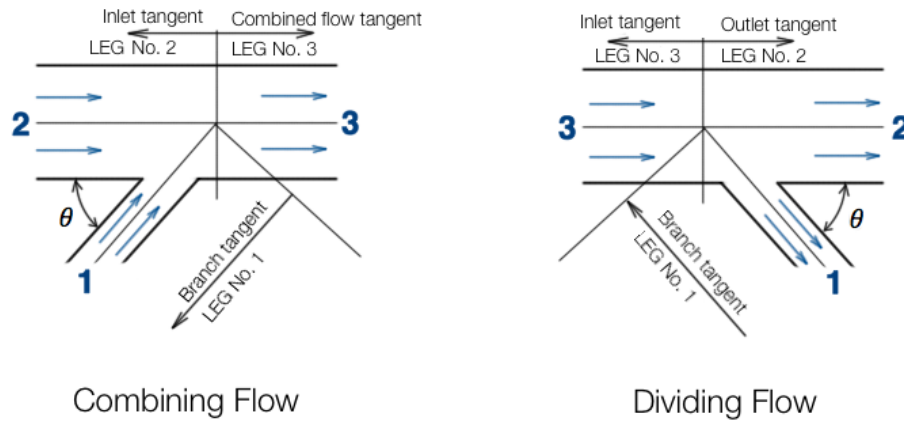


Figure 1: Notation for Combining Flow and Dividing flow

One of the most important consideration in this subject is that the cross-sectional shape of the pipes has only a secondary effect compared with the flow area ratios and with the radius at the junction of the main and branch.

The loss coefficient ζ_{ij} , for flow direction i to j , is defined as the area ratio of the total head loss between legs i to j to the mean velocity head of the combined flow.

1. Combining flow:

$$\zeta_{13} = \frac{\left(\frac{V_1^2}{2g} + h_1\right) - \left(\frac{V_3^2}{2g} + h_3\right)}{\frac{V_3^2}{2g}}$$

$$\zeta_{23} = \frac{\left(\frac{V_2^2}{2g} + h_2\right) - \left(\frac{V_3^2}{2g} + h_3\right)}{\frac{V_3^2}{2g}}$$

2. Dividing flow:

$$\zeta_{31} = \frac{\left(\frac{V_3^2}{2g} + h_3\right) - \left(\frac{V_1^2}{2g} + h_1\right)}{\frac{V_1^2}{2g}}$$

$$\zeta_{32} = \frac{\left(\frac{V_3^2}{2g} + h_3\right) - \left(\frac{V_2^2}{2g} + h_2\right)}{\frac{V_3^2}{2g}}$$

Semi empirical equations devised by Gardel have been found to be a satisfactory basis for calculating loss coefficients for tees having geometries shown in Figure 1. The equations of Gardel are:

1. Combining flow:

$$\zeta_{13} = -0,92(1 - q)^2 - q^2 \left[(1,2 - r^{1/2}) \left(\frac{\cos\theta}{a} - 1 \right) + 0,8 \left(1 - \frac{1}{a^2} \right) - (1 - a) \frac{\cos\theta}{a} \right] + (2 - a)q(1 - q)$$

$$\zeta_{23} = 0,03(1 - q)^2 - q^2 \left[1 + (1,62 - r^{1/2}) \left(\frac{\cos\theta}{a} - 1 \right) - 0,38(1 - a) \right] + (2 - a)q(1 - q)$$

2. Dividing flow:

$$\zeta_{31} = -0,95(1 - q)^2 - q^2 \left[\left(\frac{1,3 \cot(180 - \theta)}{2} - 0,3 + (0,4 - 0,1a)/a^2 \right) (1 - 0,9(r/a)^{1/2}) \right] - 0,4q(1 - q) \left(1 + \frac{1}{a} \right) \cot(180 - \theta) / 2$$

$$\zeta_{32} = -0,03(1 - q)^2 - 0,35q^2 + 0,2q(1 - q)$$

Where:

- q = ratio of flow in branch to the combined flow
- a = ratio of branch to main cross-sectional area
- r = ratio of radius at branch to main junction to the branch diameter
- θ = angle of the junction (see Figure 1)

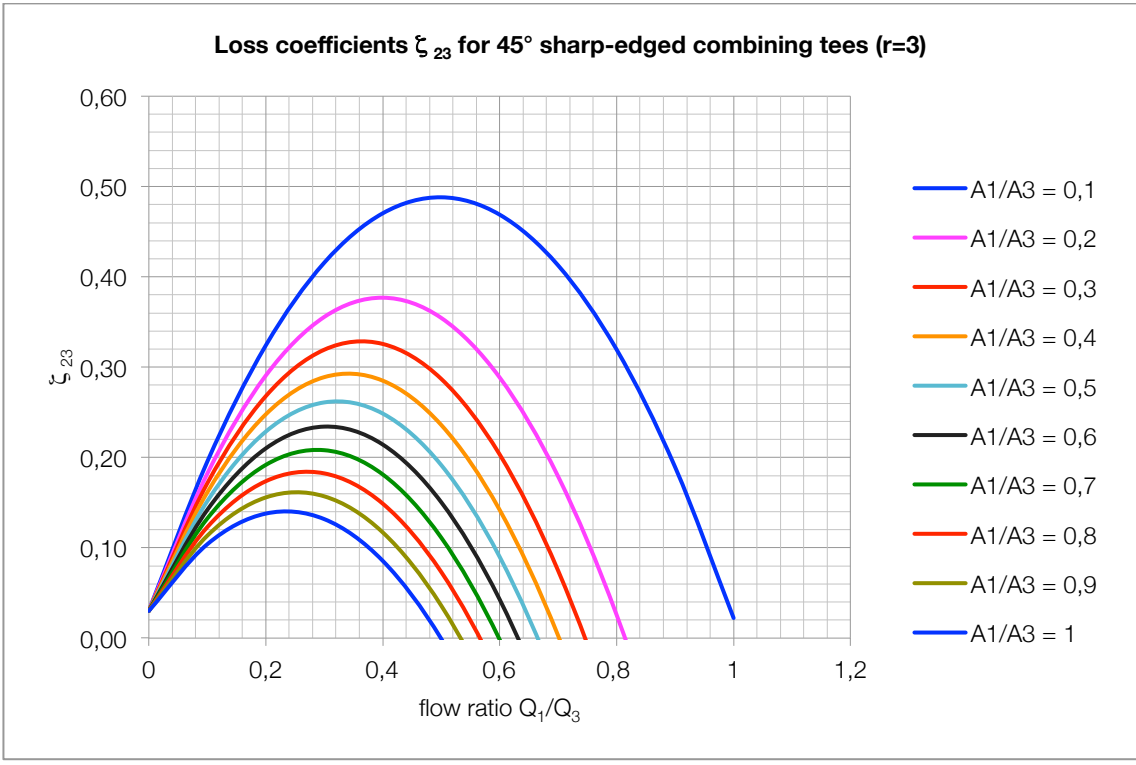
11.2 Sharp-edged combining tees

The loss coefficients for sharp-edged combining tees with a constant through flow area are shown on performance charts for the following arrangements:

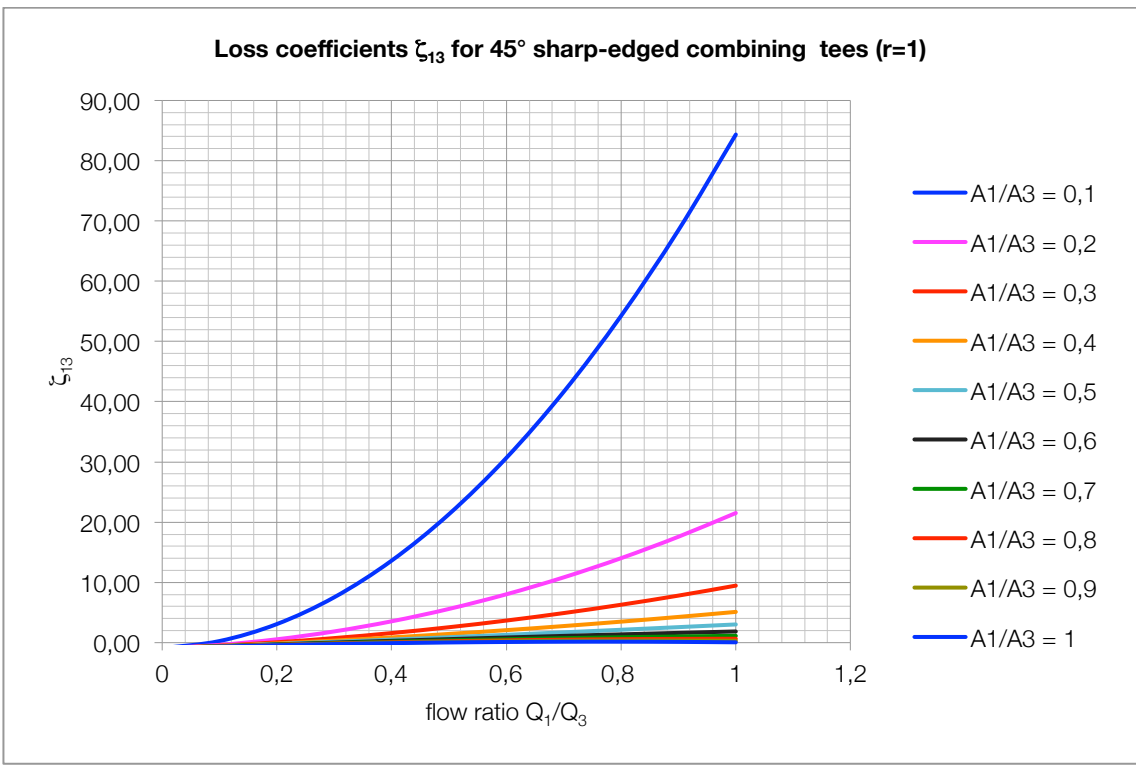
1.	45 degrees branch	ζ_{13}	Graph 2, Graph 3
2.	45 degrees branch	ζ_{23}	Graph 1
3.	90 degrees branch	ζ_{13}	Graph 5, Graph 6
4.	90 degrees branch	ζ_{23}	Graph 4

The coefficient can be used without underestimating the head loss, for tees with an outlet pipe (leg 3) of 3 diameters or more, and for the following conditions for leg 1 and 2:

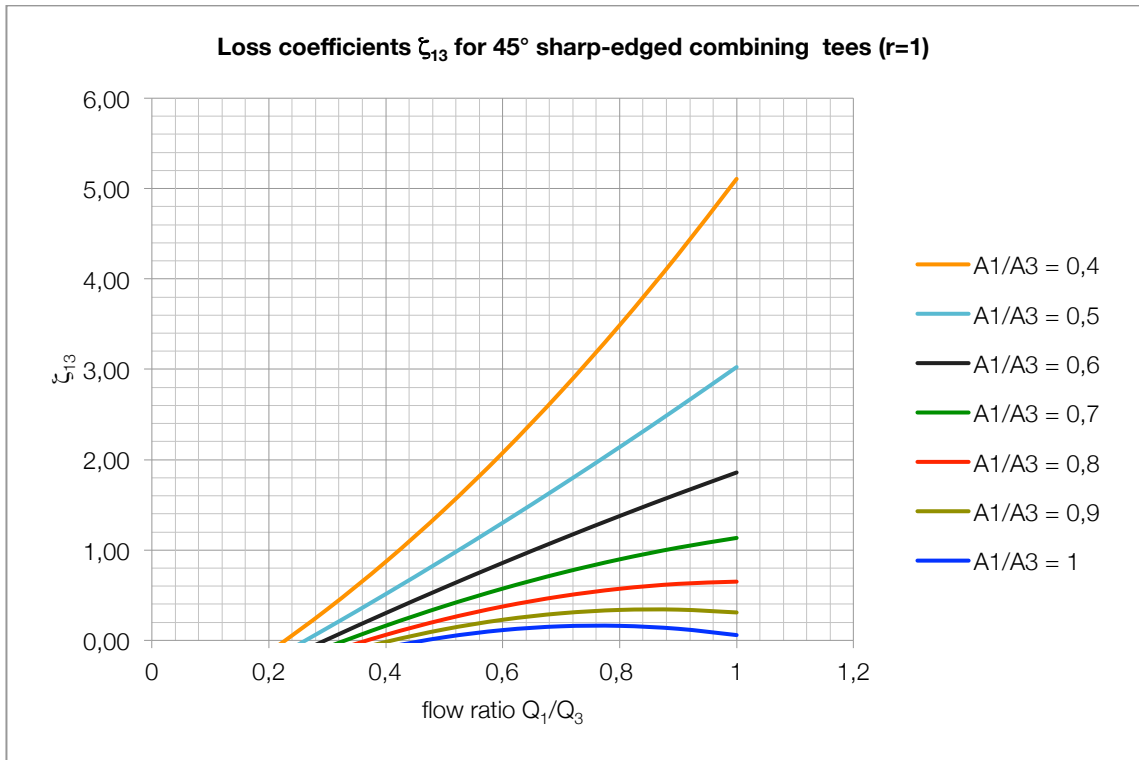
- For tees located one or more pipe diameters after a bend of radius ratio > 1 ;
- For tees located 3 or more pipe diameters after any component;



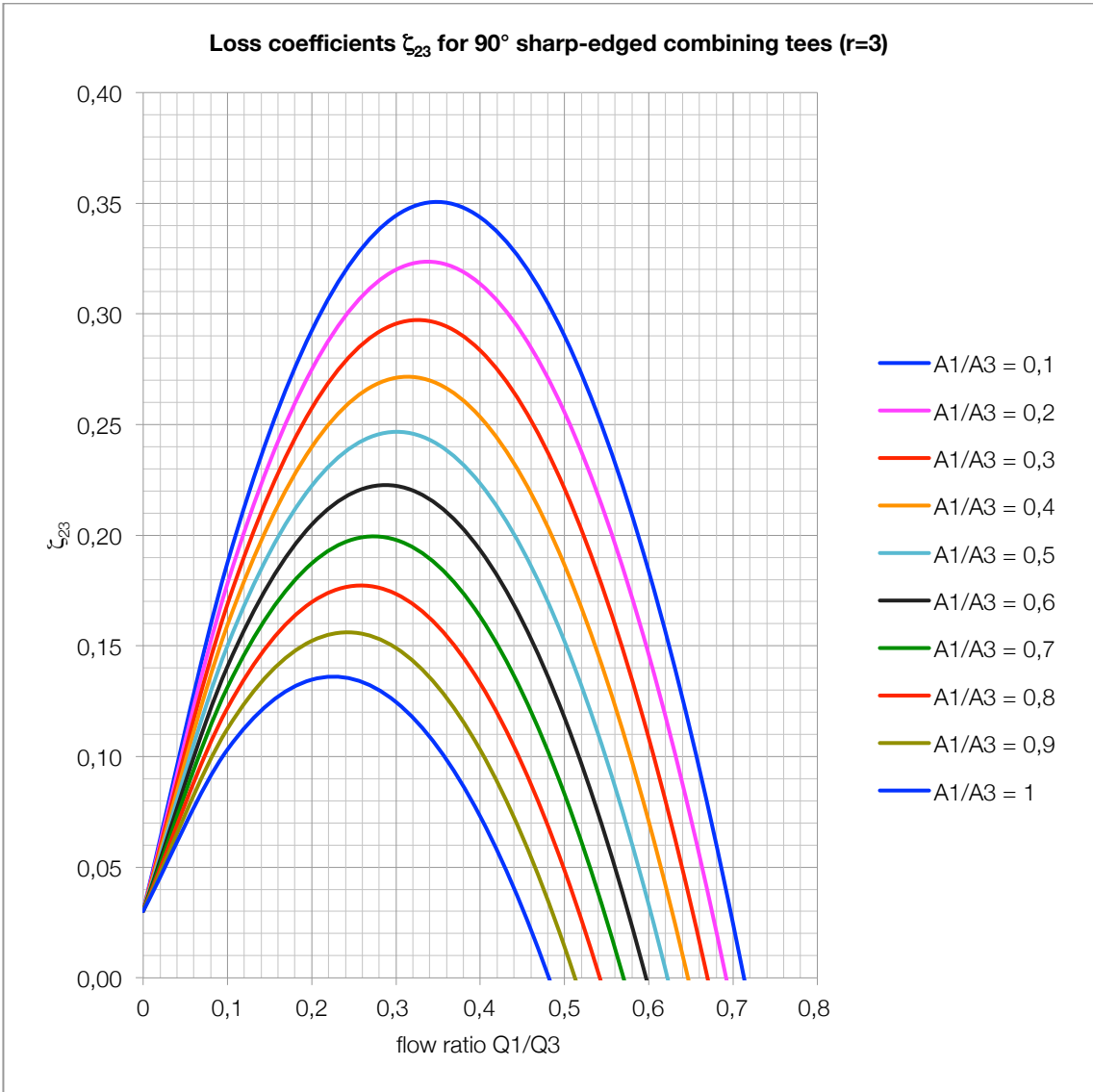
Graph 1: Loss coefficients ζ_{23} for 45 degrees sharp-edged combining tees (r=3)



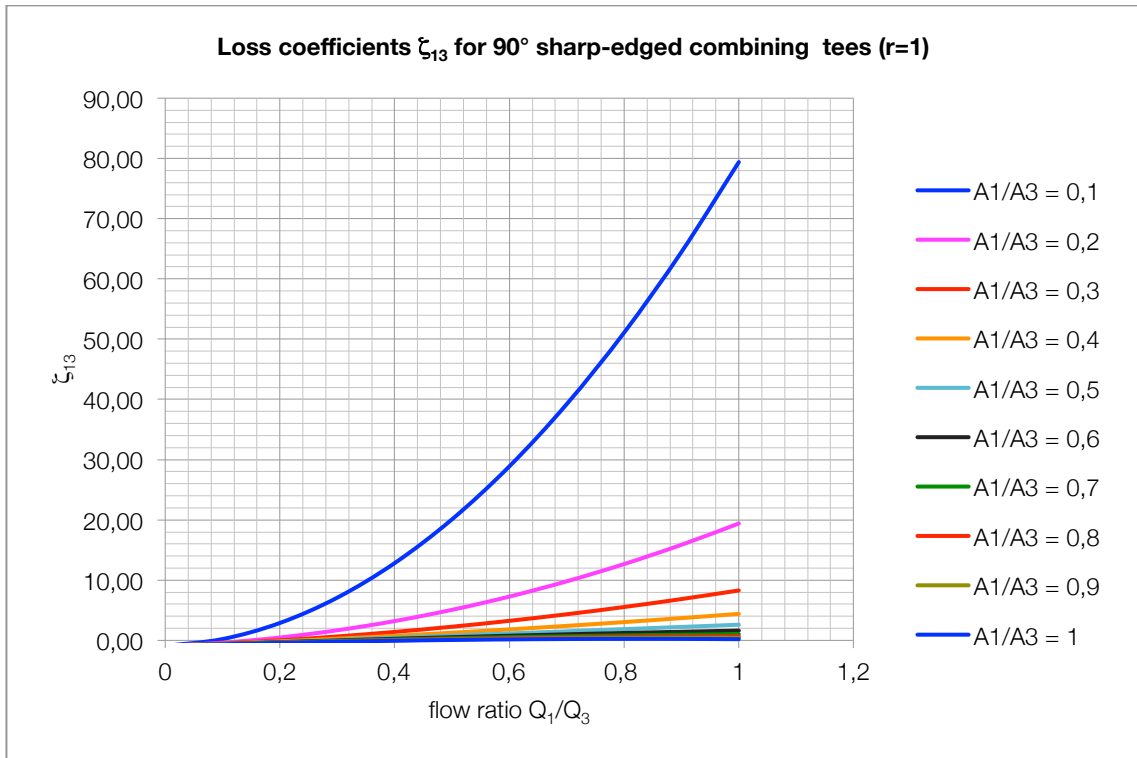
Graph 2: Loss coefficients ζ_{13} for 45 degrees sharp-edged combining tees (r=1)



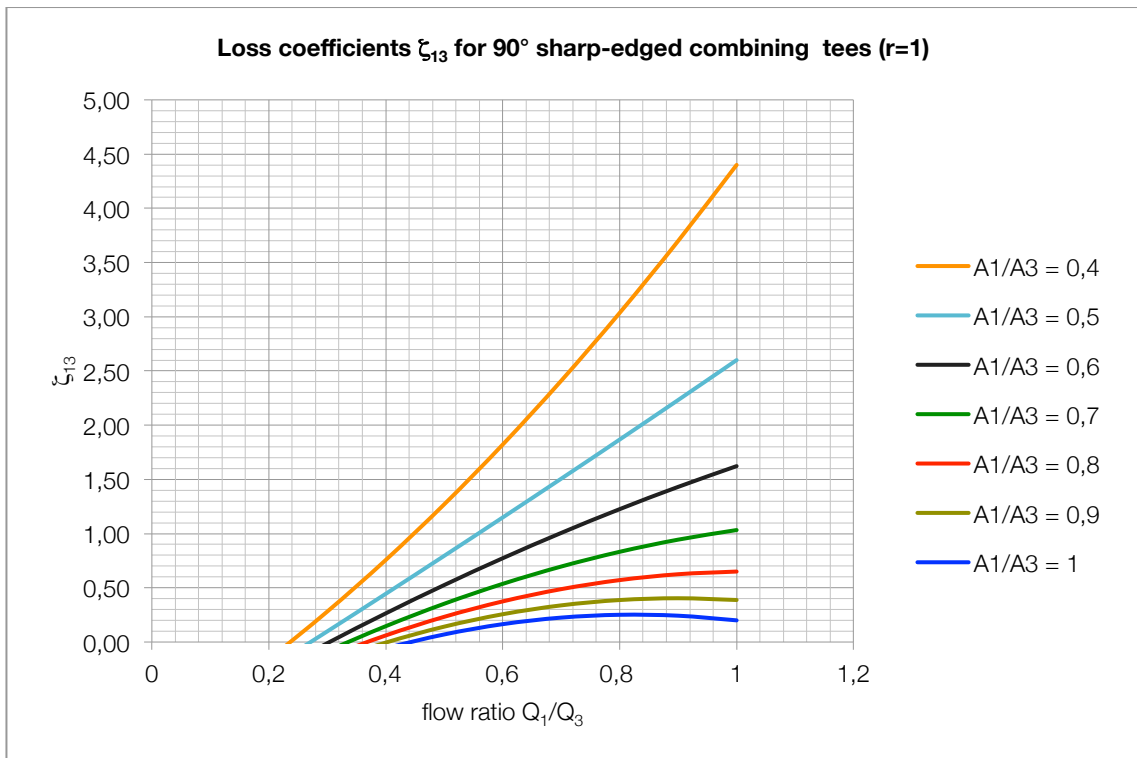
Graph 3: Loss coefficients ζ_{13} for 45 degrees sharp-edged combining tees (r=1)



Graph 4: Loss coefficients ζ_{23} for 90 degrees sharp-edged combining tees (r=3)



Graph 5: Loss coefficients ζ_{13} for 90 degrees sharp-edged combining tees ($r=1$)



Graph 6: Loss coefficients ζ_{13} for 90 degrees sharp-edged combining tees ($r=1$)

11.3 Sharp-edged dividing tees

The loss coefficients for sharp-edged dividing tees with a constant through flow area are shown on performance charts for the following arrangements:

1. 45 degrees branch ζ_{31} Graph 10, Graph 11
2. 90 degrees branch ζ_{31} Graph 8, Graph 9

The variation of the coefficient ζ_{32} is independent of the dividing flow angle and the area ratio $\frac{A_1}{A_3}$.

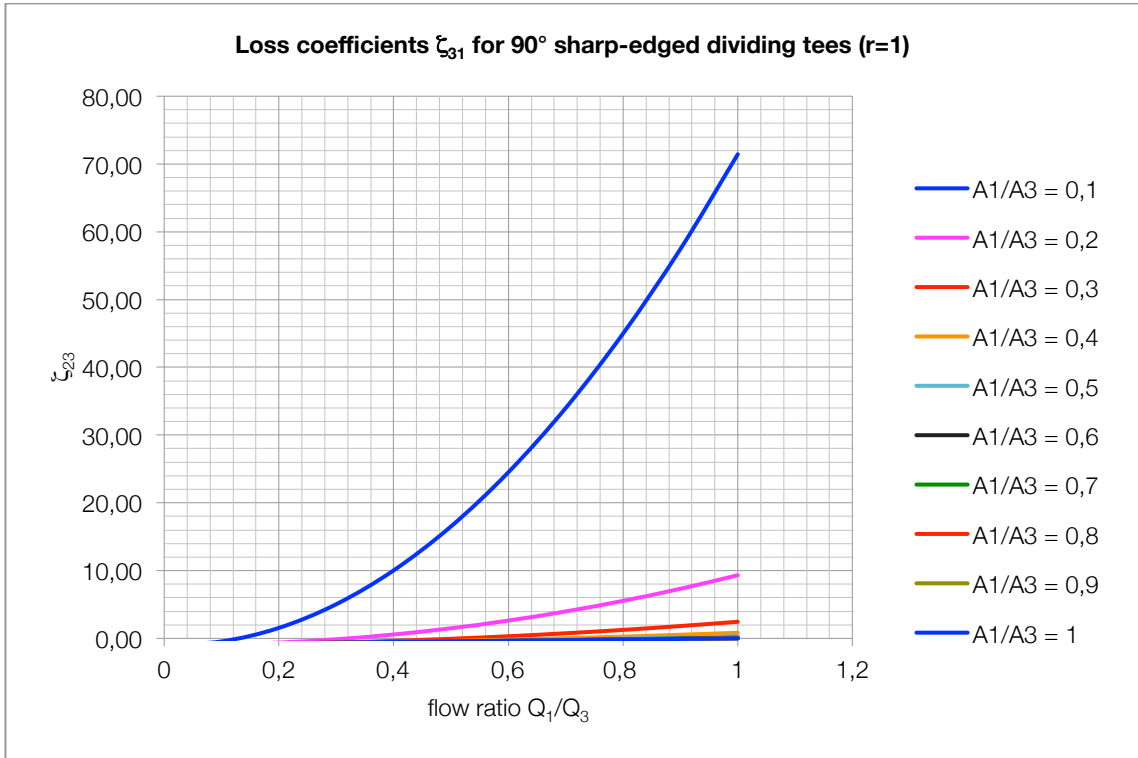
Graph 7 shows the variations of ζ_{32} with the flow ratio $\frac{Q_1}{Q_3}$.

The coefficient can be used with pipe lengths of 3 diameters or more after the tee (legs 1 and 2), and with the following inlet conditions (leg 3):

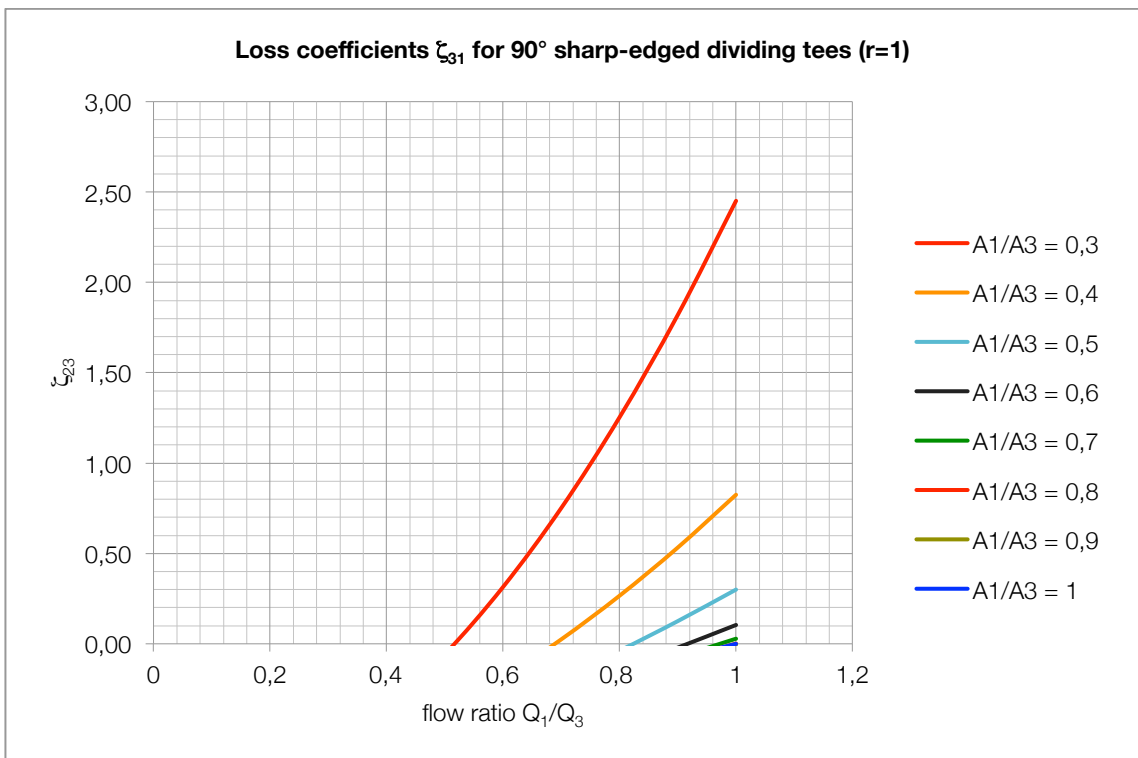
- For tees located 2 or more pipe diameters after a bend of radius ratio > 1 ;
- For tees located 4 or more diameters after any component;



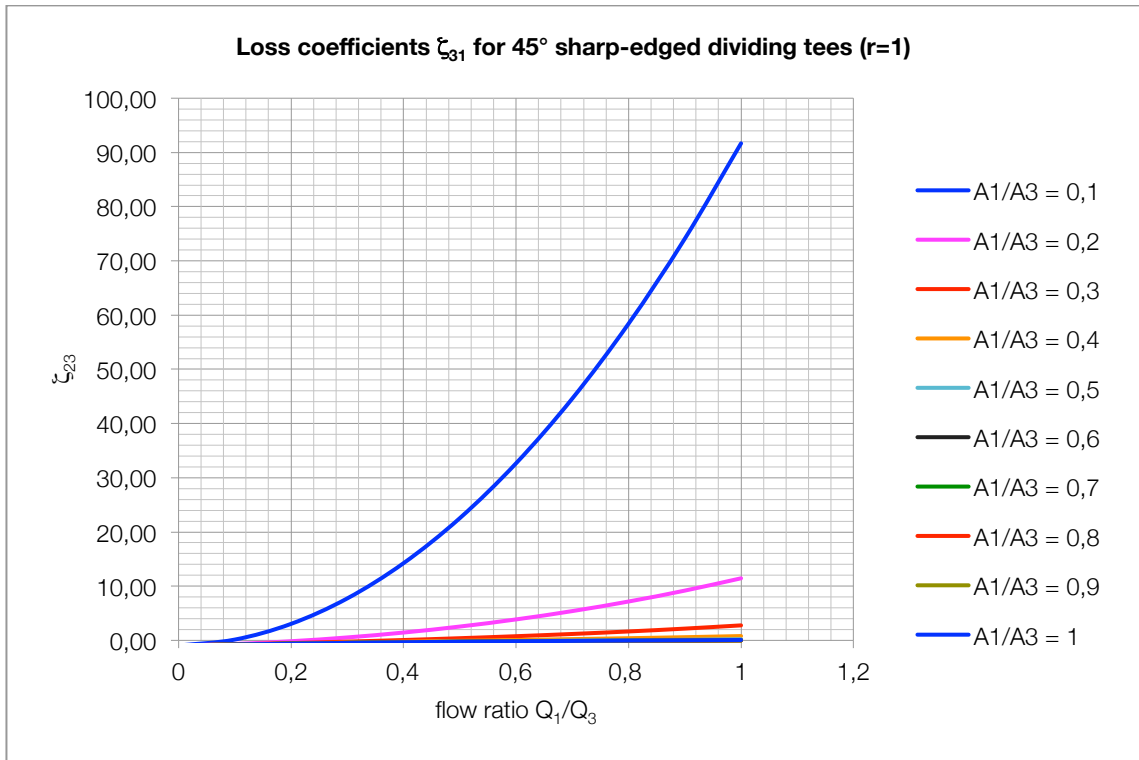
Graph 7: Loss coefficients ζ_{32} sharp-edged dividing tees



Graph 8: Loss coefficients ζ_{31} for 90 degrees sharp-edged dividing tees ($r=1$)



Graph 9: Loss coefficients ζ_{31} for 90 degrees sharp-edged dividing tees ($r=1$)



Graph 10: Loss coefficients ζ_{31} for 45 degrees sharp-edged dividing tees ($r=1$)



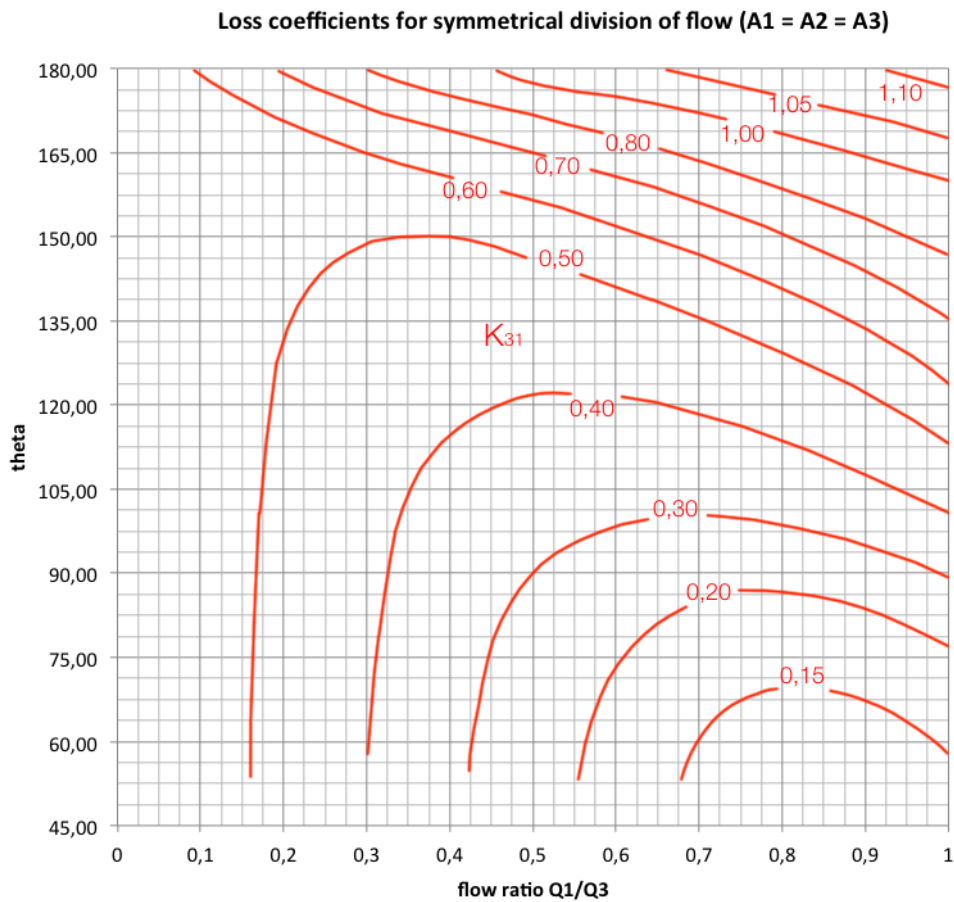
Graph 11: Loss coefficients ζ_{31} for 45 degrees sharp-edged dividing tees ($r=1$)

11.4 Symmetrical division of flow

The loss coefficients for symmetrical division of flow are shown on performance charts for the following arrangements:

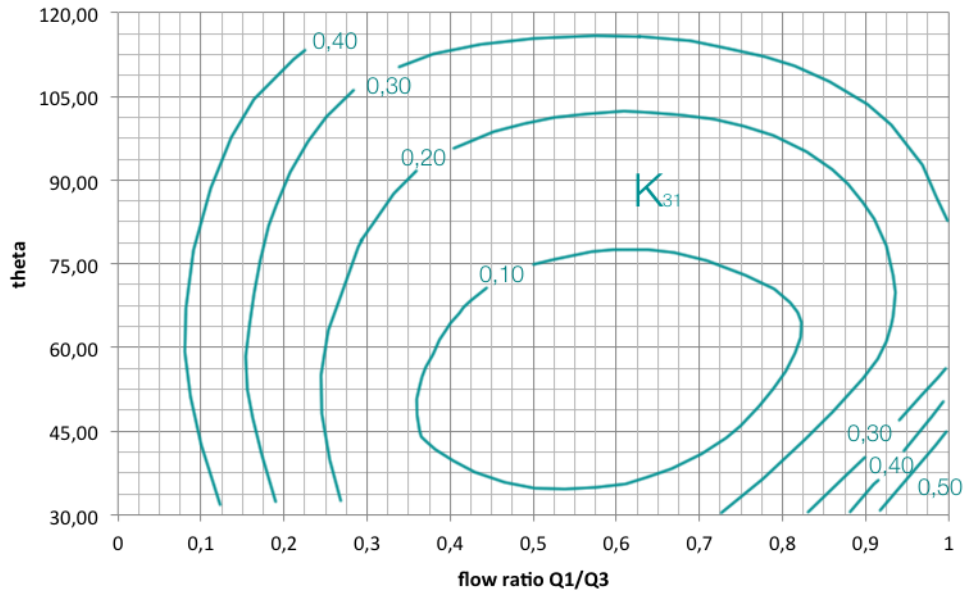
1. $A_1/A_3 = A_2/A_3 = 1,0$ Graph 12
2. $A_1 = A_2$ and $A_1+A_2 = A_3$ Graph 13

The limitation on the inlet and outlet tangent lengths are the same as for sharp-edged dividing tees.



Graph 12: Loss coefficients for symmetrical division of flow ($A_1=A_2=A_3$)

Loss coefficients for symmetrical division of flow ($A_1 = A_2$ and $A_1 + A_2 = A_3$)



Graph 13: Loss coefficients for symmetrical division of flow ($A_1=A_2$ and $A_1+A_2=A_3$)

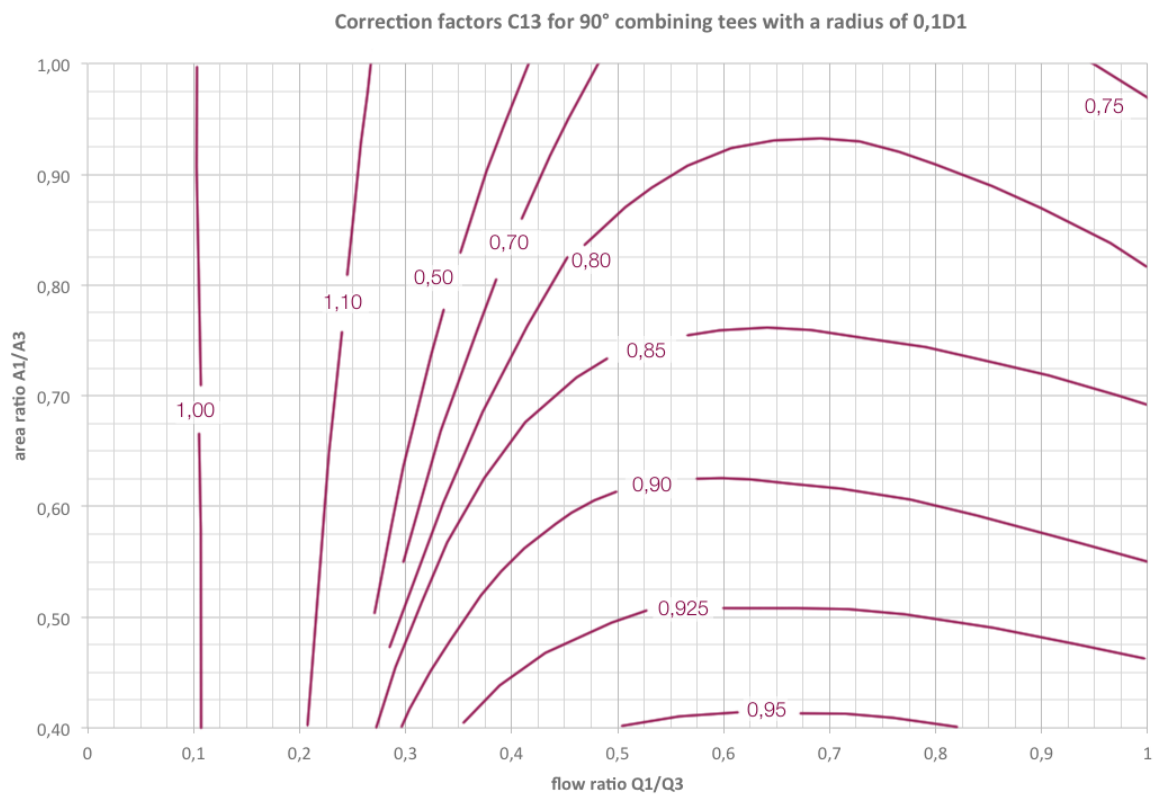
11.5 Tee junction edges

A small radius of chamfer at the junction of the main and branch has a large effect on some of the loss coefficients. For combining flow about 70% of the possible reduction is obtained with a radius of chamfer of 0,1 the branch diameter on the trailing edge of the branch.

The branch loss coefficients of dividing tees continue to fall with increase in the radius at the leading edge up to radii equal to the branch diameter.

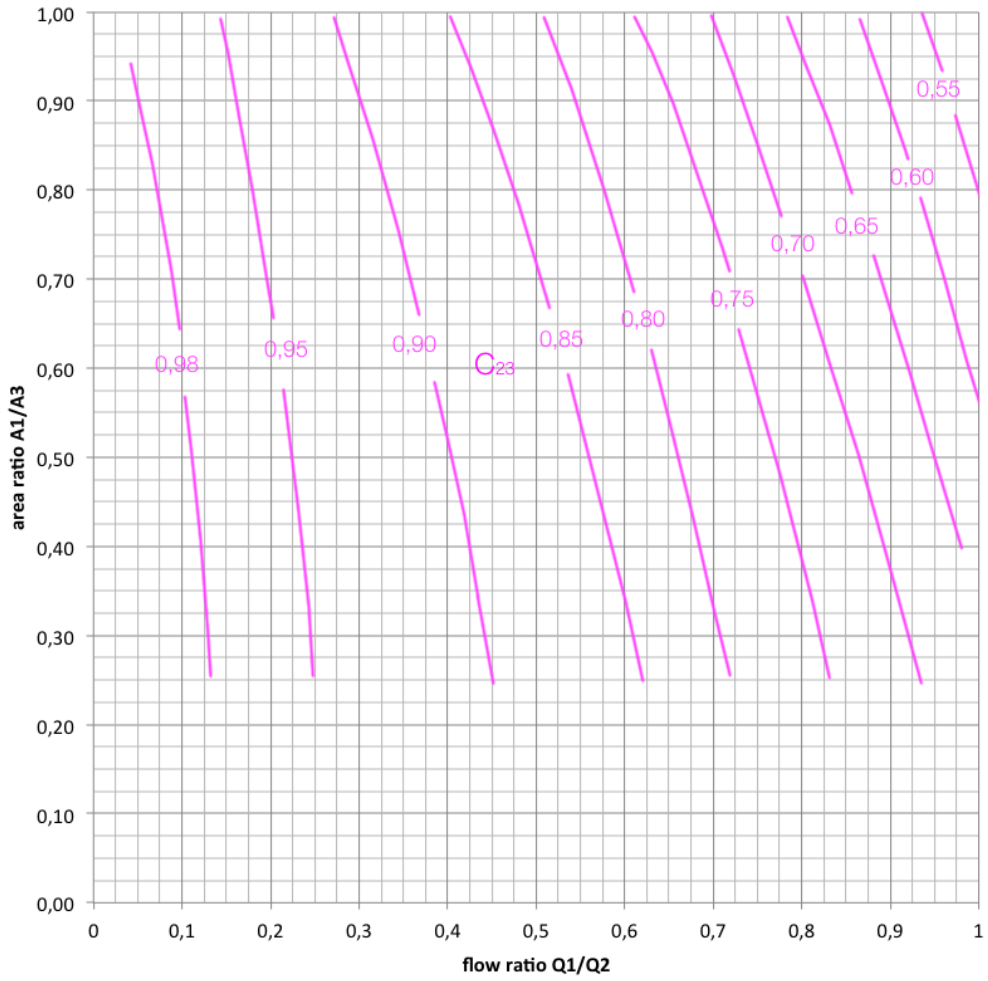
Graph 14 and Graph 15 show the combining flow correction factors, C13 and C23 respectively, to be used with the loss coefficients ζ_{13} and ζ_{23} for 90 degree sharp-edged tees with a radius of $r/d = 0,1$ at the junction of the branch leg 1 and of the through leg of the tee.

Graph 16 shows the dividing flow correction factor, C31, to be used with the loss coefficient ζ_{31} for 90 degree sharp edged tees, with a radius of $r/d = 0,1$ at the junction of the branch leg and of the through log of the tee. The loss coefficient ζ_{32} is not affected by the radius.



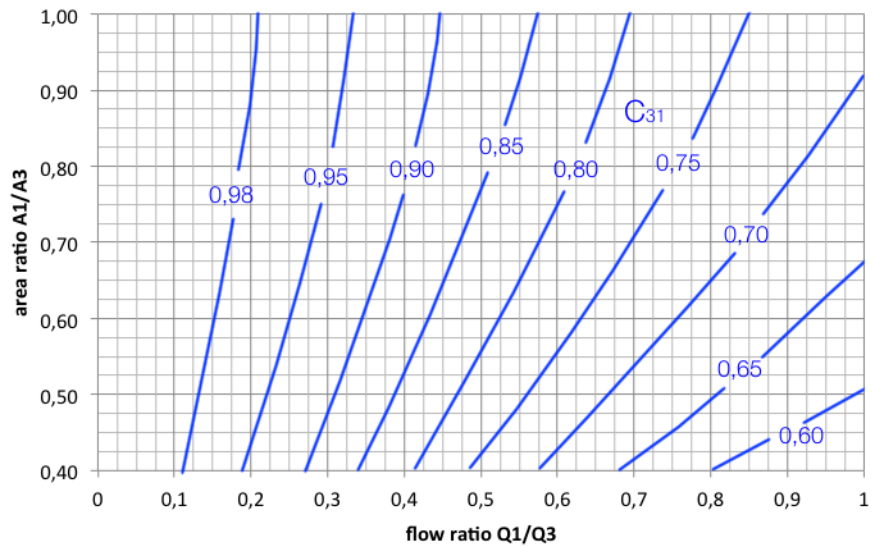
Graph 14: correction factors C13 for 90 degrees combining tees with a radius of 0,1D1

Correction factors C23 for 90° combining tees with a radius of 0,1D1



Graph 15: correction factors C23 for 90 degrees combining tees with a radius of 0,1D1

Correction factors C31 for 90° dividing tees with a radius of 0,1D1



Graph 16: correction factors C31 for 90 degrees combining tees with a radius of 0,1D1

12 Grids, screens and bar gratings

List of chapter symbols

Latin symbols:

- A = total height of the transverse elements [m];
- a_0 = width of the gap of a bar grate, radius of the orifices of a disk (plate) [m];
- c', c'' = coefficients depending on the nature of flotsam contained in the water and on the geometrical dimensions of the gratings;
- d = diameter of bracing elements [m];
- d_0 = diameter of the section of a perforated plate orifice [m];
- d_h = hydraulic diameter of the orifices of an obstruction [m];
- d_M = bar thickness [m];
- \bar{f} = cross-section coefficient;
- F_0, F_1 = flow area of the obstruction cross-section and area of the conduit section before the obstruction, respectively [m²];
- F_g = area of the obstruction front [m²];
- h = height of the intermediate support bars [m];
- k_0 = proportionality parameter for screen's losses calculation;
- k_M, k'_M = proportionality parameters for grid's and screen's losses calculation in case of Mach influence;
- k_{Re} = proportionality parameter which allow for Re Number influence in screens's losses calculation;
- l = depth of the orifices of a grid (wall thickness at the place of the orifice), of the gaps of a bar grate [m];
- S_1, S_2 = vertical and horizontal distances between the axes of adjacent bars of a grate, tubes in a bundle, etc., and also between the orifices of a perforated plate [m];
- S'_2 = diagonal distances between the orifices of a perforated plate [m];
- z = number of the orifices, of screens;
- z_1, z_2 = number of intermediate support bars and of bracing elements, respectively;

Greek symbols:

- α_0 = angle of attack of the bar in a bar grate [°];
- β_1, β_2 = coefficients which allow for the bar shape;
- ζ_M = resistance coefficient influenced by mach number for plane grids;
- θ = angle of inclination of the bar in a bar grate and of the orifices in the case of their checkerboard arrangement in a perforated plate [°];

Grids and screens represent obstructions distributed uniformly over a conduit section. For such type of flow obstacle the main source of resistance coefficient data will be Idel'chik (Idel'chik, 1966).

12.1 Grids

A plane grid placed in a straight pipe has the same resistance effect as an orifice plate: the stream contracts during its passage through the grid orifices, and its exit velocity is higher than the inlet velocity. In these devices the head losses are the result of the entrance to an orifice and with the sudden expansion at the exit.

The resistance coefficients ζ of a *plane, thin-walled grid* are function of the shape of its orifice edges, the Reynolds number Re and its cross-section coefficient \bar{f} , defined in the following expression:

$$\bar{f} = \frac{F_0}{F_g}$$

where F_0 is the flow area of the obstruction cross-section and F_g is the area of the conduit section before the obstruction.

It is calculated by the same formulas as a *restrictor*, i.e., by formulas seen in the relative chapter and listed before for different orifice shape and flow conditions.

For plane grid (perforated sheet) with sharp-edged orifices with $Re > 10^5$ and $l/d_h = 0 - 0,015$, Loss coefficients are calculate by the following formula:

$$\zeta = \frac{\Delta H}{\frac{V^2}{2g}} = \left[\left(0,707\sqrt{1-\bar{f}} \right) + 1 - \bar{f} \right]^2 \left(\frac{1}{\bar{f}} \right)^2$$

For plane grid (perforated sheet) with sharp-edged orifices with $Re < 10^5$ and $l/d_h = 0 - 0,015$ the following formula could be applied:

$$\zeta = \frac{\Delta H}{\frac{V^2}{2g}} \cong \left\{ \zeta_\varphi + \overline{\varepsilon_0^{Re}} \left[\left(1 + 0,707\sqrt{1-\bar{f}} \right) - \bar{f} \right]^2 \right\} \left(\frac{1}{\bar{f}} \right)^2$$

where ζ_φ and $\overline{\varepsilon_0^{Re}}$ are parameters depending on the orifice shape and are calculated as explained in the sudden enlargements and orifice chapter.

For grid with orifice edges beveled facing the flow or made from angle iron with $Re > 10^4$ and so turbulent flow conditions, can be applied the foloowing formula:

$$\zeta = \frac{\Delta H}{\frac{V^2}{2g}} = \left[\left(\sqrt{\zeta'(1-\bar{f})} \right) + (1-\bar{f}) \right]^2 \left(\frac{1}{\bar{f}} \right)^2$$

For thickened grid (perforated plate or laths) with $l/d_h > 0,015$, it has to be taken in account the influence of friction losses because the device length could not be neglected. The friction influence is allowed for using the λ friction coefficient, calculated for different relative roughness.

The situation is different allowing for the value of Re number:

$Re > 10^5$	$Re < 10^5$
$\zeta = \frac{\Delta H}{\frac{V^2}{2g}} \cong \left\{ \left(0,5 + \tau \sqrt{1 - \bar{f}} \right) (1 - \bar{f}) + (1 - \bar{f})^2 \right.$ $\left. + \lambda \frac{l}{d_h} \right\} \left(\frac{F_1}{F_0} \right)^2$	$\zeta = \frac{\Delta H}{\frac{V^2}{2g}} \cong \left\{ \zeta_\varphi + \overline{\varepsilon_0^{Re}} \cdot \zeta_0 + \lambda \frac{l}{d_h} \right\} \left(\frac{1}{\bar{f}} \right)^2$

Where τ is another parameter that can be determined following the sudden enlargements and orifices instructions, ζ_φ , $\overline{\varepsilon_0^{Re}}$ are the same parameters defined before and ζ_0 is defined as:

$$\zeta_0 = 1 + 0,707 \sqrt{1 - \bar{f}}$$

For grids with rounded orifices edges with $Re > 3 \times 10^5$ the loss coefficients can be computed as following:

$$\zeta = \frac{\Delta H}{\frac{V^2}{2g}} \cong \left\{ \sqrt{\zeta'(1 - \bar{f})} + (1 - \bar{f}) \right\}^2 \left(\frac{1}{\bar{f}} \right)^2$$

In the following pages are listed all the graphs and instructions to put into practice the instruction given in this short introduction.

Plane grid (perforated sheet) with sharp-edged orifices with $Re > 10^5$ and $l/d_h = 0 - 0,015$

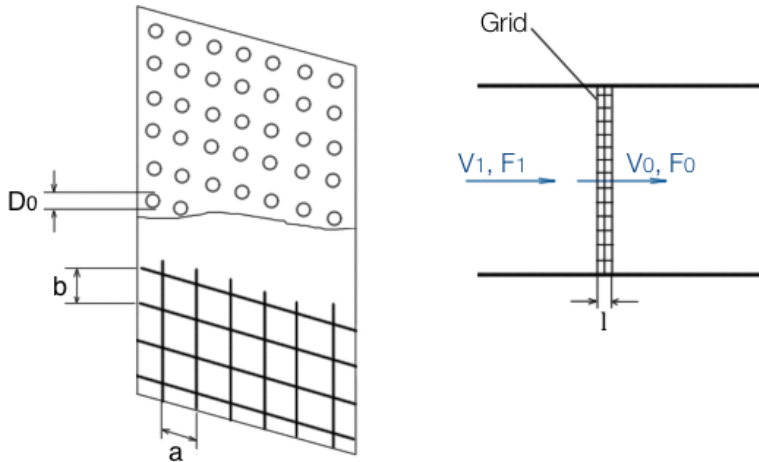


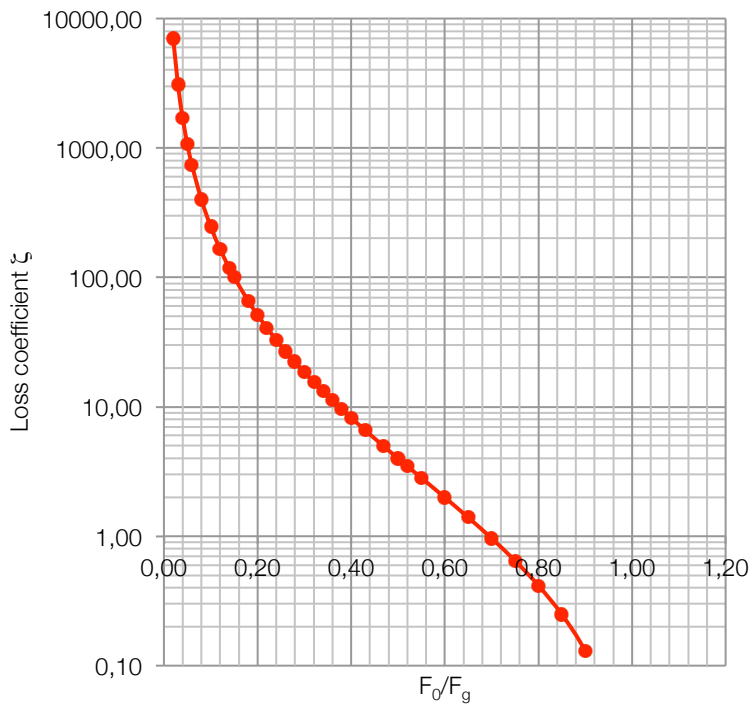
Figure 1: schematic view of a plane grid (perforated sheet)

Loss coefficients are calculate by the following formula:

$$\zeta = \frac{\Delta H}{V^2} = \left[\left(0,707\sqrt{1 - \bar{f}} \right) + 1 - \bar{f} \right]^2 \left(\frac{1}{\bar{f}} \right)^2$$

\bar{f}	ζ
0,02	7055,11
0,03	3085,11
0,04	1707,17
0,05	1074,66
0,06	733,92
0,08	399,07
0,10	246,72
0,12	165,38
0,14	117,20
0,15	100,24
0,18	65,81
0,20	51,29
0,22	40,75
0,24	32,89
0,26	26,89
0,28	22,22
0,30	18,53
0,32	15,58
0,34	13,18
0,36	11,22
0,38	9,59
0,40	8,23
0,43	6,59
0,47	4,94
0,50	4,00
0,52	3,48
0,55	2,82
0,60	1,99
0,65	1,40
0,70	0,96
0,75	0,65
0,80	0,42
0,85	0,25
0,90	0,13
0,95	0,05
1,00	0,00

Loss coefficients for plane grid (perforated sheet) with sharp-edged orifices ($Re > 10^5$)



Graph 1: loss coefficients for plane grid (perforated sheet) with sharp edged orifices and Reynolds Number $> 10^5$

Plane grid (perforated sheet) with sharp-edged orifices with $Re < 10^5$ and $l/d_h = 0 - 0,015$

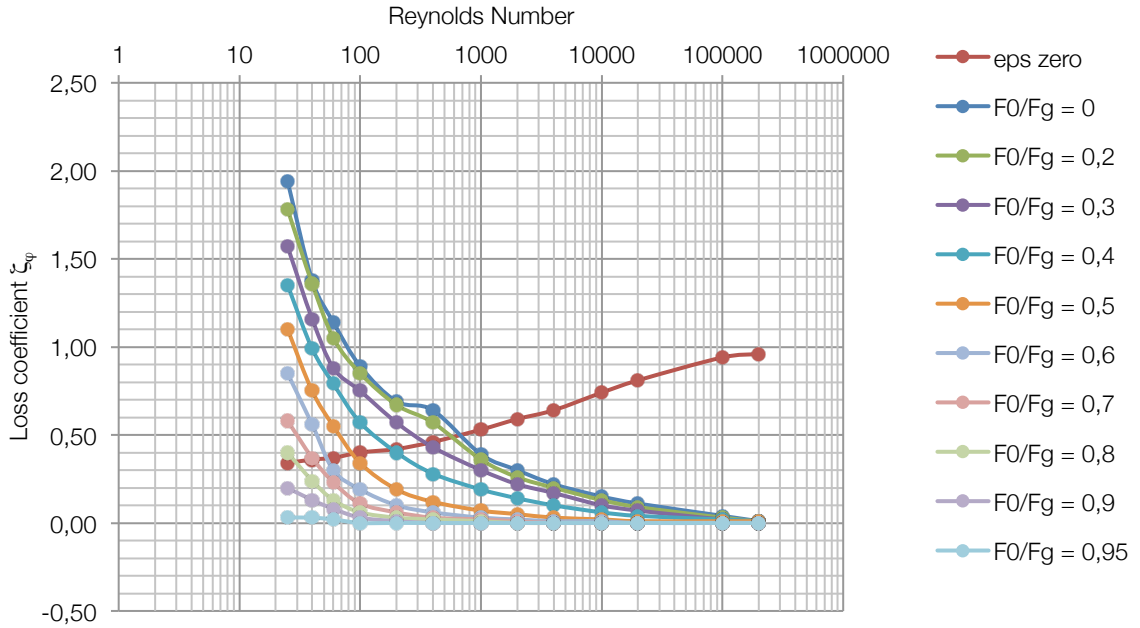
Loss coefficients are calculate by the following formula:

$$\zeta = \frac{\Delta H}{V^2} \cong \left\{ \zeta_\varphi + \overline{\varepsilon_0^{Re}} \left[\left(1 + 0,707 \sqrt{1 - \bar{f}} \right) - \bar{f} \right]^2 \right\} \left(\frac{1}{\bar{f}} \right)^2$$

Where:

ζ_φ is determined from Graph 2
 $\overline{\varepsilon_0^{Re}}$ is detrmned from Graph 2

Coefficient ζ_φ for plane grid (perforated sheet) with sharp-edged orifices ($Re < 10^5$)



Graph 2: ζ_φ coefficients for plane grid with sharped-edged orifices $Re < 10^5$

Re	$\overline{\varepsilon_0^{Re}}$	\bar{f}									
		0	0,2	0,3	0,4	0,5	0,6	0,7	0,8	0,9	0,95
25	0,34	1,94	1,78	1,57	1,35	1,10	0,85	0,58	0,40	0,20	0,03
40	0,36	1,38	1,36	1,16	0,99	0,75	0,56	0,37	0,24	0,13	0,03
60	0,37	1,14	1,05	0,88	0,79	0,55	0,30	0,23	0,13	0,08	0,02
100	0,40	0,89	0,85	0,75	0,57	0,34	0,19	0,11	0,06	0,03	0,00
200	0,42	0,69	0,67	0,57	0,40	0,19	0,10	0,06	0,03	0,01	0,00
400	0,46	0,64	0,57	0,43	0,28	0,12	0,06	0,03	0,02	0,00	0,00
1000	0,53	0,39	0,36	0,30	0,19	0,07	0,03	0,02	0,01	0,00	0,00
2000	0,59	0,30	0,26	0,22	0,14	0,05	0,02	0,01	0,00	0,00	0,00
4000	0,64	0,22	0,20	0,17	0,10	0,03	0,01	0,00	0,00	0,00	0,00
10000	0,74	0,15	0,13	0,10	0,06	0,02	0,01	0,00	0,00	0,00	0,00
20000	0,81	0,11	0,09	0,07	0,04	0,01	0,00	0,00	0,00	0,00	0,00
100000	0,94	0,04	0,03	0,02	0,02	0,01	0,00	0,00	0,00	0,00	0,00
200000	0,96	0,01	0,01	0,01	0,01	0,01	0,00	0,00	0,00	0,00	0,00

Grid with orifice edges beveled facing the flow or made from angle iron with $Re > 10^4$

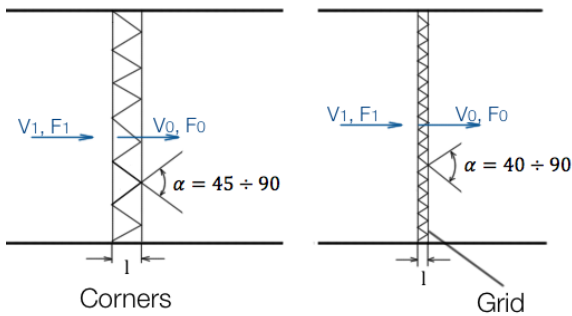


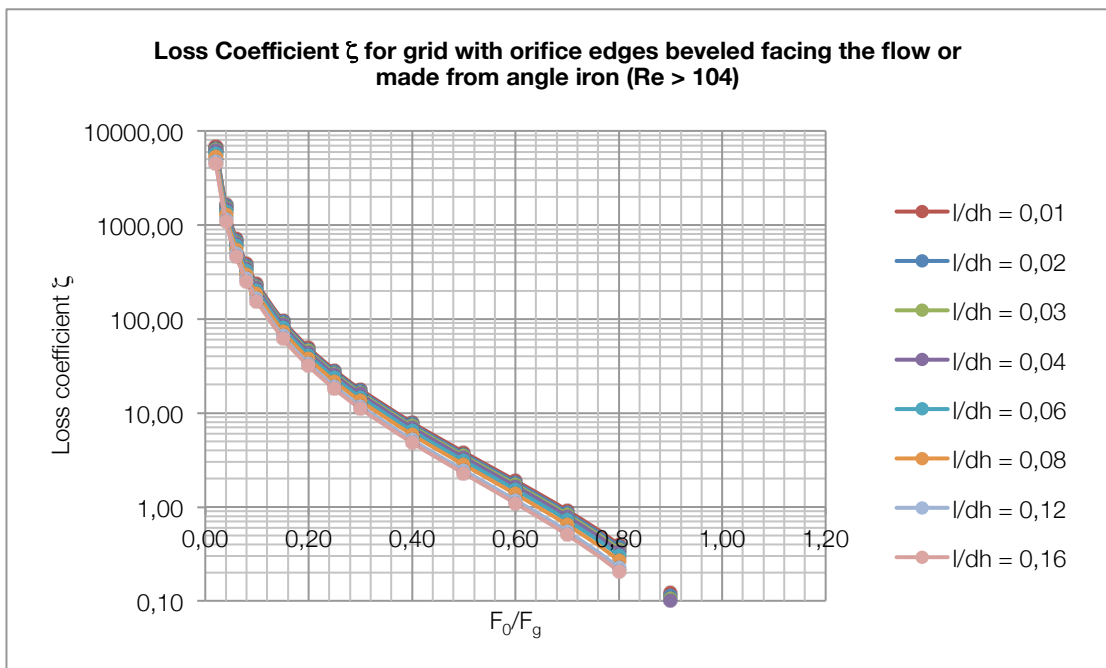
Figure 2: schematic view of beveled edges grid

Loss coefficients are calculate by the following formula:

$$\zeta = \frac{\Delta H}{V^2} = \left[\left(\sqrt{\zeta'(1-\bar{f})} \right) + (1-\bar{f}) \right]^2 \left(\frac{1}{\bar{f}} \right)^2$$

Where:

ζ' is determined with formulas in the sudden enlargement and orifice chapter as a function of l/d_h ;



Graph 3: loss coefficients fro grid with orifices edges beveled facing the flow

l/d_h	ζ'	\bar{f}													
		0,02	0,04	0,06	0,08	0,10	0,15	0,20	0,25	0,30	0,40	0,50	0,60	0,80	1,00
0,01	0,46	6818	1649	708,9	385,4	238,2	96,73	49,47	28,62	17,85	7,92	3,84	1,91	0,40	0,00
0,02	0,42	6574	1590	683,2	371,3	229,5	93,12	47,59	27,51	17,15	7,59	3,67	1,82	0,37	0,00
0,03	0,38	6322	1529	656,7	356,9	220,5	89,41	45,65	26,37	16,42	7,26	3,50	1,73	0,35	0,00
0,04	0,35	6128	1482	636,3	345,7	213,5	86,54	44,17	25,50	15,87	7,00	3,37	1,66	0,34	0,00
0,06	0,29	5724	1383	593,8	322,4	199,1	80,58	41,07	23,67	14,71	6,47	3,10	1,52	0,30	0,00
0,08	0,23	5291	1278	548,3	297,6	183,6	74,21	37,76	21,73	13,47	5,90	2,82	1,37	0,27	0,00
0,12	0,16	4733	1142	489,7	265,6	163,7	66,02	33,51	19,23	11,89	5,17	2,45	1,18	0,22	0,00
0,16	0,13	4468	1078	461,9	250,4	154,3	62,14	31,50	18,05	11,15	4,83	2,28	1,10	0,20	0,00

Thickened grid (perforated plate or laths) with $l/d_h > 0,015$

$$\zeta = \frac{\Delta H}{V^2} \cong \left\{ \left(0,5 + \tau \sqrt{1 - \bar{f}} \right) (1 - \bar{f}) + (1 - \bar{f})^2 + \lambda \frac{l}{d_h} \right\} \left(\frac{F_1}{F_0} \right)^2$$

where:

λ is the friction coefficient that can be determined following the instruction of the first chapter;

τ is another parameter that can be determined following the sudden enlargements and orifices instructions;

the results for ζ loss coefficients computed with this formula are plotted in the following diagram (Graph 4);

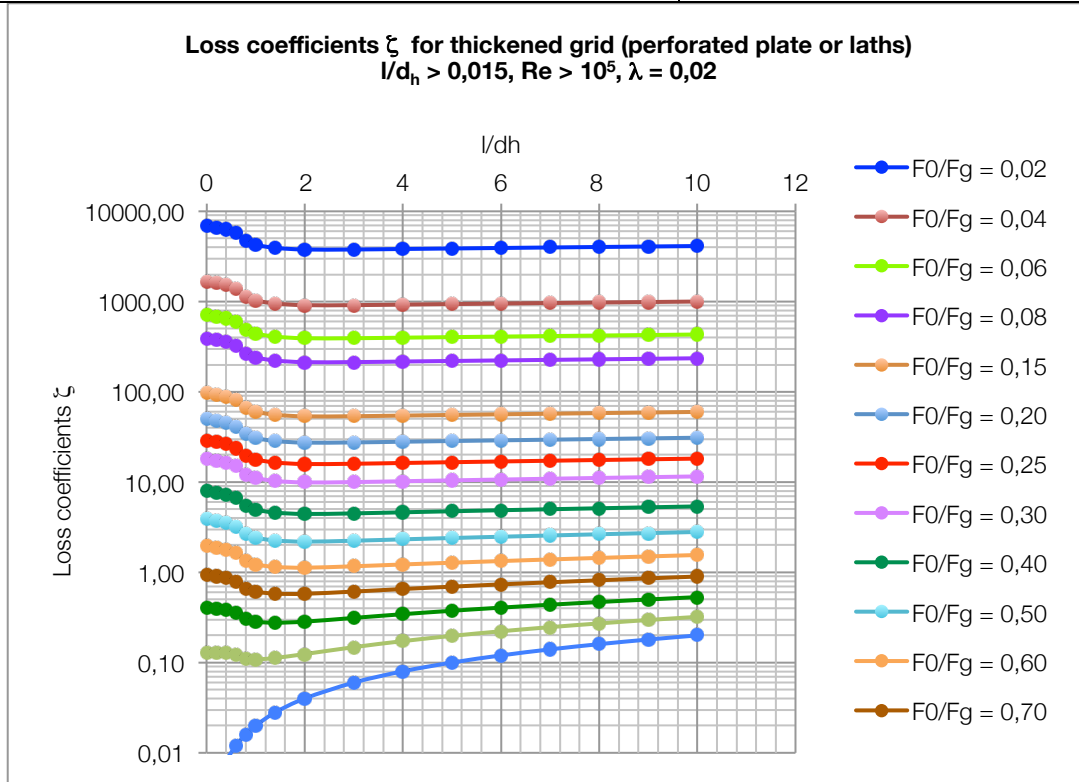
$$\zeta = \frac{\Delta H}{V^2} \cong \left\{ \zeta_\varphi + \varepsilon_0^{Re} \cdot \zeta_0 + \lambda \frac{l}{d_h} \right\} \left(\frac{1}{\bar{f}} \right)^2$$

Where:

λ is the friction coefficient that can be determined following the instruction of the first chapter;

$\zeta_\varphi, \varepsilon_0^{Re}$ are the same parameters defined before;

$$\zeta_0 = 1 + 0,707 \sqrt{1 - \bar{f}}$$



Graph 4: loss coefficients for thickened grid (perforated plate or laths) with $l/d_h > 0,015$

Grids with rounded orifices edges with $Re > 3 \times 10^5$

Loss coefficients can be computed with the following formula

$$\zeta = \frac{\Delta H}{\frac{V^2}{2g}} \cong \left\{ \sqrt{\zeta'(1-\bar{f})} + (1-\bar{f}) \right\}^2 \left(\frac{1}{\bar{f}} \right)^2$$

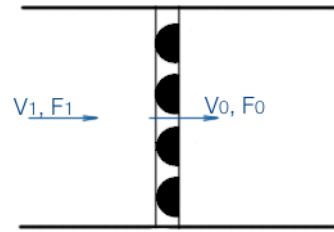
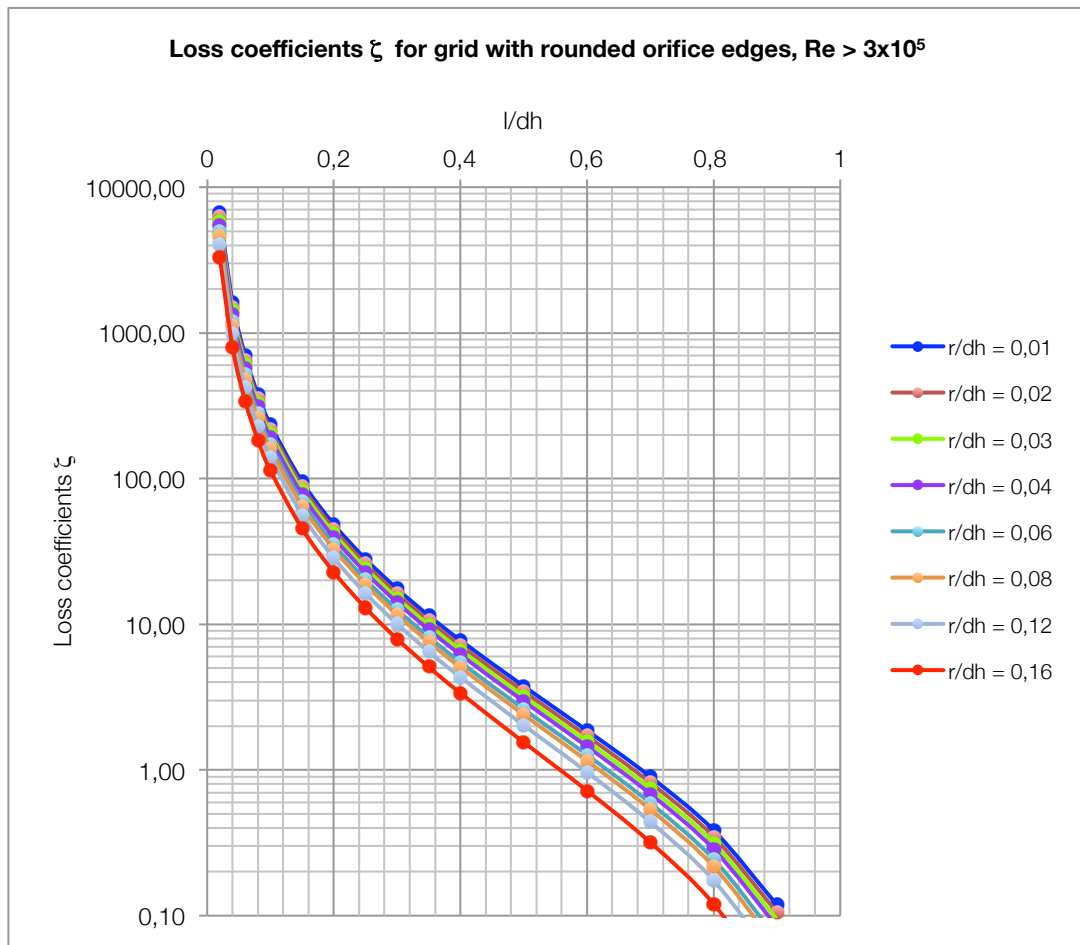


Figure 3: schematic view of rounded orifices grid

where:

ζ' is the coefficient treated and computed for sudden enlargements and orifices; in order to calculate it, it is necessary to refer to the relative chapter;

the results for ζ loss coefficients computed with this formula are plotted in the following diagram (Graph 5);



Graph 5: loss coefficients for grid with rounded orifices edges

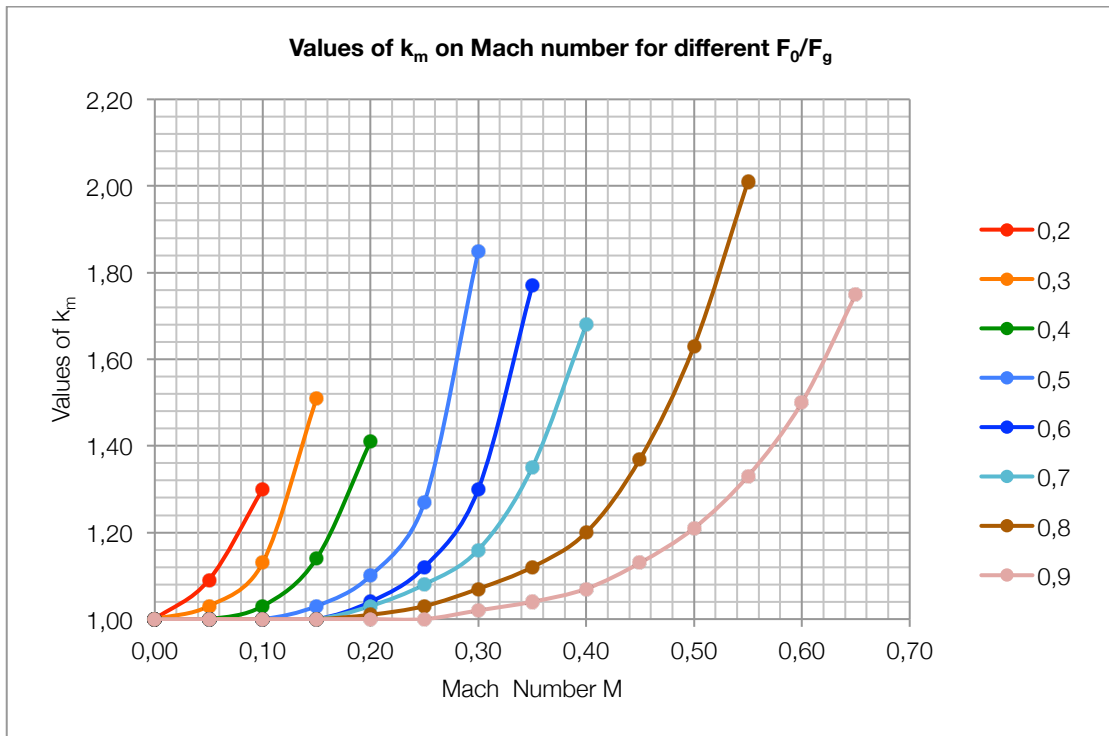
All the parameters and coefficients listed in the previous formulas can be determined following the instructions written in the sudden enlargements and orifices chapter.

The stream velocity in the narrowest section of the jets passing through the grid can turn out to be very high at small values of \bar{f} , even at low inlet velocities, and in some cases approaches the velocity of sound. Under such conditions the resistance coefficient of the grid becomes a function of the Mach number M.

This is expressed by the following formula:

$$\zeta_M = \frac{\Delta H}{V^2/2g} = \zeta \cdot k_M$$

where k_M is the corrective coefficient for the influence of the Mach number; this coefficient has been plotted in Graph 6.



Graph 6: values of k_m plotted on Mach Number varying \bar{f}

\bar{f}	Mach Number values													
	0,00	0,05	0,10	0,15	0,20	0,25	0,30	0,35	0,40	0,45	0,50	0,55	0,60	0,65
0,2	1,00	1,09	1,30	0,00	0,00	0,00	0,00	0,00	0,00	0,00	0,00	0,00	0,00	0,00
0,3	1,00	1,03	1,13	1,51	0,00	0,00	0,00	0,00	0,00	0,00	0,00	0,00	0,00	0,00
0,4	1,00	1,00	1,03	1,14	1,41	0,00	0,00	0,00	0,00	0,00	0,00	0,00	0,00	0,00
0,5	1,00	1,00	1,00	1,03	1,10	1,27	1,85	0,00	0,00	0,00	0,00	0,00	0,00	0,00
0,6	1,00	1,00	1,00	1,00	1,04	1,12	1,30	1,77	0,00	0,00	0,00	0,00	0,00	0,00
0,7	1,00	1,00	1,00	1,00	1,03	1,08	1,16	1,35	1,68	0,00	0,00	0,00	0,00	0,00
0,8	1,00	1,00	1,00	1,00	1,01	1,03	1,07	1,12	1,20	1,37	1,63	2,01	0,00	0,00
0,9	1,00	1,00	1,00	1,00	1,00	1,00	1,02	1,04	1,07	1,13	1,21	1,33	1,50	1,75

12.2 Screens

The resistance coefficients ζ a screens are calculated by the following formula:

$$\zeta = \frac{\Delta H}{V^2/2g} = k_0 \left(1 - \frac{F_0}{F_1}\right) + \left(\frac{F_1}{F_0} - 1\right)^2$$

where $k_0 = 1,3$ (according to Adamov's data) for screens made from circular metal wire not perfectly clean, but with normal surface state (neither rusty or dusty), $k_0 = 1,0$ fo new wire screens, $k_0 = 2,1$ for silk-thread screens (according to Khanzhonkov's data).

The resistance coefficient of circular-wire screens is a function of Reynolds number for $Re < 400$, and for silk-thread screens is a function of Reynolds number for $Re < 150$.

The values of screens loss coefficients for $k_0 = 1,3$ metal wires and the values of silk threads filters in condition of $Re > 400$, are plotted in Graph 7.

The influence of Reynolds number can be allowed for by the formula:

$$\zeta_{Re} = k_{Re} \cdot \zeta$$

where ζ is determined by the previous formula, and k_{Re} is determined by Graph 8.

At small values of the cross-section coefficient, the velocity in the screen orifices can approach the velocity of sound. The influence of Mach number in such conditions, is allowed for the coefficient k'_M , plotted in the Graph 9, based on Cornell's experiment:

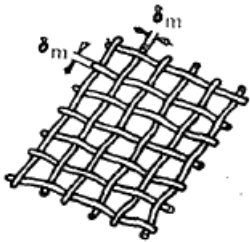
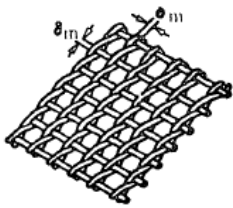
$$\zeta_M = \frac{\Delta H}{V^2/2g} = \zeta \cdot k'_M$$

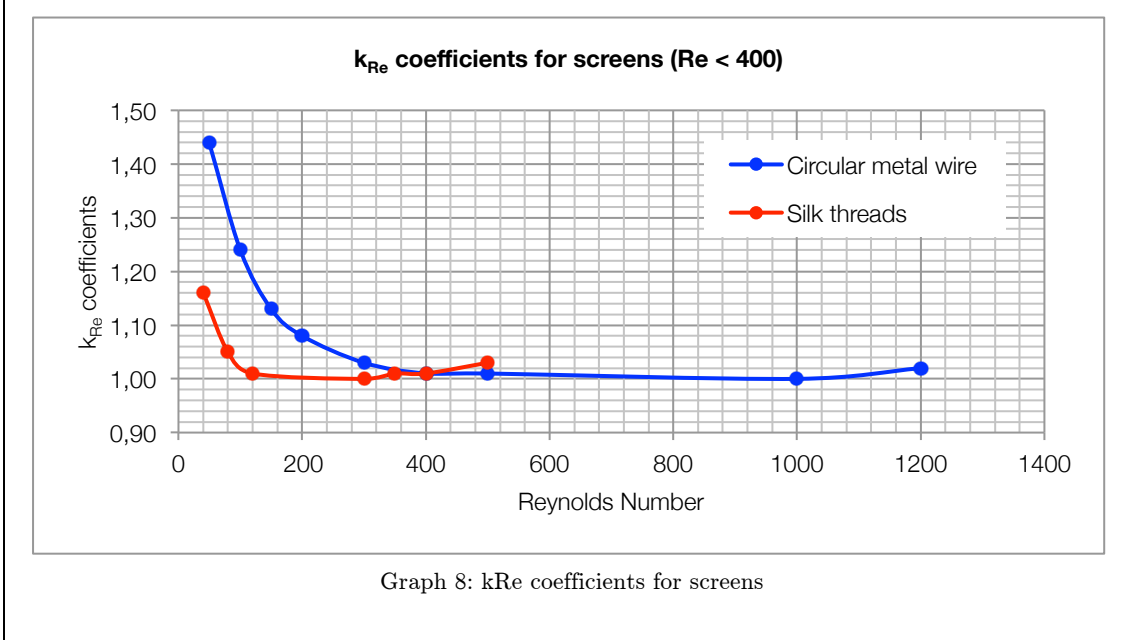
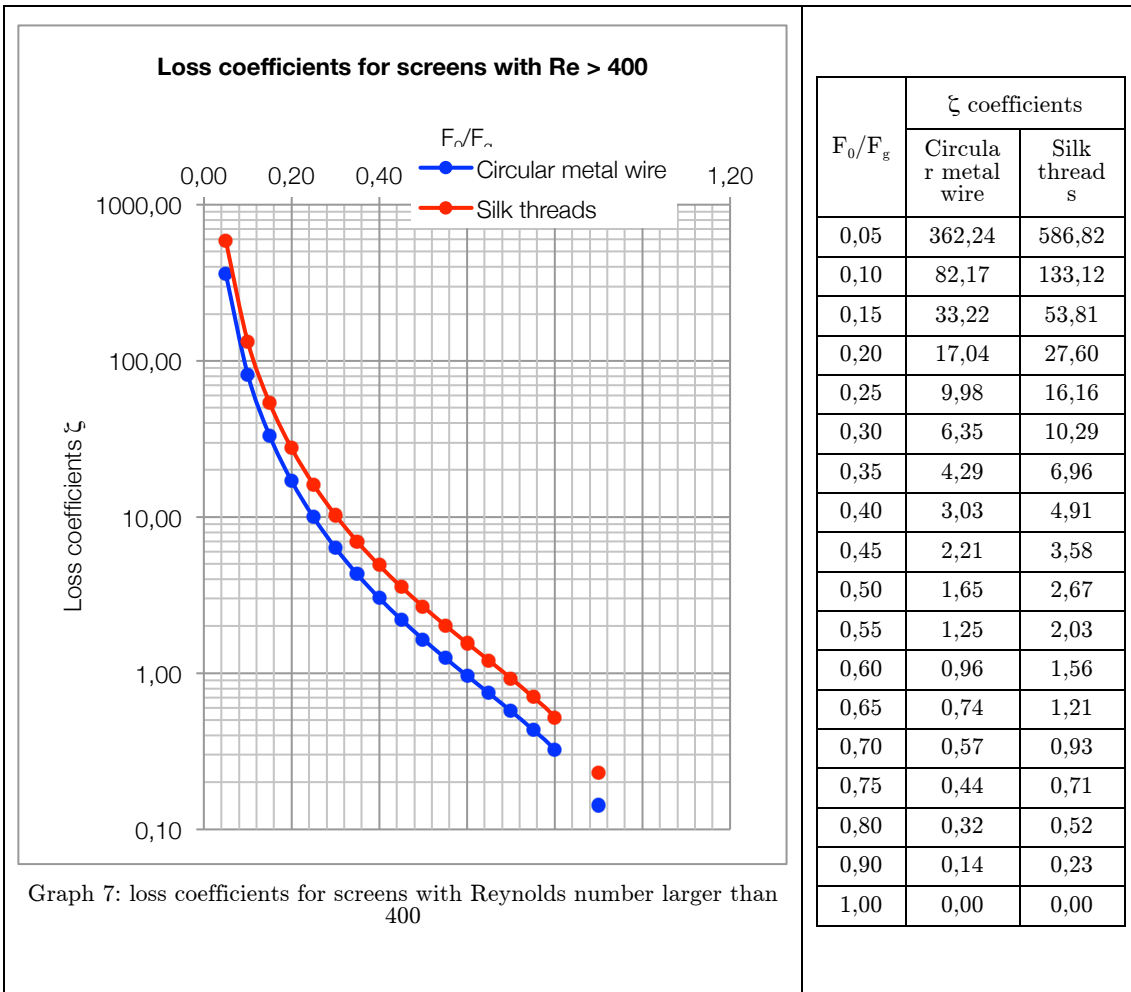
From a theoretical point of view the superposition of two screens, installed close to each other, do not lead to an increasing of the fluid resistance: if the wires of the two screens are accurately superposed the result is equivalent to one screen of doubled wire thickness in the stream direction. It follows that the resistance will increase, but rarely by a factor of two.

When the two screens are, however, installed at a distance from each other larger than 15 wire diameters, the resistance is doubled. In practical calculation the total resistance of a screen series ζ_{tot} is computed as the sum of the resistance coefficients of the single separate screens ζ_i :

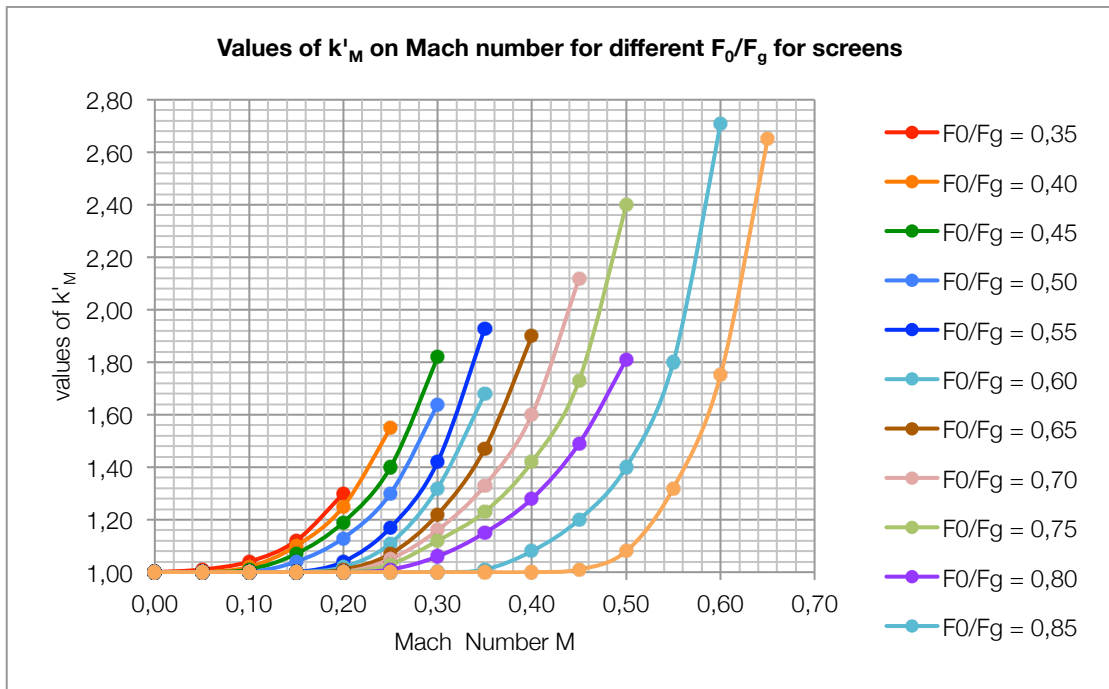
$$\zeta_{tot} = \frac{\Delta H}{V^2/2g} = \sum_i^z \zeta_i$$

Where z is the total number of screens installed.

1. Circular metal wire	2. Silk Threads
	



Re	40	50	80	100	120	150	200	300	350	400	500	1000	1200
Metal Wire	-	1,44	-	1,24	-	1,13	1,08	1,03	-	1,01	1,01	1,00	1,02
Silk Threads	1,16	-	1,05	-	1,01	-	-	1	1,01	1,01	1,03	-	-



Graph 9: values of coefficient k'_M that allow for Mach influence

\bar{f}	Mach Number values													
	0,00	0,05	0,10	0,15	0,20	0,25	0,30	0,35	0,40	0,45	0,50	0,55	0,60	0,65
0,35	1,00	1,01	1,04	1,12	1,30	-	-	-	-	-	-	-	-	-
0,40	1,00	1,00	1,02	1,10	1,25	1,55	-	-	-	-	-	-	-	-
0,45	1,00	1,00	1,01	1,07	1,19	1,40	1,82	-	-	-	-	-	-	-
0,50	1,00	1,00	1,00	1,04	1,13	1,30	1,64	-	-	-	-	-	-	-
0,55	1,00	1,00	1,00	1,00	1,04	1,17	1,42	1,93	-	-	-	-	-	-
0,60	1,00	1,00	1,00	1,00	1,02	1,11	1,32	1,68	-	-	-	-	-	-
0,65	1,00	1,00	1,00	1,00	1,01	1,07	1,22	1,47	1,90	-	-	-	-	-
0,70	1,00	1,00	1,00	1,00	1,00	1,05	1,16	1,33	1,60	2,12	-	-	-	-
0,75	1,00	1,00	1,00	1,00	1,00	1,03	1,12	1,23	1,42	1,73	2,4	-	-	-
0,80	1,00	1,00	1,00	1,00	1,00	1,01	1,06	1,15	1,28	1,49	1,81	-	-	-
0,85	1,00	1,00	1,00	1,00	1,00	1,00	1	1,01	1,08	1,2	1,4	1,8	2,71	-
0,90	1,00	1,00	1,00	1,00	1,00	1,00	1	1	1	1,01	1,08	1,32	1,75	2,65

12.3 Bar gratings

Just as for ordinary thickened grids, the total losses through bar gratings of different bar cross sections are comprised of entrance losses, frictional losses and losses with sudden expansion at exit from the section between the bars in the grating.

The resistance coefficient of gratings at $\frac{l}{d_M} = 5$ and $\frac{a_0}{S_l} \geq 0,5$ can be determined by Kirschmer's formula:

$$\zeta = \frac{\Delta H}{V^2/2g} = \beta_1 k_1 \sin \theta$$

Where β_1 is the coefficient of bar shape, determined by Table 1, θ is the inclination of the bars towards the stream and k_1 is determined by the following formula:

$$k_1 = \left(\frac{a_0}{S_l} - 1 \right)^{4/3}$$

The resistance coefficient of gratings can be determined approximately, at any value of the ratio $\frac{a_0}{S_l}$, and at any relative grating thickness $\frac{l}{a_0}$, by the following formula:

$$\zeta = \frac{\Delta H}{V^2/2g} = \beta_2 \zeta' \sin \theta$$

Where β_2 is the coefficient of bar shape, determined by table on the basis of Kirschmer's data; ζ' is the resistance coefficient of an ordinary grid or orifice plate with thick-edged orifices, determined as thickened grids; a_0 , S_l , l are gap width, distance between the axes of adjacent bars, and bar thickness in the stream direction.

The resistance coefficients of bar gratings used in hydro structures turn out to be higher than the ones determined by these formulas, due to fouling and to design peculiarities of the gratings. Accordingly it is recommended to introduce a correction coefficient c' into previous formulas whose value is to be determined as a function of the nature and amount of flotsam contained in the water, method of cleaning the grating, possibility of deposition of silt before the grating, etc.

In the case of mechanical cleaning of the gratings $c' = 1,1 - 1,3$, and in the case of manual cleaning $c' = 1,5 - 2,0$.

In order to allow for design peculiarities the same author recommends the introduction into the formulas of an additional corrective coefficient c'' :

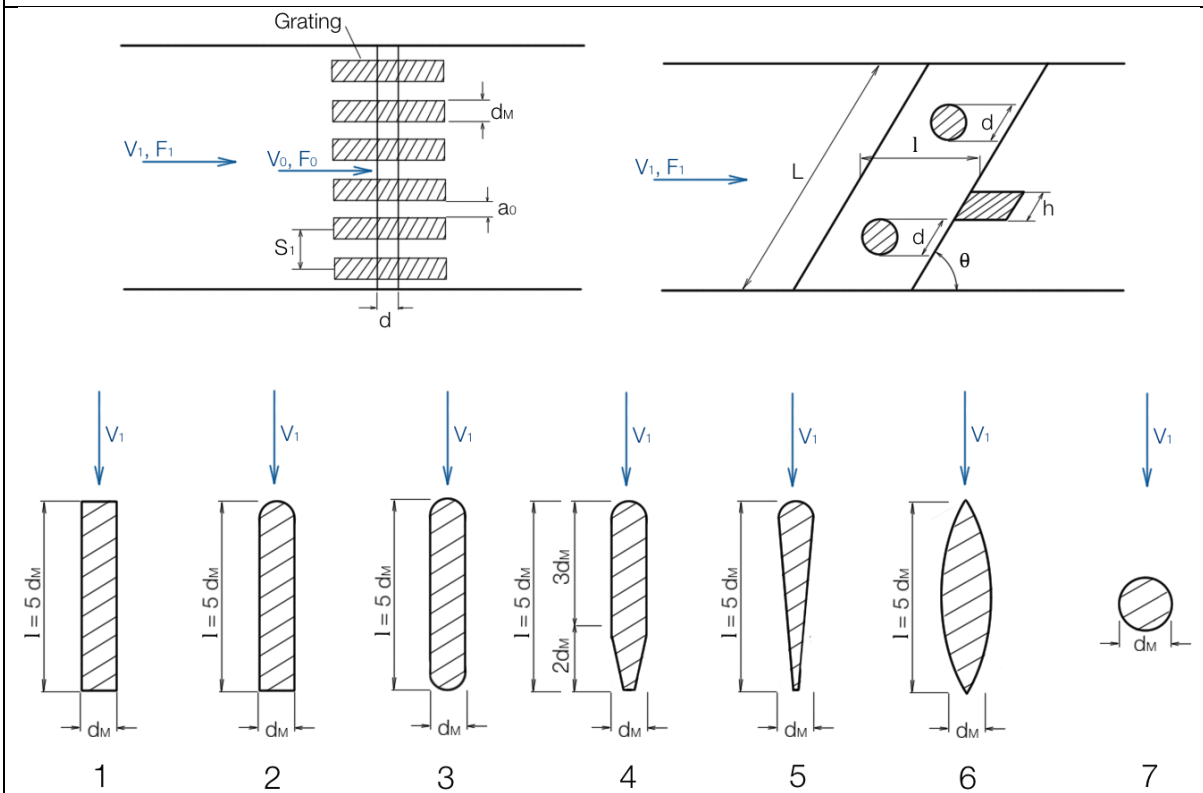
$$c'' \approx \frac{1}{\left(1 - \frac{A}{L}\right)^2}$$

where L is the internal height of the grating, A is the total height of the transverse elements that can be calculated as following:

$$A = hz_1 + dz_2$$

where h and z_1 are height and number of intermediate support bars; d and z_2 are diameter and number of bracing elements.

Bar grating with angle zero for approach, at $Re > 10^4$



Graph 10: geometrical parameters of gratings

1. Clean grating of screen

a. in case of $\frac{l}{d_M} = 5$ and $\frac{a_0}{s_l} \geq 0,5$:

$$\zeta = \frac{\Delta H}{V^2/2g} = \beta_1 k_1 \sin \theta$$

where:

$k_1 = \left(\frac{a_0}{s_l} - 1\right)^{4/3}$ can be seen in Graph 11;

β_1 can be determined from Table 1;

b. in case of any $\frac{l}{d_M}$ and any $\frac{a_0}{s_l}$

$$\zeta = \frac{\Delta H}{V^2/2g} = \beta_2 \zeta' \sin \theta$$

where:

β_2 can be determined from Table 1;

ζ' can be determined as ζ for thickened grids;

2. Clogged grating

$$\zeta_c = \frac{\Delta H}{V^2/2g} = c' \zeta$$

where:

$c' = 1,1 - 1,3$ for mechanical cleaning

$c' = 1,5 - 2,0$ for manual cleaning

3. Grating with additional frame

$$\zeta_{CF} = \frac{\Delta H}{V^2/2g} = c'' \zeta_c$$

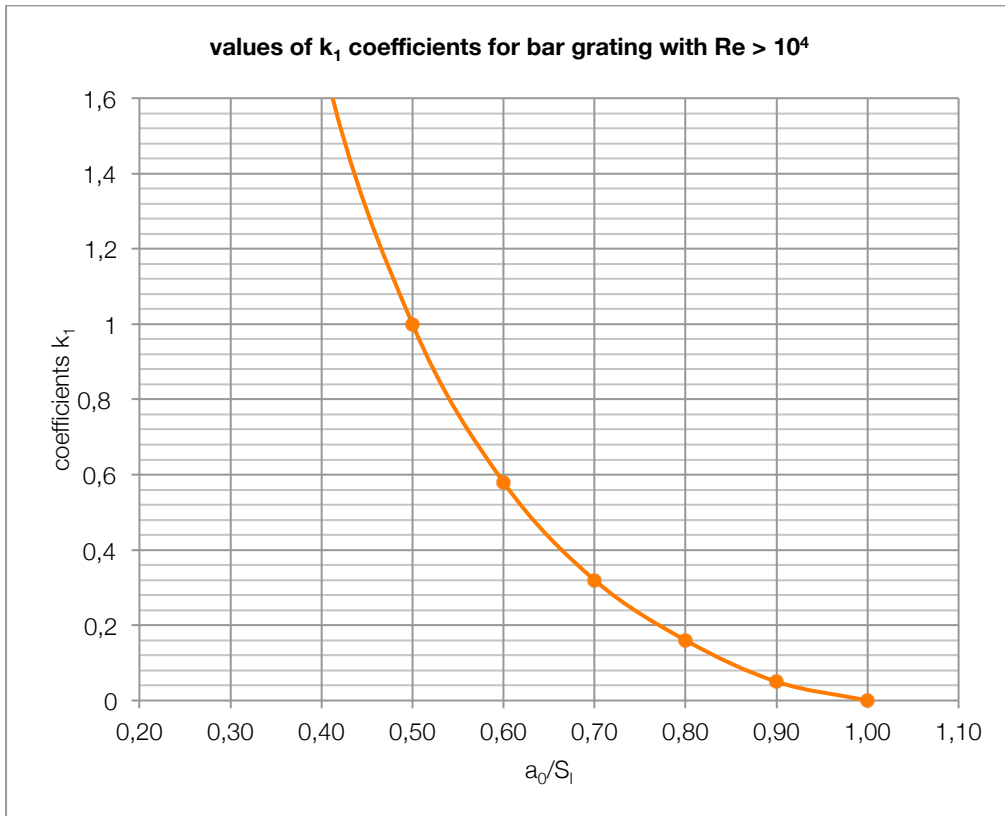
where:

$$c'' \approx \frac{1}{\left(1 - \frac{A}{L}\right)^2}$$

with $A = hz_1 + dz_2$ (see the introduction of the chapter);

Table 1: coefficients for different bar type

Type of bar	1	2	3	4	5	6	7
β_1	2,34	1,77	1,77	1,00	0,87	0,71	1,73
β_2	1,00	0,76	0,76	0,43	0,37	0,30	0,74



Graph 11: values of k_1 coefficients for bar grating ($Re10^4$)

Table 2: values of k_1

a_0/S_1	k_1
0,00	90
0,10	18,70
0,20	6,35
0,30	3,09
0,40	1,72
0,50	1,00
0,60	0,58
0,70	0,32
0,80	0,16
0,90	0,05
1,00	0

13 Valves

List of chapter symbols

Latin characters:

- b_d = width of disk flanges in disk check valves [m];
- C_C = coefficient of stream contraction;
- C_V = flow coefficient [U.S. gal/min/psi];
- D_0 = diameter of the passage cross-section of the throttling device or internal diameter of the pipe where specified [m];
- D_h = hydraulic diameter of the passage [m];
- DN = nominal diameter of the devices [mm];
- f_r = ratio of F_0 and F_S ;
- F_0 = cross-section area at the inlet of the throttling device [m²];
- F_C = cross-section area of the contracted stream after a throttle [m²];
- F_h = cross-section area of valve opening, free for the flow passage [m²];
- F_S = seat cross-section area [m²];
- G1, G2, = geometrical parameters for disk check valves;
- h = lift of the gate or valve [m];
- i = number of guide ribs;
- J = friction slope;
- J_m = friction slope in the theoretical case;
- k_{Re} = coefficient which allow for the Reynolds influence in globe valves;
- K_V = flow coefficient [m³/h/bar];
- L = generical pipe (or other device) length [m];
- m = ratio of F_h to F_C ;
- M = Mach number;
- Re = Reynolds number;
- S_{C1} = width of the guide shoulder for disk-check valves [m];
- SG = specific gravity of fluid;
- V_0 = mean stream velocity in the passage cross-section of a throttling device [m/s];
- V_m = theoretical mean stream velocity in a duct [m/s];
- x = flow velocities in VAG data technical sheets [m/s];
- y = interpolated trend of ζ values;
- Y = head drop [m];

- Z = where specified is the equivalent of ζ ;

Greek characters:

- α = opening angle of stopcocks, flaps and tilting discs [$^{\circ}$];
- β = square root of the ratio between the cross-section area at the most restricted point in the flow path, and the cross-section area of the pipe;
- β_2, β_3 = geometrical parameters for conical check valves;
- δ = opening angle of the incentrical butterfly devices [$^{\circ}$];
- Δp = pressure drop [Pa];
- ζ = head loss coefficient (see theoretical framework);
- η = relative error for butterfly valves comparisons;
- θ = convergence (or divergence) angle of pipe inlet (outlet) [$^{\circ}$];
- λ = friction coefficient (see theoretical framework);
- Π_0 = section perimeter [m];
- ψ = ratio of plug port diameter and pipe diameter;
- ω = ratio of the plug port area and the pipe area;

13.1 Introduction

Since the industrial installations usually contain a considerable number of valves, the knowledge of their resistance to the flow of fluids is necessary to determine the flow characteristics of a complete piping system.

As for the previous fittings, the aim of this chapter is to report the various resistance coefficients to flow for various commercial types of valves.

The great variety of valve designs, manufacturer, materials and the evolution in technologies applied preclude any comprehensive classification. If valves were classified according to the resistance they offer to flow, those exhibiting a straight-thru flow path such as gate, ball, plug and butterfly valves would fall in the low resistance class, and those having a change in flow path direction such as globe and angle valves would fall in the high resistance class: this is a first, very rough, classification. In order to have a more accurate classification this paper will follow the EN 736-1 standard (EN 736-1, 1995).

This standard defines valve as “piping component which influences the fluid flow by opening, closing or partially obstructing the passage of the fluid flow or by diverting or mixing the fluid flow”.

In general, the resistance coefficient of throttling and control devices is function of their design and of the shape of the inside body, which determines the stream flow, the uniformity of the section and the turbulences (Figure 1). The quality of the finishes of the inside of the body also influences in a really important way the resistance coefficient.

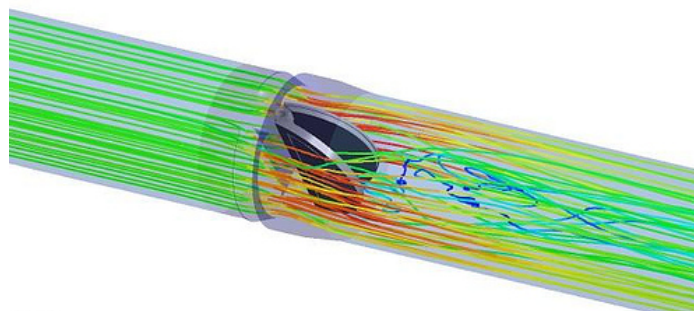


Figure 1: flow pattern and turbulences in double disk check valve

For gate valves, the resistance coefficient is similar to the resistance coefficient of the restrictor. In fact the variations in the stream flow are very similar: in both cases there's a sudden contraction followed by a sudden expansion. For the other types of valve there's a more complex obstruction that the stream has to face: sudden

contraction and expansions are more than one and abrupt variations are added. This is why, the formation of eddies is more diffused in these valves and, as a result, the resistance of this devices is bigger.

In general, the head loss produced by a valve consists of:

1. the head drop within the valve itself;
2. the head drop in the upstream pipe in excess of that which would normally occur if there were no valve in the line; this effect is very small;
3. the head drop in downstream pipe in excess of that which would normally occur if there were no valve in the line. This effect may be comparatively very large;

From an experimental point of view it is very difficult to distinguish between the three components of the head loss but the combined effect can be measured very well with known and accurate technical methods.

The resistance coefficients analyzed in the paper are given, for different types of valve, for completely open valves in dependence of the flow velocity or the nominal diameter and also for various valves' degree of opening: it's obvious that the head loss in a valve is connected also to the opening degree but in the second case, the head loss is desired.

One of the most important specifications that has to be done is that in the following pages, every head loss coefficient is computed for turbulent flow conditions, otherwise the Reynolds number will be specified.

13.1.1 Theoretical approach

From the theoretical point of view, if we want to analyze the functioning of a generic throttling device that regulates the flow in a generical pipe, the perfect example is the throttling device presented in Figure 2, which consists in a stem that moves vertically, regulated by an handle, penetrating in the flow stream.

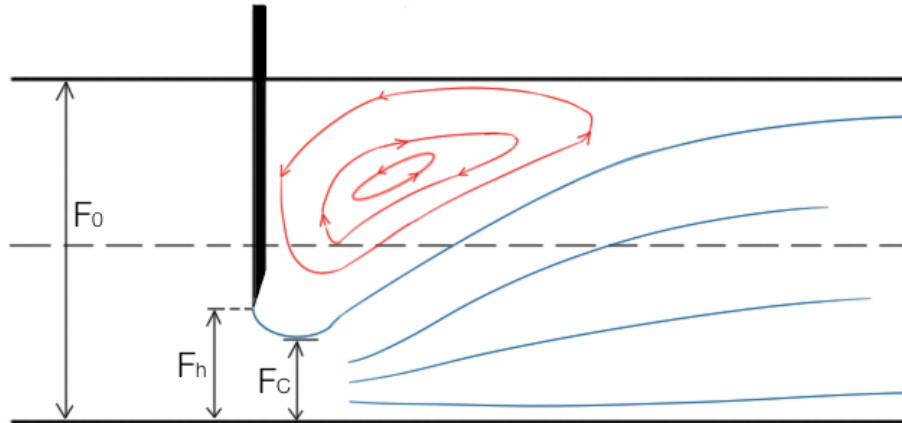


Figure 2: throttling device (gate valve)

The turbulence, that causes the energy dissipation is placed immediately after the stem and the contracted section in which we have the velocity V_c .

But, following the flow direction, it will happen a decreasing of the velocity downstream the contracted section and, in the next part of pipe the velocity will return V . For this reasoning we can compute the head loss with the Borda's formula:

$$\Delta H = \frac{(V_c - V)^2}{2g} = \frac{(V)^2}{2g} \left(\frac{1}{mC_c} - 1 \right)^2$$

where m is the throttling ratio, defined as the ratio of the free available section left by the valve F_h and the internal cross-section area F_0 :

$$m = \frac{F_h}{F_0}$$

As we said, the gate valve, but in general all the throttling components, can be used as a flow regulator.

In order to understand the way in which this regulation can be made, considering the Figure 3 we see two different tanks connected (with a smooth inlet in the section of connection, so there aren't any concentrated loss) by a duct L with interposed a gate valve S .

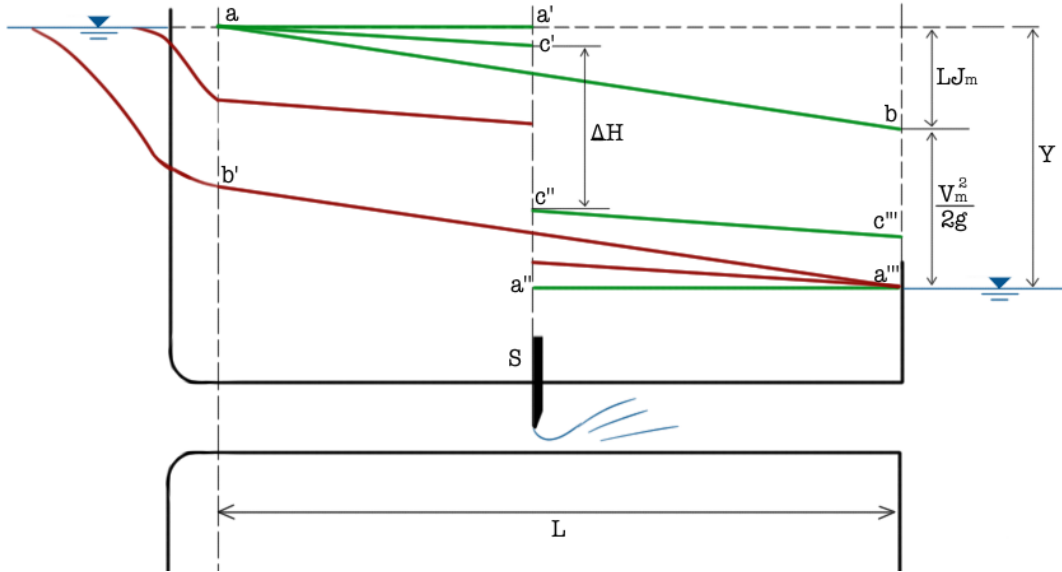


Figure 3: head lines and piezometrical lines before and after a throttling component

Calling Y the head drop between the two water levels, if we consider the gate totally closed, the head line will match the lines $a-a'$ upstream the gate and $a''-a'''$ downstream the gate.

In the opposite case (fully opened gate), the head line will match the lines $a-b$ with coefficient J_m and the piezometric line $b'-a'''$ will be parallel to the head line. Obviously the difference between the two lines is the quantity $\frac{V_m^2}{2g}$.

So we can write the following equation:

$$Y = LJ_m + \frac{V_m^2}{2g}$$

For the intermediate case, with a partial opening of the gate, it will appear a concentrated loss ΔH , that can be assimilated to the line $c'-c''$.

In this case, the head line will match the lines $a-c'$ upstream the gate and $c''-c'''$ downstream the gate, with coefficient J that is lower than the J_m coefficient seen before.

Also in this case, the piezometric lines will be parallel to the head lines, upstream and downstream the gate.

So, calling V the mean velocity in the duct, the previous equation can be written as:

$$Y = Lj + \Delta H + \frac{V^2}{2g} = \frac{V^2}{2g} \left[L \frac{\lambda}{D} + \left(\frac{1}{mC_c} - 1 \right)^2 + 1 \right]$$

This expression shows how the variation of the terms is connected with the term m .

In fact, considering the term C_c as a constant, increasing m (i.e. opening the gate) the right term of the equation has to decrease and so, the mean velocity V has to increase. In the opposite case, closing the gate and so decreasing the term m , the mean velocity has obviously to decrease.

In order to reduce the size of a gate valve and, consequently, the magnitudes of the forces involved to control it, the flow section in the valve body is usually contracted. This contraction can be symmetrical or non-symmetrical but in both cases, it increases the resistance coefficient of the valve.

13.1.2 Loss coefficient ζ and flow coefficients C_v , K_v

Head loss test data for a wide variety of valves are available from the work of numerous investigators. However, due to the time-consuming and costly nature of such testing, it is virtually impossible to obtain test data for every size and type of valve.

Commonly used concepts for giving a head loss for a certain type of valve are the “equivalent length” L/D , “the resistance coefficient” or “head loss coefficients” or simply “loss coefficient” ζ , and the “flow coefficients” K_V or C_V .

For what it concern the resistance coefficient ζ , it is expressed in terms of velocity head losses due to a valve, as it is stated in the introduction:

$$h_L = \zeta \frac{V^2}{2g}$$

Remembering that the connection between head loss and pressure drop is stated by the following formula:

$$h_L = \frac{\Delta p}{\gamma} = \frac{\Delta p}{\rho g}$$

The same loss in a straight pipe is expressed by the Darcy’s equation:

$$h_L = \lambda \frac{L}{D} \frac{V^2}{2g}$$

The ratio L/D is the equivalent length in pipe diameters of straight pipe, that will cause the same pressure drop as the obstruction under the same flow conditions. Since the resistance coefficient ζ is constant for all condition of flow, the value of L/D for any given valve must necessarily vary inversely with the change in friction factor λ for different flow conditions.

It is convenient in some branches of the valve industry, particularly in connection with control valves, to express the valve capacity and the valve flow characteristics in terms of a flow coefficient. In Europe the flow coefficient at present in use is designated K_V and it is defined as:

K_V = Rate of flow of water, in cubic meters per hour (m^3/h), at pressure drop of one kilogram force per square centimeter (kgf/cm^2) across the valve.

Another coefficient C_V is used in UK and USA and is defined as following.

C_V = Rate of flow of water, in either US or UK gallons per minute, at 60 °F (15,6 °C), at pressure drop of 1 psi across the valve.

Table 1 shows the conversion factors among UK gallons, US gallons and litres.

Table 1: conversion factors between litres, UK gallons and US gallons

	1 UK gallon	1 US gallon	1 Litre
UK gallons	1,0000 UK gal	0,8327 UK gal	0,2199 UK gal
US gallons	1,2005 US gal	1,0000 US gal	0,2642 US gal
Litres	4,5461 l	3,7854 l	1,0000 l

Mathematically the flow coefficient C_V can be expressed as:

$$C_V = Q \sqrt{\frac{SG}{\Delta p}}$$

where:

Q = rate of flow (US gallons per minute);

SG = specific gravity of fluid (water = 1);

Δp = pressure drop across valve (psi);

Mathematically the flow coefficient K_V can be expressed as:

$$K_V = \frac{Q}{\sqrt{\Delta p}}$$

where:

Q = flow (m³/h);

Δp = pressure drop across valve (kgf/cm²);

The relationship between C_V and K_V can be written as following:

Mathematically the flow coefficient C_V can be expressed as:

$$K_V = 0,865 \cdot C_V$$

The reference to test this formulas and values is the regulation coded “CEI IEC 60534-2-3: Industrial-process control valves. Flow capacity. Test procedures”.

Equation $h_L = \zeta \frac{v^2}{2g}$ is valid for computing the head loss due to valves (and fittings in general) for all conditions of flow, including laminar flow, using resistance coefficient ζ . When this equation is used to determine losses in straight pipe, it is necessary to compute Reynolds Number in order to establish the friction factor λ and to calculate ζ with the equation $\zeta = \lambda \frac{L}{D}$.

There are useful expressions to pass from flow coefficients to resistance (head loss) coefficients when the first are expressed with Uk or US units:

- Flow rate Q in UK gal/min:

$$C_V = Q \sqrt{\frac{\rho}{\Delta p(62,4)}} = \frac{24,9d^2}{\sqrt{\lambda \frac{L}{D}}} = \frac{24,9d^2}{\sqrt{\zeta}} \rightarrow \zeta = \frac{620 d^4}{C_V^2}$$

- Flow rate Q in US gal/min:

$$C_V = Q \sqrt{\frac{\rho}{\Delta P(62,4)}} = \frac{29,9d^2}{\sqrt{\lambda \frac{L}{D}}} = \frac{29,9d^2}{\sqrt{\zeta}} \rightarrow \zeta = \frac{889 d^4}{C_V^2}$$

where:

ρ = density of liquid in [lb/ft³];

Δp = pressure drop, [lbf/in²];

d = internal diameter [in];

$\frac{L}{D}$ = equivalent length of valve in pipe diameters;

λ = friction factor;

ζ = resistance coefficient;

If the units in which the flow coefficients (K_v or C_v) are in S.I. system, the formulas are different:

Table 2: coefficients conversion with diameters in [mm]

$C_v = \frac{4,62d^2}{100 \cdot \sqrt{\zeta}} \rightarrow \zeta = \frac{4,62^2 d^4}{10^4 \cdot C_v^2} = \frac{2,14 d^4}{10^3 \cdot C_v^2}$	$K_v = \frac{39,98 d^2}{1000 \cdot \sqrt{\zeta}} \rightarrow \zeta = \frac{39,98^2 d^4}{10^6 \cdot K_v^2}$ $= \frac{1,6 d^4}{10^3 \cdot K_v^2}$
--	---

where:

d = internal diameter [mm];

ζ = resistance coefficient (loss coefficient), [adim];

13.1.3 Limitation in using data

For a number of reasons the published data about valve head losses, can be only used for approximate results in computation of coefficient:

- Loss coefficients are often based on the head difference between points that are immediately before and after the component; as the influence of the valve extends thirty or more diameters downstream, the error in computation of coefficient of low impact valves (generically $\zeta < 0,5$) is often important;
- Often, different manufacturers have different devices to measure the head loss and make tests;
- Usually geometric similarity is not respected between element of different size or element made by different manufacturers;
- Usually manufacturers only make known the nominal sizes of a valve and not the real sizes; in this case, errors are important because the coefficients vary as the fourth power of the error;
- The Reynolds number effects are often neglected;
- All the plots of head loss coefficients depending on the DN are linear interpolation made by the author;
- When data are obtained from Miller book (Miller, 1973), as anticipated in the introduction to the paper, all the graphs are built graphically;
- When data are obtained from Crane book (Crane, 1999), all the formulas are built as a multiplication of a numerical factor, specific for each valve model, and the friction factor λ ; in order to select the desired value of the friction coefficient λ , in the following table there are listed value of λ for complete turbulent zone and for clean commercial steel pipe, material most commonly used in duct systems:

Table 3: friction factors for clean steel pipe in complete turbulence zone

Nominal Diameter DN [mm]																
15	20	25	32	40	50	65	80	100	125	150	200	250	300	400	450	600
Friction Factor $\lambda \times 10^2$																
2,7	2,5	2,3	2,2	2,1	1,9	1,8	1,8	1,7	1,6	1,5	1,4	1,4	1,3	1,3	1,2	1,2

13.1.4 Valves with contractions at inlet/outlet

Valves are often designed with reduced diameter, and the transition from pipe to valve ends may be either abrupt or gradual. Straight-through types, such as gate and ball valves, so designed with gradual transition are sometimes referred to as venturi valves. Crane book, refers that analysis of tests on such straight-through valves indicates an excellent correlation between test result and calculated value of ζ as a sum of ζ for a sudden contraction and a sudden enlargement.

This procedure can be applied to throttled globe and angle valves. For this case the value of β must be based upon the square root of the ratio of areas:

where:

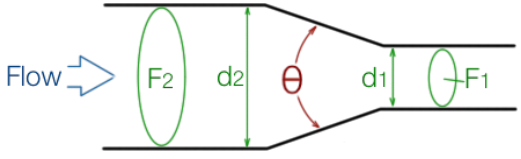
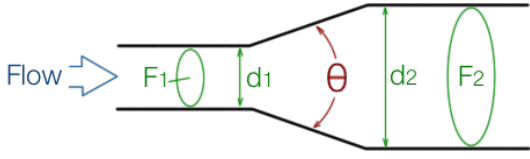
$$\beta = \sqrt{\frac{F_1}{F_0}}$$

F_1 = defines the area at the most restricted point in the flow path;

F_0 = defines the internal area of the connecting pipe;

In the following analysis for a lot of valve models will be referred also the values of resistance coefficient in the case of reduced seat design. For these cases the head loss coefficients values are computed as a sum of ζ due to enlargement, contraction and the ζ due to the valve device.

Table 4: determination of the head loss coefficient values for sudden (gradual) contraction and enlargement

Sudden and Gradual contraction		Sudden and Gradual enlargement	
			
$\theta \leq 45^\circ$	$\zeta = \frac{0,8 \sin \frac{\theta}{2} (1 - \beta^2)}{\beta^4}$	$\theta \leq 45^\circ$	$\zeta = \frac{2,6 \sin \frac{\theta}{2} (1 - \beta^2)^2}{\beta^4}$
$45^\circ < \theta \leq 180^\circ$	$\zeta = \frac{0,5 \sqrt{\sin \frac{\theta}{2}} (1 - \beta^2)}{\beta^4}$	$45^\circ < \theta \leq 180^\circ$	$\zeta = \frac{(1 - \beta^2)^2}{\beta^4}$

13.1.5 Classification of valves

As it is stated in the introduction, this paper will follow the EN 736-1 classification of the year 1995, published by the European Committee for Standardization (CEN), in order to propose the standard classification of valve types treated during the thesis.

Following the standard, the regulation stated that valves can be distinguished according to their:

- Functional features (Table 5);
- Basic design (Table 6);

Table 5: classification of valves according to functional features

Valves functional features	Type of action on the fluid	Examples
Isolating valves	Valves intended for use only in closed or fully open position.	Shutoff valves, gate valves, butterfly valves
Regulating valves	Valves intended for use in any position between closed and fully open.	Pressure reducing valves, throttle valves
Control valves	Power operated devices which change the fluid flow rate in process control systems. They consist of a valve connected to an actuator, with or without positioner, that is capable of changing the position of an obturator in the valves in response to a signal from the controlling system.	Control valves, control butterfly valves, regulating cocks, servo valves
		Level control valves
Safety valves	Valves which automatically, without the assistance of any energy other than that of the fluid concerned, discharge a certified quantity of the fluid so as to prevent a predetermined safe pressure being exceeded, and which are designed to reclose and prevent further flow of fluid after normal pressure conditions of service have been restored.	Outlet valves, safety valves, safety shut off valves
Bursting disc safety devices	Non-reclosing pressure relief devices actuated by differential pressure and designed to function by the bursting of the bursting disc(s). They are the complete assembly of installed components including, where appropriate, bursting disc holders.	Bursting disc safety devices
Check valves	Valves which automatically open by fluid flow in a defined direction and which automatically close to prevent fluid flow in the reverse direction.	Check valves and non-return valves
Diverting valves	Valves intended to influence the proportion of two or more output flows from a common input flow by changing the position of the obturator.	
Mixing valves	Valves intended to influence the proportion of two or more input flows to produce a common output flow by changing the position of the obturator.	
Automatic steam traps	Self-contained valves which automatically drain the condensate from a steam-containing enclosure whilst remaining tight to live steam or, if necessary, allowing steam to flow at a predetermined rate.	

This chapter will follow the indication of the basic design characteristics for the classification. In this sense valve types are distinguished by:

- a) The operating motion of the obturator;
- b) The direction flow in the seating area;

According to these two characteristics it is possible to classify the valves in the following basic types, listed in Table 6:

- *Gate Valves*: valves in which the obturator movement is linear and, in the seating area, at right angle of the direction flow;
- *Globe Valves*: valves in which the obturator movement is linear and, in the seating area, in the direction of flow;
- *Plug and Ball valves*: valves in which the obturator rotates about an axis at right angle to the direction of flow and, in the open position, the flow passes through the obturator;
- *Butterfly valve and eccentric plug valves*: valves in which the obturator rotates about an axis at right angle to the direction of flow and, in the open position, the flow passes around the obturator;
- *Diaphragm valves*: valves in which the fluid flow passage through the valve is changed by deformation of a flexible obturator;

Table 6: classification of valves according to their basic design

Working mechanism of the closure device				
Linear	Turning around the axis perpendicular to the direction of flow		Deformation of a flexible component	
Direction of flow in the connection area				
Perpendicular to the movement of the closure device	In the direction of movement of the closure device	Through the closure device	Around closure device	Different depending on design
Designation of basic designs				
Gate Valves	Globe (Control) Valves	Plug and Ball Valves	Butterfly and eccentric plug Valves	Diaphragm Valves
Models listed in the paper				
Gate valves	Globe valves Lift check valves Stop check valves Ball check valves Disc check valves Conical check valves Nozzle valves	Plug valves Ball valves Stopcocks	Butterfly valves Flaps Swing check valves Tilting disc check valves	Diaphragm valves

13.2 Gate Valves

Gate valves are used for large nominal diameter ($DN > 100$). They are characterized by their low flow resistance and short physical height. Valve plates, usually of double design, move back and forth to open, to regulate and to close these valves, using a handle. Nowadays this mechanism can be electromagnetically actuated.

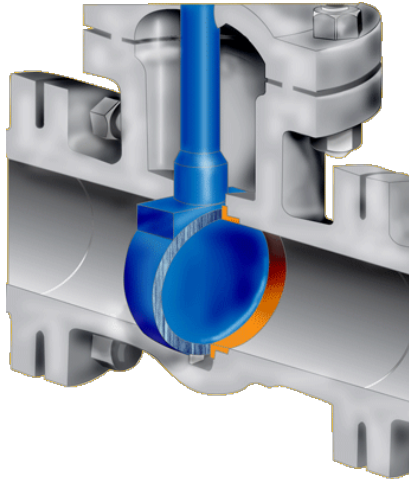


Figure 4: gate valve closure member

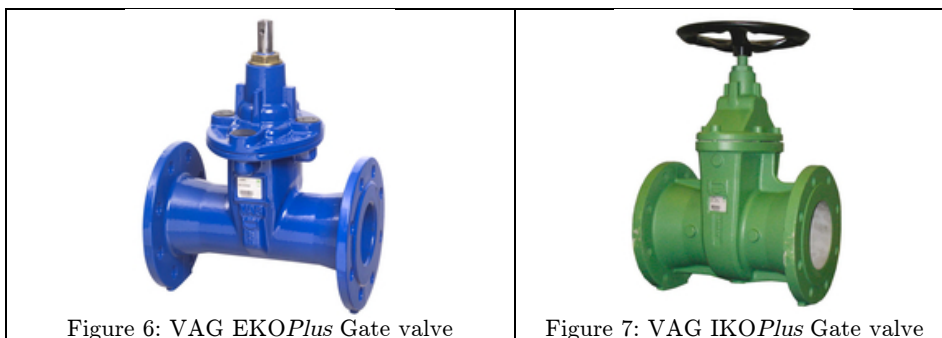


Figure 5: VAG BETA@ 200 Gate Valve

There is another important differentiation that is necessary to be explained for gate valve types concerning the material of the seat and the closure member.

In order to exemplify the concept, it is possible to analyze the behaviour of two gate valves with different material technologies available from VAG production, listed in Table 7: VAG EKO@*plus* gate valve and VAG IKO@*plus* gate valve.

Table 7: VAG Gate valves products



The most important difference in this sense between the two valve models is recognizable in the materials used for closure member and seat construction.

In EKO model body, cover and shut-off wedge are made by cast iron and the valve is resilient seated. In IKO model body, cover and shut-off wedge are made by ductile iron but the valve is metallic sealing.



Figure 8: EKO and IKO VAG models schematic view

This difference brings to sensible discrepancies in terms of concentrated head loss and will be clear looking at Graph 3, where is represented the trend of ζ values for each valve plotted against the nominal values of the diameter (in mm).

It is visible that the metallic sealing and the difference in composition of IKO model, brings to larger values of head loss coefficients for every nominal diameter value. This comparison brings to the conclusion that metallic gate valves entails greater concentrated head loss in fully open position than resilient sealing ones.

In literature, it is very difficult to found these type of differentiation and the gate valves are often presented without talking about materials and proposing one formula or one series of values valid for both types.

13.2.1 Fully open gate valves

Making a great simplification, the most of internet web sites, technical report and literature associate to gate valves a single head loss coefficient range of values from 0,10 to 0,30 for fully open throttling device.

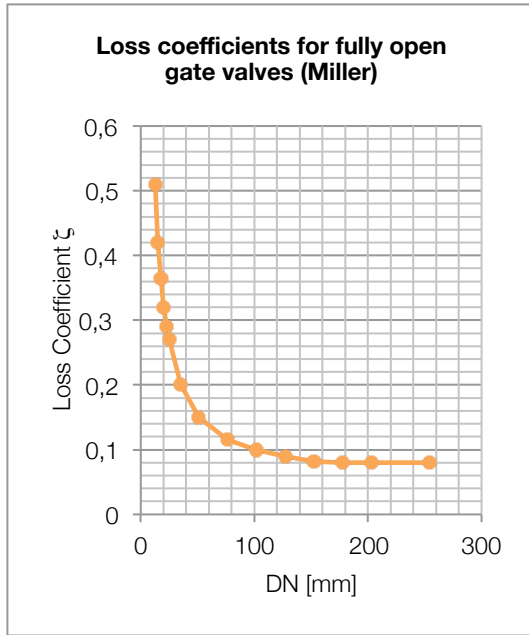
In Table 8 are listed all these single values and ranges of values from different sources:

Table 8: examples of approximate minor loss coefficient associated to standard gate valve from different sources

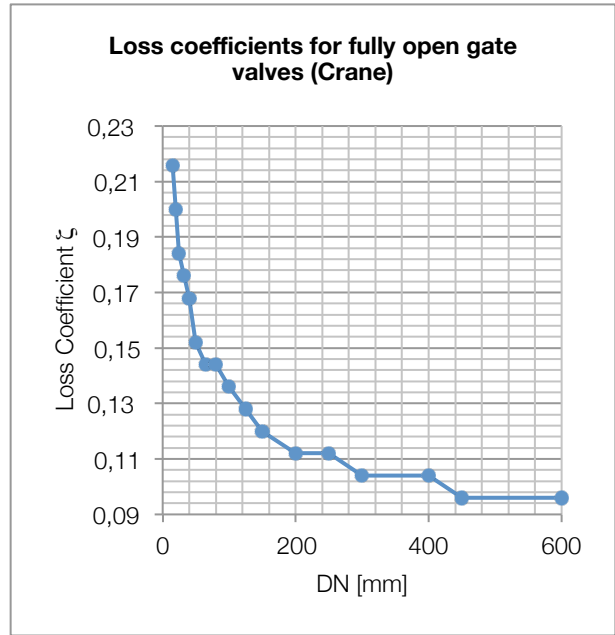
Source	ζ value
Bianchi, Sanfilippo, 2001	0,15
Engineeringtoolbox.com	0,15
Globalsupplyline.com	0,15
Austin University	0,17
I.E. Idel'chik, 1966	0,20
wikiengineer.com	0,20
Zappe R. W., 1998	0,10 – 0,30

Graph 1 shows mean loss coefficients for fully open gate valves with the same flow area as the pipe for Reynolds Number above 5×10^3 (turbulent flow regime). It is not unusual for quoted loss coefficients to vary by a factor or two for valve size under 3 inches (70 mm).

In the Crane book of losses for fully open gate valves the used formula is $\zeta = 8\lambda$ and in the Graph 2 are plotted the values of head loss coefficients found in Crane book (Crane, 1999).

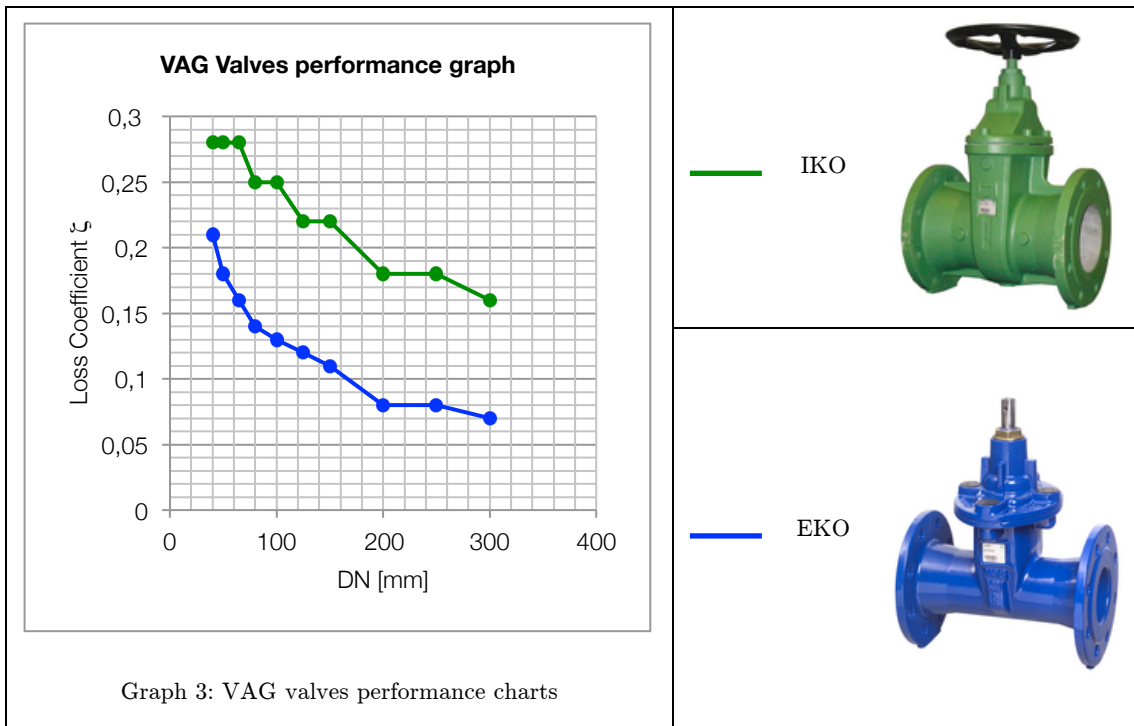


Graph 1: loss coefficients for fully open gate valves



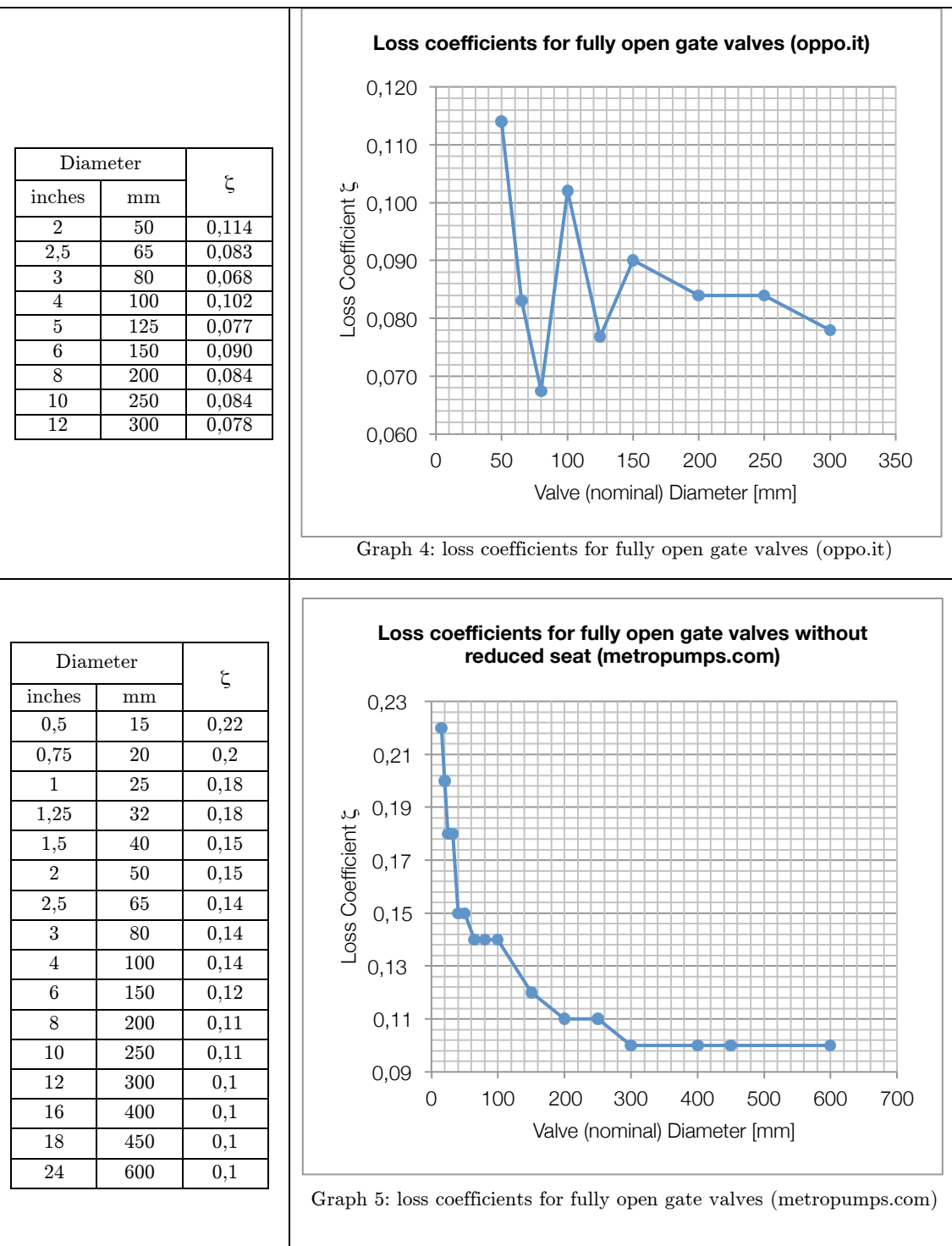
Graph 2: loss coefficients for fully open gate valves (Crane)

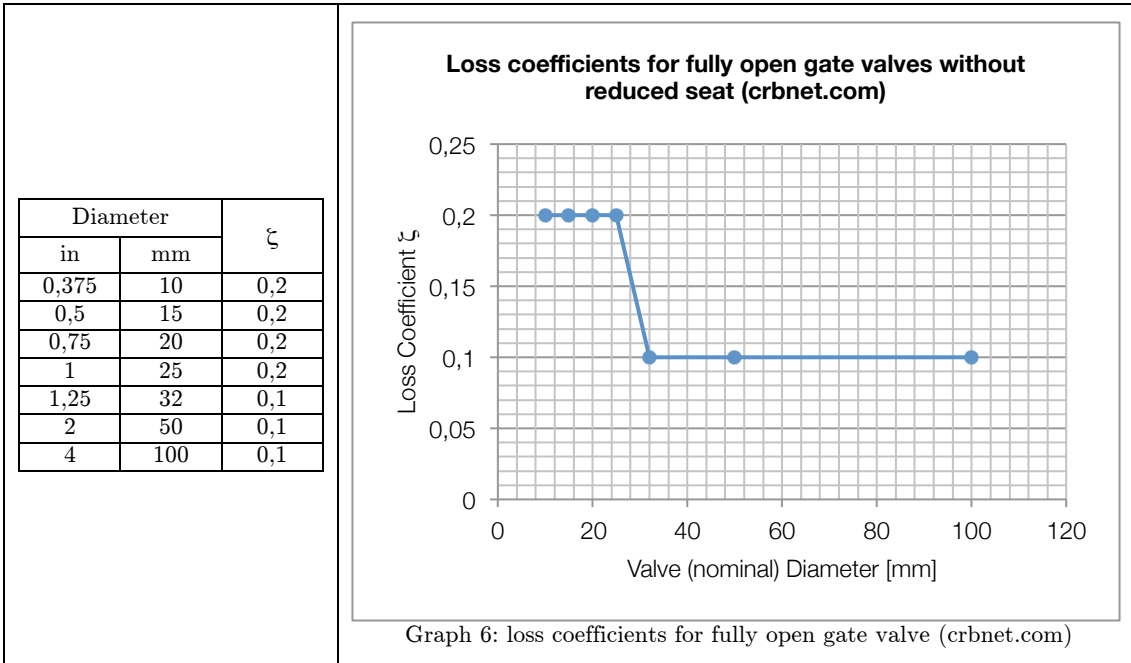
In Graph 3 are represented the trend of ζ values for VAG Valve models IKO and EKO against the Nominal Value of the diameter (in mm). It is graphically confirmed that the metallic sealing IKO causes greater head losses than resilient seated EKO.



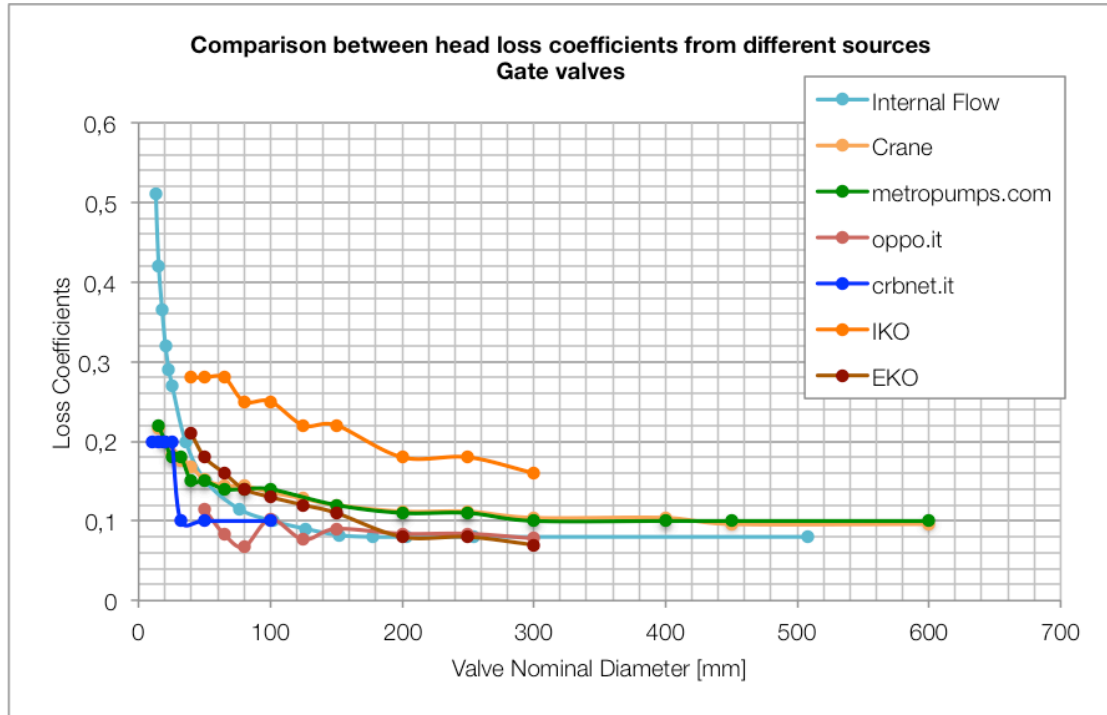
Graph 3: VAG valves performance charts

Researching on internet websites a lot of tables can be found, containing different values of the loss coefficient ζ (sometimes direct values, sometimes in other forms as equivalent length) for fully open gate valves. In the Graph 4, Graph 5 and Graph 6, there is a summary of the main valid results that can be found with the corresponding web site:





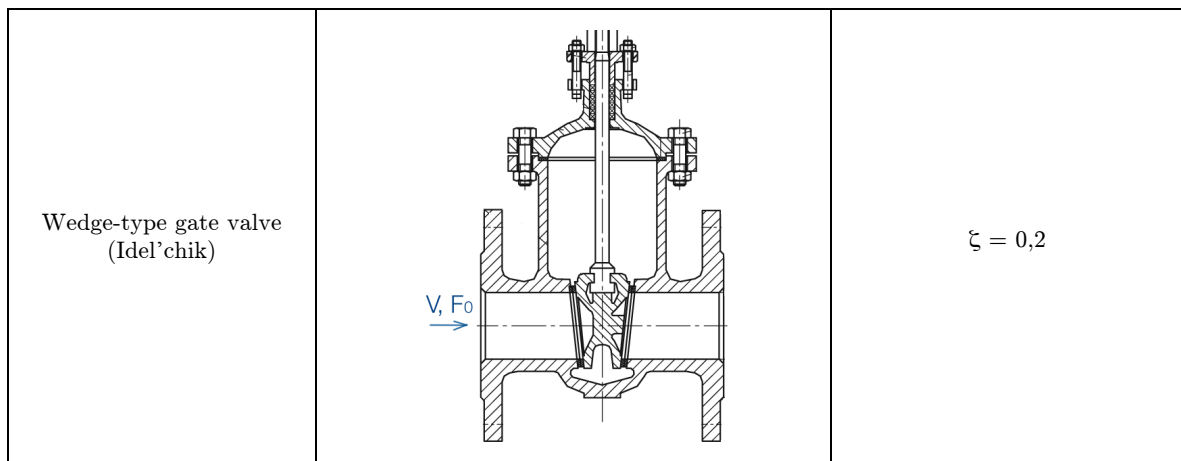
In Graph 7 there is a comparison between the loss coefficients for fully open gate valves from the different sources (literature and website). It is clear that the results are very similar, in particular for nominal diameters between 100 and 600 mm. For low values of nominal diameter Miller book (Miller, 1973) gives results that are higher than the other sources but in the book itself it's stated that for quoted values of loss coefficients at these value of DN is not unusual to vary by a factor or two. A more complete analysis will be executed in the conclusive chapter.



Graph 7: comparison between head loss coefficients from different gate valves's sources

For all the VAG valves there's a clear correspondence between the data taken from technical data sheets and the values find from websites and literature. Only VAG IKOplus Gate Valve, that is metallic-sealing gate valve for use in hot-water pipelines, shows loss coefficients greater than the others.

Also from Idel'chik restance book there's a note aboute wedge-type (metallic sealing) valves, and there's listed a different coefficient from rubber sealing one:



As it is stated in the introductive valves sub-chapter, valves are often designed with a contraction/enlargement and so there are applied to the entrance and to the end of the valve a gradual contraction/enlargement and the coefficient is the resultant of the sum of the single loss coefficient of the valve and the two contraction.

As for the globe valves, turning back on the Crane book, there are other formulas that let to compute the resistance coefficient in this situation of symmetric contraction:

Table 9: formulas for calculating loss coefficient for gate valves

$\beta < 1; \theta \leq 45^\circ$	$\beta < 1; 45^\circ < \theta \leq 180^\circ$
$\zeta = \frac{8\lambda}{\beta^4} + \frac{0,8 \sin \frac{\theta}{2} (1 - \beta^2)}{\beta^4} + \frac{2,6 \sin \frac{\theta}{2} (1 - \beta^2)^2}{\beta^4}$	$\zeta = \frac{8\lambda}{\beta^4} + \frac{0,5 \sqrt{\sin \frac{\theta}{2}} (1 - \beta^2)}{\beta^4} + \frac{(1 - \beta^2)^2}{\beta^4}$

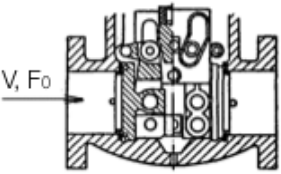
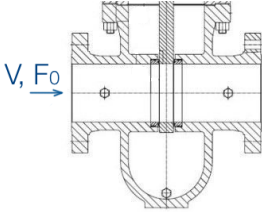
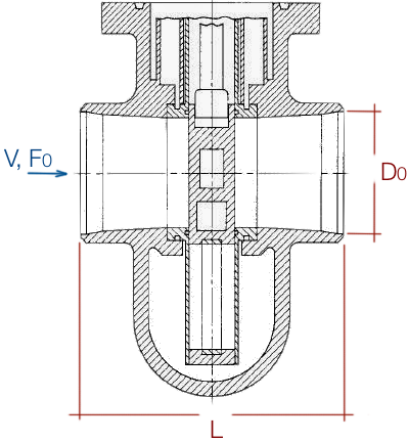
To use this formulas it has to be computed β factor, the ratio between the inside diameter and the outside diameter.

This table can be applied to gate valves standard, wedge disk gate valves, double disk or plug type to compute the complete loss coefficient ζ .

13.2.2 Other types of gate valves

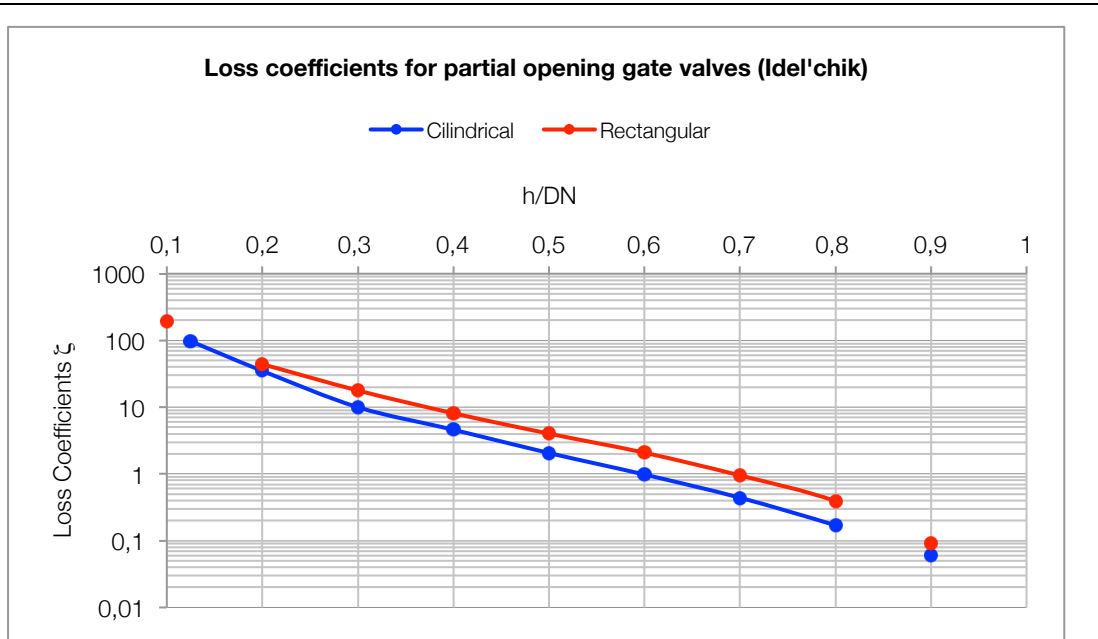
Other types of gate valves with their associated loss coefficients, are listed in **Error! Reference source not found.** The values of ζ are taken from Idel'chik (Idel'chik, 1966) but they are not been object of comparisons or other elaboration of data because of the field of application is different: steam and gas.

Table 10: particular types of gate valve

Valve type	Sectional view	Loss coefficient ζ
Steam gate valve with lever gate		$\zeta = 0,75$
Conduit-type gate valve		$\zeta = 0,30 \div 2,20$
Gate valve with symmetric contraction		$\zeta = 0,40 \div 1,80$

13.2.3 Partial opening of gate valves

All of the ζ seen till now, are values taken for fully open gate valves. Obviously a throttling device as a gate valve has always datasheets and performance graphs that plot loss coefficients against the opening percentage or other equivalent parameters. In particular there's a lot of literature referring to this topic as the Idel'chik book (Idel'chik, 1966) which make a distinguish between cylindrical pipe and rectangular pipe for computing loss coefficients that are plotted in Graph 8:



Graph 8: loss coefficients for gate valves

h/DN	ζ Cylindrical	ζ Rectangular
0,1	-	193
0,125	97,8	-
0,2	35	44,5
0,3	10	17,8
0,4	4,6	8,12
0,5	2,06	4,02
0,6	0,98	2,08
0,7	0,44	0,95
0,8	0,17	0,39
0,9	0,06	0,09
1	0	0

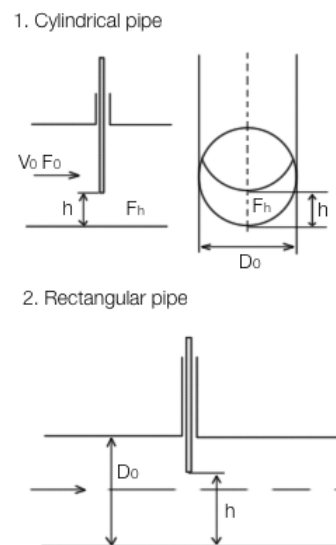
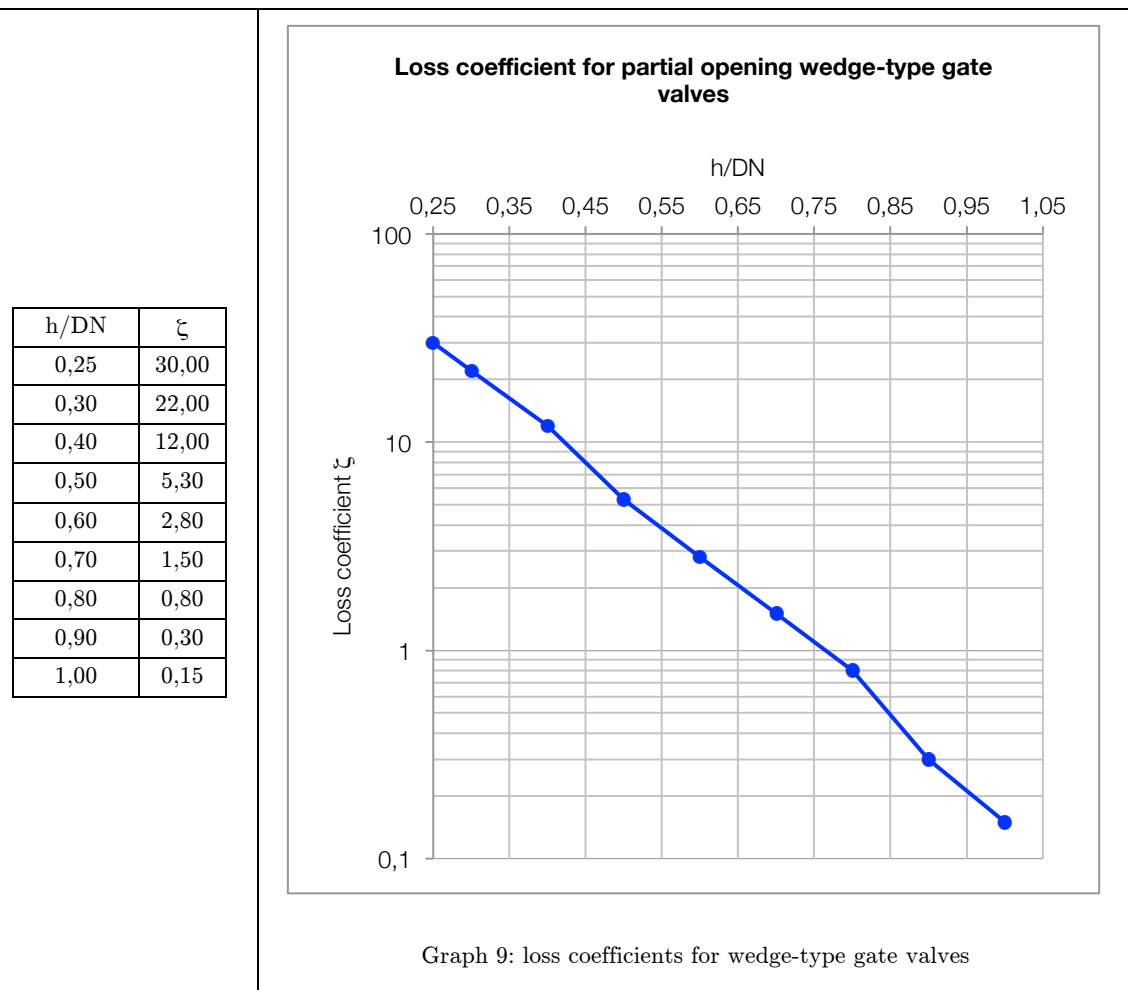


Figure 9: geometrical parameters associated with gate valves

Idel'chik (Idel'chik, 1966) has also plotted loss coefficients for wedge-type gate valve which are the metallic seating, that are reported in the Graph 9:



13.3 Globe valves

Globe valves are simple on concept, relatively easy and inexpensive to manufacture and are able to handle a wide variety of liquids and gasses. Globe valves can be counted in the high-resistance valves: the shape of the valve, a “globe,” makes it very strong and able to withstand very high pressures. They are closing-down valves in which the closure member is moved up and down on the seat. The usual way to define his closure member is to associate it to a disk. The way in which this disk is moving up and down determines the opening of the valve and so the variation of the flow. Globe valves, however, are not particularly good in applications where the valve must be opened and closed frequently.

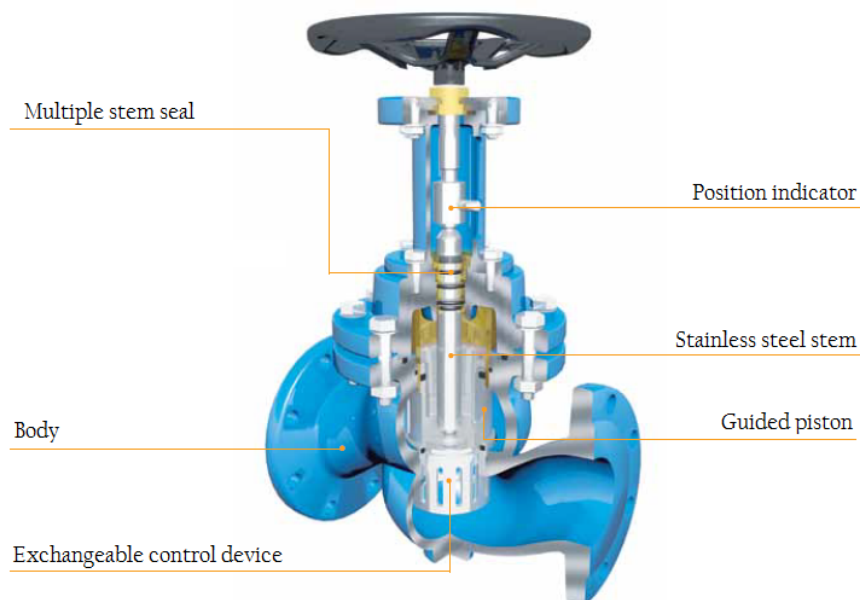


Figure 10: VAG Dura control globe valve

Globe valves, even when they are fully open, provide a significant restriction to the flow through them. The flowing material must round several bends to get through the valve which adds resistance to flow. For this reason, globe valves often need to be sized based on the orifice size (the minimum diameter of the seat) in addition to the pipe size. In short, a valve that fits a certain sized pipe, if it does not have a large enough orifice, may not allow sufficient flow in some applications.

Finally, globe valves are not good at regulating flow but, may, of course, be used for on-off duty, where this tortuous flow passage can be accepted: they work best fully open or fully closed and can't provide a consistently regulated flow when partially open.

The wide range of duties has led to the development of numerous variations of globe valve designed to meet a particular duty at the lowest cost. An effective classification of this type of valve can be the Zappe's (Zappe, 1998) one:

- Angle pattern; Figure 11 a)
- Oblique pattern; Figure 11 b)
- Standard pattern; Figure 11 c)

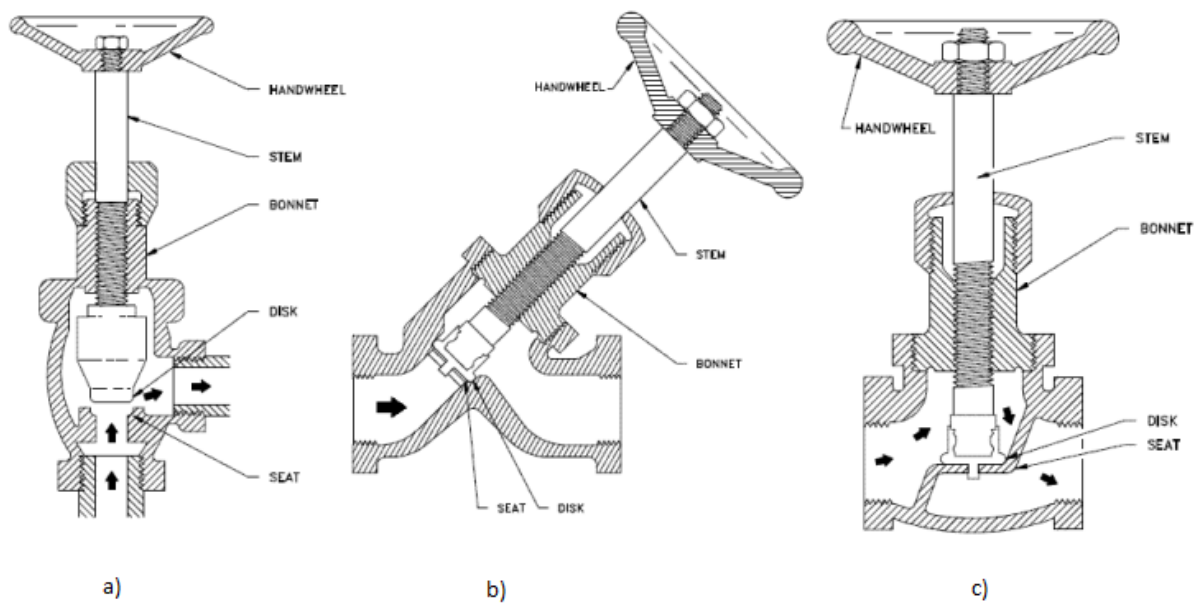


Figure 11: Different types of globe valves

Globe valves may be provided with either metal seating or soft seating. In the case of metal seating, the seating stress must not only be high but also circumferentially uniform to achieve the desired degree of fluid tightness. These requirements have led to a number of seating designs, showed in Figure 12.

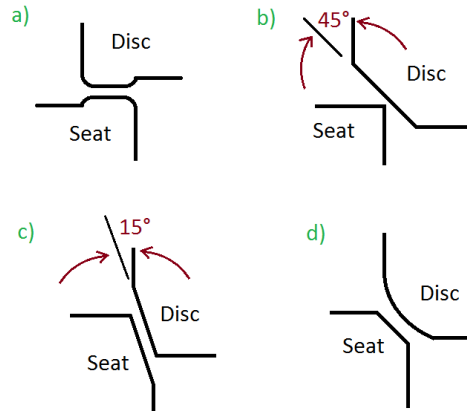


Figure 12: seating configuration frequently employed in Globe valves

In general, all the values listed in this paper for all the types of globe valves are given for turbulent flow condition and for friction factors taken for commercial smooth steel. If other boundary condition were applied, there would be the corresponding specification.

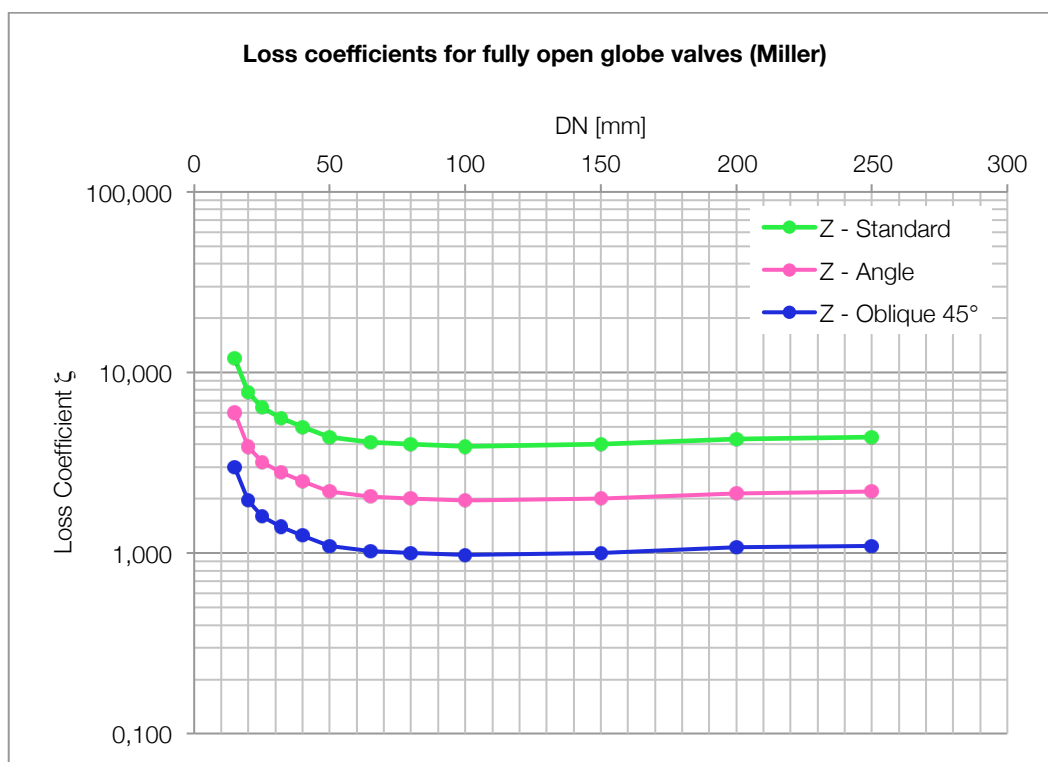
13.3.1 Fully open globe valves

In a lot of websites and other sources the main value for ζ coefficient that appears characterizing globe valve in general (not even specified if straight-way, angle or oblique) is 10. There are also more detailed data from other sources which are resumed in Table 11.

Table 11: examples of approximate minor loss coefficient associated to standard globe valve from different sources

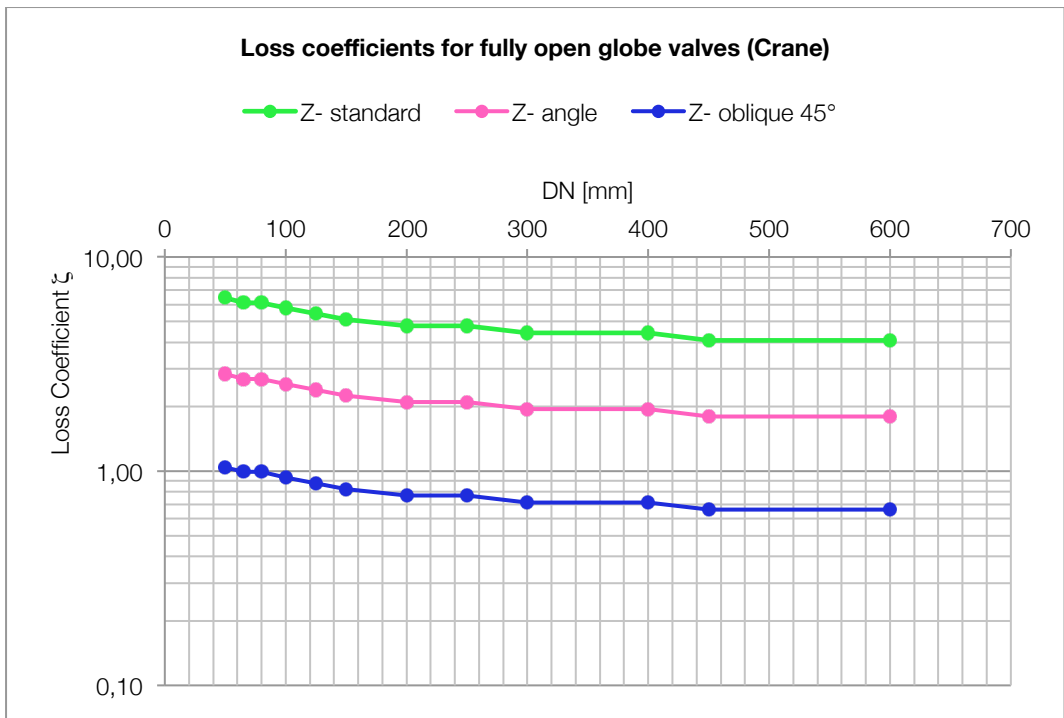
Source	ζ value
lmnoeng.com	10,0
baen.tamu.edu	10,0
Zappe (1998)	<p>Globe valve, standard pattern</p> <p>Full bore seat, cast: 4,0 – 10,0 Full bore seat, forged (small size): 5,0 – 13,0</p> <p>Globe valve, 45°</p> <p>oblique pattern: Full bore seat, cast: 1,0 – 3,0 Globe valve, angle pattern: Full bore seat, cast: 2,0 – 5,0 Full bore seat, forged (small size): 1,5 – 3,0</p>

In Graph 10 are represented the values of loss coefficient for the three types of gate valve described before and taken from Miller book. The trends of the three types are very similar but there are differences in the values: in particular Miller states that loss coefficients for fully open angle valves can be taken as half of the standard valve ones and coefficients of fully open oblique valve (“Y-valve”) are a quarter of the corresponding values in standard valves.

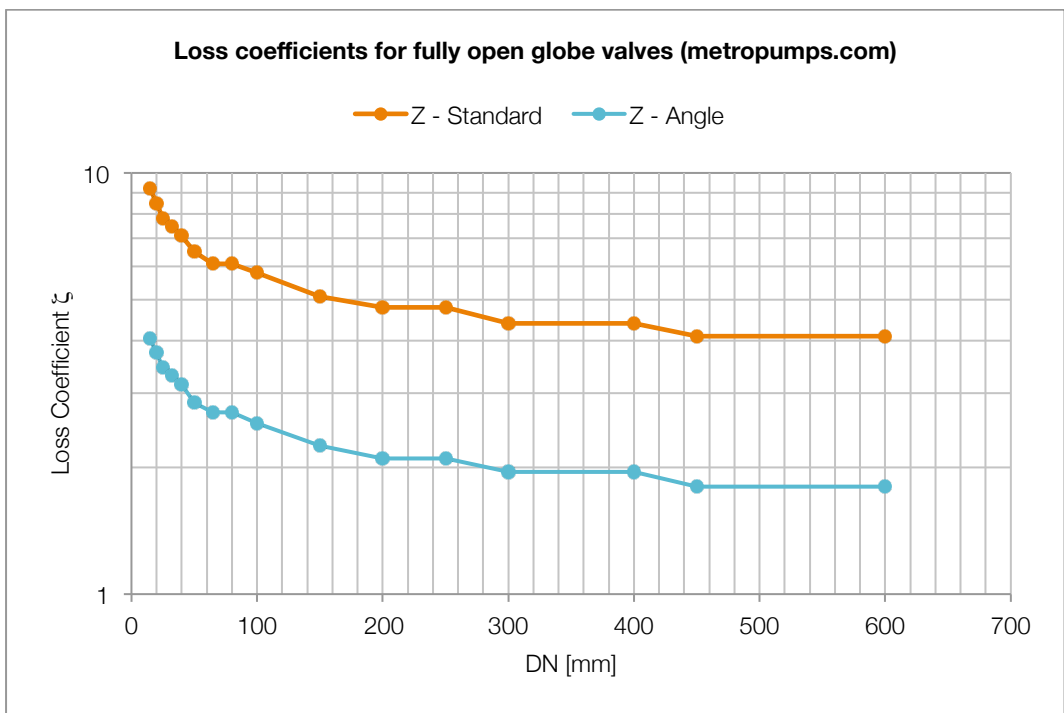


Graph 10: loss coefficients for fully open globe valves three types (Miller)

Researching on internet websites and in literature a lot of tables can be found, containing different values of the loss coefficient ζ (sometimes direct values, sometimes in other forms as equivalent length) for fully open globe valves. In the following graphs, there is a summary of the main valid results that can be found with the corresponding source.



Graph 11: loss coefficients for fully open globe valves three types (Miller)



Graph 12: loss coefficients for fully open globe valves (metropumps.com)

Crane book

Valve DN		λ (clean steel pipe)	ζ standard	ζ angle	ζ oblique
[inches]	[mm]				
2	50	0,019	6,46	2,85	1,05
2 1/2	65	0,018	6,12	2,70	0,99
3	80	0,018	6,12	2,70	0,99
4	100	0,017	5,78	2,55	0,94
5	125	0,016	5,44	2,40	0,88
6	150	0,015	5,10	2,25	0,83
8	200	0,014	4,76	2,10	0,77
10	250	0,014	4,76	2,10	0,77
12	300	0,013	4,42	1,95	0,72
16	400	0,013	4,42	1,95	0,72
18	450	0,012	4,08	1,80	0,66
24	600	0,012	4,08	1,80	0,66

ζ standard
= 340 λ
 ζ angle
= 155 λ
 ζ oblique
= 55 λ

metropumps.com

Valve DN		ζ standard	ζ angle
[inches]	[mm]		
1/2	15	9,2	4,05
3/4	20	8,5	3,75
1	25	7,8	3,45
1 1/4	32	7,5	3,30
1 1/2	40	7,1	3,15
2	50	6,5	2,85
2 1/2	65	6,1	2,70
3	80	6,1	2,70
4	100	5,8	2,55
6	150	5,1	2,25
8	200	4,8	2,10
10	250	4,8	2,10
12	300	4,4	1,95
16	400	4,4	1,95
18	450	4,1	1,80
24	600	4,1	1,80

Miller book

Valve DN		ζ standard	ζ angle	ζ oblique
[inches]	[mm]			
1/2	15	12,00	6,00	3,00
3/4	20	7,80	3,90	1,95
1	25	6,40	3,20	1,60
1 1/4	32	5,60	2,80	1,40
1 1/2	40	5,00	2,50	1,25
2	50	4,40	2,20	1,10
2 1/2	65	4,10	2,05	1,025
3	80	4,00	2,00	1,00
4	100	3,90	1,95	0,975
6	150	4,00	2,00	1,00
8	200	4,30	2,15	1,075
10	250	4,40	2,20	1,10

In the following pages there are the coefficients taken from Idel'chik handbook of hydraulic resistance (Idelchik, 1966). Idel'chik makes a distinction between two patterns of standard globe valves, looking at the inclination of the interface between the closure member and the seat: 45° or 90°.

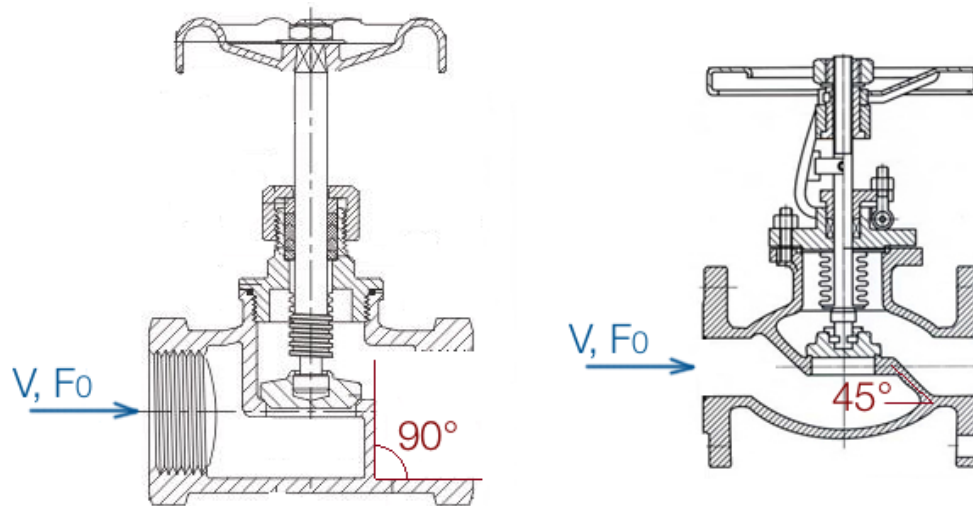
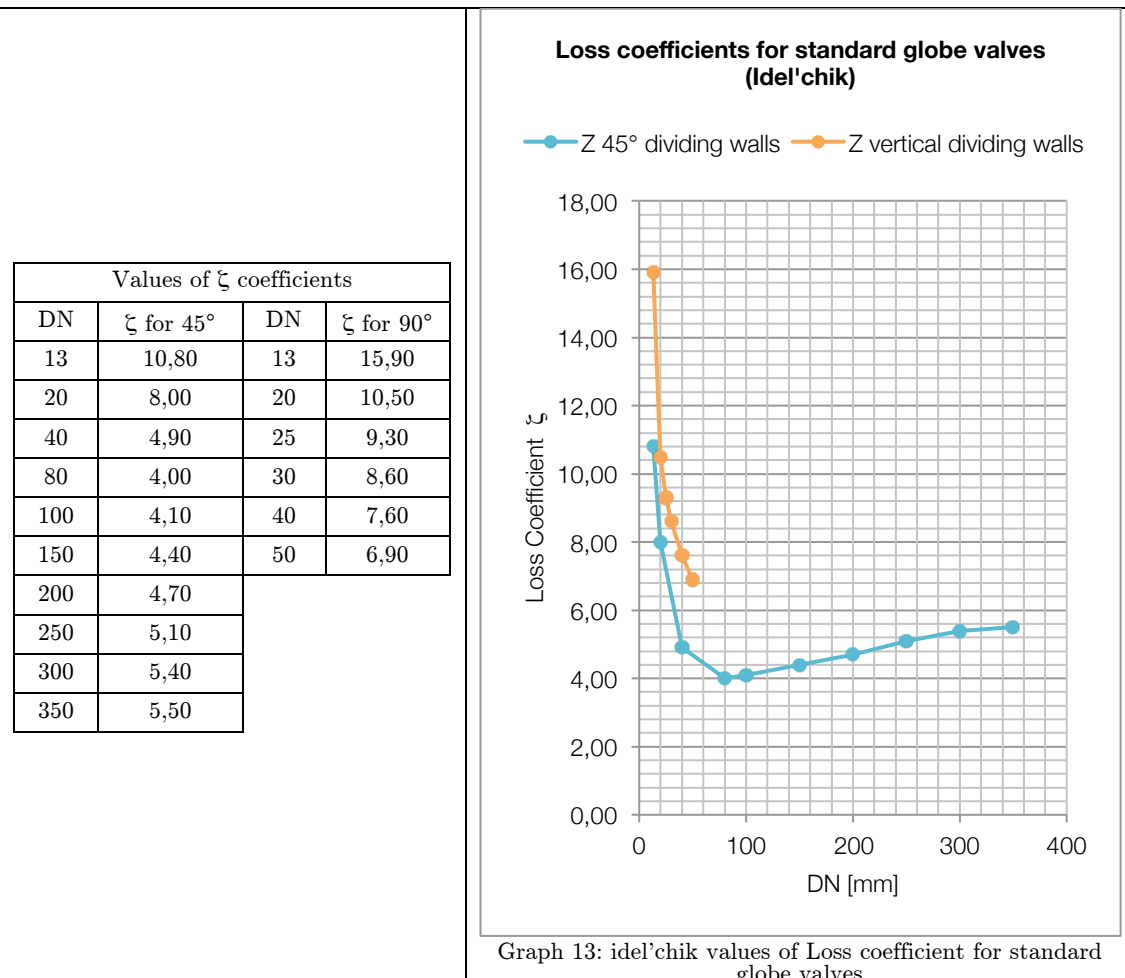
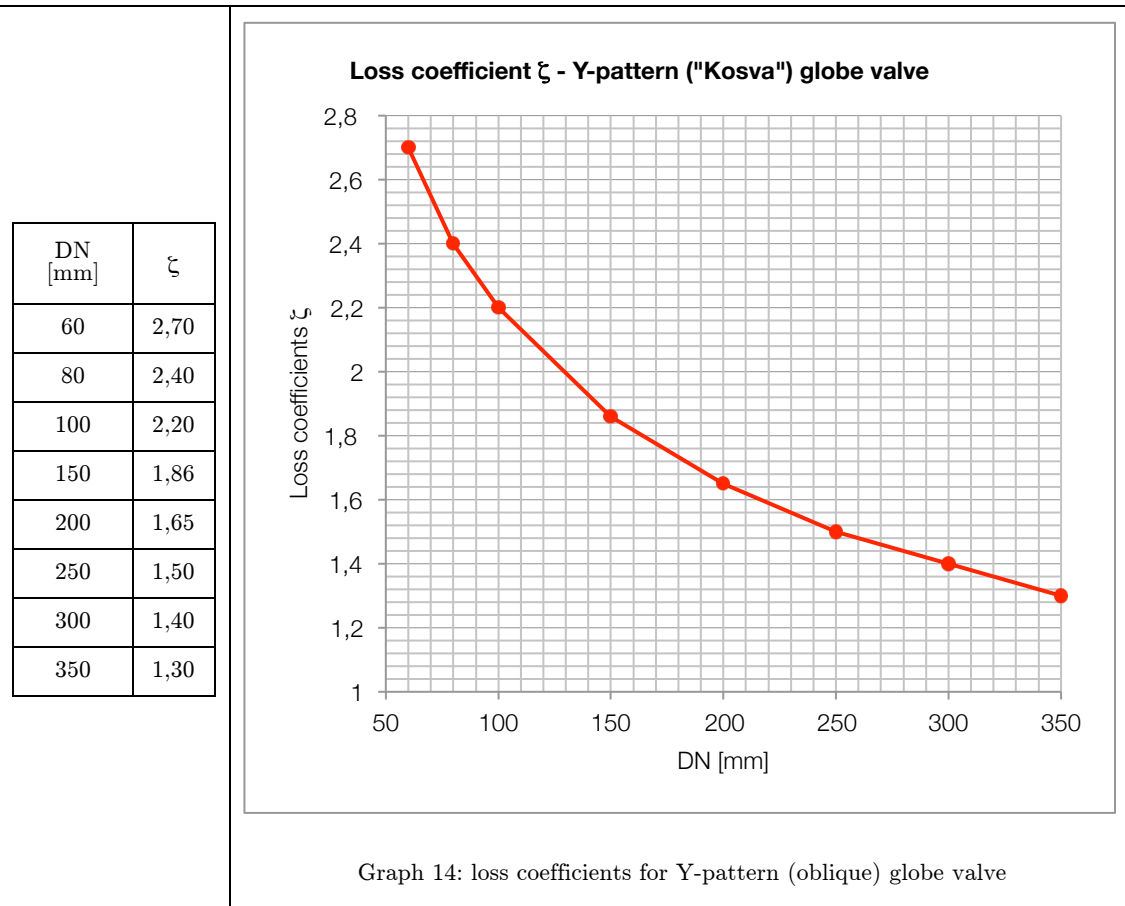


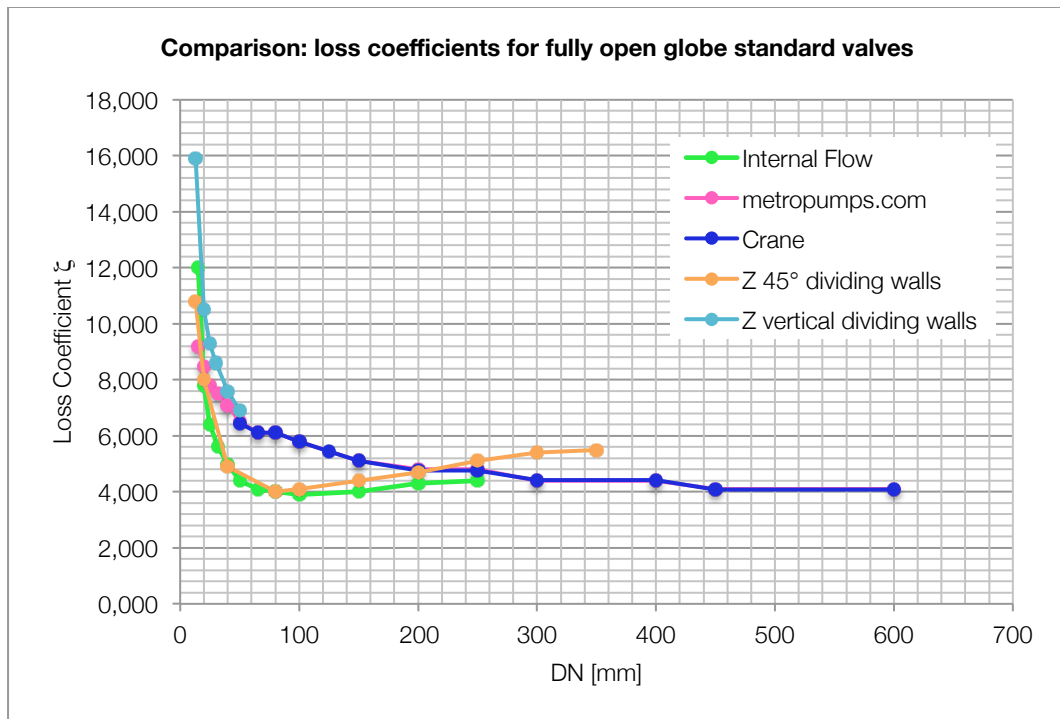
Figure 13: standard globe valve models: vertical (90°) and 45° walls



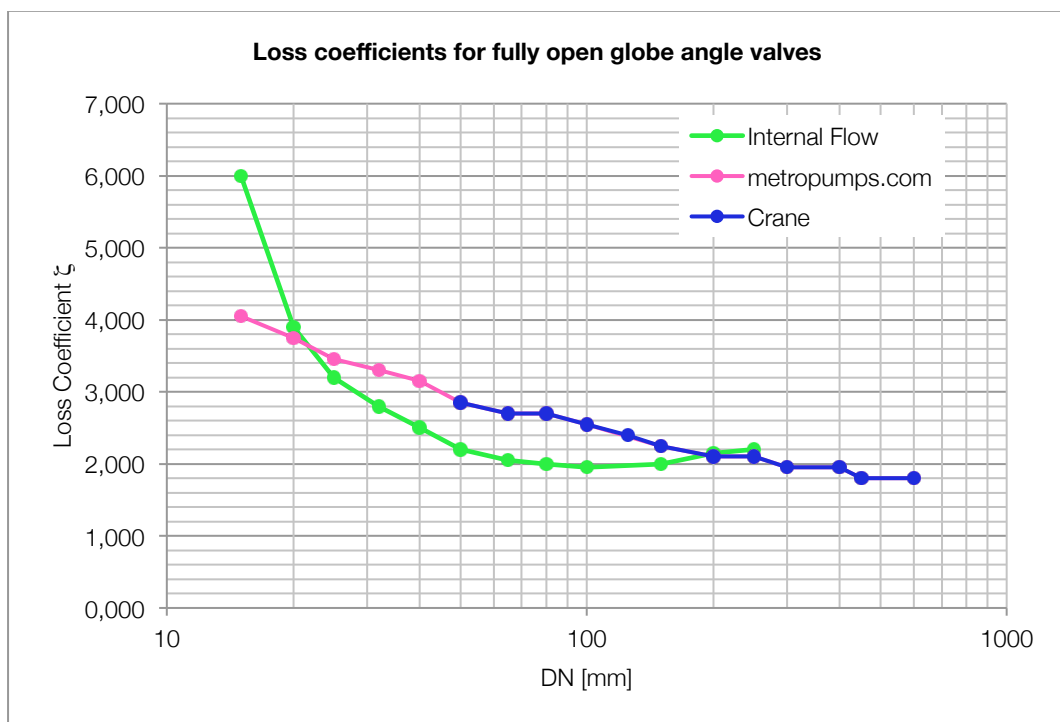
Idel'chik (idel'chik, 1966) lists also ζ values for two types of a particular type of globe oblique valve (Y-pattern), named "Kosva" in the book, plotted against diameter (real) values in the Graph 14:



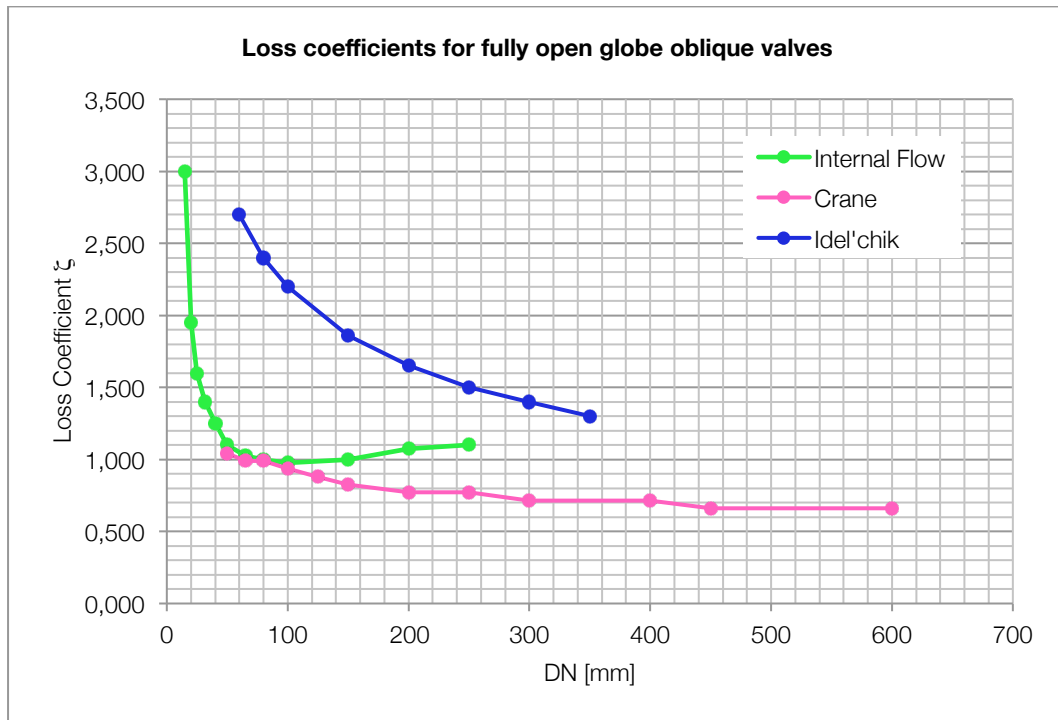
In the Graph 15, Graph 16 and Graph 17 are plotted the comparisons between the different sources for every type of globe valve (standard-pattern, angle-pattern and oblique-pattern).



Graph 15: loss coefficients for fully open globe standard values



Graph 16: loss coefficients for fully open globe angle valves



Graph 17: loss coefficients for fully open oblique valves

It's clear that the values for standard-pattern are very similar for every sources. In particular it can be noticed that there are two principal trends: one characterized by the values from Idel'chik 45° degrees dividing walls and from Miller's Internal Flow, and the other for metropumps.com, Idel'chik vertical dividing walls and Crane book.

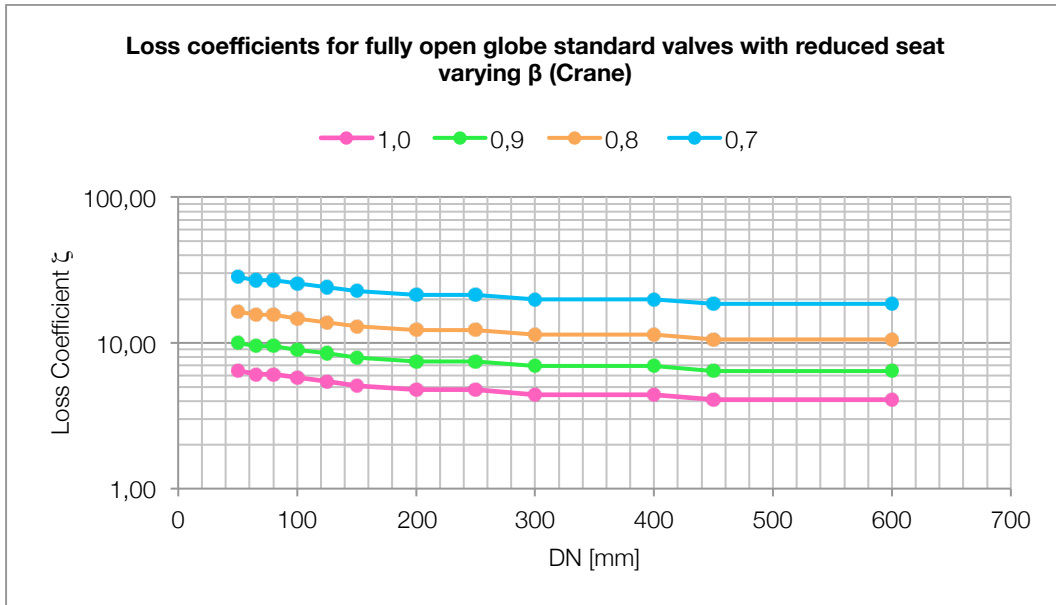
For the angle valves the Crane's trend and metropumps.com are practically overlapped.

For oblique valve the trends are a little bit more different than the other models. This is explainable if we think about the great variety of the Y-pattern models of the valves. There are a lot of parameters that can vary between the models, for example the angle itself, the flow direction, the manufacturing of the seat. For this type of valve is very difficult to analyze the behavior of the head losses from the theoretical point of view.

A more detailed comparison between each pattern of this valve's type are made in the conclusive chapter.

13.3.2 Globe valves with contractions at inlet and outlet

In idel'chik book of resistance and in Crane there are data about computation of the head loss coefficients for standard globe valve with a contraction before and after in the inlet and outlet. In particular is possible to analyze the behavior of the standard globe valve defining the coefficient β as in Crane book: it is the ratio between the diameter of the pipe and the diameter of the reduced seat of the valve.



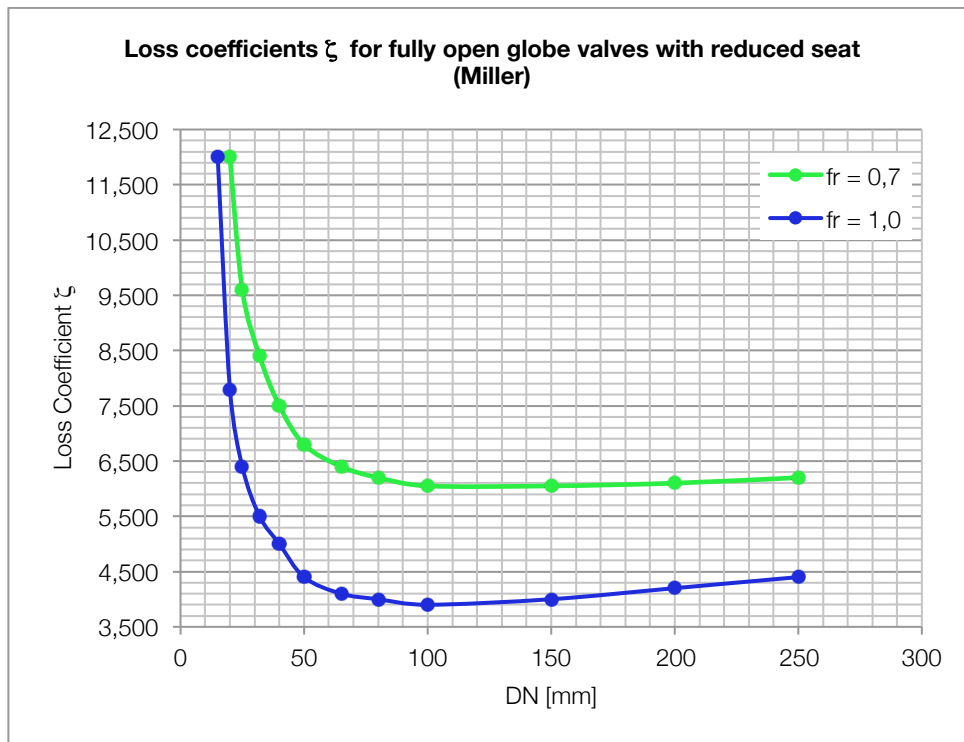
Graph 18: loss coefficients for open globe standard valves with reduced seat for Crane

Nominal diameter [mm]	ζ loss coefficients for standard globe valve			
	$\beta = 1,0$	$\beta = 0,9$	$\beta = 0,8$	$\beta = 0,7$
50	6,46	10,03	16,38	28,41
65	6,12	9,51	15,55	26,99
80	6,12	9,51	15,55	26,99
100	5,78	8,99	14,72	25,58
125	5,44	8,47	13,89	24,16
150	5,10	7,95	13,06	22,74
200	4,76	7,43	12,23	21,33
250	4,76	7,43	12,23	21,33
300	4,42	6,92	11,40	19,91
400	4,42	6,92	11,40	19,91
450	4,08	6,40	10,57	18,49
600	4,08	6,40	10,57	18,49

13.3.3 Globe valves with reduced seat

In Miller book (Miller, 1973), there's a graph which plots the head loss coefficients ζ at different nominal diameter values, for reduced seat globe valves (Graph 19).

Defining the ratio f_r of the cross sectionl inlet area of the pipe F_0 and the seat area F_s , in the following graph there's the comparison between the curves corresponding to $f_r = 0,7$ and $f_r = 1,0$ (no reduced seat).

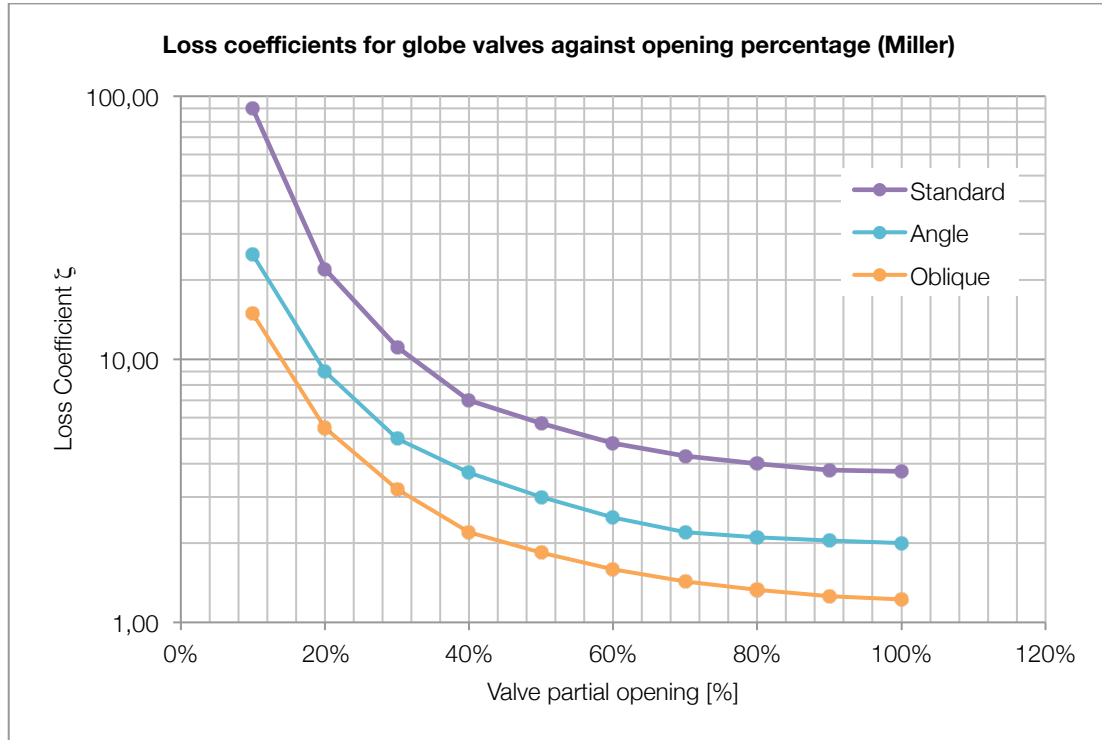


Graph 19: loss coefficients for open globe standard valves with reduced seat for Miller

Loss coefficients ζ	
$f_r = 0,7$	$f_r = 1,0$
inf	12,00
12,00	7,80
9,60	6,40
8,40	5,50
7,50	5,00
6,80	4,40
6,40	4,10
6,20	4,00
6,05	3,90
6,05	4,00
6,10	4,20
6,20	4,40

13.3.4 Partial opening of globe valves

Idel'chik book of resistance (Idel'chik, 1966) plots the Graph 20 for the three main types of globe valve regarding the head losses against the opening percentage of the valve:



Graph 20: loss coefficients for the three models of globe valve against opening percentage

Partial Opening	ζ values		
	Standard	Angle	Oblique
10%	90,00	25,00	15,00
20%	22,00	9,00	5,50
30%	11,10	5,00	3,20
40%	7,00	3,70	2,20
50%	5,70	3,00	1,84
60%	4,80	2,50	1,59
70%	4,30	2,20	1,43
80%	4,00	2,10	1,33
90%	3,80	2,05	1,26
100%	3,75	2,00	1,22

From this point of view it is clear that the best performer is the oblique-pattern globe valve but a more detailed comparison is made in the conclusive chapter.

13.3.5 Other types of globe valves

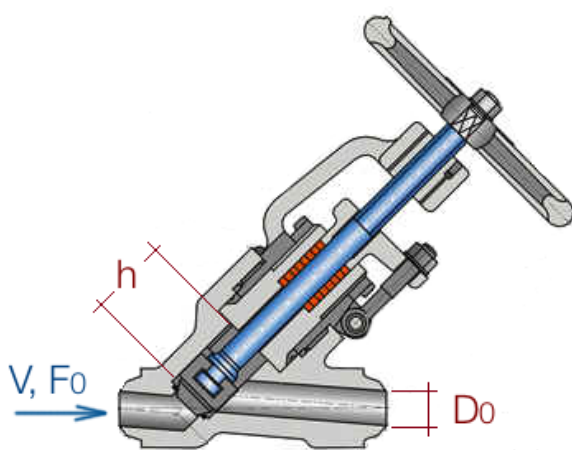
Direct-flow globe valves

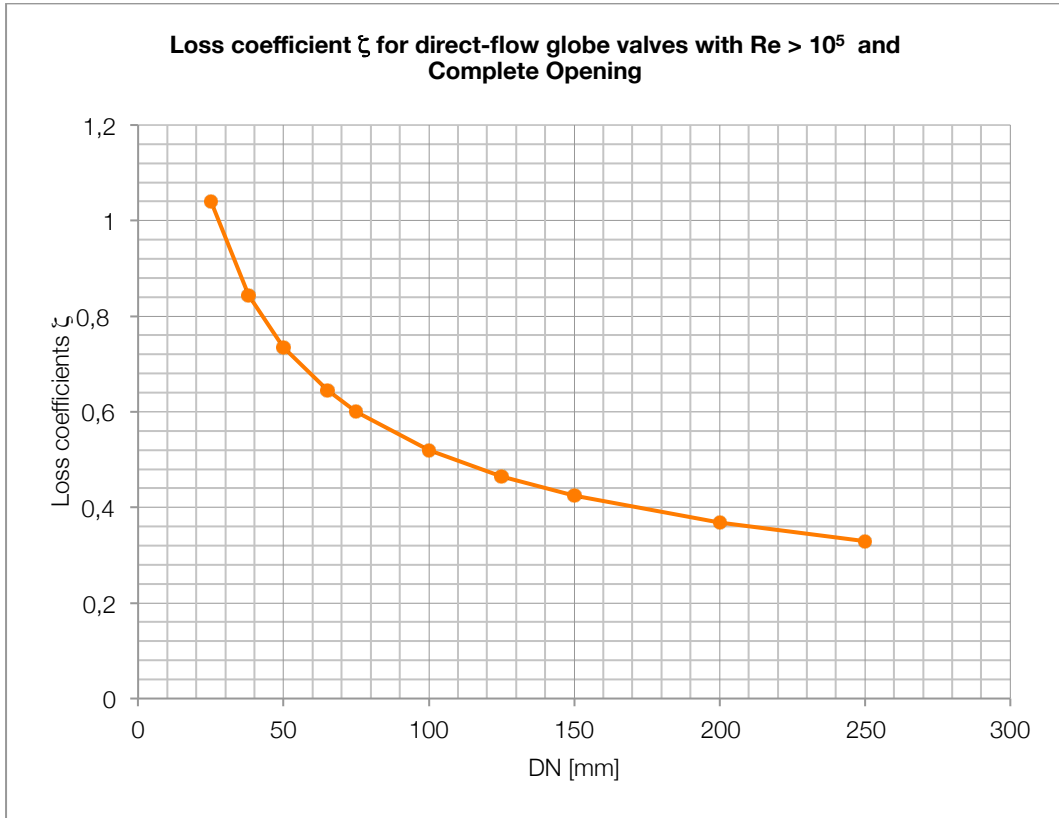
For idel'chik book (idel'chik, 1966) , the best design for minimizing fluid resistance is that of a straight-way globe valve. The resistance coefficient of this valve type, depends mostly on the Reynolds number value: at small Re the coefficient decreases rapidly with the increase of Re till the minimum value for $Re = 5 \times 10^4$. After that point it begins a slow increase until, finally, it becomes constant and independent of Re.

The resistance coefficient for straight-way globe valve, can be determined by Murin formulas for the cases listed in the Table 12.

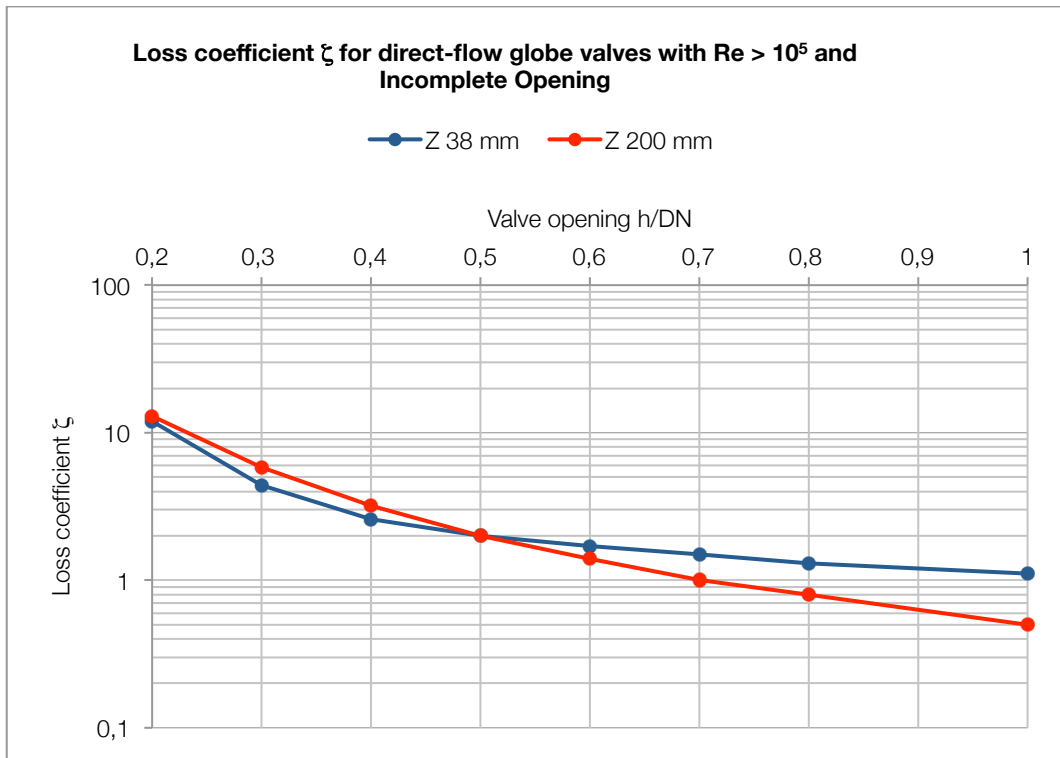
Table 12: resistance coefficient for straight-way globe valves formulas

As a function of the valve lift h/DN , at $DN = 38$ mm	$\zeta = \frac{\Delta H}{\frac{V_0^2}{2g}} = 1,28 + \frac{0,084}{\left(\frac{h}{DN}\right)^2}$
As a function of the valve lift h/DN , at $DN = 200$ mm	$\zeta = \frac{\Delta H}{\frac{V_0^2}{2g}} = \frac{0,51}{\left(\frac{h}{DN}\right)^2}$
At full opening within the limits $25 \text{ mm} < DN < 200 \text{ mm}$	$\zeta = \frac{\Delta H}{\frac{V_0^2}{2g}} = \frac{5,2}{\sqrt{DN}}$

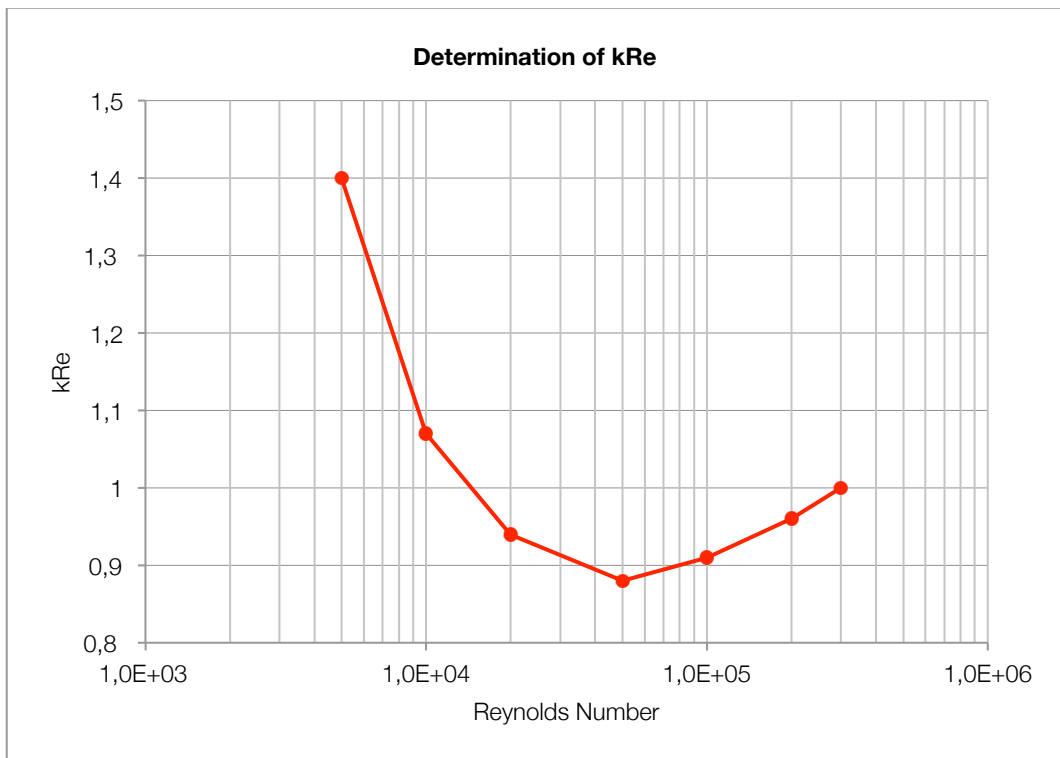
 <p>Figure 14: direct-flow globe valve with geometrical parameters</p>	$Re > 3 \times 10^5$ Incomplete opening	
	$D_0 = 38 \text{ mm}$	$\zeta = 1,28 + \frac{0,084}{\left(\frac{h}{DN}\right)^2}$
	$D_0 = 200 \text{ mm}$	$\zeta = \frac{0,51}{\left(\frac{h}{DN}\right)^2}$
	$Re > 3 \times 10^5$ Complete opening	
	$25 \text{ mm} < D_0 < 200 \text{ mm}$	$\zeta = \frac{5,2}{\sqrt{DN}}$
	$Re < 3 \times 10^5$ Incomplete opening	
$\zeta_{laminar} = k_{Re} \zeta_{turbulent}$		



Graph 21: loss coefficients for direct-flow globe valve, $Re > 3 \times 10^5$ for complete opening



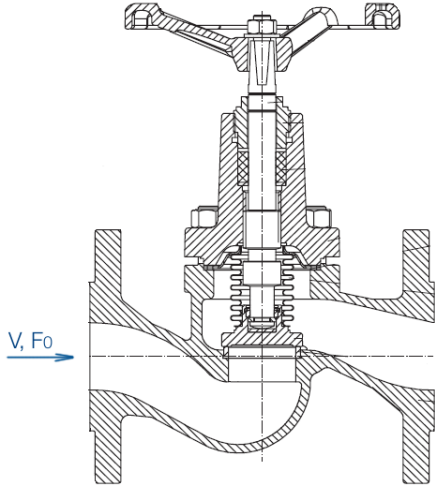

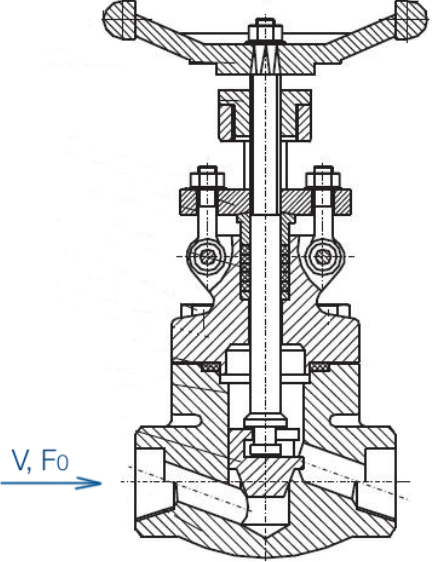

Graph 22: loss coefficients for direct-flow globe valve, $Re > 3 \times 10^5$ for incomplete opening



Graph 23: Determination of k_{Re}

Other types of globe valves with their associated loss coefficients are listed in the following table. The values of ζ are taken from Idel'chik book of hydraulic resistance.

Table 13: particular globe valve types

Valve type	Sectional view		Loss coefficient ζ
Straight way globe valve			$\zeta = 3,4$
Forged globe valve			$\zeta = 7,8$

13.4 Lift check valves

A lift-check valve is a check valve in which the disk, sometimes called *lift*, can be lifted up off its seat by higher pressure of inlet or upstream fluid to allow flow to the outlet or downstream side. A guide keeps motion of the the closure member in these valves in the direction normal to the plane of the seat, so the valve can later reseal properly. When the pressure is no longer higher, gravity or higher downstream pressure will cause the disk to lower onto its seat, shutting the valve to stop reverse flow.

In the following pages are plotted, in the Graph 24 and Graph 25 the trends of the head loss coefficient for this type of valve from the different sources.

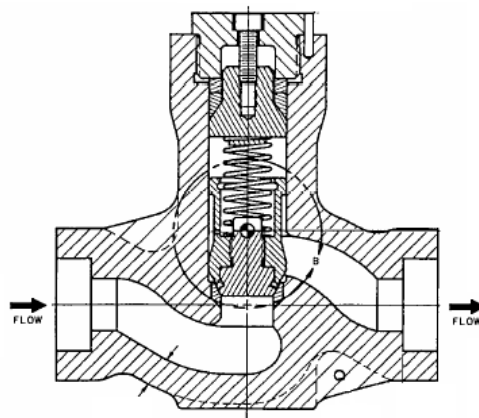
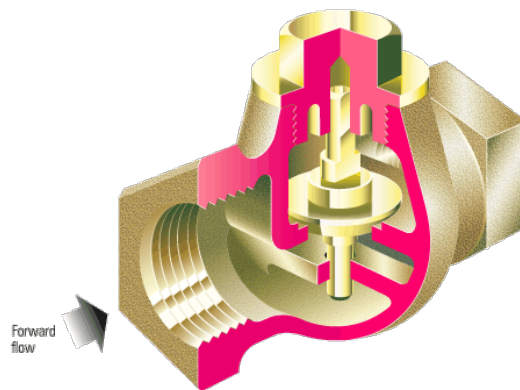


Figure 15: schematic representation and section view of a lift check valve (standard pattern)

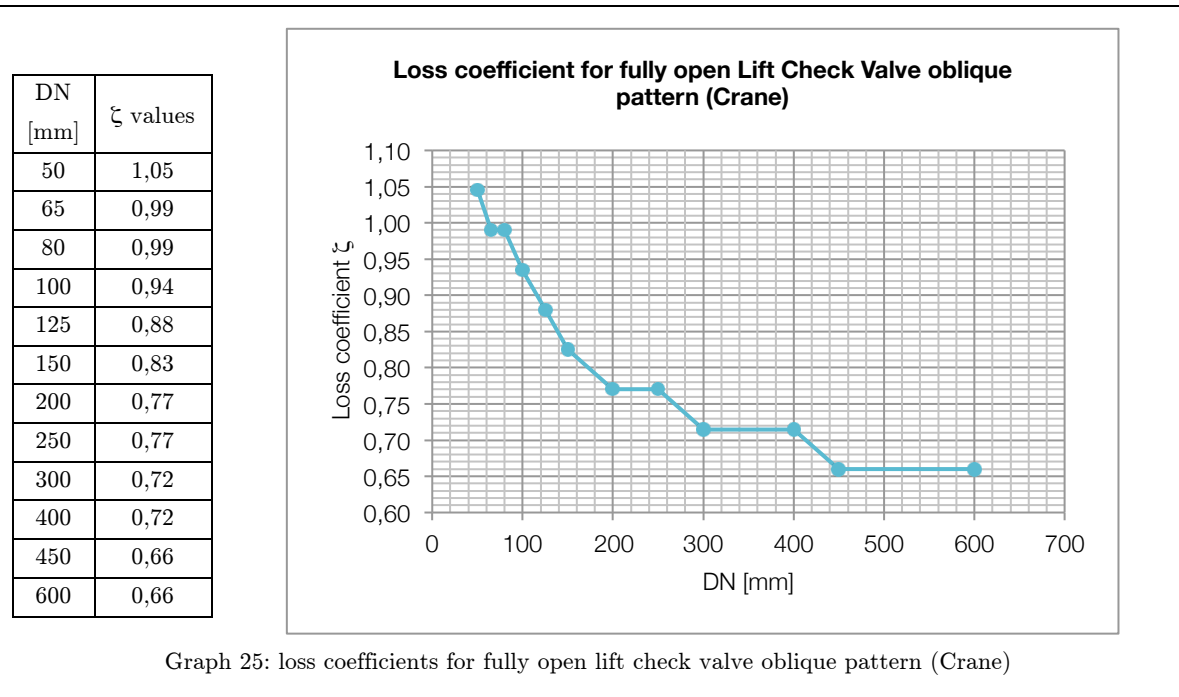
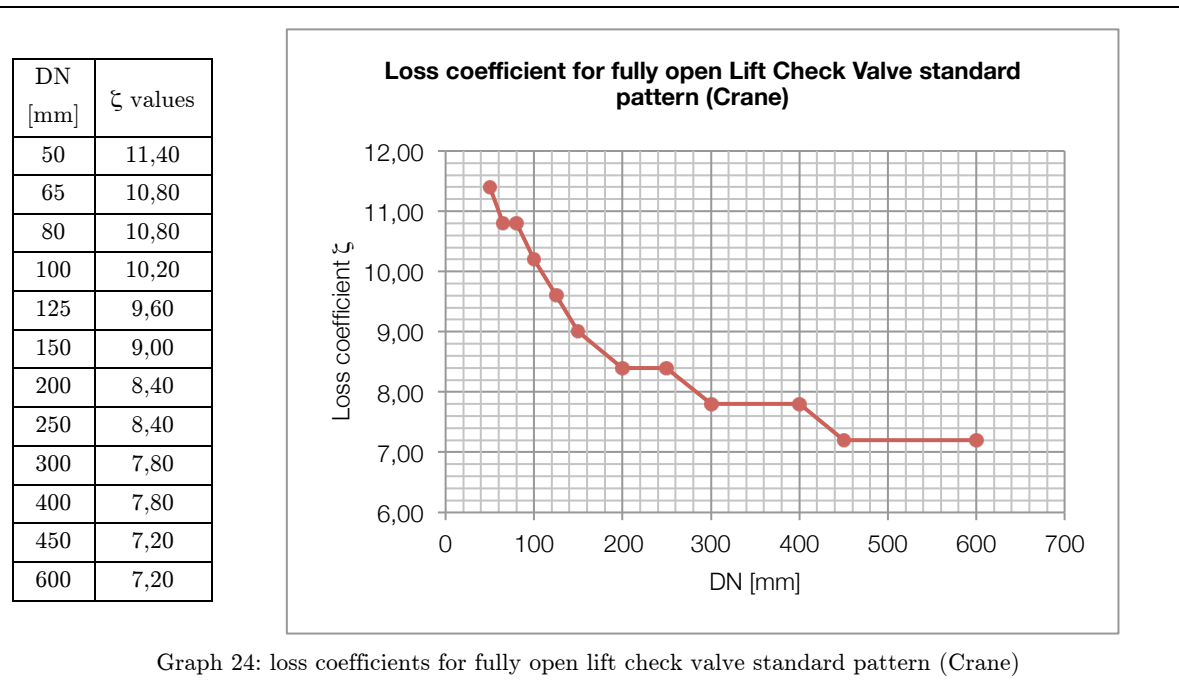


In this category of valves it is possible to include two main patterns of valve: the standard lift check valves, which is perfectly in line with the previous description, and the ball check valve, in which the body and the flow direction is similar but closure member is literally a ball.

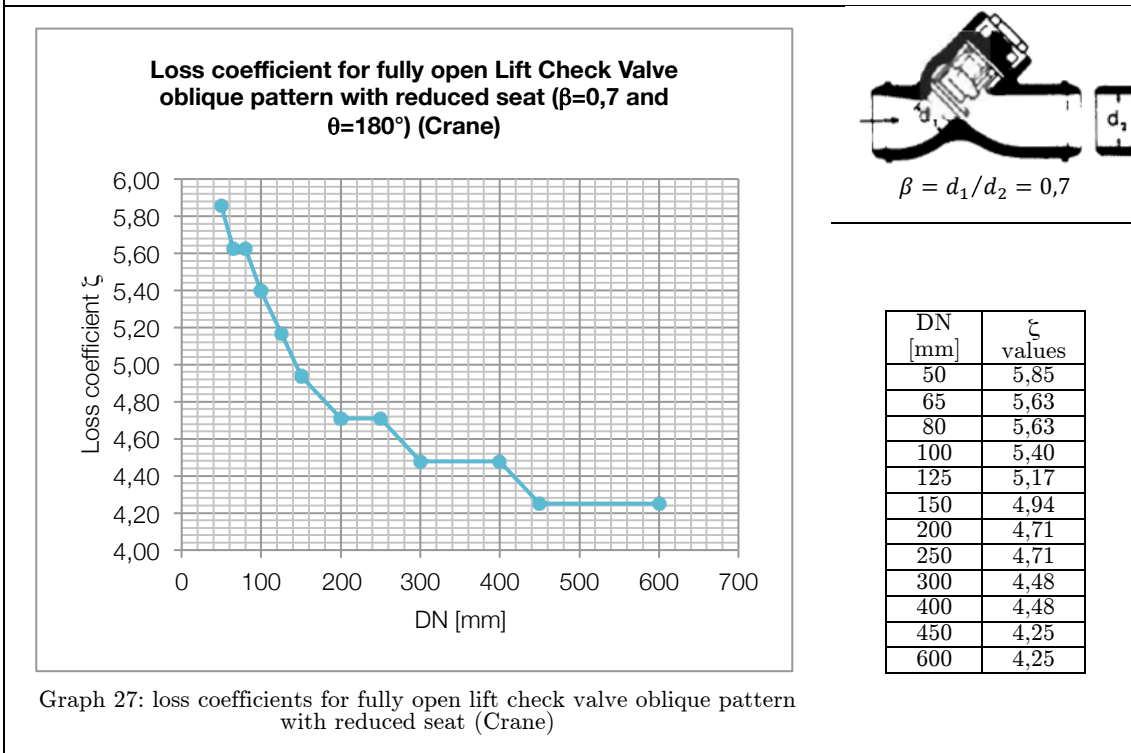
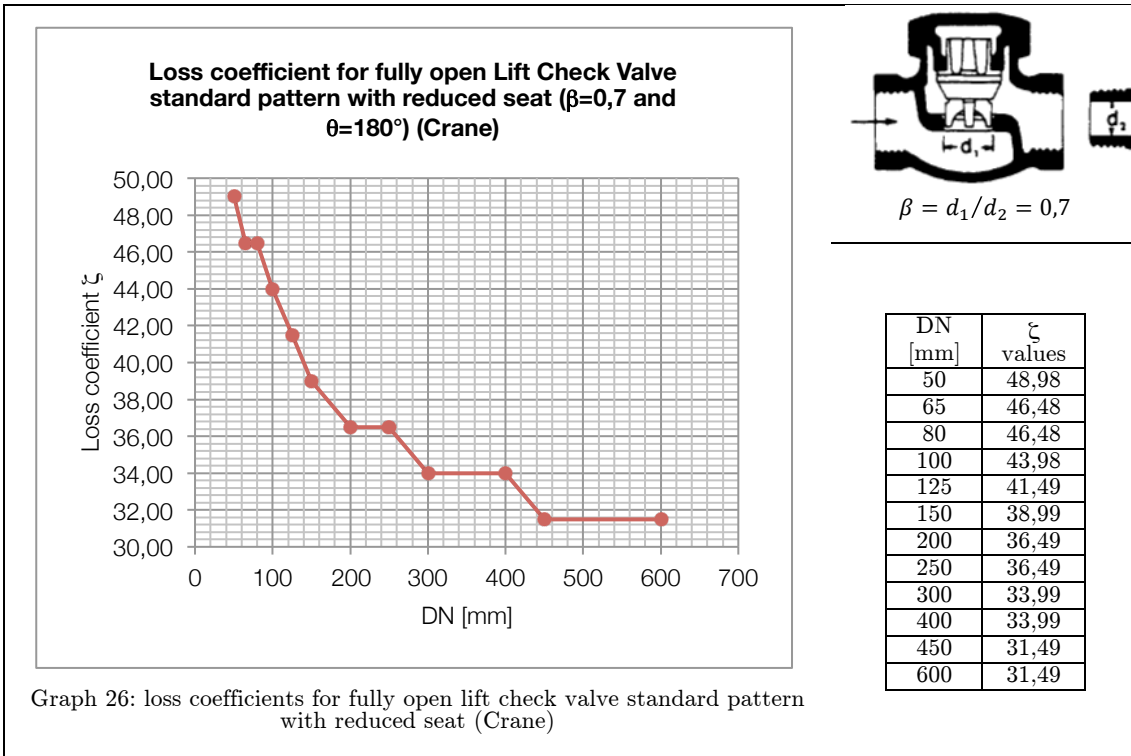
13.4.1 Standard Lift Check Valves

The geometry, materials and constructive particulars are very similar to the standard, angle and oblique globe valves. For Miller (Miller, 1973) check valves of similar design to globe and angle valve have similar loss coefficients in the fully open position.

In the following graphs are plotted the results given by Crane (Crane, 1999) about this type of valves:

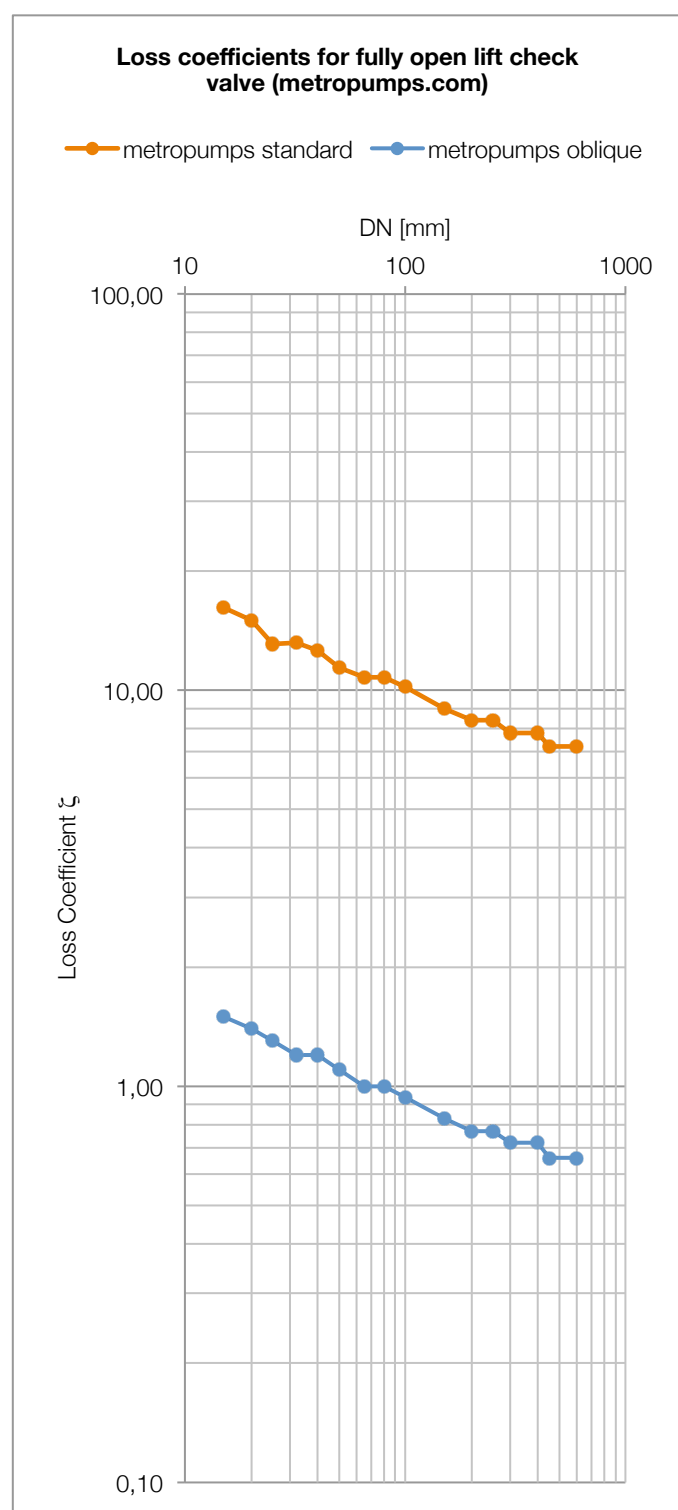


Crane technical book (Crane, 1999) also refers the values of coefficients for lift check valves with contraction at inlet and outlet, computed for divergence angle $\theta = 180^\circ$ (abrupt enlargement) and $\beta = 0,7$. These values are plotted in the Graph 26 and in the Graph 27.



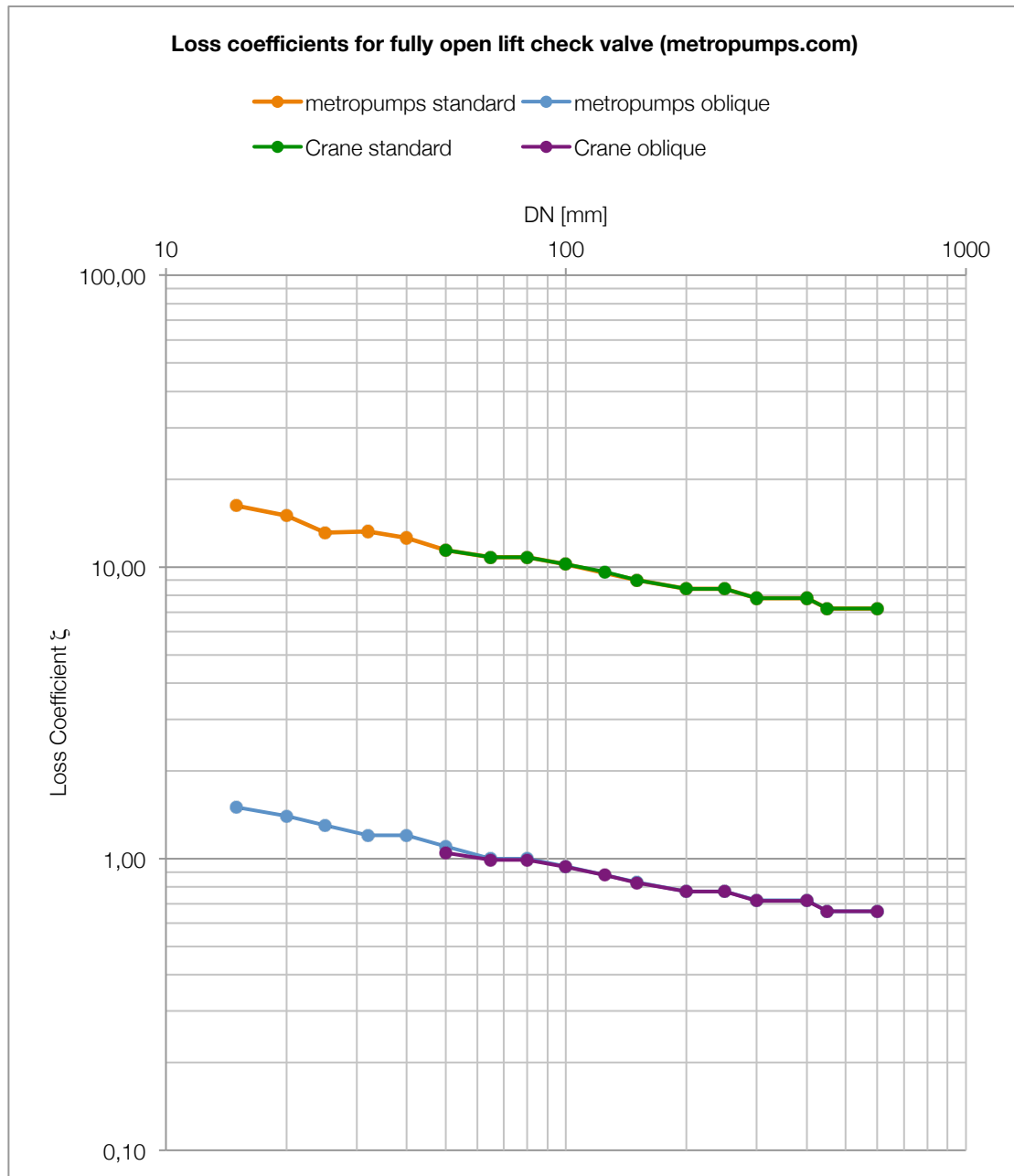
The site metropumps.com refers the values of coefficients for fully open standard lift check valves plotted in Graph 28.

DN [mm]	ξ standard	ξ oblique
15	16,20	1,50
20	15,00	1,40
25	13,08	1,30
32	13,20	1,20
40	12,60	1,20
50	11,40	1,10
65	10,80	1,00
80	10,80	1,00
100	10,20	0,94
150	9,00	0,83
200	8,40	0,77
250	8,40	0,77
300	7,80	0,72
400	7,80	0,72
450	7,20	0,66
600	7,20	0,66



Graph 28: loss coefficient values for fully open lift check valves

In the Graph 29 there is the comparison between the values from the two sources:



Graph 29: comparison between Crane data and metropumps.com data

It's clear that the values are practically overlapped for the two types of valves with similar diameters but a more complex analysis of the comparison will be made in the conclusive chapter.

13.4.2 Ball Check Valves

This consists of a rubber-coated ball that is normally seated on the inlet to the valve, sealing off the inlet. When pressure is exerted on the ball, it is moved off its seat along a guide rail, allowing fluid to pass through the inlet. When the fluid pressure drops, the ball slides back into its position on the inlet seat. There is a great variety in the ball check valves and the main discriminating of the classifications is recognizable in the direction of the guide rails compared to the flow direction: oblique, perpendicular or, more rarely, axial. Both of the available sources treat only oblique rail guides.



Figure 16: VAG KRV ball check-valve

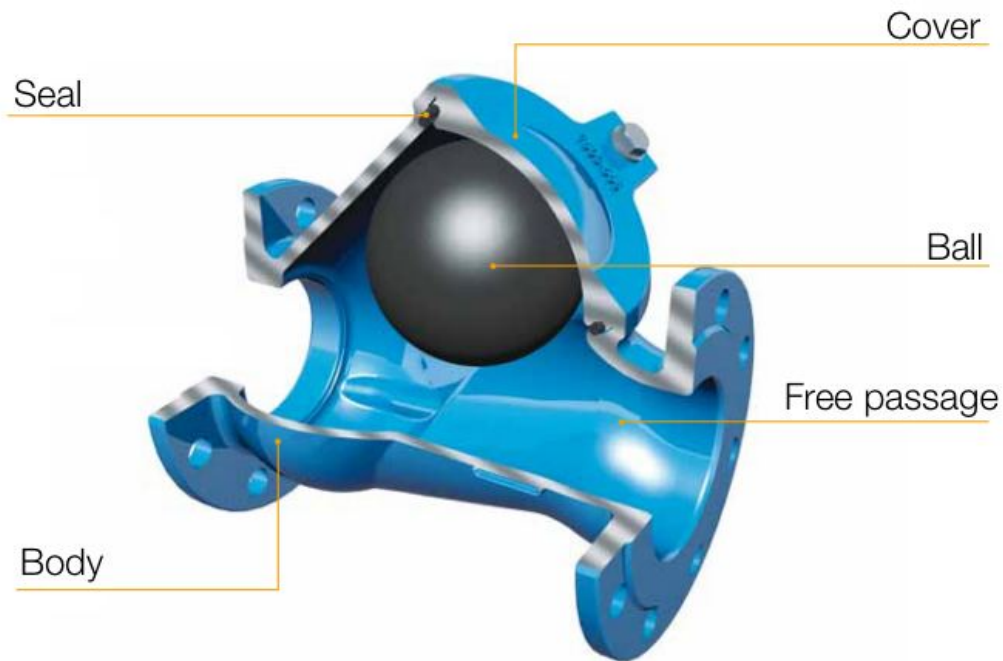
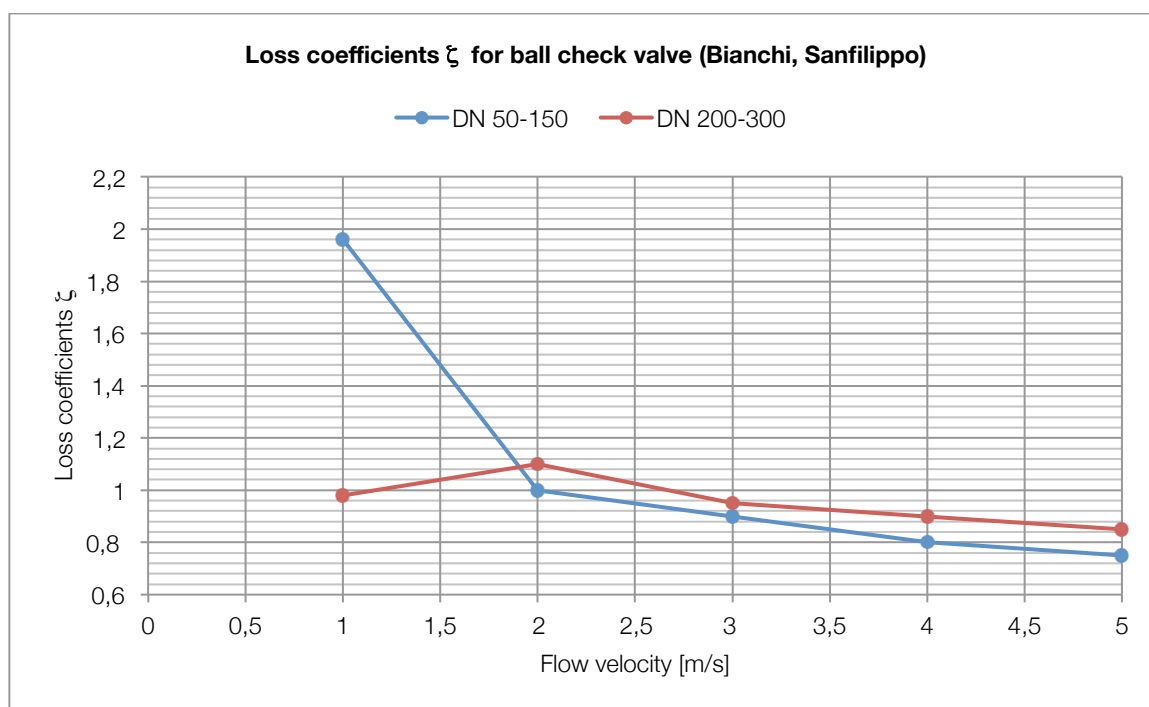
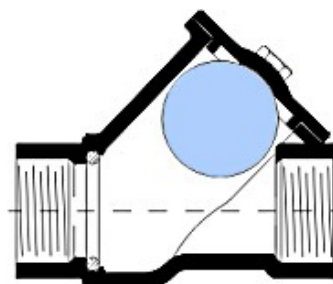


Figure 17: schematic view of VAG KRV ball check-valve

For this valve type are found only head loss coefficient values against the flow velocity in the pipe: this is an obvious choice because we're talking about a check-valve, which is open and regulated by the flow itself. From Bianchi (Bianchi, Sanfilippo, 2001) we can refer the following values for this type of valve, with oblique lift seat, plotted in the Graph 30:

Flow velocity	DN [mm]	ζ values
$V_0 \leq 1$ m/s	DN 50 ÷ 150	$\Delta H = 0,10$ m
	DN 200 ÷ 300	$\Delta H = 0,05$ m
$V_0 \leq 2$ m/s	DN 50 ÷ 150	1,00
	DN 200 ÷ 300	1,10
$V_0 \leq 3$ m/s	DN 50 ÷ 150	0,90
	DN 200 ÷ 300	0,95
$V_0 \leq 4$ m/s	DN 50 ÷ 150	0,80
	DN 200 ÷ 300	0,90
$V_0 \leq 5$ m/s	DN 50 ÷ 150	0,75
	DN 200 ÷ 300	0,85



Graph 30: loss coefficients ζ for ball check valve (Bianchi, Sanfilippo)

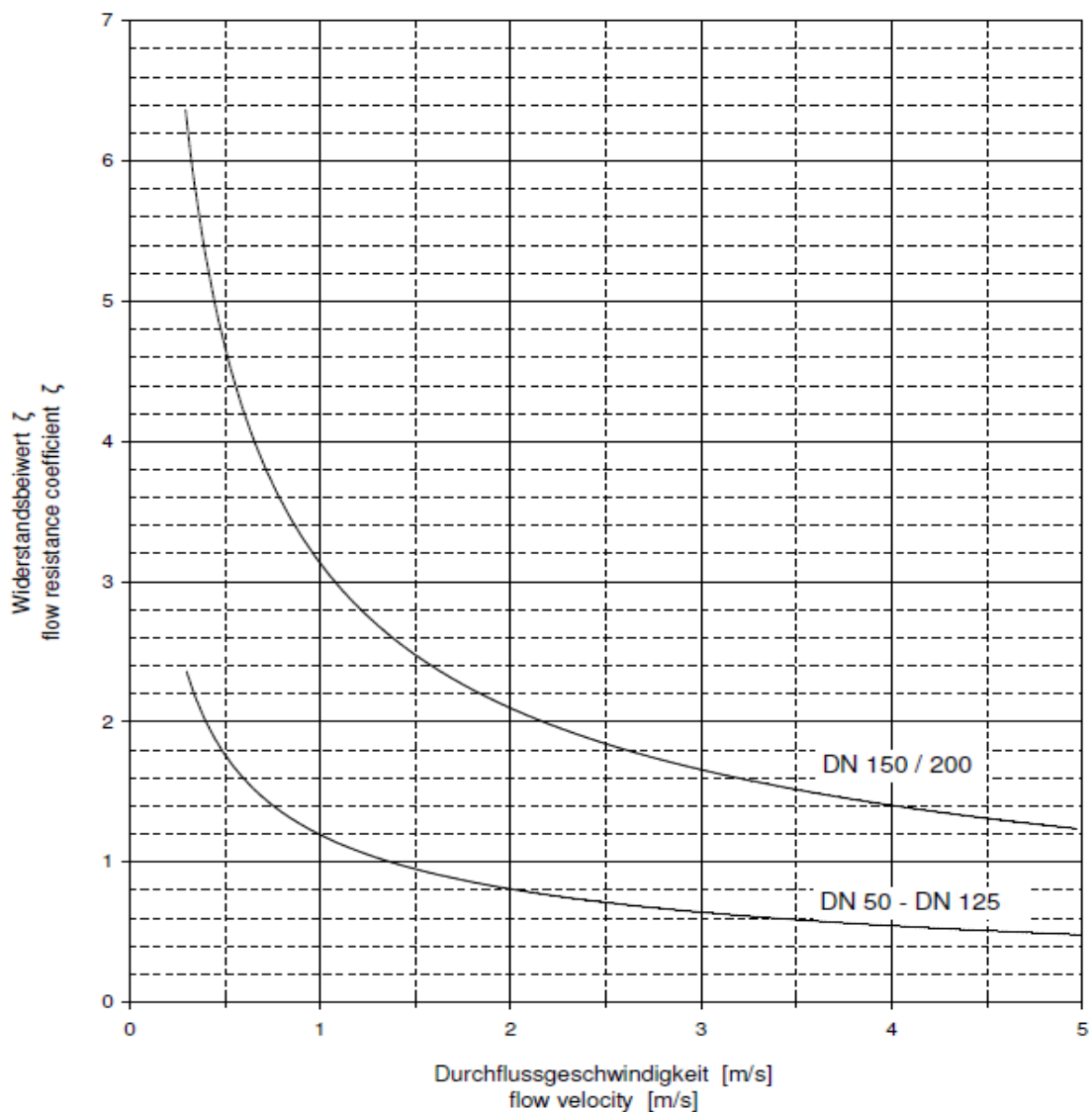
From technical sheets of VAG VALVES we take Graph 31 where there are plotted the head loss coefficients values ζ on flow velocity for the following product:



Figure 18: VAG KRV Ball Check Valve

Product features and benefits:

- Resilient seated in accordance with EN 12334
 - No mechanically moving parts
 - Easy to maintain
- Prevention of back flow via ball check principle
- Little risk of blockage due to full bore type
 - Applicable at low differential pressure
 - Low friction losses
 - With sinking ball



Graph 31: head loss coefficients for different values of flow velocity (ball check valve VAG)

13.5 Disk Check Valves

The disc check valve consists of four main components: the body, a disc, a spring and a spring retainer. The disc moves in a plane at right angles to the flow of the fluid, resisted by the spring that is held in place by the retainer.

The body is designed to act as an integral centring collar that facilitates installation. Where a 'zero leakage' seal is required, a soft seat can be included.

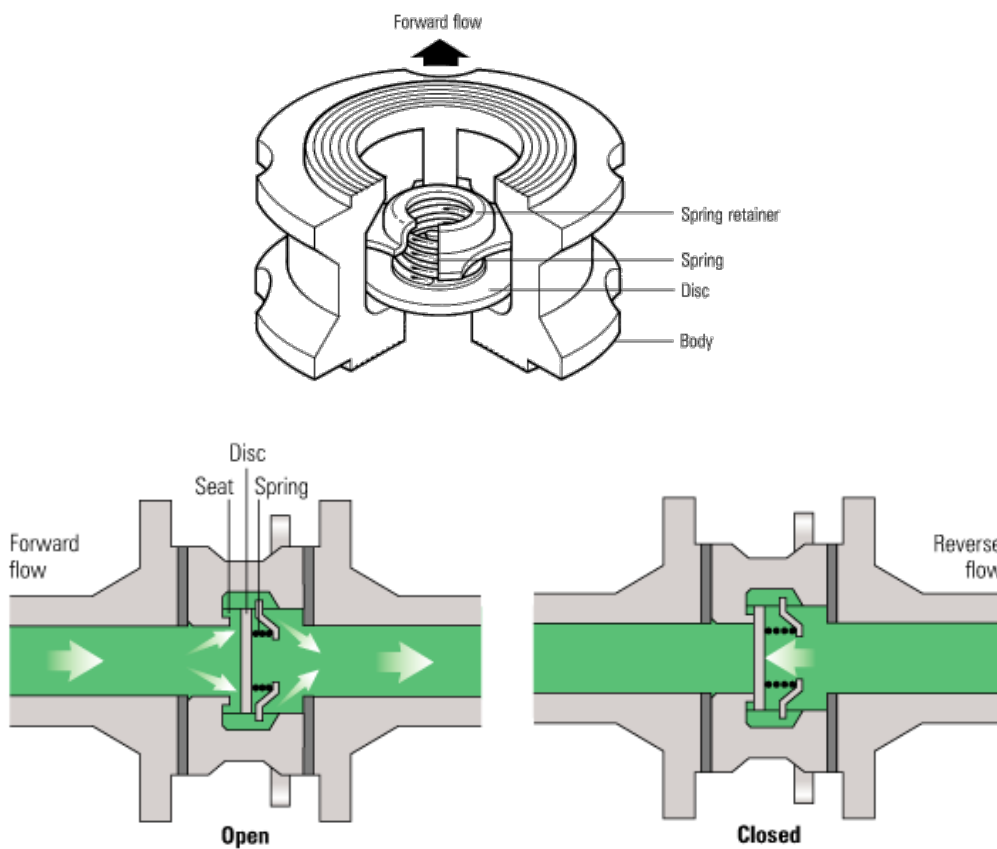


Figure 19: schematic functioning of disk check valves

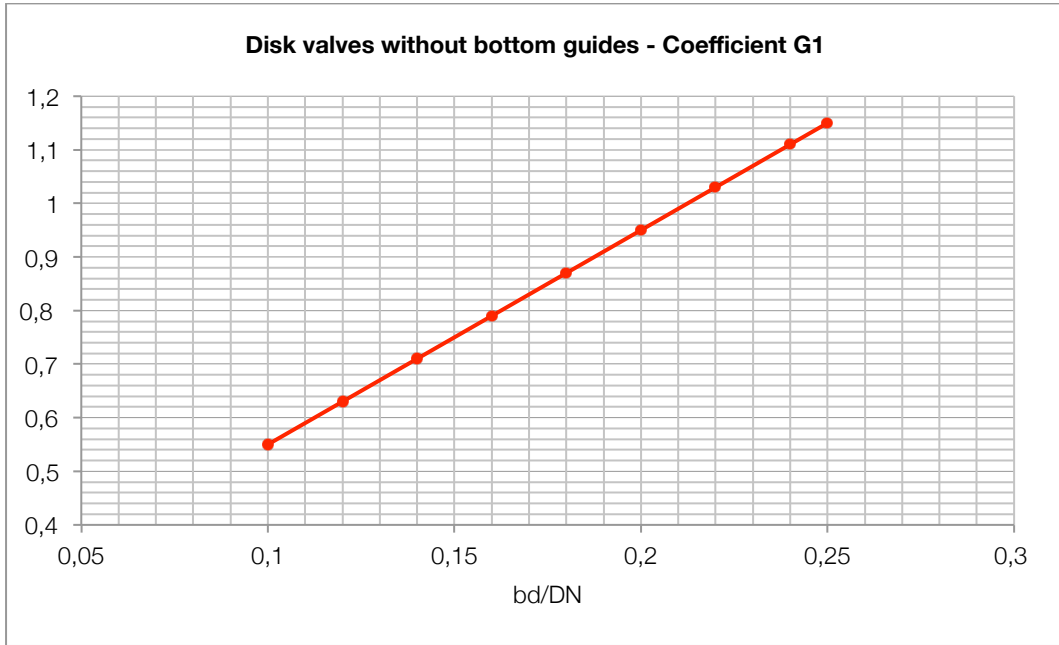
Taking from Idel'chik book of resistance (idel'chik, 1966), the resistance coefficient of axial check disk valves type can be determined by the following formula (proposed by *Bach*) within the limits $0,1 < \frac{h}{DN} < 0,25$ and $0,1 < \frac{b_d}{DN} < 0,25$:

$$\zeta = \frac{\Delta H}{V^2} = \left[0,55 + 4 \left(\frac{b_d}{DN} - 0,1 \right) + \frac{0,155}{\left(\frac{h}{DN} \right)^2} \right] = G1 + G2$$

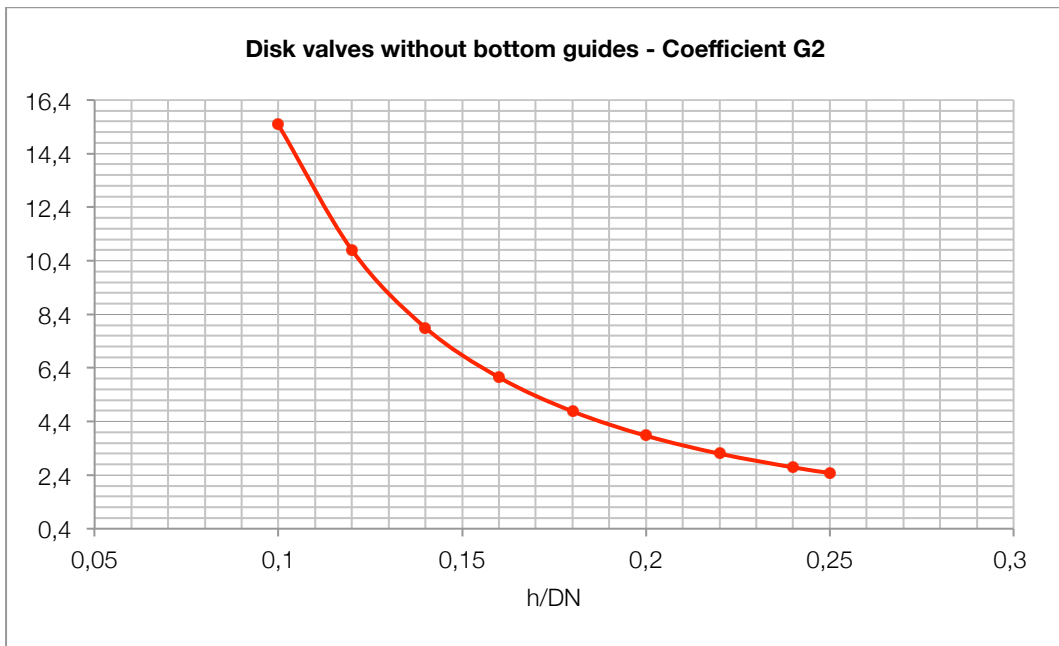
where

- h distance between disk and seat [m];
- b_d width of the disk flange, [m],
- $G1 = 0,55 + 4 \left(\frac{b_d}{DN} - 0,1 \right)$
- $G2 = \frac{0,155}{\left(\frac{h}{DN} \right)^2}$

the graphical representation of the parameters present in the previous formula is proposed in Graph 32, Graph 33 and Graph 34.



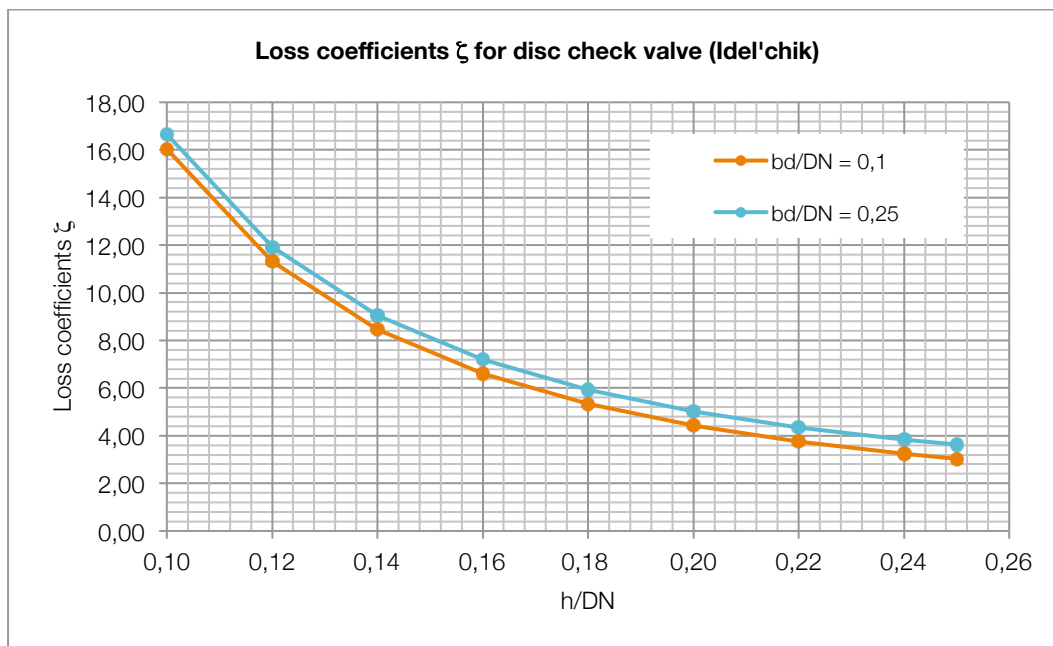
Graph 32: values of coefficient G1 for disk valves with bottom guides



Graph 33: values of coefficient G2 for disk valves with bottom guides

b_d/DN	G1	h/DN	G2
0,1	0,55	0,1	15,5
0,12	0,63	0,12	10,8
0,14	0,71	0,14	7,9
0,16	0,79	0,16	6,05
0,18	0,87	0,18	4,78
0,2	0,95	0,2	3,87
0,22	1,03	0,22	3,2
0,24	1,11	0,24	2,69
0,25	1,15	0,25	2,48

In the Graph 34 there are plotted the loss coefficient for the extreme value of the range for G1 ($b_d/DN=0,1$ and $b_d/DN=0,25$):



Graph 34: Loss coefficient for disk check valves (idel'chik)

h/DN	ζ values	
	bd/DN = 0,1	bd/DN = 0,25
0,1	16,05	16,65
0,12	11,31	11,91
0,14	8,46	9,06
0,16	6,60	7,20
0,18	5,33	5,93
0,2	4,43	5,03
0,22	3,75	4,35
0,24	3,24	3,84
0,25	3,03	3,63

13.6 Conical Check Valves

Conical valve is a sort of nozzle valve, in which the closure member has a conical dimension, and moves forward and backward, in axial direction (parallel to flow direction) closing the passage of the stream when it touches the valve seating.

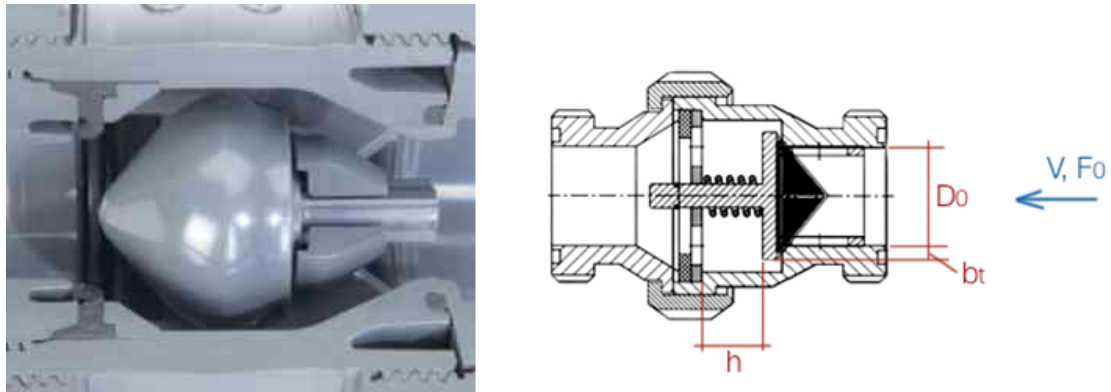
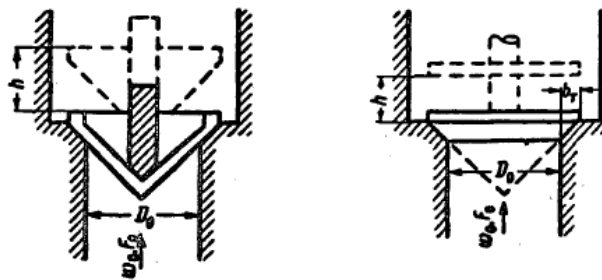


Figure 20: Conical valve with geometric parameters

Following the Idel'chik book of resistance, it is possible to identify two types of conical valve:

1. Conical valve with conical seat;
2. Conical valve with flat seat;



1. Conical seat

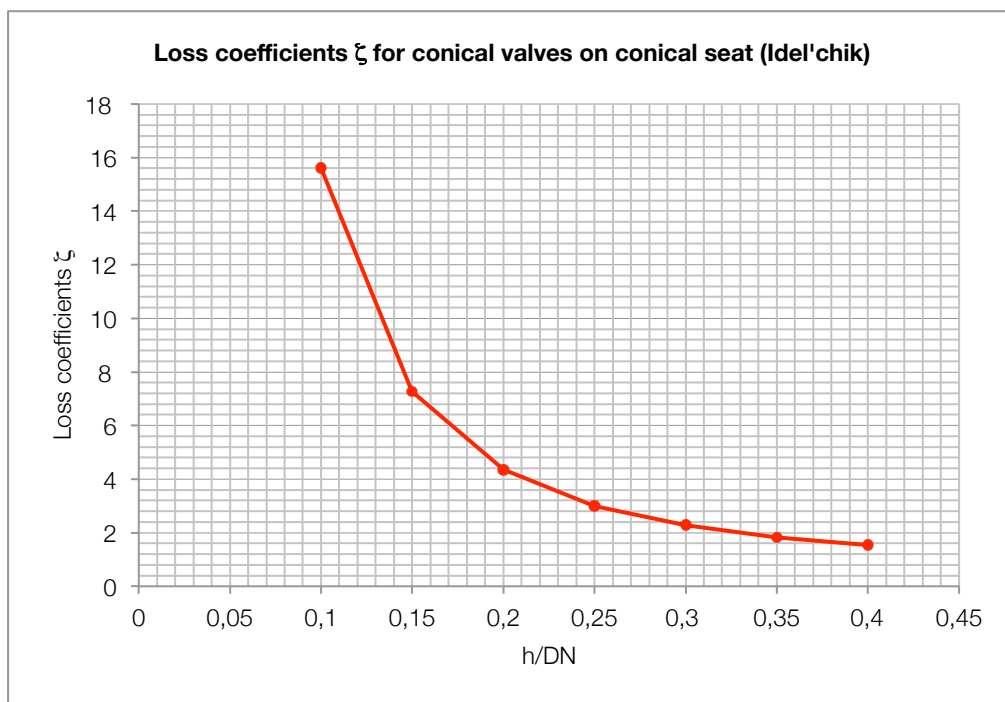
2. Flat seat

Figure 21: conical valve types with geometrical parameters

The loss coefficient for conical valve with conical seat within the limits $0,125 < \frac{h}{DN} < 0,4$ is determined by the following expression, represented in Graph 35.

$$\zeta = \frac{\Delta H}{\frac{V^2}{2g}} = \left[0,6 + \frac{0,15}{\left(\frac{h}{DN}\right)^2} \right]$$

h/DN	ζ values
0,10	15,60
0,15	7,27
0,20	4,35
0,25	3,00
0,30	2,27
0,35	1,82
0,40	1,54



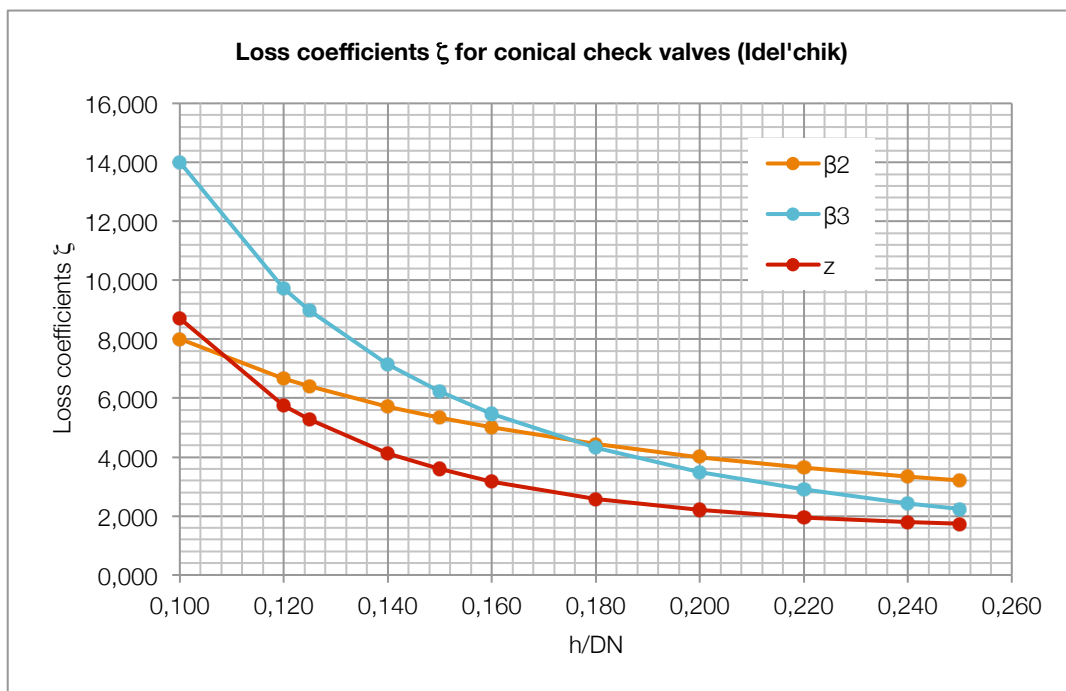
Graph 35: loss coefficients for conical valve on conical seat (Idel'chik)

The loss coefficients ζ for conical valve with flat seat within the limits $0,1 < \frac{h}{DN} < 0,25$ and for $\frac{b_d}{D_0} = 0,1$ are calculated by the following formula, and they are represented with the letter “z” in the Graph 36 (values obtained for values of $b_d/DN = 0,1$).

h/DN	β_2	β_3	ζ values
0,10	8,00	14,00	8,70
0,12	6,66	9,73	5,75
0,14	5,71	7,15	4,13
0,16	5,00	5,46	3,17
0,18	4,44	4,32	2,58
0,20	4,00	3,50	2,20
0,22	3,63	2,90	1,96
0,24	3,33	2,43	1,80
0,25	3,20	2,24	1,74

$$\zeta = \frac{\Delta H}{V^2} = 2,7 - \frac{0,8}{DN} + \frac{0,14}{\left(\frac{h}{DN}\right)^2} = 2,7 - \beta_2 + \beta_3$$

$$\text{where } \beta_2 = \frac{0,8}{DN} \text{ and } \beta_3 = \frac{0,14}{\left(\frac{h}{DN}\right)^2}$$



Graph 36: loss coefficients ζ for conical valve on flat seat (Idel'chik)

13.7 Nozzle check valves

Nozzle valves are specifically designed for fast-reversing systems where backflow is a constant concern. In such critical service applications, nozzle check valves offer the following benefits:

- Minimize the damaging effects of water hammer in fluid systems;
- Protects rotating equipment from damage due to flow reversal;
- Minimizes pressure loss in piping systems;
- Provides quick dynamic response reducing reverse velocity

The particular form of the spindle inside the valve seating makes the flow path inside the valve free for turbulences around the closure member. This design form is the main responsible of the low pressure drops in this axial valve type. Low pressure loss can be equated with energy savings in the plant or more throughout, making the axial type valve a competitive check valve solution when considering full lifecycle costs. This is a complex technology that is improving year after year and there are a lot of models of this valve type, but it is possible to recognize two main nozzle valve types:

1. Solid disc nozzle valve;
2. Ring disc nozzle valve;

In the following pages there will be plotted for both valve types an image to identify them and then the loss coefficients, obtained for different velocity values and for different nominal diameters.

For nozzle check valves there are a lot of sources of data available online and in literature and in the following pages will be listed and plotted data from both sources.

From literature it is possible to plot from Bianchi and Sanfilippo (Bianchi and Sanfilippo, 2001) book and from Idel'chik book of resistance (Idel'chik, 1966): both of these sources reports data for the solid disc nozzle valve and Idel'chik specifies that the seal member of the valve has a spherical shape.

For Idel'chik the head loss coefficient can be computed with the following formula, valid with the ratio h/DN included between 0,1 and 0,25 values:

$$\zeta = \frac{\Delta H}{V^2/2g} = 2,7 - \frac{0,8}{\frac{h}{DN}} + \frac{0,14}{\left(\frac{h}{DN}\right)^2}$$

where h is the distance between the sealing member and the seat , [m].

It is interesting to note that this formula is the same as the conical check valve one, used for the same objective.

The manufacturer data are taken from the following sites, corresponding to the relative industries which makes available their data sheet for a free download:

Goodwin International	http://www.checkvalves.co.uk/nozzle.html
NoReVa GmbH	http://www.noreva.de
Crane Chem Pharma Energy	http://www.cranecpe.com
Erhard	http://www.erhard.de

13.7.1 Solid disc nozzle check valves

The axial design allows for a streamlined flow path around the closure member which is the entire solid disc that moves forward and backward towards the seating zone, minimizing pressure drop across the valve. This efficient design, combined with a good responsive non-slam operation, make this valve ideal for high head values and pump applications.

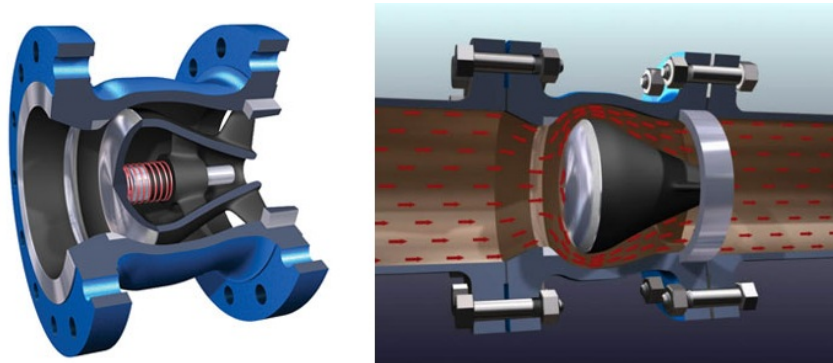
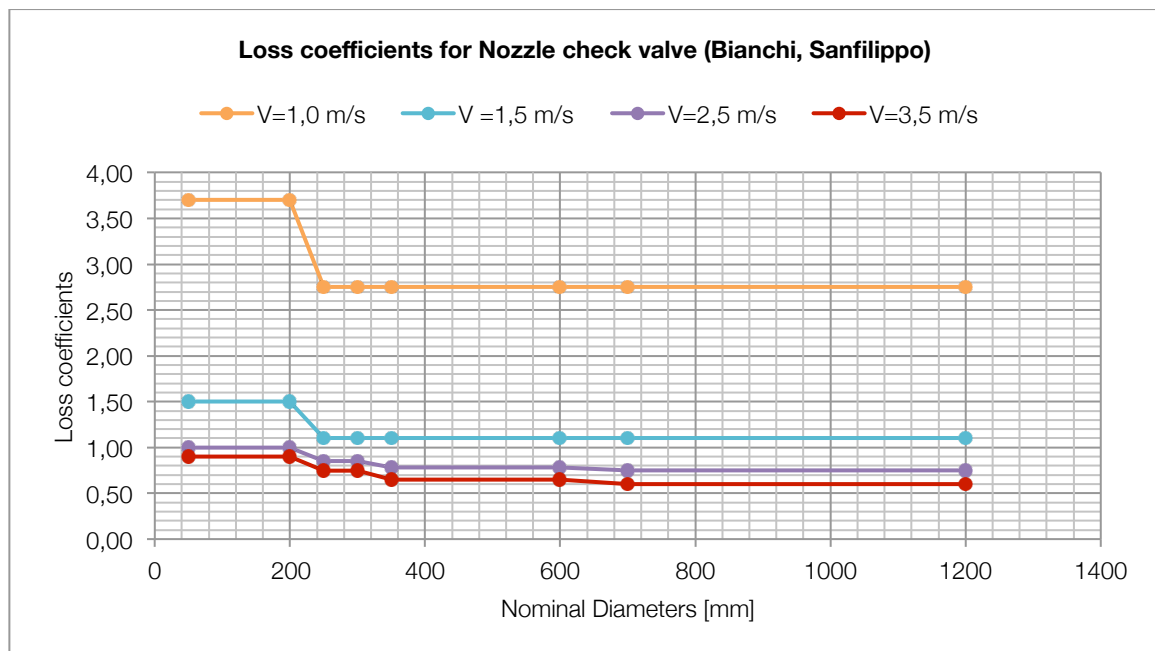


Figure 22: solid disc nozzle check valve

In the following pages are plotted the list of diagrams and graphs for the different types of solid disc nozzle valve.



Graph 37: loss coefficients for nozzle check valves (Bianchi and Sanfilippo)

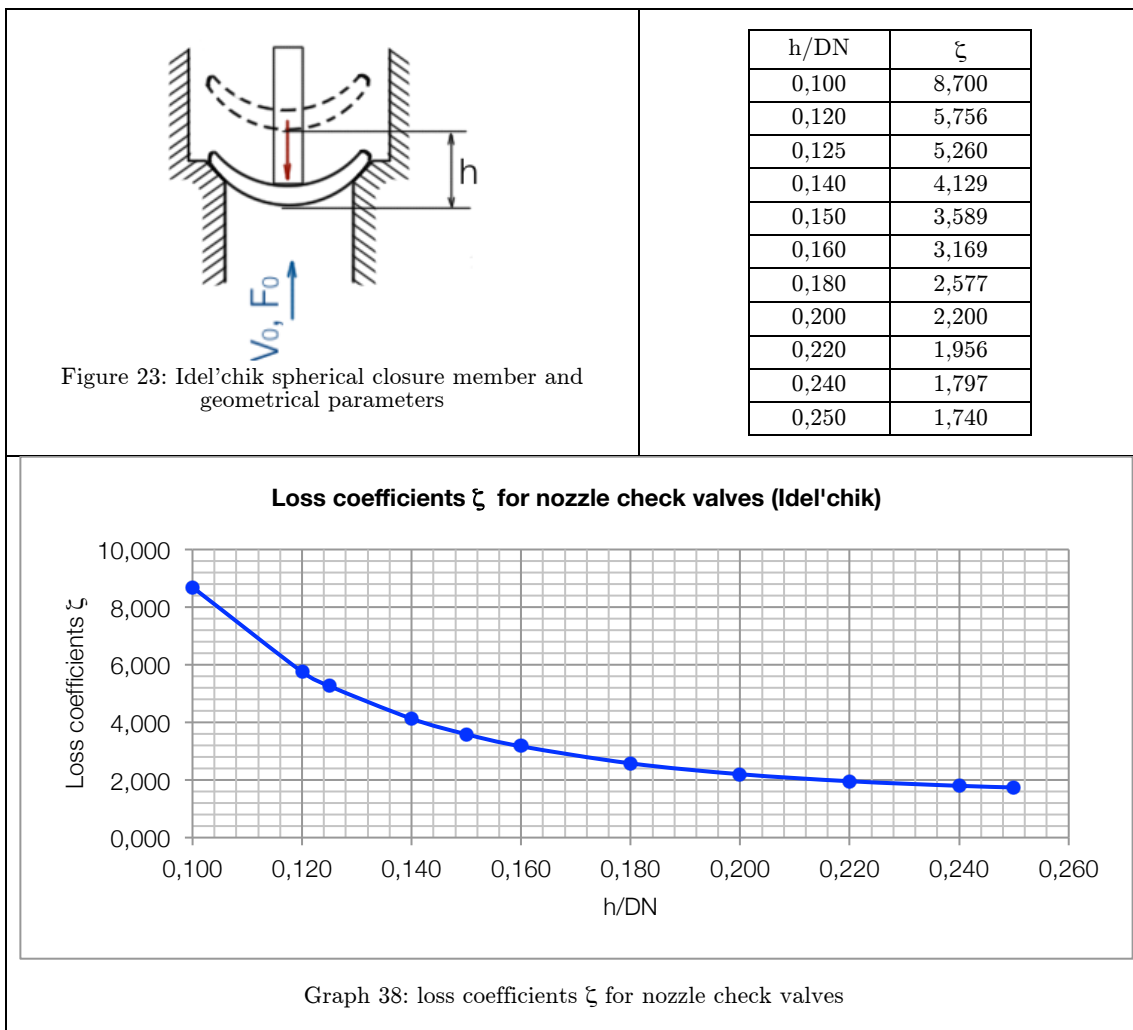
Idel'chik (Idel'chik, 1966), gives the head loss coefficients values against the opening percentage of the valve $\frac{h}{DN}$. Putting equal to the unit this value, and so considering the fully open position of the valve, the head loss is equal to:

$$\zeta = \frac{\Delta H}{V^2/2g} = 2,7 - \frac{0,8}{1} + \frac{0,14}{(1)^2} = 2,04$$

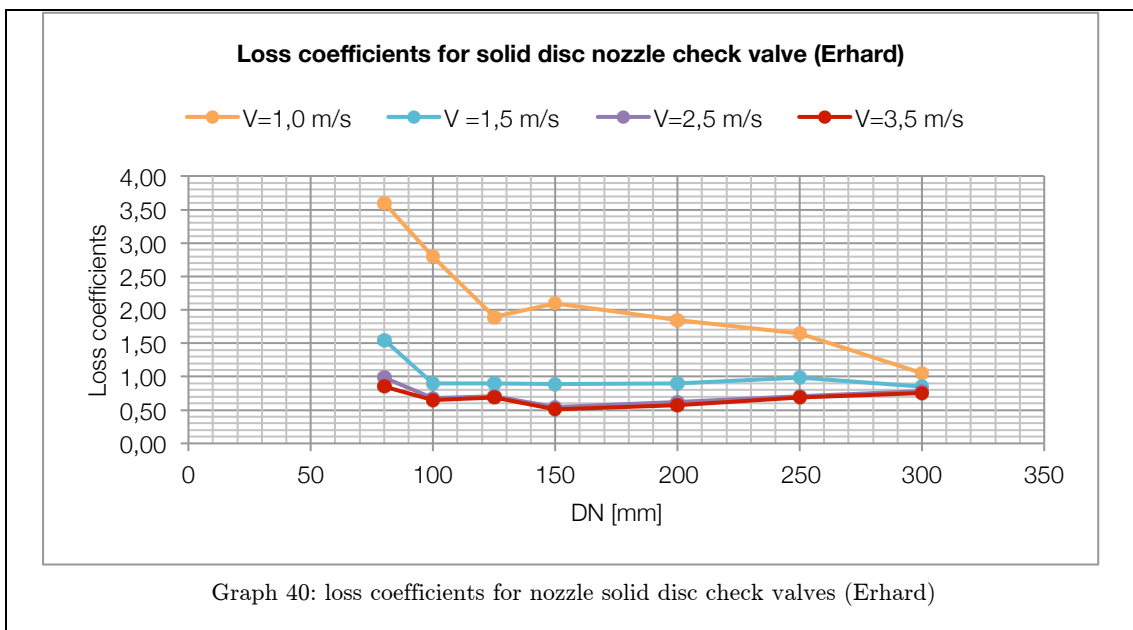
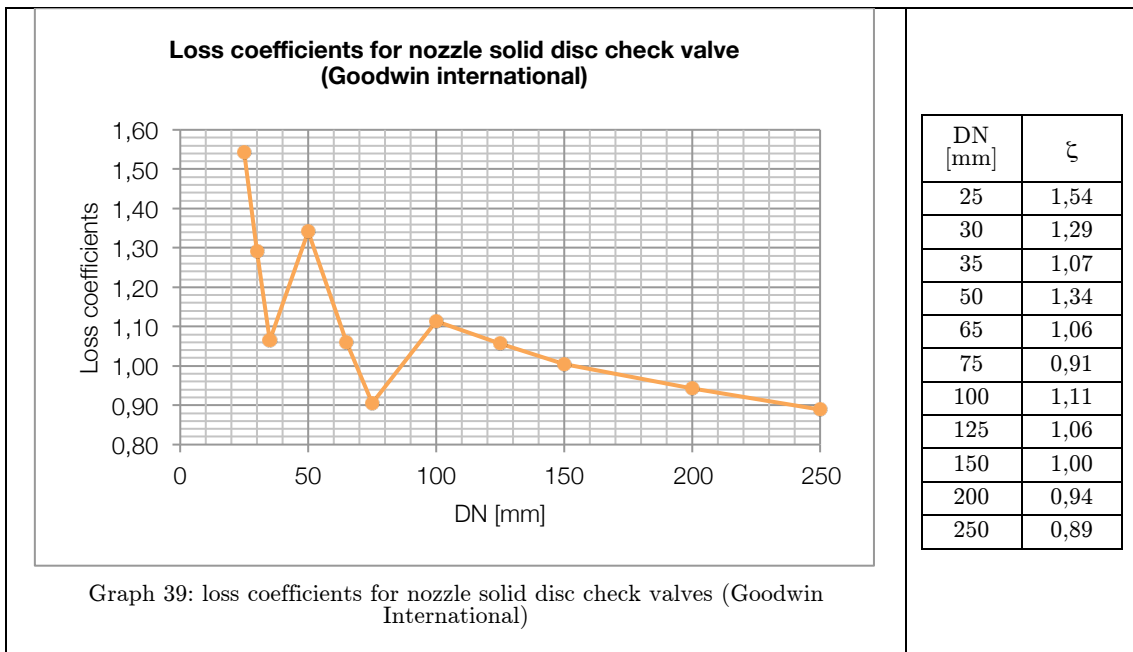
Idel'chik's (Idel'chik, 1966) head loss coefficients can be computed with the following formula, valid for $0,1 < \frac{h}{DN} < 0,25$, and the values are plotted in the Graph 38.

$$\zeta = \frac{\Delta H}{V^2/2g} = 2,7 - \frac{0,8}{\frac{h}{DN}} + \frac{0,14}{\left(\frac{h}{DN}\right)^2}$$

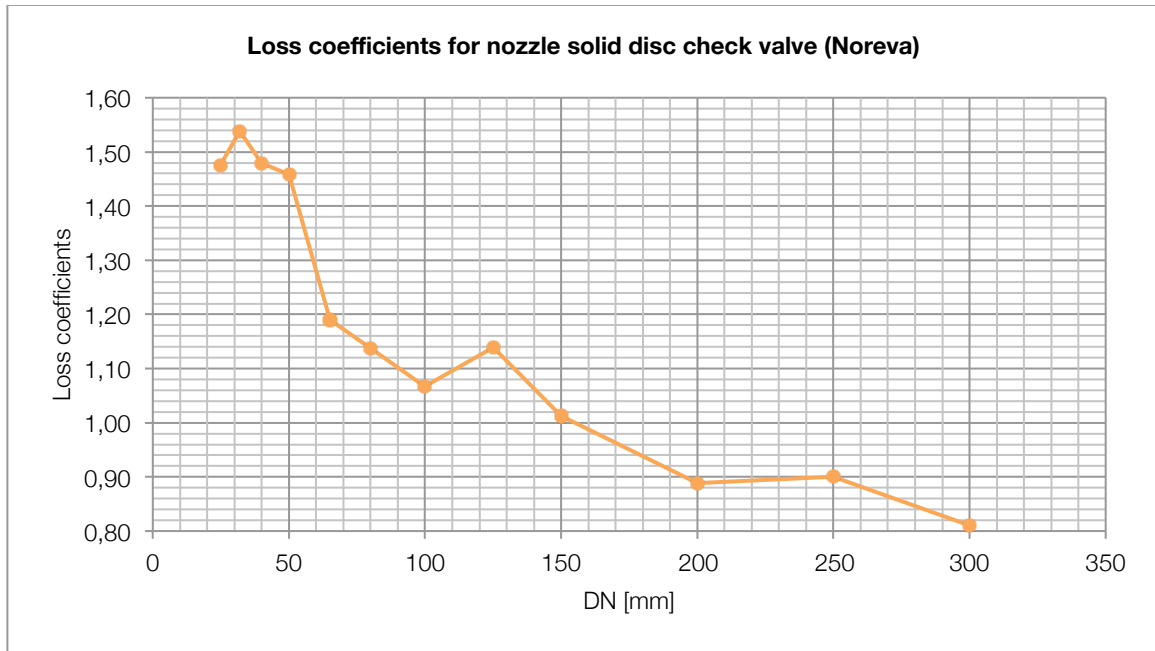
where h is the distance between the sealing member and the seat, [m].



In the Graph 39 and in the Graph 40 are plotted the head loss coefficients ζ from Goodwin international and from Erhard respectively.



DN [mm]	ζ values			
	V=1,0 m/s	V =1,5 m/s	V=2,5 m/s	V=3,5 m/s
80	3,60	1,55	0,98	0,85
100	2,80	0,90	0,68	0,65
125	1,90	0,90	0,71	0,69
150	2,10	0,89	0,54	0,51
200	1,85	0,90	0,62	0,57
250	1,65	0,98	0,71	0,69
300	1,05	0,85	0,78	0,75



Graph 41: loss coefficients for solid disc check valve (NoReVa)

DN [mm]	Flow rate [l/min]	Flow rate [U.S. gal/min]	ΔH [mbar]	ΔH [psi]	C_v	ζ
25	100	26,42	85,00	1,23	23,78	1,48
32	100	26,42	33,00	0,48	38,16	1,54
40	100	26,42	13,00	0,19	60,79	1,48
50	200	52,83	21,00	0,31	95,67	1,46
65	200	52,83	6,00	0,09	178,97	1,19
80	400	105,67	10,00	0,15	277,26	1,14
100	500	132,09	6,00	0,09	447,43	1,07
125	2000	528,34	42,00	0,61	676,45	1,14
150	2000	528,34	18,00	0,26	1033,30	1,01
200	4000	1056,69	20,00	0,29	1960,54	0,89
250	9000	2377,55	42,00	0,61	3044,03	0,90
300	20000	5283,44	90,00	1,31	4621,04	0,81

The head loss values plotted in the Graph 41 are obtained from the pressure loss curves in the technical data sheets of NoReVa, that represent ΔH [mbar] and at different flow rate, plotted for different DN values. From these data is possible to compute the flow coefficients C_v , and then it is immediate to obtain the head loss coefficient ζ .

13.7.2 Ring disc nozzle check valves

In this valve's type, the closure member is the ring positioned around the closure member that moves towards the seat when closed position is required.

The ring disc design ensures that the disc remains light and responsive even in large sizes. Mounted on a multiple helical spring and radial guide assembly, the disc moves freely without any of the frictional forces associated with the solid disc and shaft design.

With a flow path both around and through the center of the disc the flow capacity of the valve is great. Due to excellent pressure recovery properties of the diffuser, the minimal pressure drop across the valves gives lifetime energy savings when compared to more conventional check valve designs.

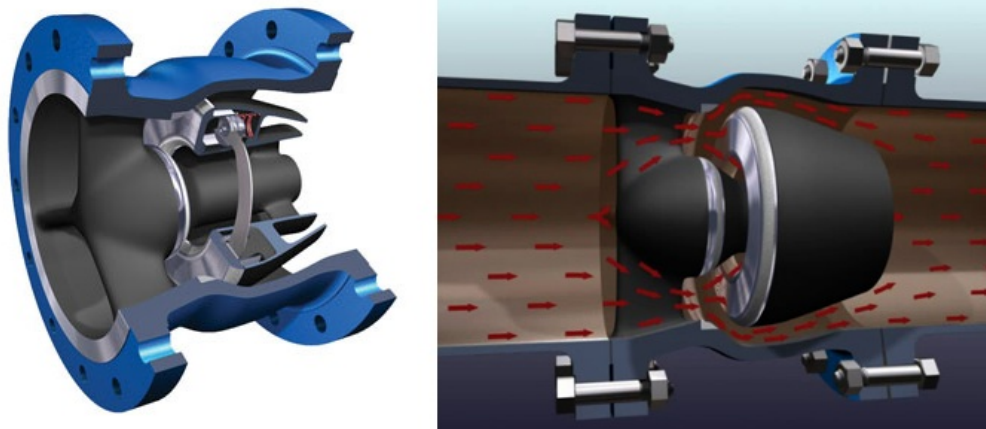
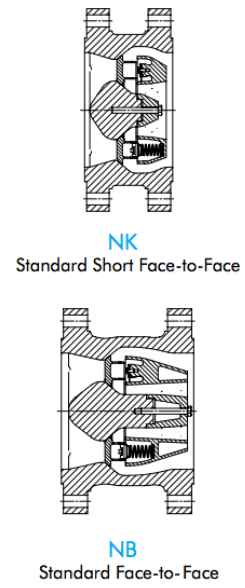
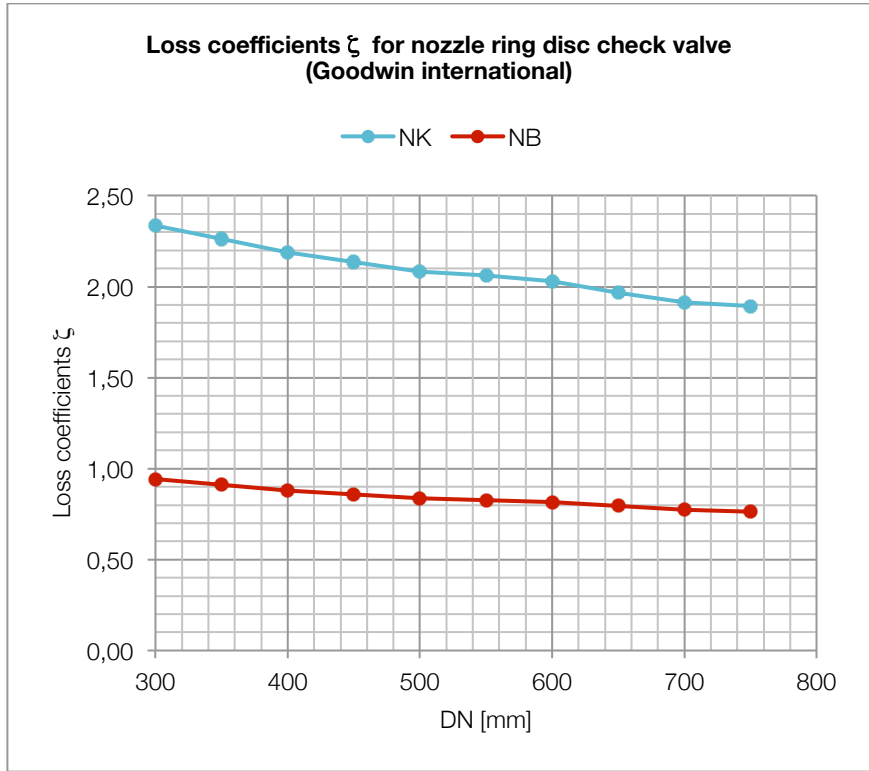


Figure 24: ring disc nozzle check valves

For this valve type the data plotted in the Graph 42 are from Goodwin international. From this manufacturer there are two different model of ring disc nozzle valve: NK and NB (schematic representation in Graph 42). The difference is essentially in the dimension of the ring positioned up to the closure member: the former is shorter than in the second.



Graph 42: loss coefficients ζ for nozzle ring disc check valve (Goodwin international)

13.8 Plug Valves

Plug Valves are manual valves, belonging to the group that use the rotating method to control the flow regulation. The throttling device in this type of valves is a plug-shaped closure member that rotates itself through increments of 90° to engage or disengage a porthole or hole in the plug with the ports in the valve body.



Figure 25: Schematic View of a plug valve

The shape of this plug may thereby be cylindrical. There are other rotary valves with spherical-shaped rotary element belonging to plug valves group, but are conventionally referred to as ball valves (not to be confused with check-ball valves). These valves are treated separately in the following pages. Plug valves are best suited for stopping and starting flow and for flow diversion, though they are also used for moderate throttling.



Figure 26: Throttling positions of plug valves

Plug valves can be classified as:

1. Cylindrical plug valves;
2. Tapered plug valves;
3. Three-way plug-valves;

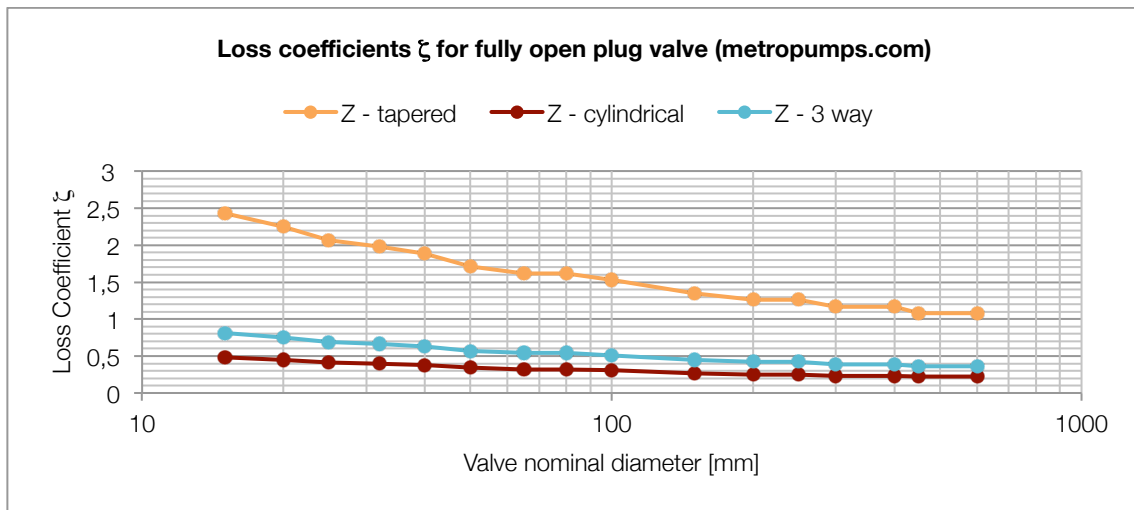
For every type of this devices there are a lot of literature and websites that provides a lot of information about minor loss coefficient ζ (sometimes indicated by the letter “Z”).

13.8.1 Fully open plug valves

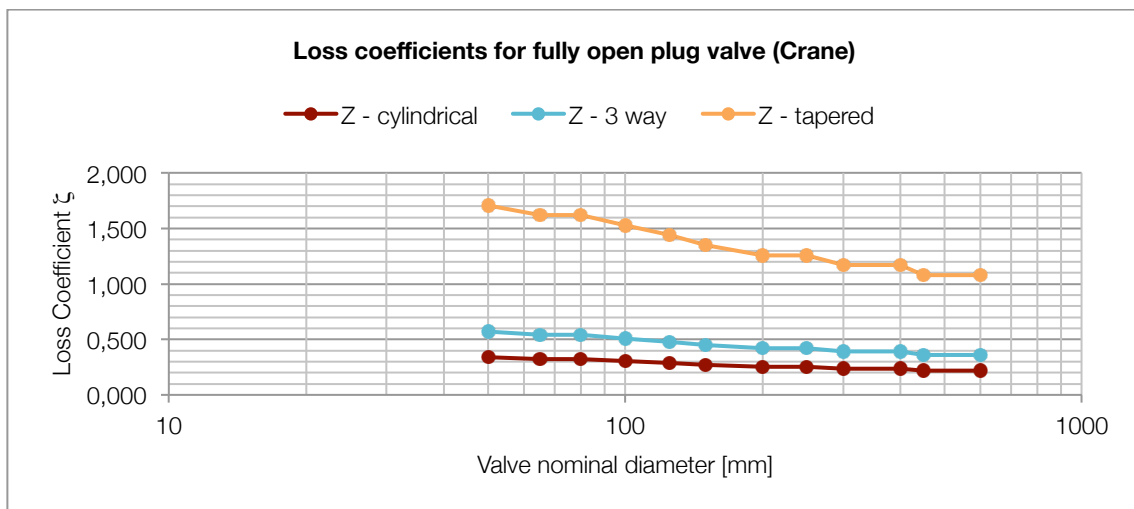
In Table 14, in the Graph 43 and in the Graph 44 are plotted the head loss coefficient values from Miller (Miller, 1973), from metropumps.com website, and from Crane (Crane, 1999) respectively. For Crane (Crane, 1999) and metropumps are represented the coefficients for all the three types of fully open valves.

Table 14: Head loss coefficients ζ for plug valves

Source	Head Loss Coefficients ζ	
	Miller (Miller, 1973) ($\omega = \text{Plug Port Area/Pipe Area}$)	$\omega = 1,0$
	$\omega = 0,7$	$\zeta = 1,0$

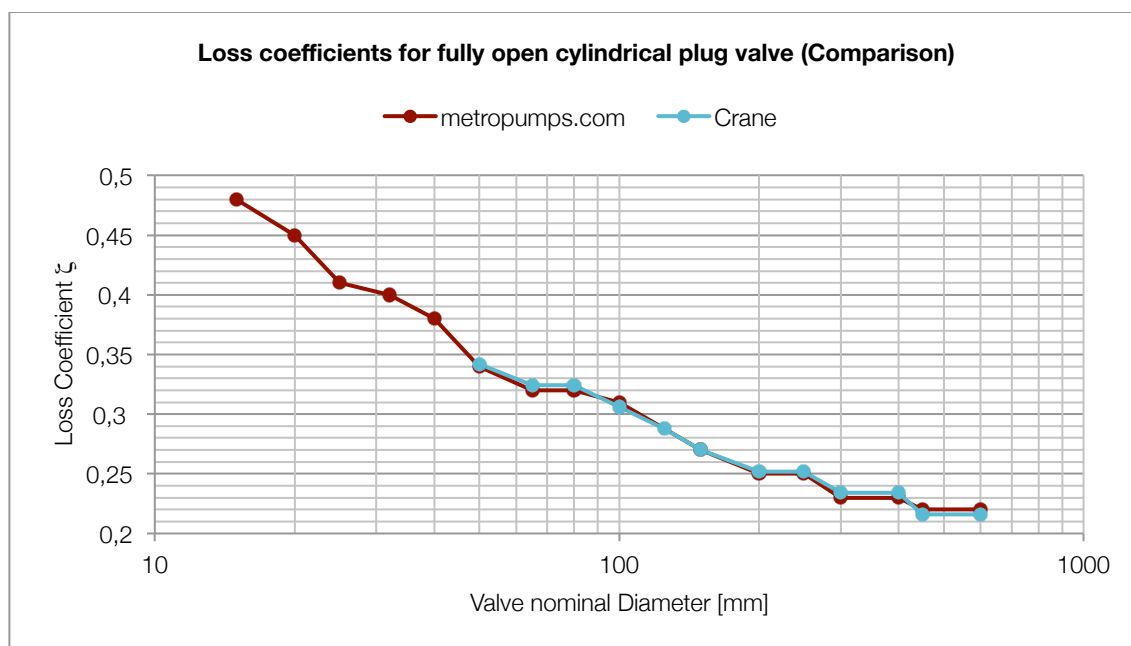


Graph 43: loss coefficients ζ for plug valves (metropumps.com)

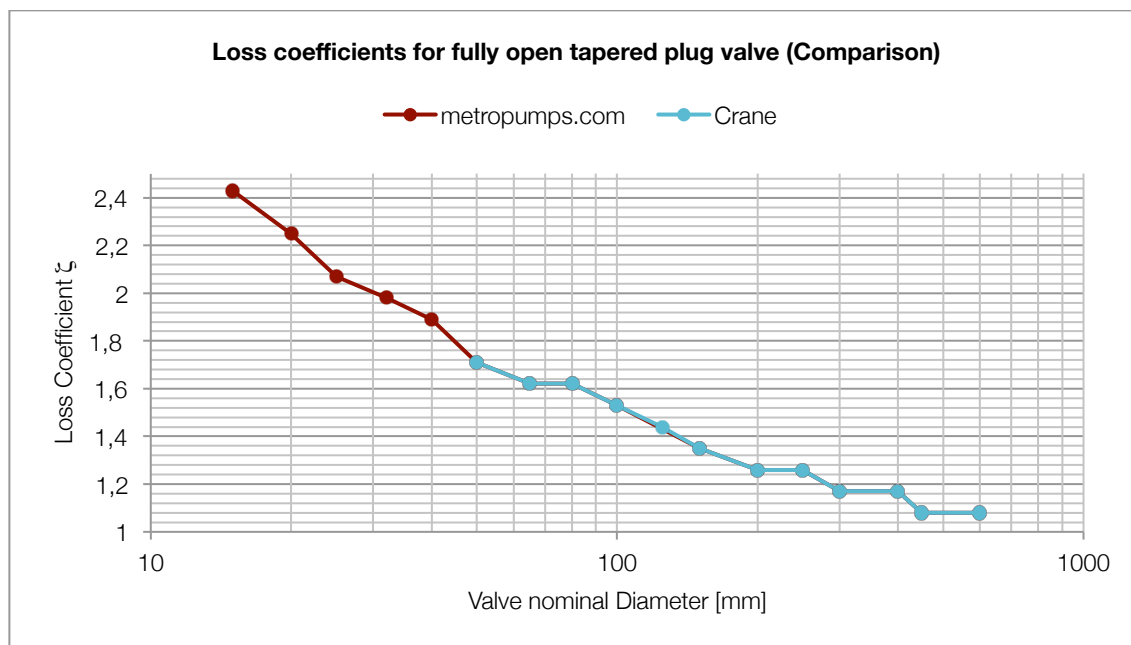


Graph 44: loss coefficient for plug valves (Crane book)

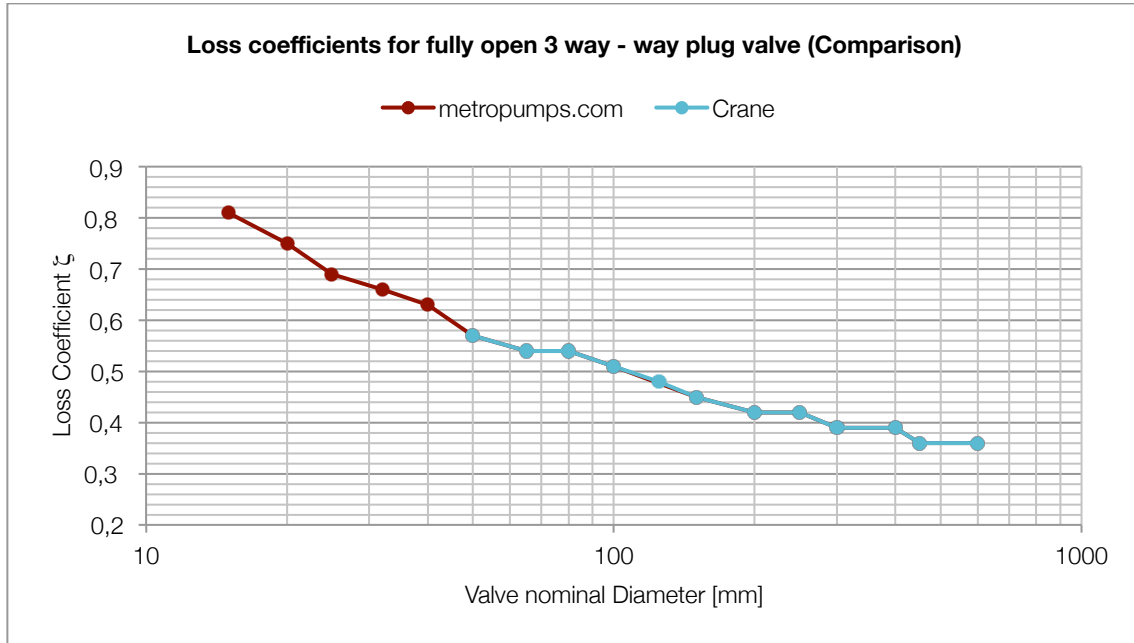
In Graph 45, Graph 46 and in Graph 47 are plotted the comparisons between the head loss coefficients from Crane (Crane, 1999) and metropumps.com for the cylindrical, tapered and 3-way patterns respectively.



Graph 45: comparison between Crane book and metropumps.com for cylindrical open plug valves



Graph 46: comparison between Crane book and metropumps.com for tapered open plug valves

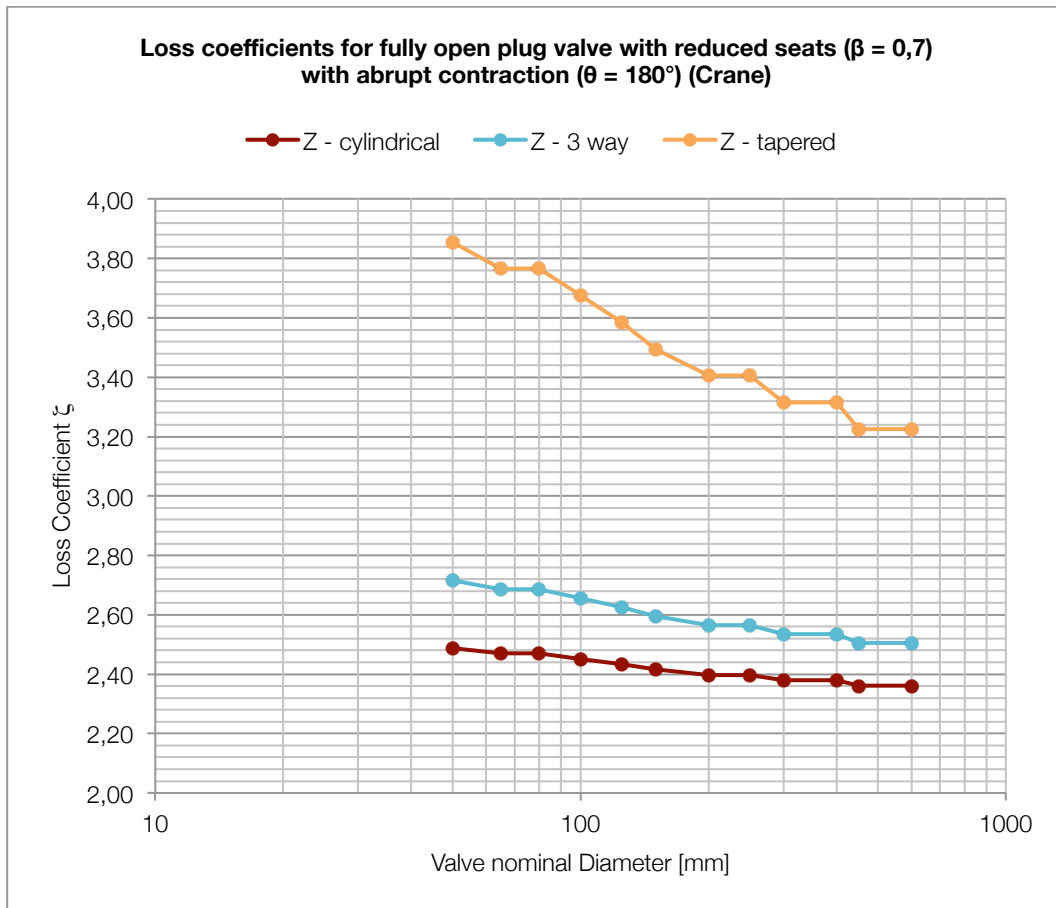


Graph 47: comparison between Crane book and metropumps.com for 3-way open plug valves

This is only a graphical representation to have a look on the perfect overlapping of the data, which is a confirmation of the reliability of them. A more complete comparison between values for all the plug valve pattern's is presented in the conclusive chapter.

13.8.2 Plug valves with contractions at inlet and outlet

In Crane (Crane, 1999) there's an additional analysis for plug valves with contractions and enlargements at inlet and outlet of the valve. Making the hypothesis of commercial steel pipe as the main material of production, the results for $\beta = 0,7$ and $\theta = 180^\circ$ (divergence angle) are plotted in the following graph.



Graph 48: loss coefficient for fully open plug valves

DN [mm]	50	65	80	100	125	150	200	250	300	400	450	600
Cylindrical	2,49	2,47	2,47	2,45	2,43	2,42	2,40	2,40	2,38	2,38	2,36	2,36
3-way	2,72	2,69	2,69	2,66	2,63	2,60	2,57	2,57	2,54	2,54	2,51	2,51
Tapered	3,86	3,77	3,77	3,68	3,59	3,50	3,41	3,41	3,32	3,32	3,23	3,23

13.9 Ball valves

Ball valves, also called spherical valves (not to confuse with ball check valve), are included in the same category as the plug valves because the direction of the flow in the seating area is the same, the movement of the closure device is rotational and the flow passes through the closure member itself. They are, substantially, particular plug valves with a spherical-shaped closure member with an excellent sealing.

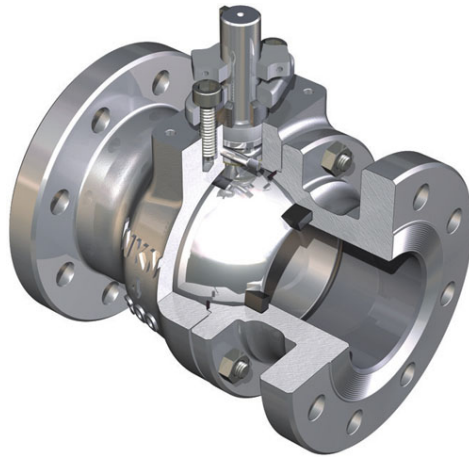


Figure 27: ball valve

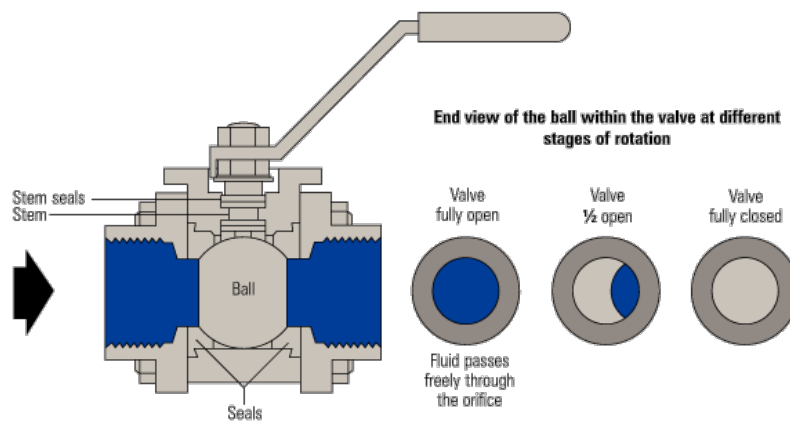


Figure 28: Functioning of a ball valve

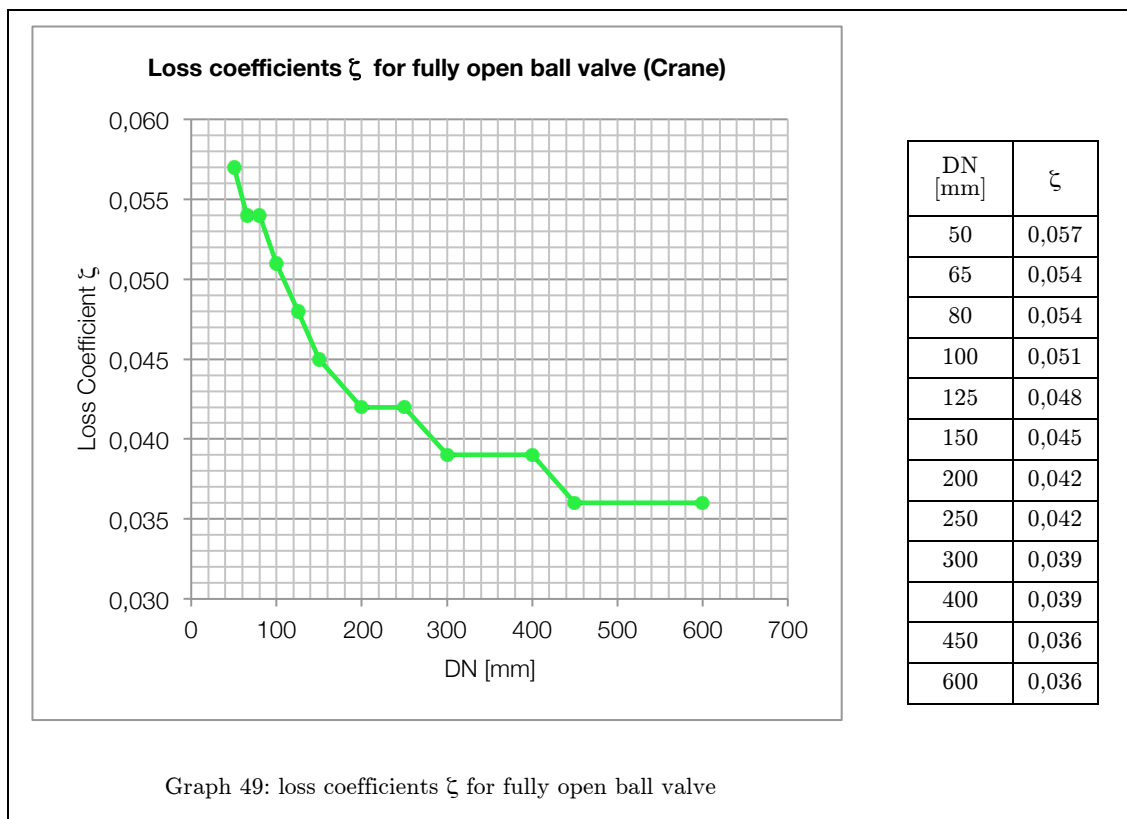
13.9.1 Fully open ball valves

In the Table 15 are plotted punctual values founded in the corresponding literature or websites. The values from engineering toolbox are collected also for partially closed valve.

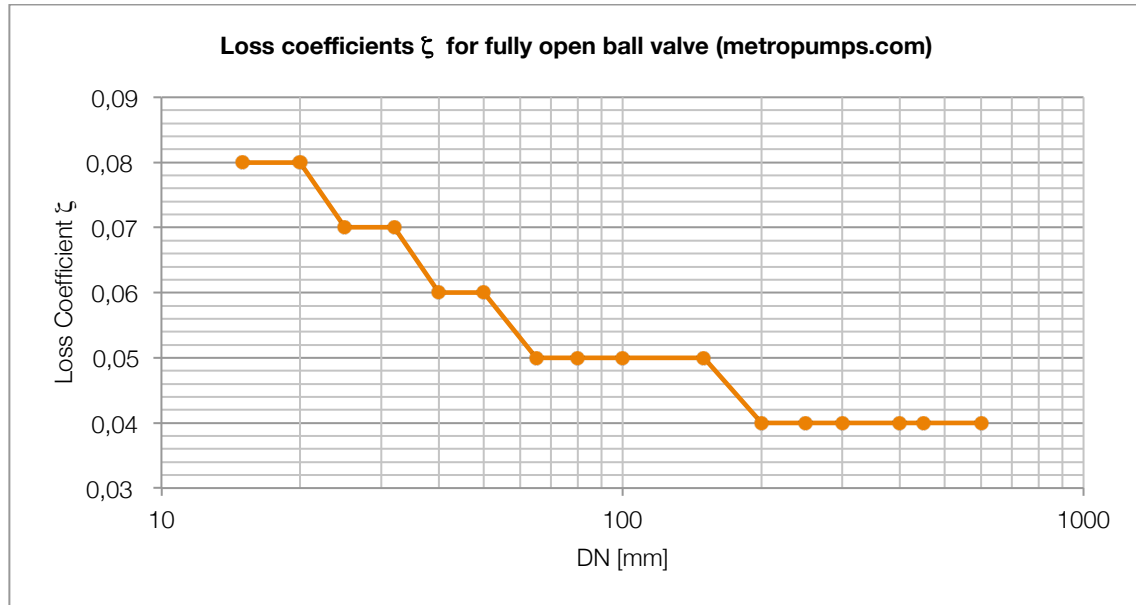
Crane (Crane, 1999) plots a perfect analysis of the head loss in this type of valve. Making the hypothesis of commercial steel pipe as the main material of production, for fully open ball valve the head loss coefficients are plotted in Graph 49.

Table 15: Head loss coefficients for ball valves

Source	Head Loss Coefficients ζ	
	engineeringtoolbox.com	Fully Open
1/3 closed		5,50
2/3 closed		200
Miller (Miller, 1973)	0,2	
Bianchi (Bianchi, Sanfilippo, 2001) (ψ = plug port diameter/pipe diameter)	$\psi = 0,84$	0,6

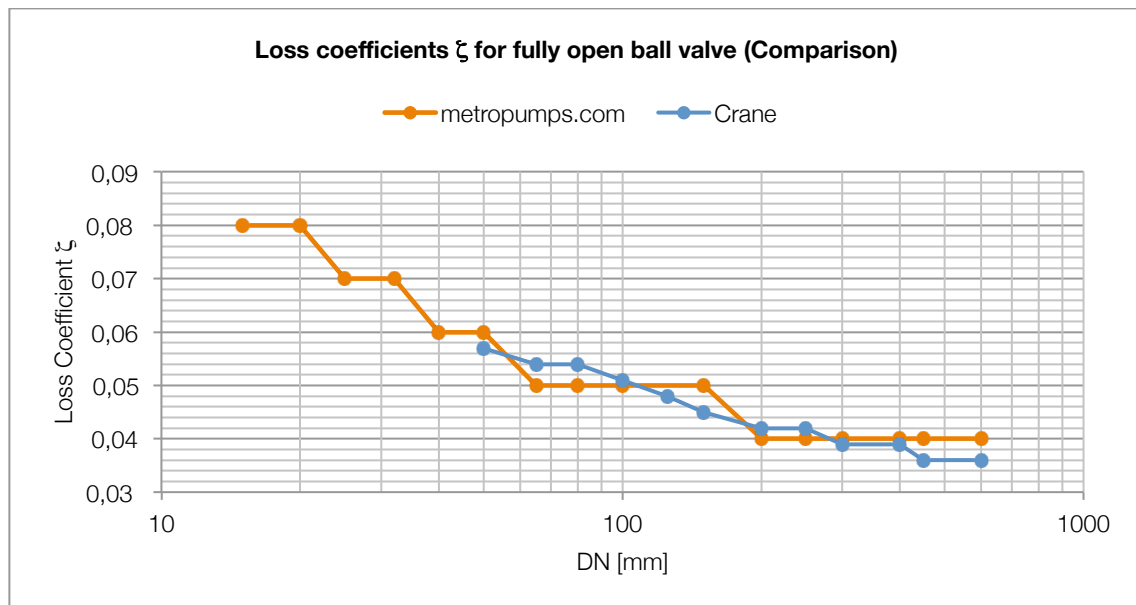


The website metropumps.com plots a similar performance graph for ball valve (Graph 50):



Graph 50: loss coefficients ζ for fully open ball valve (metropumps.com)

In the the Graph 51 is plotted the comparison between the two sources. It is clear that the trend of the two sites is very similar with percentage error always under the 10%.



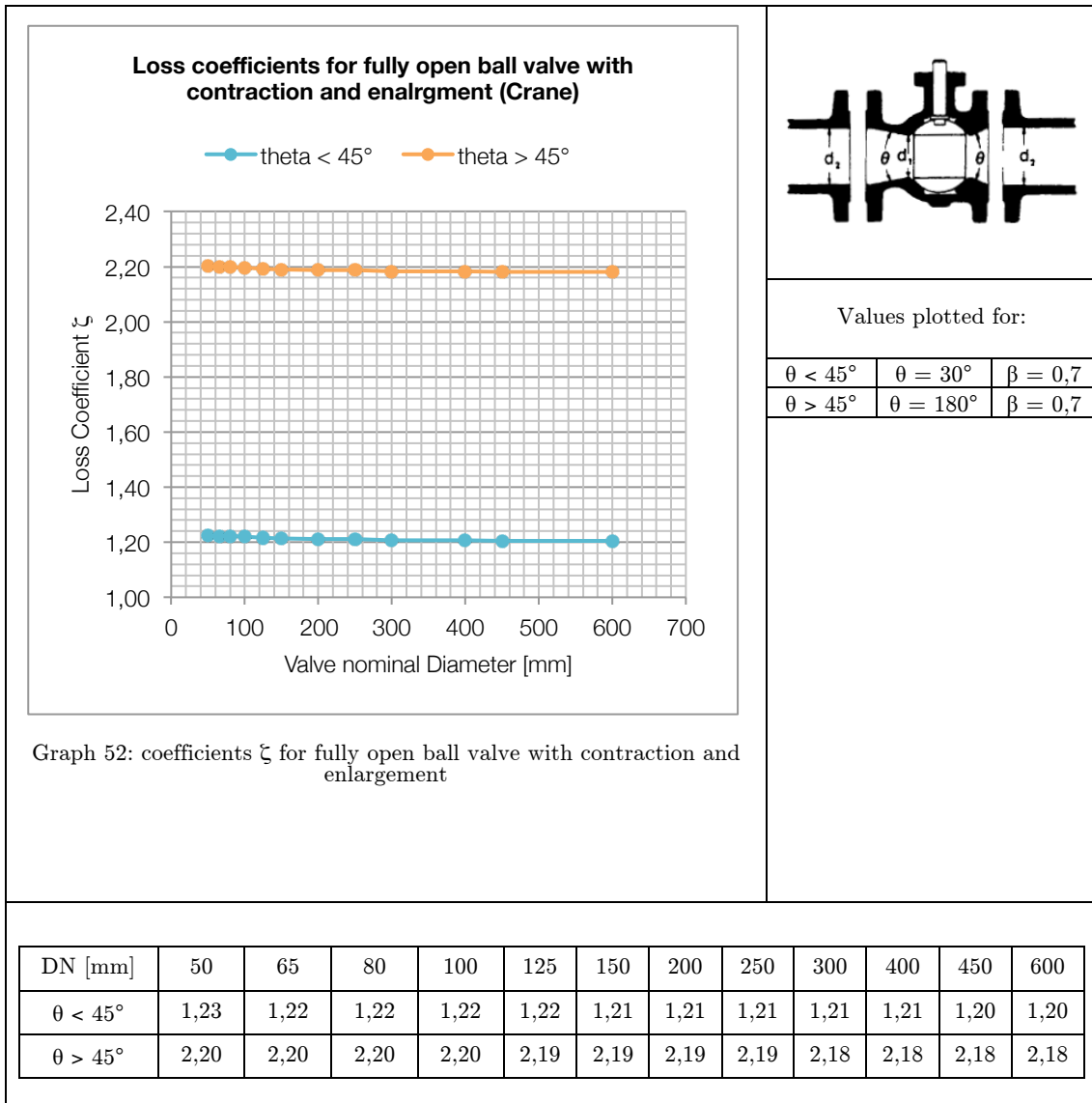
Graph 51: comparison between the two sources for head loss coefficient of fully open ball valve

In the conclusive chapter is reported a more complete analysis of the comparison between different sources.

13.9.2 Ball valves with contractions at inlet and outlet

Crane (Crane, 1999) has analyzed also the situation with the contractions and enlargments at inlet and outlet of the valve respectively. The values plotted are obtained for two ranges: $\theta < 45^\circ$ and $\theta > 45^\circ$. To represent the ranges the author's choice is to use $\theta = 30^\circ$ and $\theta = 180^\circ$ respectively, with $\beta = 0,7$.

The results are plotted in Graph 52.



13.10 Stopcocks

Stopcocks are particular types of small plug valves. For this kind of devices, Idel'chik (Idel'chik, 1966) has a particular section which plots the head loss coefficients against the angle of opening α [°] of the valve distinguishing between two types of conduit: rectangular and cylindrical. The data are plotted in Graph 53.

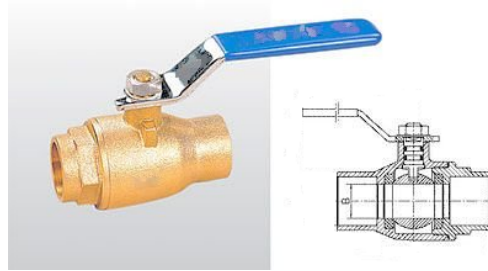
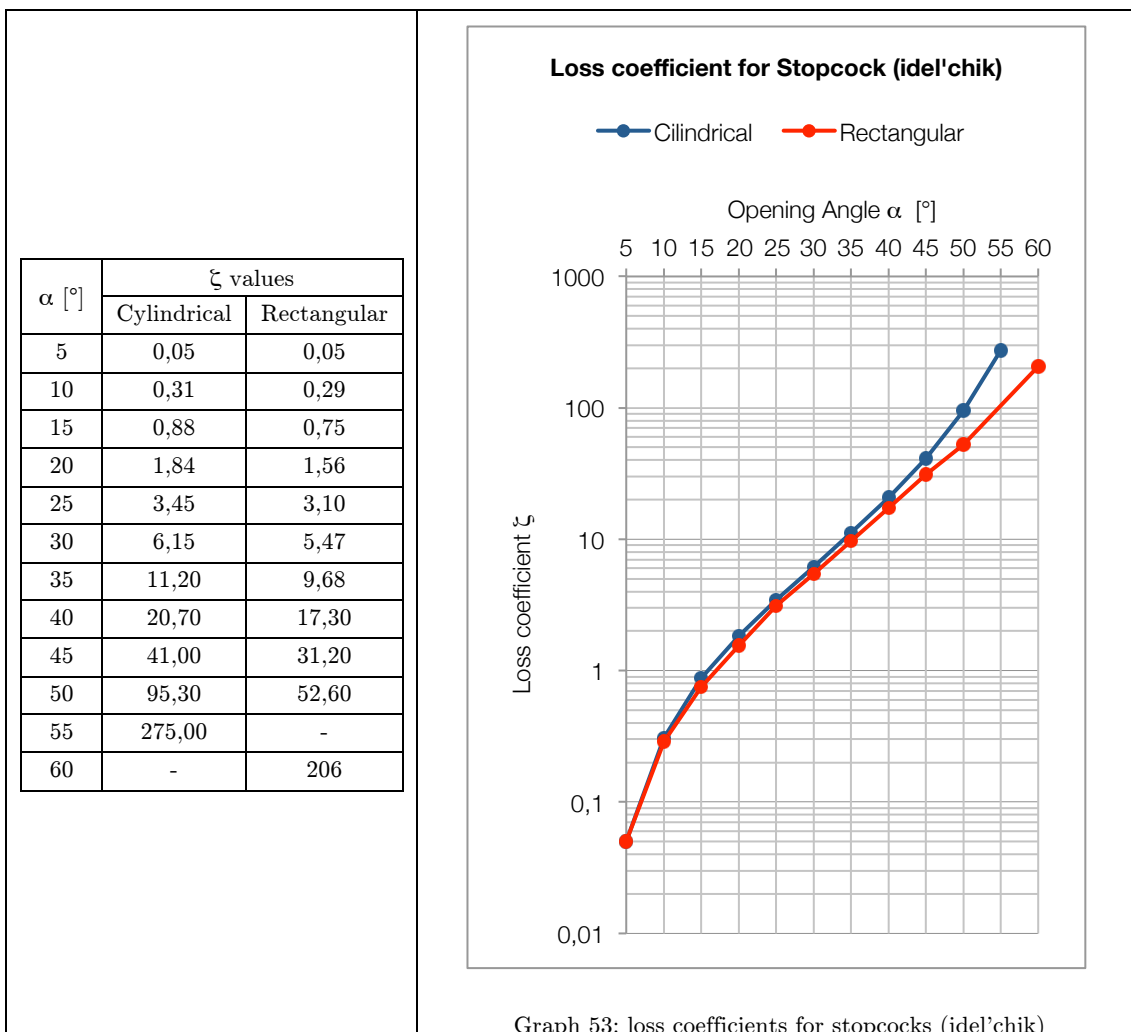


Figure 29: stopcock with its schematic opening angle representation



13.11 Butterfly valves

Butterfly valves are commonly used in industrial applications to control the internal flow of both compressible and incompressible fluids. A butterfly valve typically consists of a metal disk formed around a central shaft, which acts as its axis of rotation.



Figure 30: VAG Cerex 300-L Butterfly valve

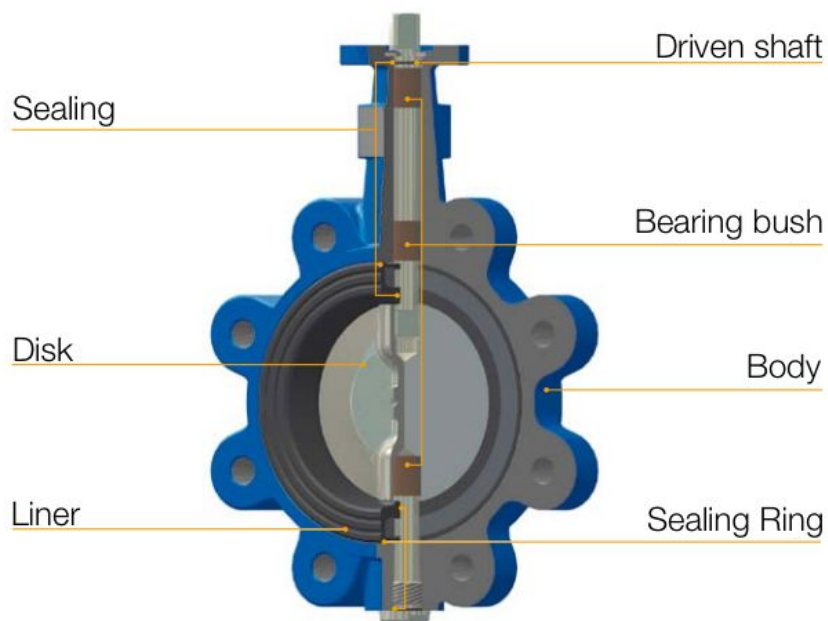


Figure 31: schematic view of the VAG Cerex-L butterfly valve

As the valve's opening angle, δ , is increased from 0° (fully open) to 90° (fully closed), fluid is able to more readily flow past the valve.

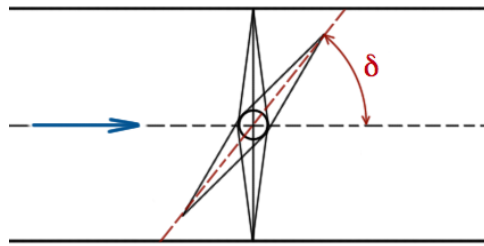


Figure 32: definition of opening angle for butterfly valves

There are in literature and in websites a lot of ways and parameters to state the butterfly valves performances such as pressure drop, hydrodynamic torque, flow coefficient, loss coefficient and torque coefficient. The reasons are different but it is important to say that head losses in butterfly valves can be related to a lot a different factors depending on geometrical aspects and manufacturing aspects. Variations in the loss coefficients of valves from different manufacturers are greater than the variations in loss coefficients for different sizes of valves from the same manufacturer.

A general classification is not so easy to be done because there's a great variety between the butterfly valves models in commerce in terms of manufacturing, dimensions, geometrical aspects and materials. From the point of seat tightness, butterfly valves may be divided into nominal-leakage valves, low-leakage valves, and tight shut-off valves. The nominal and low-leakage valves are used mainly for throttling or flow control duty, while tight shut-off butterfly valves may be used for tight shut-off, throttling, or flow control duty.

From the disc design point of view, butterfly valves can be divided in two main groups, one with single disk and other with double disk.

Fisher (Fischer, 2004), divides valves into three categories: swing-through, lined and high-performance. The most rudimentary is the swing-through design. Rather like a stovepipe damper, but considerably more sophisticated, the valve disk in this valve design swings close to, but clear of body's inner wall. Such a valve is used for throttling applications that do not require shut-off tighter than about one percent of full flow.

In this paper, considering all of this possible classification, butterfly valves are divided into two main categories based on the position of the closure member:

1. central pattern;
2. double eccentric pattern;

In the central pattern, the disc, with its axis of rotation, is positioned perfectly centered in the body of the butterfly valve (Figure 30).

The technological innovation proved that this design choice has two main disadvantages:

1. High friction during the whole stroke of the closure member (Figure 33);
2. High deformation of the rubber in fully open position;

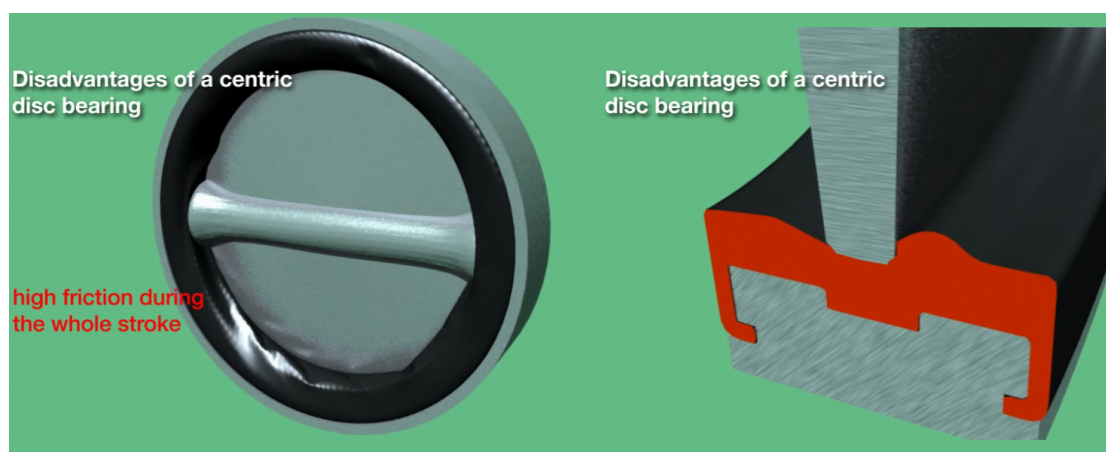


Figure 33: high friction during the stroke of the closure member

The first of this two problems is caused by the incenteral position of the disc in the horizontal plane; moving the rotation point of the closure member back from its original position (Figure 34), is possible to avoid friction and to obtain a more durable resilient seating zone.

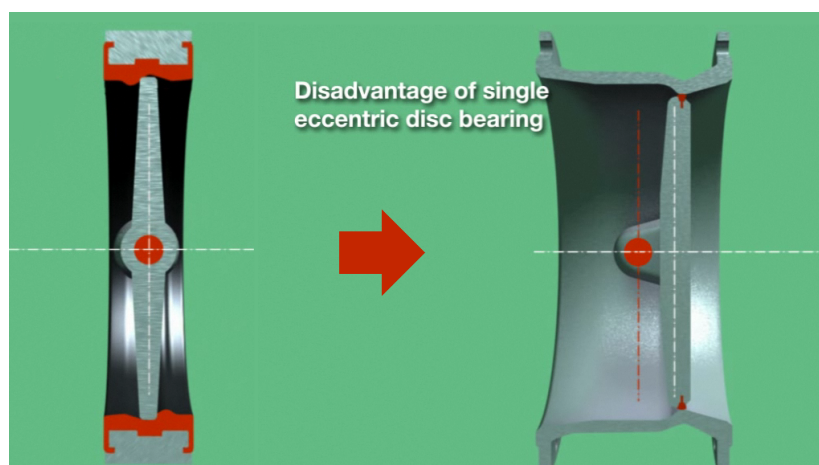


Figure 34: moving the center of rotation back

This trick brings to the second problem stated before: the single eccentric rotation of the disc implies the rubbing between the metallic seat of the valve and the rubber that surrounds the closure member.

This situation implies the damage of the rubber with the passing of time and, consequently, the imperfect watertight in closed position (Figure 35).

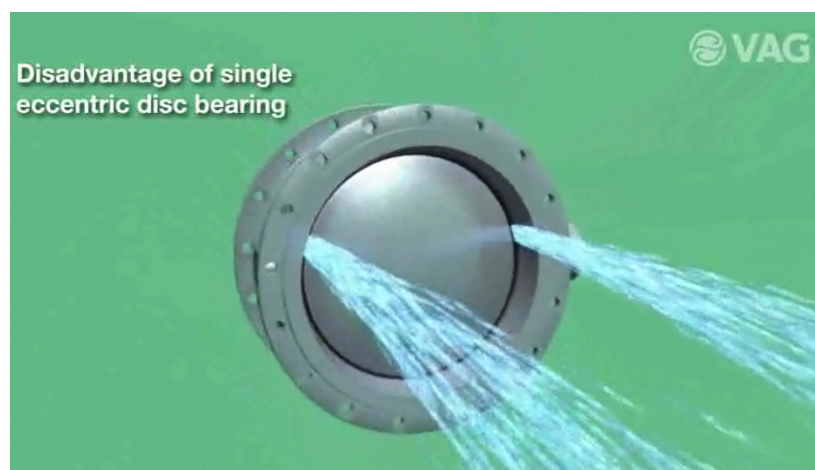


Figure 35: imperfect watertight closure

This situation can be solved with a second moving of the rotation line of the closure member in vertical direction (Figure 36).

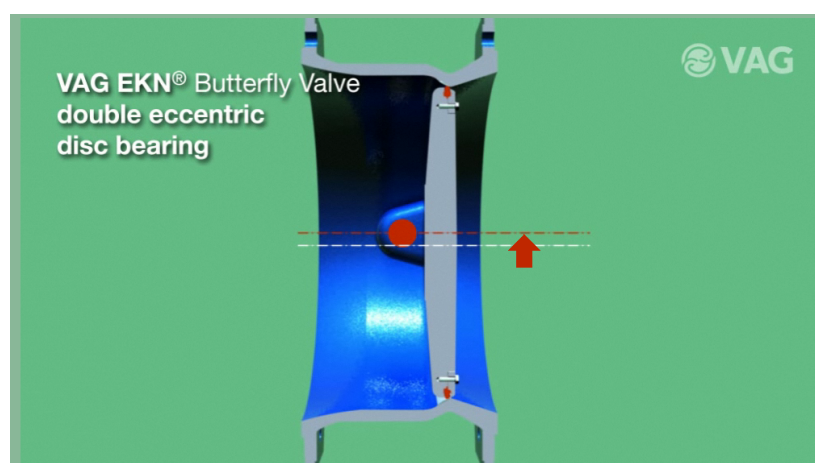


Figure 36: vertical moving of the rotation line of the closure member

This play will make the friction between the rubber of the closure member and the sealing materials more soft, and so will help watertight of the valve.

In this sense, VAG developed the EKN Butterfly valve model (Figure 37 and Figure 38), which is a double eccentric pattern of butterfly valve. The head loss coefficients of this valve will be presented in the relative section in the Graph 61.

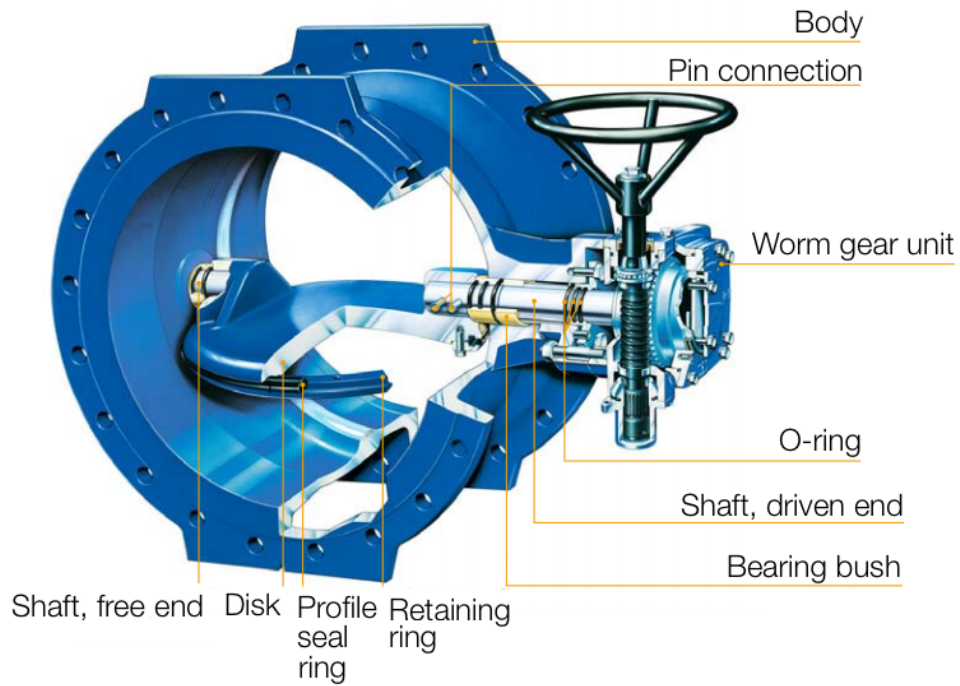


Figure 37: VAG EKN Butterfly Valve schematic

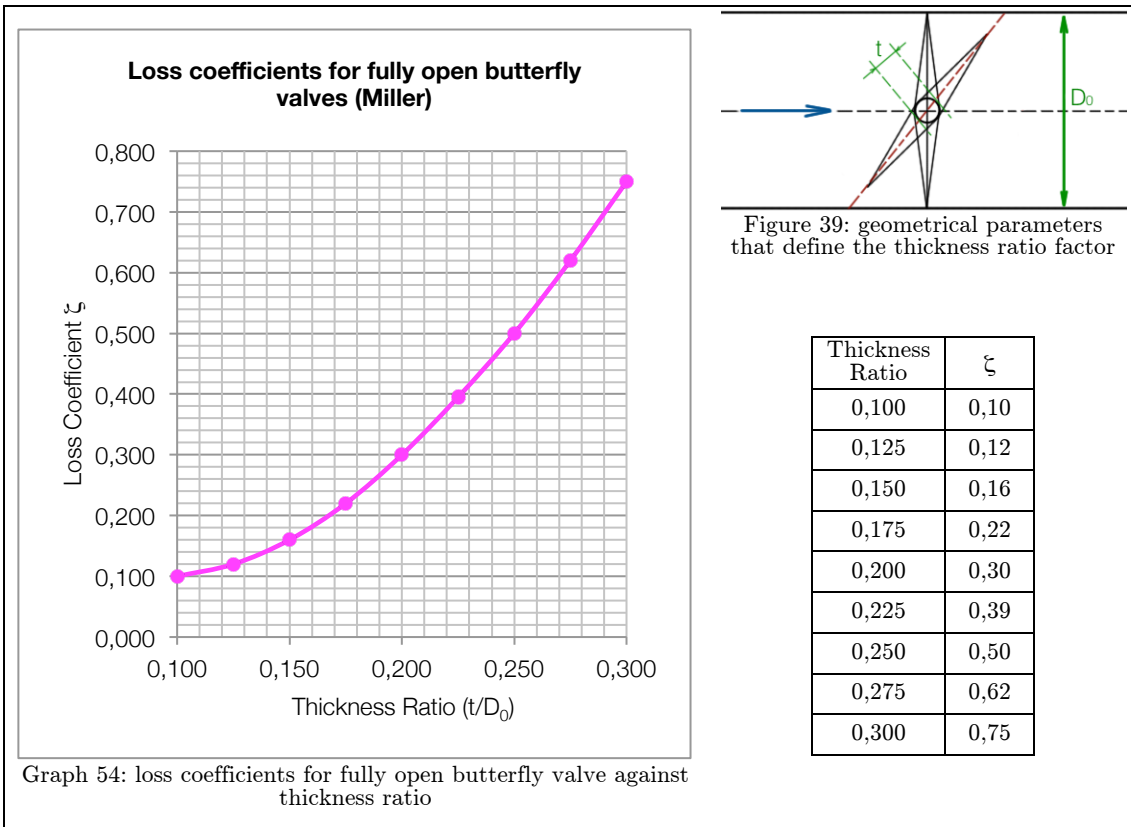


Figure 38: VAG EKN Butterfly Valve

13.11.1 Fully open central pattern

Against thickness ratio

In the following graphs are plotted the values ζ for butterfly valves fully open against the thickness ratio parameter. The thickness ratio is defined as a ratio of the dimension “t” of the disk shaft and the duct diameter D_0 (Figure 39). The graph is taken from Miller (Miller, 1973), for Reynolds number above 5×10^3 . The plotted curve represents a mean of the fully open valve loss coefficients given for all the sizes.



The trend in this graph is monotone increasing and this is what is clear from the theoretical approach: the greater are the geometrical dimensions of the disk, the greater are the turbulences that causes largest head losses.

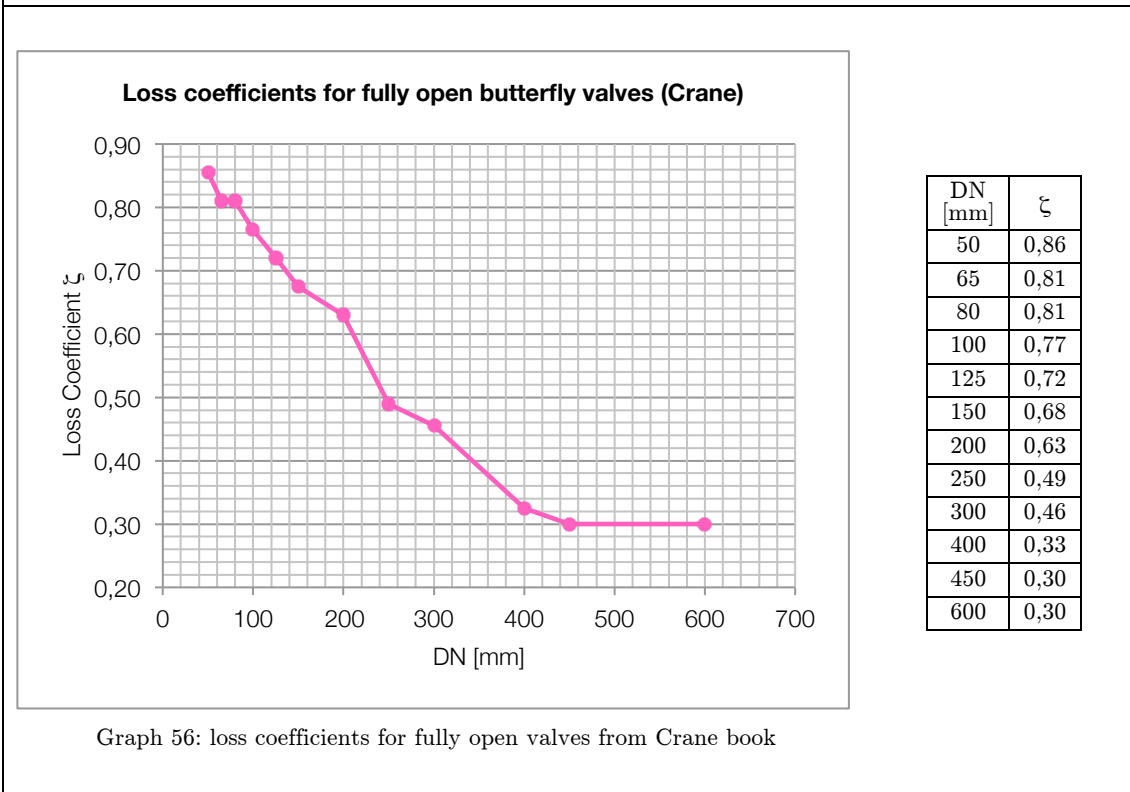
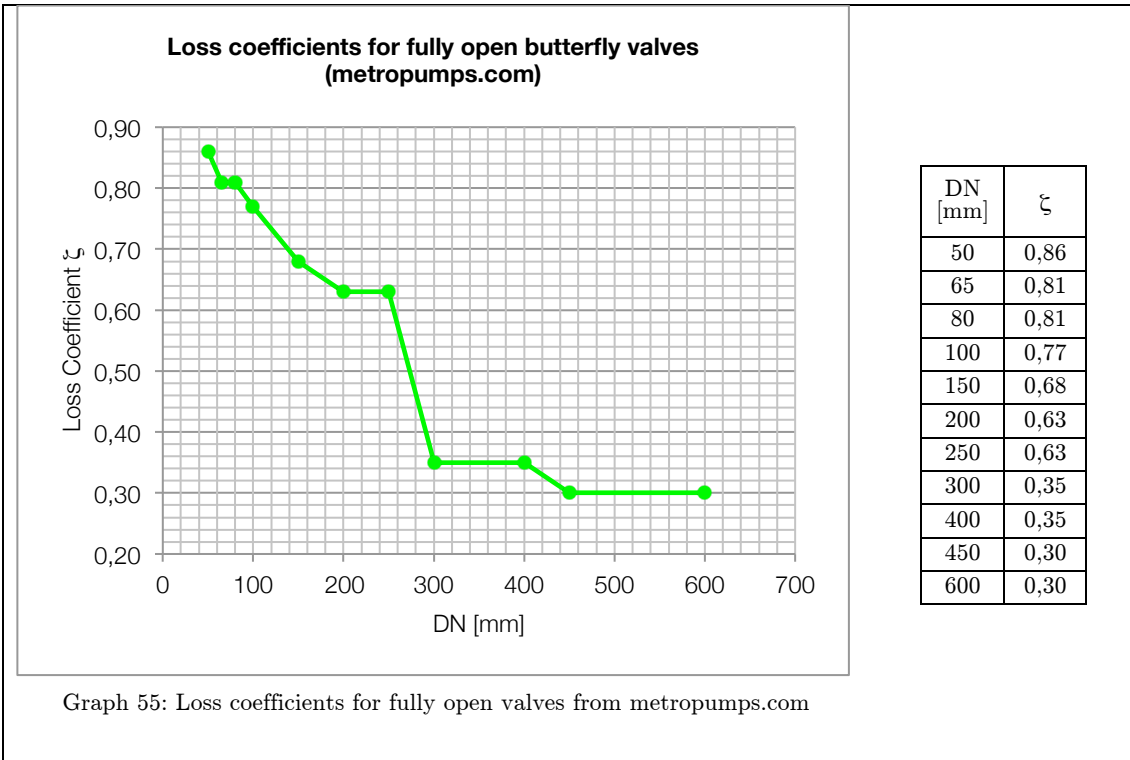
From Bianchi (Bianchi, Sanfilippo 2001) we have the values plotted in the Table 16, which are little bit higher than Miller:

Table 16: Bianchi and Sanfilippo values of loss coefficients

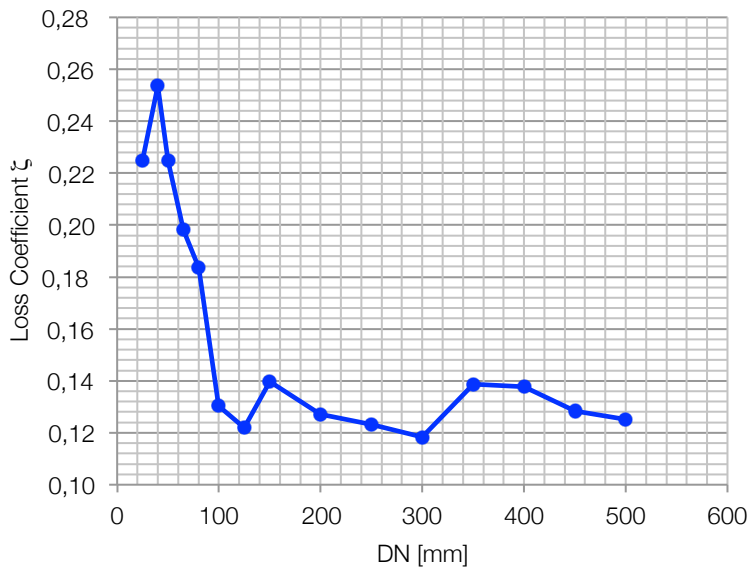
Thickness Ratio	Commercial
0,150	0,28
0,200	0,44
0,250	0,72
Usual values	0,6 – 0,7

Against Nominal Diameter

In the following graphs (Graph 55, Graph 56, Graph 57, Graph 58) it is represented the head loss coefficients for fully open valves, against the nominal diameter value DN. For every graph is shown the source and the peculiarities of the curves.



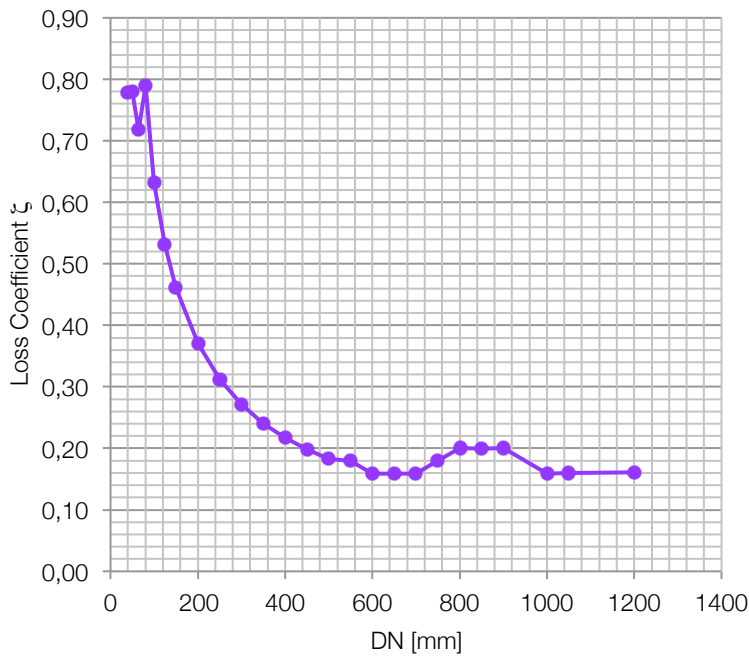
**Loss coefficients for fully open butterfly valves
(Valvias.com)**



DN [mm]	ζ
50	0,86
65	0,81
80	0,81
100	0,77
150	0,68
200	0,63
250	0,63
300	0,35
400	0,35
450	0,30
600	0,30

Graph 57: loss coefficients for fully open valves from valvias.com

**Loss coefficients for fully open butterfly valves
(valvemate.com)**



DN [mm]	ζ
40	0,78
50	0,78
65	0,72
80	0,79
100	0,63
125	0,53
150	0,46
200	0,37
250	0,31
300	0,27
350	0,24
400	0,22
450	0,20
500	0,18
550	0,18
600	0,16
650	0,16
700	0,16
750	0,18
800	0,20
850	0,20
900	0,20
1000	0,16
1050	0,16
1200	0,16

Graph 58: loss coefficients for fully open valves from valvemate.com

Another source of loss coefficients data for the central pattern of butterfly valve are VAG technical data sheets for the following valve products. The head loss coefficients are plotted against the DN values in the Graph 59.

VAG CEREX® 300-L Butterfly valve

VAG CEREX® 300-W Butterfly valve

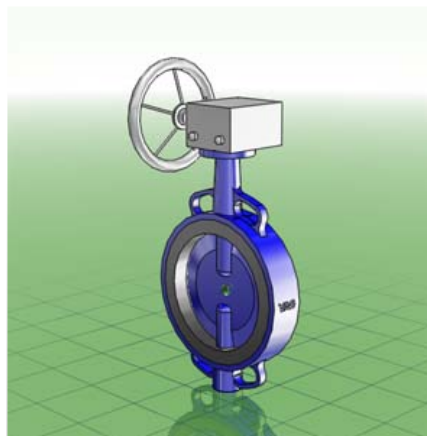


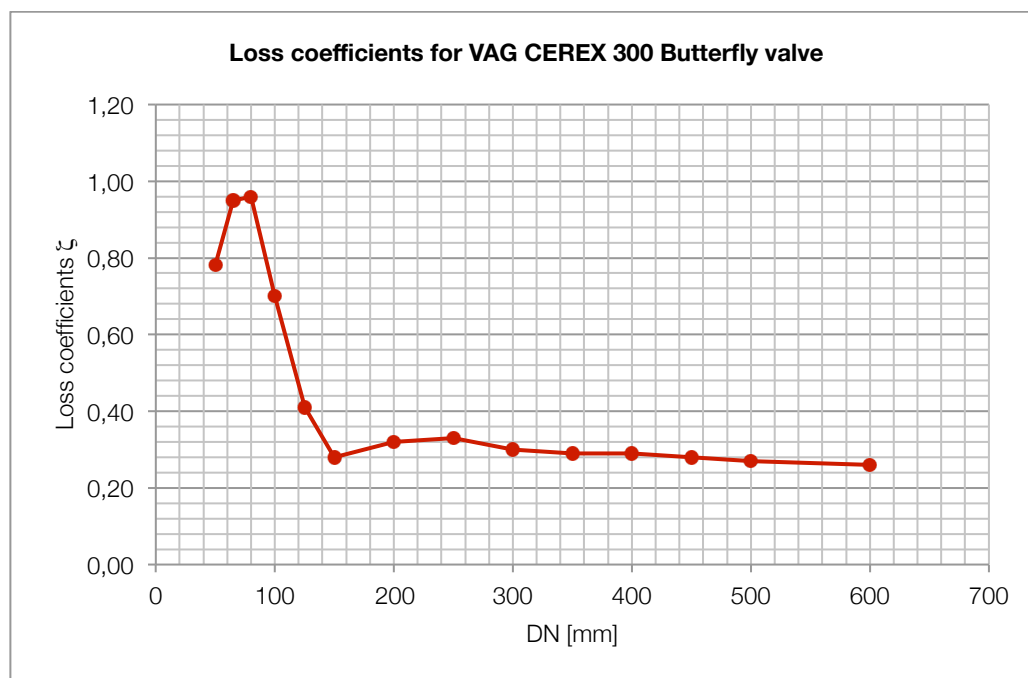
Figure 40: VAG CEREX-L Butterfly Valve

Figure 41: VAG CEREX-W Butterfly Valve

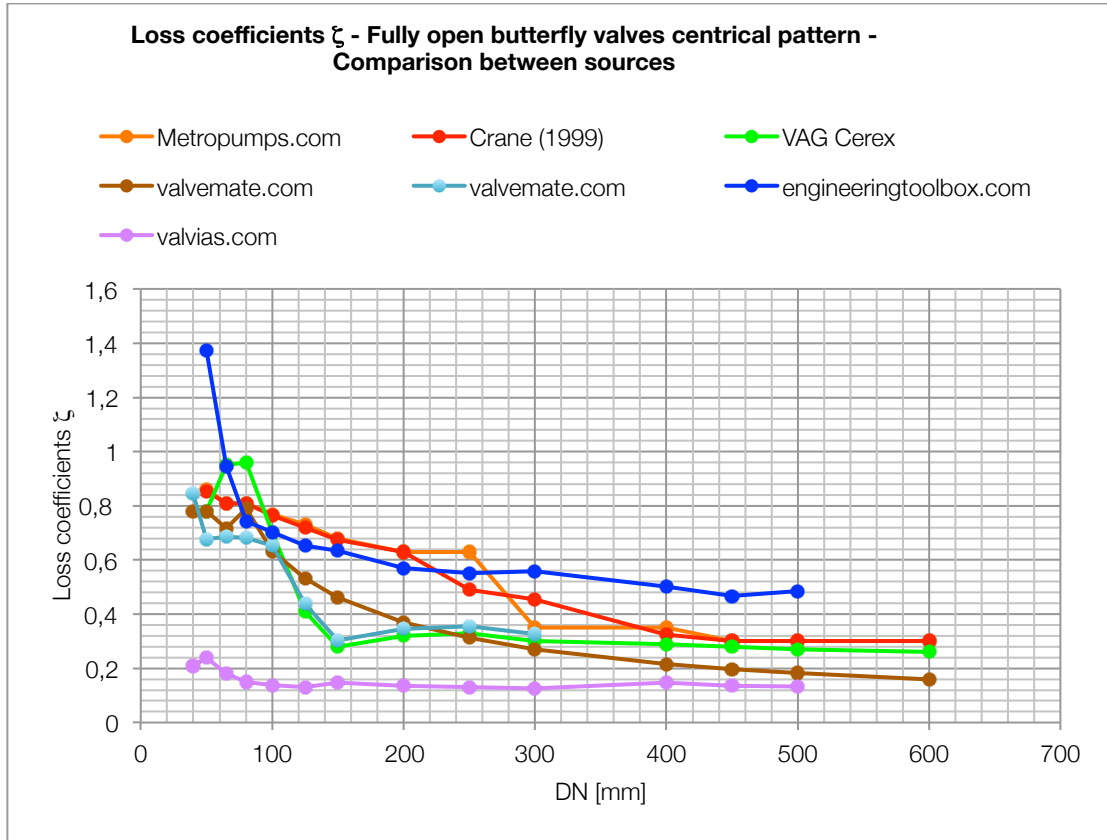
Operation data:

Maximum flow velocity in fully open position:

- PN 16: 4 m/s
- PN 10: 3 m/s



Graph 59: loss coefficients for fully open VAG CEREX Butterfly Valve



Graph 60: comparison between loss coefficients of central pattern of butterfly valves

Graph 60 summarizes the differences between all the results taken from the previous sources. It's clear that the trend is very similar in all the cases: high values are concentrated in small values of nominal diameter, than there is a decreasing that is fast in the first part and lower in the second. Loss coefficients of Crane (Crane, 1999), metropumps.com and valvemate.com are similar also in the absolute values, in particular the percentage difference between Crane (Crane, 1999) and metropumps.com are always under 28%. A more complete comparison will be executed in the finale conclusive chapter.

13.11.2 Fully open double eccentric pattern

As stated before, the values of the head loss coefficient ζ for this valve pattern are taken from VAG data sheet belonging to VAG EKN model. The data are plotted in the Graph 61, at different nominal pressures PN (associated to different velocities).

This valve is used in underground installation, chamber installation and installation in plants.

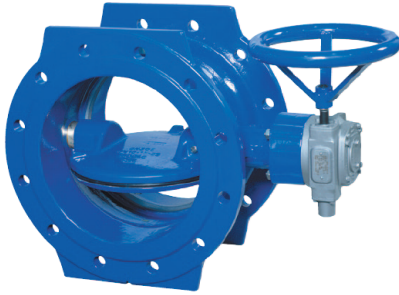


Figure 42: VAG EKN Butterfly Valve

There are different type of valve basing on PN 6, 10, 16, 25 and 40 and powered by different actuator as handwheel, electric actuator, pneumatic actuator, hydraulic actuator.

Operation data:

Maximum flow velocity in fully open position:

- PN 40: 6 m/s
- PN 25: 5 m/s
- PN 16: 4 m/s
- PN 10: 3 m/s
- PN 6: 2,5 m/s

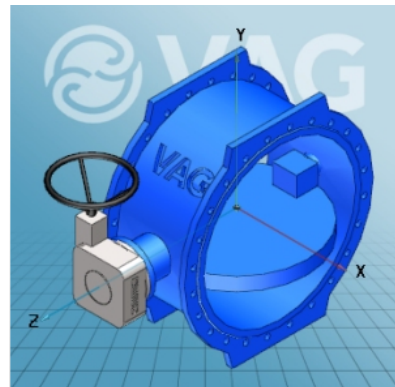
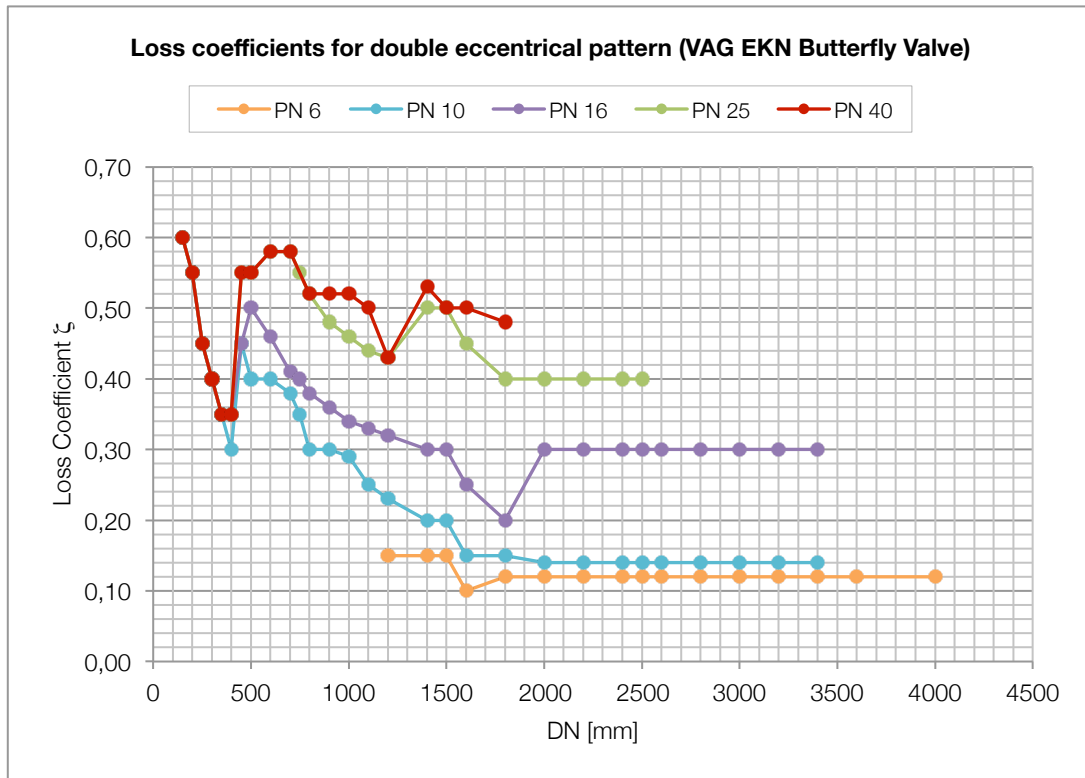


Figure 43: 3D view of VAG EKN Butterfly valve

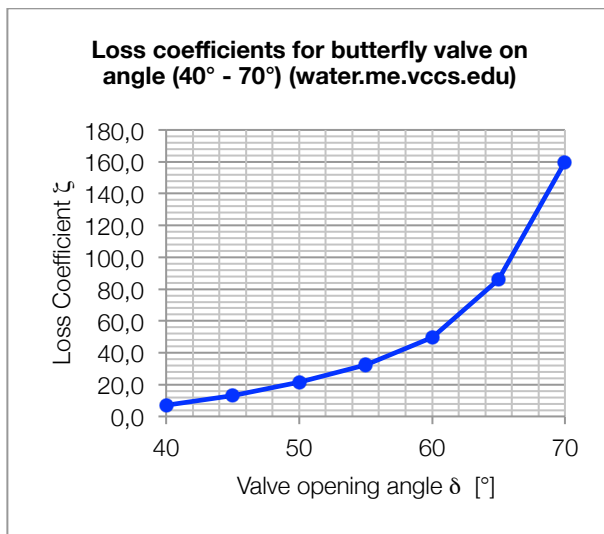


Graph 61: VAG EKN Butterfly Valve loss coefficients

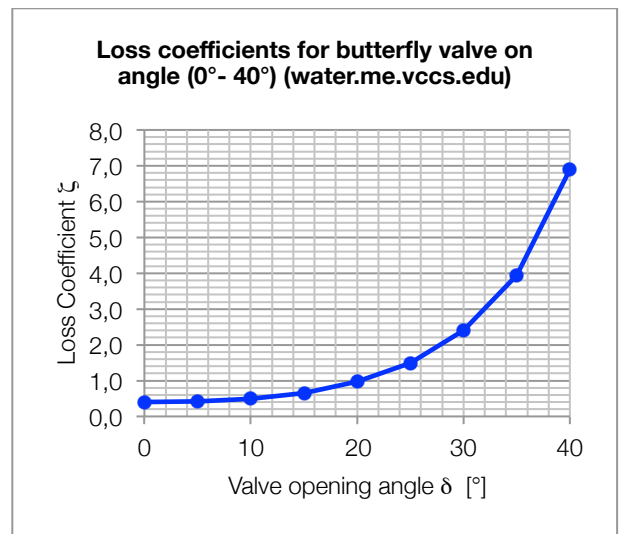
A comparison between the data of the double eccentric pattern and the data for the central pattern will be made in the final chapter.

13.11.3 Partial opening of butterfly valves

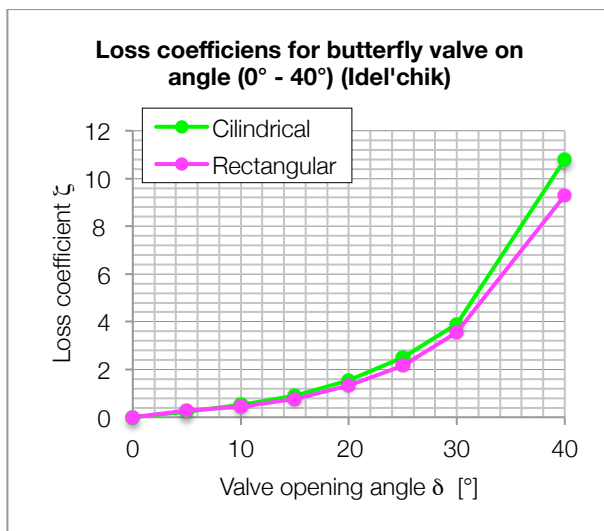
In the following graphs are plotted the values of the head loss against the valve opening percentage (opening angle δ). In general, butterfly valves give little resistance to flow when fully open and sensitive flow control when open between about 15° and 70° . Graph 62 and Graph 63 plot the result of the website water.me.vccs.edu for butterfly valves completely open varying the opening angle. Graph 64 and Graph 65 are the results taken from Idel'chik (Idel'chik, 1966), that makes a difference from Rectangular conduit and cylindrical conduit.



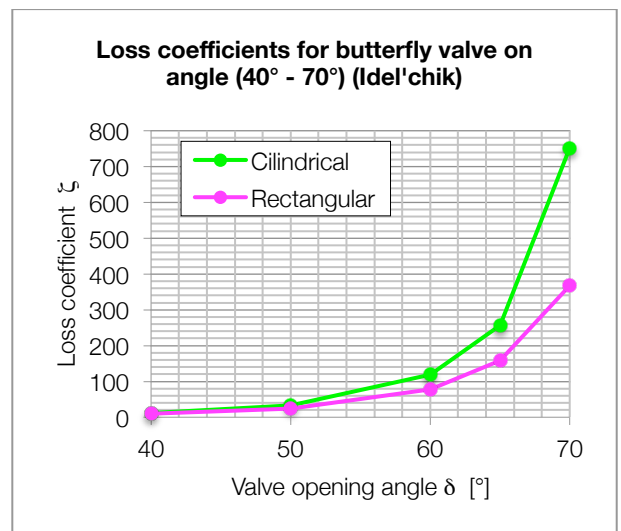
Graph 62: loss coefficients for butterfly valve against opening angle values between 40° and 70° (water.me.vccs.edu)



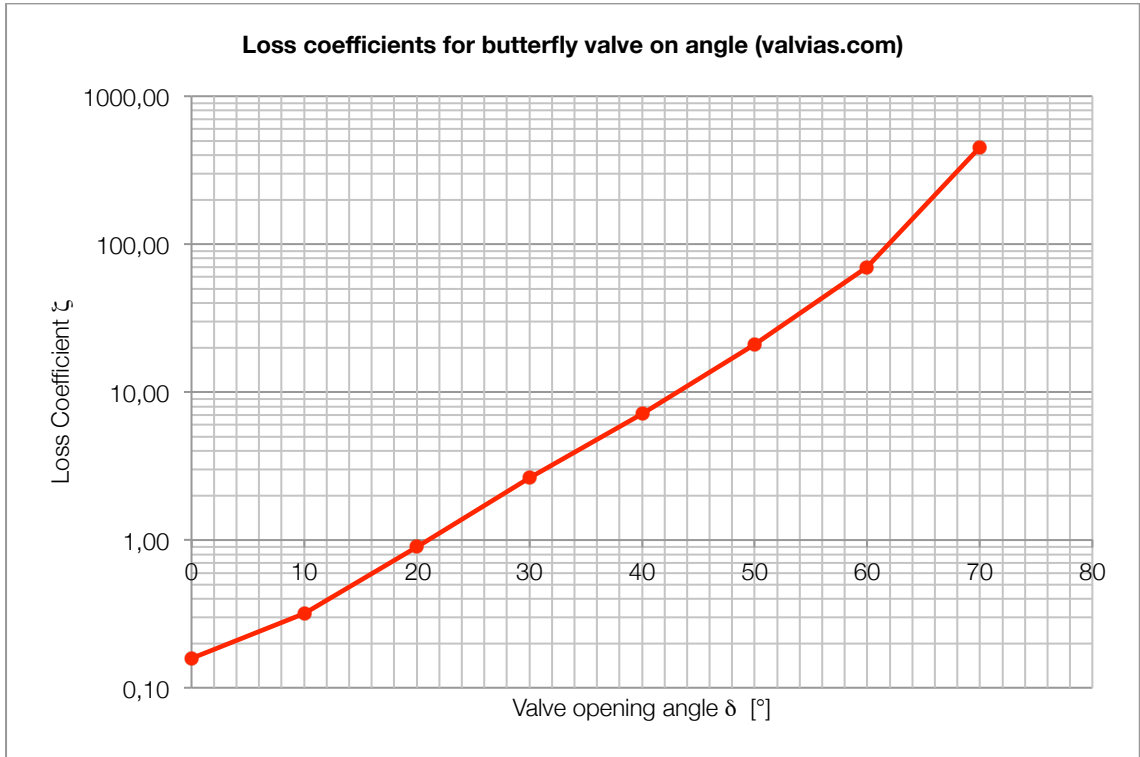
Graph 63: Loss coefficients for butterfly valve against opening angle values between 0° and 40° (water.me.vccs.edu)



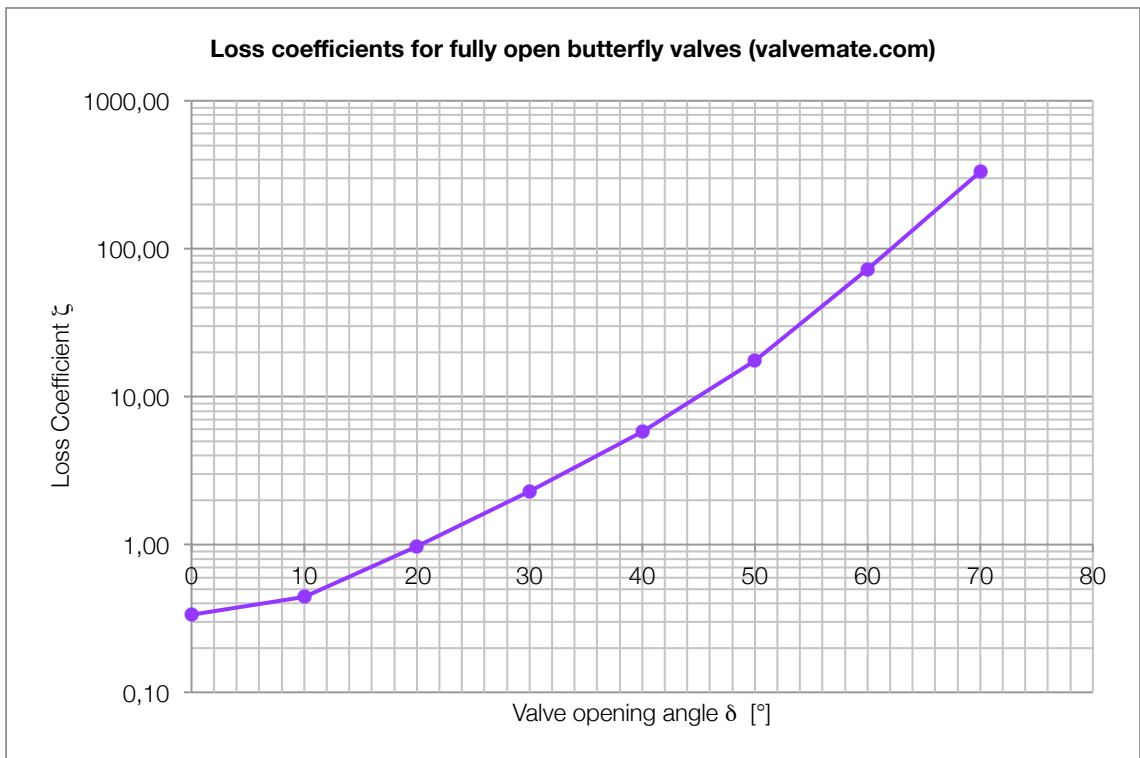
Graph 64: Loss coefficients for butterfly valve against opening angle values between 0° - 40° (Idel'chik)



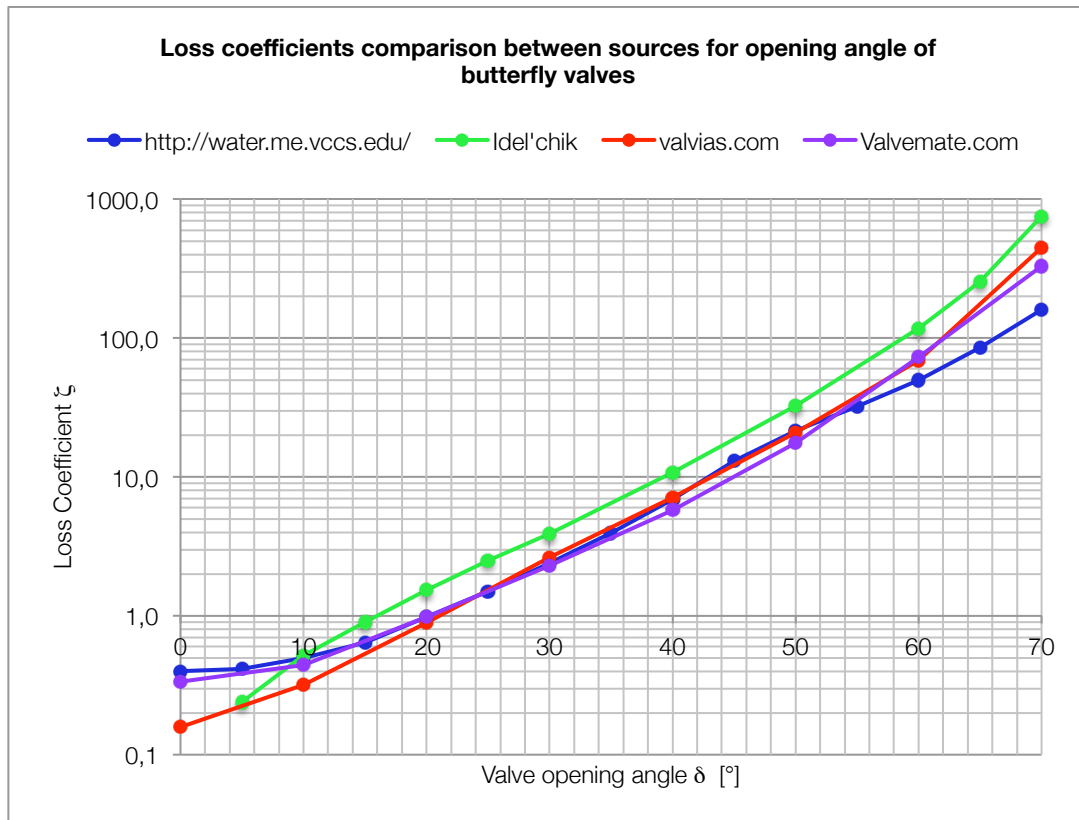
Graph 65: Loss coefficients for butterfly valve against opening angle values between 40° - 70° (Idel'chik)



Graph 66: Loss coefficients for butterfly valve against opening angle (valvias.com)



Graph 67: Loss coefficients for butterfly valve against opening angle (valvemat.com)



Graph 68: Comparison between loss coefficients of different sources (opening percentage)

Graph 66 is created by the average values of valvias.com, which refers the variation of the coefficient varying the nominal diameter.

Graph 68 underlines that if we make a comparison between the results, it's easy to see that the trend is very similar in the four cases. The values in the case of Idel'chik book are a little higher than the others but there's no information about the sources adopted and so looking for the reason of this is very hard.

The variation angle in which the results are best matched are the "central", in particular between 20° and 60°. This is another noticeable result: for bigger or smaller opening angles values the turbulence is very high and all the measurement are less accurate.

A more complete comparison will be performed in the last conclusive chapter.

13.12 Flaps

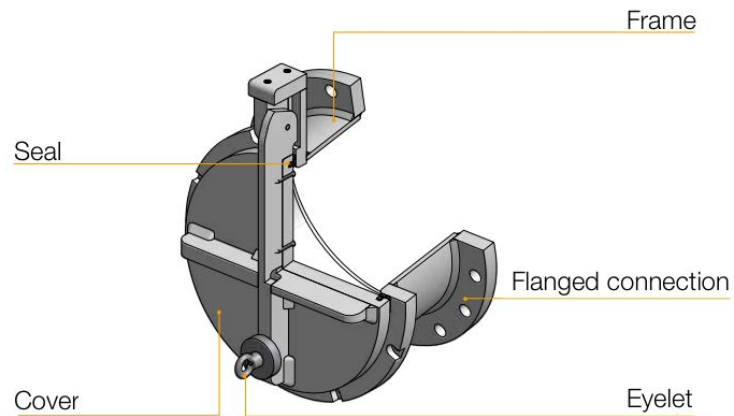
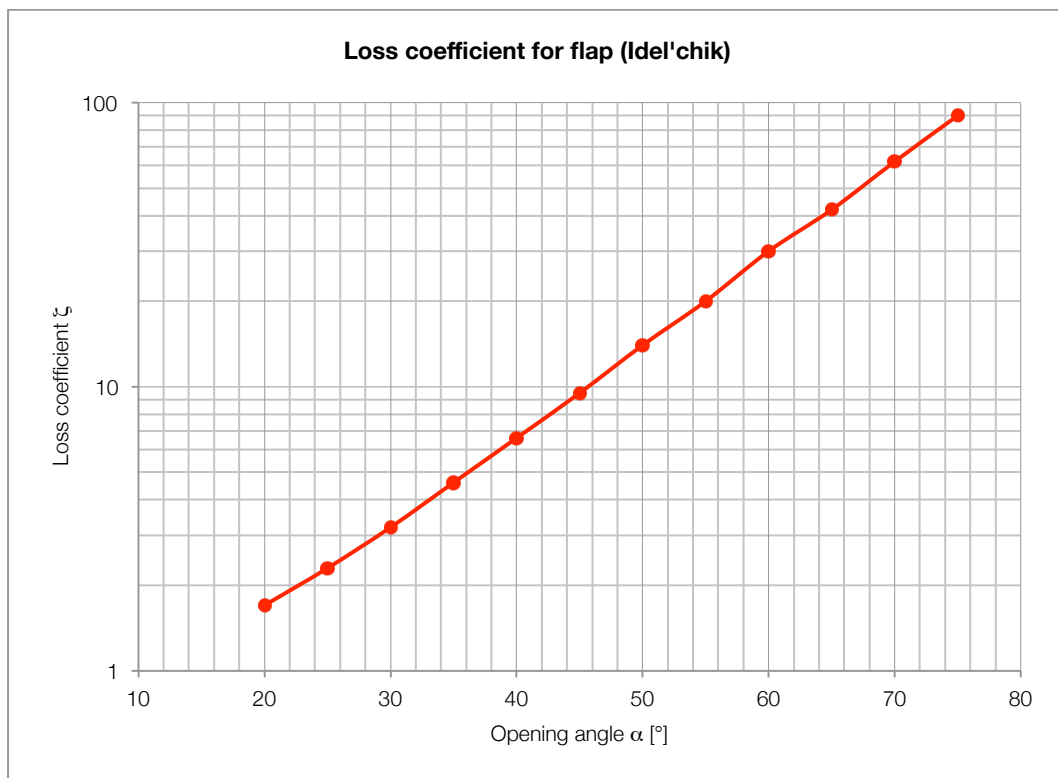


Figure 44: flap valve

In the Graph 69 is plotted the trend of the loss coefficient for flap valve against the opening angle α , in logarithmic scale and standard view, from Idel'chik resistance book (Idel'chik, 1966).



Graph 69: Loss coefficient for flap valves in logarithmic scale (Idel'chik)

α [°]	20	25	30	35	40	45	50	55	60	65	70	75
ζ	1,7	2,3	3,2	4,6	6,6	9,5	14	20	30	42	62	90

13.13 Swing check valves

A swing check valve consists of a flap or disc of the same diameter as the pipe bore, which hangs down in the flow path. With flow in the forwards direction, the pressure of the fluid forces the disc to hinge upwards, allowing flow through the valve. Reverse flow will cause the disc to shut against the seat and stop the fluid going back down the pipe. In the absence of flow, the weight of the flap is responsible for the closure of the valve; however, in some cases, closure may be assisted by the use of a weighted lever. Most swing check valves can be installed in horizontal or vertical, upward flow, piping.

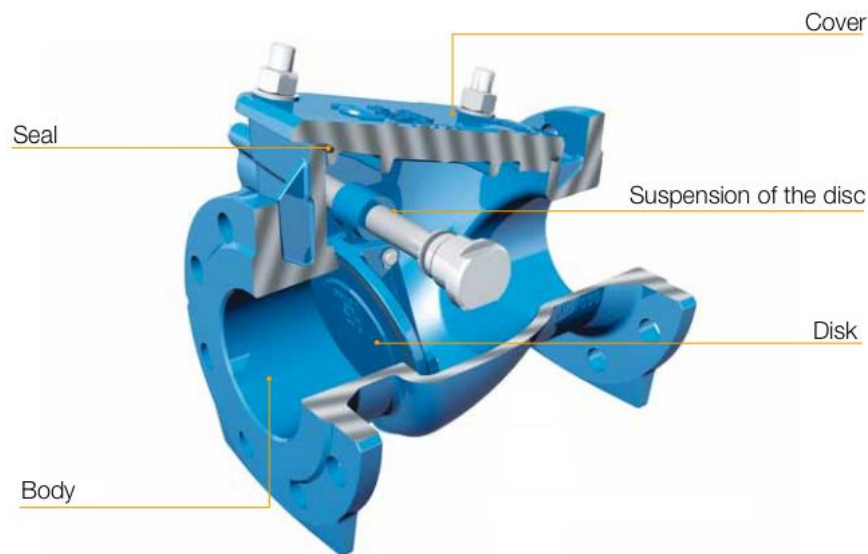


Figure 45: VAG RSK Check valve

They offer low resistance to flow and are particularly suited to low velocity service. The closure member swings about a hinge, which is mounted outside the seat.

Swing valves can be considered, from a certain point of view, as butterfly valves with an eccentric position of their closure member: the functioning principle is the same, activated by an hinging of a disc down, blocking the flow path.

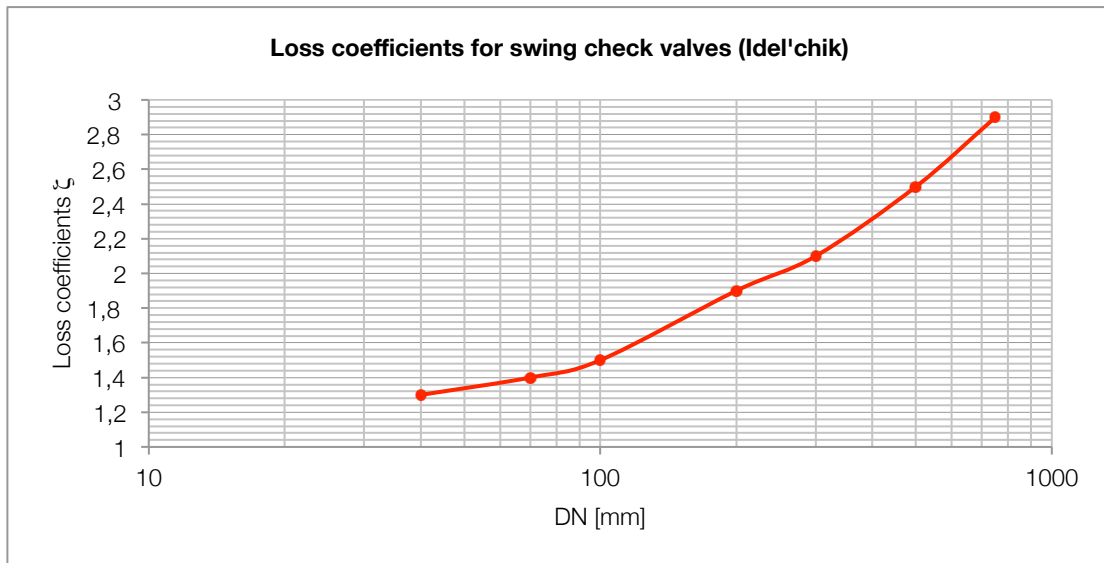
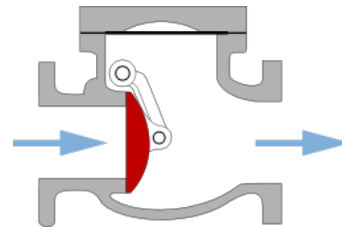
In the following pages will be treated the two main patterns of the swing check valves: clapet check valves and wafer check valves.

In the Graph 70 are plotted the head loss coefficient values taken from Idel'chik (Idel'chik, 1966) for fully open swing check valves.



Figure 46: VAG RSK Disk Check valve (swing check valve)

DN [mm]	40	70	100	200	300	500	750
ζ	1,3	1,4	1,5	1,9	2,1	2,5	2,9



Graph 70: loss coefficients for swing check valves (Idel'chik)

From Bianchi (Bianchi, Sanfilippo, 2001) we can refer the following ζ values for the same type of valve:

flow velocity $V_0 \leq 2$ m/s	With counterweight	1,00
	Without counterweight	2,50
flow velocity $V_0 > 2$ m/s	DN 80 ÷ 150	1,20
	DN 200 ÷ 600	0,70
	DN 700 ÷ 1800	0,41

In particular there are a lot of differences in these values. For values of velocity greater than 2 m/s and for diameter values between 80 and 150 mm the value is similar. For larger diameter values the differences are considerable: it is clear that for Idel'chik the trend is increasing with the diameters value and for Bianchi is decreasing.

Miller, for this type of valve, reports that for velocities above 2 m/s, when most commercial valves are fully open, a loss coefficient of 1,0 may be assumed. The loss coefficient increases rapidly at velocities below those necessary to hold the valve in fully open position. When multiple door valves are used, a loss coefficient of 1,5 may tentatively be assumed.

VAG Valves data sheets presents its swing check valve model with Graph 71, in which are presented head loss coefficients against the flow inlet velocity.

It is clear that for this valve type, turbulences and eddies are caused, in the open position, by the geometrical abrupt change immediately after the inlet cross-section: the disc, in open position, represents an obstacle to the regular stream flow because it breaks the regular geometry of the pipe. In this sense the field which it is possible to set in is the reduction of the geometrical differences between the cross-section in the valve in open position and the pipe cross-section. VAG Valves has developed "VAG RETO-STOP Non-Return Valve" a valve model which minimizes this difference, and reports its head loss data in Graph 72.

VAG RSK Disk Check Valve AL

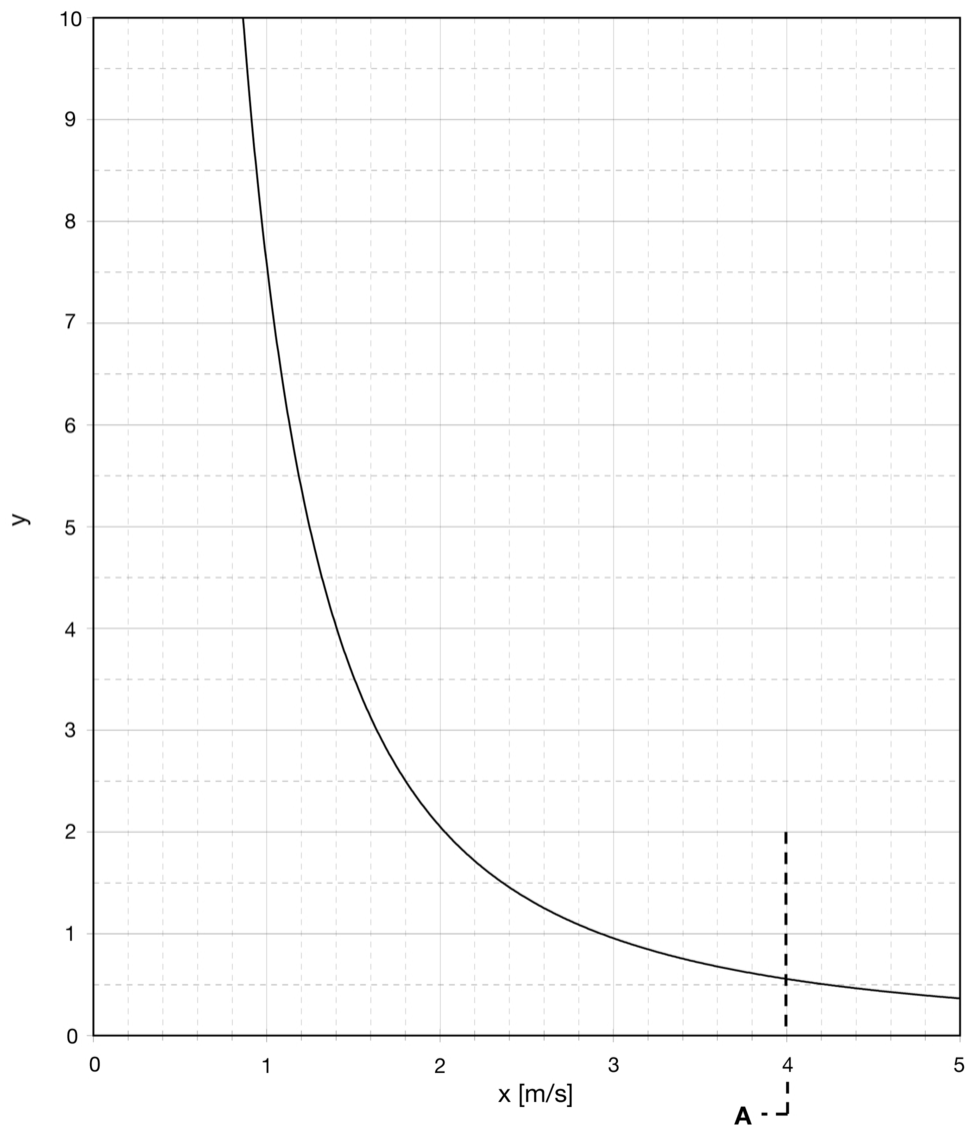


Figure 47: VAG RSK Disk Check Valve AL

Product characteristics:

- Resilient seated in accordance with EN 12334
- Face-to-face length acc. to EN 558-1, basic series 48 (DIN 3202, F6)
- With flange ends on both sides acc. to EN 1092-2
- With lever and weight (located on the right in flow direction)
- Lever and weight useable for position indicator
- For horizontal and vertical (flow from bottom upwards) pipelines

NB x is the flow velocity and y are the loss coefficient values ζ



Graph 71: Loss coefficients for VAG RSK Disk Check Valve AL

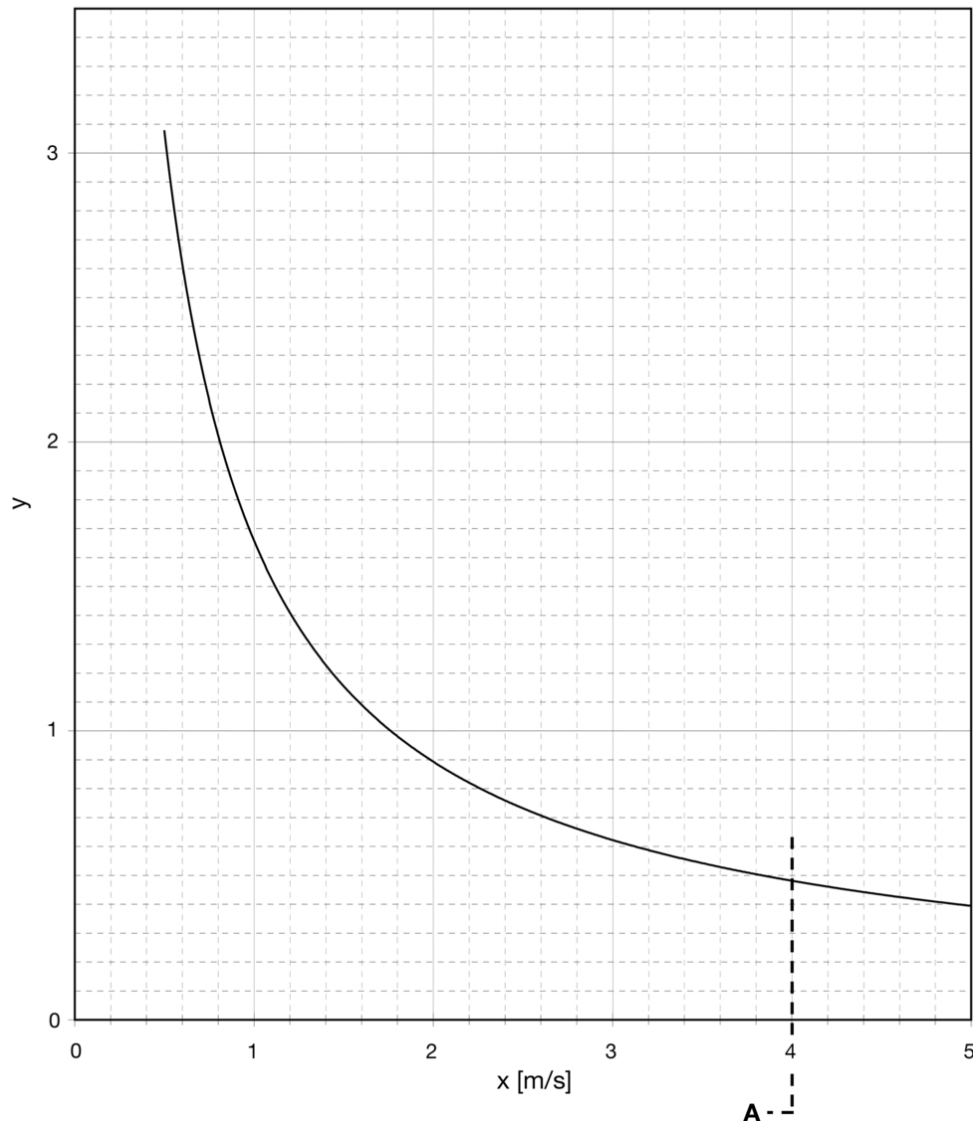
VAG RETO-STOP Non-Return Valve



Figure 48: VAG RETO-STOP Non-Return Valve

- Resilient seated in accordance with EN 12334
- Face-to-face length acc. to EN 558-1, basic series 48 (DIN 3202, F6)
- With flange ends on both sides acc. to EN 1092-2
- Double service life due to turnable disk
- Integrated limit stops in the disk to protect the seal
- No bearing friction due to integrated suspension of disk
- Pre-stressed disk closing due to rubber suspension
- Incrustation and corrosion-free rubber lined disk

NB x is the flow velocity and y are the loss coefficient values ζ



Graph 72: Loss coefficients for VAG RETO-STOP Non-Return Valve

13.14 Wafer Check Valves

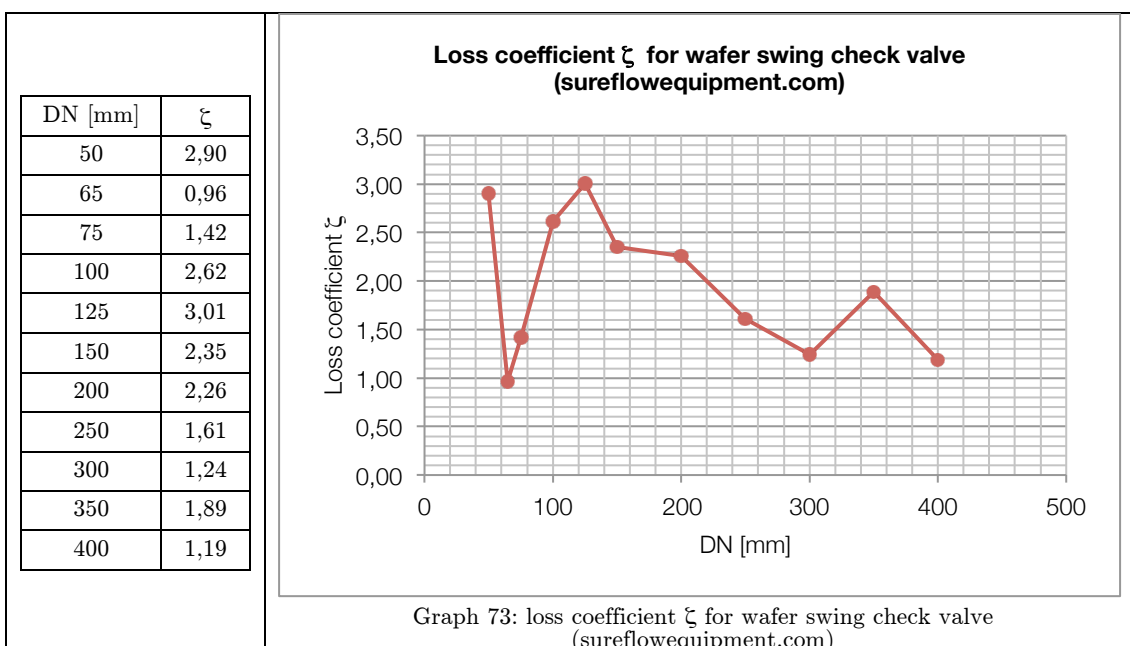
Both lift and swing check valves tend to be bulky which limits their size and makes them costly. To overcome this, wafer check valves have been developed. By definition wafer check valves are those that are designed to fit between a set of flanges. This broad definition covers a variety of different designs, including double disc wafer check valves.

13.14.1 Swing type wafer check valves



Figure 49: sectional view of a wafer check valve

These are similar to the standard swing check valves, but do not have the full-bodied arrangement, instead, when the valve opens, the flap is forced into the top of the pipeline. Subsequently, the flap must have a smaller diameter than that of the pipeline, and because of this, the pressure drop across the valve, which is often high for swing type valves, is further increased. In the Graph 73 are plotted the head loss coefficients for this valve type, from the sureflowequipment.com website.



Another source of data is Bianchi (Bianchi, Sanfilippo, 2001), for which it is possible to refer that the value for wafer check valve for flow velocities above 2 m/s is $\zeta = 1,1$.

13.14.2 Split disk wafer check valves

The split disc check valve or dual plate check valve (Figure 50) is designed to overcome the size and pressure drop limitations of the swing and disc type wafer check valves. The flap of the swing check valve is essentially split and hinged down its centre, such that the two disc plates will only swing in one direction. The disc plates are held against the seat by a torsion spring mounted on the hinge.

In order to hold the hinge in the centre of the flow path, externally mounted retainer pins can be used. These retainer pins are a common source of leakage from the valve. An improved design secures the hinge internally, and as the valve mechanism is entirely sealed within the body, leakage to atmosphere is prevented.



Figure 50: VAG ZETKA Non-return valve

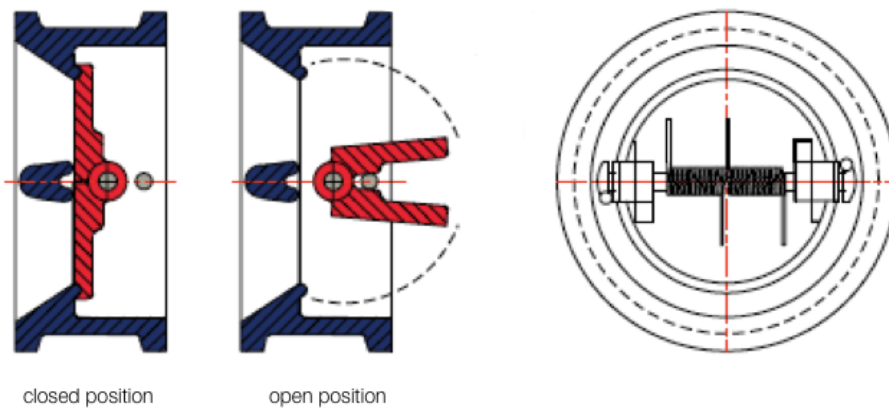


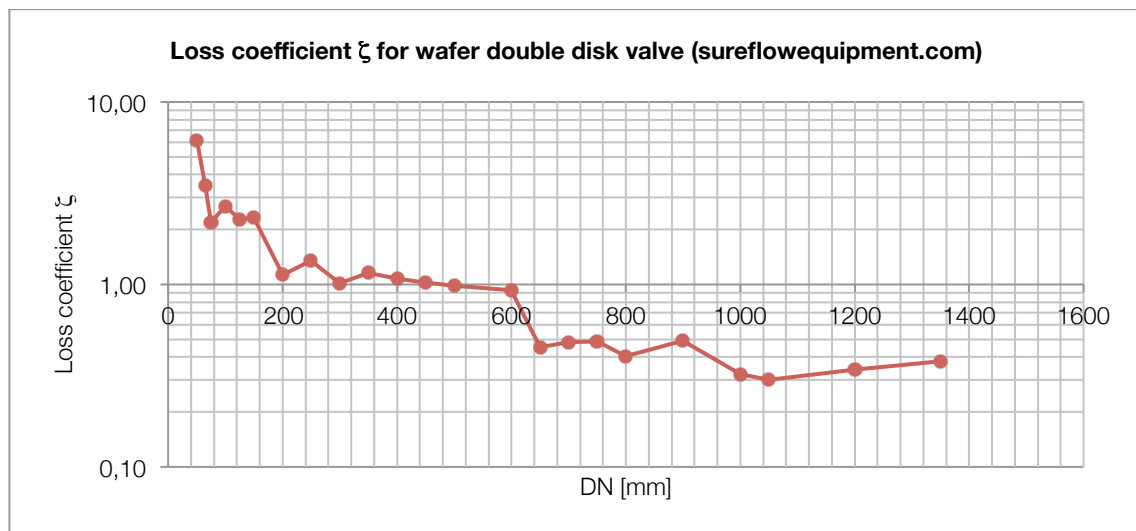
Figure 51: wafer double disk check valve schematic view

The frequent opening and closing of the split disc check valve would soon cause seat damage if the heels of the disc plates were allowed to scuff against the seat during opening. To overcome this, the heel of the disc plates lift during the initial opening of the valve and the plates rotate purely on the hinge as opposed to the seat face.

The split disc type of check valve has several advantages over other types of check valves:

- The split disc design is not limited in size and these valves have been produced in sizes of up to DN5400;
- The pressure drop across the split disc check valve is significantly lower than across other types;
- They are capable of being used with lower opening pressures;
- Split disc check vales can be installed in any position, including vertical pipelines;

For this valve type there are data available online on the site www.sureflowequipment.com, which is a manufacturer of this valve type and others. Data from this site are plotted in the Graph 74:



Graph 74: loss coefficients for wafer double disk valve (sureflowequipment.com)

DN [mm]	50	65	75	100	125	150	200	250	300	350	400	450	500	600	650
ζ	6,17	3,47	2,20	2,69	2,28	2,32	1,13	1,35	1,02	1,16	1,08	1,03	0,99	0,93	0,45

DN [mm]	700	750	800	900	1000	1050	1200	1350
ζ	0,48	0,49	0,40	0,49	0,32	0,30	0,34	0,38

13.15 Tilting-disk check valves

Tilting Disk check valves (Figure 52 and Figure 53) consist of a cylindrical housing, with a pivoted circular disk. The pivots are located just above the center of the disk, and offset from the plane of the body seat. The closure member tilts about a hinge, which is mounted near, but above, the center of the seat; This design gives a bell-crank action to the disk. The seat is of circular bevel type and the disk drops in or out of contact without rubbing or sliding.

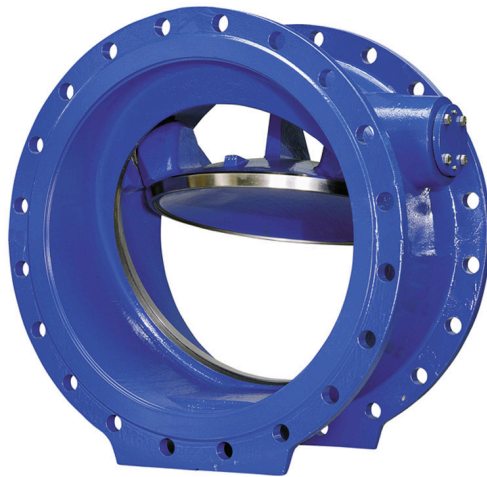


Figure 52: VAG SKR Slanted Seat Tilting-disk check valve



Figure 53: VAG SKR Slanted Seat Tilting-disk check valve (CUT VIEW)

13.15.1 Fully open tilting disk check valves

In the Graph 75 and Graph 76 are plotted the head loss coefficients values (indicated with the letter “Z”) for $\alpha = 5^\circ$ and $\alpha = 15^\circ$, taken from Crane (Crane, 1999) and from the site metropumps.com:

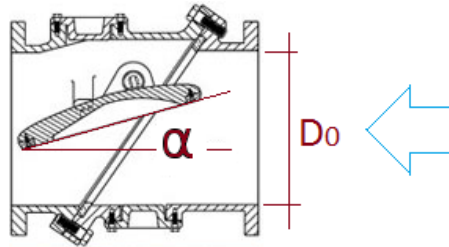
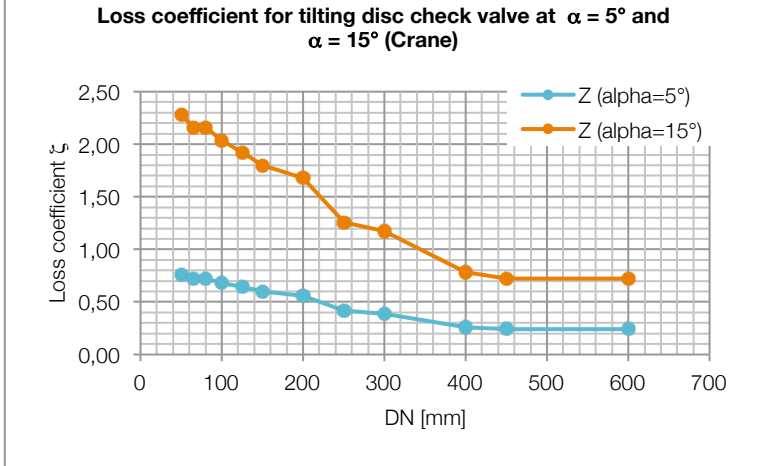
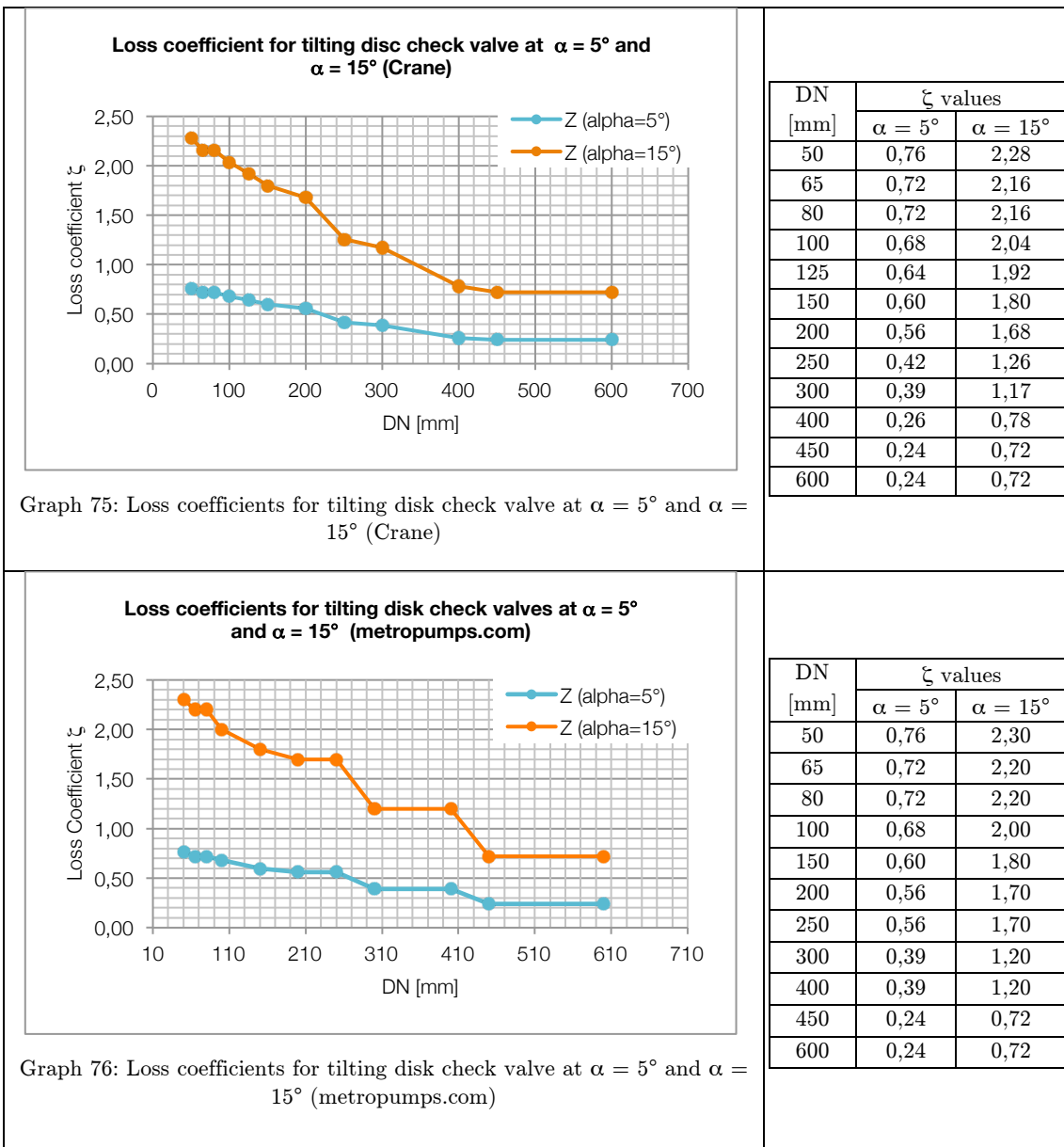
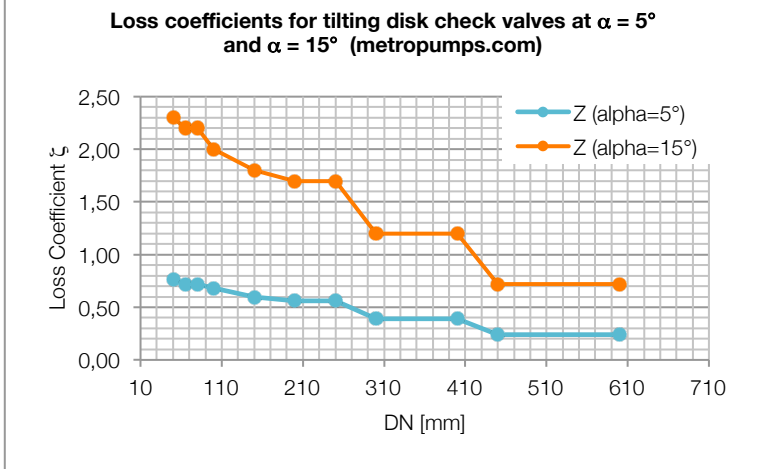


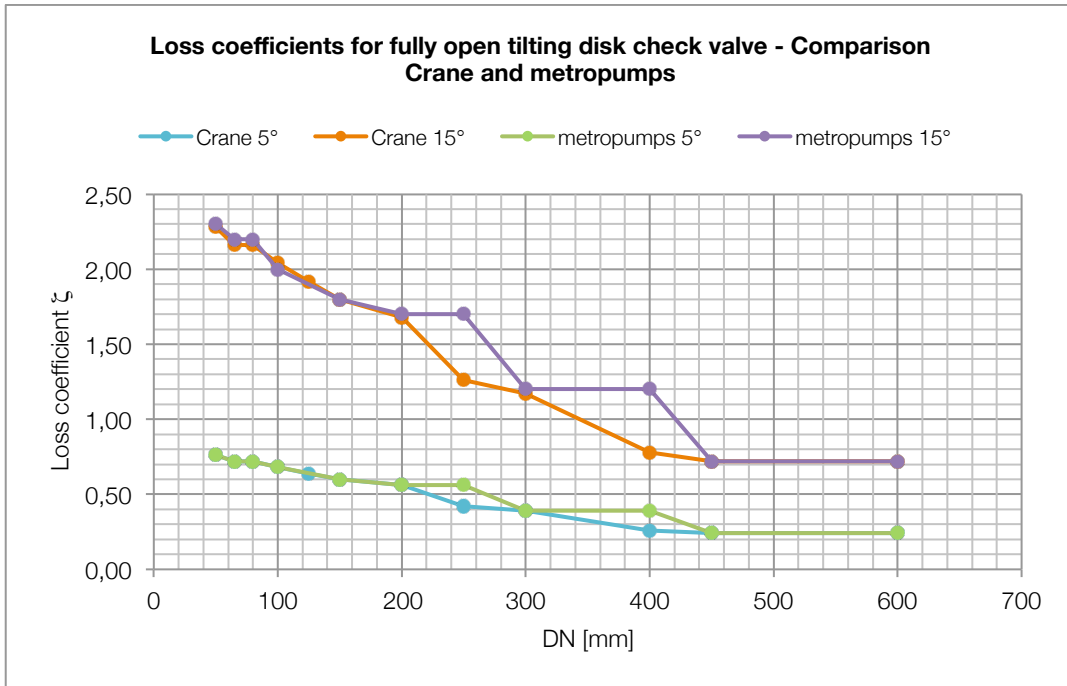
Figure 54: tilting-disk valve opening angle definition



Graph 75: Loss coefficients for tilting disk check valve at $\alpha = 5^\circ$ and $\alpha = 15^\circ$ (Crane)



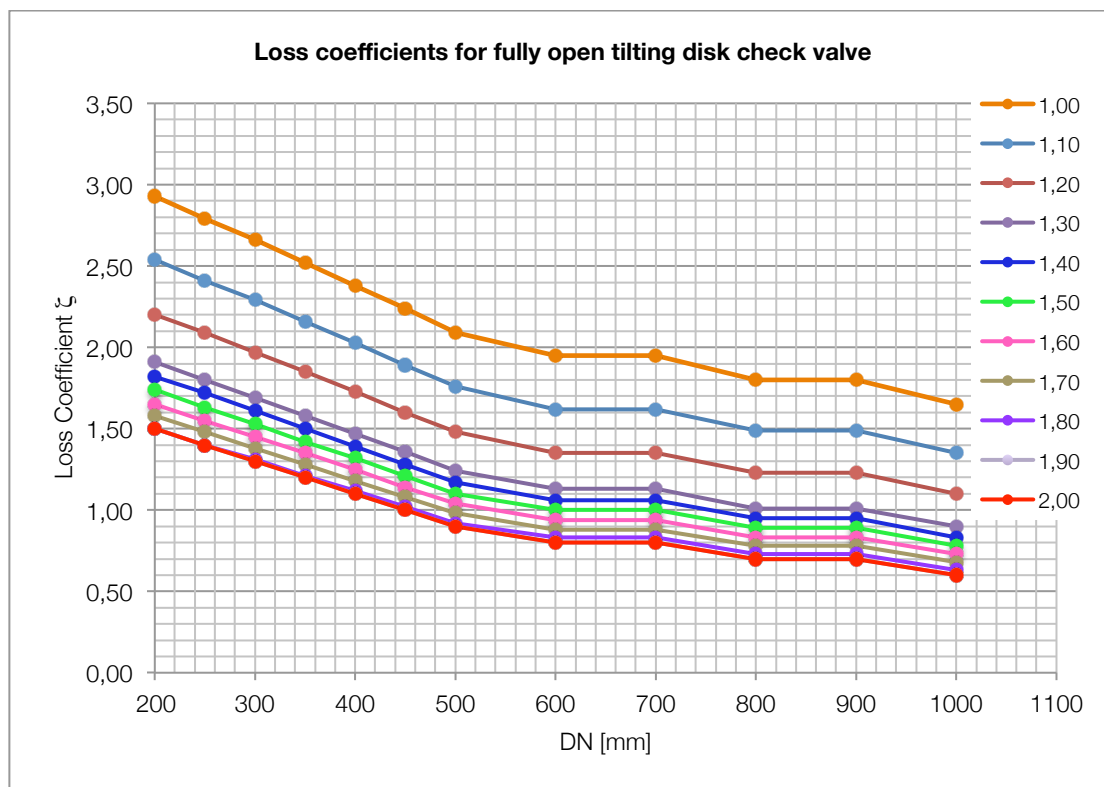
Graph 76: Loss coefficients for tilting disk check valve at $\alpha = 5^\circ$ and $\alpha = 15^\circ$ (metropumps.com)



Graph 77: comparison between head loss values from metropumps.com and Crane

If we compare the results between the two sources, it is clear that the trends for the two values of α are very similar. The largest differences between values are concentrated on 400 and 250 DN values but the other are practically overlapped.

In the Graph 78 and in the Table 17 are plotted the results taken from VAG technical reports about this type of valve, for VAG SKR slanted seat tilting disk check valve, against the nominal diameter and against the flow velocity for the fully open position.



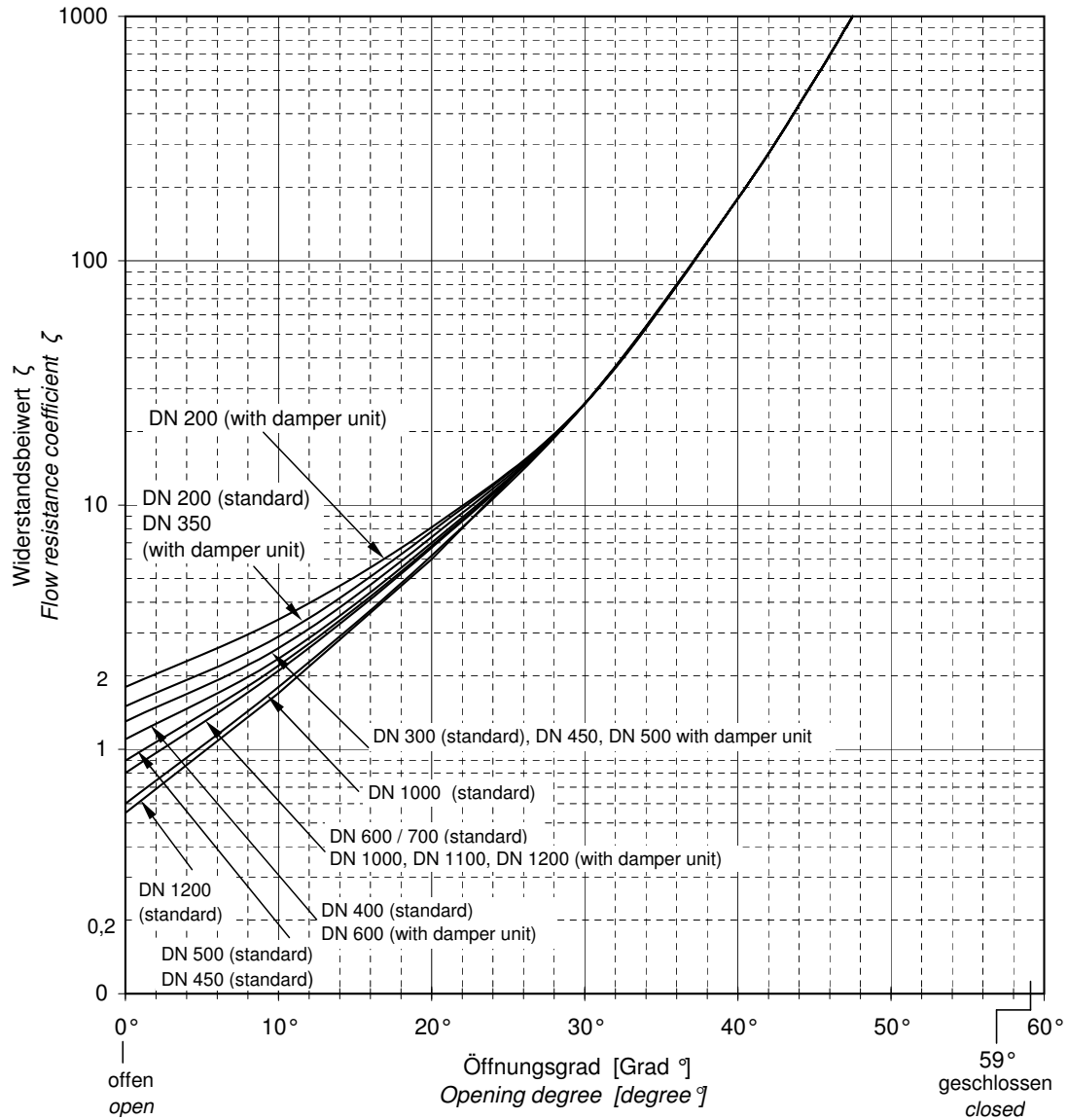
Graph 78: head loss coefficients for VAG SKR slanted seat tilting disk check valve

Table 17: VAG VALVES data for tilting disk check valve without damper unit

DN [mm]	velocity [no u.d.m.]										
	1,00	1,10	1,20	1,30	1,40	1,50	1,60	1,70	1,80	1,90	2,00
200	2,93	2,54	2,20	1,91	1,82	1,74	1,65	1,58	1,50	1,50	1,50
250	2,79	2,41	2,09	1,80	1,72	1,63	1,55	1,48	1,40	1,40	1,40
300	2,66	2,29	1,97	1,69	1,61	1,53	1,45	1,38	1,31	1,30	1,30
350	2,52	2,16	1,85	1,58	1,50	1,42	1,35	1,28	1,21	1,20	1,20
400	2,38	2,03	1,73	1,47	1,39	1,32	1,25	1,18	1,12	1,10	1,10
450	2,24	1,89	1,60	1,36	1,28	1,21	1,14	1,08	1,02	1,00	1,00
500	2,09	1,76	1,48	1,24	1,17	1,10	1,04	0,98	0,92	0,90	0,90
600	1,95	1,62	1,35	1,13	1,06	1,00	0,94	0,88	0,83	0,80	0,80
700	1,95	1,62	1,35	1,13	1,06	1,00	0,94	0,88	0,83	0,80	0,80
800	1,80	1,49	1,23	1,01	0,95	0,89	0,83	0,78	0,73	0,70	0,70
900	1,80	1,49	1,23	1,01	0,95	0,89	0,83	0,78	0,73	0,70	0,70
1000	1,65	1,35	1,10	0,90	0,83	0,78	0,73	0,68	0,63	0,60	0,60

13.15.2 Partial opening of tilting disc-check valves

The same data on loss coefficients are plotted in VAG technical data sheet against the opening angle α of the closure member for every commercial diameter treated:



Graph 79: loss coefficients against opening angle for tilting disk check valve

DN	200	250	300	350	400	450	500	600	700	800	900	1000	1200
ζ -Wert (standard)	1,5	1,4	1,3	1,2	1,1	1,0	0,9	0,8	0,8	0,7	0,7	0,6	0,55
ζ -Wert (with damper unit)	1,8	1,7	1,6	1,5	1,4	1,3	1,2	1,1	1,0	0,9	0,9	0,8	0,7

13.16 Diaphragm valves

Diaphragm valves (or membrane valves) consists of a valve body with two or more ports, a diaphragm, and a “weir or saddle” or seat upon which the diaphragm closes the valve.



Figure 55: schematic view of VAG TOP-STOP valve

There are two main categories of diaphragm valves: one type seals over a “weir” (saddle) and the other, sometimes called “straight-way” or “full bore” seals over a seat. The weir or saddle type is the most common in process applications and the seat-type is more commonly used in slurry applications.

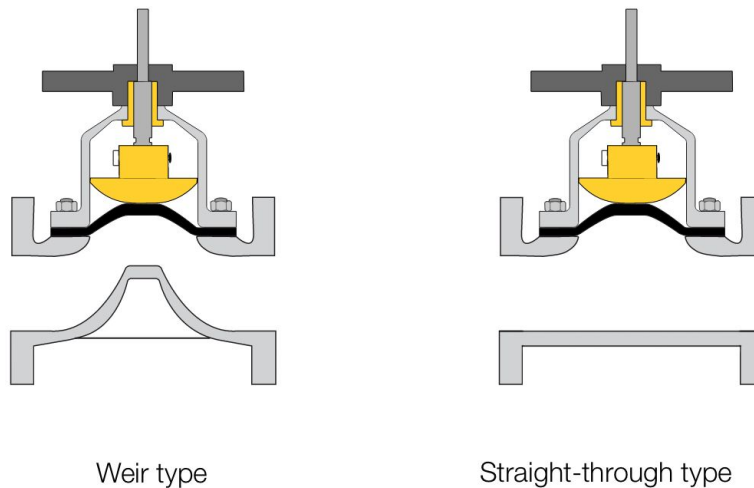


Figure 56: difference between straight-through type and the weir type of diaphragm valve

While diaphragm valves usually come in two-port forms, they can also come with three ports or more and can be manual or automated and their application is generally as shut-off valves in process systems.

In the Graph 80 is plotted the performance graph of the VAG TOP-STOP diaphragm valve, in which are represented the head loss coefficient values ζ depending on the flow velocity at the inlet of the valve indicated with the symbol x . This valve model is represented in Figure 57 and Figure 58.

Miller (Miller, 1973), for the weir type of this valve, in condition of fully open, refers the ζ coefficients which are listed in the

Zappe (Zappe, 1998) lists the following head loss coefficients for both types of the diaphragm valves in the



Figure 57: VAG TOP-STOP Diaphragm Non-Return Valve

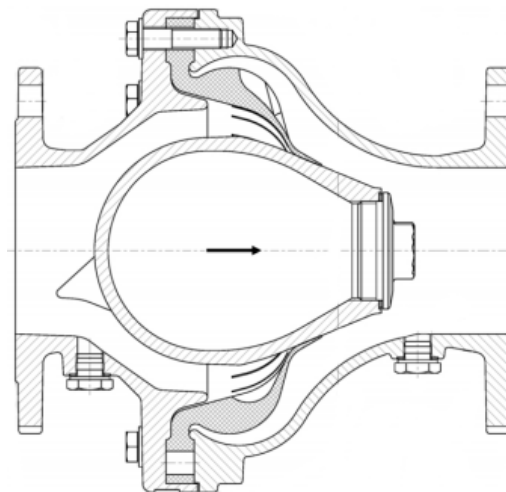


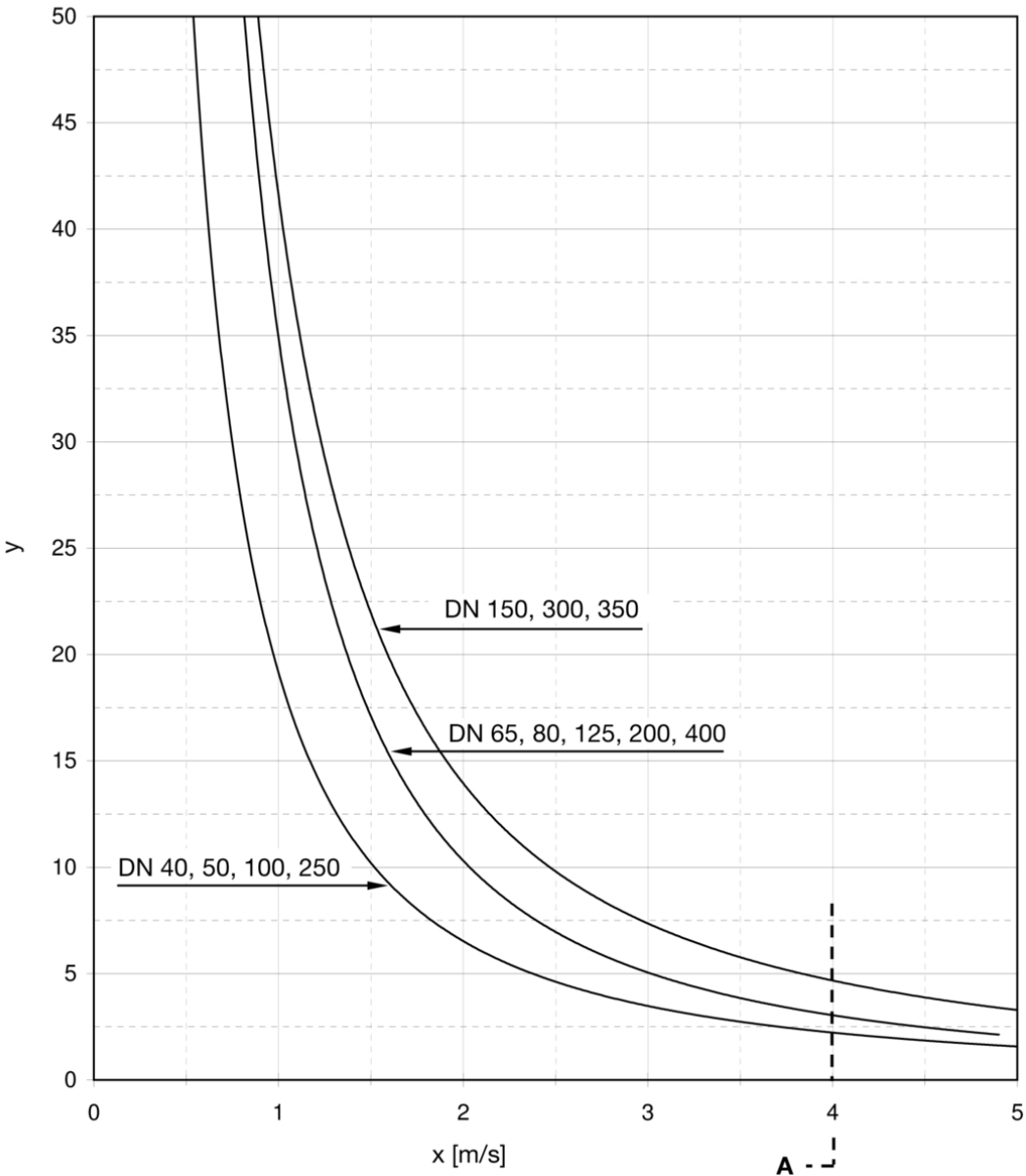
Figure 58: VAG TOP-STOP diaphragm non-return valve (technical illustration)

Table 18: head loss coefficients from Miller (1973)

weir height = pipe diameter	$\zeta = 2,5$
weir height = half pipe diameter	$\zeta = 1,0$
weir as a part of venturi section	$\zeta = 0,5$

Table 19: head loss coefficients from Zappe (1998)

Weir type	$\zeta = 2,0 \div 3,5$
Straight-through type	$\zeta = 0,6 \div 0,9$



Graph 80: Loss coefficients for VAG TOP-STOP Diaphragm Non-Return Valve

Where x is the flow velocity and y is the loss coefficient ζ .

14 New valve introduction

14.1 Main inlet valve for hydro power turbine

VAG Main Inlet Valve can be included in the butterfly valve's category. Looking at Figure 59 it is clear that the closure member is a disc actuated by a rotation movement of an actuator, as for the butterfly valves.

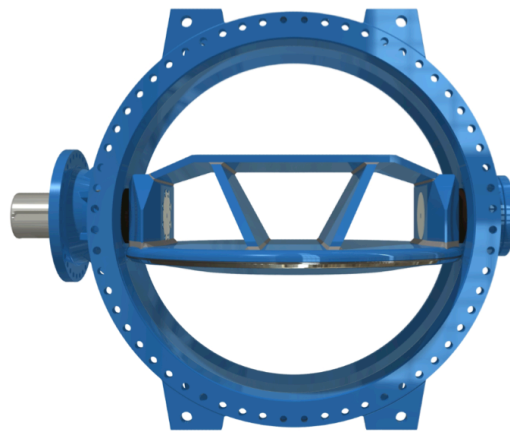


Figure 59: VAG Main Inlet Valve

In Figure 60 are also presented all the components of this valve type. The nominal diameter range of production is from DN 600 to DN 3000, and the nominal pressure range is from PN 4 to PN 15.

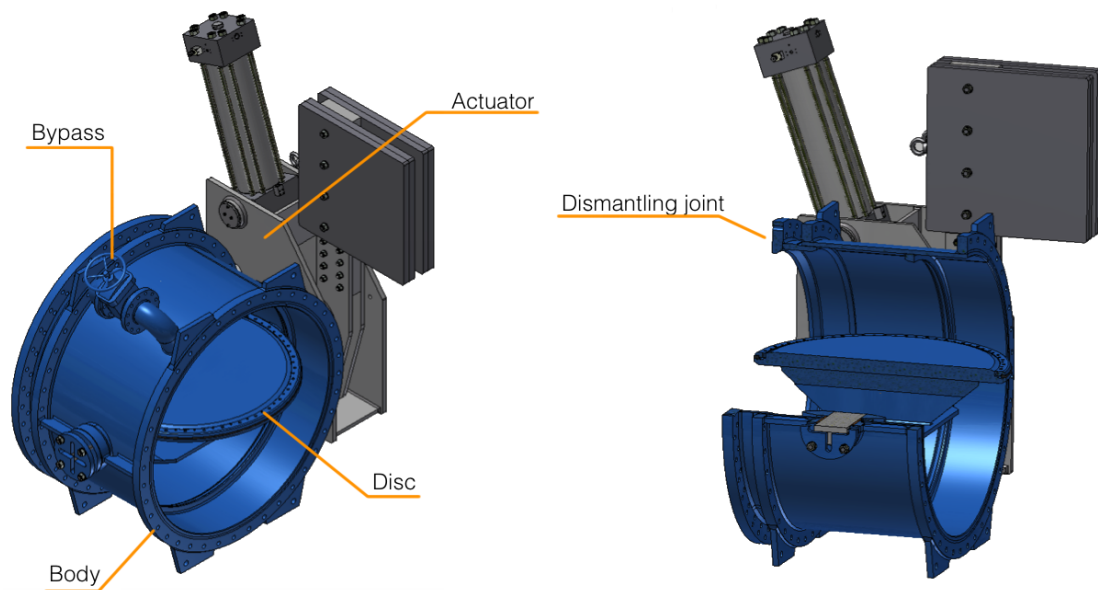


Figure 60: components of Main Inlet Valve

This valve model is still in a design project phase. In particular in Figure 61 is plotted the CFD calculation of the velocities. CFD, that stands for computational fluid dynamics, is a branch of fluid mechanics that uses numerical methods and algorithms to solve and analyze problems that involve fluid flows. Computers are used to perform the calculations required to simulate the interaction of liquids and gases with surfaces defined by boundary conditions.

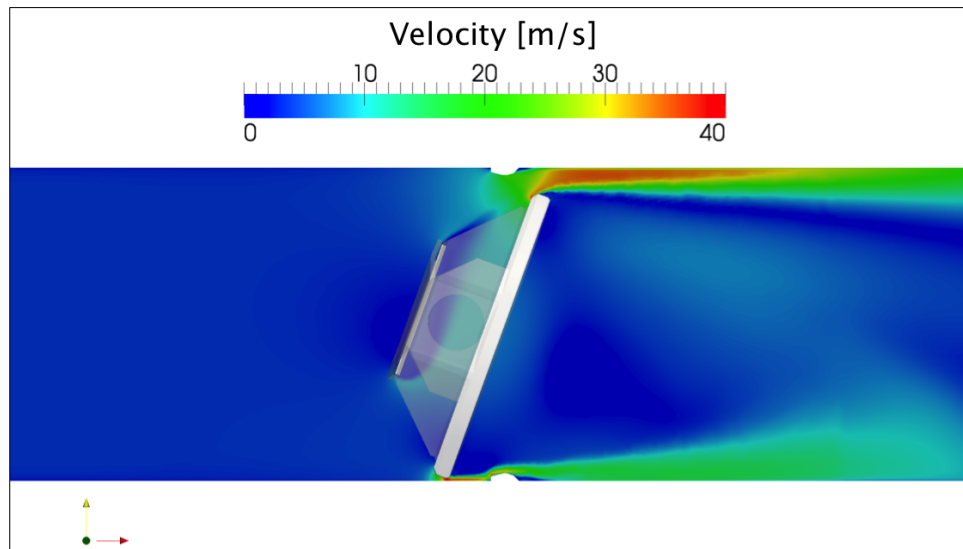


Figure 61: CFD computation of velocity

This valve model is particularly suited for hydro power turbines' field of application.

14.2 VAG CHECKtronic Pump Safety Valve

The CHECKtronic Pump Control Valve has evolved from VAG's extensive experience in the design of automatic control valves to control surges associated with the starting and stopping of pumps. The valve, which is illustrated in Figure 62, is as a combined-pump-start-up and pump protecting device for waste water pumping stations.



Figure 62: VAG CHECKtronic Pump Safety Valve

Its innovative design incorporates a fail-safe check feature into an electric motor operated valve, providing the ideal combination of surge control and positive closure for power failure or other emergencies. CHECKtronic Pump Control Valve for its capability to control pressure surges associated with pumping operations at the higher gradient, its flow efficient design and the integral fail-safe check-feature represents a real innovation.

The main peculiarity in the functioning of this valve type is the electrical actuation, that allows start up of pump against closed valve and provides slow opening and slow closing for normal pump operation; the electric actuator eliminates complicated hydraulic controls, minimizes installation costs, and reduces maintenance. The spring-assisted disc closes in event of pump, motor or power failure and it is independent of the electric actuation. The stroke time of open and close can be adjusted in order to suit the operating conditions.

Technical features

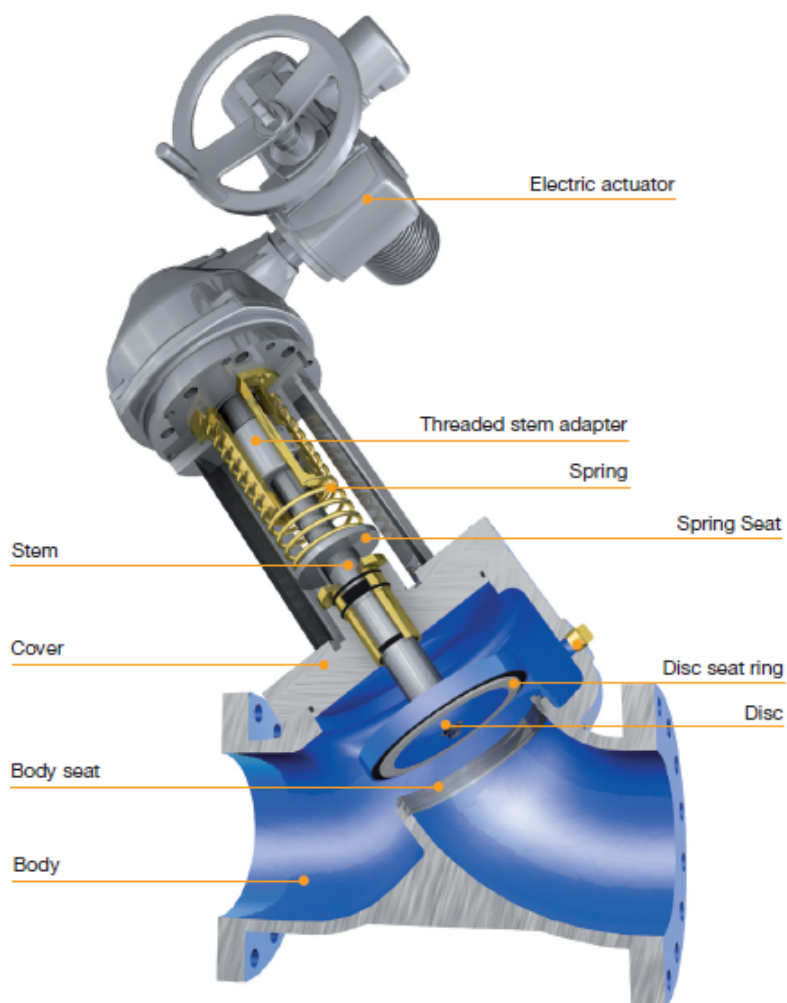


Figure 63: Checktronic valve features illustration

In the Figure 63 are illustrated the sectional view and the main material's features of this valve's type. CHECKtronic valve is produced for PN 10, PN 16 and PN 25 and for a range of nominal diameters DN from 80 mm to 600 mm.

The standard model is made by ductile iron in its body, cover and disc, by stainless steel in its seat and the disc is made by ultra high molecular weight polyethylene.

There are special versions available of this valve depending on the commercial request: higher pressure, bigger sizes, other materials, different flange systems.

In the Figure 64 and Figure 65 are illustrated the two technical schemes for the two main pattern of the valves: in the Figure 64 is represented the VAG CHECKtronic pump safety valve with gearbox and electric actuator, in the Figure 65 is represented the same valve without the gearbox.

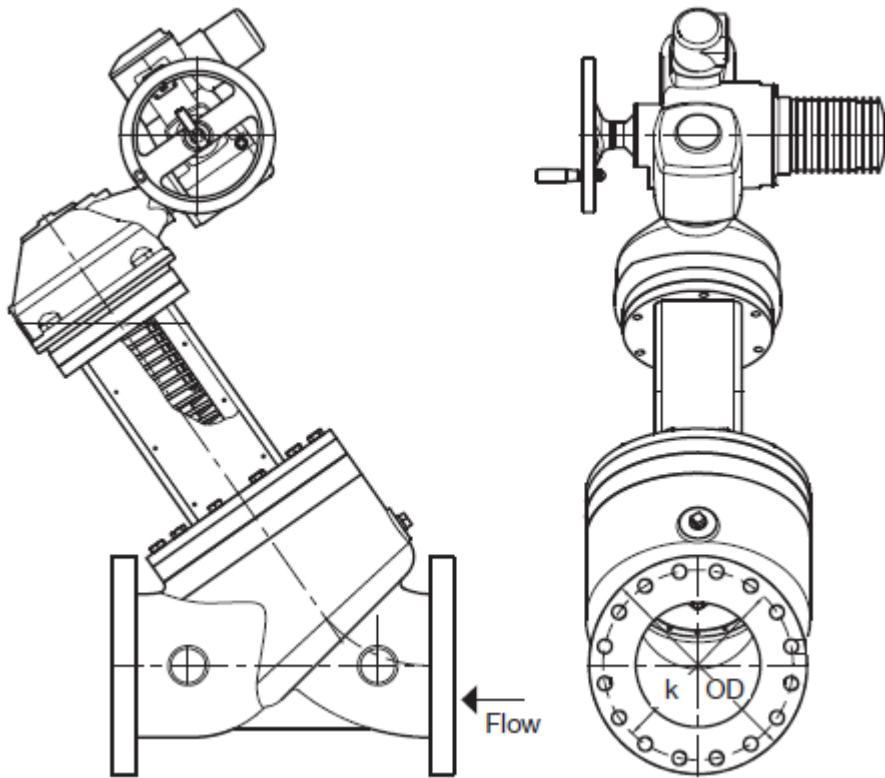


Figure 64: VAG CHECKtronic pump safety valve with gearbox and electric actuator

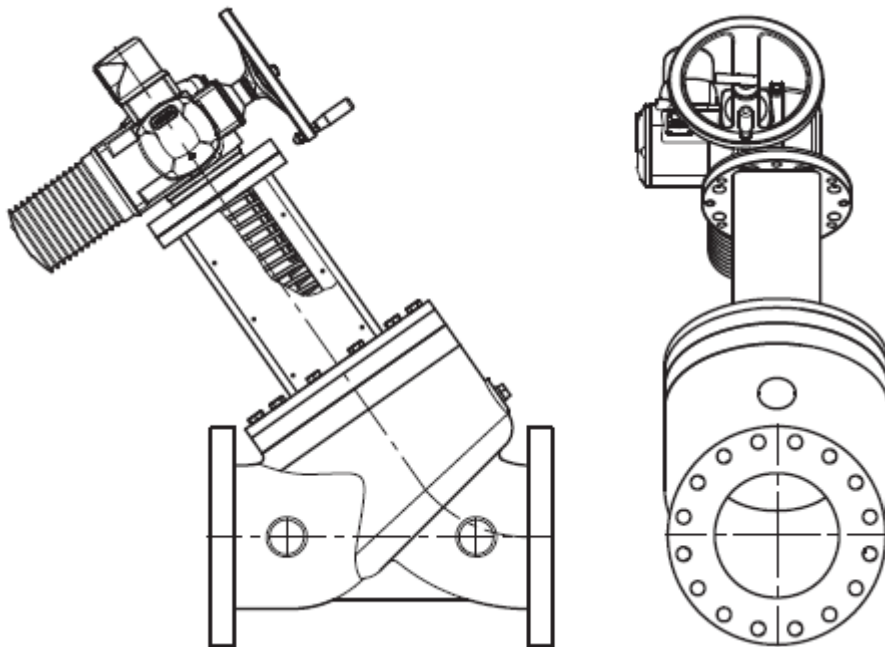


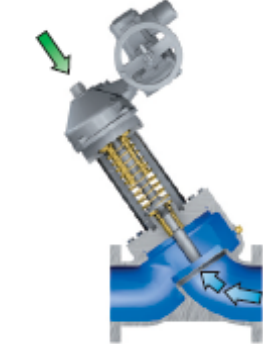



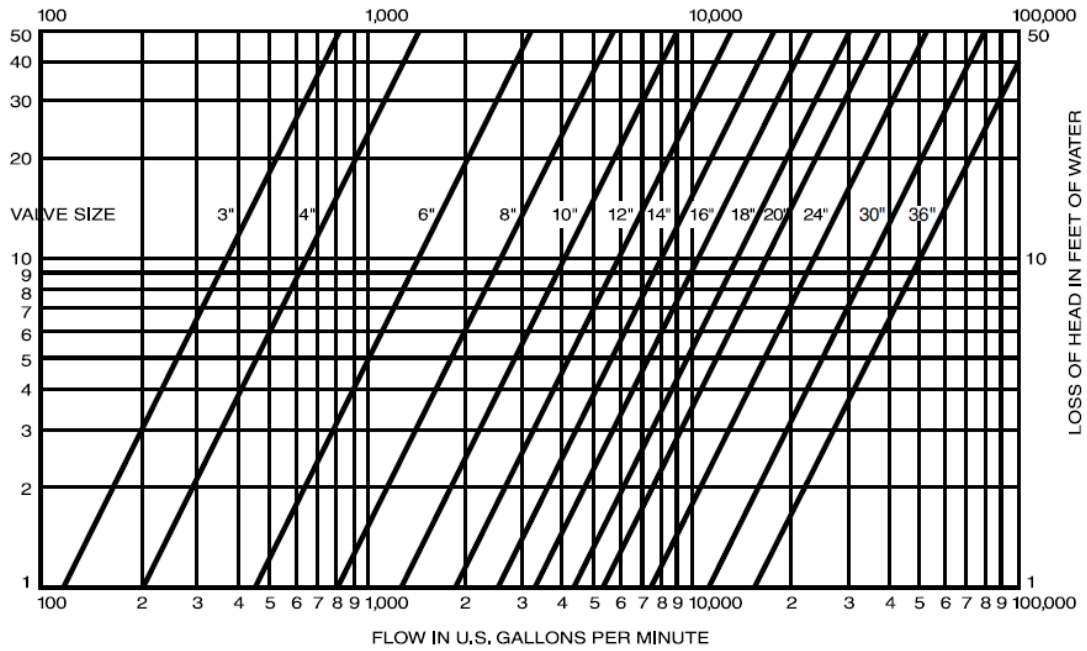
Figure 65: VAG CHECKtronic pump safety valve with electric actuator and without gearbox

Functioning of the valve

<p style="text-align: center;"><i>Pump start</i></p> <p>The electric actuator holds the valve closed against the starting pump. After the pump is up to speed, the electric actuator slowly opens the valve and controls how fast the fluid column accelerates to flowing velocity in order to minimize pump start-up surges.</p>	
<p style="text-align: center;"><i>Normal pump running</i></p> <p>The valve is fully open during normal pump running. In this phase, its streamlined body produces very low headloss and handles sewage or debris-laden water without clogging.</p>	
<p style="text-align: center;"><i>Normal pump shutdown</i></p> <p>While the pump runs the electric actuator begins slowly closing the valve to control how fast the fluid column decelerates in order to minimize column separations and pressure surges. The pump motor disengages after the valve is fully seated and the fluid has been brought to rest.</p>	
<p style="text-align: center;"><i>Pump or power failure</i></p> <p>If the valve is open and there is a loss of power to the pump the integral spring-assisted “stop-check” automatically separates from the electric actuator and quickly closes to prevent backflow through the pump.</p>	

Head loss coefficients

In Graph 81 is plotted the trend of the head losses curves for CHECKtronic valve. This graph is available from VAG data sheet with the head losses (in feet of water) associated to the rate of flow Q (in U.S. gallons per minute).



Graph 81: local head losses of CHECKtronic valve against the flow

Table 20: head loss coefficients computation

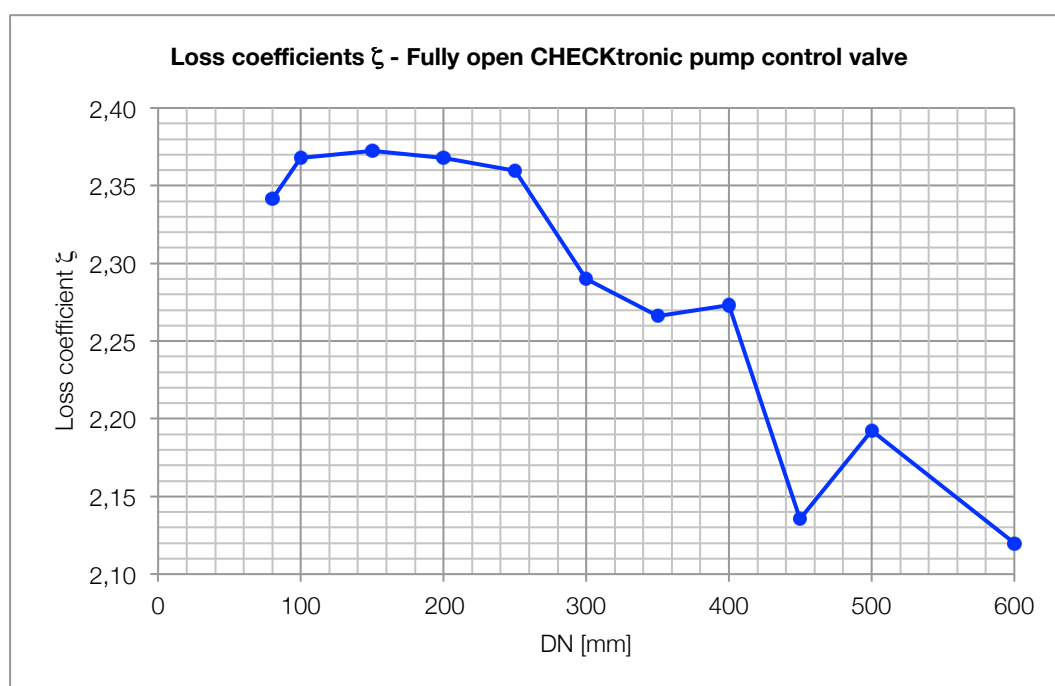
DN		hL	hL	Q	Cv	ζ
[in]	[mm]	[ft _{H₂O}]	psi	US gal/min	US gal/min/(psi ^{0,5})	
3	80	3,00	1,30	200,00	175,4	2,34
4	100	6,00	2,60	500,00	310,0	2,37
6	150	19,00	8,24	2000,00	696,9	2,37
8	200	6,00	2,60	2000,00	1240,1	2,37
10	250	30,00	13,01	7000,00	1941,0	2,36
12	300	4,50	1,95	4000,00	2863,8	2,29
14	350	7,50	3,25	7000,00	3882,0	2,27
16	400	9,00	3,90	10000,00	5062,6	2,27
18	450	1,90	0,82	6000,00	6611,0	2,14
20	500	32,00	13,87	30000,00	8054,5	2,19
24	600	29,00	12,57	40000,00	11281,1	2,12

From Graph 81 it is possible to obtain the head losses in feet of waters against the rate of flow Q for every valve size. From these values it is possible to compute the Flow coefficient C_V for each dimension and from C_V it is possible to compute the head loss coefficient associated ζ with the following expression:

$$\zeta = \frac{889 \cdot DN^4}{C_V^2}$$

The result of the computation is listed in the Table 20.

In the Graph 82 are plotted the values obtained for the head loss coefficients ζ of the CHECKtronic valves in fully open position, depending on the nominal diameter DN.

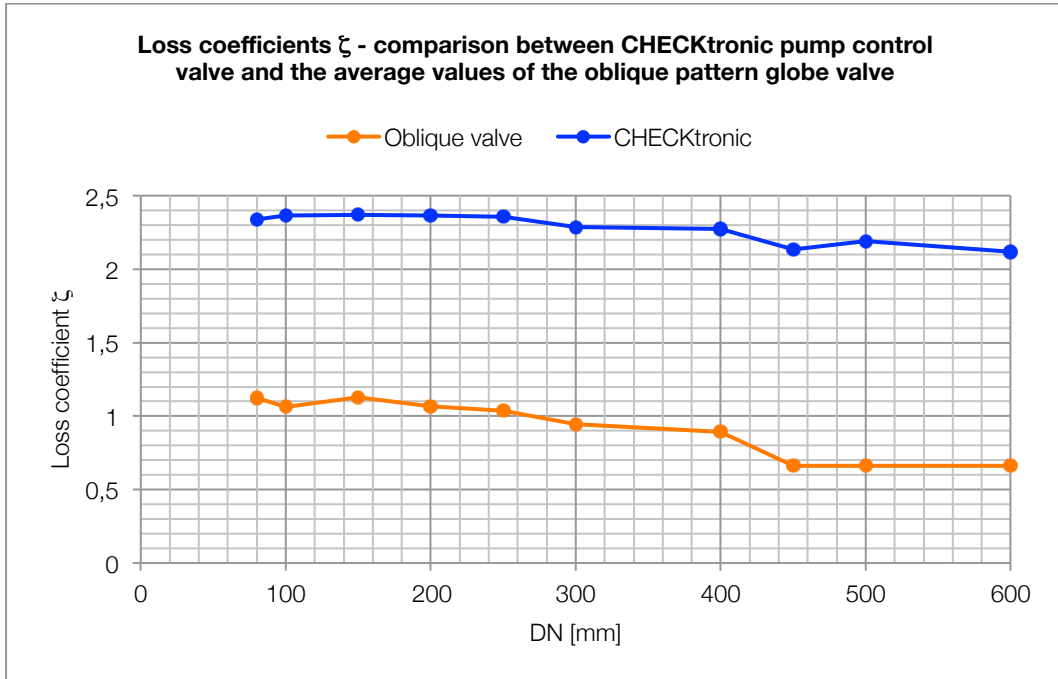


Graph 82: loss coefficients ζ for CHECKtronic valve

The trend of the curve is decreasing with the increasing of the DN, except for the stretch of curve from DN 450 to DN 500. The average value of the loss coefficients μ is 2,28 with a standard deviation σ of 0,09.

The internal features of this valve allow to include this valve in the globe valve category, mre precisely in the oblique pattern. It is interesting to compare the head loss coefficient values obtained to the average ones for the oblique pattern of a globe valve.

Graph 83 contains the comparison between the CHECKtronic valve and the oblique pattern average values of loss coefficients. The trend of the two curves is very similar (they are practically parallels) but it is clear that the CHECKtronic valve causes higher head losses than the oblique pattern's one.



Graph 83: comparison between loss coefficients ζ of a standard globe valve oblique pattern and the CHECKtronic valve

In Table 21 is plotted the comparison between the noticeable statistical parameters for the CHECKtronic valve and the oblique standard pattern.

Table 21: comparison between statistical parameters of CHECKtronic and globe oblique pattern

CHECKtronic valve	$\mu_A = 2,28$
	$\sigma_M = 0,09$
Globe oblique pattern	$\mu_A = 1,02$
	$\sigma_M = 0,26$

The standard deviation σ_M computed on different nominal diameters is very lower in the CHECKtronic pattern, and so it is possible to state that using the only value μ_A instead of the right value associated to the DN request implies a lower error for CHECKtronic.

15 Conclusions

List of the chapter symbols

Latin characters:

- b, c, c_n = constant parameters which determine the equation trend-line model;
- DN = nominal diameter [mm];
- f_r = ratio of F_0 and F_S ;
- F_0 = cross-section area at the inlet of the throttling device [m^2];
- F_S = seat cross-section [m^2];
- n_{DN} = number of head loss coefficient considered for the same nominal diameter;
- R^2 = coefficient of determination;
- x = variable which is equivalent to the DN;
- y = trend-line equation;

Greek characters:

- ζ = head loss coefficient;
- η = percentage error;
- μ = arithmetic mean;
- μ_A = arithmetic mean of average values;
- μ_i = arithmetic mean of head loss coefficients associated to the i -th nominal diameter;
- μ_{SD} = arithmetic mean of the standard deviations;
- σ = standard deviation;
- σ_M = standard deviation of the mean values;

15.1 Introduction

The final chapter of this paper has the aim to describe and compare the results obtained for the valve's head loss computation. The paper, as stated in the introductory chapter, is born for the practical reason to have the availability of data and formulas to compute immediately the head loss for different pipe devices, flow conditions and geometrical parameter of the pipe itself. In the valve's chapter are collected a large amount of these data for every valve's type and for every flow conditions from different sources. This large collection of data could be impractical and, in this sense, could be described better with statistical tools.

It is important to specify that all the data and all the name references that the reader will find in this chapter are the same used in the previous chapter, and it is possible to compare all the values and the names.

It is also interesting and useful to have a simple estimation of the reliability of these data, based on a rough statistical analysis performed by the program Microsoft Excel. This analysis could be seen as the aim of the paper. It is important to underline that all the parameters, the tools and the way in which data are presented are an subjective choice of the author.

This statistical analysis performed in the following chapter is based on the following parameters, which are computed and presented for the main valve's type:

- μ : arithmetic mean value (or average value);
- σ : standard deviation;
- $y =$ trend-line equation;
- $R^2 =$ coefficient of determination;
- $\mu_A =$ arithmetic mean of average values;
- $\mu_{SD} =$ arithmetic mean of the standard deviations;
- $\sigma_M =$ standard deviation of the mean values;

The arithmetic mean μ is given for different values of the nominal diameter DN for fully open valves. The choice of this parameter comes from the desire to give a practical list of values for all the diameters and it is obtained allowing for all the sources and giving them the same importance. In this sense, the standard deviation σ is important as much as the arithmetic mean value: it is necessary for the reader to have an idea of the reliability of the arithmetic mean and it gives the measure of how the single data are far from μ . A factor that can be critical reading this parameter is the amount of data obtained for the same nominal diameter DN: a large amount of data could determine a larger standard deviation σ than a small amount of data but this fact does not imply that μ is less accurate.

Using the arithmetic mean values and the values of the standard deviation founded for every DN, it is possible to built a sort of confidence interval adding and subtracting the σ values for every DN to the μ values. This operation is useful to have an immediate visual reference in order to understand which are the most reliable values.

The trend-line y and the coefficient of determination R^2 are strictly correlated: they are determined by the program using the least squares method. The least square method determines the trend-lines minimizing the sum of squared residuals between the given data and an equation model chosen by the following:

- exponential: $y = ce^{bx}$;
- linear: $y = mx + b$;
- logarithmic: $y = c \ln(x) + b$;
- polynomial (from 2nd to 3rd degree): $y = b + c_1x + c_2x^2 + c_3x^3$;
- power: $y = cx^b$;

where b , c and c_n are constant parameters. The mathematical form of the equation is evidently $y = f(x)$ where y is, as stated before, the trend-line function and x is the nominal diameter DN.

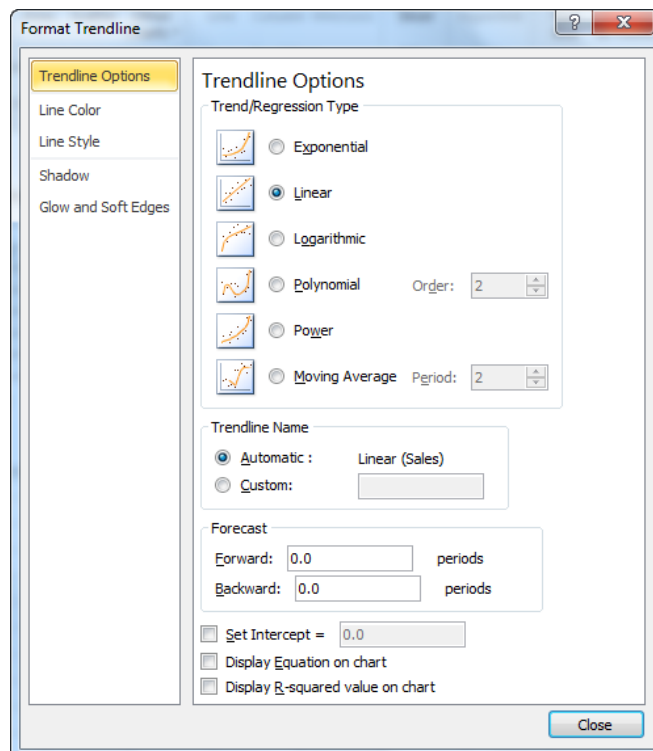


Figure 1: Excel screenshot choosing the trend-lines' model

The trend-line equation y is given for two main reasons: the first is to allow the reader to compute the head loss coefficient value ζ for nominal diameters not considered in the paper and the second is to have a practical tool faster than the research in the web data or paper.

The measure of the precision of fitting of the trend-line is given by the coefficient of determination R^2 : It provides a measure of how well the obtained data are replicated by the model. This parameter is important for some reasons. First of all R^2 is the discriminating parameter on which is based the choice of the equation model for the trend-line: the higher is the more the model is correct to fit the data. Secondly, the coefficient of determination gives an important information on the reliability of the data because a correct mathematical description implies an high value of R^2 .

The arithmetic mean of average values μ_A is a parameter given for every valve's type considered and is determined by the following formula:

$$\mu_A = \frac{\sum_i \mu_i}{n_{DN}}$$

where n_{DN} is the number of the head loss coefficients considered for the same diameter and μ_i is the i -th arithmetic mean value associated to the i -th DN value. This parameter can give an immediate head loss coefficient for all the diameters which can be used for preliminary projects in the very initial step of a design work.

Associated to μ_A is reported also the σ_M which is the standard deviation calculated for the μ_A parameter. This coefficient gives information about the variability of the average head loss coefficient values μ_i against the i -th diameter, and so the reader can understand immediately if the arithmetic mean μ_A could be used allowing for the precision required.

The last parameter given is the arithmetic mean of the standard deviations μ_{SD} . This parameter gives an additional information about the reliability of the data: if μ_{SD} is high for a particular valve's type it means that there's an high discordance between the data collected and the average values computed.

All the curves determined from punctual data are linear interpolations except for the data obtained by formulas.

15.2 Valves comparisons and conclusions

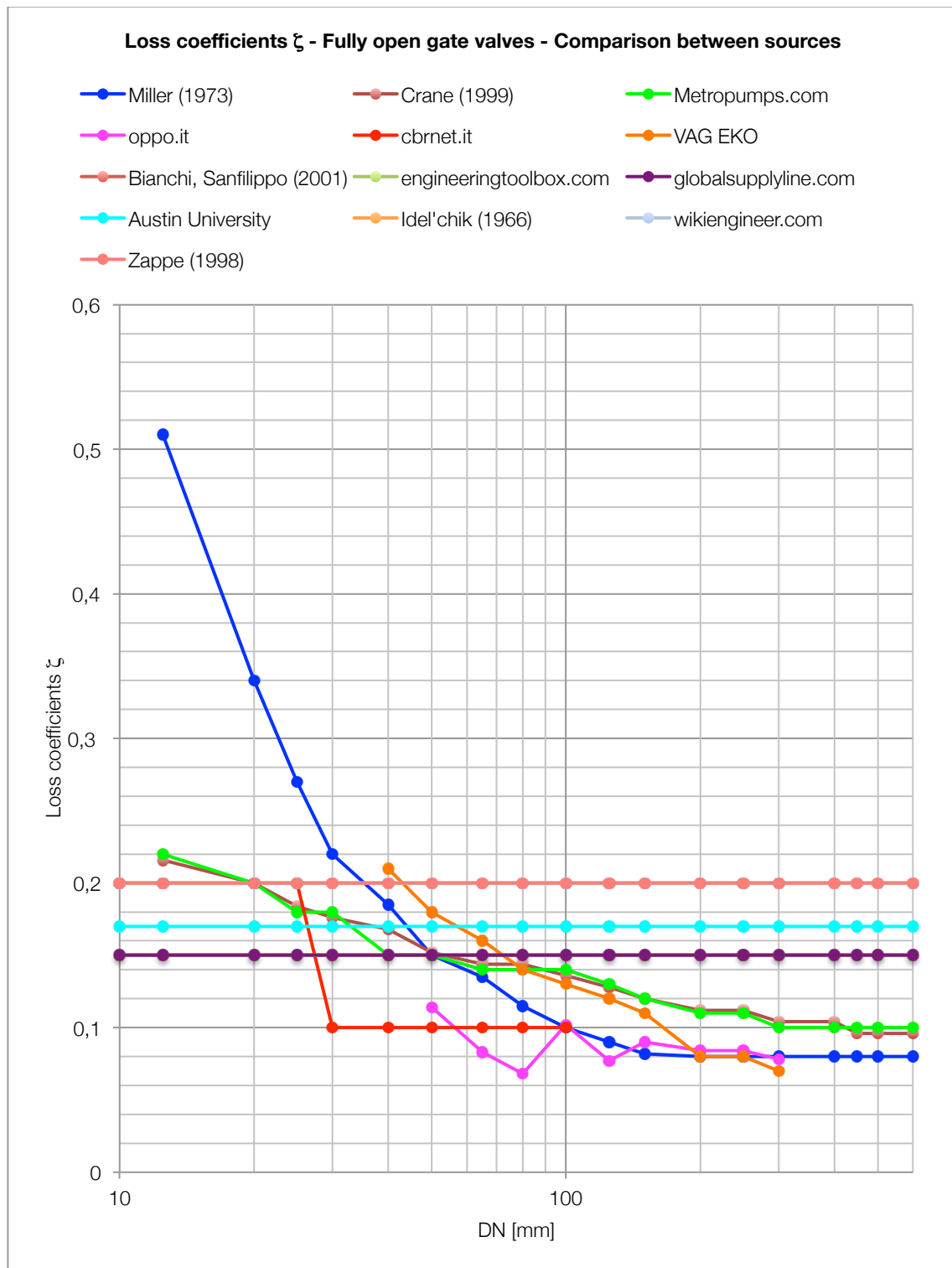
In the following pages are quoted the data with the statistical comparison described before. For every valve's model, the structure of the chapter is composed in the same way, as following:

- the graph in which are plotted all the head loss coefficients value against the DN for fully open models;
- the table in which are listed the data plotted;
- a graph in which are plotted the arithmetic mean μ , the standard deviation σ and the consequent confidence interval against the nominal diameter DN;
- the graph(s) in which are built the trend-lines y with the equation used and the coefficient of determination R^2 ;
- a table which summarizes the main statistical parameters met before in the graphs and the parameters μ_A , μ_{SD} and σ_M ;

Over and above the elements listed, other comparisons with graphs and tables are also presented, that are peculiar for each valve's type. This additional elements will be explained as they will appear in the following pages.

After the graph and the tables listed before, a series of comments is collected, referring to the related valve's type. This notes are the real conclusions of the paper and the choice to break them into pieces is due to make their contents immediatly verifiable looking at the graph and the tables in the related paragraph.

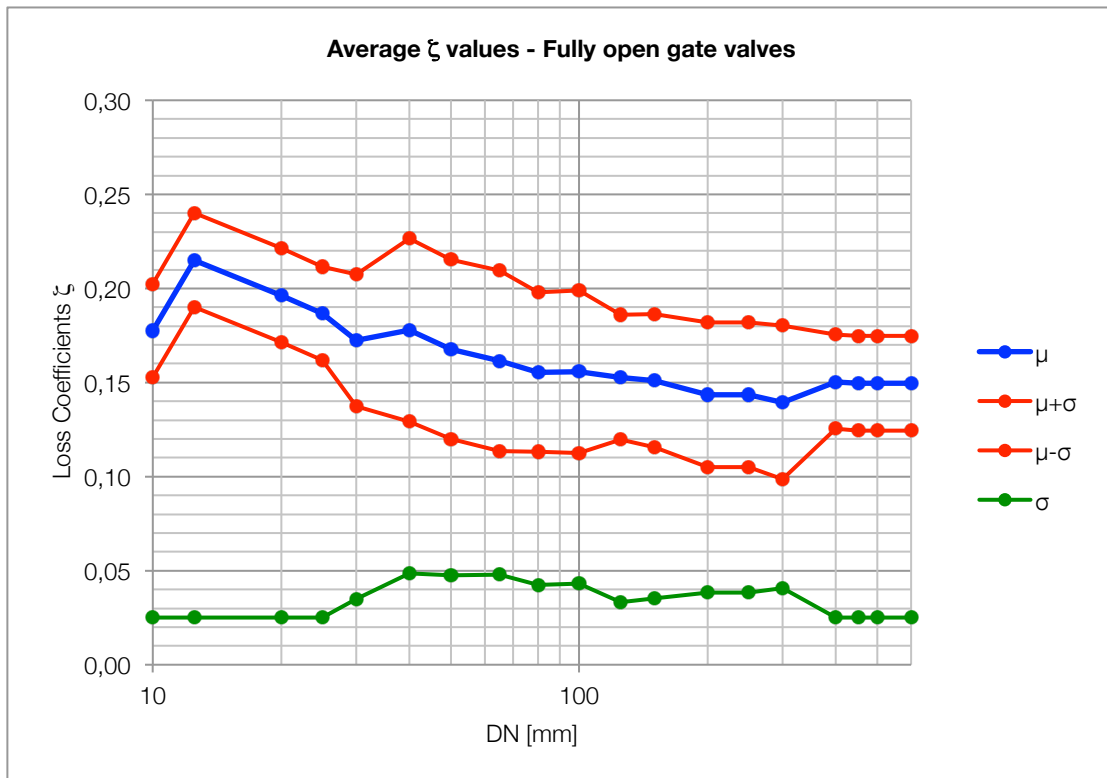
15.2.1 Gate valves



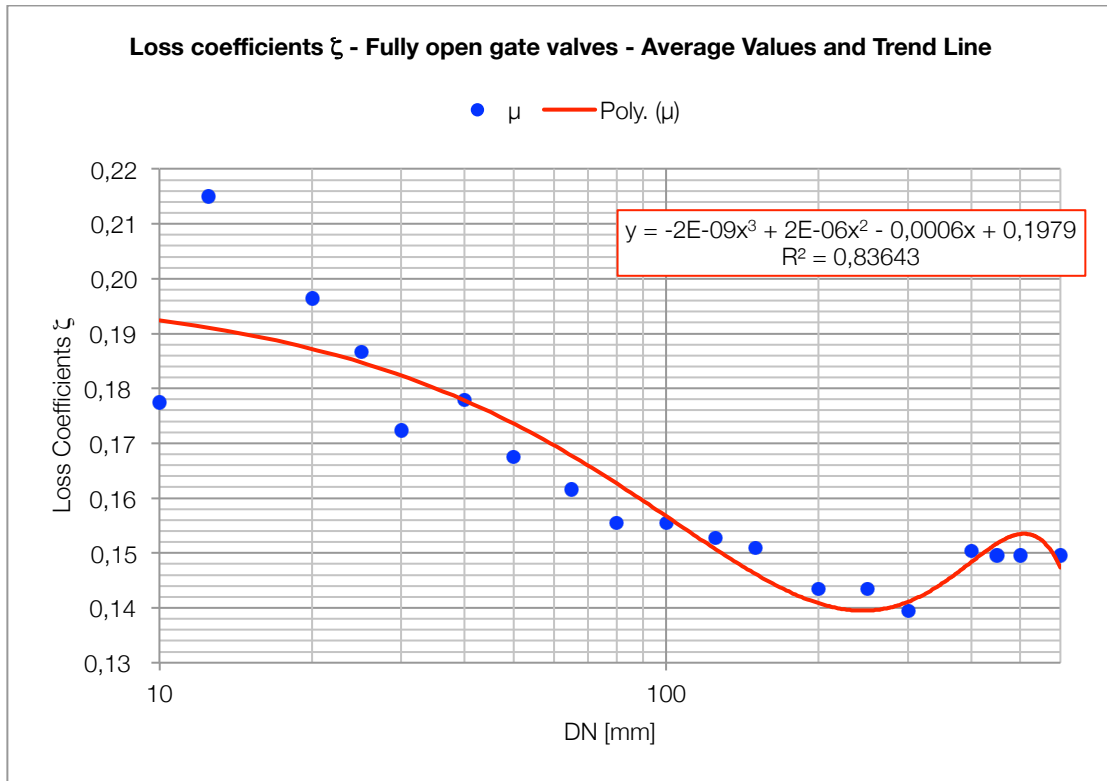
Graph 1: Loss coefficients ζ for fully open gate valves - comparison between sources

Table 1: average ζ values for fully open gate valves

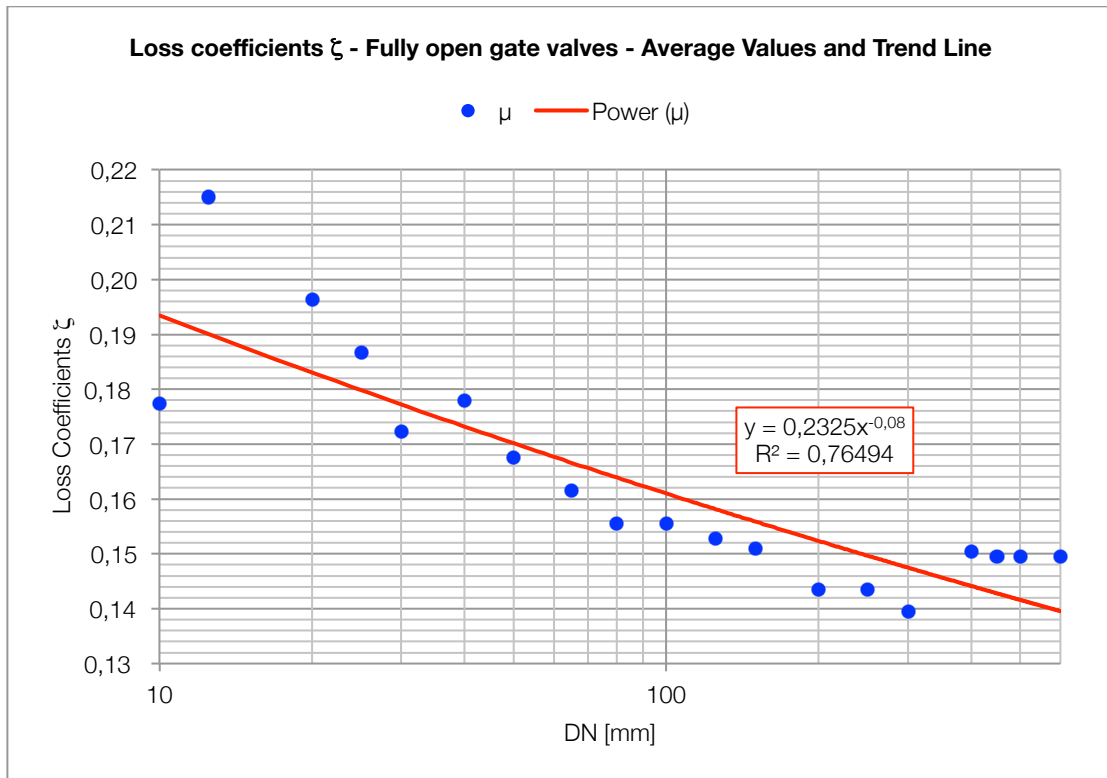
DN [mm]	μ	σ	$\mu+\sigma$	$\mu-\sigma$
10	0,18	0,0249	0,2024	0,1526
15	0,22	0,0249	0,2400	0,1902
20	0,20	0,0249	0,2213	0,1714
25	0,19	0,0249	0,2117	0,1618
30	0,17	0,0351	0,2074	0,1373
40	0,18	0,0486	0,2266	0,1293
50	0,17	0,0476	0,2151	0,1200
65	0,16	0,0479	0,2095	0,1137
80	0,16	0,0423	0,1978	0,1132
100	0,16	0,0432	0,1988	0,1124
125	0,15	0,0332	0,1859	0,1195
150	0,15	0,0353	0,1862	0,1156
200	0,14	0,0384	0,1820	0,1051
250	0,14	0,0384	0,1820	0,1051
300	0,14	0,0408	0,1801	0,0986
400	0,15	0,0251	0,1755	0,1253
450	0,15	0,0251	0,1747	0,1245
500	0,15	0,0251	0,1747	0,1245
600	0,15	0,0251	0,1747	0,1245



Graph 2: average ζ values for fully open gate valves



Graph 3: average values ζ and trend-line y for fully open gate valves



Graph 4: average values ζ and trend-line y for fully open gate valves

Table 2: statistical parameters for fully open gate valves

Trend-line equation:	$y = 2 \cdot 10^{-9}DN^3 + 2 \cdot 10^{-6}DN^2 - 0,0006DN + 0,1979$
Coefficient of determination	$R^2 = 0,83643$
Trend-line equation:	$y = 0,2325 \cdot DN^{-0,08}$
Coefficient of determination	$R^2 = 0,76494$
Arithmetic mean of average values	$\mu_A = 0,16$
Arithmetic mean of the standard deviations	$\mu_{SD} = 0,03$
Standard deviation of the mean values	$\sigma_M = 0,02$

Comments

Looking at Graph 1, the number of sources used for the gate valves is the highest in the chapter. The great amount of data makes the results really variable between them but it is possible to recognize the same trend in all the series of data: the higher the DN is the lower is the head loss coefficient value ζ .

In the Graph 1 it is possible to recognize, in some sources, stretch of curves which are substantially plane: if the values used are experimentally founded, it is possible that the author had maintained the same valve body (and so the head loss is constant) but changed the DN, applying contraction device at inlet and a diffuser at outlet of the valve. There are also sources for which the head loss coefficient is invariant on the nominal diameter for all the range of DN.

The range of the nominal diameters DN considered is from 10 to 600. The values are quite similar specially for DN values between 50 mm and 300 mm. Above and under these values it is possible to recognize some high differences, concentrated in some sources, for example Miller's values (Miller, 1973) are much larger than the other sources for small diameters DN.

The range of the head loss coefficient founded for this valve's type is quantifiable from 0,06 (oppo.it) to 0,5 (Miller). In general it is possible to say that the gate valve, regardless of the DN value, is a low resistance valve when used in fully open position.

The Table 1 and the Graph 2 plot the average values μ of the head loss coefficients ζ , the standard deviation σ and the confidence interval obtained. Looking at the graph is possible to recognize points in which the decreasing trend of the single sources is not respected. For example from DN 10 to DN 15 there is an increase and the same from DN 300 to DN 400. It is interesting to recognize that in these points there's the maximum value of the standard deviation σ : this fact is explainable with the variety

of the “constant” sources, which can make the average values μ decreasing in the range of high head losses and increasing in the low head losses.

In general, the confidence interval is near to the average curve and has a regular trend all over the DN range considered. This fact is the consequence of the trend of the standard deviation curve, which is regular itself. From a statistical point of view, this fact is good because it means that the errors are more or less the same all over the diameter range and so the average curve can be considered nearly reliable. However, the values of the standard deviation curve are not negligible because its values are comparable to the average values of the head loss: this fact is another time caused by the variety of the sources.

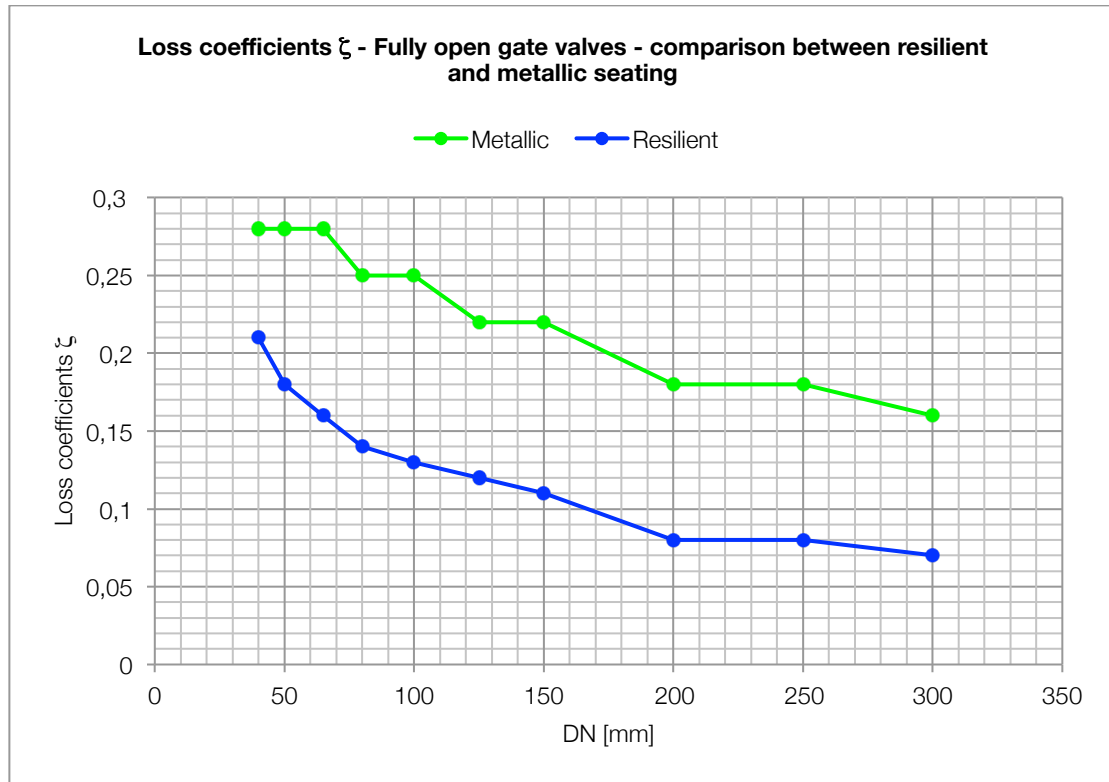
In the Graph 3 and in the Graph 4 are presented the trend lines obtained using two different equation models: polynomial at the 3rd degree and power, respectively. The two trend lines match the average value curve nearly well, considering the R^2 factor which is higher in the polynomial curve but noticeable also for the power curve. The choice to use two different trend lines belongs to a simple consideration: the polynomial curve is more effective in data fitting but there are stretch of the curves which are not completely corresponding to the theoretical aspects. This means that polynomial curve is less practical than the power curve, which is less accurate in fitting data but it is simpler to use.

In Table 2 are presented the other parameters useful to the statistical interpretation: the arithmetic mean of average values μ_A , the arithmetic mean of the standard deviations μ_{SD} and the standard deviation of the mean values σ_M .

Looking at the value of μ_A it is possible to say that it is very similar to the value reported by the “constant” sources. The very small value of σ_M means that the μ_A is very similar to the other μ values and so, from a practical point of view, it is possible to use it instead of the average values without committing a great error.

The value of the arithmetic mean of the standard deviations μ_{SD} confirms that, for all the range of DN, it is not possible to neglect it but its value is low compared to the other head loss values and so the μ values are reliable.

15.2.1.1 Comparison between resilient and metallic seating

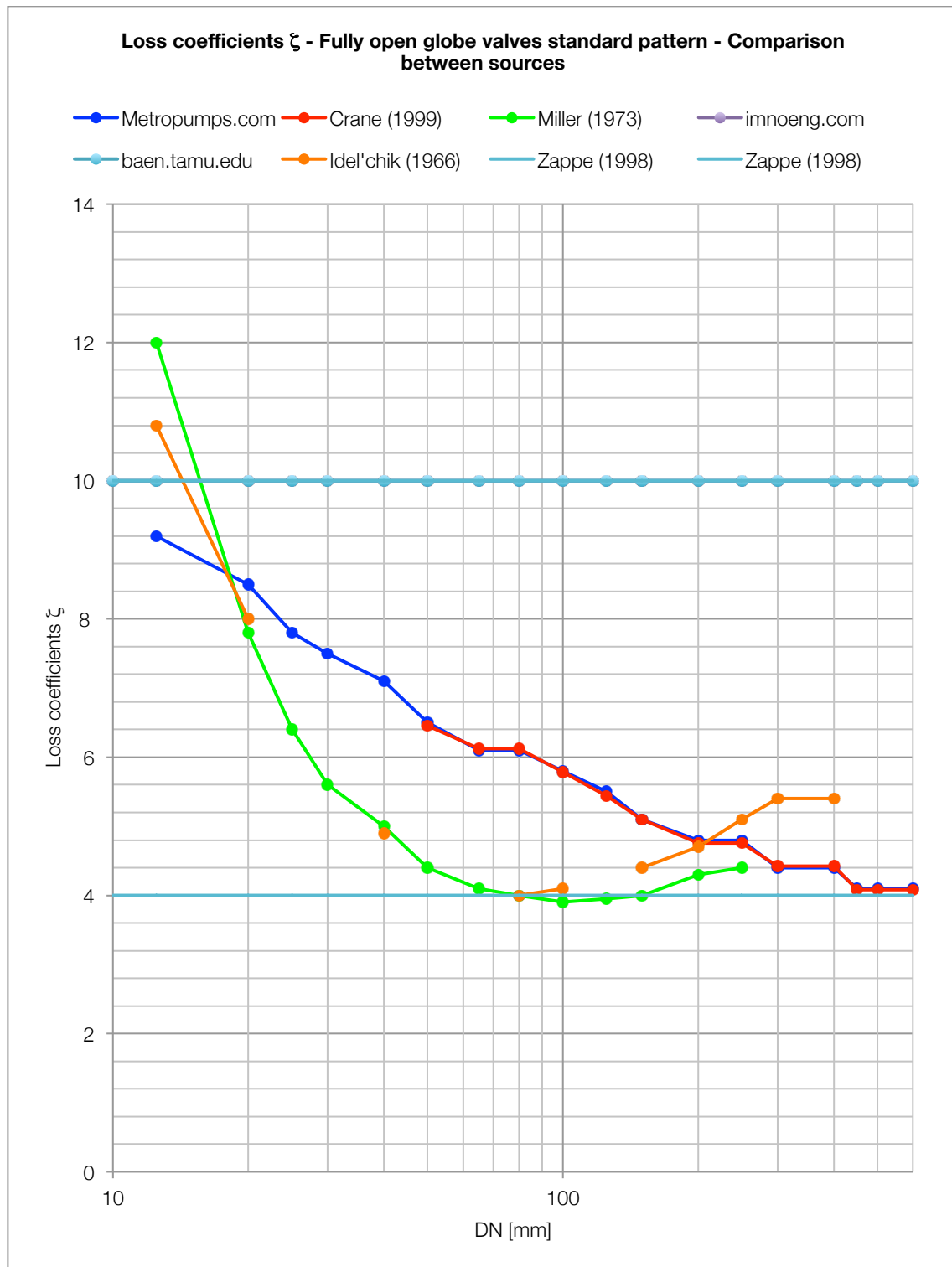


Graph 5: comparisons between metallic and resilient type of gate valves

In Graph 5 is presented another peculiar comparison between different gate valve's type: resilient-seated and metallic-sealing gate valves. This comparison is taken from VAG data sheets is done for fully open valves and shows clearly that the head loss coefficients of the metallic-sealing gate valve are higher than the resilient-seated valve for all the range of diameter considered. In general the resilient-seated data are very similar to the mean values μ computed and the metallic-sealing data are higher: a metallic-sealing valve implies higher head losses.

15.2.2 Globe valves

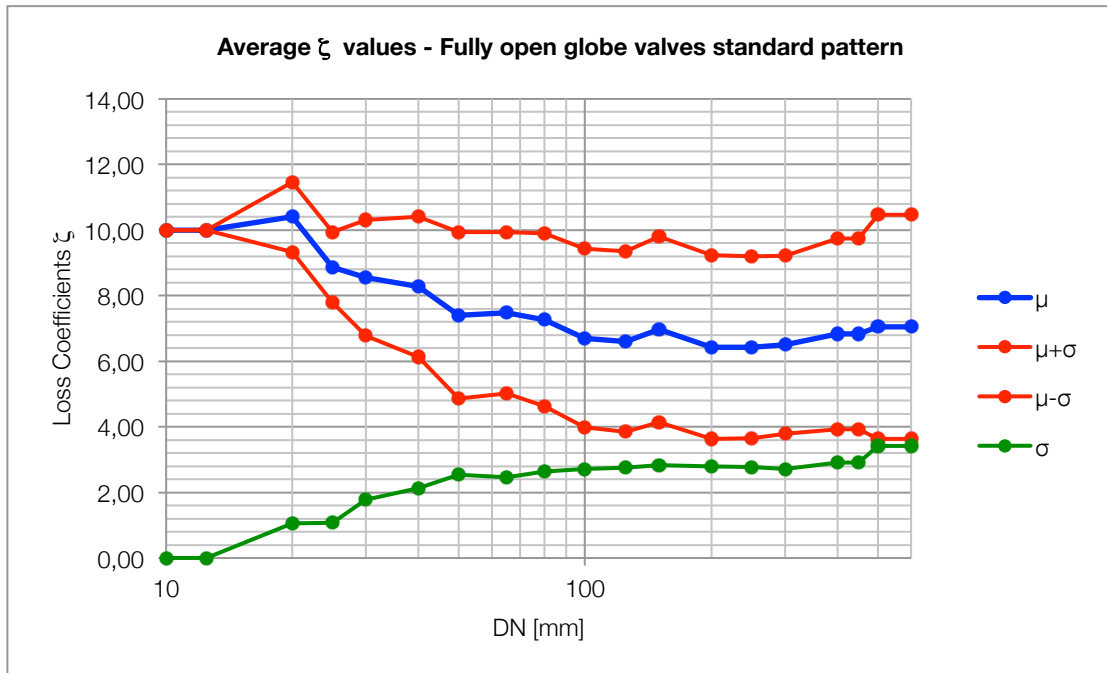
15.2.2.1 Standard pattern



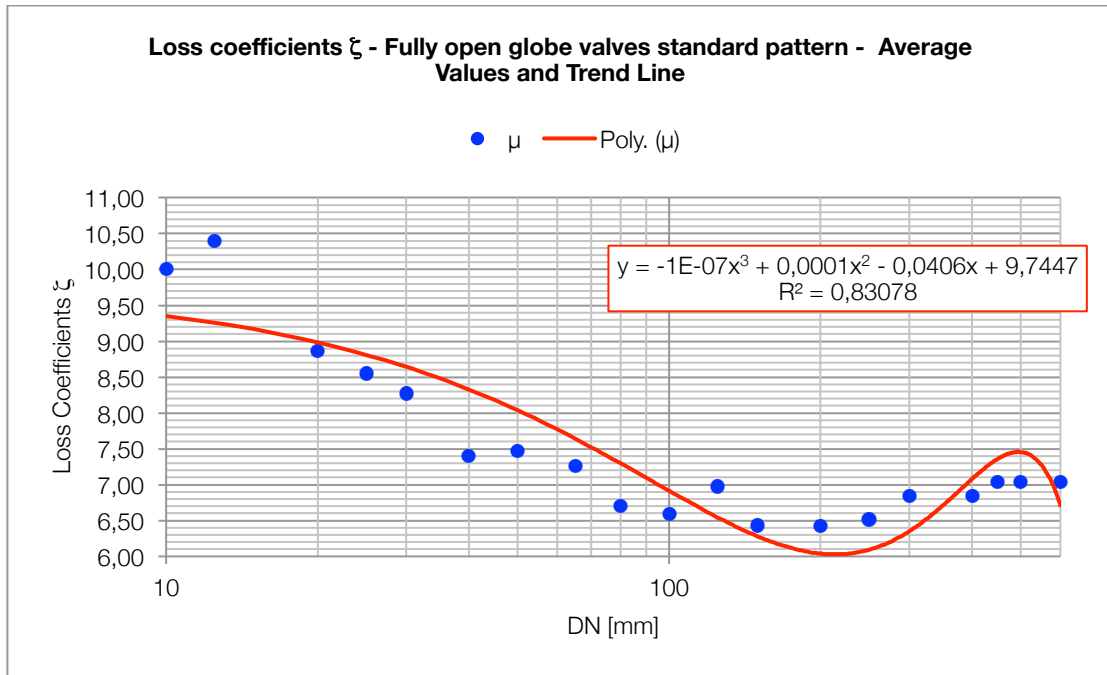
Graph 6: Loss coefficients ζ for fully open globe valves standard pattern - comparison between sources

Table 3: average ζ values for fully open globe valves (standard pattern)

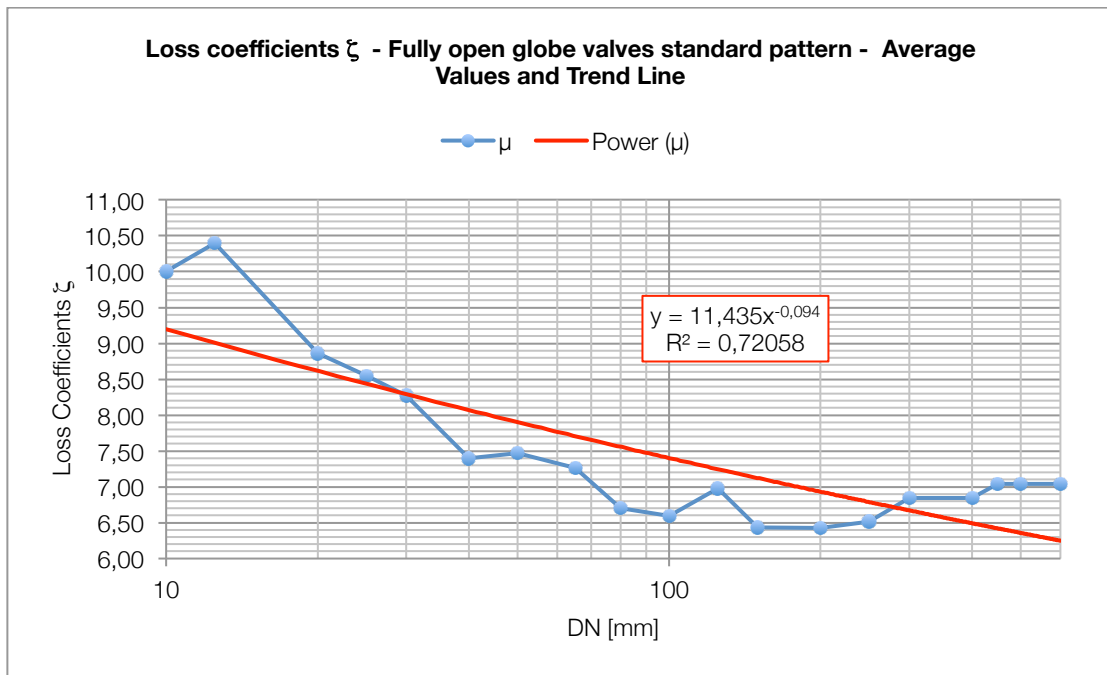
DN [mm]	μ	σ	$\mu+\sigma$	$\mu-\sigma$
6	1,44	0,0000	1,4400	1,4400
10	0,86	0,0000	0,8576	0,8576
15	1,72	1,1829	2,8996	0,5338
20	1,26	0,7549	2,0163	0,5065
25	1,08	0,6303	1,7141	0,4535
30	1,00	0,5387	1,5376	0,4602
40	0,92	0,5007	1,4178	0,4164
50	0,88	0,3683	1,2496	0,5129
65	1,19	0,8764	2,0628	0,3101
80	1,12	0,7758	1,8978	0,3462
100	1,06	0,7002	1,7642	0,3638
125	0,91	0,0577	0,9711	0,8556
150	1,13	0,4942	1,6230	0,6345
200	1,07	0,4149	1,4811	0,6514
250	1,04	0,3468	1,3818	0,6882
300	0,95	0,3940	1,3390	0,5510
400	0,90	0,3074	1,2024	0,5876
450	0,66	0,0000	0,6600	0,6600
500	0,66	0,0000	0,6600	0,6600
600	0,66	0,0000	0,6600	0,6600



Graph 7: average ζ values for fully open globe valves (standard pattern)



Graph 8: average values ζ and trend-line y for fully open globe valves (standard pattern)



Graph 9: average values ζ and trend-line y for fully open globe valves (standard pattern)

Table 4: statistical parameters for fully open globe valves (standard pattern)

Trend-line equation:	$y = -10^{-7}DN^3 + 0,0001DN^2 - 70,0406DN + 9,7447$
Coefficient of determination	$R^2 = 0,83078$
Trend-line equation:	$y = 11,435 \cdot DN^{-0,094}$
Coefficient of determination	$R^2 = 0,72058$
Arithmetic mean of average values	$\mu_A = 7,63$
Arithmetic mean of the standard deviations	$\mu_{SD} = 2,31$
Standard deviation of the mean values	$\sigma_M = 1,27$

Comments

The statistical analysis for globe valves is presented for the three pattern of the valve: standard, oblique and angle.

In the Graph 6 is presented the amount of data for the standard pattern of fully open globe valve. The sources used for this valve type are lower in number than the ones used for the gate valves but anyway relevant.

The range of the DN considered is from DN 6 to DN 600, another time very similar to gate valves, but the head loss coefficients are very different from before: their range is spaced between 12 to 4. However, the trend is similar to before, high values for small diameters and low values for high diameters. This is a constant fact for all the sources except for Idel'chik (Idel'chik, 1966) and Miller (Miller, 1966) which present an increasing stretch of curve after DN 100. It is immediatly recognizable a perfect match between the sources metropumps.com and Crane book (Crane, 1999).

There are also sources which present constant values of the head loss coefficients for all the range of nominal diameters DN. In particular, for the globe valve type some sources, for example Zappe (Zappe, 1998), present a range of values and not only one constant values. It is interesting to see that all the values from all the sources are substantially enclosed in this range.

Looking at the Graph 7, it is plotted the average curve μ for the range of nominal diameter. The trend of the curve is substantially decreasing with the diameters as expected from the single sources values, except for the values corresponding to DN 20 and DN 150 which present a little increasing stretch.

On the contrary, the trend of the standard deviation σ is clearly increasing for higher values of the nominal diameters DN. Consequently, the confidence interval obtained gradually opens with the increasing of DN values. This means that values for lower diameters, practically under DN 50, are more reliable but also that there are less data

for this low DN. For high DN values, practically for diameters above DN 100, the values of the standard deviation is nearly touching the confidence interval: the uncertainty increases with the increasing of the DN values.

In the Graph 8 and in the Graph 9 are presented the trend lines obtained for the average values μ . In this case there are presented two different trend lines obtained from a polynomial equation and a power equation model respectively. Looking at the values of R^2 for the two equation is possible to say that in general are both good fitting data but polynomial is better. However, as for the gate valves, the polynomial equation is at 3rd degree with very small coefficients, and so it is possible that present computational problem for the high number and exponential derived. The power equation is less fitting but it has an easier practical application.

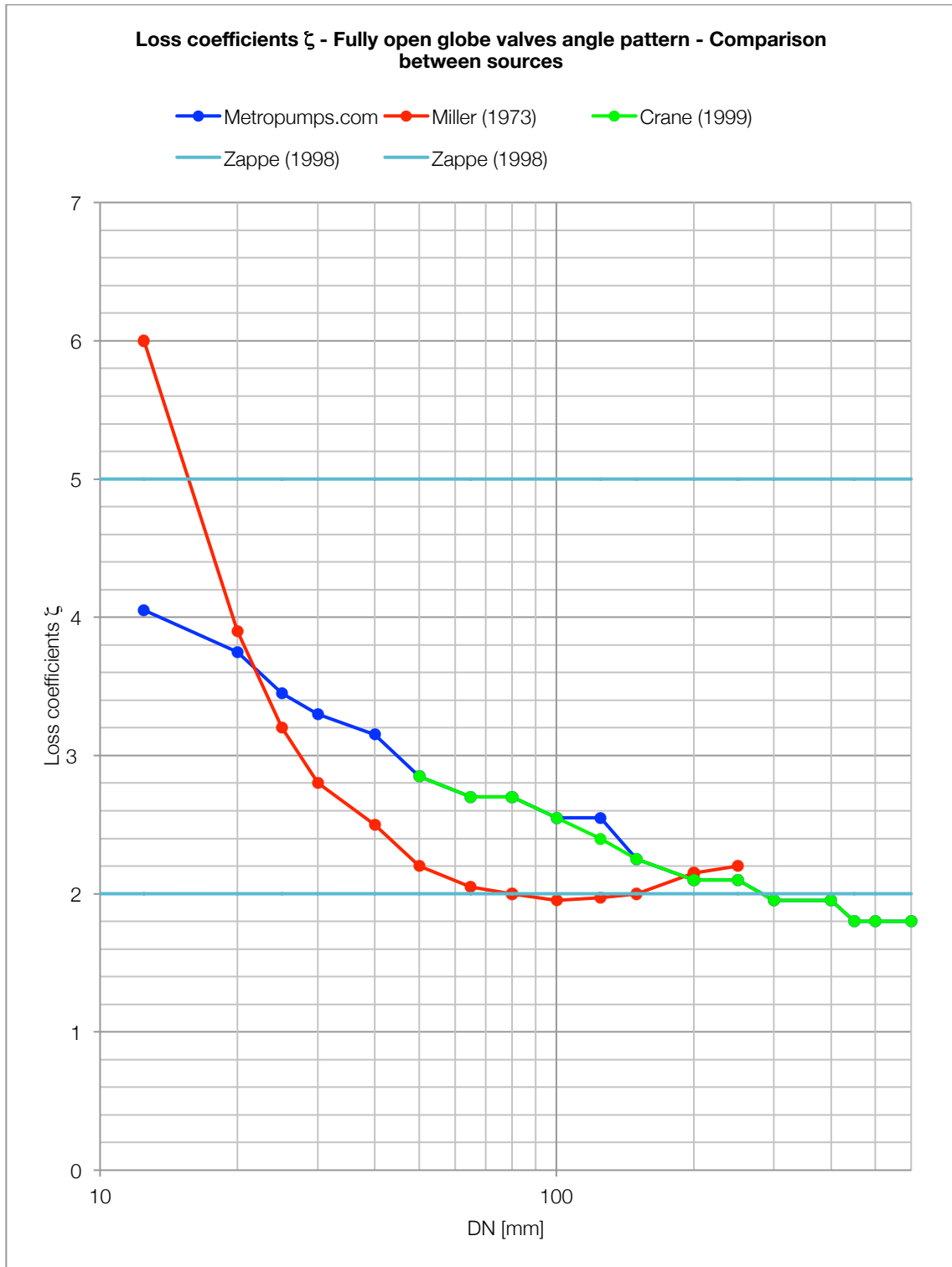
In Table 4 are presented the other parameters useful to the statistical interpretation: the arithmetic mean of average values μ_A , the arithmetic mean of the standard deviations μ_{SD} and the standard deviation of the mean values σ_M .

Looking at the value of μ_A , really higher than in the gate valves, it is confirmed that globe valves are high resistance valves.

The value of σ_M tells that there are considerable differences between μ_A and the other μ values and so, from a practical point of view, it is not possible to use μ_A instead of the average values without committing a noticeable error.

The value of the arithmetic mean of the standard deviations μ_{SD} confirms that, for all the range of DN, it is not possible to neglect it but its value is low compared to the other head loss values and so the μ values are reliable.

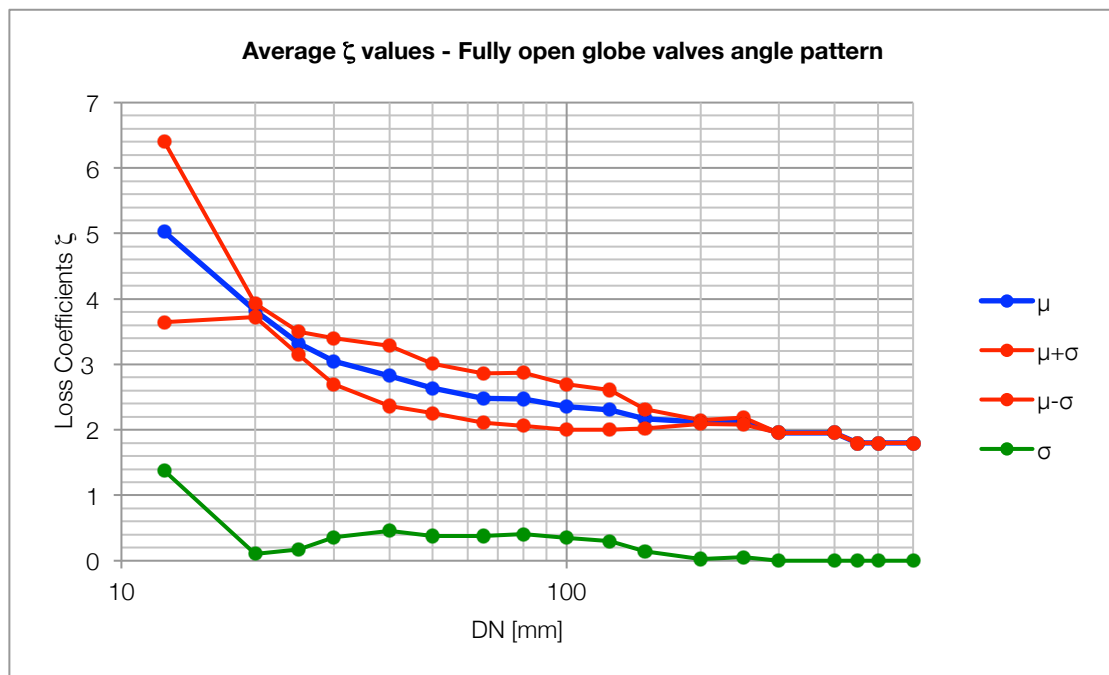
15.2.2.2 Angle pattern



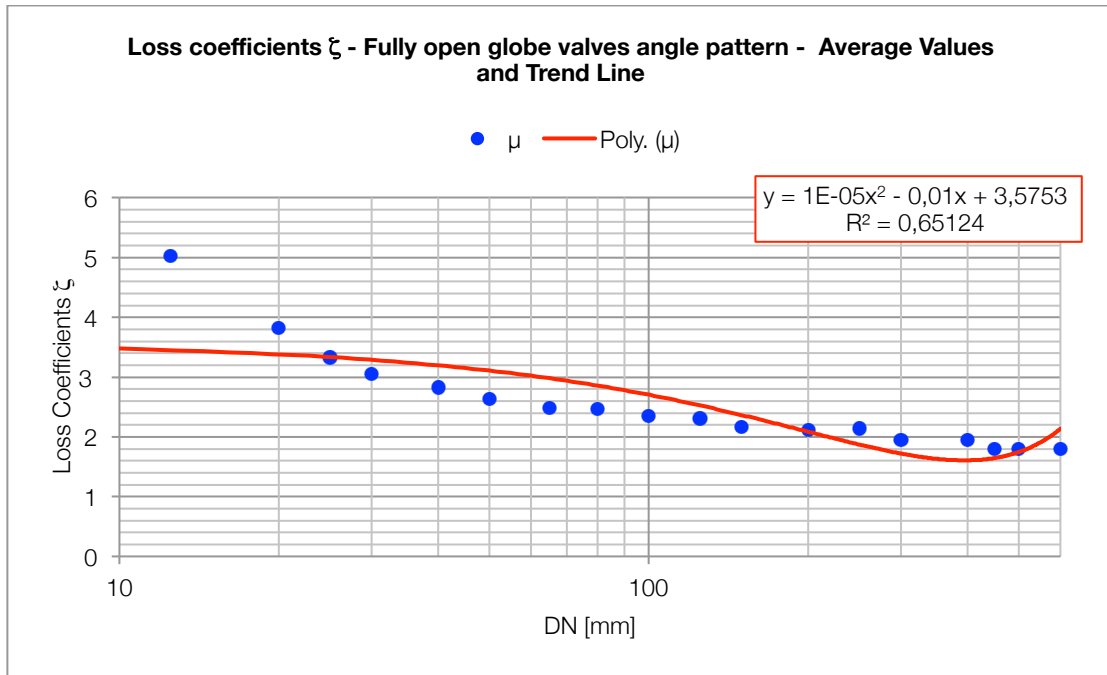
Graph 10: Loss coefficients ζ for fully open globe valves angle pattern - comparison between sources

Table 5: average ζ values for fully open globe valves (angle pattern)

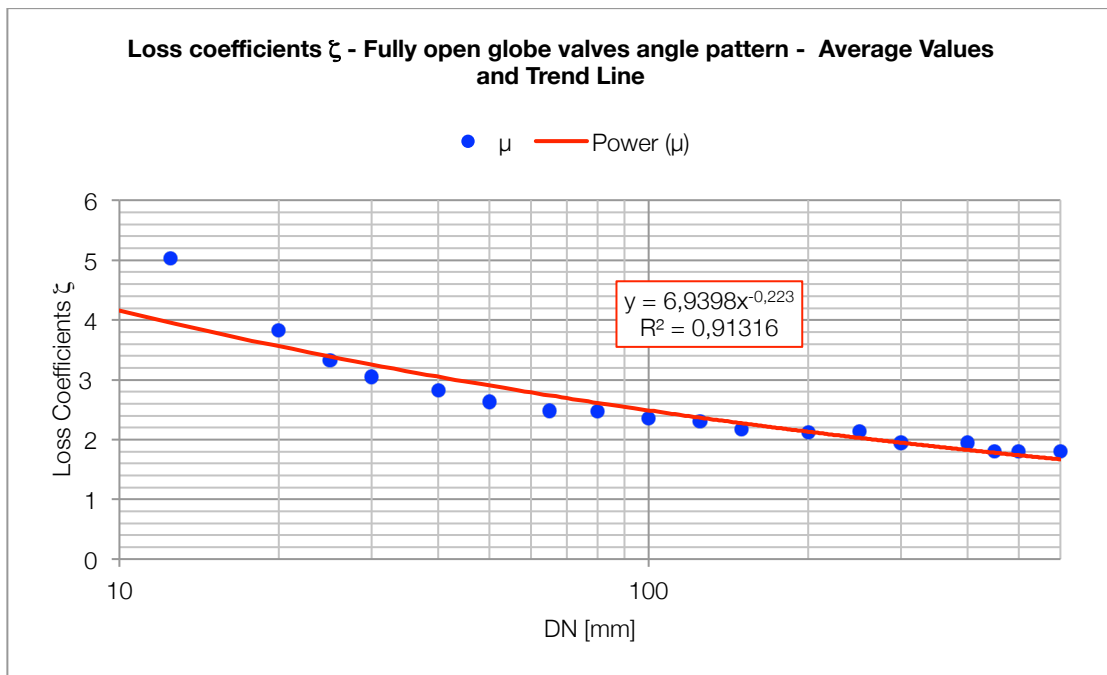
DN [mm]	μ	σ	$\mu+\sigma$	$\mu-\sigma$
15	5,03	1,3789	6,4039	3,6461
20	3,83	0,1061	3,9311	3,7189
25	3,33	0,1768	3,5018	3,1482
30	3,05	0,3536	3,4036	2,6964
40	2,83	0,4596	3,2846	2,3654
50	2,63	0,3753	3,0086	2,2581
65	2,48	0,3753	2,8586	2,1081
80	2,47	0,4041	2,8708	2,0625
100	2,35	0,3464	2,6964	2,0036
125	2,31	0,3011	2,6077	2,0056
150	2,17	0,1443	2,3110	2,0223
200	2,12	0,0289	2,1455	2,0878
250	2,13	0,0577	2,1911	2,0756
300	1,95	0,0000	1,9500	1,9500
400	1,95	0,0000	1,9500	1,9500
450	1,80	0,0000	1,8000	1,8000
500	1,80	0,0000	1,8000	1,8000
600	1,80	0,0000	1,8000	1,8000



Graph 11: average ζ values for fully open globe valves (angle pattern)



Graph 12: average values ζ and trend-line y for fully open globe valves (angle pattern)



Graph 13: average values ζ and trend-line y for fully open globe valves (angle pattern)

Table 6: statistical parameters for fully open globe valves (angle pattern)

Trend-line equation:	$y = 10^{-5}DN^2 - 0,01DN + 3,5753$
Coefficient of determination	$R^2 = 0,65124$
Trend-line equation:	$y = 6,9398 \cdot DN^{-0,223}$
Coefficient of determination	$R^2 = 0,91316$
Arithmetic mean of average values	$\mu_A = 2,56$
Arithmetic mean of the standard deviations	$\mu_{SD} = 0,25$
Standard deviation of the mean values	$\sigma_M = 0,83$

Comments

In the Graph 10 is presented the amount of data for the angle pattern of fully open globe valve. The number of sources for the angle pattern is similar to the standard pattern and so it is expected to have the same reliability.

The range of the DN considered is from DN 15 to DN 600 and the head loss coefficients are definitely lower than the globe standard's ones: their range is spaced between 6 and 2. However, the trend is decreasing with the diametes, exactly as before. This is a constant fact for all the sources except for Miller (Miller, 1966) which presents an increasing stretch of curve after DN 100. Again, it is immediatly recognizable a perfect match between the sources metropumps.com and Crane book (Crane, 1999).

There is again the range of values presented by Zappe (Zappe, 1998) which presents constant values of the head loss coefficients for all the range of nominal diameters DN. In particular, for Zappe (Zappe, 1998), it is stated that all the head loss coefficients have to be included between the value 2 and the value 5.

Looking at the Graph 11, it is plotted the average curve μ for the range of nominal diameter. The trend of the curve is decreasing with the diameters as expected from the single sources values, except for the value corresponding to DN 250 which presents a little plane stretch.

The trend of the standard deviation σ is nearly inline with the trend of the average values μ . In particular there are very small values of the standard deviation for high values of DN. This is the consequence of the small amount of data for high diamters but also of the matching percentage of these data. In the "middle zone" in particular from diameter 20 to the diameter 125, there's a little opening of the confidence interval. Indeed, this opening is really small and the confidence interval is reduced

and near to the trend of the μ curve. For angle pattern models, in the end, it is possible to argue that values of μ are more reliable than standard pattern.

In the Graph 12 and in the Graph 13 are presented the trend lines obtained for the average values μ . Also in this case there are presented two different trend lines obtained from a polynomial equation and a power equation model respectively.

Looking at the values of R^2 for the two equation is possible to say that for the first time the polynomial one has a bad fitting with the data. This fact is the consequence of the shape of the μ curve, very close to what the author expected from the single sources: a gradual decreasing of the middle values, very fitting to a power equation.

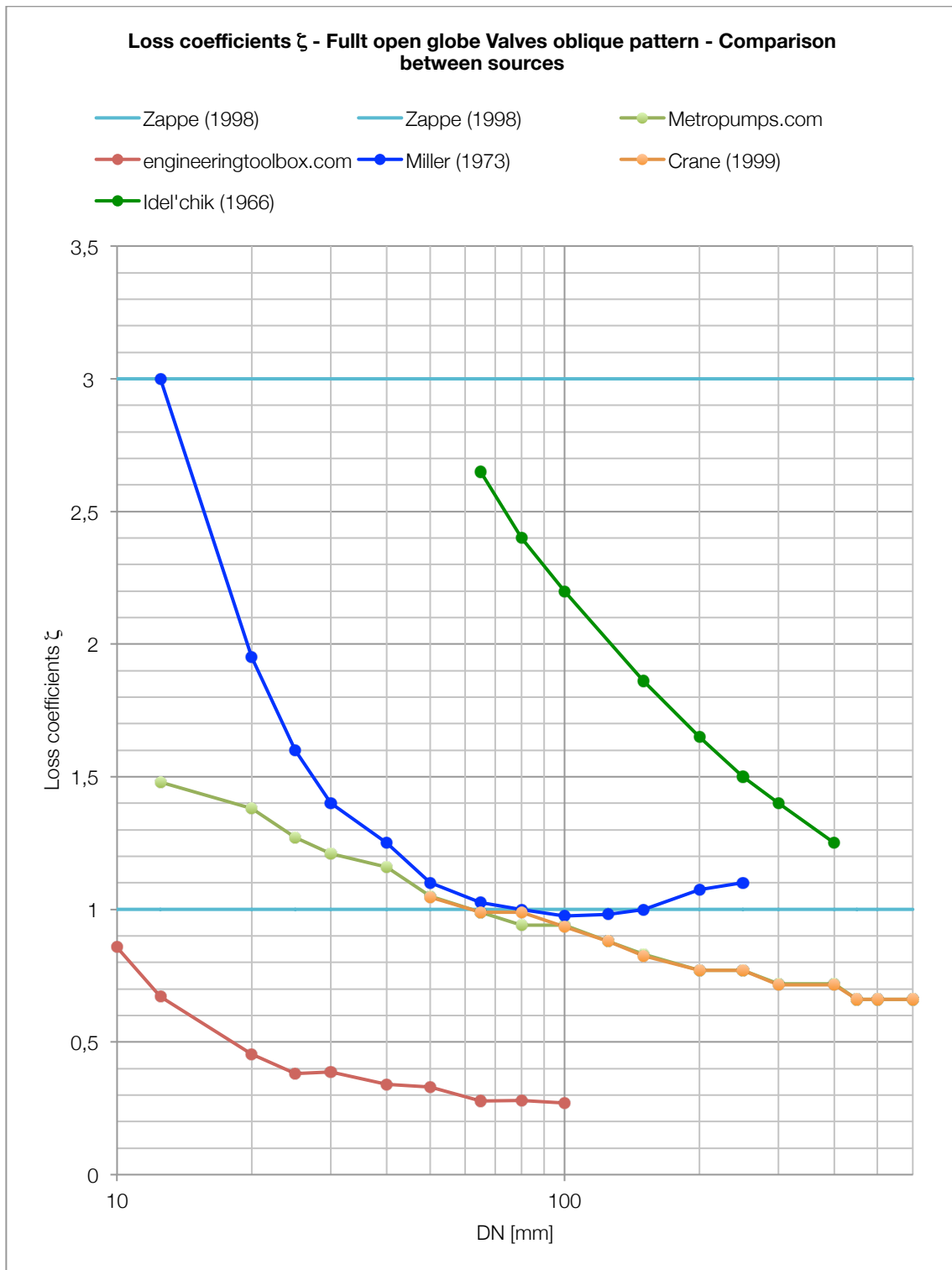
In Table 6 are presented the other parameters useful to the statistical interpretation: the arithmetic mean of average values μ_A , the arithmetic mean of the standard deviations μ_{SD} and the standard deviation of the mean values σ_M .

Looking at the value of μ_A , really higher than in the gate valves, it is confirmed that globe valves are high resistance valves but the angle pattern is very lower than the standard pattern.

The value of the arithmetic mean of the standard deviations μ_{SD} confirms that, for all the range of DN the μ values are reliable because its value is lower than the μ_A value.

The value of σ_M tells that there are considerable differences between the average head loss coefficient values among the different DN and so, from a practical point of view, it is not possible to use μ_A instead of the average values without committing a noticeable error.

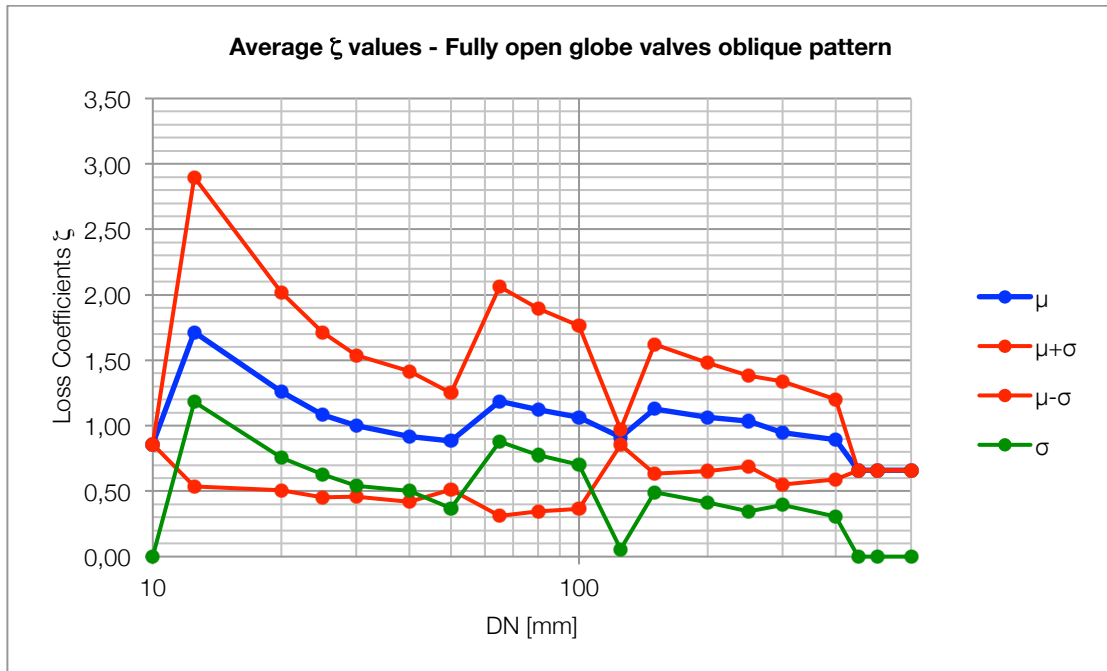
15.2.2.3 Oblique pattern



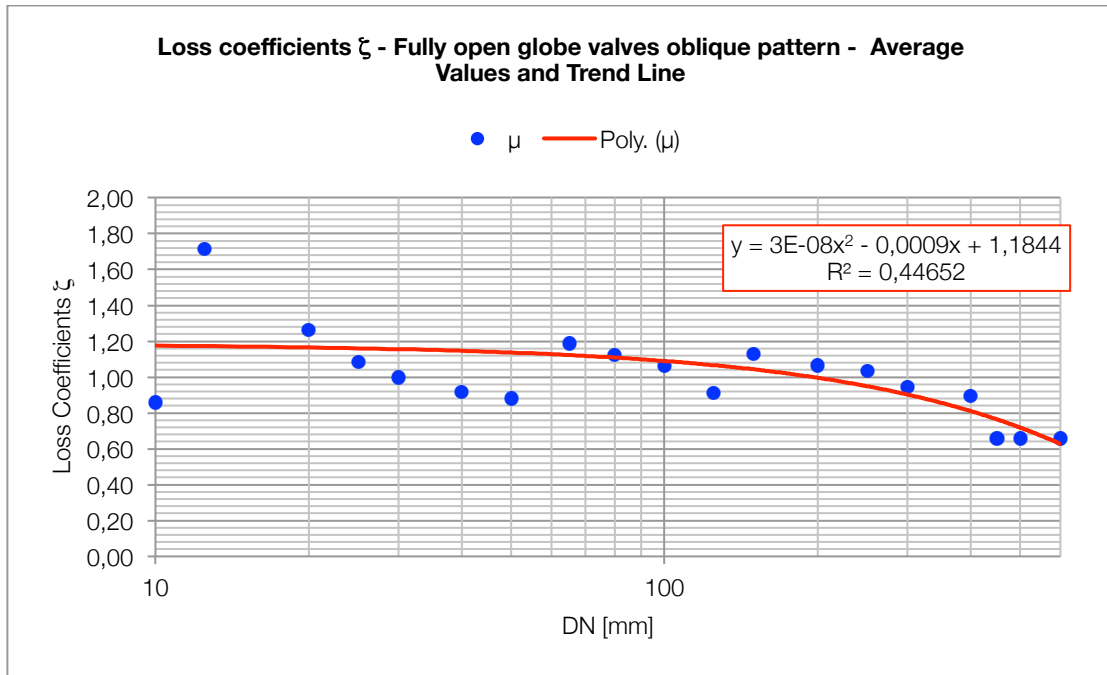
Graph 14: loss coefficients ζ for fully open globe valves oblique pattern - comparison between sources

Table 7: average ζ values for fully open globe valves (oblique pattern)

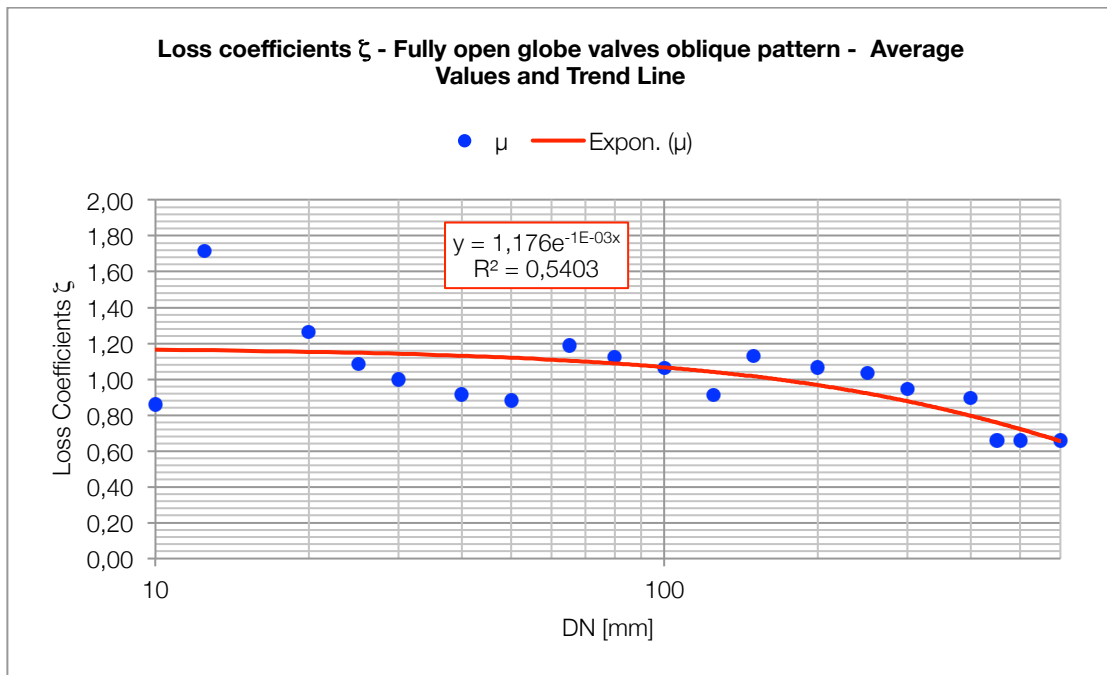
DN [mm]	μ	σ	$\mu+\sigma$	$\mu-\sigma$
6	1,44	0,0000	1,4400	1,4400
10	0,86	0,0000	0,8576	0,8576
15	1,72	1,1829	2,8996	0,5338
20	1,26	0,7549	2,0163	0,5065
25	1,08	0,6303	1,7141	0,4535
30	1,00	0,5387	1,5376	0,4602
40	0,92	0,5007	1,4178	0,4164
50	0,88	0,3683	1,2496	0,5129
65	1,19	0,8764	2,0628	0,3101
80	1,12	0,7758	1,8978	0,3462
100	1,06	0,7002	1,7642	0,3638
125	0,91	0,0577	0,9711	0,8556
150	1,13	0,4942	1,6230	0,6345
200	1,07	0,4149	1,4811	0,6514
250	1,04	0,3468	1,3818	0,6882
300	0,95	0,3940	1,3390	0,5510
400	0,90	0,3074	1,2024	0,5876
450	0,66	0,0000	0,6600	0,6600
500	0,66	0,0000	0,6600	0,6600
600	0,66	0,0000	0,6600	0,6600



Graph 15: average ζ values for fully open globe valves (oblique pattern)



Graph 16: average values ζ and trend-line y for fully open globe valves (oblique pattern)



Graph 17: average values ζ and trend-line y for fully open globe valves (oblique pattern)

Table 8: statistical parameters for fully open globe valves (oblique pattern)

Trend-line equation:	$y = 3 \cdot 10^{-8}DN^2 - 0,0009DN + 1,1814$
Coefficient of determination	$R^2 = 0,44652$
Trend-line equation:	$y = 1,176 \cdot e^{-0,003DN}$
Coefficient of determination	$R^2 = 0,5403$
Arithmetic mean of average values	$\mu_A = 1,02$
Arithmetic mean of the standard deviations	$\mu_{SD} = 0,42$
Standard deviation of the mean values	$\sigma_M = 0,26$

Comments

In the Graph 14 is presented the amount of data for the oblique pattern of fully open globe valve. The number of sources for the angle pattern is the same as for the angle pattern but it is immedialy evident that there are some differences in the trend of the curves presented. In the standard pattern and in the angle pattern all the data were similar in trends and there were a lot of overlapping points between the curves. In the oblique pattern data are very spread in the graph and this is an indication of poorer reliability than the previous patterns. Another difference immediatly found is the range of values: for the DN the range is the same (from DN 6 to DN 600) as the angle pattern, but the loss coefficient values are enclosed between 0,4 and 3,0 that are significantly smaller values than before.

Looking at the Graph 15, it is plotted the average curve μ for the range of nominal diameter. The trend of the curve is not so regular as before, and this is a consequence which was expected looking at the spread of values in the previous graph. However, it is possible to recognize the same decreasing trend, except for some particular values of DN (DN 15, DN 65 and DN 150).

The trend of the standard deviation σ is nearly parallel to the average values found before. The values of the standard deviation are really high and can be safely compared to the average value of the curve μ . This is another time a consequence of the great spread between the single sources curves. Finally it is possible to state that head loss coefficient values found for the oblique pattern of globa valves are strongly less accurate than before, and the use of the average curves implies higher errors than before. This could be the consequence of the higher variability between the models of the same valve: it is clear that standard patterns and angle patterns are geometrically shaped in the same way, except for the internal materials and dimensions, but the oblique patterns are very different between themselves.

In the Graph 16 and in the Graph 17 are presented the trend lines obtained for the average values μ . Another time it is possible to recognize a consequence of the spread of data: both of the trend lines, the polynomial one and the exponential one, have a bad fitting for the average curves.

Looking at the values of R^2 for the two equation is possible to say that are both very small if compared to the one seen before and so it is not recommended to use this practical equations.

In Table 8 are presented the other parameters useful to the statistical interpretation: the arithmetic mean of average values μ_A , the arithmetic mean of the standard deviations μ_{SD} and the standard deviation of the mean values σ_M .

Looking at the value of μ_A , really higher than in the gate valves, it is confirmed that globe valves are high resistance valves but the angle pattern is very lower than the standard pattern.

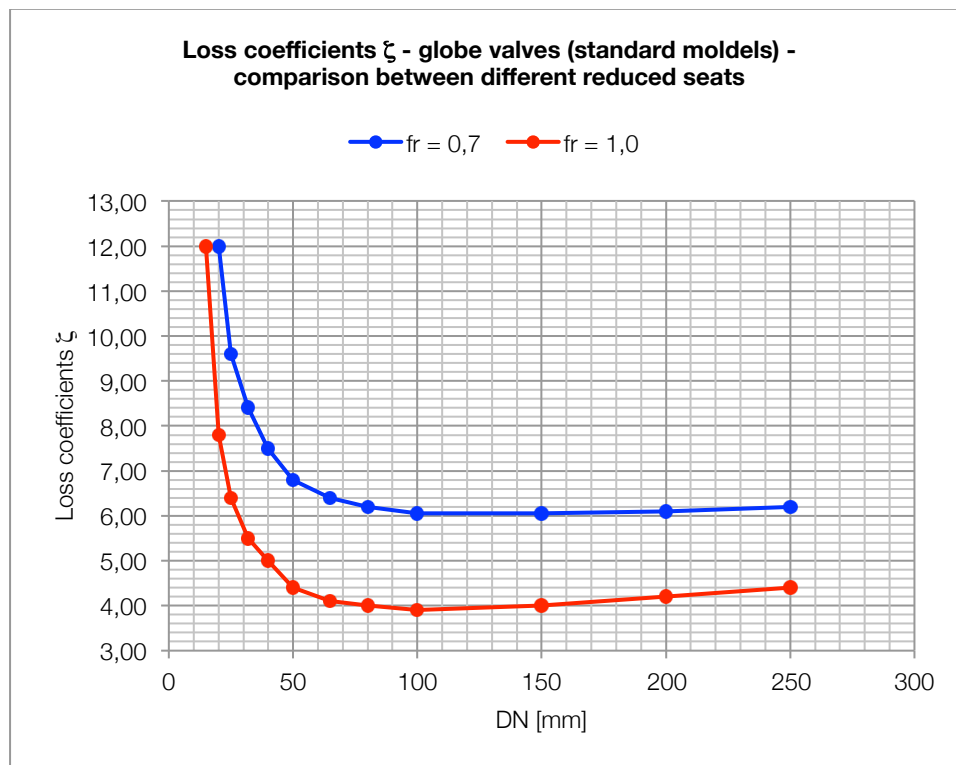
The value of the arithmetic mean of the standard deviations μ_{SD} is very high as expected and confirms that, for all the range of DN the μ values aren't reliable.

The value of σ_M tells that there are considerable differences between the average head loss coefficient values among the different DN and so, from a practical point of view, it is not possible to use μ_A instead of the average values without committing a noticeable error.

15.2.2.4 Comparison between standard seating globe valves and reduced seating globe valves (standard pattern)

Table 9: comparison between head loss coefficients from standard and reduced seat globe valves (standard models)

DN [mm]	$f_r = 0,7$	$f_r = 1,0$
15	-	12,00
20	12,00	7,80
25	9,60	6,40
32	8,40	5,50
40	7,50	5,00
50	6,80	4,40
65	6,40	4,10
80	6,20	4,00
100	6,05	3,90
150	6,05	4,00
200	6,10	4,20
250	6,20	4,40

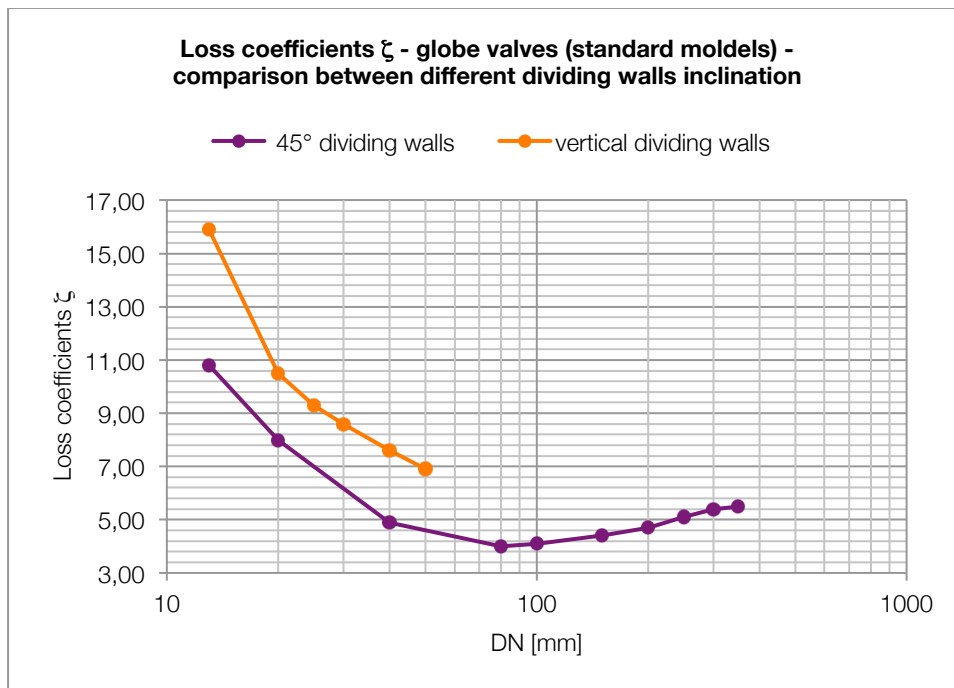


Graph 18: comparison between head loss coefficients from standard and reduced seat globe valves (standard models)

15.2.2.5 Comparison between vertical dividing walls and 45° dividing walls for standard globe valves

Table 10: comparison between vertical dividing walls and 45° dividing walls for standard globe valves

45° dividing walls		vertical dividing walls	
DN [mm]	ζ	DN [mm]	ζ
13	10,80	13	15,90
20	8,00	20	10,50
40	4,90	25	9,30
80	4,00	30	8,60
100	4,10	40	7,60
150	4,40	50	6,90
200	4,70		
250	5,10		
300	5,40		
350	5,50		

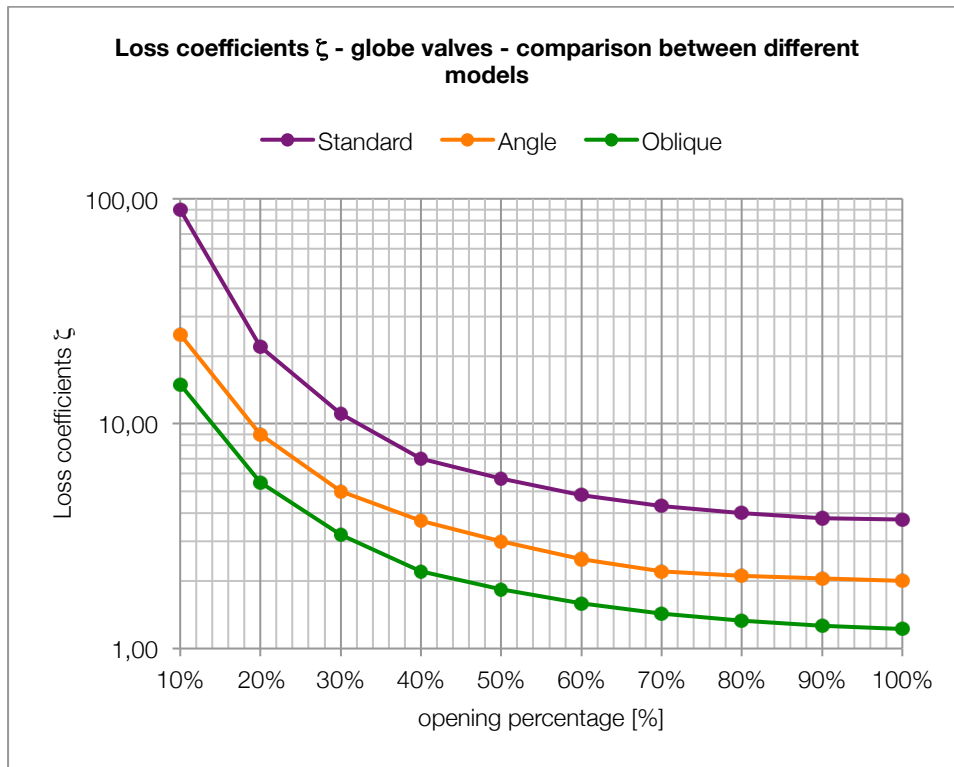


Graph 19: comparison between vertical dividing walls and 45° dividing walls for standard globe valves

15.2.2.6 Comparison of loss coefficient values at different opening percentage between different globe valve models

Table 11: comparison of loss coefficient values ζ at different opening percentage between different globe valve models

Partial Opening	ζ values		
	Standard	Angle	Oblique
10%	90,00	25,00	15,00
20%	22,00	9,00	5,50
30%	11,10	5,00	3,20
40%	7,00	3,70	2,20
50%	5,70	3,00	1,84
60%	4,80	2,50	1,59
70%	4,30	2,20	1,43
80%	4,00	2,10	1,33
90%	3,80	2,05	1,26
100%	3,75	2,00	1,22

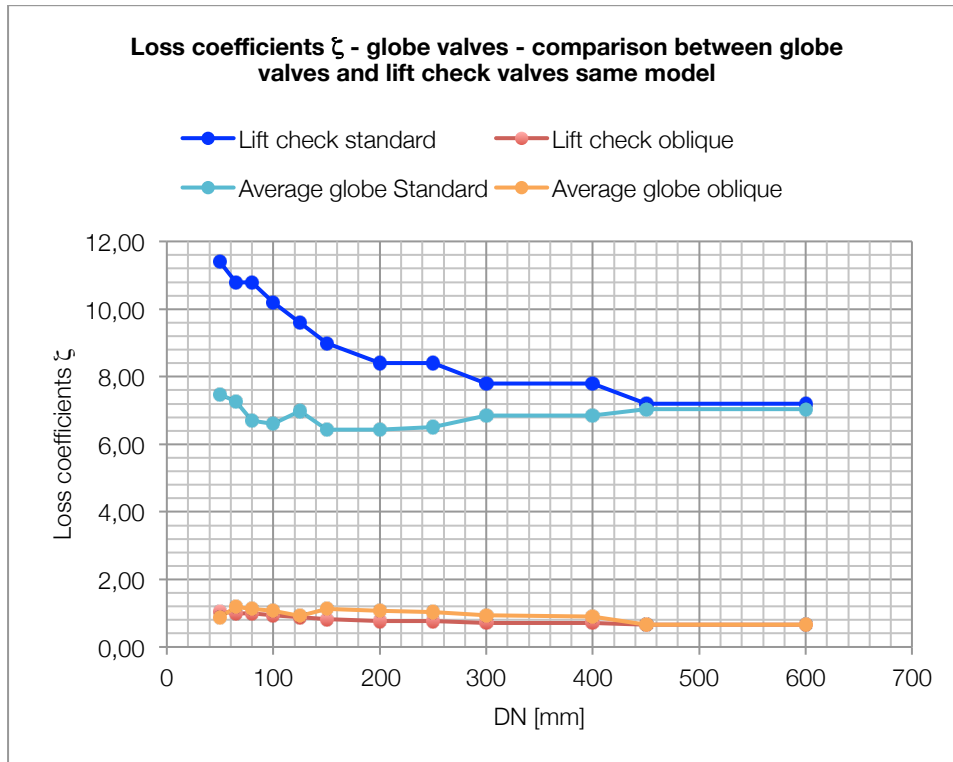


Graph 20: comparison of loss coefficient values ζ at different opening percentage between different globe valve models

15.2.2.7 Comparison between corresponding models of lift-check valves and globe valves

Table 12: comparison between corresponding models of lift-check valves and globe valves

DN [mm]	Head loss coefficient values ζ				Percentage error η	
	Lift check standard	Lift check oblique	Average globe Standard	Average globe oblique	standard	oblique
50	11,40	1,05	7,47	0,88	34,46%	15,67%
65	10,80	0,99	7,26	1,19	32,74%	19,84%
80	10,80	0,99	6,70	1,12	37,93%	13,33%
100	10,20	0,94	6,60	1,06	35,33%	13,80%
125	9,60	0,88	6,98	0,91	27,31%	3,79%
150	9,00	0,83	6,43	1,13	28,52%	36,82%
200	8,40	0,77	6,43	1,07	23,49%	38,47%
250	8,40	0,77	6,51	1,04	22,50%	34,42%
300	7,80	0,72	6,84	0,95	12,26%	32,17%
400	7,80	0,72	6,84	0,90	12,26%	25,17%
450	7,20	0,66	7,05	0,66	2,15%	0,00%
600	7,20	0,66	7,05	0,66	2,15%	0,00%



Graph 21: comparison between corresponding models of lift-check valves and globe valves

15.2.2.8 Other comments

Comparison between standard seats and reduced seats globe valves

In the Graph 18 and in the Table 9 are presented the data found in Idel'chik book (Idel'chik, 1966) which derive from a comparison between standard patterns of globe valves with different f_r ratio. In particular it is possible to recognize that the curve associated to the globe valve without the reduced seat is lower than the one with $f_r=0,7$. This is what is expected from the theoretical chapter because a reduced seat causes more turbulences in the flow and, consequently, more head losses.

Comparison between walls of different inclinations (globe valves standard pattern)

In the Graph 19 and in the Table 10 are presented the data found in Idel'chik book (Idel'chik, 1966) which derive from a comparison between different inclination of the dividing walls of the standard patterns globe valves. In particular there are two main inclinations of the dividing walls: 45° and 90° . It is possible to recognize that the curve associated to the 45° is lower than the 90° one.

Comparison between different opening percentage (globe valves standard pattern)

In the Graph 20 and in the Table 11 are presented the data found in Idel'chik book (Idel'chik, 1966) which derive from a comparison between the head loss coefficients of different globe valve patterns versus the opening percentage. The range of opening is from 10% and 100%, which corresponds to the complete opening. It is interesting to see that the trend of the curves is perfectly inline of what it is expected from the theory: the more the valve is open the more the head loss coefficient has a low value. It is respected also the comparison between different valve's patterns: comparing the μ_A values previously found it is clear that the standard pattern valve has the highest values of head loss coefficients, the angle is the second and in the third position it is found the oblique pattern. This trend is respected also at different percentage of opening: the standard curve is the highest, the second is the angle and the lowest is the oblique pattern.

Comparison between globe valves and lift check valves

In the Table 12 and in the Graph 21 is presented the last comparison in the field of globe valve is done for globe valves, with the standard function of controlling the flow (control valves) and the globe valves used for non-return function, the lift-check valves. The shape, the materials and the geometrical aspects of these two valves type are the same: the only difference is the functioning of the shut-off member. From the

theoretical point of view it is expected that the differences are minimal between the two valves.

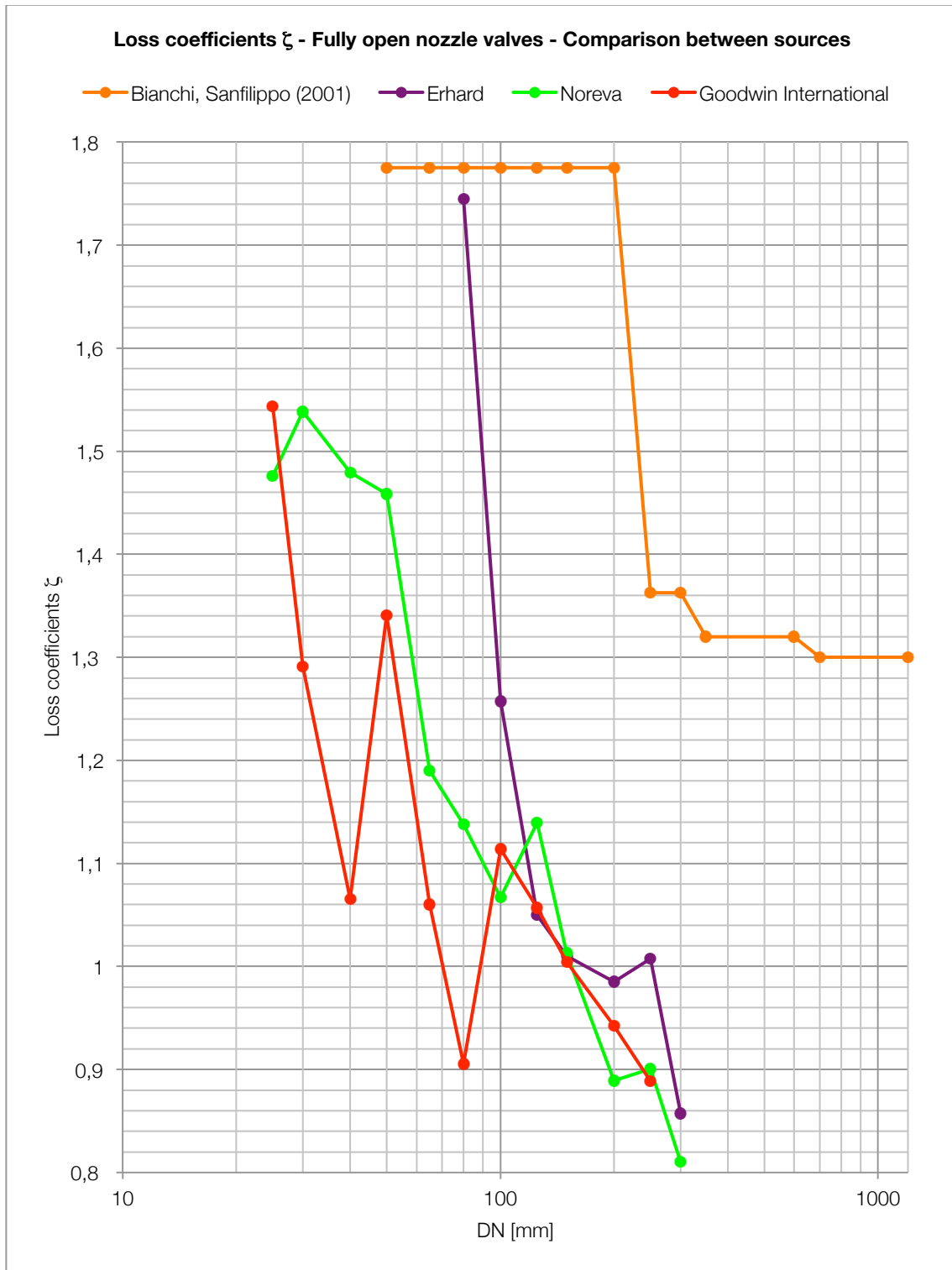
The comparison is made graphically in the Graph 21 and with the help of the factor η in the Table 12, and it is made for standard pattern and oblique pattern.

For the standard pattern and for diameter enclosed in the range between 50 mm and 150 mm the percentage error is more or less quantified in the 30%. This is a sensible difference, confirmed graphically in the Graph 21. After DN 150 the percentage error is gradually reducing till the value of 2% more or less.

For the oblique pattern the trend of the percentage error η is completely opposite: for the diameter range enclosed between DN 50 and DN 125 the values of η is more or less 15%. After DN 150 there's an increasing of the value to more or less the 30%, except for the DN 450 and DN 600 which is near to zero.

This values state that there's a sensible difference between the lift-check valves and the globe control valves in terms of the head losses.

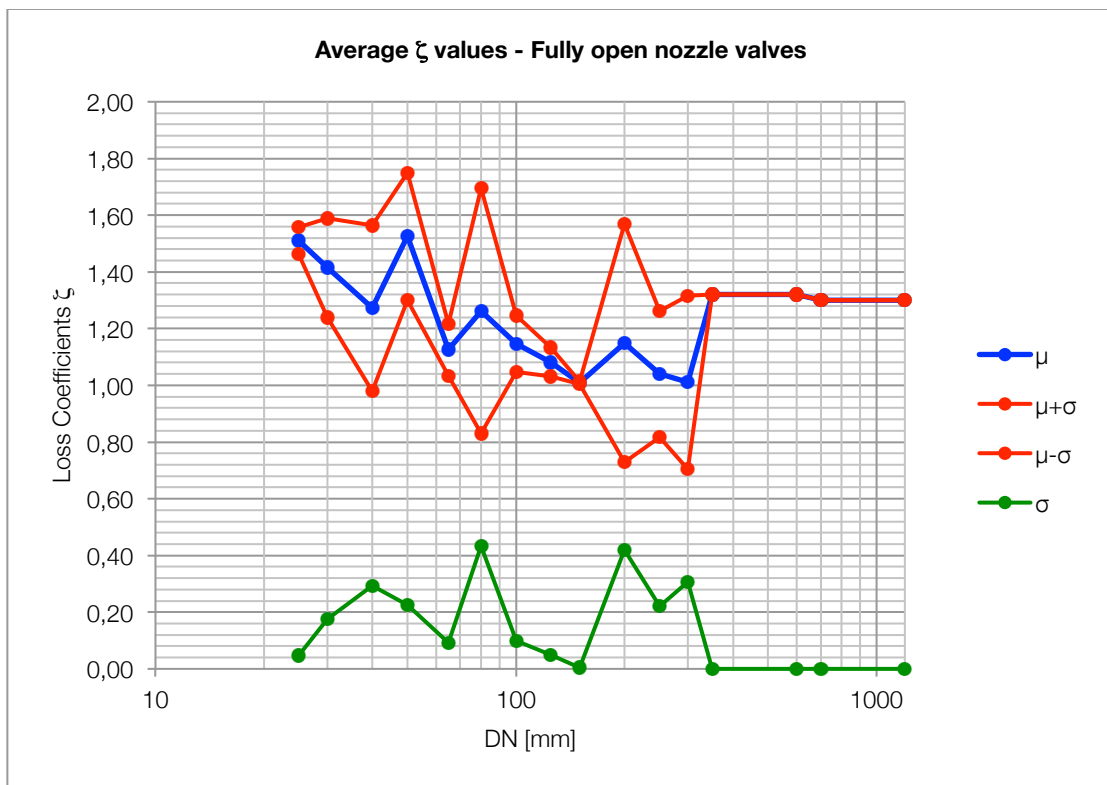
15.2.3 Nozzle valves



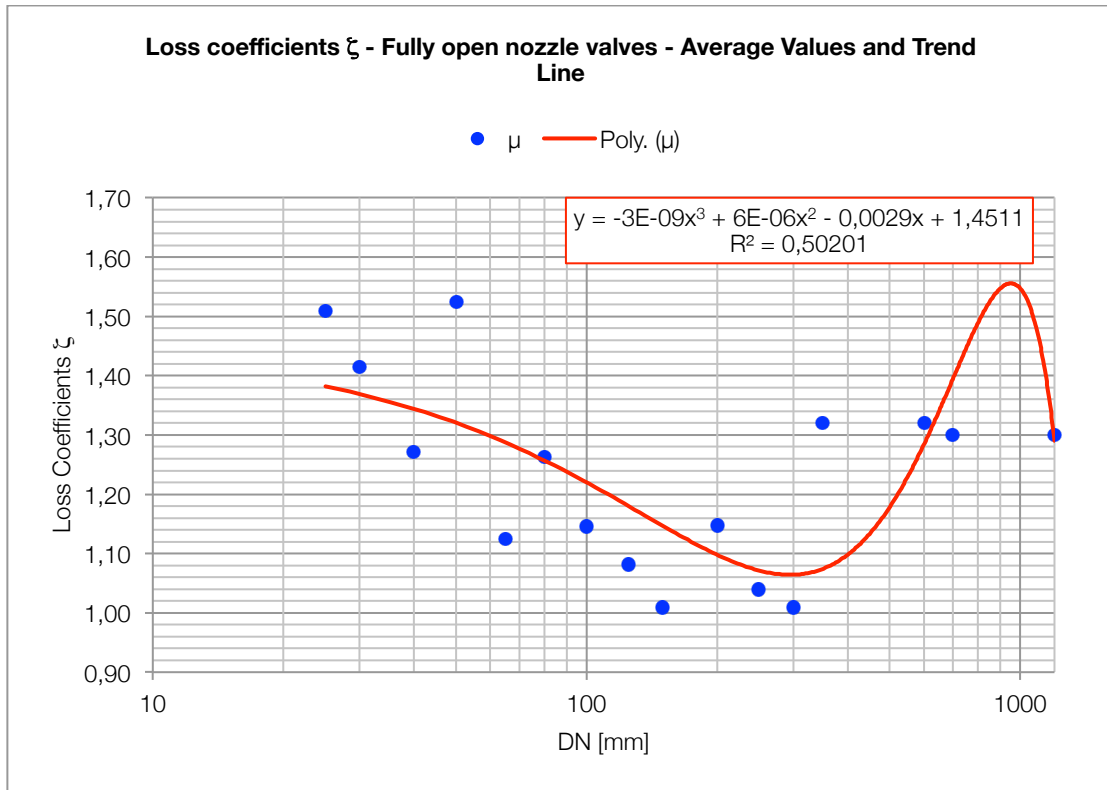
Graph 22: loss coefficients ζ for fully open nozzle valves - comparison between sources

Table 13: average ζ values for fully open nozzle valves

DN [mm]	μ	σ	$\mu+\sigma$	$\mu-\sigma$
25	1,51	0,0477	1,5574	1,4620
30	1,41	0,1747	1,5894	1,2400
40	1,27	0,2929	1,5652	0,9794
50	1,52	0,2246	1,7493	1,3002
65	1,34	0,3808	1,7226	0,9609
80	1,39	0,4368	1,8277	0,9540
100	1,30	0,3247	1,6281	0,9786
125	1,26	0,3488	1,6042	0,9066
150	1,20	0,3830	1,5835	0,8175
200	1,15	0,4200	1,5678	0,7278
250	1,04	0,2217	1,2615	0,8180
300	1,01	0,3061	1,3162	0,7039
350	1,32	0,0000	1,3200	1,3200
600	1,32	0,0000	1,3200	1,3200
700	1,30	0,0000	1,3000	1,3000
1200	1,30	0,0000	1,3000	1,3000



Graph 23: average ζ values for fully open nozzle valves



Graph 24: average values ζ and trend-line y for fully open nozzle valves

Table 14: statistical parameters for fully open nozzle valves

Trend-line equation:	$y = -3 \cdot 10^{-9}DN^3 + 6 \cdot 10^{-6}DN^2 - 0,0029 \cdot DN + 1,4511$
Coefficient of determination	$R^2 = 0,50201$
Arithmetic mean of average values	$\mu_A = 1,23$
Arithmetic mean of the standard deviations	$\mu_{SD} = 0,18$
Standard deviation of the mean values	$\sigma_M = 0,18$

Comments

Looking at Graph 22, the number of sources used for the nozzle valves is very similar to the globe valves. The trend of the curves is not so regular as before: it is possible to recognize a decreasing of the head loss coefficient values with the increasing of the DN values but no source has a monotonically trend.

The range of the nominal diameters DN is wider than before: it is considered a range from 25 to 1200. Defining a first sub-range from DN 25 to DN 100 it is possible to recognize a spread between values that are really different between themselves: this spread between values can suggest that there will be high values of the standard deviations σ and so a unreliable value of the μ . But from the DN 100 there is a decreasing of this spread and the curves begin to be very similar, with same overlapping points. For this second-sub-range the head loss coefficients ζ are more similar and so it is expected a lower value of σ .

The range of the head loss coefficients ζ founded for this valve's type is quantifiable from 0,8 (Noreva) to 1,75 (Bianchi, Sanfilippo, 2001). In general it is possible to say that nozzle valves, specially looking at the dimensions of the closure member, are low-resistance valves.

The Table 13 and the Graph 23 plot the average values μ of the head loss coefficients ζ , the standard deviation σ and the confidence interval obtained. Looking at the graph is possible to recognize a very irregular trend of the values against the nominal diameter. The irregular trend is repeated also for the standard deviation values σ . This combination brings to a very irregular trend of the confidence interval which is very open for DN 80 and DN 200 but very closed for DN 150 and DN 250.

The values of the standard deviation curve are not only irregular but also they are not negligible also if its values are sensibly lower than the average values.

In the Graph 24 is presented the trend line obtained for nozzle valve: its type is polynomial but, looking at the value of R^2 there isn't a good fit of the data. This is a consequence of the great irregularity of the average head loss curve: it is impossible to create a good fit curve using an equation model without sensible errors.

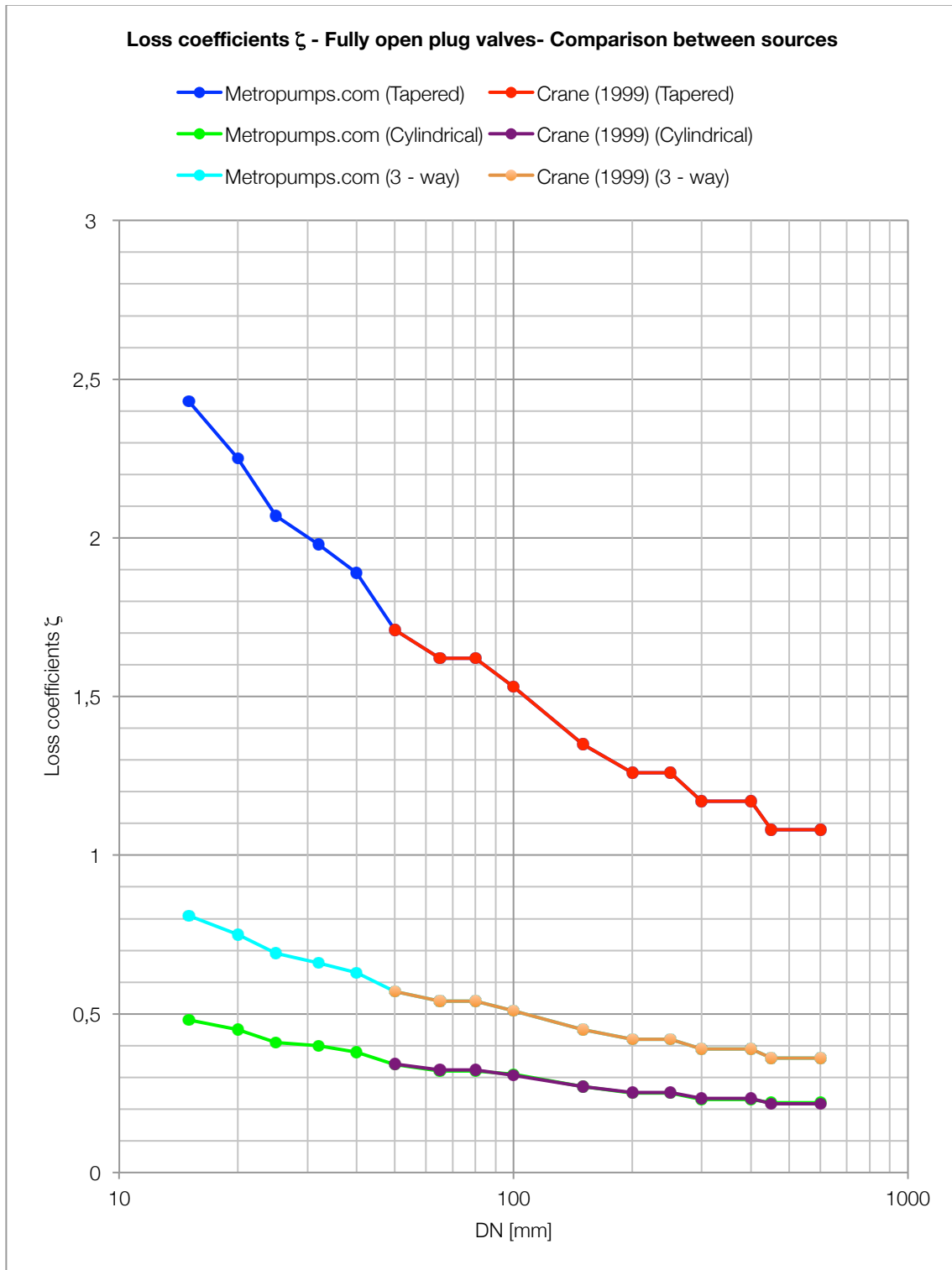
In Table 14 are presented the other parameters useful to the statistical interpretation: the arithmetic mean of average values μ_A , the arithmetic mean of the standard deviations μ_{SD} and the standard deviation of the mean values σ_M .

Looking at the value of μ_A it is possible to say that it is very reduced, as it is stated before (low-resistance valve). The value of σ_M is not so high, which means that the μ_A is very similar to the other μ values and so, from a practical point of view, it is

possibile to use it instead of the average values without committing a great error (from the hydraulic point of view).

The value of the arithmetic mean of the standard deviations μ_{SD} states that, for all the range of DN, it is not possibile to neglect it but its value is low compared to the other head loss values and so the μ values are reliable. This is not what was expected but a good confirm from the practical point of view.

15.2.4 Plug valves



Graph 25: loss coefficients ζ for fully open plug valves - comparison between sources

Comments

In the Graph 25 are plotted the head loss coefficient curves for the three patterns of plug valves: tapered pattern, cylindrical pattern and 3-way pattern. It is immediately recognizable the same trend in all the three patterns: the head loss curve is decreasing with the increasing of the nominal diameter values DN. Another thing that is evident is the perfect overlapping of the curves from different sources but same pattern: this will bring to a negligible values of the standard deviation σ and a perfect reliability of the data (basing on the sources used that are only two).

The range of the nominal diameters DN is from 15 mm to 600 mm for all the three patterns. The range of the head loss coefficients ζ founded for these valve's types are quantifiable in the following table:

Table 15: comparison between ranges of different plug valve's patterns

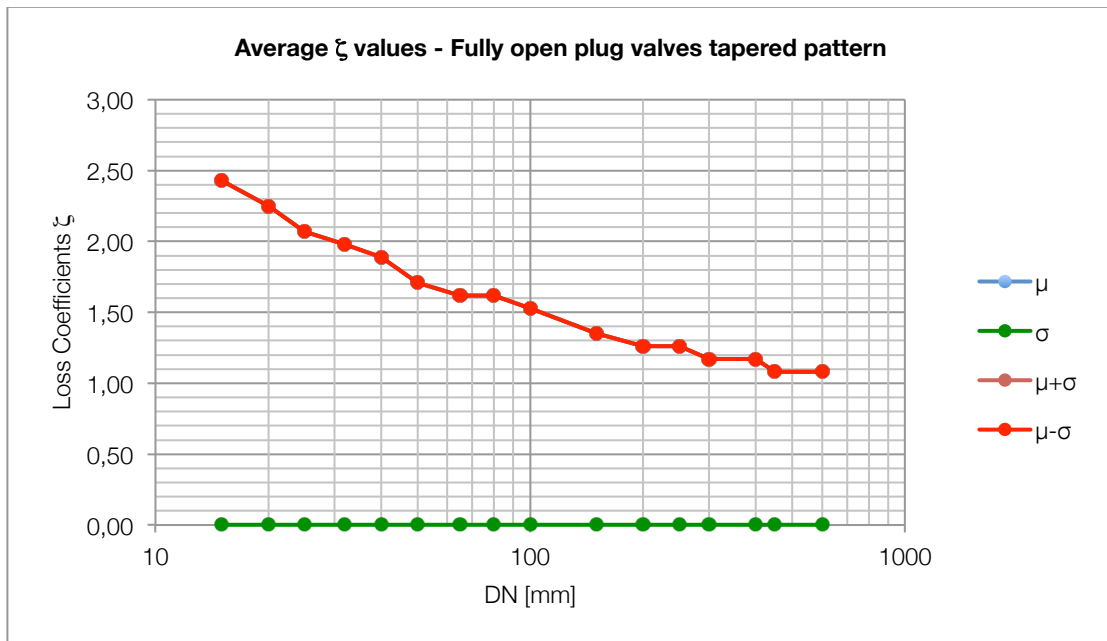
<i>Plug valve pattern</i>	<i>Range of values</i>
Tapered model	1,08 ÷ 2,43
Cylindrical model	0,22 ÷ 0,48
3-way model	0,36 ÷ 0,81

The values of the 3-way pattern and the cylindrical pattern are not the same but there are small differences between the curves, which are parallel (and so they don't overlap themselves) but very close. The tapered pattern has head loss coefficients which are definitely higher while parallel. In general it is possible to recognize a perfect parallelism between different patterns' curves: although the values are very different between themselves, the trend of the linear interpolation between them is the same.

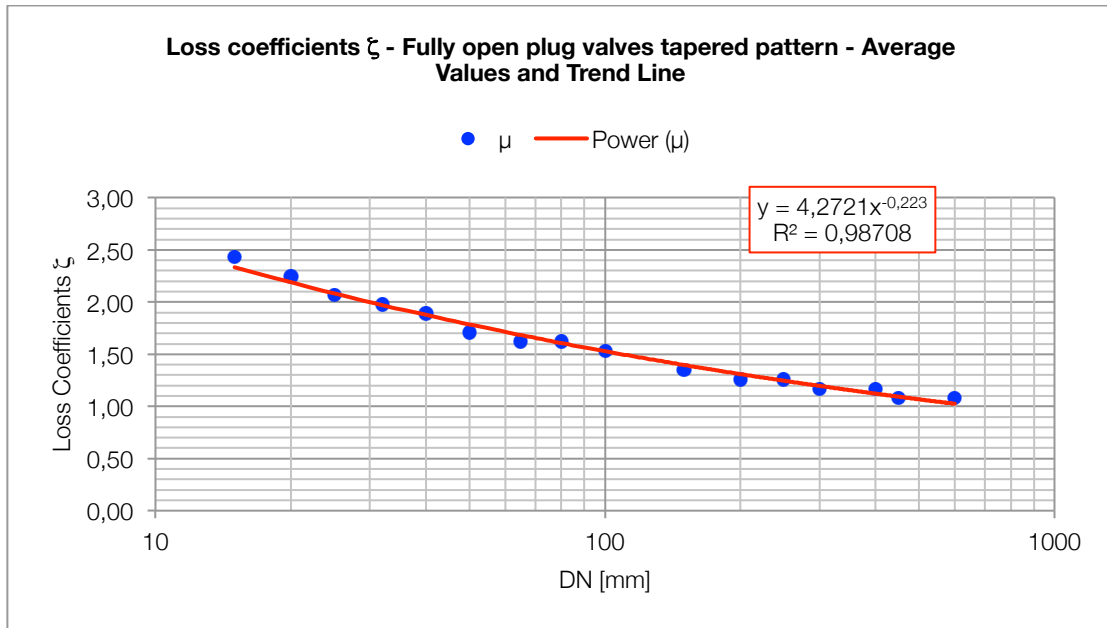
15.2.4.1 Tapered pattern

Table 16: average ζ values for fully open plug valves (tapered pattern)

DN [mm]	μ	σ	$\mu+\sigma$	$\mu-\sigma$
15	2,43	0,0000	2,4300	2,4300
20	2,25	0,0000	2,2500	2,2500
25	2,07	0,0000	2,0700	2,0700
32	1,98	0,0000	1,9800	1,9800
40	1,89	0,0000	1,8900	1,8900
50	1,71	0,0000	1,7100	1,7100
65	1,62	0,0000	1,6200	1,6200
80	1,62	0,0000	1,6200	1,6200
100	1,53	0,0000	1,5300	1,5300
150	1,35	0,0000	1,3500	1,3500
200	1,26	0,0000	1,2600	1,2600
250	1,26	0,0000	1,2600	1,2600
300	1,17	0,0000	1,1700	1,1700
400	1,17	0,0000	1,1700	1,1700
450	1,08	0,0000	1,0800	1,0800
600	1,08	0,0000	1,0800	1,0800



Graph 26: average ζ values for fully open plug valves (tapered pattern)



Graph 27: average values ζ and trend-line y for fully open plug valves (tapered pattern)

Table 17: statistical parameters for fully open plug valves (tapered pattern)

Trend-line equation:	$y = 4,2721 \cdot DN^{-0,223}$
Coefficient of determination	$R^2 = 0,98708$
Arithmetic mean of average values	$\mu_A = 1,59$
Arithmetic mean of the standard deviations	$\mu_{SD} = 0,00$
Standard deviation of the mean values	$\sigma_M = 0,43$

Comments

The Table 16 and the Graph 26 plot the average values μ of the head loss coefficients ζ , the standard deviation σ and the confidence interval obtained for the tapered pattern of plug valve. Looking at the Graph 26 is possible to recognize a very regular trend of the values against the nominal diameter, a consequence of the perfect initial overlapping of the data from different sources. The regular trend is repeated also for the standard deviation values σ which are equal to zero for all the range of DN considered. From DN 40 the sources considered are two but the standard deviation is again near to zero because of the perfect overlapping of the sources.

In the Graph 27 is presented a trend line obtained for tapered pattern valve. The very regular trend of the head loss values fits almost perfectly with the power trend line plotted and the extremely high value of R^2 is the confirm of that fact: it is possible to create a very good fit curve this equation model without committing sensible errors.

In Table 17 are presented the other parameters useful to the statistical interpretation: the arithmetic mean of average values μ_A , the arithmetic mean of the standard deviations μ_{SD} and the standard deviation of the mean values σ_M .

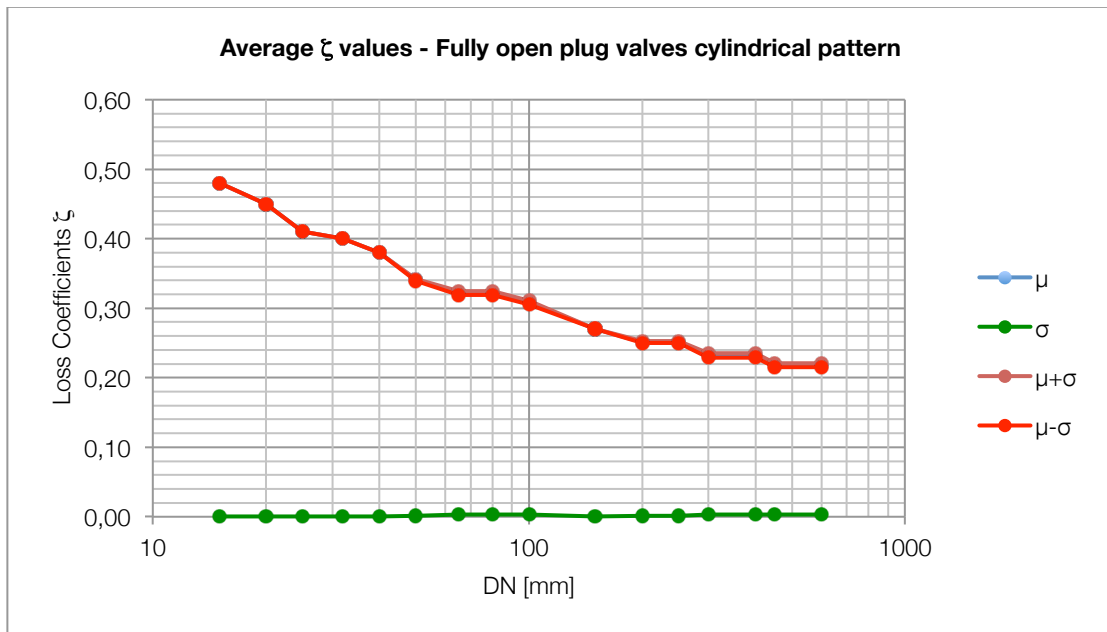
Looking at the value of μ_A it is possible to say that it is very reduced, as it is stated before (low-resistance valve). The value of σ_M is not so high, which means that the μ_A is very similar to the other μ values and so, from a practical point of view, it is possible to use it instead of the average values without committing a great error (from the hydraulic point of view).

The zero value of the arithmetic mean of the standard deviations μ_{SD} states that, for all the range of DN, it is possible to neglect it and so the μ values are reliable. This is not what was expected but a good confirm from the practical point of view.

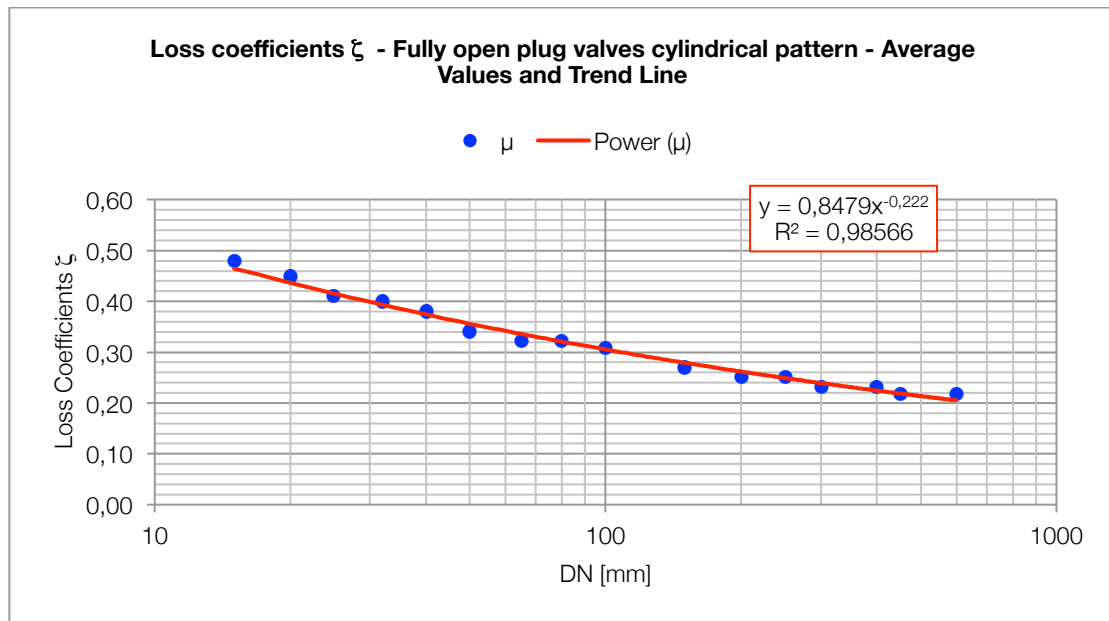
15.2.4.2 Cylindrical pattern

Table 18: average ζ values for fully open plug valves (cylindrical pattern)

DN [mm]	μ	σ	$\mu+\sigma$	$\mu-\sigma$
15	0,48	0,0000	0,4800	0,4800
20	0,45	0,0000	0,4500	0,4500
25	0,41	0,0000	0,4100	0,4100
32	0,40	0,0000	0,4000	0,4000
40	0,38	0,0000	0,3800	0,3800
50	0,34	0,0014	0,3424	0,3396
65	0,32	0,0028	0,3248	0,3192
80	0,32	0,0028	0,3248	0,3192
100	0,31	0,0028	0,3108	0,3052
150	0,27	0,0000	0,2700	0,2700
200	0,25	0,0014	0,2524	0,2496
250	0,25	0,0014	0,2524	0,2496
300	0,23	0,0028	0,2348	0,2292
400	0,23	0,0028	0,2348	0,2292
450	0,22	0,0028	0,2208	0,2152
600	0,22	0,0028	0,2208	0,2152



Graph 28: average ζ values for fully open plug valves (cylindrical pattern)



Graph 29: average values ζ and trend-line y for fully open plug valves (cylindrical pattern)

Table 19: statistical parameters for fully open plug valves (cylindrical pattern)

Trend-line equation:	$y = 0,8479 \cdot DN^{-0,222}$
Coefficient of determination	$R^2 = 0,98566$
Arithmetic mean of average values	$\mu_A = 0,32$
Arithmetic mean of the standard deviations	$\mu_{SD} = 0,00$
Standard deviation of the mean values	$\sigma_M = 0,09$

Comments

The observations that could be made for the cylindrical pattern of plug valves are very similar to the tapered ones. In the Table 18 and in the Graph 28 are plotted the average values μ of the head loss coefficients ζ , the standard deviation σ and the confidence interval obtained for this valve. Looking at the Graph 28 is possible to recognize a very regular trend of the values against the nominal diameter, a consequence of the perfect initial overlapping of the data from different sources. The regular trend is repeated also for the standard deviation values σ which are practically negligible for all the range of DN considered: the highest value is 0,0028 which represent 1% compared to the corresponding mean value μ of 0,23. The consequence of this fact is that the confidence interval curves are practically

overlapped to the mean curve and there's no question about the reliability of these data.

In the Graph 29 is presented the trend line obtained for cylindrical pattern valve. The very regular trend of the head loss values fits almost perfectly with the power trend line plotted and the extremely high value of R^2 is the confirm of this fact: it is possible to create a very good fit curve this equation model without committing sensible errors.

In Table 19 are presented the other parameters useful to the statistical interpretation: the arithmetic mean of average values μ_A , the arithmetic mean of the standard deviations μ_{SD} and the standard deviation of the mean values σ_M .

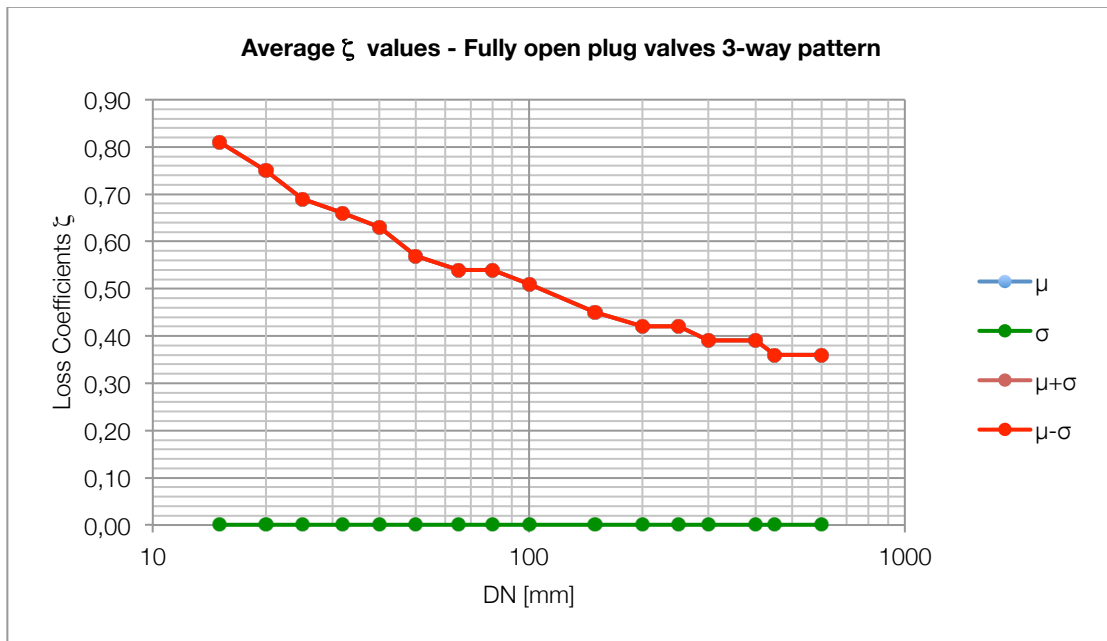
As for the tapered pattern, looking at the value of μ_A it is possible to say that it is very reduced, and it is even the 30% of the tapered valve pattern and so it is confirmed that the valve is a low-resistance valve. The value of σ_M is very reduced too and it means that the μ_A is very similar to the other μ values and so, from a practical point of view, it is possible to use the μ_A value independently from the diameter chosen, without without committing a sensible error (from the hydraulic point of view).

The zero value of the arithmetic mean of the standard deviations μ_{SD} states that, for all the range of DN, it is possible to neglect it and so the μ values are reliable. This is not what was expected but a good confirm from the practical point of view.

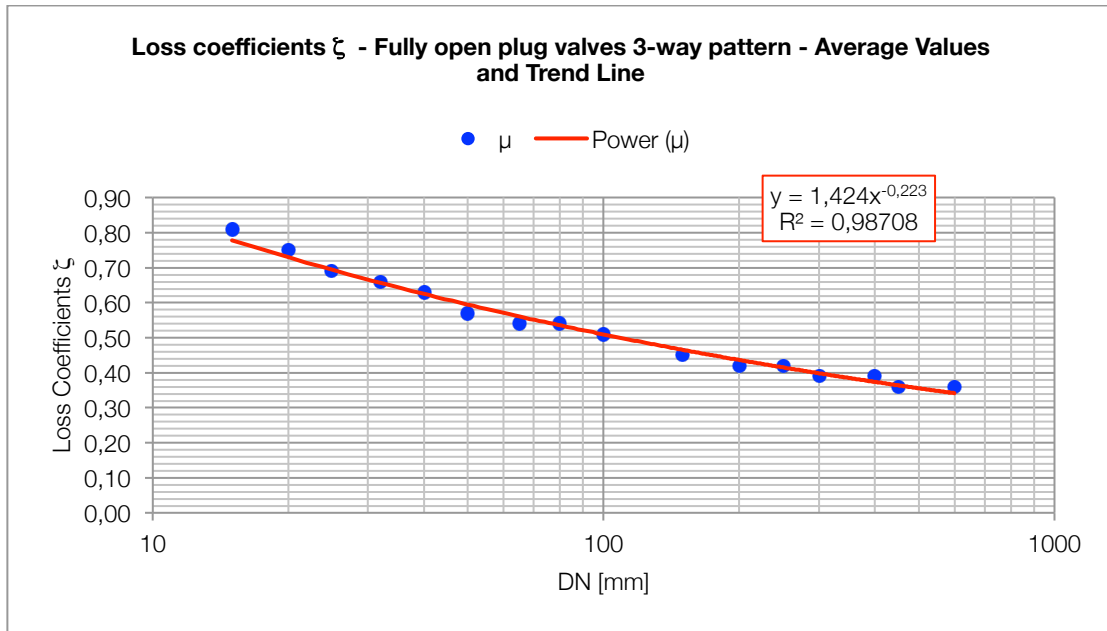
15.2.4.3 3-way pattern

Table 20: average ζ values for fully open plug valves (3-way pattern)

DN [mm]	μ	σ	$\mu+\sigma$	$\mu-\sigma$
15	0,81	0,0000	0,81	0,81
20	0,75	0,0000	0,75	0,75
25	0,69	0,0000	0,69	0,69
32	0,66	0,0000	0,66	0,66
40	0,63	0,0000	0,63	0,63
50	0,57	0,0000	0,57	0,57
65	0,54	0,0000	0,54	0,54
80	0,54	0,0000	0,54	0,54
100	0,51	0,0000	0,51	0,51
150	0,45	0,0000	0,45	0,45
200	0,42	0,0000	0,42	0,42
250	0,42	0,0000	0,42	0,42
300	0,39	0,0000	0,39	0,39
400	0,39	0,0000	0,39	0,39
450	0,36	0,0000	0,36	0,36
600	0,36	0,0000	0,36	0,36



Graph 30: : average ζ values for fully open plug valves (3-way pattern)



Graph 31: average values ζ and trend-line y for fully open plug valves (3-way pattern)

Table 21: statistical parameters for fully open plug valves (3-way pattern)

Trend-line equation:	$y = 1,424 \cdot DN^{-0,223}$
Coefficient of determination	$R^2 = 0,98708$
Arithmetic mean of average values	$\mu_A = 0,53$
Arithmetic mean of the standard deviations	$\mu_{SD} = 0,00$
Standard deviation of the mean values	$\sigma_M = 0,14$

Comments

Again, most of the observations that could be made for the 3-way pattern of plug valves are very similar to the tapered and the cylindrical ones. In the Table 20 and in the Graph 30 are plotted the average values μ of the head loss coefficients ζ , the standard deviation σ and the confidence interval obtained for this valve. The standard deviation is equal to zero for all the nominal diameters values DN and so there's a perfect overlapping between the average curve and the confidence interval curves. The trend of the μ curve is the same as before, decreasing with the increasing of the DN values.

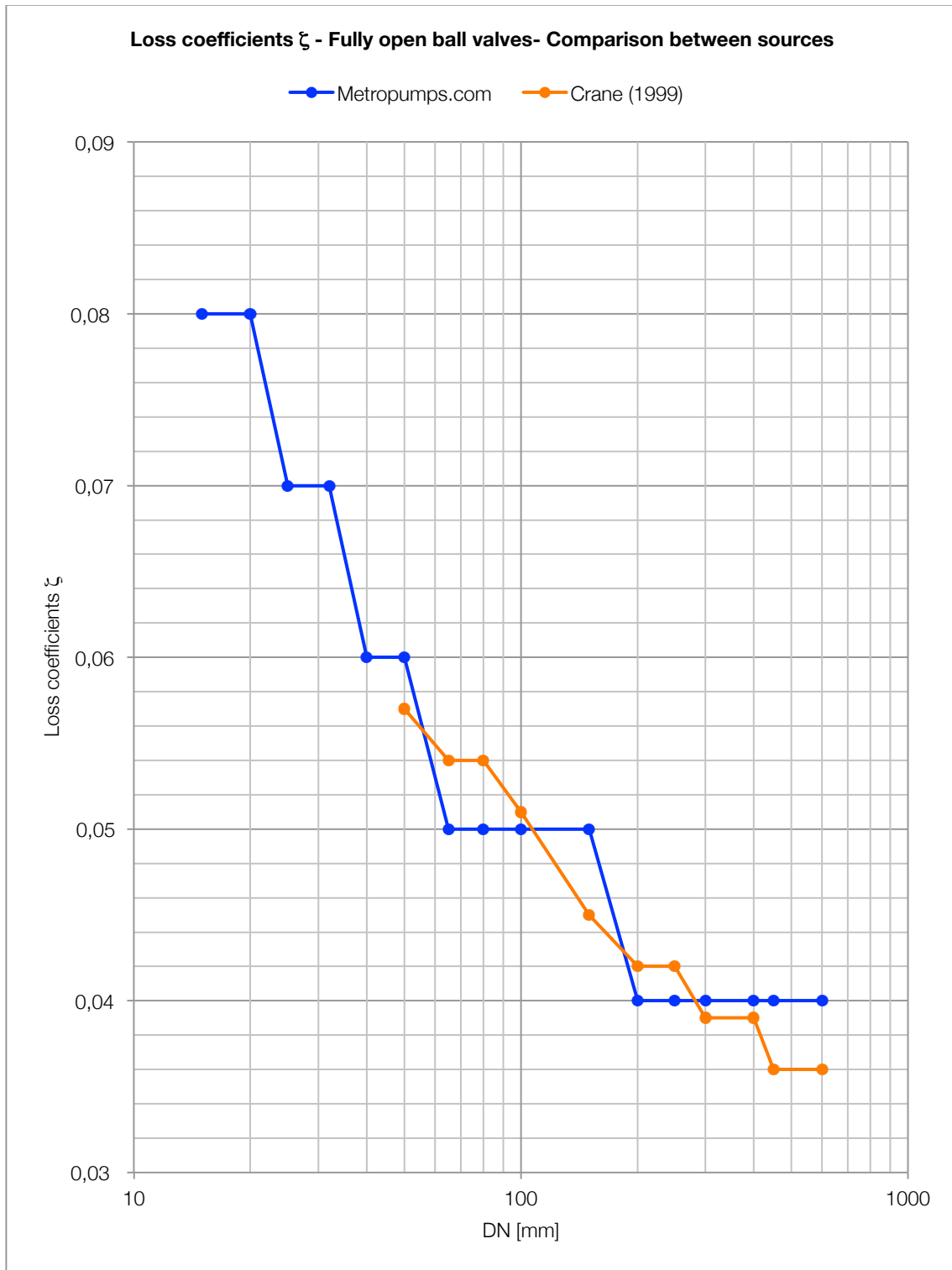
In the Graph 31 is presented the trend line obtained for cylindrical pattern valve which is made from a power equation model, as for the other pattern of plug valve. Again, the very regular trend of the head loss values fits almost perfectly with the power trend line plotted and the extremely high value of R^2 is the confirm of this fact: it is possible to create a very good fit curve this equation model without committing sensible errors.

In Table 21 are presented the other parameters useful to the statistical interpretation: the arithmetic mean of average values μ_A , the arithmetic mean of the standard deviations μ_{SD} and the standard deviation of the mean values σ_M .

As for the tapered pattern, looking at the value of μ_A it is possible to say that it is very reduced, and it is even the 30% of the tapered valve pattern and so it is confirmed that the valve is a low-resistance valve. The value of σ_M is very reduced too and it means that the μ_A is very similar to the other μ values and so, from a practical point of view, it is possible to use the μ_A value independently from the diameter chosen, without without committing a sensible error (from the hydraulic point of view).

The zero value of the arithmetic mean of the standard deviations μ_{SD} states that, for all the range of DN, it is possible to neglect it and so the μ values are reliable. This is not what was expected but a good confirm from the practical point of view.

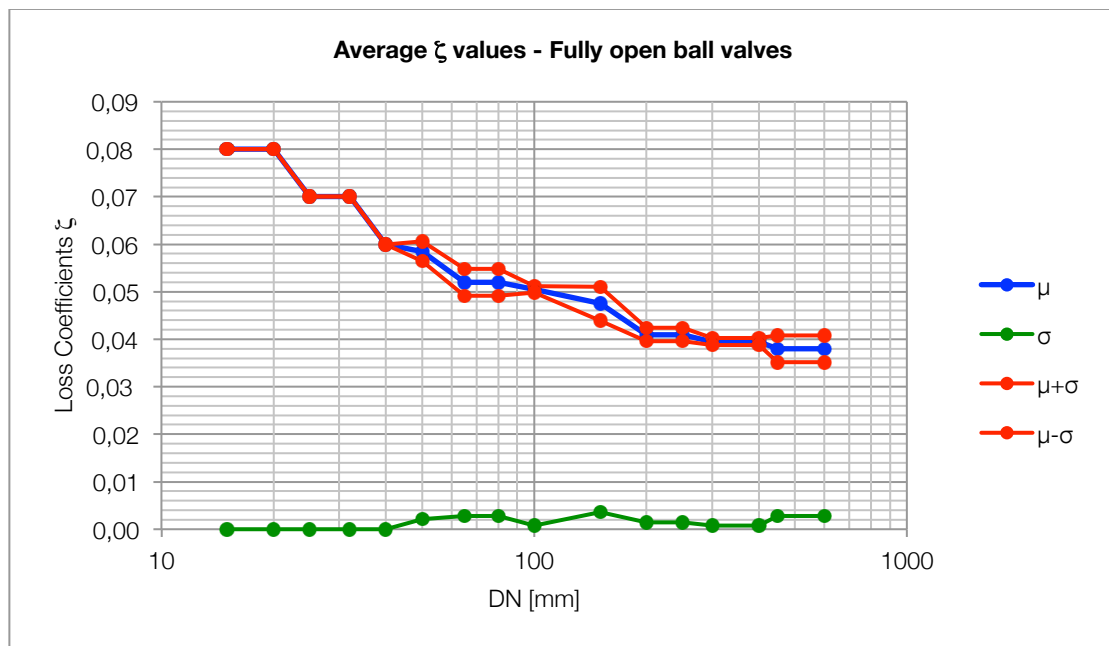
15.2.5 Ball valves



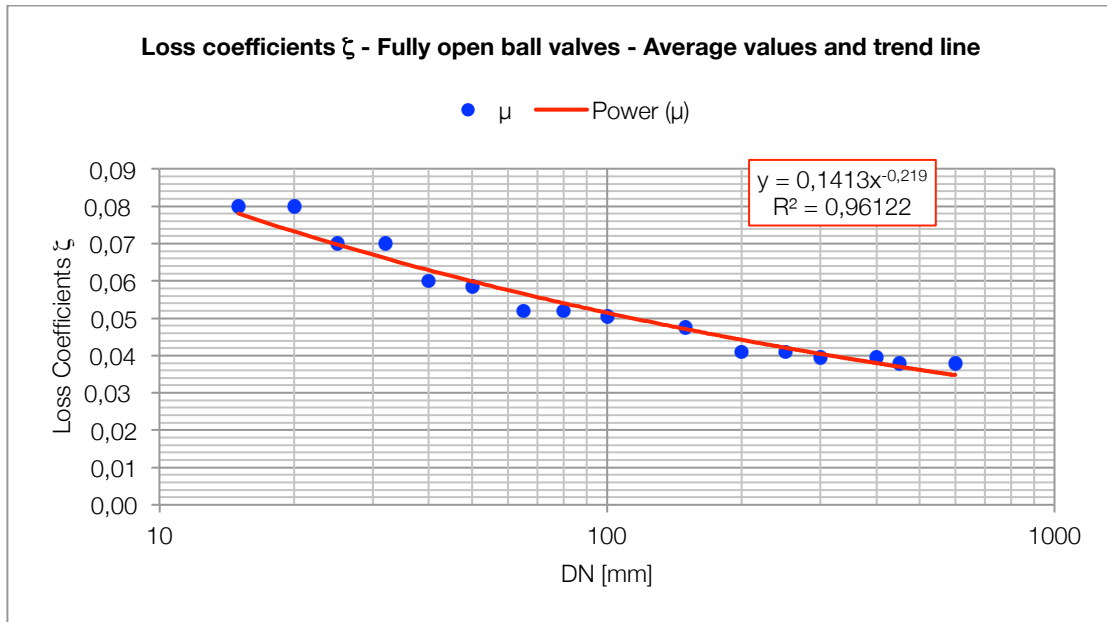
Graph 32: loss coefficients ζ for fully open ball valves - comparison between sources

Table 22: average ζ values for fully open ball valves

DN [mm]	μ	σ	$\mu+\sigma$	$\mu-\sigma$
15	0,08	0,0000	0,0800	0,0800
20	0,08	0,0000	0,0800	0,0800
25	0,07	0,0000	0,0700	0,0700
32	0,07	0,0000	0,0700	0,0700
40	0,06	0,0000	0,0600	0,0600
50	0,06	0,0021	0,0606	0,0564
65	0,05	0,0028	0,0548	0,0492
80	0,05	0,0028	0,0548	0,0492
100	0,05	0,0007	0,0512	0,0498
150	0,05	0,0035	0,0510	0,0440
200	0,04	0,0014	0,0424	0,0396
250	0,04	0,0014	0,0424	0,0396
300	0,04	0,0007	0,0402	0,0388
400	0,04	0,0007	0,0402	0,0388
450	0,04	0,0028	0,0408	0,0352
600	0,04	0,0028	0,0408	0,0352



Graph 33: average ζ values for fully open ball valves



Graph 34: average values ζ and trend-line y for fully open ball valves

Table 23: statistical parameters for fully open ball valves

Trend-line equation:	$y = 0,1413 \cdot DN^{-0,219}$
Coefficient of determination	$R^2 = 0,96122$
Arithmetic mean of average values	$\mu_A = 0,05$
Arithmetic mean of the standard deviations	$\mu_{SD} = 0,00$
Standard deviation of the mean values	$\sigma_M = 0,01$

Comments

In the Graph 32 are plotted the data found in the two sources for ball valves. even if there is not a perfect overlapping as for the plug valves (all the patterns), it is possible to say that there's a very congruent trend of the head loss coefficient ζ lines. The trend is decreasing with the increasing of the diameters, a confirmation of what it is expected from the theoretical approach. From both sources there are stretches of the curves which are practically plane: this means that the same head loss coefficients is used for different diameters and this could be the result of using the same valve at different diameters with different flanges. The aspect which hits is the fact that both of the sources presents very low coefficients: the range is from 0,03 to 0,08. This implies that the ball valve is a very low resistance valve. The range of nominal diameters DN considered is from 15 mm to 600 mm.

In the Table 22 and in the Graph 33 are plotted the average values μ of the head loss coefficients ζ , the standard deviation σ and the confidence interval obtained for this valve. The trend is again decreasing with the nominal diameters, as expected from the Graph 32. The values found for the standard deviation are really low if compared to the average values of the curve μ : the most noticeable value of the standard deviation is the 0,035 corresponding to DN 150. For this DN the loss coefficient is 0,05 and the standard deviation is the 7% of this value. The first consequence of this fact is that the confidence interval is very close to the average curve μ . The second consequence of this graph is that the values are really reliable and the average trend of the line is very similar to the trend of the single sources lines.

In the Graph 34 is presented the trend line obtained for fully open ball valves. The equation model chosen in this case is the power model which, looking at the high value of R^2 (0,96122) is a very good fitting of the average data computed: it is possible to use practically the fitting curve without committing sensible errors.

In Table 23 are presented the other parameters useful to the statistical interpretation: the arithmetic mean of average values μ_A , the arithmetic mean of the standard deviations μ_{SD} and the standard deviation of the mean values σ_M .

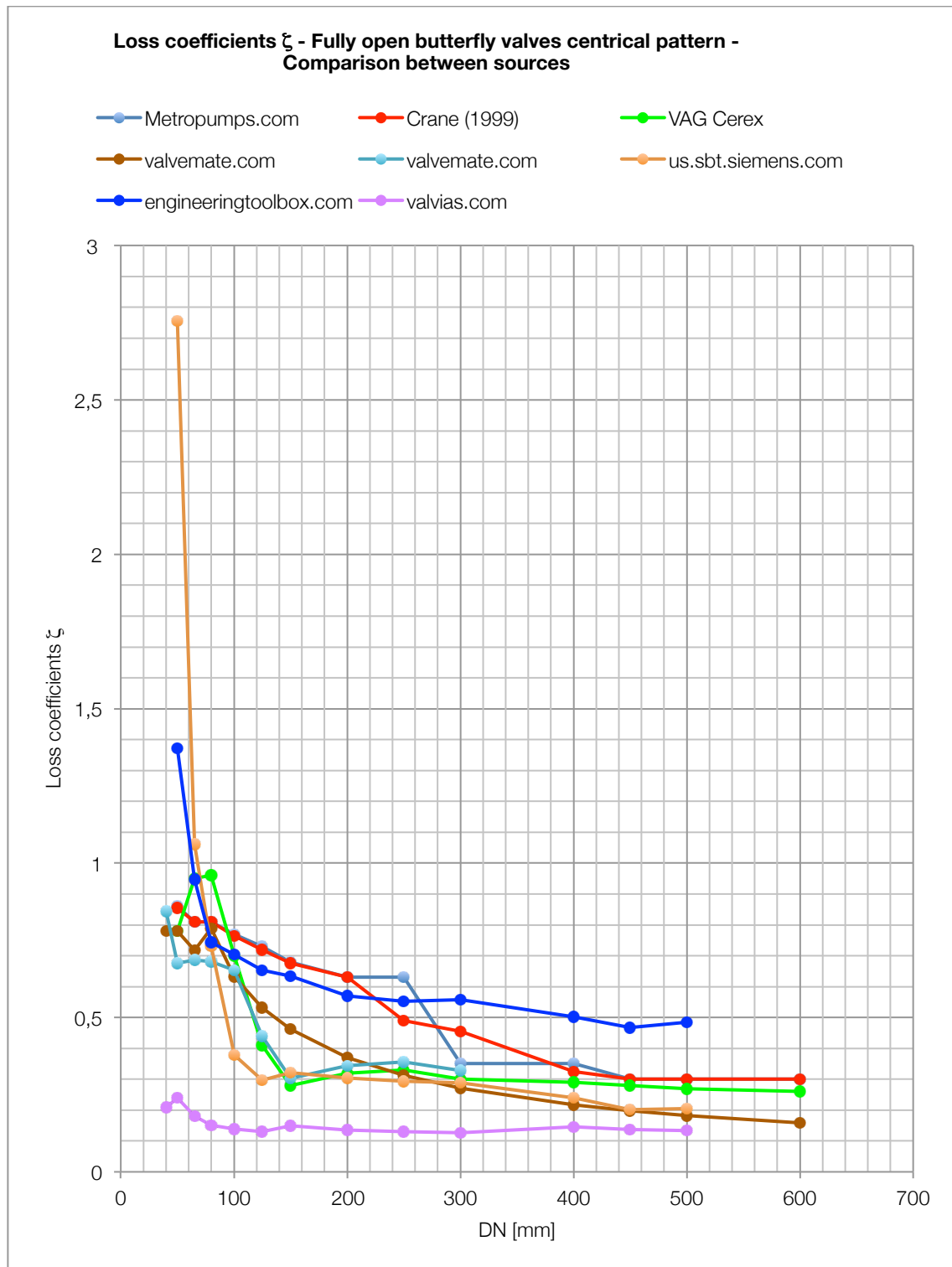
As for the plug valves, looking at the value of μ_A it is possible to say that it is very reduced and so it is confirmed that the valve is a very low-resistance valve. The value of σ_M practically zero and this means that there's almost no difference in using the parameter μ_A instead of the μ calculated with the trend line or the one of the curve.

The zero value of the arithmetic mean of the standard deviations μ_{SD} states that, for all the range of DN, it is possible to neglect it and so the μ values are reliable. This is not what was expected but a good confirm from the practical point of view.

In general another observation which can be made is that the trend lines, the average values, the trend of the curves and the statistical parameters of the ball valves are very similar to the plug valves. This is what it is expected from the theoretical approach because the head loss coefficients in valves have great dependence on geometrical factors and inside shapes of the components and plug valves and ball valves are very similar from all of these points of view: the functioning is the same, the approach to the flow is the same and the geometrical aspects are very similar.

15.2.6 Butterfly valves

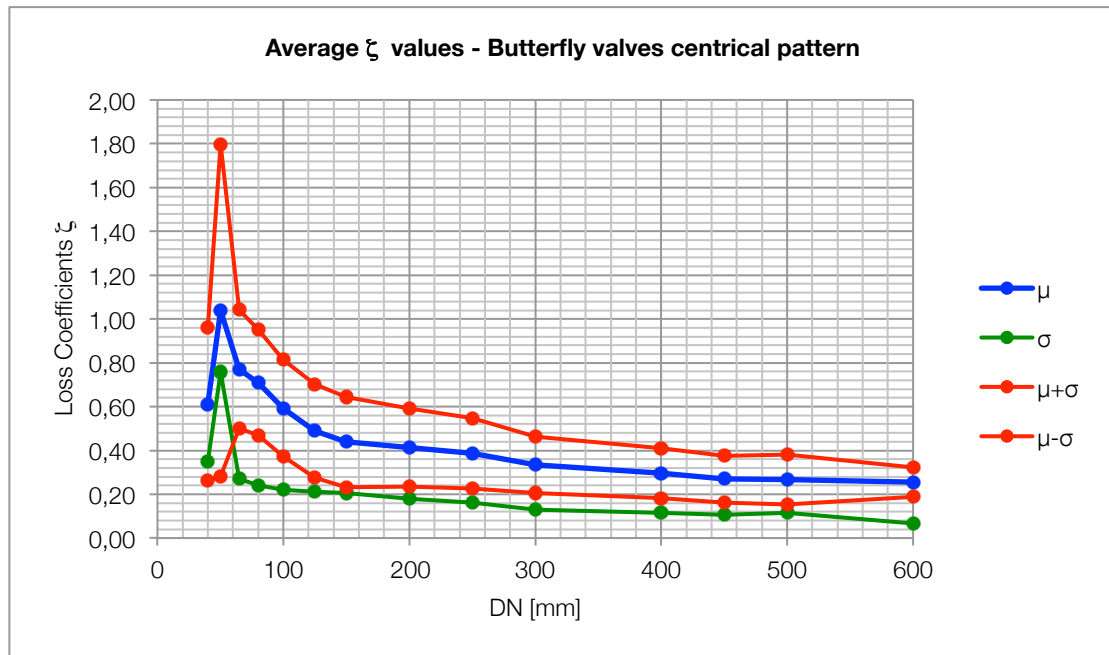
15.2.6.1 Fully open (central pattern)



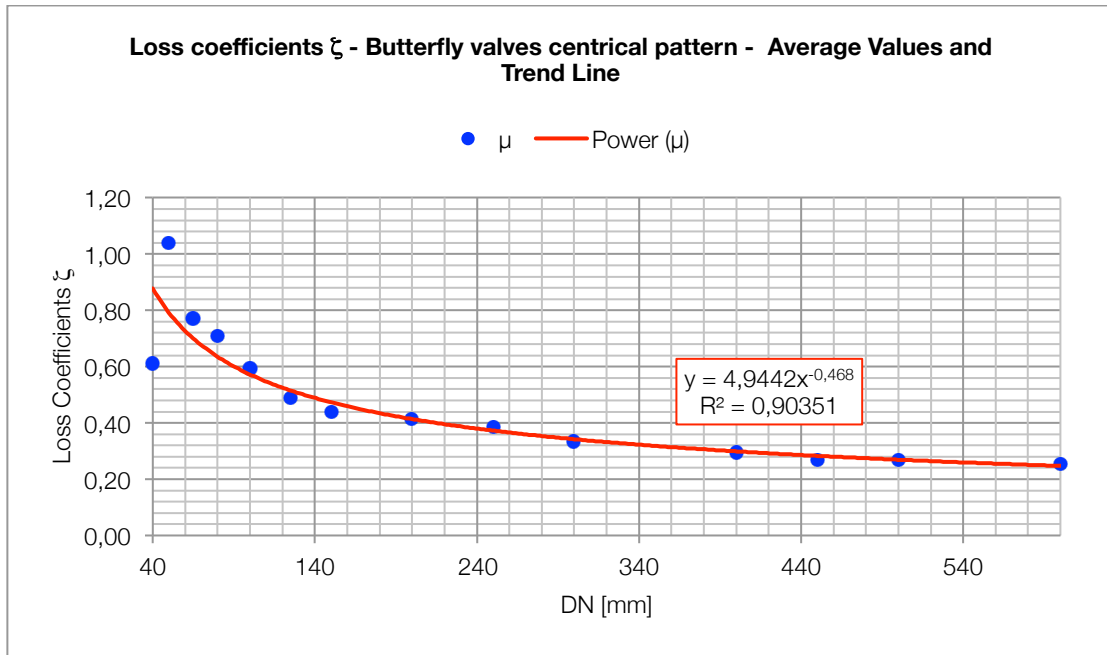
Graph 35: loss coefficients ζ for fully open butterfly valves (central pattern) - comparison between sources

Table 24: average ζ values for fully open butterfly valves (central pattern)

DN [mm]	μ	σ	$\mu+\sigma$	$\mu-\sigma$
40	0,61	0,3500	0,9607	0,2607
50	1,04	0,7587	1,7986	0,2812
65	0,77	0,2698	1,0401	0,5004
80	0,71	0,2402	0,9498	0,4694
100	0,59	0,2211	0,8138	0,3717
125	0,49	0,2121	0,7011	0,2769
150	0,44	0,2051	0,6433	0,2330
200	0,41	0,1786	0,5916	0,2344
250	0,39	0,1609	0,5477	0,2260
300	0,33	0,1286	0,4630	0,2059
400	0,30	0,1138	0,4096	0,1819
450	0,27	0,1070	0,3759	0,1620
500	0,27	0,1145	0,3825	0,1535
600	0,25	0,0667	0,3214	0,1879



Graph 36: average ζ values for fully open butterfly valves (central pattern)



Graph 37: average values ζ and trend-line y for fully open butterfly valves (central pattern)

Table 25: statistical parameters for fully open butterfly valves (central pattern)

Trend-line equation:	$y = 4,9442 \cdot DN^{-0,468}$
Coefficient of determination	$R^2 = 0,90351$
Arithmetic mean of average values	$\mu_A = 0,49$
Arithmetic mean of the standard deviations	$\mu_{SD} = 0,22$
Standard deviation of the mean values	$\sigma_M = 0,23$

Comments

In the Graph 35 are plotted the data found from all the sources used for central butterfly valves in fully open position. The amount of data is noticeable and comparable to the other two most important valve's patterns (gate and globe) analyzed in the paper. It is immediately recognizable a trend which all the curves have: the head loss coefficient values ζ are decreasing with the increasing of the nominal diameter value DN.

It is evident that there are two sources which present data that are definitely out of the middle range of the others: us.sbt.siemens.com present the highest value (2,75) of

the graph and the website valvias.com plot a curve which is very low compared to the others. Excluding these two sources the range of the head loss coefficients is enclosed between the values 0,15 and 1,38 which put the butterfly valve in the category of the low resistance valves. the range of nominal diameters DN analyzed is from 40 mm to 600 mm.

In the Table 24 and in the Graph 36 are plotted the average values μ of the head loss coefficients ζ , the standard deviation σ and the confidence interval obtained for this valve. The trend is again decreasing with the nominal diameters, as expected from the Graph 35. This trend is respected except for one value, corresponding to the DN 50: for this DN the μ value is 1,04 which is an increase looking at the 0,61 found for DN 40. This “anomaly” is caused by the head loss coefficient corresponding to DN 50 from the source us.sbt.siemens.com which increase definitely the trend of the curve.

The values found for the standard deviation σ can be compared to the average values of the curve μ as graphically confirmed. For example in the DN 500 the value of the average head loss coefficient μ is 0,27 and the standard deviation corresponding is 0,1145 which is the 42% of the value.

This is a consequence of different factors: the great amount of data, the great amount of different manufacturing models of this valve type and the evolution of the technology associated makes the data really spreading between themselves and the reliability is affected.

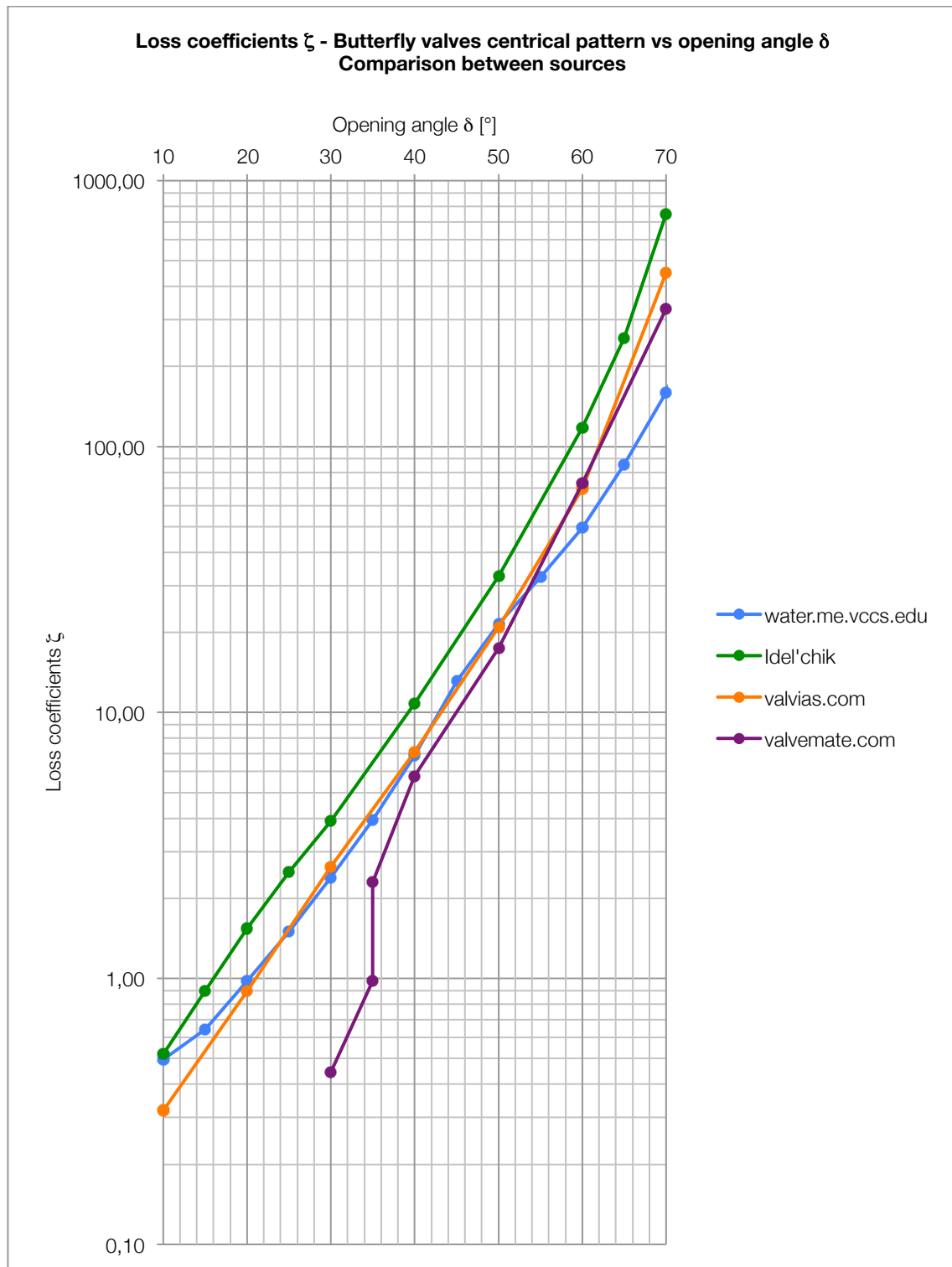
In the Graph 37 is presented the trend line obtained for fully open butterfly valves. The equation model chosen in this case is the power model which, looking at the high value of R^2 (0,90351) is a very good fitting of the average data computed: it is possible to use practically the fitting curve without committing sensible errors.

In Table 25 are presented the other parameters useful to the statistical interpretation: the arithmetic mean of average values μ_A , the arithmetic mean of the standard deviations μ_{SD} and the standard deviation of the mean values σ_M .

The value of μ_A tells that the impact in a flow of a butterfly valve is higher for example than the plug valves or ball valves but it is not so high. The value of σ_M is not negligible, representing almost the 50% of the μ value. This fact means that there is a sensible difference using the parameter μ_A instead of the μ calculated with the trend line or the one of the curve $\mu(DN)$.

The 0,22 value of the arithmetic mean of the standard deviations μ_{SD} states that, for all the range of DN, μ values are not very reliable and it is necessary to make further analysis to select the correct values of the head loss coefficients.

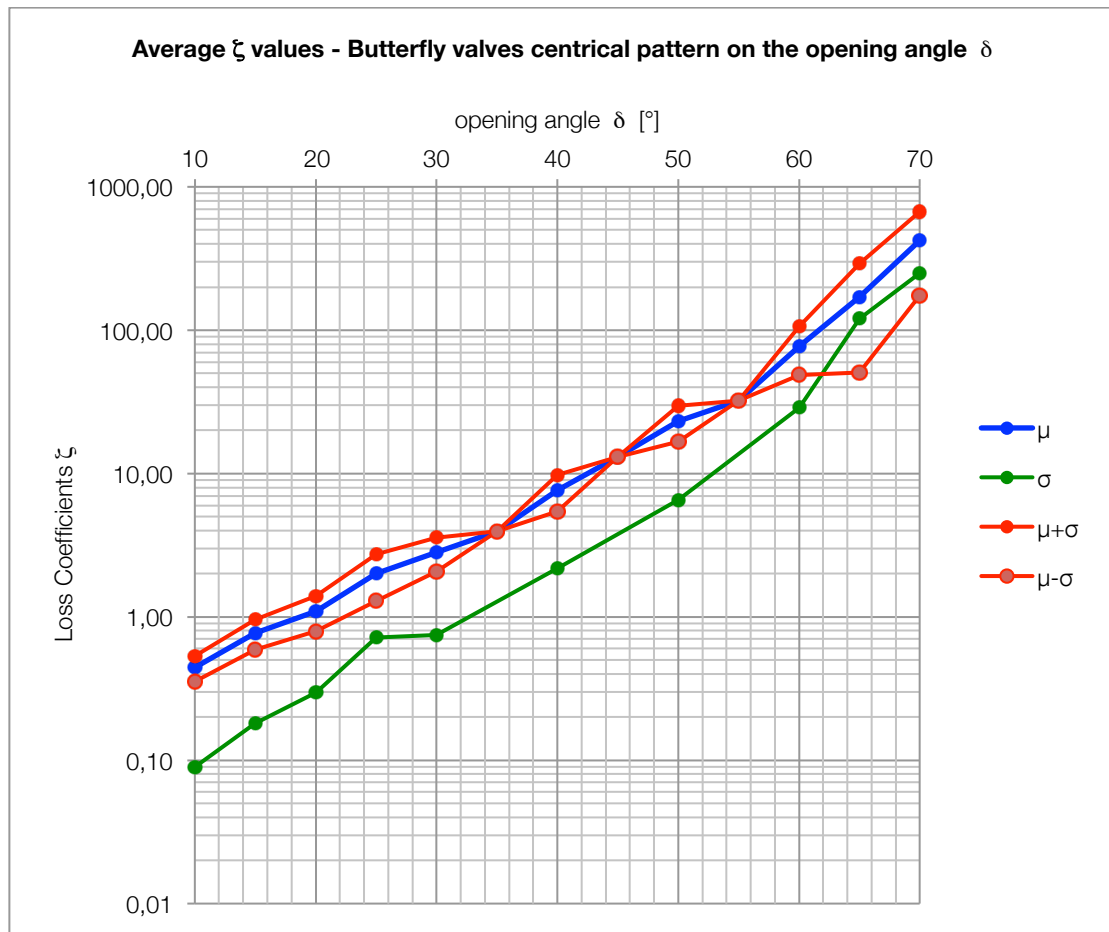
15.2.6.2 Opening angle δ (central pattern)



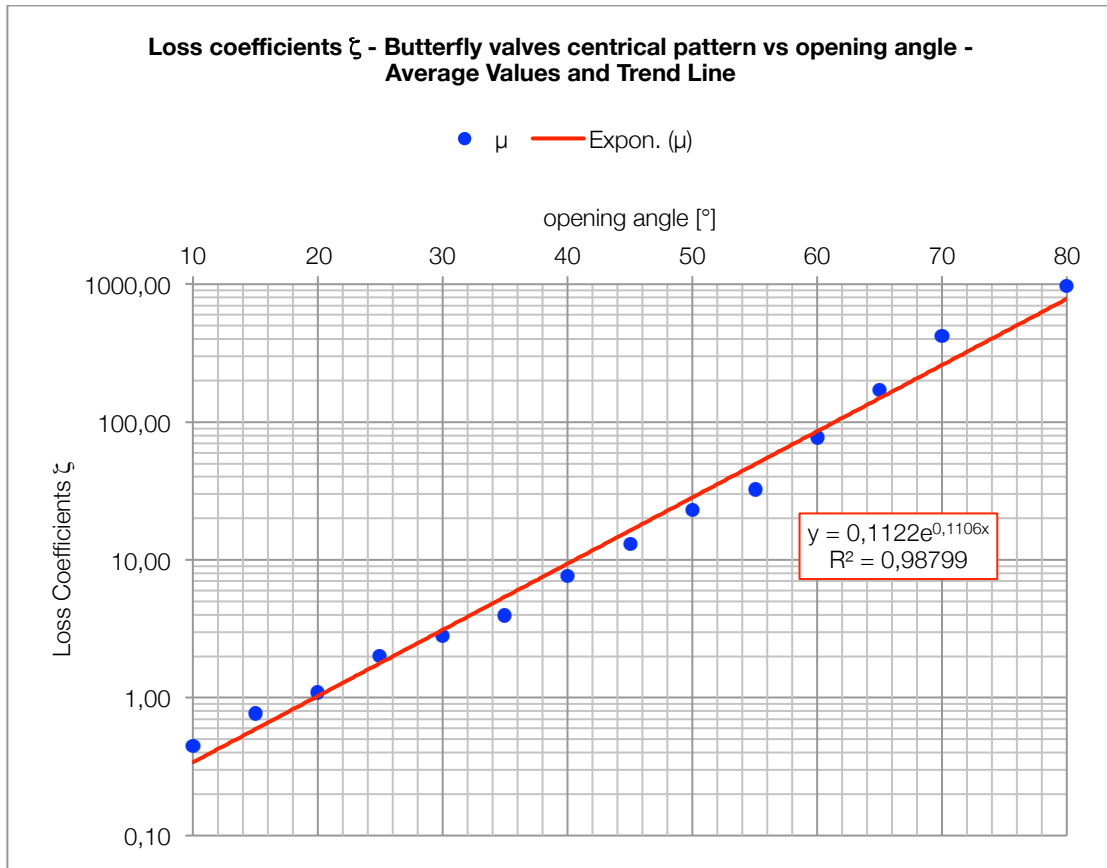
Graph 38: loss coefficients ζ for butterfly valves (central pattern) on the opening angle δ - comparison between sources

Table 26: average ζ values for butterfly valves (central pattern) on the opening angle δ

δ [°]	μ	σ	$\mu+\sigma$	$\mu-\sigma$
80	976,00	0,0000	976	976
70	422,95	249,0813	672	173,87
65	170,85	120,4203	291	50,43
60	77,52	28,8824	106,4	48,64
55	32,30	0,0000	32,30	32,30
50	23,16	6,5381	29,70	16,63
45	13,10	0,0000	13,10	13,10
40	7,64	2,1866	9,828	5,455
35	3,94	0,0000	3,940	3,940
30	2,81	0,7467	3,556	2,062
25	2,01	0,7142	2,719	1,291
20	1,10	0,2977	1,395	0,799
15	0,77	0,1810	0,953	0,591
10	0,44	0,0898	0,534	0,354



Graph 39: average ζ values for butterfly valves (central pattern) on the opening angle δ



Graph 40: average values ζ and trend-line y for butterfly valves (central pattern) against the opening angle δ

Table 27: statistical parameters for fully open butterfly valves (central pattern)

Trend-line equation:	$y = 0,1122 \cdot e^{0,1106DN}$
Coefficient of determination	$R^2 = 0,98799$

Comments

For the butterfly valves it is performed an additional statistical comparing analysis, similar to the one done for fully open valves, but depending on the opening angle δ .

In the Graph 38 are plotted the head loss coefficients data found from all the sources used for central butterfly valves against the opening angle. It is obviously recognizable a common trend: the more the opening angle is high the more the head loss coefficients are high.

The range of the opening angle is from 10° to 70° . This choice derives from some considerations: a smaller value of the opening angle brings to coefficients practically equal to the fully open ones and higher angles causes head losses too high to be compared exactly.

The range of the head loss is really high because the closing of the shut-off member of the butterfly valves causes great amount of turbulences and, consequently, great energy loss.

In the Table 26 and in the Graph 39 are plotted the average values μ of the head loss coefficients ζ , the standard deviation σ and the confidence interval obtained for this valve. The trend is obviously the same as the single sources, increasing with the opening angle value. There's a lot of spread between the low angle coefficients and the high angle coefficient: in the range $10^\circ \div 70^\circ$ there is a difference of three orders of magnitude.

The standard deviation values are really high and increasing with the opening angle, except for the values corresponding to DN 55, DN 45 and DN 35, for which there's only one availability of sources and so the standard deviation is obviously zero.

In the Graph 40 is plotted the trend line obtained for fully open butterfly valves. The equation model chosen in this case is the exponential model which is obviously graphically straight in the logarithmic scale of the Graph 40.

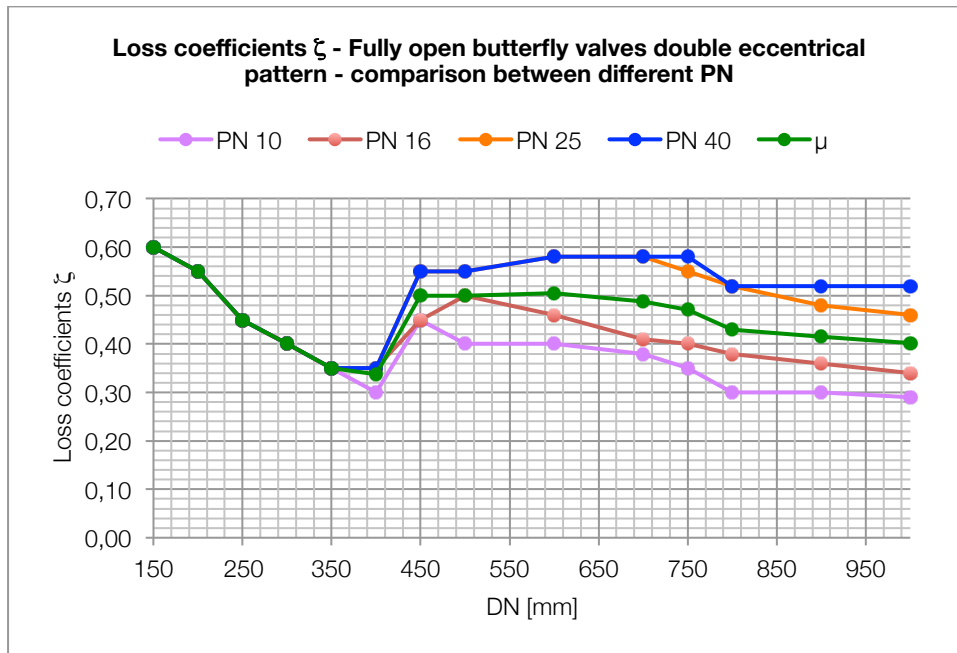
The value of the coefficient of determination is really high, $R^2=0,98799$, and this is the confirmation that the exponential is a very good fitting of the average data computed.

Obviously there is no sense in computing the arithmetic mean of average values μ_A , the arithmetic mean of the standard deviations μ_{SD} and the standard deviation of the mean values σ_M : comparison can be made only between the same angles and a parameter which means all the angles is no-sense.

15.2.6.3 Comparison between central and double eccentric pattern (VAG)

Table 28: loss coefficients ζ for fully open butterfly valve double eccentric pattern

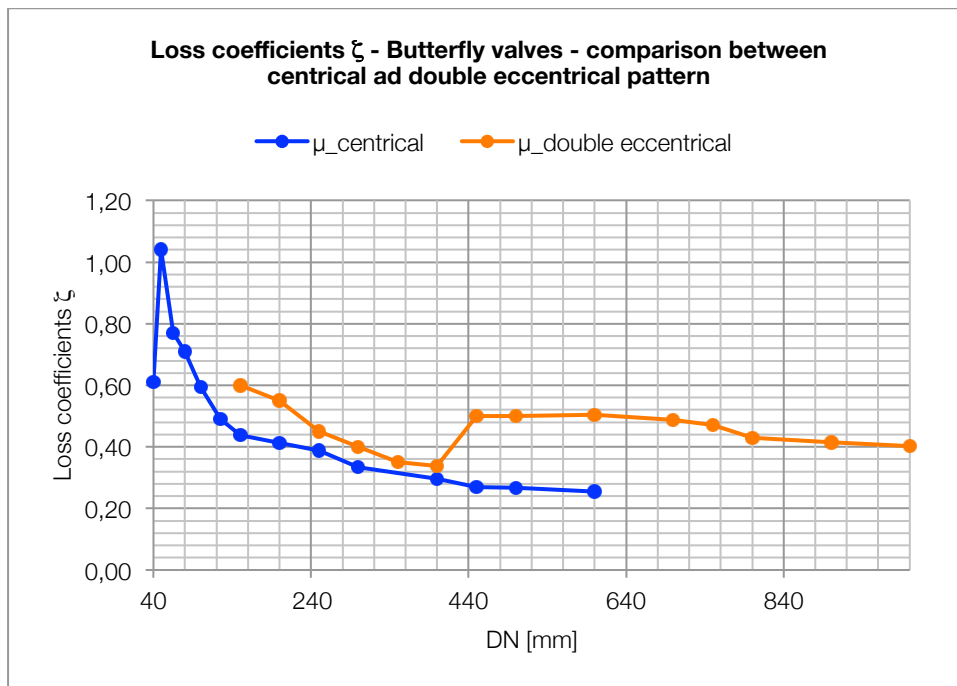
DN [mm]	PN 10	PN 16	PN 25	PN 40	μ double eccentric
150	0,60	0,60	0,60	0,60	0,60
200	0,55	0,55	0,55	0,55	0,55
250	0,45	0,45	0,45	0,45	0,45
300	0,40	0,40	0,40	0,40	0,40
350	0,35	0,35	0,35	0,35	0,35
400	0,30	0,35	0,35	0,35	0,34
450	0,45	0,45	0,55	0,55	0,50
500	0,40	0,50	0,55	0,55	0,50
600	0,40	0,46	0,58	0,58	0,51
700	0,38	0,41	0,58	0,58	0,49
750	0,35	0,40	0,55	0,58	0,43
800	0,30	0,38	0,52	0,52	0,43
900	0,30	0,36	0,48	0,52	0,42
1000	0,29	0,34	0,46	0,52	0,40



Graph 41: loss coefficients ζ for fully open butterfly valve double eccentric pattern at different PN

Table 29: comparison between loss coefficients ζ for central model and double eccentric model and percentage differences at same DN

DN [mm]	μ central	DN [mm]	μ double eccentric	DN [mm]	η
40	0,61	150	0,60	150	36,94%
50	1,04	200	0,55	200	33,16%
65	0,77	250	0,45	250	16,33%
80	0,71	300	0,40	300	19,61%
100	0,59	350	0,35	400	14,10%
125	0,49	400	0,34	450	14,10%
150	0,44	450	0,50	500	85,89%
200	0,41	500	0,50	600	86,59%
250	0,39	600	0,51	700	98,30%
300	0,33	700	0,49		
400	0,30	750	0,47		
450	0,27	800	0,43		
500	0,27	900	0,42		
600	0,25	1000	0,40		



Graph 42: comparison between loss coefficients ζ for central model and double eccentric model

Comments

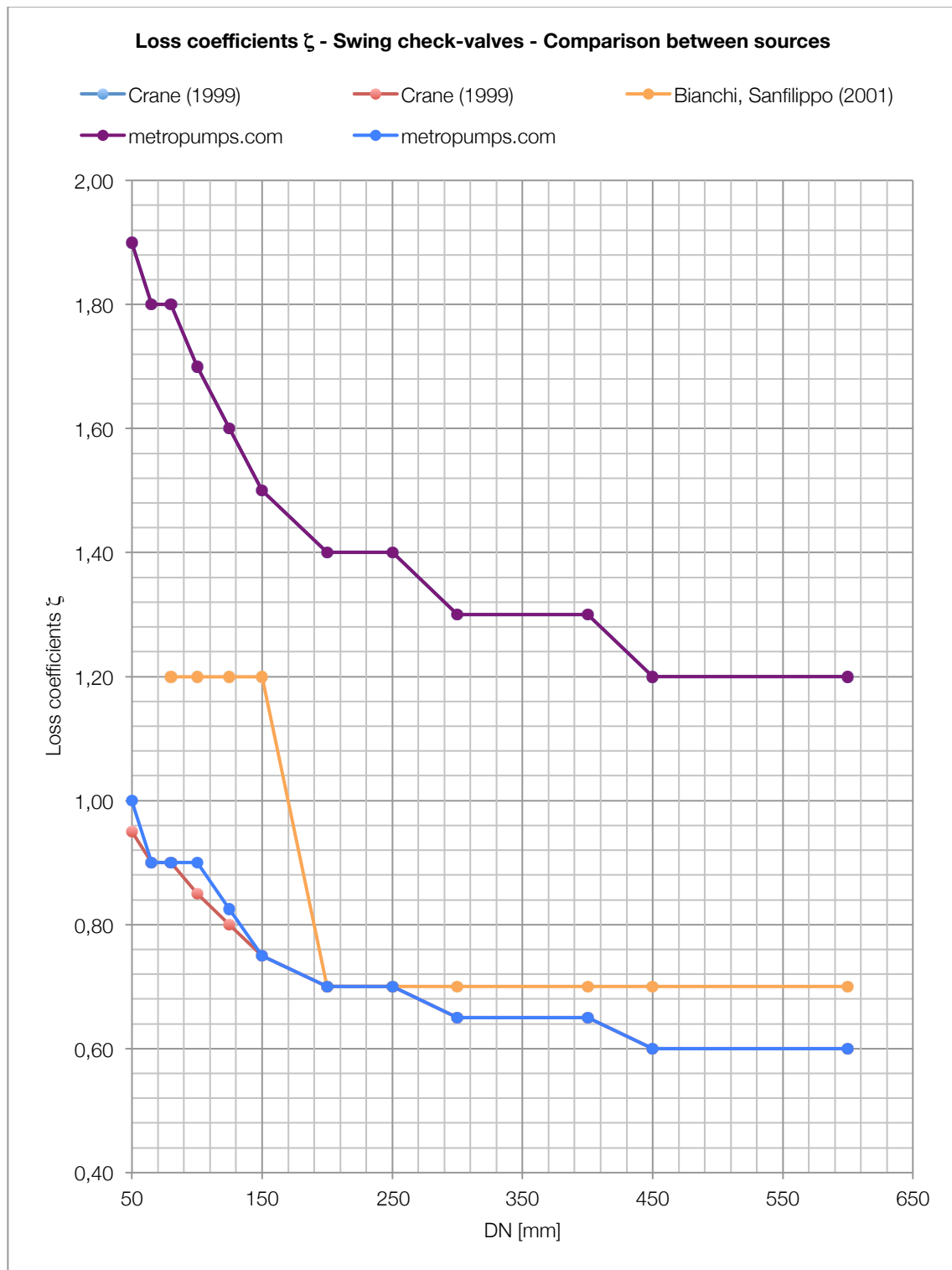
A very interesting comparison can be made for butterfly valve, between fully open central patterns and double eccentric patterns. The data of the double eccentric pattern are available thanks to the VAG data sheet which plot the head loss curves for different PN, depending on the nominal diameter values DN.

In Table 28 and in the Graph 41 are plotted all the different values of the head loss coefficients for different PN of the double eccentric pattern of the valve and there's also the mean value curve μ associated computed on this data. The trend of this curve is really curious because there is a decreasing with the increasing of the diameters till the value of DN 400, then a rapid increasing and then again a substantial constant value of the head losses. The range of the nominal diameters considered is the same as it is found in VAG data sheets, from 150 mm to 1000 mm and the head losses are always included between 0,60 and 0,29 values.

In Table 29 and in the Graph 42 is plotted the comparison between the average curve μ obtained for the central pattern and the curve μ obtained for the double eccentric pattern. The trend, in the first part of the double eccentric curve, from DN 150 to DN 300 is very similar and decreasing with the increasing of the DN values. The two curves are substantially parallel, and the double eccentric one is sensibly higher than the central: the percentage differences η between the two models in this stretch are equal to the 15% more or less. From the DN 500 there is an abrupt increasing of the percentage differences η between the two curves, a consequence of the abrupt increasing of the double eccentric μ curve: here the differences are equal to the 85% more or less.

The conclusions of this comparison is that the double eccentric pattern has a sensibly higher impact on the flow in terms of head losses. This difference has to be taken in account in the preliminary step of a design work because can imply money losses. On the other hand, as specified in the relative chapter, the double eccentric pattern could bring great advantages in terms of durability and so economic benefits. This two factors has to be compared in design phase.

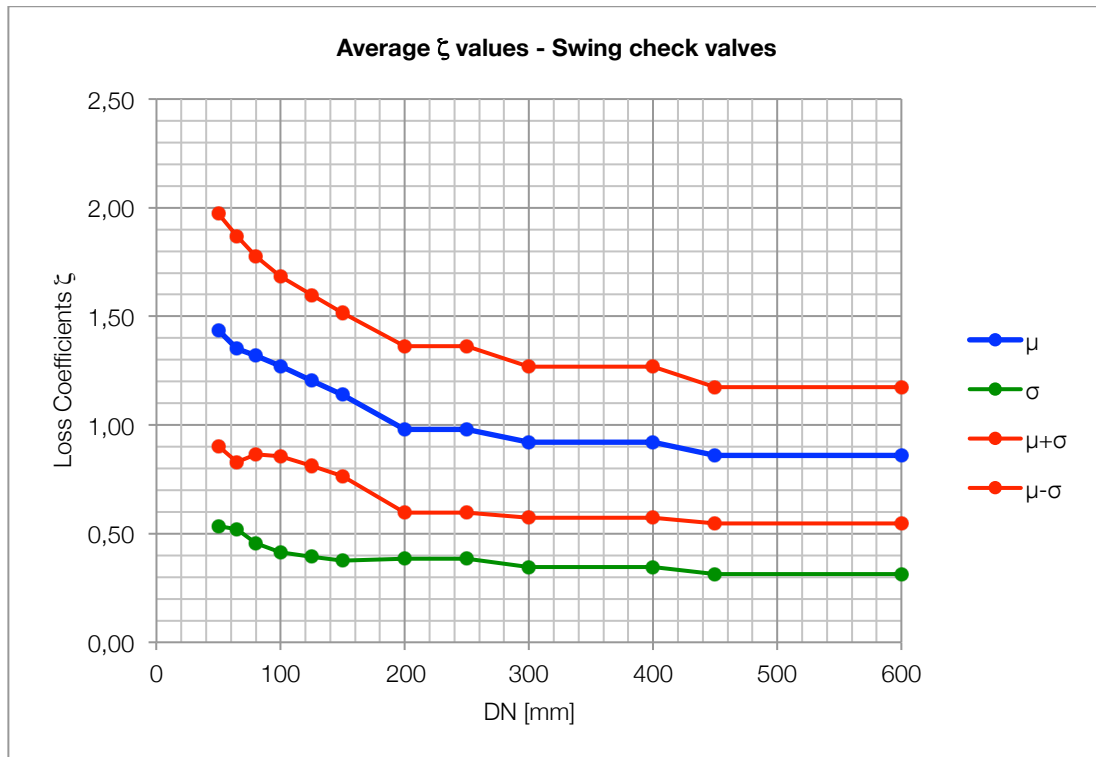
15.2.7 Swing check valves



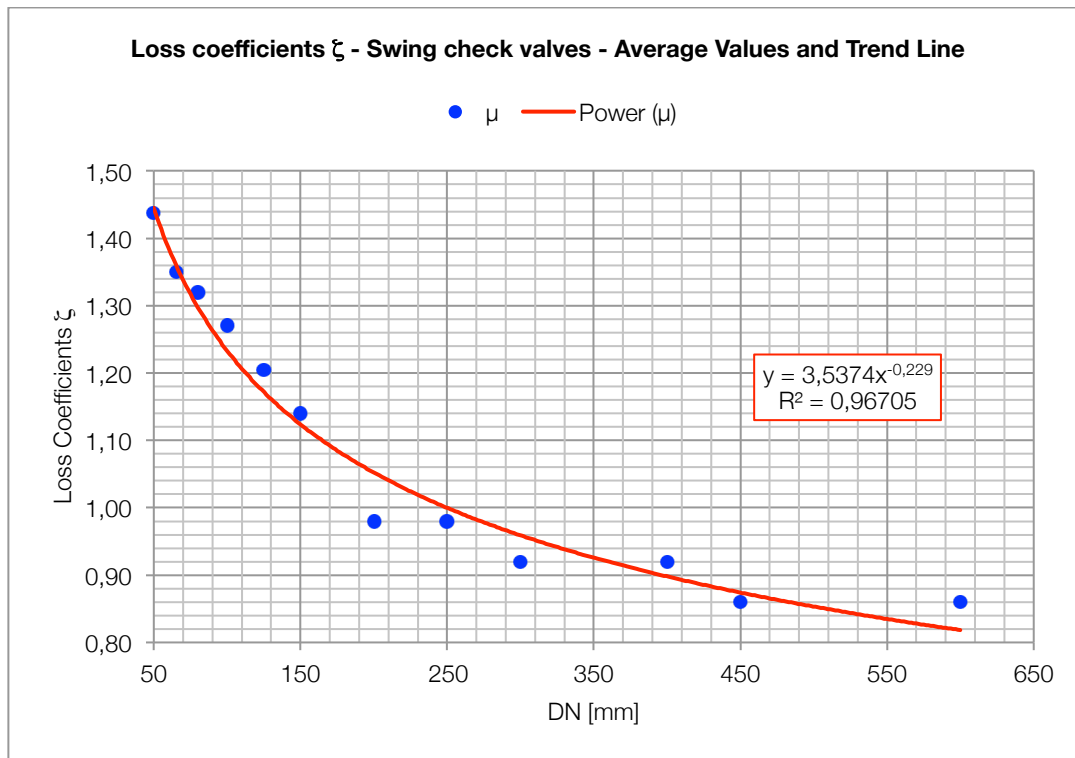
Graph 43: loss coefficients ζ for fully open swing check valves - comparison between sources

Table 30: average ζ values for swing check valves

DN [mm]	μ	σ	$\mu+\sigma$	$\mu-\sigma$
50	1,44	0,5344	1,9719	0,9031
65	1,35	0,5196	1,8696	0,8304
80	1,32	0,4550	1,7750	0,8650
100	1,27	0,4147	1,6847	0,8553
125	1,21	0,3939	1,5989	0,8111
150	1,14	0,3765	1,5165	0,7635
200	0,98	0,3834	1,3634	0,5966
250	0,98	0,3834	1,3634	0,5966
300	0,92	0,3475	1,2675	0,5725
400	0,92	0,3475	1,2675	0,5725
450	0,86	0,3130	1,1730	0,5470
600	0,86	0,3130	1,1730	0,5470



Graph 44: average ζ values for swing check valves



Graph 45: average values ζ and trend-line y for swing check valves

Table 31: statistical parameters for swing check valves

Trend-line equation:	$y = 3,5374 \cdot DN^{-0,229}$
Coefficient of determination	$R^2 = 0,96705$
Arithmetic mean of average values	$\mu_A = 1,00$
Arithmetic mean of the standard deviations	$\mu_{SD} = 0,34$
Standard deviation of the mean values	$\sigma_M = 0,32$

Comments

In the Graph 43 are plotted the head loss coefficient values founded for the swing check-valves depending on the nominal diameter DN. The trend of all the sources is perfectly evident: the head loss coefficients are decreasing with the increasing of the nominal diameter values for all the sources.

The metropumps.com source plots a series of data that are sensibly higher than the others, but the other data are extremely similar, with a lot of overlapping situations.

In all sources there are stretches of the curves which are practically plane: this means that the same head loss coefficients is used for different diameters and this could be the result of using the same valve at different diameters with different flanges.

The range of the nominal diameters considered is from 50 mm to 600 mm and for these diameters the range of head loss coefficients is enclosed from 0,60 (for high diameter values) to 1,90 (for low diameter values).

In the Table 30 and in the Graph 44 are plotted the average values μ of the head loss coefficients ζ , the standard deviation σ and the confidence interval obtained for this valve. The trend of the average curve μ is again decreasing with the nominal diameters, as expected from the Graph 43. The values found for the standard deviation are sensibly low if compared to the average values of the curve μ and there's a little bit decreasing with the increasing of the diameter values. But the rate of this decreasing is very low and the consequence of this is that the confidence interval is practically parallel to the average curve μ . The standard deviation values are enclosed from 0,5344 to 0,3130 corresponding to DN 50 and DN 600. These values represent the 37% and the 36% of the corresponding average value, respectively. This means that the value cannot be negligible but at the same the reliability of the average data is safe.

In the Graph 45 is presented the trend line obtained for fully open swing check valves. The trend of the average value curve μ suggests that the perfect fitting equation model is the power. In fact looking at the high value of R^2 (0,96705) there is the confirmation of the good fitting of the average data computed: it is possible to use practically the fitting curve without committing sensible errors.

In Table 31 are presented the other parameters useful to the statistical interpretation: the arithmetic mean of average values μ_A , the arithmetic mean of the standard deviations μ_{SD} and the standard deviation of the mean values σ_M .

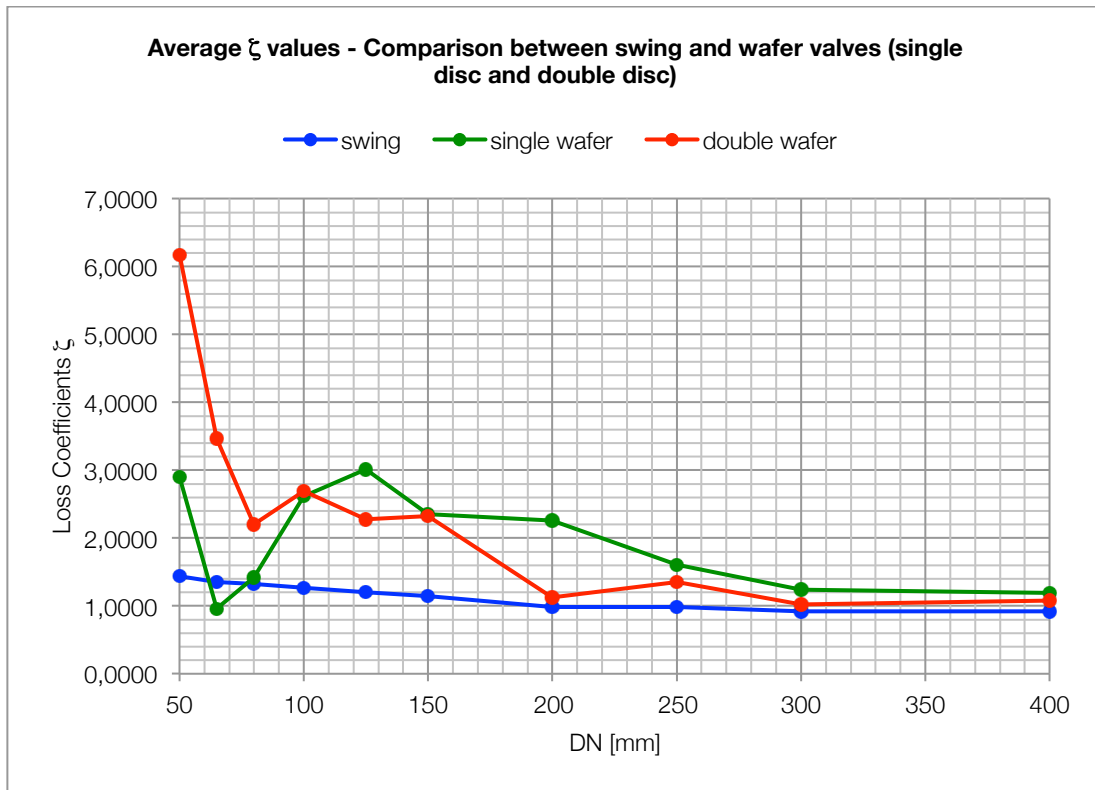
The value of σ_M is 0,32 and means that there's a sensible difference in using the parameter μ_A instead of the μ calculated with the trend line or the one of the curve.

The value of the arithmetic mean of the standard deviations μ_{SD} is very similar to the σ_M and, as stated before, it confirms the quite good reliability of the average data μ .

15.2.7.1 Comparisons between swing check valves and wafer check-valves (single and double pattern)

Table 32: comparison between average ζ values for swing check valves, single wafer check valves and double wafer check valves

DN [mm]	ζ values		
	Swing-check valves	single wafer	double wafer
50	1,44	2,90	6,17
65	1,35	0,96	3,47
80	1,32	1,42	2,2
100	1,27	2,62	2,69
125	1,21	3,01	2,28
150	1,14	2,35	2,32
200	0,98	2,26	1,13
250	0,98	1,61	1,35
300	0,92	1,24	1,02
400	0,92	1,19	1,08



Graph 46: comparison between average ζ values for swing check valves, single wafer check valves and double wafer check valves

Comments

The swing check-valves and the wafer check-valves can both be considered as butterfly valves with an extreme eccentrical closure member. This fact can suggest that a comparison between their loss coefficient values could be a good issue.

From the functional point of view, the two valves are practically the same: the shut-off member of both valves, rotates on a pivot fixed on the high wall of the valve.

The noticeable difference between the two valve patterns is represented by the dimension of the body: the swing's one is bigger, while the wafer is reduced.

The comparison is made also with the double wafer valve, which has a different rotation moving of the closure member but is considered in the same field of application.

The Graph 46 plots the head loss coefficient values for the three valve pattern. In particular, the range of values for the three pattern is the following table (Table 33):

Table 33: comparison between ranges of different plug valve's patterns

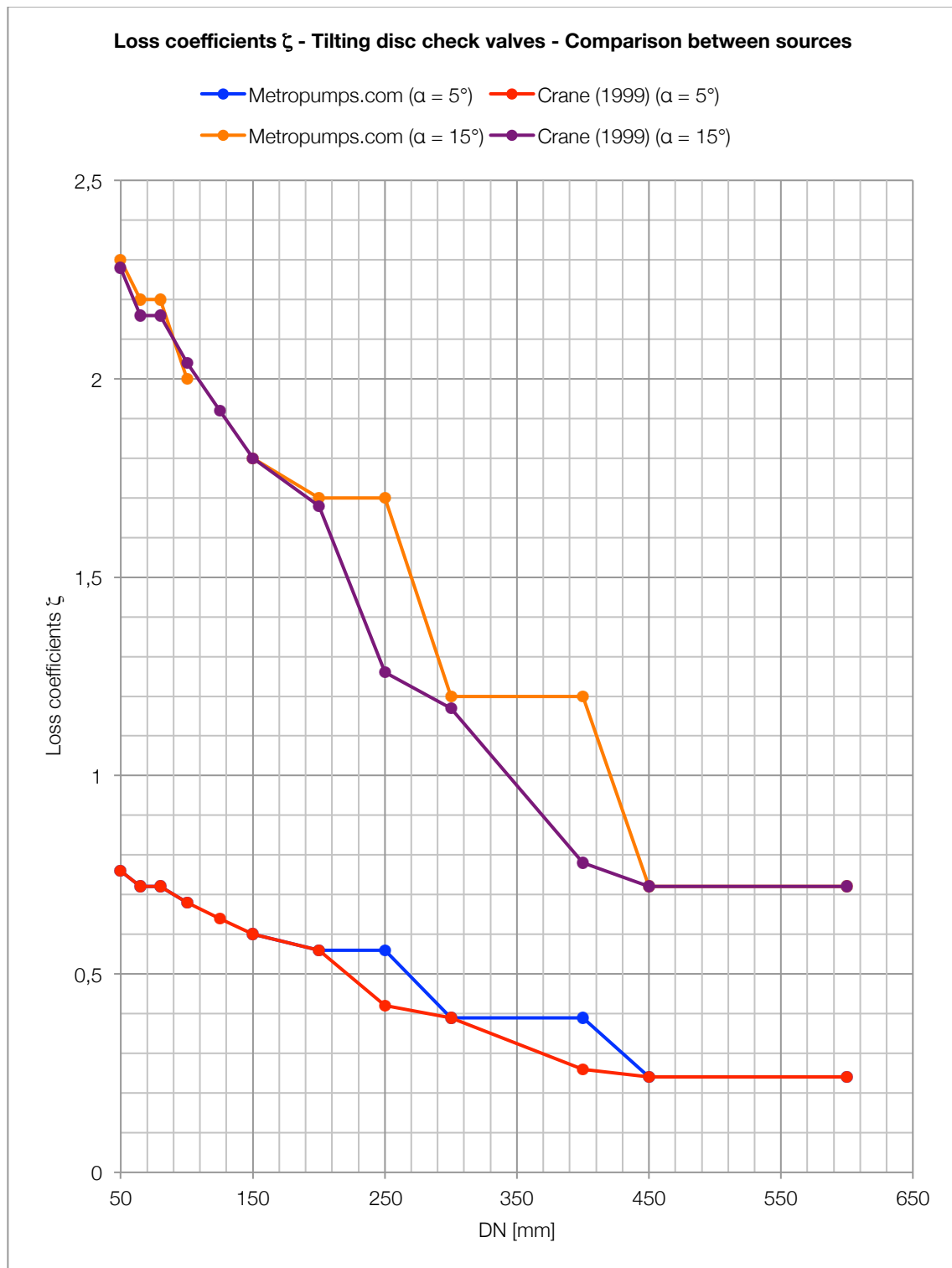
<i>Valve pattern</i>	<i>Range of values</i>
Swing-check	0,92 ÷ 1,44
Single wafer	1,19 ÷ 3,01
Double wafer	1,08 ÷ 6,17

It is clear that the trend of three pattern is the same: increasing with the decreasing of the diameter values. However, there are differences between the models:

- the double wafer has a wider range of values considering the same range of DN;
- the trend of the swing check valves is nearly constant (though decreasing) and lower than the others;
- in the wafer trends there is an increasing of the values for DN 125, an “anomaly” towards the rest of the graph;

Nevertheless, for high nominal diameter values the head loss coefficient are quite similar and there are overlapping situations for DN 100, DN 150 and DN 200.

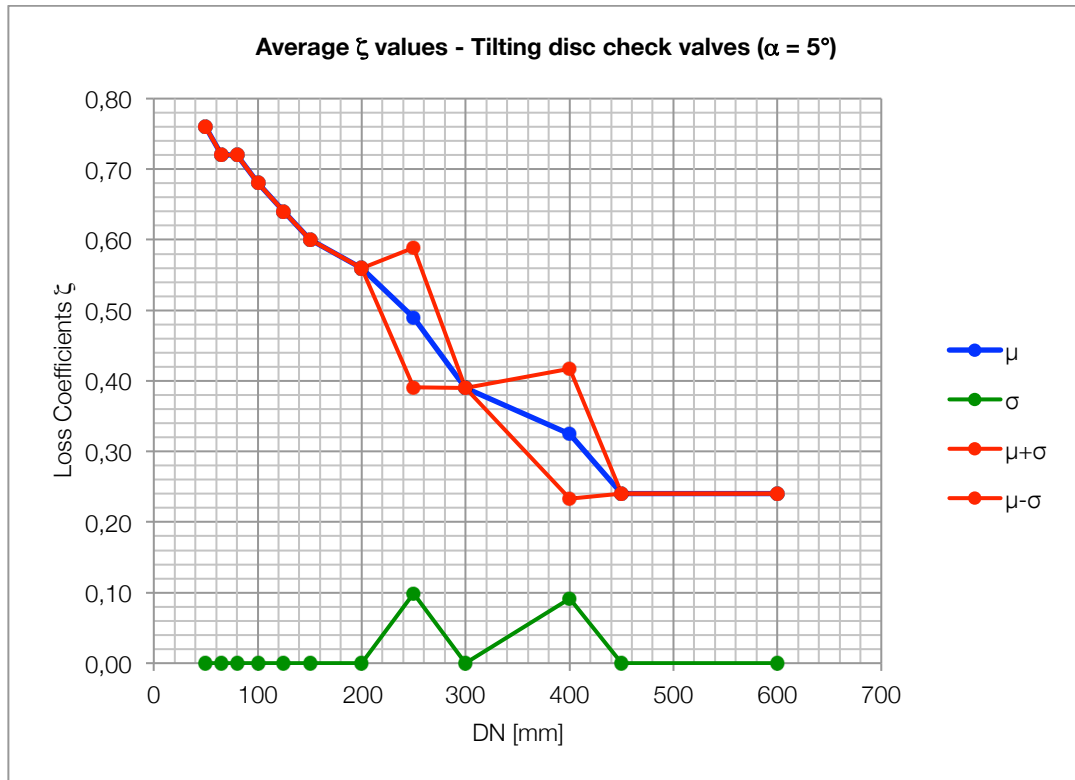
15.2.8 Tilting disc check valves



Graph 47: loss coefficients ζ for tilting disc check valves - comparison between sources

Table 34: average ζ values for tilting disc check valves ($\alpha = 5^\circ$)

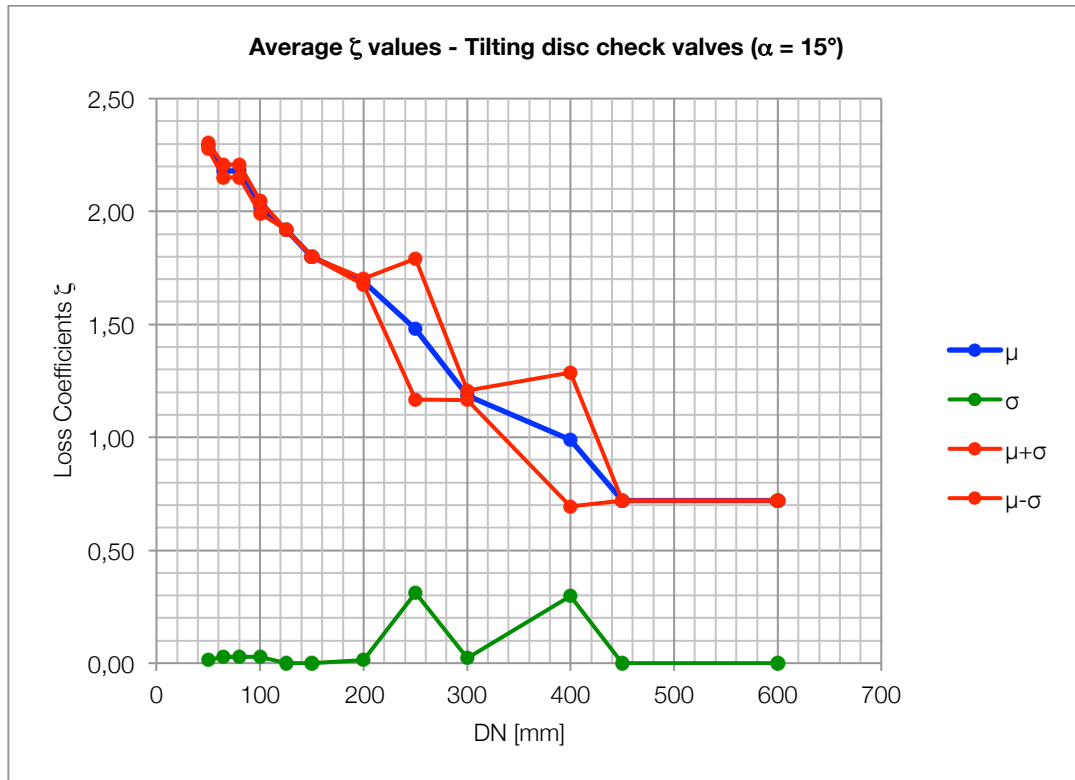
DN [mm]	μ	σ	$\mu + \sigma$
50	0,76	0,0000	0,7600
65	0,72	0,0000	0,7200
80	0,72	0,0000	0,7200
100	0,68	0,0000	0,6800
125	0,64	0,0000	0,6400
150	0,60	0,0000	0,6000
200	0,56	0,0000	0,5600
250	0,49	0,0990	0,5890
300	0,39	0,0000	0,3900
400	0,33	0,0919	0,4169
450	0,24	0,0000	0,2400
600	0,24	0,0000	0,2400



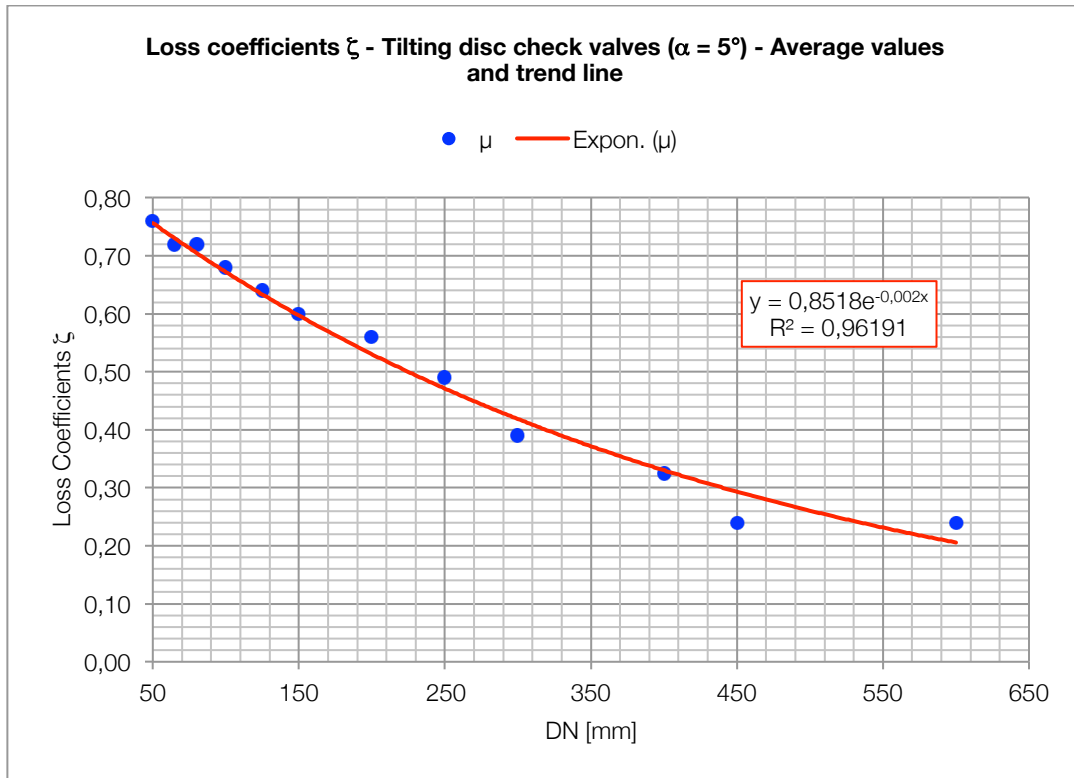
Graph 48: average ζ values for tilting disc check valves ($\alpha = 5^\circ$)

Table 35: average ζ values for tilting disc check valves ($\alpha = 15^\circ$)

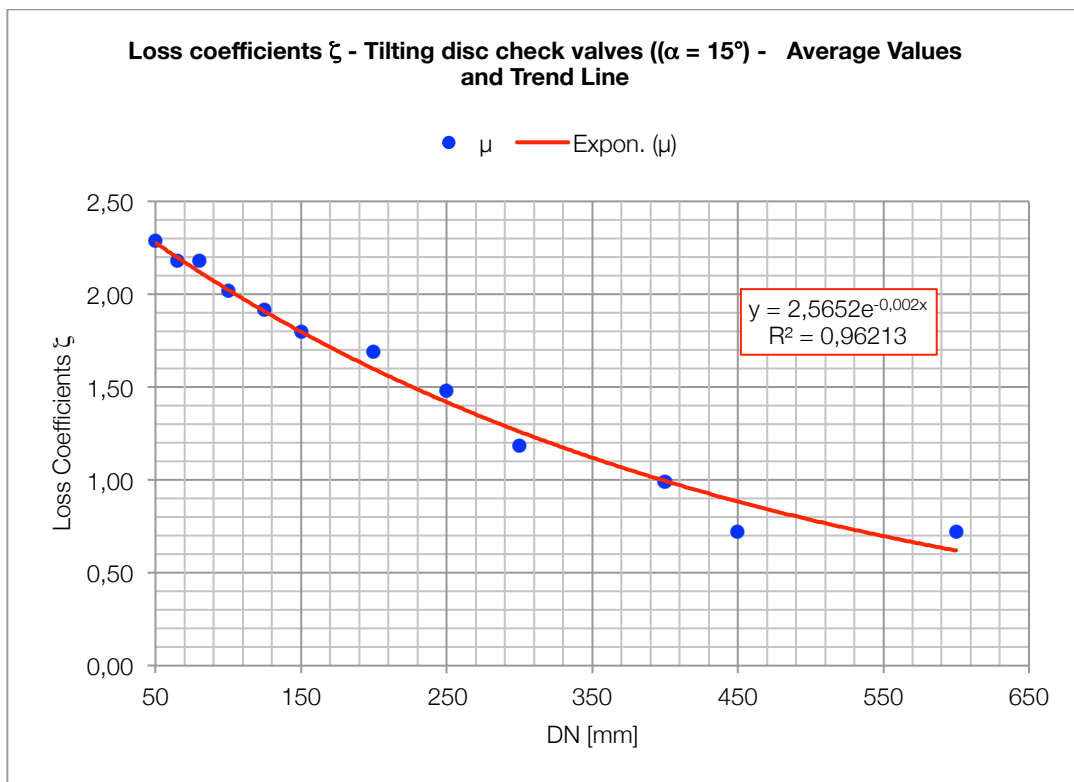
DN [mm]	μ	σ	$\mu + \sigma$
50	2,29	0,0141	2,3041
65	2,18	0,0283	2,2083
80	2,18	0,0283	2,2083
100	2,02	0,0283	2,0483
125	1,92	0,0000	1,9200
150	1,80	0,0000	1,8000
200	1,69	0,0141	1,7041
250	1,48	0,3111	1,7911
300	1,19	0,0212	1,2062
400	0,99	0,2970	1,2870
450	0,72	0,0000	0,7200
600	0,72	0,0000	0,7200



Graph 49: average ζ values for tilting disc check valves ($\alpha = 15^\circ$)



Graph 50: average values ζ and trend-line y for tilting disc check valves ($\alpha = 5^\circ$)



Graph 51: average values ζ and trend-line y for tilting disc check valves ($\alpha = 15^\circ$)

Table 36: statistical parameters for tilting-disc check valves

	$\alpha = 5^\circ$	$\alpha = 15^\circ$
Trend-line equation:	$y = 0,8518 \cdot e^{-0,002DN}$	$y = 2,5652 \cdot e^{-0,002DN}$
Coefficient of determination	$R^2 = 0,96191$	$R^2 = 0,96213$
Arithmetic mean of average values	$\mu_A = 0,53$	$\mu_A = 1,60$
Arithmetic mean of the standard deviations	$\mu_{SD} = 0,02$	$\mu_{SD} = 0,06$
Standard deviation of the mean values	$\sigma_M = 0,19$	$\sigma_M = 0,57$

Comments

In the Graph 47 are plotted the head loss coefficient trends for both of the opening of the tilting disc check valves: α equal to 5° and 15° .

In both of the opening and for both of the sources, the trend is very regular and decreasing with the increasing of the nominal diameter values. As expected, the trends of the $\alpha=15^\circ$ are higher than $\alpha=5^\circ$.

The differences between the sources are extremely reduced, in fact there's an almost perfect overlapping for all the point in the Graph 47. The only sensible differences are concentrated in the values corresponding to the DN 250 and DN 400. In both cases the metropumps.com website plots higher values than Crane (Crane, 1999). These values are equal to the corresponding ones found for the previous diameter (DN 300). This fact can suggest that in the metropumps.com site is considered the same valve although the nominal diameter is different.

The range of nominal diameters considered is enclosed from DN 50 to DN 600 and the head loss range of values is $0,24 \div 0,76$ for $\alpha=5^\circ$ and $0,72 \div 2,29$ for $\alpha=15^\circ$.

In the Table 34, in the Graph 48 and in the Table 35 and in the Graph 49 are plotted the average values μ of the head loss coefficients ζ , the standard deviation σ and the confidence interval respectively for $\alpha=5^\circ$ and $\alpha=15^\circ$. The trend of the average curve μ is again decreasing with the nominal diameters, as expected from the Graph 47. The values found for the standard deviation are extremely low if compared to the average values of the curve μ and this fact is the consequence of the overlapping seen in Graph 47. The only two noticeable values of σ are 0,09 and 0,09 for $\alpha=5^\circ$, 0,31 and 0,29 for $\alpha=15^\circ$ corresponding to DN 250 and DN 400 respectively

as expected. The other values are almost completely negligible, although the σ values for $\alpha=15^\circ$ are higher than the $\alpha=5^\circ$ values.

In the Graph 50 and in the Graph 51 are presented the trend lines obtained for $\alpha=5^\circ$ and for $\alpha=15^\circ$ for the tilting disc check valves. The trends of both of the average curves μ suggest that the perfect fitting equation model is the exponential. In fact looking at the high value of R^2 for both of the curves (for $\alpha=5^\circ$, $R^2=0,96191$ and for $\alpha=15^\circ$, $R^2=0,96213$) there is the confirmation of the good fitting of the average data computed: it is possible to use practically the fitting curve without committing sensible errors.

In Table 36 are presented the other parameters useful to the statistical interpretation: the arithmetic mean of average values μ_A , the arithmetic mean of the standard deviations μ_{SD} and the standard deviation of the mean values σ_M for both of the α values.

The value of the arithmetic mean of the standard deviations μ_{SD} is very similar in both of the α values and is very low as expected: they confirm the quite good reliability of the average data μ .

The value of σ_M is very different between the two models and this means that there's a sensible difference in using the parameter μ_A instead of the μ calculated with the trend line or the one of the curve.

15.3 Future developments

In this paragraph are collected all the aspects that, in the opinion of the author, can be the objects of future developments.

In the introductory chapters are explained all the limitation caused by the arbitrary choices of the author or by the context in which the sources (literature and websites) were created. One of the aspect that can be improved in this sense is the collection of a larger amount of data: the number of sources considered can be improved and extended, in order to have more points of view and a better estimate of the curves founded by comparison for the valves.

This comparative analysis, which is executed only on the valve chapter because of the requests, can be made for all the devices quoted in the paper: it can be so interesting to have a comparative analysis also for the other fittings, in order to understand the reliability of the literature and website data as for the valves.

The hydraulic engineering, which is the field of application of this paper, in particular the control of pressure, is a place of continuous technological innovation. It could be interesting to use the same approach used in this paper in order to estimate the improvements brought by the new technologies in the field of head losses and in the uncertainty associated with them.

Another point which can be developed is the equation models used in the comparison between data: in the present paper the program used for the analysis is Microsoft Excel but can be executed with other softwares which can be more “open” in order to interfere in the equation models. Insisting on this point it is possible to use other statistical parameters which can estimate better the precision of the data and the accuracy of the equation models used.

This paper provides all the tools necessary to make all the comparisons also between different types of valve. In the paper, except for the swing check valves compared with the wafer patterns, the only comparisons executed are made between different sources but on the same valve’s pattern. If the head losses are the most important factor in the design of a piping system, it is possible to use this paper to compare the head losses of different valve’s type in order to choose the most fitting.

Another important need that a design stage has is the economical aspect: the minimization of the disbursements and the maximization of the earnings is often the most important boost in the planning stage.

As stated in the introductory chapter, in a piping system, head losses mean money losses and this is why the head loss coefficient of a fitting has to be as accurate as possible. This paper is born in order to supply to this need and can be furthermore developed in order to provide the tools to make the correct choices in the initial stage of the project.

For example, starting from the statistical parameters found for the valves, it is possible to have a rough estimation of the economic uncertainty connected with the hydraulic uncertainty of the head losses.

It could be very important also to have an experimental confirm of the data collected in this paper: all the equation models and all the data computed in the paper can be experimentally confirmed or disproved but in both cases it is important to have an experimental reply.

Bibliography

Literature

AA:VV.: “Manuale dell’ingegnere”, 82a edizione, U. Hoepli editore, 1990.

Ballio F., Guadagnini A., Larcan E., Malavasi S., Orsi E., Riva M.: “note del corso di Idraulica”, Politecnico di Milano.

Ballio F., Guadagnini A., Malavasi S., Orsi E., Riva M.: “note degli insegnamenti di: Meccanica dei Fluidi I – parte G: Correnti”, Politecnico di Milano.

Bianchi A., Sanfilippo U.: “Pompe e impianti di sollevamento”, Hoepli, 2001.

Citrini D., Nosedà G.: “Idraulica”, seconda edizione, Casa Editrice Ambrosiana, 1987.

Crane CO.: “Flow of Fluids through valves, fittings and pipe, Metric Edition - SI Units”, Crane Co., 1999.

Del Toro A.: “Computational fluid dynamics analysis of butterfly valve performance factors”, Utah State University, 2012.

EN 736-1: “Valves – Terminology – Part 1: Definition of types of valves”, 1995.

Fischer: “Control valve sourcebook”, Emerson process management, 2004.

I.E. Idel’chik: “Handbook of hydraulic resistance – Coefficients of local resistance and friction”, Israel Program for Scientific Translations Ltd., 1966.

KSB Italia S.p.A.: “Formazione Tecnica Valvole”, 2004.

Malavasi S.: “note del corso di Meccanica dei Fluidi– Moto nelle condotte in pressione”, Politecnico di Milano, 1999.

Miller S. Donald: “Internal Flow - A guide to losses in pipe and duct systems”, 1973.

Piccioli Cappelli P.: “Perdite di carico attraverso griglie e filtri commerciali”, Politecnico di Milano, 1995.

Sure flow equipment Inc: “Check valves”, 2010.

VAG-Armaturen GmbH: “VAG Valves – Technical Datasheets”, 2011.

VAG-Armaturen GmbH: “VAG Valves – Flyers”, 2011.

Zappe R. W.: “Valve Selection Handbook”, 4th edition, Gulf publishing Company, 1998.

Websites

<https://build.openmodelica.org>

<http://coastalhydraulicslaboratory.tpub.com>

<http://kypipe.com>

<http://m.iopscience.iop.org>

<http://udel.edu>

<http://water.me.vccs.edu>

<http://wordpress.novanumeric.com>

<http://www.accutech2000.com.au>

<http://www.arenahome.org>

<http://www.asia-valve.com>

<http://www.crbnet.it>

<http://www.cs.cdu.edu.au>

<http://www.crp.co.uk>

<http://www.diiar.polimi.it>

<http://www.emergencyplumber.uk.com>

<http://www.engineeringtoolbox.com>

<http://www.global-manufacturer.com>

<http://www.irritrol.it>

<http://www.katmarsoftware.com>

<http://www.larapedia.com>

<http://www.lmnoeng.com>

<http://www.metropumps.com>

<http://www.oppo.it>

<http://www.pfeiffer-vacuum.com>

<http://www.pipeflowcalculations.com>

<http://www.vag-armaturen.com>

<http://www.valvias.com>

<http://www.valmade.com>

<http://www.valmate.com.tw>

<https://www.wikipedia.org>

<http://www.weramc.org>

Acknowledgements

Per prima cosa vorrei ringraziare il professor Alberto Bianchi per l'opportunità che mi ha concesso, assegnandomi il compito di redigere questo elaborato che si è rivelato un lavoro stimolante e formativo.

Desidero inoltre ringraziare sentitamente l'azienda VAG-Armaturen GmbH per il supporto che mi è stato fornito per tutto il periodo di elaborazione dello scritto. In particolare ringrazio l'ing. Emiliano Veronese, sempre sollecito nel fornirmi gli strumenti, i dati e i consigli necessari. Allo stesso modo ringrazio il sig. Anton Rienmüller, per l'interesse e per la disponibilità mostrati.

Ci sono molte altre persone che hanno partecipato alla stesura di questo elaborato in maniera meno diretta ma ugualmente importante. Citare tutti e tutti gli aspetti in cui mi hanno aiutato è impossibile, ma desidero ugualmente provare a dedicar loro un piccolo ringraziamento.

Innanzitutto voglio ringraziare la mia famiglia; senza il loro supporto costante e il loro esempio non avrei avuto né i mezzi né l'ispirazione per arrivare a concludere la laurea in Ingegneria. Spero che il percorso che ho intrapreso, che si conclude in questo lavoro, li abbia resi orgogliosi tanto quanto loro rendono orgoglioso me.

Ringrazio Marta la quale, fra le molte altre cose, mi ha regalato quotidianamente la serenità e la consapevolezza che mi hanno spinto in questo periodo della mia vita.

Ringrazio i miei amici, che non sto a nominare uno per uno perché sanno già che mi riferisco a loro. Con la loro presenza e la loro vicinanza hanno alleggerito i momenti critici e reso i momenti felici, ancora più felici.

Ringrazio infine i miei insostituibili compagni di studio, i quali hanno reso il percorso accademico l'occasione di incontrare delle grandi persone e dei veri amici.